ERDC/EL TR-04-13

Environmental Laboratory

US Army Corps of Engineers®
Engineer Research and Development Center

Three-Dimensional Eutrophication Model of the Lower St. Johns River, Florida

Dottie H. Tillman, Carl F. Cerco, Mark R. Noel, James L. Martin, and John Hamrick

August 2004

20041105 088

Approved for public release; distribution is unlimited.

BEST AVAILABLE COPY

ERDC/EL TR-04-13
August 2004

Three-Dimensional Eutrophication Model of the Lower St. Johns River, Florida

Dottie H. Tillman, Carl F. Cerco, and Mark R. Noel

Environmental Laboratory
U.S. Army Engineer Research and Development Center
3909 Halls Ferry Road
Vicksburg, MS 39180-6199

James L. Martin

Department of Civil Engineering
Mississippi State University
Mississippi State, MS 39762

John Hamrick

Tetra Tech Incorporated
Fairfax, VA 22030

Final report

Approved for public release; distribution is unlimited.

Prepared for St. Johns River Water Management District
4049 Reid Street
Palatka, FL 32177

Under CRDA 02-EL-03

ABSTRACT: The CE-QUAL-ICM three-dimensional eutrophication model was applied to the lower, estuarine, portion of the St. Johns River, Florida. Transport processes were obtained from the Environmental Fluid Dynamics Code. Model application period was December 1996 through November 1998. The model activated 28 state variables in the water column including physical variables, three algal groups, multiple forms of carbon, nitrogen, phosphorus and silica, and dissolved oxygen. Several features were added to the model for this application. These included representation of the internal algal phosphorus pool, distinction of labile and refractory organic matter, and representation of nitrogen fixation. The water column was coupled to a predictive sediment diagenesis model that computed sediment-water fluxes of dissolved oxygen, chemical oxygen demand, ammonium, nitrate, phosphate, and silica, based on computed inputs of particulate organic matter. Model results were compared to an extensive suite of observations in the water column and benthic sediments.

DISCLAIMER: The contents of this report are not to be used for advertising, publication, or promotional purposes. Citation of trade names does not constitute an official endorsement or approval of the use of such commercial products. All product names and trademarks cited are the property of their respective owners. The findings of this report are not to be construed as an official Department of the Army position unless so designated by other authorized documents.

DESTROY THIS REPORT WHEN IT IS NOT LONGER NEEDED. DO NOT RETURN TO THE ORIGINATOR.

Contents

Conversion Factors, Non-SI to SI Units of Measurement xii

Preface xiii

1—Introduction 1-1

Background 1-1
St. Johns River 1-2
Study Objective 1-3
References 1-3

2—Data Bases 2-1

Observed Data 2-1
Light Attenuation Data 2-3
Meteorological Data 2-7

3—Hydrodynamic Model 3-1

Introduction 3-1
Summary of CE-QUAL-ICM Linkage Interface Procedure 3-2
Summary of Implementation 3-6
Testing of the EFDC/CE-QUAL-ICM Model Linkage 3-7

4—Loads and Boundary Conditions 4-1

Introduction 4-1
Boundary Conditions 4-1
Point and Non-point Source Loads 4-7
References 4-28

5—Water Quality Model Formulation 5-1

Introduction 5-1
Conservation of Mass Equation 5-1
State Variables 5-2
Algae 5-4
Organic Carbon 5-20
Phosphorus 5-23
Nitrogen 5-29
Silica 5-34
Chemical Oxygen Demand 5-36
Dissolved Oxygen 5-36
Temperature 5-39
Inorganic (Fixed) Solids 5-40

Salinity 5-41
Parameter Values 5-41
References 5-44

6—Water Column Calibration Results 6-1

The Calibration Period 6-1
Presentation Formats 6-3
Temperature 6-9
Salinity 6-9
Chlorophyll 6-72
Ammonia and Nitrate 6-72
Total Nitrogen 6-73
Dissolved Inorganic Phosphate 6-74
Total Phosphorus 6-75
TOC and DOC 6-75
Dissolved Oxygen 6-76
Total Suspended Solids 6-77
References 6-77

7—Modeling Processes at the Sediment-Water Interface 7-1

Introduction 7-1
Coupling With the Sediment Diagenesis Model 7-2
Field and Laboratory Program 7-5
Data Analyses 7-7
Parameter Specification 7-9
Model Results 7-11
References 7-19

8—Analysis of Water Column Kinetics 8-1

Introduction 8-1
Droop Kinetics 8-1
Nitrogen Fixation 8-15
Labile and Refractory Dissolved Organic Matter 8-27
Primary Production and Respiration 8-43
References 8-48

9—Light Attenuation 9-1

The Data Base 9-1
The Model 9-1
Model Results 9-2
Discussion 9-8
References 9-9

10—Analysis 10-1

Limiting Nutrients 10-1
Variables With No Observed Data 10-5
Transport Across Boundaries and Nutrient Budgets 10-23
Reference 10-37

Appendix A: Acronyms A1

SF 298

List of Figures

Figure 1-1 Lower St . Johns River Basin 1-4

Figure 3-1 Lower St. Johns River EFDC numerical grid 3-8

Figure 3-2 Comparison of CE-QUAL-ICM predictions at midpoint of each day to EFDC predictions and observations for the simulation period at Shands Bridge (surface) 3-10

Figure 3-3 Comparison of CE-QUAL-ICM predictions at midpoint of each day to EFDC predictions and observations for the simulation period at Shands Bridge (bottom) 3-10

Figure 3-4 Comparison of CE-QUAL-ICM predictions at midpoint of each day to EFDC predictions and observations for the simulation period at Buckman Bridge (surface) 3-11

Figure 3-5 Comparison of CE-QUAL-ICM predictions at midpoint of each day to EFDC predictions and observations for the simulation period at Buckman Bridge (bottom) 3-11

Figure 3-6 Comparison of CE-QUAL-ICM predictions at midpoint of each day to EFDC predictions and observations for the simulation period at Acosta Bridge (surface) 3-12

Figure 3-7 Comparison of CE-QUAL-ICM predictions at midpoint of each day to EFDC predictions and observations for the simulation period at Acosta Bridge (bottom) 3-12

Figure 3-8 Comparison of CE-QUAL-ICM predictions at midpoint of each day to EFDC predictions and observations for the simulation period at Dames Bridge (surface) 3-13

Figure 3-9 Comparison of CE-QUAL-ICM predictions at midpoint of each day to EFDC predictions and observations for the simulation period at Dames Bridge (bottom) 3-13

Figure 3-10 Comparison of CE-QUAL-ICM predictions at midpoint of each day to EFDC predictions and observations for the simulation period at Bar Pilot (surface) 3-14

Figure 3-11 Comparison of CE-QUAL-ICM predictions at midpoint of each day to EFDC predictions and observations for the simulation period at Bar Pilot (bottom) 3-14

Figure 4-1 Six colored reaches represent segmentation of the St . Johns River, showing location of observed water quality stations 4-9

Figure 4-2 Mean monthly TP PS loads into Segment 1, 1996-1998 4-10

Figure 4-3 Mean monthly TP PS loads into Segment 2, 1996-1998 4-10

Figure 4-4 Mean monthly TP PS loads into Segment 3, 1996-1998 4-11
Figure 4-5 Mean monthly TP PS loads into Segment 4, 1996-1998 4-11
Figure 4-6 Mean monthly TP PS loads into Segment 5, 1996-1998 4-12
Figure 4-7 Mean monthly TP PS loads into Segment 6, 1996-1998 4-12
Figure 4-8 Mean monthly TN PS loads into Segment 1, 1996-1998 4-13
Figure 4-9 Mean monthly TN PS loads into Segment 2, 1996-1998 4-13
Figure 4-10 Mean monthly TN PS loads into Segment 3, 1996-1998 4-14
Figure 4-11 Mean monthly TN PS loads into Segment 4, 1996-1998 4-14
Figure 4-12 Mean monthly TN PS loads into Segment 5, 1996-1998 4-15
Figure 4-13 Mean monthly TN PS loads into Segment 6, 1996-1998 4-15
Figure 4-14 Mean monthly TP NPS loads into Segment 1, 1996-1998 4-20
Figure 4-15 Mean monthly TP NPS loads into Segment 2, 1996-1998 4-20
Figure 4-16 Mean monthly TP NPS loads into Segment 3, 1996-1998 4-21
Figure 4-17 Mean monthly TP NPS loads into Segment 4, 1996-1998 4-21
Figure 4-18 Mean monthly TP NPS loads into Segment 5, 1996-1998 4-22
Figure 4-19 Mean monthly TP NPS loads into Segment 6, 1996-1998 4-22
Figure 4-20 Mean monthly TN NPS loads into Segment 1, 1996-1 998 4-23
Figure 4-21 Mean monthly TN NPS loads into Segment 2, 1996-1998 4-23
Figure 4-22 Mean monthly TN NPS loads into Segment 3, 1996-1998 4-24
Figure 4-23 Mean monthly TN NPS loads into Segment 4, 1996-1998 4-24
Figure 4-24 Mean monthly TN NPS loads into Segment 5, 1996-1998 4-25
Figure 4-25 Mean monthly TN NPS loads into Segment 6, 1996-1998 4-25
Figure 5-1 Production versus irradiance relationship 5-6
Figure 5-2 Effect of temperature and nutrient limitation on carbon-to-chlorophyll ratio 5-7
Figure 5-3 Effect of irradiance and temperature on carbon-to-chlorophyll ratio 5-8
Figure 5-4 Effect of nutrient limitation and irradiance on carbon-to-chlorophyll ratio 5-8
Figure 5-5 Monod formulation for nutrient-limited growth 5-9
Figure 5-6 Droop formulation for nutrient-limited growth 5-10
Figure 5-7 Algal biomass with fixed and variable internal phosphorus 5-12
Figure 5-8 Dissolved phosphate with fixed and variable internal phosphorus 5-12
Figure 5-9 Biomass and cell quota for algae with variable internal phosphorus 5-13

Figure 5-10 Internal and external phosphorus for simulation with variable internal phosphorus 5-13
Figure 5-11 Relation of algal production to temperature 5-14
Figure 5-12 Combined effects of light and nutrient limitations 5-15
Figure 5-13 Relation of algal metabolism to temperature 5-17
Figure 5-14 Algal ammonium preference 5-19
Figure 5-15 Model carbon cycle 5-20
Figure 5-16 Model phosphorus cycle 5-24
Figure 5-17 Effect of algal biomass and nutrient concentration on phosphorus mineralization 5-26
Figure 5-18 Model nitrogen cycle 5-30
Figure 5-19 Effect of DO and ammonium on nitrification rate 5-32
Figure 5-20 Model silica cycle 5-35
Figure 5-21 DO sources and sinks 5-37
Figure 5-22 Computed and tabulated values of Rv 5-38
Figure 6-1 Wind speed for both simulation years 6-2
Figure 6-2 Time-series plots at Fulton Point for top, middle, and bottom layers for all water quality constituents 6-10
Figure 6-3 Time-series plots at Pine Point for top, middle, and bottom layers for all water quality constituents 6-29
Figure 6-4 Time-series plots at Picolata top, middle, and bottom layers for all water quality constituents 6-42
Figure 6-5 Longitudinal water quality results for August 1997 and 1998 6-49
Figure 6-6 Cumulative distribution results for all water quality constituents 6-64
Figure 7-1 Sediment model schematic 7-1
Figure 7-2 Sediment model elevation 7-3
Figure 7-3 Location of sediment-water flux and interstitial water measurements 7-6
Figure 7-4 Computed and observed sediment diagenesis flux 7-12
Figure 7-5 Computed and observed sediment-water ammonium flux 7-12
Figure 7-6 Computed and observed sediment oxygen demand 7-13
Figure 7-7 Computed and observed sediment phosphate flux 7-14
Figure 7-8 Observed versus computed interstitial ammonium concentration 7-14
Figure 7-9 Observed versus computed interstitial nitrate concentration 7-15
Figure 7-10 Observed versus computed interstitial phosphate concentration. 7-16
Figure 7-11 Observed versus computed interstitial sulfide concentration 7-16

Figure 7-12 Observed versus computed interstitial silica concentration 7-17
Figure 7-13 Observed versus computed sediment bulk nitrogen concentration 7-17
Figure 7-14 Observed versus computed sediment bulk organic carbon concentration 7-18
Figure 7-15 Observed versus computed sediment bulk inorganic phosphorus concentration 7-18
Figure 7-16 Observed versus computed sediment bulk phosphorus concentration 7-19
Figure 8-1 Computed limits to algal production at Racey Point 8-6
Figure 8-2 Computed limits to algal production at Talleyrand 8-7
Figure 8-3 Computed cell quota at Racey Point 8-8
Figure 8-4 Computed cell quota at Talleyrand 8-9
Figure 8-5 Computed and observed chlorophyll at Racey Point 8-11
Figure 8-6 Computed and observed chlorophyll at Talleyrand 8-12
Figure 8-7 Computed and observed DIP at Racey Point 8-13
Figure 8-8 Computed and observed DIP at Talleyrand 8-14
Figure 8-9 Computed and observed relationship between temperature and nitrogen fixation 8-17
Figure 8-10 Computed and observed relationship between salinity and nitrogen fixation 8-18
Figure 8-11 Computed and observed relationship between DIN and nitrogen fixation 8-19
Figure 8-12 Effect of parameter Khnfix on nitrogen limitation computed for KHn = 0.02 g N m^3 8-20
Figure 8-13 Computed and observed relationship between chlorophyll and nitrogen fixation 8-22
Figure 8-14 Computed and observed chlorophyll concentration, with nitrogen fixation, along river axis, August 1998 8-23
Figure 8-15 Computed and observed total nitrogen concentration, with nitrogen fixation, along river axis, August 1998 8-23
Figure 8-16 Computed and observed chlorophyll concentration, without nitrogen fixation, along river axis, August 1998 8-24
Figure 8-17 Computed and observed total nitrogen concentration, without nitrogen fixation, along river axis, August 1998 8-24
Figure 8-18 Computed salinity along river axis, August 1998 8-25
Figure 8-19 Chlorophyll ME with and without nitrogen fixation 8-26
Figure 8-20 Total nitrogen ME with and without nitrogen fixation 8-27
Figure 8-21 Computed labile and refractory DOC at Picolata 8-29

Figure 8-22 Computed labile and refractory DON at Picolata 8-29
Figure 8-23 Computed labile and refractory DOP at Picolata 8-30
Figure 8-24 Computed and observed DOC at Picolata for calibration, all labile, all refractory, and average splits 8-32
Figure 8-25 System-wide cumulative distributions of computed and observed DOC for calibration, all labile, all refractory, and average splits 8-33
Figure 8-26 Computed and observed DO at Picolata for calibration, all labile, all refractory, and average splits 8-34
Figure 8-27 System-wide cumulative distributions of computed and observed DO for calibration, all labile, all refractory, and average splits 8-35
Figure 8-28 Computed and observed DIN at Picolata for calibration, all labile, all refractory, and average splits 8-36
Figure 8-29 System-wide cumulative distributions of computed and observed DIN for calibration, all labile, all refractory, and average splits 8-37
Figure 8-30 Computed and observed chlorophyll at Picolata for calibration, all labile, all refractory, and average splits 8-39
Figure 8-31 System-wide cumulative distributions of computed and observed chlorophyll for calibration, all labile, all refractory, and average splits 8-40
Figure 8-32 Computed and observed DIP at Picolata for calibration, all labile, all refractory, and average splits 8-41
Figure 8-33 System-wide cumulative distributions of computed and observed DIP for calibration all labile, all refractory, and average splits 8-42
Figure 8-34 Observed and computed monthly mean GAP at Federal Point ... 8-44
Figure 8-35 Observed and computed monthly mean GAP at Picolata 8-44
Figure 8-36 Observed and computed monthly mean GAP at Mandarin Point 8-45
Figure 8-37 Observed and computed monthly mean VCR at Federal Point ... 8-46
Figure 8-38 Observed and computed monthly mean VCR at Picolata 8-46
Figure 8-39 Observed and computed monthly mean VCR at Mandarin Point 8-47
Figure 9-1 Computed and observed light attenuation at Palatka 9-3
Figure 9-2 Computed and observed light attenuation at Racey Point 9-3
Figure 9-3 Computed and observed light attenuation at Picolata 9-4
Figure 9-4 Computed and observed light attenuation at Mandarin Point 9-4
Figure 9-5 Computed and observed light attenuation at Piney Point 9-5

Figure 9-6 Computed and observed light attenuation at Talleyrand 9-5
Figure 9-7 Computed and observed light attenuation at Fulton Point..... 9-6
Figure 9-8 Computed and observed light attenuation at Bar Pilot 9-6
Figure 9-9 Mean computed and observed light attenuation at eight stations .. 9-7
Figure 9-10 Components of modeled light attenuation 9-7
Figure 9-11 Observed mean light attenuation versus salinity at nine stations in the modeled domain 9-8
Figure 10-1 Limiting factors of algal growth at seven stations on the St . Johns River 10-1
Figure 10-2 Fulton Point computed water quality constituents that have no observed data available 10-6
Figure 10-3 Piney Point computed water quality constituents that have no observed data available 10-13
Figure10-4 Picolata computed water quality constituents that have no observed data available 10-20
Figure 10-5 TN budget by segments for both simulation years 10-25
Figure 10-6 TP budget by segments for both simulation years 10-31

List of Tables

Table 2-1 CE-QUAL-ICM Water Quality Model State Variables 2-1
Table 2-2 St. Johns River Water Quality Main Stem Stations 2-2
Table 2-3 Available Continuously Monitored Water Quality Main Stem Data 2-3
Table 2-4 Light Attenuation Stations on the St. Johns River 2-4
Table 2-5 Available 1997-1998 Meteorological Data 2-5
Table 4-1 Correspondence of CE-QUAL-ICM State Variables and Point-Source Concentration Data 4-2
Table 4-2 Specification of West and East Bank Tributary Stations for Water Temperatures 4-2
Table 4-3 Point Loading Sources Included in Model Simulations 4-7
Table 4-4 Point-Source Concentration Data Provided by the SJRWWMD With Partitioning Fractions for Corresponding Water Quality Variables 4-16
Table 4-5 Non-point Loading Sources Included in Model Simulations 4-18
Table 4-6 Atmospheric Loads to St Johns River 4-29
Table 5-1 Water Quality Model State Variables 5-2
Table 5-2 Properties of Well-Mixed System 5-11

Table 5-3 Parameters in Kinetics Equations 5-41
Table 6-1 Combined Water Quality Statistics for All Stations 6-5
Table 6-2 Combined Water Quality Statistics for All Stations -1996-1997 .. 6-5
Table 6-3 Combined Water Quality Statistics for All Stations -1997-1998 .. 6-6
Table 6-4 Statistics for All Water Quality Constituents at Each Station 6-6
Table 6-5 Comparison of Water Quality RE Statistics at Five CE-QUAL-ICM Study Sites 6-71
Table 7-1 Sediment Model State Variables and Fluxes 7-2
Table 7-2 Summary of Sediment-Water Fluxes 7-8
Table 7-3 Routing Organic Particles Into Sediment Classes 7-10
Table 8-1 Parameters in Droop Kinetics 8-5
Table 8-2 Dissolved Organic Matter Mineralization Rates 8-31
Table 8-3 Observed and Computed Annual-Average Production and Respiration 8-45
Table 10-1 Variables With No Observed Data 10-5

Conversion Factors, Non-SI to SI Units of Measurement

Non-SI units of measurement used in this report can be converted to SI units as follows:

Multiply	By	To Obtain
miles (U.S. statute)	1.609347	kilometers
square miles	2,589,998	square meters

Preface

This study was conducted as part of a feasibility cost share agreement between the U.S. Army Engineer District, Jacksonville, and the St. Johns River Water Management District related to protecting and restoring the Lower St. Johns River. The project was assigned to the U.S. Army Engineer Research and Development Center (ERDC) under the purview of the Environmental Laboratory (EL).

This report was prepared by the Water Quality and Contaminant Modeling Branch, Environmental Processes and Effects Division, EL. The study was supervised by Barry Bunch, Chief, Water Quality and Contaminant Modeling Branch, Environmental Processes and Effects Division, EL. General supervision was provided by Dr. Edwin A. Theriot, Director, EL. Technical reviewers were Toni Toney, Carlos Ruiz, and Billy Johnson.

COL James R. Rowan, EN, was Commander and Executive Director of ERDC. Dr. James R. Houston was Director.

1 Introduction

Background

The U.S. Army Engineer District, Jacksonville (CESAJ)[1] and the St. Johns River Water Management District (SJRWMD) have a feasibility cost share agreement related to protecting and restoring the Lower St. Johns River (LSJR). The agreement includes a need to identify maximum acceptable levels of point and nonpoint source pollutant loadings. As designated in the 1987 Surface Water Improvement and Management (SWIM) Act, the Lower St. Johns River basin is in need of restoration and special protection. The Florida Department of Environmental Protection (FDEP) and the U.S. Environmental Protection Agency (EPA) have listed it as an impaired waterbody, which requires the establishment of a Total Maximum Daily Load (TMDL) (303d listed for nutrients, total suspended solids, turbidity, coliform bacteria, and other causes). As part of Phase 3, Amendment 4 in the cost share agreement, written specifications for an LSJR water quality model have been determined and described. The U.S. Army Engineering Research and Development Center, Environmental Laboratory (EL) was requested by CESAJ to support development of a three-dimensional (3D) hydrodynamic and water quality model for the LSJR system.

In addition to determining acceptable levels of pollutant loadings and assessing the effects of these loadings on the LSJR, the model will be used as a means to separate natural variations from human impacts. Other potential model uses are:

a. Gaining a basic understanding of the physical and some of the chemical and biological dynamics of the river.

b. Evaluating the sensitivity of the river to changes in tributary inflows and pollutant loadings.

c. Ranking areas for load reductions in accordance with management priorities.

d. Developing recommendations for practical and feasible river restoration actions and plans for management.

[1] For convenience unusual abbreviations used in this report are listed and defined in Appendix A, Acronyms.

e. Developing recommendations to the Florida Department of Environmental Protection in support of Total Maximum Daily Loads and other pollutant loading limitations.

To meet the requirements of the CESAJ/SJRWMD scope-of-work (SOW), the modeling system had to contain coupled, 3D hydrodynamic and water quality models that were capable of running multi-year simulations on workstations. The hydrodynamic model (HM) had to include salinity transport and baroclinic coupling to momentum. The SOW also requested that the 3D finite difference models use a boundary-fitted grid, and the grid for the water quality model (WQM) must be the same as for the HM. The modules in the WQM had to include kinetics for: (1) water column eutrophication processes including multiple phytoplankton groups; (2) littoral processes involving growth of submerged aquatic vegetation (SAV) and organic matter flux; and (3) sediment dynamics including deposition and resuspension, flocculation of organic matter, sediment diagenesis, and dissolved oxygen (DO) and nutrient fluxes between bottom sediments and the water column.

St. Johns River

The SJRWMD manages the LSJR basin, which represents approximately 22 percent of the SJRWMD managed area. The LSJR flows from the confluence of Florida's Ocklawaha River to the north and east toward Jacksonville, eventually flowing into the Atlantic Ocean (Figure 1-1). Due to the large tidal range near its mouth, the St. Johns has never been precisely flow-gauged, though mean annual discharge is believed to be between 170 to 225 m^3/s (Morris 1995). In periods of low water, tides may cause a reverse flow as far south as Lake Monroe, 161 miles upstream from the river's mouth.

The St. Johns River is the longest northern flowing river in the United States and the longest river in Florida at 300 miles in length. The LSJR represents approximately one-third of the total length of the St. Johns River (100 miles) and less than one-third of the total watershed area of 9,562 sq miles. The water surface area of the LSJR is 34,817 ha (85,967 acres) including tributary mouths below tide head (Hendrickson and Konwinski 1998). Hendrickson and Konwinski (1998) segment the LSJR into three riverine salinity and limnologic zones: a fresh tidal lacustrine zone extending from Palatka to Orange Park; a predominantly oligohaline, lacustrine zone extending from Orange Park north toward Fuller Warren Bridge (Interstate 95) in Jacksonville; and a mesohaline, riverine zone extending from Jacksonville to the Atlantic Ocean.

The LSJR basin is between the subtropical climate of southern Florida and the humid continental climate of the southeastern United States. Its climate is classified as humid subtropical, having an average summer maximum daily temperature of 32.2 °C (90 °F). During the winter season, below freezing temperatures occur 10-15 times per year. The average annual rainfall in the LSJR basin is approximately 132 cm (52 in.) with most of the precipitation occurring June through September from convective activity.

Land use patterns within the basin vary from the southern portion to the northern portion. The southern portion is predominantly rural with land uses ranging from forestry to row crop agriculture. In the northern portion of the basin, the heavily urbanized cities of Jacksonville, Orange Park, and Middleburg dominate land uses. Approximately three quarters (64 to 82 percent) of the heavily urbanized areas of the LSJR drain to the oligohaline and mesohaline zones of the river, compared with the 62 to 98 percent of agricultural land draining to the fresh tidal lacustrine zone (Hendrickson and Konwinski 1998).

Water quality of the LSJR varies depending on location (e.g., poor in the urbanized areas to good in the sparsely populated areas). Water quality problems identified on the LSJR include low DO, excessive nutrients that induce algal blooms (confined to the area from Palatka to 15 miles north at Tocoi Creek and from Doctor's Inlet north to the Fuller Warren Bridge), and elevated bacterial populations. The primary culprits causing degradation are point and nonpoint sources such as industrial dischargers, municipal water treatment plants, stormwater runoff from agriculture and dairy farms, and septic tanks (SAD and SJRWMD 1994).

Study Objective

The objective of this 2-year study was the development of a 3D calibrated water quality model, with the capabilities discussed above coupled to the SJRWMD hydrodynamic model of the LSJR. For the 2-year simulation period, the SJRWMD selected December 1996 through November 1998 because more observed data had been collected during this period for the water quality constituents of interest.

Reference

Hendrickson, J. C., and Konwinski., J. (1998). "Seasonal nutrient import-export budgets for the lower St. Johns River, Florida," Final report under Contract No. WM598, Florida Department of Environmental Protection, Tallahassee, FL.

Morris, F. W. (1995). "Lower St. Johns River Basin Reconnaissance: Hydrodynamics and salinity of surface water," St. Johns River Water Management District Technical Publication SJ95-9, Vol 3, St. Johns River Water Management District, Palatka, FL.

U.S. Army Corps of Engineers, Jacksonville (South Atlantic Division (SAD)), and St. Johns River Water Management District. (1994). "St. Johns River, Florida Water Quality Feasibility Study, Phase I Interim Report, Volume IV: Estimated Natural Discharge and Chemical-Constituent Loading from the Upper Floridian Aquifer to the Lower St. Johns River, Northern Florida," Special Publication SJ94-SP15, Palatka, FL.

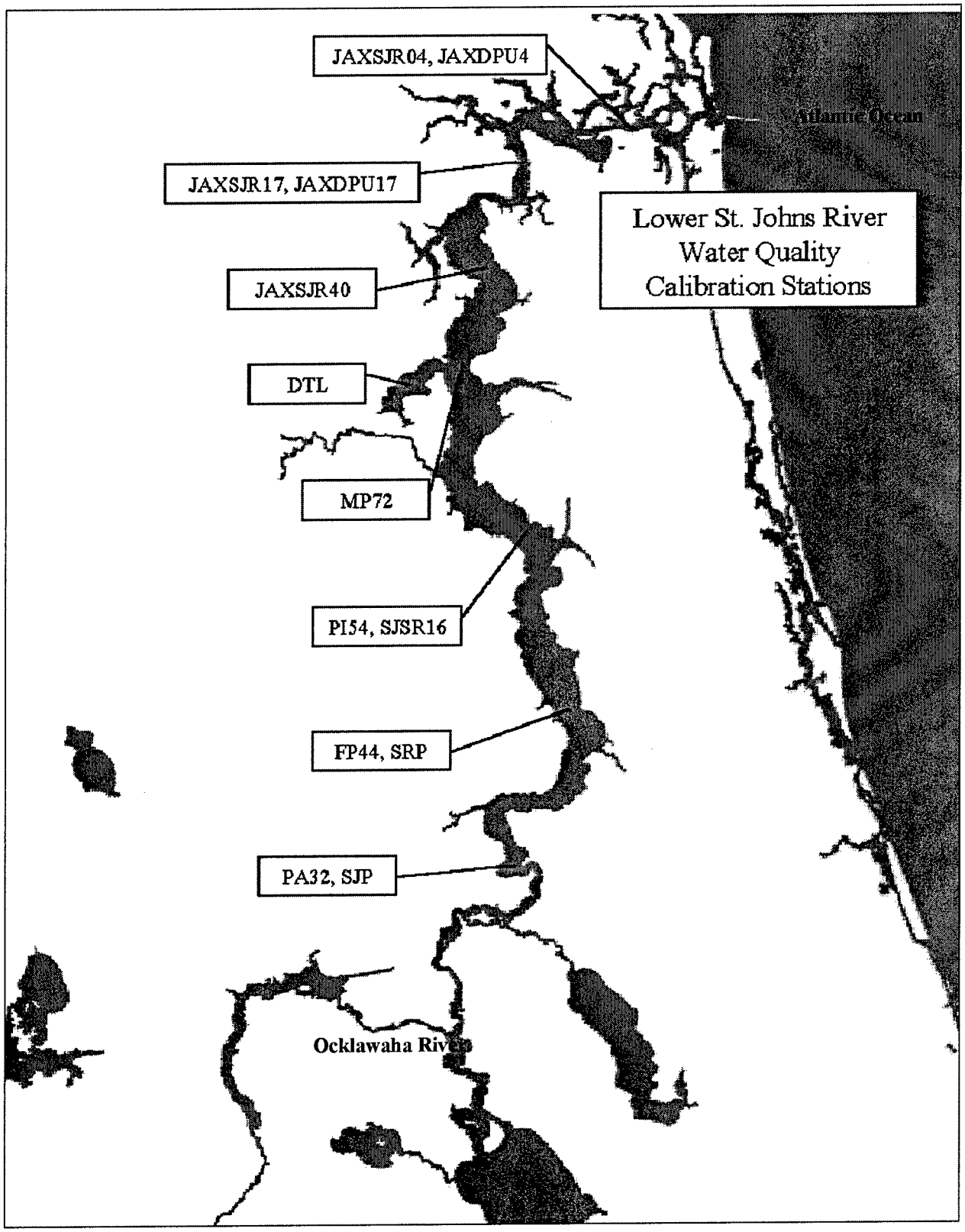

Figure 1-1. Lower St. Johns River Basin

2 Data Bases

Observed Data

Observed water quality data are required by Corps of Engineers Integrated Compartment Water Quality Model (CE-QUAL-ICM) to set initial and boundary conditions for each constituent modeled in a simulation. Observed data (preferably water column profile data) are also required to evaluate model performance. The SJRWMD provided all observed data for this study. Much of the data were extracted from STOrage and RETrieval (STORET) into a Microsoft® Excel spreadsheet. This file contained data for 50 water quality parameters at 303 stations on the St. Johns River and its tributaries. Although data span many years (1959-1999), not every water quality constituent was measured each year. Of the 50 water quality parameters, only data for constituents being modeled (Table 2-1) were extracted from the spreadsheet and plotted to examine data trends and consistency. A Statistical Analysis System (SAS) program was run on the data to calculate mean, maximum, and minimum values for each year. Most observed data were measured in the surface layer, although a few stations had observations at middle and bottom depths.

Table 2-1
CE-QUAL-ICM Water Quality Model State Variables

Temperature	Salinity
Fixed Solids	Cyanobacteria
Diatoms	Other Phytoplankton
Zooplankton Group 1	Zooplankton Group 2
Labile Dissolved Organic Carbon	Refractory Dissolved Organic Carbon
Labile Particulate Organic Carbon	Refractory Particulate Organic Carbon
Ammonium	Nitrate + Nitrite Nitrogen
Refractory Dissolved Organic Nitrogen	Labile Dissolved Organic Nitrogen
Refractory Particulate Organic Nitrogen	Labile Particulate Organic Nitrogen
Labile Dissolved Organic Phosphorus	Total Phosphate
Labile Particulate Organic Phosphorus	Refractory Dissolved Organic Phosphorus
Internal Phosphorus, Algal Group 2	Refractory Particulate Organic Phosphorus
Chemical Oxygen Demand	Internal Phosphorus, Algal Group 1
Dissolved Silica	Internal Phosphorus, Algal Group 3
Particulate Biogenic Silica	Dissolved Oxygen

The SJRWMD identified two consecutive simulation periods to be modeled during this study, 1 December 1996 to 30 November 1997 and 1 December 1997 to 30 November 1998. Table 2-2 was generated from data extracted from the Excel spreadsheet provided by SJRWMD and contains a number of observations for each modeled water quality constituent for each water level of the main stem stations (Figure 1-1) used for comparison during calibration.

Table 2-2
St. Johns River Water Quality Main Stem Stations (Hendrickson 1999)

Station ID	River Mile	NH4D		NH4T		NOXT		NOXD		TPT		TPD		PO4D		TOC		DOC		CL		CHLA		CHLAC	
		97	98	97	98	97	98	97	98	97	98	97	98	97	98	97	98	97	98	97	98	97	98	97	98
JAXDPU4	07a	-	-	-	-	-	-	-	-	-	-	-	-	-	-	-	-	-	-	-	-	-	-	-	-
JAXSJR04	07b	31	65	34	65	-	16	-	65	34	65	31	65	-	65	34	65	30	65	-	59	34	65	34	65
JAXDPU5	08	-	-	-	-	-	-	-	-	-	-	-	-	-	-	-	-	-	-	-	-	-	-	-	-
JAXDPU13	13	-	-	-	-	-	-	-	-	-	-	-	-	-	-	-	-	-	-	-	-	-	-	-	-
JAXDPU14	14a	-	-	-	-	-	-	-	-	-	-	-	-	-	-	-	-	-	-	-	-	-	-	-	-
JAXSJR14	14b	33	-	36	-	-	-	-	-	36	-	33	-	-	-	36	-	33	-	-	-	36	-	36	-
JAXSJR17	17	30	70	33	70	-	18	-	70	33	70	30	70	-	70	33	70	30	70	-	64	33	70	33	70
JAXDPU17	18	-	-	-	-	-	-	-	-	-	-	-	-	-	-	-	-	-	-	-	-	-	-	-	-
OR81	25a	-	-	-	-	-	-	-	-	-	-	-	-	-	-	-	-	-	-	-	-	-	-	-	-
OR82	25b	-	-	-	-	-	-	-	-	-	-	-	-	-	-	-	-	-	-	-	-	-	-	-	-
MP72	36	13	13	13	13	-	3	13	13	13	13	13	13	13	13	13	13	13	13	13	12	13	13	13	13
SJRHBP	42	20	20	22	20	2	-	22	20	22	20	20	20	22	20	22	20	20	20	22	20	22	20	22	20
PP62	46	11	13	11	13	-	3	11	13	11	13	11	13	11	13	11	13	11	13	11	12	11	13	11	13
SJGCE	50a	11	12	12	12	1	-	11	12	12	12	11	12	11	12	12	12	11	12	12	12	12	12	12	12
SJSR16	50b	11	12	12	12	1	-	12	12	12	12	10	12	12	12	12	12	11	12	12	12	12	12	12	12
PI52	55a	-	-	-	-	-	-	1	-	-	-	-	-	1	-	-	-	-	-	1	-	1	-	-	-
SJCM25	55b	11	12	12	12	1	-	12	12	12	12	11	12	12	12	12	12	11	12	12	12	12	12	12	12
FP44	60	12	12	12	12	-	3	12	12	12	12	12	12	12	12	11	12	12	12	12	11	12	12	12	12
SRP	63	11	12	12	12	1	-	12	12	12	12	11	12	12	12	12	12	11	12	12	12	12	12	12	12
SJM37	67	11	12	12	12	1	-	11	12	12	12	11	12	12	12	12	12	11	12	12	12	12	12	12	12
FP42	70	11	13	11	13	-	3	11	13	11	13	11	13	11	13	11	13	11	13	11	12	11	13	11	13
SJRCC	75	11	11	12	11	1	-	11	11	12	11	11	11	12	11	12	11	11	11	12	11	12	11	12	11

Note:

NH4D: Ammonium-Dissolved MG/L as N
NH4T: Ammonium-Total MG/L as N
NOXT: Nitrate&Nitrite-Total MG/L as N
NOXD: Nitrate&Nitrite-Diss. MG/L as N
TPT: Total Phosphorus-T MG/L as P
TPD: Total Phosphorus-D MG/L as P
PO4D: Ortho-Phosphate-D MG/L as P
TOC: Total Organic Carbon MG/L as C
DOC: Dissolved Organic Carbon MG/L as C
CL: Chloride MG/L
CHLA: Chlorophyll-A MG/M3
CHLAC: Chlorophyll-Corrected MG/M3

In addition to the Excel spreadsheet, the SJRWMD provided files containing continuous monitored data by the U.S. Geological Survey (USGS) for the following constituents:

- Temperature,
- DO,
- Salinity,
- Barometric pressure,
- Air temperature,
- Relative humidity,
- Net radiation,
- Photo-active radiation,
- Rainfall,
- Wind speed/wind direction.

Table 2-3 lists the station names and locations, water levels and time periods of salinity, DO, and temperature samples.

Table 2-3
Available Continuously Monitored Water Quality Main Stem Data Provided by SJRWMD

Station Name	Dates	River Miles	Salinity			DO			Water Temp		
			S	M	B	S	M	B	S	M	B
Dames Point	10/4/95-9/30/98	10	X	X	X	X	X	X	X	X	X
Acosta Bridge	10/4/95-9/30/98	26	X	X	X	X	X	X	X	X	X
Shands Bridge	10/4/95-9/30/98	50	X	X	X	X	X	X	X	X	X
Buckman Bridge	10/4/95-9/30/98	58	X	X	X	X	X	X	X	X	X
Dancy Point	10/4/95-9/30/98	70	X		X	X		X	X		X
Buffalo Bluff	10/4/95-9/30/98	89	X			X			X		

Note: S = surface; M = middle; B = bottom.

Light Attenuation Data

SJRWMD provided light attenuation observations for a number of stations on the LSJR (Table 2-4). A designation of N/A for a segment number in Table 2-4 indicates the station was outside the study grid. Comparisons of light attenuation values predicted by CE-QUAL-ICM were made to data collected at stations designated on Figure 1-1. Data collection at most of the stations used in comparisons began mid-1997 or later and continued into late 2000. Some stations did not have any data collected during the simulation period.

Table 2-4
Light Attenuation Stations on the St. Johns River

Station ID	Collection Period	Segment #
SAVBOLSO	10/21/1997 - 04/02/2001	4
SAVBUCBO	10/21/1997 – 12/15/1999	4
SAVCRL10	10/08/1997 – 12/16/1999	N/A
SAVCRL20	10/08/1997 – 04/03/2001	N/A
SAVCRL30	10/08/1999 - 12/16/1999	N/A
SAVDRLKO	10/21/1997 – 04/02/2001	5
SAVFERPO	10/22/1997 – 09/29/1998	5
SAVBOLSO	10/21/1997 – 04/02/2001	4
SAVFPLO	10/08/1997 – 12/16/1999	6
SAVHOLCO	11/19/1997 – 12/15/1999	5
SAVHRTBO	10/21/1997 – 12/15/1999	4
SAVLKGRO	01/19/2000 – 04/03/2001	N/A
SAVMILCO	10/21/1997 – 03/08/2001	2
SAVMOCSO	10/21/1997 – 12/15/1999	4
SAVPTLVO	10/21/1997 – 09/19/2000	4
SAVRICNO	10/08/1997 – 04/03/2001	6
SAVSCRAO	10/22/1997 – 04/03/2001	5
SAVWARCO	10/22/1997 – 12/16/1999	6
SAVWELKO	10/22/1997 – 09/20/2000	3
HCC	01/14/1997 – 03/15/2001	5
SJCM25	01/14/1997 – 03/15/2001	5
SJM37	01/14/1997 – 03/15/2001	6
SJP	06/10/1997 – 03/15/2001	6
SJRCC	01/14/1997 – 03/15/2001	6
SJRCE	03/10/1999 – 03/15/2001	N/A
SJRCW	03/10/1999 – 03/15/2001	6
SJRHBP	02/11/1997 – 03/15/2001	5
SJSR16	01/14/1997 – 03/15/2001	5
SRB	10/09/1997 – 12/14/2000	6
SRP	02/11/1997 – 03/15/2001	4
BB22	04/05/1999 – 10/26/2000	6
CRESLM	04/05/1999 – 02/27/2001	N/A
DEEPCC	04/29/1999 – 02/27/2001	5
DTL	04/29/1999 – 02/26/2001	4
FP42	04/29/1999 – 02/27/2001	6
FP44	04/29/1999 – 02/27/2001	5
JAXSJR04	03/08/1999 – 02/26/2001	2
JAXSJR17	03/08/1999 – 02/26/2001	4
JAXSJR40	04/02/1999 – 02/26/2001	4
LG12	04/05/1999 – 02/27/2001	3
MP72	04/02/1999 – 02/26/2001	4
MSJLGM	04/05/1999 – 10/25/1999	3
MSJLGN	04/05/1999 – 10/25/1999	3
MSJLGS	04/05/1999 – 10/25/1999	3

(Sheet 1 of 3)

Table 2-4 (Continued)

Station ID	Collection Period	Segment #
OCKLRM	04/27/1999 – 02/27/2001	3
PA32	04/29/1999 – 02/27/2001	6
PALMOC	04/29/1999 – 10/26/1999	4
OCKLRM	04/02/1999 – 10/26/1999	4
PI54	04/29/1999 – 02/26/2001	5
PP62	04/29/1999 – 08/26/1999	5
SJR40	04/27/1999 – 10/25/1999	N/A
SJRHBP	11/22/1999 – 02/26/2001	5
SJWSIL	04/29/1999 – 10/30/2000	5
JAXSJR01	03/09/2000 – 02/12/2001	N/A
JAXSJR04	03/09/2000 – 02/12/2001	2
JAXSJR09	03/09/2000 – 02/12/2001	N/A
JAXSJR14	03/09/2000 – 02/12/2001	3
JAXSJR17	03/09/2000 – 02/12/2001	4
JAXSJR21	03/09/2000 – 02/12/2001	4
JAXSJR26	03/09/2000 – 02/12/2001	4
JAXSJR30	03/09/2000 – 02/12/2001	4
JAXSJR34	03/09/2000 – 02/12/2001	4
JAXSJR40	03/09/2000 – 02/12/2001	4
AOESJR	09/21/2000 – 01/18/2001	1
AONSJR	09/21/2000 – 01/18/2001	1
AOSSJR	09/21/2000 – 01/18/2001	1
DTL	04/07/1999 – 10/26/1999	4
JULCM	04/07/1999 – 09/29/1999	N/A
ORTRM	04/07/1999 – 09/29/1999	N/A
SAVBOLSI	04/07/1999 – 09/29/1999	4
SAVBUCBI	04/07/1999 – 09/29/1999	4
SAVDRLKI	05/051999 – 09/29/1999	5
SAVMOCSI	04/07/1999 – 09/29/1999	4
SAVPTLVI	04/07/1999 – 09/29/1999	4
SJNDTLIE	04/07/1999 – 09/29/1999	4
SJNOBBLZ	04/07/1999 – 09/29/1999	4
SJNPPLZ	04/07/1999 – 09/29/1999	4
SJRM27C	04/07/1999 – 09/29/1999	4
SJRM27E	04/07/1999 – 09/29/1999	4
SJRM27W	04/07/1999 – 09/29/1999	4
SJRM30C	04/07/1999 – 09/29/1999	4
SJRM30E	04/07/1999 – 09/29/1999	4
SJRM30W	04/07/1999 – 09/29/1999	4
SJRM35C	04/07/1999 – 09/29/1999	4
SJRM40E	04/07/1999 – 09/29/1999	4
SJRM40W	04/07/1999 – 09/29/1999	4
SJRM54B	08/16/2000 – 08/30/2000	N/A
SJRM54C	08/10/2000 – 08/30/2000	N/A
SJRM54D	08/16/2000 – 08/30/2000	N/A

(Sheet 2 of 3)

Table 2-4 (Concluded)

Station ID	Collection Period	Segment #
SJRM54E	08/16/2000 – 08/30/2000	N/A
SJRM54W	08/16/2000 – 08/30/2000	N/A
SJRM58B	08/02/2000 – 08/30/2000	N/A
SJRM58C	08/02/2000 – 08/30/2000	N/A
SJRM58D	08/02/2000 – 08/30/2000	N/A
SJRM58E	08/02/2000 – 08/30/2000	N/A
SJRM58W	08/02/2000 – 08/30/2000	N/A
SJRM62B	06/21/2000 – 08/23/2000	N/A
SJRM62C	06/21/2000 – 08/30/2000	N/A
SJRM62D	06/21/2000 – 08/23/2000	N/A
SJRM62E	06/21/2000 – 08/23/2000	N/A
SJRM62W	06/21/2000 – 08/23/2000	N/A
SJRM66B	06/14/2000 – 08/30/2000	N/A
SJRM66C	06/14/2000 – 08/30/2000	N/A
SJRM66D	06/14/2000 – 08/30/2000	N/A
SJRM66E	06/14/2000 – 08/30/2000	N/A
SJRM66W	06/07/2000 – 08/23/2000	N/A
SJRM70B	06/07/2000 – 08/23/2000	N/A
SJRM70C	06/14/2000 – 08/23/2000	N/A
SJRM70D	06/14/2000 – 08/23/2000	N/A
SJRM70E	06/14/2000 – 08/23/2000	N/A
SJRM70W	06/14/2000 – 08/23/2000	N/A
SJRM74B	06/07/2000 – 07/26/2000	N/A
SJRM74C	06/07/2000 – 07/26/2000	N/A
SJRM74D	06/07/2000 – 07/26/2000	N/A
SJRM74E	06/07/2000 – 07/26/2000	N/A
SJRM74W	06/07/2000 – 07/26/2000	N/A
SJRM78B	06/07/2000 – 07/19/2000	N/A
SJRM78C	06/07/2000 – 07/19/2000	N/A
SJRM78D	06/07/2000 – 07/19/2000	N/A
SJRM78E	06/07/2000 – 07/19/2000	N/A
SJRM78W	06/07/2000 – 07/19/2000	N/A
MILLCSJR	02/08/2000 – 10/24/2000	N/A
MTPTNCTR	02/08/2000 – 05/02/2000	N/A
SAVBOLSO	11/16/1999 – 10/24/2000	4
SAVCRL20	11/17/1999 – 05/03/2000	N/A
SAVDRLKO	11/16/1999 – 10/24/2000	5
SAVRICNO	11/17/1999 – 10/25/2000	6
SAVSCRAO	11/17/1999 – 10/25/2000	5
SAVWELKO	11/17/1999 – 10/25/2000	3

(Sheet 3 of 3)

Meteorological Data

Table 2-5 contains station name and locations where meteorological data were supplied by the SJRWMD. Specific meteorological data (e.g., dew point temperature and cloud cover) not provided by the SJRWMD were requested from the Air Force Combat Climatology Center in order to calculate heat exchange coefficients and equilibrium temperatures required by CE-QUAL-ICM. Data were requested for Jacksonville and Gainesville, FL. A comparison of the parameters at these two stations showed minimal difference; thus information at the Jacksonville Airport was used in the calculations.

Table 2-5
Available 1997-1998 Meteorological Data Provided by SJRWMD

Station Name	Dates	River Miles	RF	AT	RH	BP	WD	WS	NR	PAR
Dames Point	10/4/95-9/30/98	10	X	X	X	X	X	X	X	X
Acosta Bridge	10/4/95-9/30/98									X
Shands Bridge	10/4/95-9/30/98	50	X	X	X	X	X	X		X
Buckman Bridge	10/4/95-9/30/98	58								X
Dancy Point	10/4/95-9/30/98	70								
Buffalo Bluff	10/4/95-9/30/98	89	X	X	X	X	X	X	X	X

Note: X indicates availability at station; RF = rainfall; AT = air temperature; RH = relative humidity; BP = barometric pressure; WD = wind direction; WS = wind speed; PAR = photo active radiation.

3 Hydrodynamic Model

Introduction

The foundation of the CE-QUAL-ICM model is the solution to the 3D mass-conservation equation for a control volume. The CE-QUAL-ICM control volumes correspond to cells on the model grid. CE-QUAL-ICM solves, for each volume and for each state variable, the equation:

$$\frac{\delta V_j C_j}{\delta t} = \sum_{k=1}^{n} Q_k C_k + \sum_{k=1}^{n} A_k D_k \frac{\delta C}{\delta x_k} + \Sigma \; S_j \tag{3-1}$$

in which:

V_j = volume of jth control volume (m^3)
C_j = concentration in j^{th} control volume (g m^{-3})
t, x = temporal and spatial coordinates
n = number of flow faces attached to j^{th} control volume
Q_k = volumetric flow across flow face k of jth control volume (m^3 s^{-1})
C_k = concentration in flow across face k (g m^{-3})
A_k = area of flow face k (m^2)
D_k = diffusion coefficient at flow face k (m^2 s^{-1})
S_j = external loads and kinetic sources and sinks in j^{th} control volume (g s^{-1})

CE-QUAL-ICM is an integrated compartment model that uses an unstructured grid. The user can specify the grid and transport information for the solution of the discretized form of Equation 3-1. More typically, the grid structure and transport information is derived from the application of a hydrodynamic model and the information passed to CE-QUAL-ICM through linkage files. The linkage information required includes:

- Mapping information to identify relative cell locations,
- Geometry information such as interface areas and lengths,
- Rates of flows and dispersion across cell boundaries, and
- Cell volumes for comparison with computed volumes.

The linkage information is provided to CE-QUAL-ICM in three input files. A map file contains the flow and cell mapping between the hydrodynamic model's volumetric elements and unstructured CE-QUAL-ICM model. A geometry file contains cell-mapping information (e.g., cells numbers above particular cells). A binary linkage file contains time-variable geometry (interfacial areas and volumes) as well as rates of flow and diffusion.

CE-QUAL-ICM has previously been linked with a variety of hydrodynamic models. One of the most frequently used hydrodynamic models is CH3D. Initial project plans called for SJRWMD to apply CH3D to the Lower St. Johns River. However, prior to the initiation of the current phase of the CE-QUAL-ICM project, the SJRWMD successfully applied the Environmental Fluid Dynamics Code (EFDC), developed by Dr. John Hamrick (Tetra Tech), to the Lower St. Johns River. Rather than switch to CH3D, it was decided following the initial project in October 1999 that the SJRWMD would continue the use of EFDC and that linkage routines would be developed between EFDC and CE-QUAL-ICM. The linkage was supported in part by U.S. EPA Region 4 with funding for Dr. Hamrick to assist in the linkage development. The initial linkage was developed by Dr. Hamrick and then tested and modified by EL. This chapter describes the development and testing of the linkage. A summary of the linkage procedure developed by Dr. Hamrick is provided below, followed by a summary of the linkage's implementation and testing.

Summary of CE-QUAL-ICM Linkage Interface Procedure

The volume continuity equation in EFDC can be written as:

$$\frac{dV_{l,k}}{dt} = Q_{lw,k} - Q_{le,k} + Q_{ls,k} - Q_{ln,k} + Q_{l,k-1} - Q_{l,k} + S_{l,k} \tag{3-2}$$

where V is the cell column, the first four Qs on the right side are the horizontal flows in compass notation, the fifth and sixth Qs are the vertical flows, and S is a volume source term that includes volumetric inflows and outflows including direct rainfall and water surface evaporation. The cell volume is given by:

$$V_{l,k} = A_l \Delta_k H \tag{3-3}$$

where A_l is the horizontal cell area, Δ_k is the dimensionless sigma layer thickness, and H is the water column depth. The sigma layer formulation requires that the vertical flows at the bottom of the lowest layer ($k = 1$, in EFDC) and at the top surface layer ($k = K$, in EFDC) be identically zero:

$$\begin{aligned} Q_{l,0} &= 0 \\ Q_{l,K} &= 0 \end{aligned} \tag{3-4}$$

The discrete form of Equation 3-2 over a hydrodynamic model time step is:

$$\frac{\left(V_{l,k}^{n} - V_{l,k}^{n-1}\right)}{\theta} = \left(Q_{lw,k} - Q_{le,k} + Q_{ls,k} - Q_{ln,k} + Q_{l,k-1} - Q_{l,k} + S_{l,k}\right)^{n,n-1} \tag{3-5}$$

where n,n-1 denotes an average of the right side variables over the time interval θ between time levels n-1 and n. The interface procedure is based on averaging Equation 3-5 over N time steps. For example, over the first N time steps of the simulation the result is:

$$\frac{\left(V_{l,k}^{N} - V_{l,k}^{0}\right)}{N\theta} = \frac{1}{N}\sum_{n=1}^{N}\left(Q_{lw,k} - Q_{le,k} + Q_{ls,k} - Q_{ln,k} + Q_{l,k-1} - Q_{l,k} + S_{l,k}\right)^{n,n-1} \tag{3-6}$$

or

$$\frac{\left(V_{l,k}^{N} - V_{l,k}^{0}\right)}{N\theta} = \tilde{Q}_{lw,k} - \tilde{Q}_{le,k} + \tilde{Q}_{ls,k} - \tilde{Q}_{ln,k} + \tilde{Q}_{l,k-1} - \tilde{Q}_{l,k} + \tilde{S}_{l,k} \tag{3-7}$$

where the tilde denotes the corresponding average.

To provide continuity consistent interface information, EFDC accumulates only the horizontal flows and the volume source term. Equation 3-7 can be rewritten as:

$$\tilde{Q}_{l,k} - \tilde{Q}_{l,k-1} + \frac{V_{l,k}^{N}}{N\theta} = \frac{V_{l,k}^{0}}{N\theta} + \tilde{Q}_{lw,k} - \tilde{Q}_{le,k} + \tilde{Q}_{ls,k} - \tilde{Q}_{ln,k} + \tilde{S}_{l,k} \tag{3-8}$$

where the terms on the right include the known initial volume and the accumulated averages. Note that had the averaged vertical flows been accumulated and combined with the final volume on the left side of Equation 3-8, the equation would not likely have been satisfied due to round off in the averaging process. An alternate implemented in the EFDC interfaces is determination of the vertical flows and the final volume such that Equation 3-8 is satisfied to machine precision. Equation 3-8 for the bottom layer of a cell stack is:

$$\tilde{Q}_{l,1}^{*} = \tilde{Q}_{l,1} + \frac{A_l \Delta_1 H_l^{N}}{N\theta} = \frac{V_{l,1}^{0}}{N\theta} + \tilde{Q}_{lw,1} - \tilde{Q}_{le,1} + \tilde{Q}_{ls,1} - \tilde{Q}_{ln,1} + \tilde{S}_{l,1} \tag{3-9}$$

where * denotes a readily calculated temporary variable. Combining Equation 3-8 written for the second layer with Equation 3-9 gives:

$$\tilde{Q}_{l,2}^{*} = \tilde{Q}_{l,2} + \frac{A_l(\Delta_1 + \Delta_2)H_l^N}{N\theta} = \frac{V_{l,1}^0}{N\theta} + \frac{V_{l,2}^0}{N\theta} + \tilde{Q}_{lw,1} - \tilde{Q}_{le,1} + \tilde{Q}_{ls,1} - \tilde{Q}_{ln,1} + \tilde{S}_{l,1} + \tilde{Q}_{lw,2} - \tilde{Q}_{le,2} + \tilde{Q}_{ls,2} - \tilde{Q}_{ln,2} + \tilde{S}_{l,2} \quad (3\text{-}10)$$

and identifies the general recursion

$$\tilde{Q}_{l,k}^{*} = \tilde{Q}_{l,k} + \frac{A_l H_l^N}{N\theta}\sum_{j=1}^{k}\Delta_j = \sum_{j=1}^{k}\left(\frac{V_{l,j}^0}{N\theta} + \tilde{Q}_{lw,j} - \tilde{Q}_{le,j} + \tilde{Q}_{ls,j} - \tilde{Q}_{ln,j} + \tilde{S}_{l,j}\right) \quad (3\text{-}11)$$

For the top layer, $k = K$, Equation 3-11 gives

$$\tilde{Q}_{l,K}^{*} = \frac{A_l H_l^N}{N\theta} = \sum_{j=1}^{K}\left(\frac{V_{l,j}^0}{N\theta} + \tilde{Q}_{lw,j} - \tilde{Q}_{le,j} + \tilde{Q}_{ls,j} - \tilde{Q}_{ln,j} + \tilde{S}_{l,j}\right) \quad (3\text{-}12)$$

due to Equation 3-4 and the summation of D over K being unity. Thus Equation 3-12 is readily solved for the interface corrected depth at the end of the averaging interval. The interior vertical flows for $k = 1, K - 1$ are then determined from:

$$\tilde{Q}_{l,k} = \tilde{Q}_{l,k}^{*} - \frac{A_l H_l^N}{N\theta}\sum_{j=1}^{k}\Delta_j \quad (3\text{-}13)$$

The issue of determining the water column depth at the end of the averaging period, simultaneously with the vertical flows, rather than using the value provided directly by the hydrodynamic simulation deserves some clarification. First, reconsider Equation 3-8:

$$\tilde{Q}_{l,k} - \tilde{Q}_{l,k-1} + \frac{V_{l,k}^N}{N\theta} = \frac{V_{l,k}^0}{N\theta} + \tilde{Q}_{lw,k} - \tilde{Q}_{le,k} + \tilde{Q}_{ls,k} - \tilde{Q}_{ln,k} + \tilde{S}_{l,k} \quad (3\text{-}8, \text{bis})$$

which corresponds to a system of K equations. If the volume at the end of the averaging interval determined by hydrodynamic model is used in Equation 3-8, the equation is appropriately written as:

$$\tilde{Q}_{l,k} - \tilde{Q}_{l,k-1} = \frac{V_{l,k}^0}{N\theta} - \frac{V_{l,k}^{Nhyd}}{N\theta} + \tilde{Q}_{lw,k} - \tilde{Q}_{le,k} + \tilde{Q}_{ls,k} - \tilde{Q}_{ln,k} + \tilde{S}_{l,k} \quad (3\text{-}14)$$

which is a system of K equations with K - 1 unknowns if the $k = 0$ and $k = K$ vertical flows are presumed identically zero consistent with the sigma formulation. The problem posed by Equation 3-14 is over-determined, having fewer unknowns than equations. Note also that summing Equation 3-14 over the vertical layer stack to give an external model continuity equation

$$0 = \frac{A_l}{N\theta}\left(H_l^{Nhyd} - H_l^0\right) - \sum_{k=1}^{K}\left(\tilde{Q}_{lw,k} - \tilde{Q}_{le,k} + \tilde{Q}_{ls,k} - \tilde{Q}_{ln,k} + \tilde{S}_{l,k}\right) \tag{3-15}$$

does not necessarily resolve the problem in that, even though the external continuity equation is solved identically over each hydrodynamic time step, rounding errors can accumulate in the averaging of the depth integrate horizontal transports with Equation 3-15 not being identically satisfied. Alternately, Equation 3-15 can be solved for the interface corrected depth at the end of the averaging interval

$$\frac{A_l}{N\theta} H_l^N = \frac{A_l}{N\theta} H_l^0 + \sum_{k=1}^{K}\left(\tilde{Q}_{lw,k} - \tilde{Q}_{le,k} + \tilde{Q}_{ls,k} - \tilde{Q}_{ln,k} + \tilde{S}_{l,k}\right) \tag{3-16}$$

and subtracted from the first K - 1 equations of the set (Equation 3-8) giving

$$\begin{aligned} &\tilde{Q}_{l,k} - \tilde{Q}_{l,k-1} = \tilde{Q}_{lw,k} - \tilde{Q}_{le,k} + \tilde{Q}_{ls,k} - \tilde{Q}_{ln,k} + \tilde{S}_{l,k} \\ &-\sum_{k=1}^{K}\left(\tilde{Q}_{lw,k} - \tilde{Q}_{le,k} + \tilde{Q}_{ls,k} - \tilde{Q}_{ln,k} + \tilde{S}_{l,k}\right) \;:\quad k = 1, K-1 \end{aligned} \tag{3-17}$$

which is in principle identical to the procedure defined by Equations 3-11 to 3-13 but involves more arithmetic operations.

The interfacing is expanded to subsequent averaging periods by saving the interface-corrected water column depth at the end of the previous averaging period to define the initial volume at the start of the next averaging period. As a final overall check, the interface procedure essentially implements a secondary continuity tracking to that of the hydrodynamic model. If the procedure is robust, one would expect that water column depths predicted by the hydrodynamic model after m averaging periods would be consistent with the final interface-adjusted depths locally

$$\left|H_l^{mNhyd} - H_l^{mN}\right| \le \varepsilon \tag{3-18}$$

and globally

$$\left|\sum_{l=1}^{L} A_l H_l^{mNhyd} - \sum_{l=1}^{L} A_l H_l^{mN}\right| \le \varepsilon_g \tag{3-19}$$

Summary of Implementation

The implementation of the linkage was accomplished in an interface program and a subroutine of EFDC. The interface program is run first and used to create input files for both EFDC and CE-QUAL-ICM. The EFDC program reads these files and, during its execution, creates the binary linkage files read by CE-QUAL-ICM.

Interface program

The interface program reads two input files, a general input file (EFDC_ICM.INP), and a map file. The map file (CELL.INP) contains the I and J coordinates for the EFDC grid, where the number at a particular I, J location designates the type of cell (0=dry land cell not bordering a water cell, 9=dry land cell bordering a water cell), and where 1 ≤number ≥ 5 indicates a water cell. The general input file contains:

a. Grid and flow transfer parameters, such as the I (pseudo X), J (pseudo Y) and K (pseudo Z) dimensions of the grid.

b. The number and I,J coordinates of the flow boundary conditions.

c. The number and I,J coordinates of the open boundary conditions.

d. The number and I,J coordinates of the EFDC cells that are not included in the CE-QUAL-ICM grid. This input was included to allow elimination of EFDC cells not needed for the CE-QUAL-ICM grid, such as the upstream "sponge" for Buffalo Bluff. The elimination of the sponge cells results in there not being a one-one correspondence in the numbering of the EFDC and CE-QUAL-ICM grid cells.

The output from the interface program includes two files read by EFDC and two by CE-QUAL-ICM. The output files used for EFDC input include an EFDC to CE-QUAL-ICM cell mapping file (EFDC_C_ICM) and a flow mapping file (EFDC_F_ICM). Files are also created to aid in generating the map (MAP_W_ICM) and geometry files (GEO_W_ICM) read by CE-QUAL-ICM. Once the interface program is run and the output files are created, they are copied to directories for input to EFDC or CE-QUAL-ICM, as appropriate. An additional output file (TESTGRID.PRN) contains the cell numbers at each I,J location for comparison of the EFDC and CE-QUAL-ICM grids.

EFDC

A subroutine developed for EFDC by Dr. Hamrick and modified by EL reads the input files created by the interface program and creates the binary linkage files read by CE-QUAL_ICM. An additional input file (EFDC.ICM) controls the linkage. This file contains:

a. Control information (controlling creation of diagnostic files).

b. Number of ICM cells, horizontal and vertical flow faces.

c. I,J locations of tributaries in EFDC input and flag indicating if they are to be written to CE-QUAL-ICM.

d. Flag for mapping internal EFDC boundaries to CE-QUAL-ICM open boundaries for areas where the EFDC cells are not used in CE-QUAL-ICM simulations.

Within the main EFDC input file (EFDC.INP), flags indicate whether a linkage file is to be created (variable ISWASP), and a variable indicates the number of reference time steps over which the variables written to the linkage file are averaged. During the execution of EFDC, two binary linkage files are created and updated. The first file (EFDCRME.INP) contains the net rates of precipitation and evaporation over the averaging period. The second file (EFDCHYD.INP) contains both time-invariant and time-variant information. The time-invariant data for the sigma grid include:

- Surface areas,
- Vertical water column interfacial areas,
- Cell dimensions, and
- Sigma layer thickness (fraction).

The time-variant data include:

- Rates of flow and diffusion,
- Total water column volumes (converted to cell volumes), for comparison with ICM predictions (computed from continuity).

Additional files may be output containing diagnostic information and the results of EFDC salinity and dye tracer simulations for comparison with CE-QUAL-ICM predictions.

Testing of the EFDC/CE-QUAL-ICM Model Linkage

The linkage between EFDC and CE-QUAL-ICM was tested using four grids developed for the Lower St. Johns River. They included:

a. A grid consisting of 5,230 water cells in the horizontal and 5 vertical layers, with 15 open boundary and 79 tributary inflows for each layer, developed by the SJRWMD and modified by Dr. Hamrick. The CE-QUAL-ICM grid was a one-one overlay.

b. A grid consisting of 5,230 EFDC cells in the horizontal with 8 vertical layers, with 17 open boundary and 76 tributary inflows for each layer, developed by the SJRWMD. The CE-QUAL-ICM grid was a one-one overlay.

c. A grid consisting of 2,210 EFDC cells in the horizontal with 8 vertical layers, with 17 open boundary and 76 tributary inflows for each layer, developed by the SJRWMD. The CE-QUAL-ICM grid was a one-one overlay.

d. A grid consisting of 2,210 EFDC cells in the plan, with 6 layers and with 17 open boundary cells and 76 tributary inflows for each layer. For CE-QUAL-ICM, by eliminating the cells used to represent volume

upstream of Palatka, the number of horizontal cells was reduced to 2,120, and tributary inflows reduced to 64. This was the final grid (Figure 3-1) and will be used in all further CE-QUAL-ICM simulations.

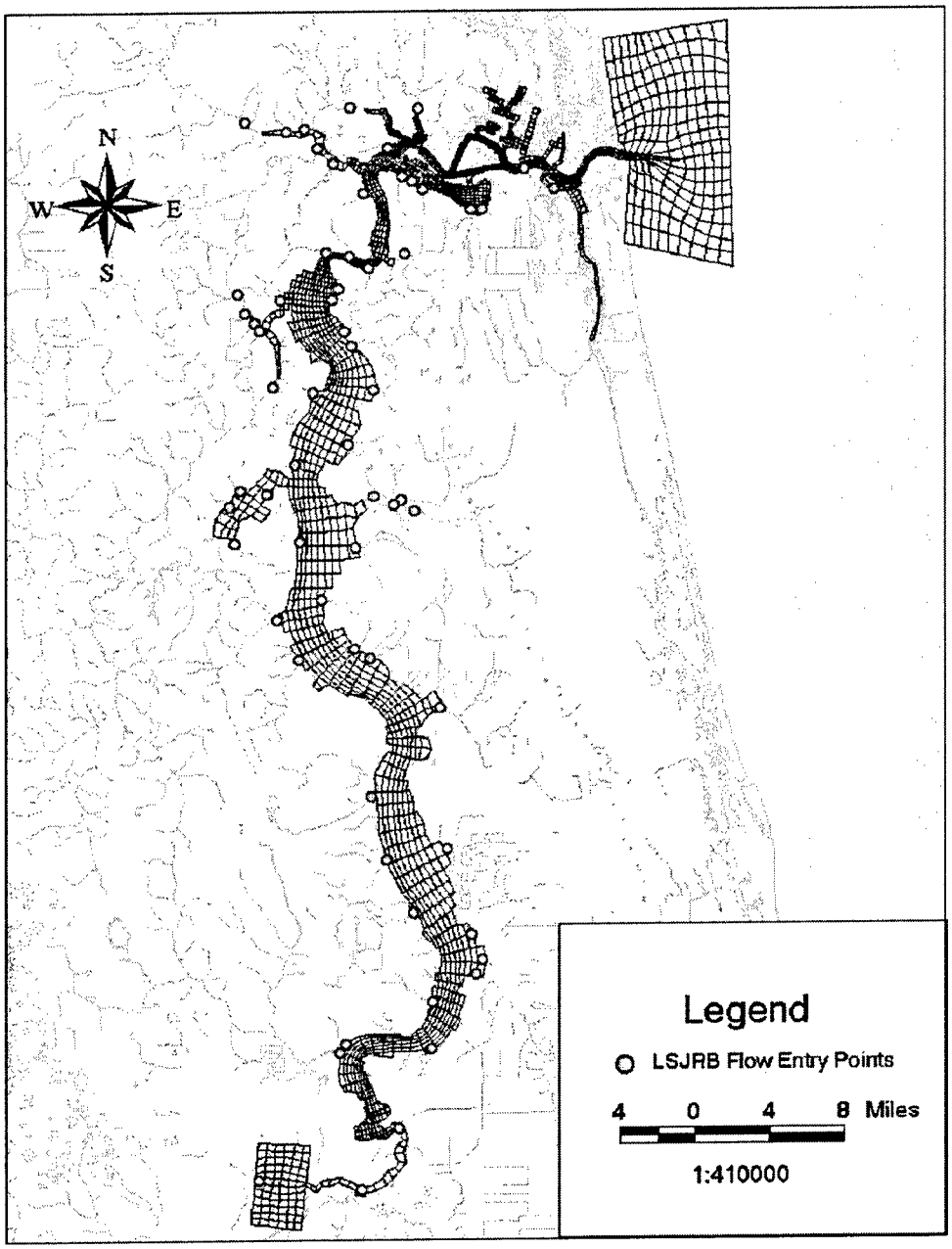

Figure 3-1. Lower St. Johns River EFDC numerical grid

For each of the above grids, the EFDC model was executed and linkage files created. CE-QUAL-ICM input files were developed for the simulation of salinity and a conservative tracer.

Testing first consisted of comparisons of volumes predicted by EFDC with those predicted by CE-QUAL-ICM after a 60-day simulation period. CE-QUAL-ICM takes the initial volumes from the linkage file and then computes new volumes from continuity using the flows contained in the linkage file. The volumes were compared at the end of simulations for the entire grid and over time for individual model cells. For selected cells, all flows and volume changes were output and examined.

Initial simulations with EFDC indicated a volume imbalance. This was reported and the EFDC linkage routines modified by Dr. Hamrick to correct the volume imbalance.

For the corrected EFDC, the total volume at the end of the 396-day simulation for the period of 1 October 1997 to 31 October 1998 for the 2210 X 6 layer grid (the final grid) was 3.82E+09 m^3, with a difference in total grid volume between EFDC and CE-QUAL-ICM of -7.8E-04 percent. The maximum difference between the computed EFDC and CE-QUAL-ICM volumes for any cell was 0.08 percent. Similar differences were noted in other simulations, indicating that the volume balance was acceptable (near machine accuracy).

Comparisons were also made between salinities and dye tracer concentrations predicted by EFDC and CE-QUAL-ICM. In general, the predicted concentrations were very similar but not identical. Generally, CE-QUAL-ICM predicted stronger gradients than those predicted by EFDC. This was attributed to the numerical solution technique used in CE-QUAL-ICM being less dispersive than that used in EFDC. Representative comparisons of salinities predicted by CE-QUAL-ICM and EFDC, and observed data, are provided in Figures 3-2 to 3-11. Note in these figures that the CE-QUAL-ICM predictions are at the mid-point of each day, while the EFDC predictions are hourly.

Predicted concentrations and volumes were sufficiently close to conclude that the linkage was successfully completed.

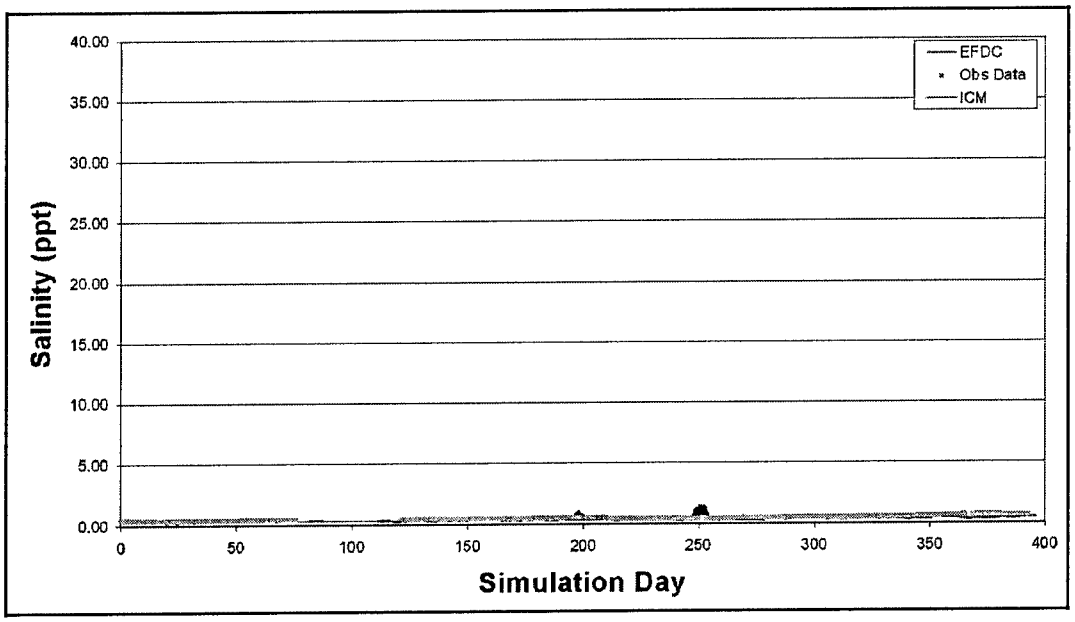

Figure 3-2. Comparison of CE-QUAL-ICM predictions at midpoint of each day to EFDC predictions and observations for the simulation period at Shands Bridge (surface)

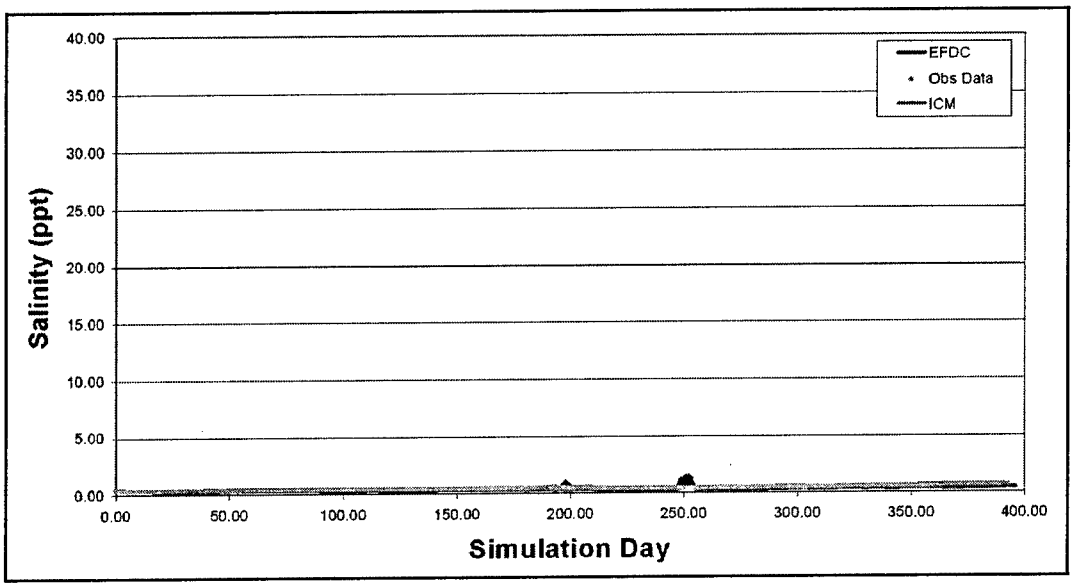

Figure 3-3. Comparison of CE-QUAL-ICM predictions at midpoint of each day to EFDC predictions and observations for the simulation period at Shands Bridge (bottom)

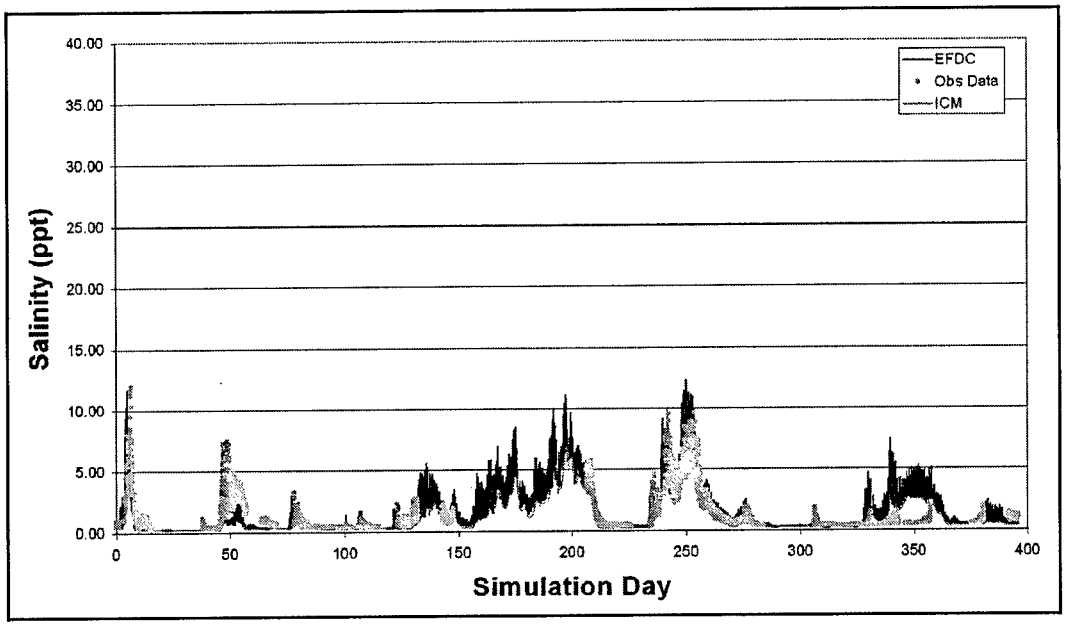

Figure 3-4. Comparison of CE-QUAL-ICM predictions at midpoint of each day to EFDC predictions and observations for the simulation period at Buckman Bridge (surface)

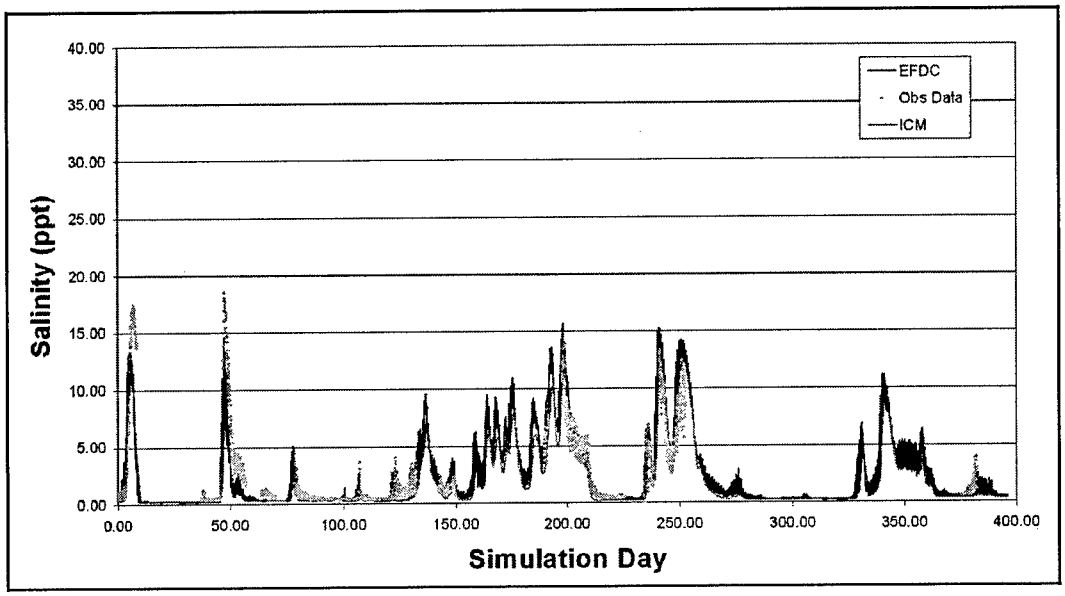

Figure 3-5. Comparison of CE-QUAL-ICM predictions at midpoint of each day to EFDC predictions and observations for the simulation period at Buckman Bridge (bottom)

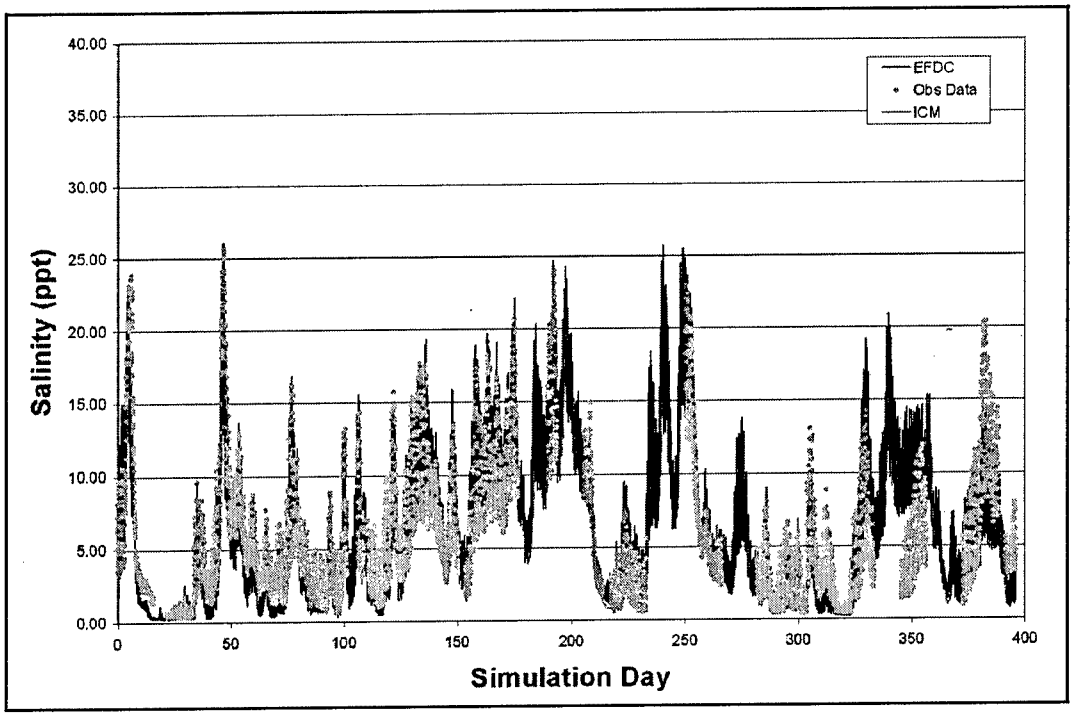

Figure 3-6. Comparison of CE-QUAL-ICM predictions at midpoint of each day to EFDC predictions and observations for the simulation period at Acosta Bridge (surface)

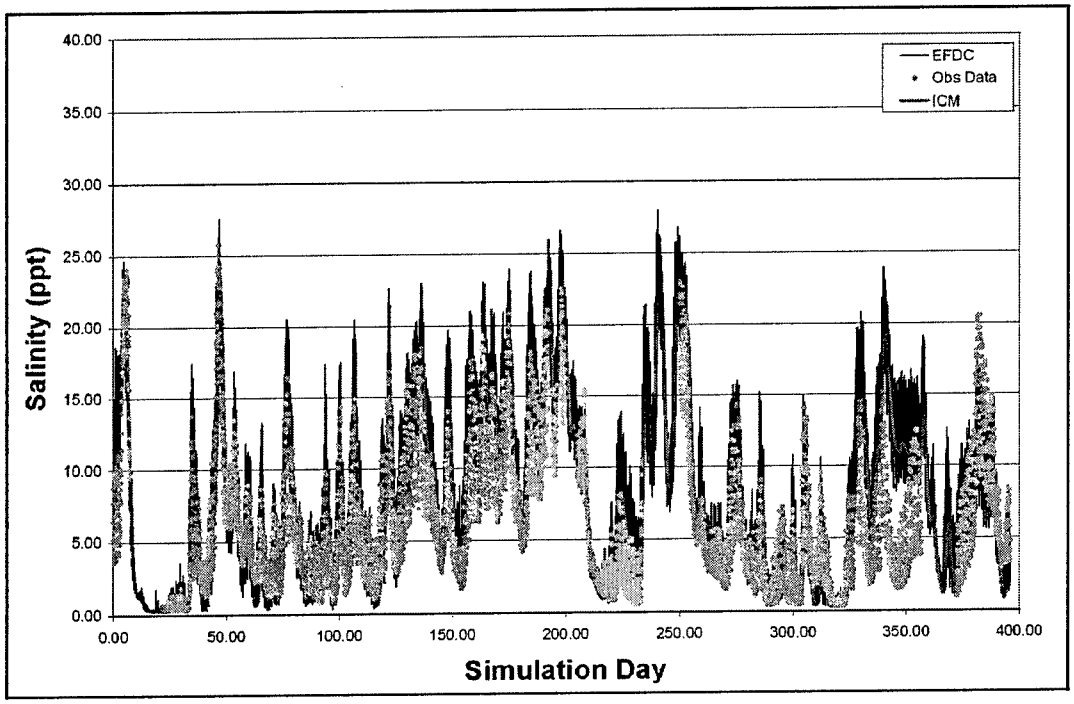

Figure 3-7. Comparison of CE-QUAL-ICM predictions at midpoint of each day to EFDC predictions and observations for the simulation period at Acosta Bridge (bottom)

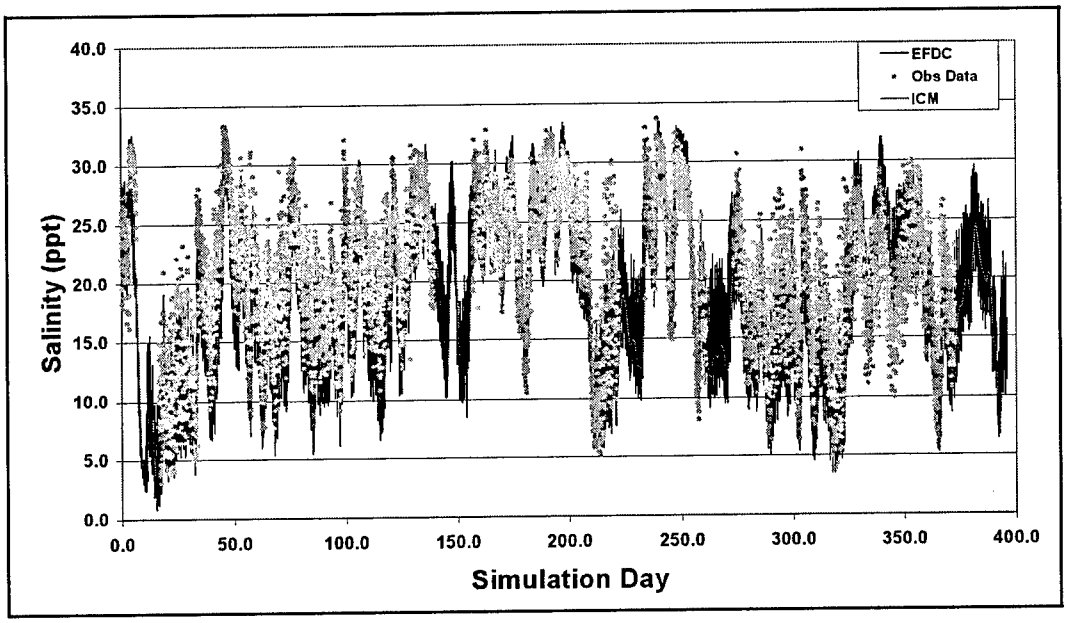

Figure 3-8. Comparison of CE-QUAL-ICM predictions at midpoint of each day to EFDC predictions and observations for the simulation period at Dames Bridge (surface)

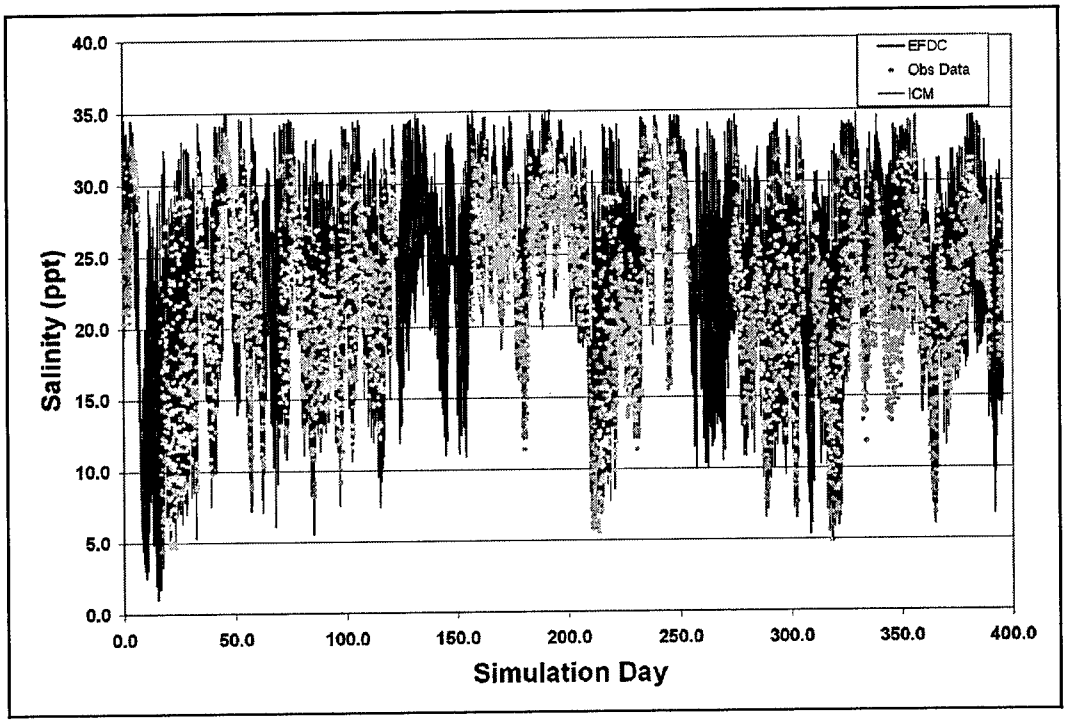

Figure 3-9. Comparison of CE-QUAL-ICM predictions at midpoint of each day to EFDC predictions and observations for the simulation period at Dames Bridge (bottom)

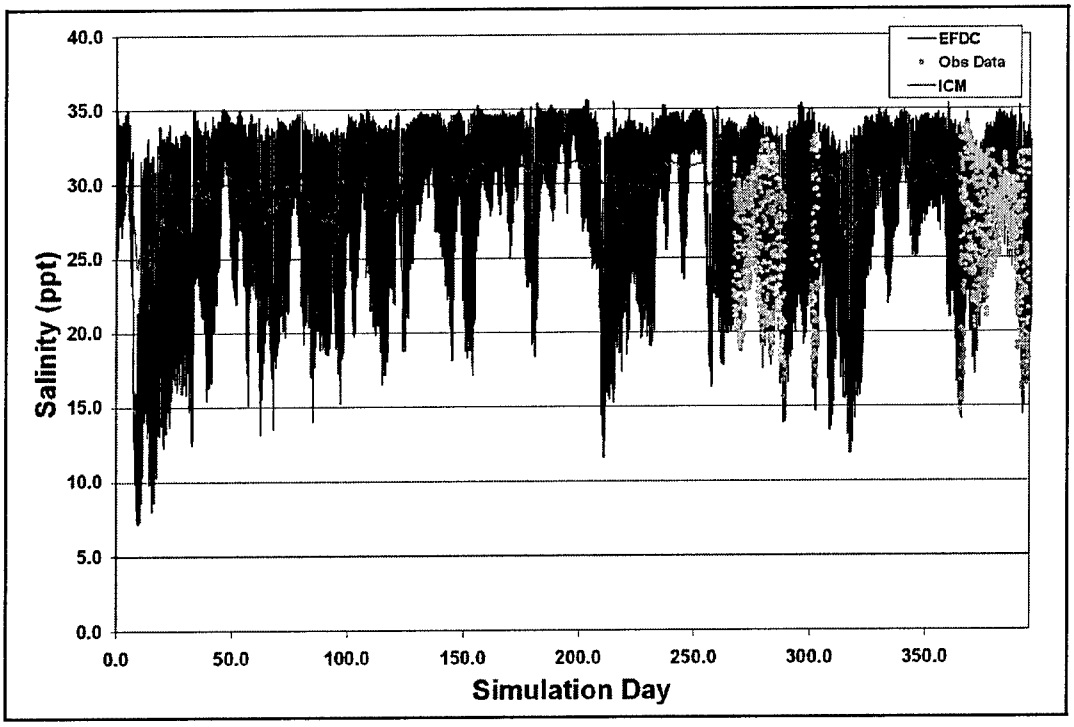

Figure 3-10. Comparison of CE-QUAL-ICM predictions at midpoint of each day to EFDC predictions and observations for the simulation period at Bar Pilot (surface)

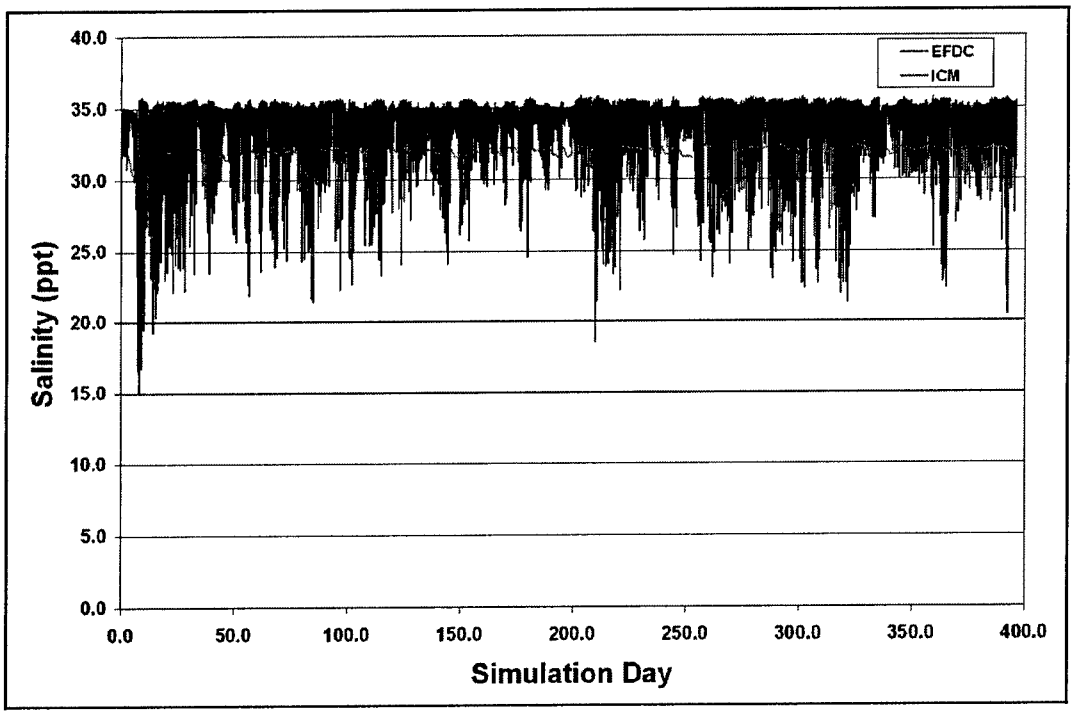

Figure 3-11. Comparison of CE-QUAL-ICM predictions at midpoint of each day to EFDC predictions and observations for the simulation period at Bar Pilot (bottom)

4 Loads and Boundary Conditions

Introduction

Boundaries and loads provided the forcing functions for water quality in the application of CE-QUAL-ICM to the Lower St. Johns River Estuary. Loads are the product of Q and C, where Q (V/T) is the rate of water flow and C (M/V) the constituent concentration. The loads (M/T) can be provided directly to ICM. This would be required, for example, where the rates of inflow are not specified to the ICM model through the hydrodynamic linkage file. Alternatively, where the rates of inflow are included in the hydrodynamic linkage file, the concentrations can be specified as a boundary condition and the load (QC) computed internally.

In the application of CE-QUAL-ICM to the Lower St. Johns River Estuary, boundary conditions or loads were provided for the 17 horizontal segments comprising the ocean boundary, 36 point sources (PS), and 65 tributaries or non-point sources (NPS). For each of these locations, boundary conditions or loads were also specified for each of the six vertical layers in the model grid.

For PS, the rates of inflow were not considered in the EFDC hydrodynamic simulations. For these sources, all forcings were included as loads in this application. For the ocean boundary, all forcings were specified as boundary conditions. For tributaries and NPS, the forcings were specified as either loads or boundary conditions, based upon either convenience or the form of the data supplied by the SJRWMD. A series of boundary and loading files were developed for each source and constituent simulated, and the correspondence of the constituents and input files tabulated in Table 4-1. For time-varying data, individual files were created for each of the 2 years of simulation: 1 December 1996 to 30 November 1997 and 1 December 1997 to 30 November 1998 (indicated by 9* in Table 4-1). The methods and assumptions to create these files are discussed in the following sections.

Boundary Conditions

Boundary conditions were specified at the 17 horizontal segments comprising the ocean boundary and for selected constituents for the 65 NPS. Boundary conditions were also specified for each of the six vertical layers

Table 4-1
Correspondence of CE-QUAL-ICM State Variables and Point-Source Concentration Data Provided by the SJRWMD

Variable Number	Variable Name	Buffalo Bluff and Dunn's Creek	Other NPS	PS	Ocean Boundary
1	Temperature	Temp9*_BC.NPT	Temp9*_BC.NPT	None	Temp9*_BC.NPT
2	Salinity	SAL96_BC.NPT (0.0 assumed for Buffalo Bluff)	none	None	OCN_BC.NPT
3	Suspended Solids	BUFF9*B.NPT, DUNN9*_B.NPT	NPS_96B.NPT	PS1_9*.NPT, PS29*.NPT	OCN_BC.NPT
4	Algae Type 1	BUFF9*B.NPT, DUNN9*_B.NPT	NPS_96B.NPT	PS1_9*.NPT	OCN_BC.NPT
5	Algae Type 2	BUFF9*B.NPT, DUNN9*_B.NPT	NPS_96B.NPT	PS1_9*.NPT	OCN_BC.NPT
6	Algae Type 3	BUFF9*B.NPT, DUNN9*_B.NPT	NPS_96B.NPT	PS1_9*.NPT	OCN_BC.NPT
7	Zooplankton Type 1	not simulated	not simulated	not simulated	not simulated
8	Zooplankton Type 2	not simulated	not simulated	not simulated	not simulated
9	Labile DOC	BUFF9*B.NPT, DUNN9*_B.NPT	NPS_96B.NPT	PS1_9*.NPT	OCN_BC.NPT
10	Refractory DOC	BUFF9*B.NPT, DUNN9*_B.NPT	NPS_96B.NPT	PS1_9*.NPT	OCN_BC.NPT
11	Labile POC	BUFF9*B.NPT, DUNN9*_B.NPT	NPS_96B.NPT	PS1_9*.NPT	OCN_BC.NPT
12	Refractory POC	BUFF9*B.NPT, DUNN9*_B.NPT	NPS_96B.NPT	PS1_9*.NPT	OCN_BC.NPT
13	Ammonium	BUFF9*B.NPT, DUNN9*_B.NPT	NPS_96B.NPT	PS1_9*.NPT	OCN_BC.NPT
14	Nitrate	BUFF9*B.NPT, DUNN9*_B.NPT	NPS_96B.NPT	PS1_9*.NPT	OCN_BC.NPT
15	Urea	Not simulated	Not simulated	Not simulated	Not simulated
16	Labile DON	BUFF9*B.NPT, DUNN9*_B.NPT	NPS_96B.NPT	PS1_9*.NPT	OCN_BC.NPT
17	Refractory DON	BUFF9*B.NPT, DUNN9*_B.NPT	NPS_96B.NPT	PS1_9*.NPT	OCN_BC.NPT
18	Labile PON	BUFF9*B.NPT, DUNN9*_B.NPT	NPS_96B.NPT	PS1_9*.NPT	OCN_BC.NPT
19	Refractory PON	BUFF9*B.NPT, DUNN9*_B.NPT	NPS_96B.NPT	PS1_9*.NPT	OCN_BC.NPT
20	Total Phosphate	BUFF9*B.NPT, DUNN9*_B.NPT	NPS_96B.NPT	PS1_9*.NPT	OCN_BC.NPT
21	Labile DOP	BUFF9*B.NPT, DUNN9*_B.NPT	NPS_96B.NPT	PS1_9*.NPT	OCN_BC.NPT

(Continued)

Table 4-1 (Concluded)

Variable Number	Variable Name	Buffalo Bluff and Dunn's Creek	Other NPS	PS	Ocean Boundary
22	Refractory DOP	BUFF9*B.NPT, DUNN9*_B.NPT	NPS_96B.NPT	PS1_9*.NPT	OCN_BC.NPT0
23	Labile POP	BUFF9*B.NPT, DUNN9*_B.NPT	NPS_96B.NPT	PS1_9*.NPT	OCN_BC.NPT
24	Refractory POP	BUFF9*B.NPT, DUNN9*_B.NPT	NPS_96B.NPT	PS1_9*.NPT	OCN_BC.NPT
25	Particulate Inorganic P	Not simulated	Not simulated	Not simulated	Not simulated
26	COD	None	None	None	None
27	DO	BUFF9*B.NPT, DUNN9*_B.NPT	DOX9*BC.NPT	None	OCN_BC.NPT
28	Particulate Si	BUFF9*B.NPT, DUNN9*_B.NPT	Si_BC.NPT	PS1_9*.NPT	OCN_BC.NPT
29	Dissolved Si	BUFF9*B.NPT, DUNN9*_B.NPT	Si_BC.NPT	PS1_9*.NPT	OCN_BC.NPT
30	Internal P1	None	None	None	None
31	Internal P2	None	None	None	None
32	Internal P3	None	None	None	None

in the model grid. Typically, all boundary conditions are specified to CE-QUAL-ICM in a single time-varying file. The structure of the standard file allows specification of the boundary locations for each water quality constituent followed by a time series of concentrations for those constituents and locations. The standard approach requires that all updates be at the same frequency. For the application of CE-QUAL-ICM to the Lower St. Johns Estuary, where the frequency of updates varied between sources from hourly to monthly values, reducing all data for the large number of sources to the same update frequency for incorporation into a single loading file would have resulted in an excessively large file. Instead, the CE-QUAL-ICM model was modified to allow specification of multiple boundary condition files. The files used and the assumptions used in their development are described below.

Salinity

All salinities were specified in boundary condition files. Separate files were developed for the salinities at the ocean boundary, Dunns Creek, and Buffalo Bluff. As with the EFDC hydrodynamic model, the salinities for all other sources were assumed to be zero.

Time-varying salinities, extracted from the input file (SSER.INP) to the EFDC hydrodynamic model, for Dunns Creek and Buffalo Bluff were specified in the boundary condition files DUNN96_N.NPT or DUNN97_N.NPT and BUFF96_N.NPT or BUFF97_N.NPT for the 2 years of simulation. The

frequency of the updates varied but averaged 6 to 12 hours. The salinities were assumed to be constant with depth.

The ocean salinities used in the water quality simulations were also extracted from input (SSER.INP) to the hydrodynamic model. The salinities for each of the six layers, from the surface downward, were 35.00, 35.10, 35.25, 35.50, 35.75, and 36.00 ppt. The salinities were assumed to remain constant and were specified in the boundary file OCN_BC.NPT.

Water temperature

All water temperatures were specified as boundary conditions in a single file for each year simulated (TEMP96_BC.NPT and TEMP97_BC.NPT) based upon observed data provided by SJWMD. For each of these files, the update frequency for water temperatures was hourly. The water temperatures were assumed constant with depth.

Since PS flows were not included in hydrodynamic simulations, no boundary conditions were specified for these sources. Hourly varying temperature values were specified at the ocean boundary, Buffalo Bluff, and Dunns Creek. The ocean temperatures were based upon National Oceanic and Atmospheric Administration (NOAA) data collected at Jacksonville Beach. For the remaining 63 tributaries and NPS, the SJRWMD estimated hourly temperatures based upon the best fit for stations located on the east or west bank of the estuary. The west bank stations used to create time-series included:

- NBC - North Fork of Black Creek
- BSF - South Fork of Black Creek
- BLC - Black Creek @ Hwy 209
- SPCR - Swimming Pen Creek
- PTC - Peters Creek @ Hwy 209
- RCB - Rice Creek @ US 17

The east bank stations used to create time-series included:

- SMC – Six Mile Creek @ SR 13
- MOB - Moccasin Branch @ SR 13
- DPB - Deep Creek @ RR
- OHD - Hastings Drainage District Outlet
- DCH - Deep Creek Headwaters
- DBR - Dog Branch

The estimated temperatures were then assigned to east or west bank stations as indicated in Table 4-2.

Table 4-2
Specification of West and East Bank Tributary Stations for Water Temperatures

West Bank Tributaries					East Bank Tributaries				
Trib. No.	Cell No.	IC	JC	Name	Trib. No.	Cell No.	IC	JC.	Name
3	134	171	20	Rice Creek	2	1216	182	31	Mill Branch
5	126	158	20	Mason Branch	4	1015	162	27	Dog Branch
6	1152	154	29	Deep Creek	7	1151	153	29	Moccasin Branch
9	122	148	20	Cedar Creek	8	1096	152	28	McCullough Creek
11	121	140	20	Clarkes Creek	10	1149	145	29	Tocoi Creek
14	119	122	20	Governors Creek	12	1187	133	30	Sixmile Creek
15	92	118	19	Black Creek	13	1078	125	28	Orange Grove Branch
17	77	114	18	Swimming Pen Creek	16	1185	113	30	Cunningham Creek
18	45	112	16	Drs Lake West	26	1584	43	54	Gin House Creek
19	43	110	16	Lucy Branch	27	1124	61	29	Pottsburg Creek
20	72	109	18	Drs Lake East	28	1215	110	31	Julington Creek
21	27	92	12	Ortega River	31	1080	127	28	Kendall Creek
22	14	79	12	Cedar River	32	841	117	26	Kentucky Branch
23	1	46	2	Trout River	34	1215	110	31	Durbin Creek
24	10	29	11	Broward River	35	1215	110	31	Flora Branch
25	1189	15	31	Dunn Creek	36	1215	110	31	Cormorant Creek
29	133	170	20	Moccasin Creek	37	1181	83	30	Unnamed Creek
30	195	144	21	Unnamed Creek	38	1139	94	29	Christopher Bran
33	264	112	22	Peters Branch	39	1138	91	29	New Rose Creek
49	452	37	24	Drummond Creek	40	1230	80	32	Craig Creek
50	37	46	15	Moncrief Creek	41	934	64	27	Miller Creek
51	13	46	12	Ribault River	42	1244	41	33	Unnamed Creek
52	7	46	8	Block House Creek	43	1283	41	36	Unnamed Creek
53	4	46	5	West Branch	44	1306	41	38	New Castle Creek
54	483	68	24	Hogan Creek	45	1540	43	52	Jones Creek
55	338	50	23	Long Branch	46	1562	43	53	Cow Head Creek
56	489	74	24	McCoy Creek	47	1777	31	67	Unnamed Creek

(Continued)

Table 4-2 (Concluded)

West Bank Tributaries					East Bank Tributaries				
Trib. No.	Cell No.	IC	JC	Name	Trib. No.	Cell No.	IC	JC	Name
57	51	84	17	Big Fishweir Creek	48	1842	35	76	Mt Pleasant Creek
58	15	80	12	Williamson Creek	63	1142	97	29	Goodbys Creek
59	19	84	12	Butcher Pen Creek	64	1065	101	28	Deep Bottom Creek
60	21	86	12	Fishing Creek					
61	114	99	20	Unnamed Creek					
62	257	105	22	Orange Park Slough					

Other ocean boundary conditions

Concentrations of other water quality constituents simulated were specified as boundary input at the ocean boundary. These conditions were based on analysis by the SJRWMD, where averaged conditions were computed from a limited number of samples collected over six dates near the ocean model boundary. The averaged values were assumed to remain constant over the 2-year period of simulation and were assumed to be constant with depth. They were specified in the input file OCN_BC.NPT. Boundary conditions were specified for total suspended solids, each of the three algal groups, Labile dissolved organic carbon (DOC), Refractory DOC, Labile dissolved organic phosphorus (POC), Refractory POC, Ammonium, Nitrate, Labile dissolved organic nitrogen (DON), Refractory DON, Labile PON, Refractory PON, Total Phosphorus (TP), Labile DOP, Refractory DOP, Labile POP, Refractory POP, DO, Particulate Si (silica), and Dissolved Si. Since only dissolved silica data were available, the total and particulate fractions were estimated based upon the assumption that 70 percent of the silica was in the dissolved form.

Other boundary conditions for Buffalo Bluff and Dunns Creek

Concentrations of other water quality constituents simulated were specified as boundary input for Buffalo Bluff and Dunns Creek based upon data provided by the SJRWMD. These time-varying conditions were based on data collected at varying frequencies, but averaging approximately two to three weeks. The time-varying values were assumed to remain constant with depth, and were specified in the input files BUFF96_B.NPT, BUFF97_B.NPT, DUNN96_B.NPT and DUNN97_B.NPT. Boundary conditions were specified for total suspended solids, each of the three algal groups, Labile DOC, Refractory DOC, Labile POC, Refractory POC, Ammonium, Nitrate, Labile DON, Refractory DON, Labile PON, Refractory PON, Total P, Labile DOP, Refractory DOP, Labile POP, Refractory POP, DO, Particulate Si, and Dissolved Si. As discussed above, only dissolved silica data were available, so the total and particulate fractions were estimated based upon the assumption that 70 percent of the silica was in the dissolved form.

Other boundary conditions for non-point sources

Concentrations of silica and DO were also specified separately as boundary conditions for 63 of the tributaries and NPS (see Table 4-2). Silica and DO concentrations for Buffalo Bluff, Dunns Creek ,and ocean boundary were specified separately, as described above. No boundary conditions were provided for PS, as PS flows were not included in hydrodynamic simulations.

DO concentrations for the 63 tributaries and NPS were based on single monthly averages of DNC and RCB observed values. These averages were assumed to be applicable to all of the 63 NPS and assumed constant with depth. The monthly values were specified in the files TRBC9697.NPT and TRBC9798.NPT for the two simulation years.

Total estimated silica concentrations were provided by the SJRWMD for 63 of the tributaries and NPS. These values were assumed constant with time and over the six modeled layers. The total silica was subdivided into dissolved and particulate fractions based upon the assumption that 70 percent of the silica was in the dissolved form. The estimated values were provided to the model in the input file SI_BC.NPT.

Point and Non-point Source Loads

Point source loads

Data were provided by the SJRWMD for the 36 point sources listed in Table 4-3. Also listed in Table 4-3 are the facility locations, I and J grid coordinates, and the surface cell number in the ICM model grid corresponding

Table 4-3
Point Loading Sources Included in Model Simulations

Facility ID	Facility Name	Data Freq.	Facility Latitude	Facility Longitude	IC	JC	ICM Surface Grid #
FL0023493	MANDARIN WWTF	Daily	30.17903	-81.62241	100	28	1064
FL0026000	BUCKMAN STREET WWTF	Daily	30.35232	-81.62898	55	24	470
FL0026441	ARLINGTON EAST WWTF	Daily	30.34665	-81.54316	39	48	1464
FL0026450	JAX DISTRICT II WWTF	Daily	30.42293	-81.61842	36	24	451
FL0026468	SOUTHWEST DISTRICT WWTF	Daily	30.23276	-81.72250	90	20	112
FL0000400	STONE CONTAINER CORPORATION	Monthly	30.41900	-81.60420	28	21	141
FL0000892	JEFFERSON SMURFIT CORPORATION	Monthly	30.36670	-81.62500	51	24	466

(Continued)

Table 4-3 (Concluded)

Facility ID	Facility Name	Data Freq.	Facility Latitude	Facility Longitude	IC	JC	ICM Surface Grid #
FL0002763	GEORGIA PACIFIC, PALATKA	Monthly	29.68247	-81.68278	171	20	134
FL0020231	JACKSONVILLE BEACH	Monthly			31	81	1900
FL0020427	NEPTUNE BEACH WWTF	Monthly	30.31558	-81.42007	31	81	1900
FL0020915	GREEN COVE SPRINGS, CITY OF	Monthly	30.00724	-81.69646	121	20	118
FL0022489	WESLEY MANOR RETIRMNT VILL-JAX	Monthly	30.11390	-81.60610	110	31	1215
FL0023248	BUCCANEER WWTF	Monthly	30.36976	-81.41157	31	81	1900
FL0023604	MONTEREY WWTF	Monthly	30.33060	-81.60116	59	27	929
FL0023621	HOLLY OAKS SUBDIVISION	Monthly	30.35752	-81.52208	43	54	1584
FL0023663	SAN JOSE SUBDIVISION	Monthly	30.24698	-81.62258	94	28	1059
FL0023671	JACKSONVILLE HEIGHTS	Monthly	30.24100	-81.75670	86	12	21
FL0023922	TOWN OF ORANGE PARK	Monthly	30.18241	-81.70981	103	21	170
FL0024767	SAN PABLO WWTF	Monthly	30.27763	-81.43065	53	78	1874
FL0025151	MILLER STREET WWTP	Monthly	30.17820	-81.71228	103	21	170
FL0025828	ORTEGA HILLS SUBDIVISION	Monthly	30.21869	-81.70962	92	12	27
FL0026751	ROYAL LAKES	Monthly	30.21389	-81.54440	96	29	1141
FL0026778	BEACON HILLS WWTF	Monthly	30.38379	-81.52166	31	57	1631
FL0026786	WOODMERE SUBDIVISION	Monthly	30.37987	-81.60245	44	27	914
FL0030210	SOUTH GREEN COVE SPRINGS WWTF	Monthly	29.98259	-81.66759	125	21	183
FL0032875	FLEMING OAKS WWTP	Monthly	30.07463	-81.70457	115	22	267
FL0038776	ATLANTIC BEACH WWTF	Monthly	30.33551	-81.40882	31	81	1900
FL0040061	PALATKA, CITY OF	Monthly	29.61582	-81.65123	182	42	1352
FL0041530	ANHEUSER BUSCH MAIN ST. LAND APP.	Monthly	30.45278	-81.65000	29	11	10
FL0042315	CITY OF HASTINGS	Monthly	29.72500	-81.50000	154	29	1152
FL0043591	JULINGTON CREEK WWTP	Monthly	30.10634	-81.62597	113	30	1185
FL0043834	FLEMING ISLAND SYSTEM WWTP	Monthly	30.09279	-81.71982	113	22	265
FL0117668	UNITED WATER FL - ST. JOHNS NORTH	Monthly	30.09556	-81.61089	113	30	1185
FLA011427	USN NS MAYPORT	Monthly	30.39690	-81.39750	31	94	1967
FLA011429	USN NAS JACKSONVILLE	Monthly	30.24138	-81.67580	91	20	113

to the loading location. The St. Johns River study area was divided into six segments as denoted on Figure 4-1. Monthly PS loads for Total P and Total N were summed for each segment and are presented in Figures 4-2 through 4-13. As noted in Figures 4-2 through 4-7, segment 4 received the majority of the Total P loads (approximately 1,200 kg/day) while the Total P loads to the other segments ranged from 30 to 210 kg/day. Similar to Total P loads, maximum Total N loads (approximately 4,200 kg/day) to the system were received in segment 4 as shown in Figure 4-11, while loads to the other segments range from 60 to 950 kg/day (Figures 4-8 through 4-13 except Figure 4-11).

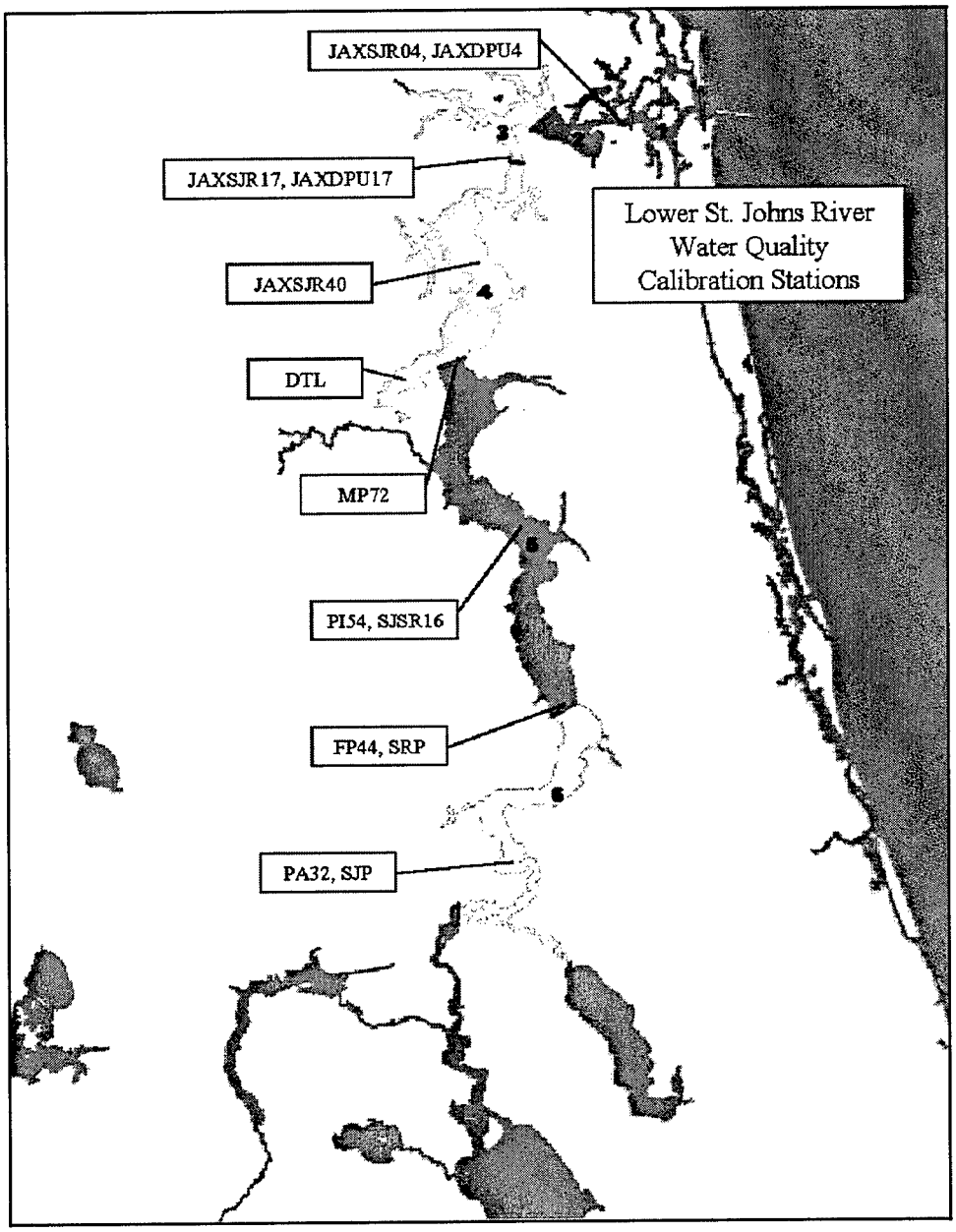

Figure 4-1. Six colored reaches represent segmentation of the St. Johns River, showing location of observed water quality stations

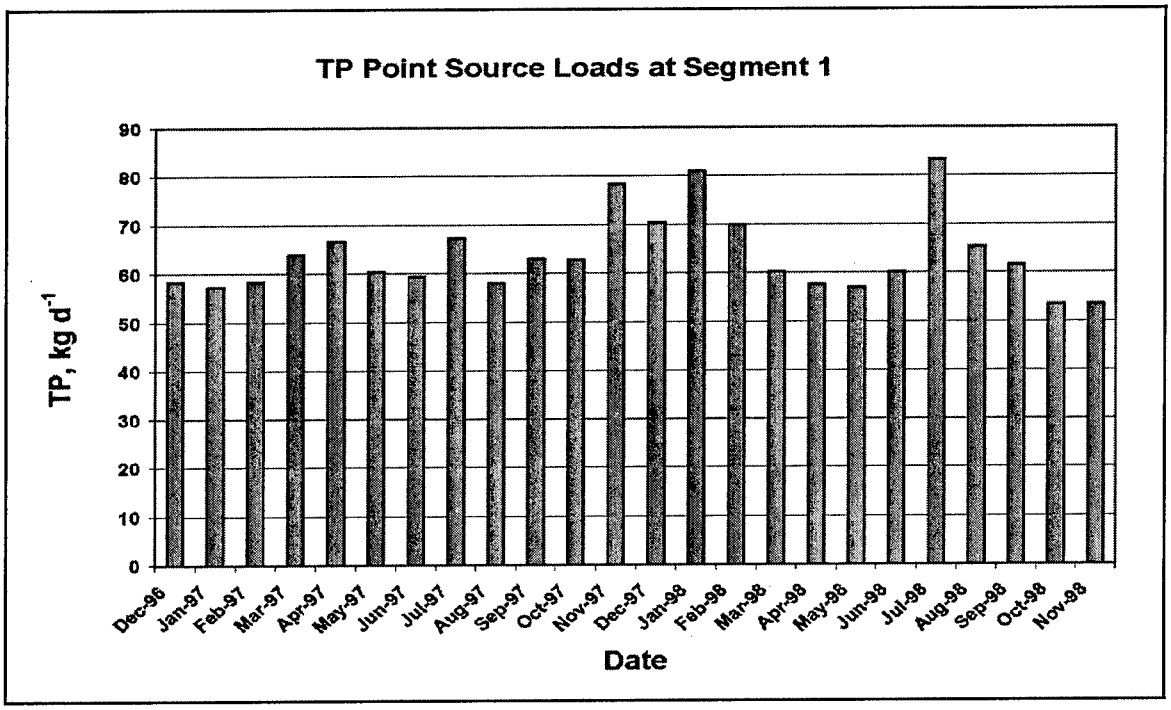

Figure 4-2. Mean monthly TP PS loads into Segment 1, 1996-1998

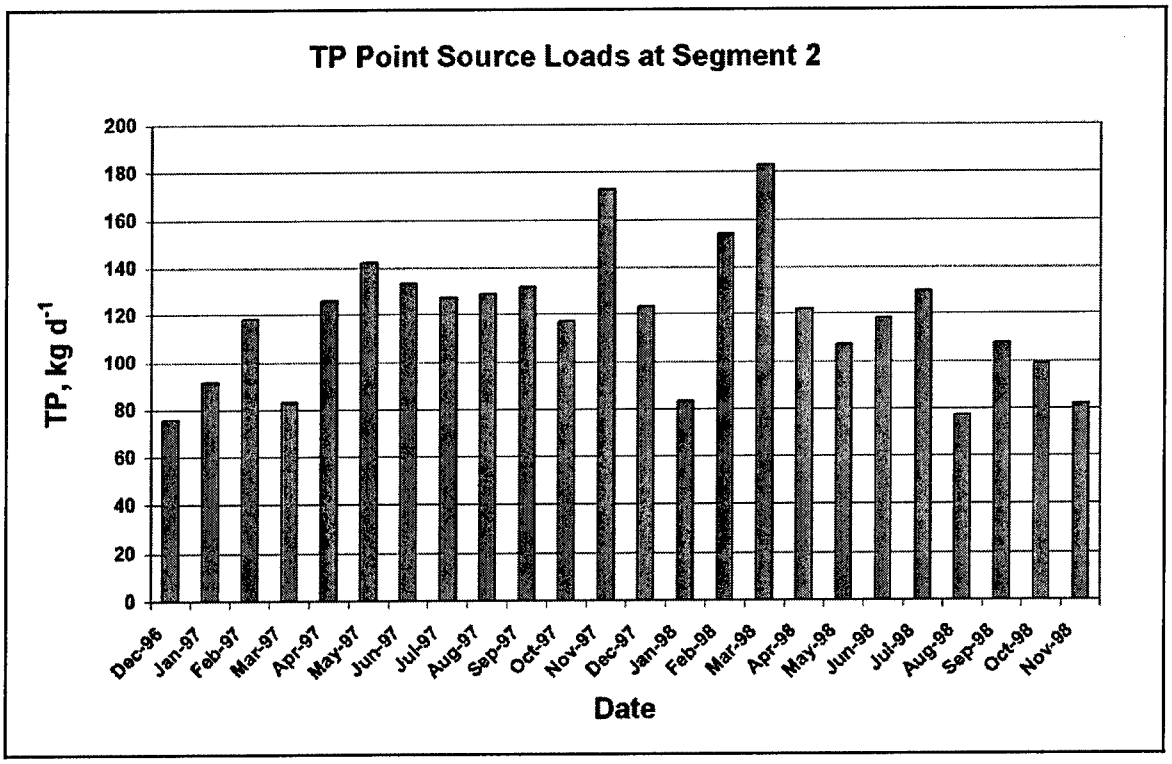

Figure 4-3. Mean monthly TP PS loads into Segment 2, 1996-1998

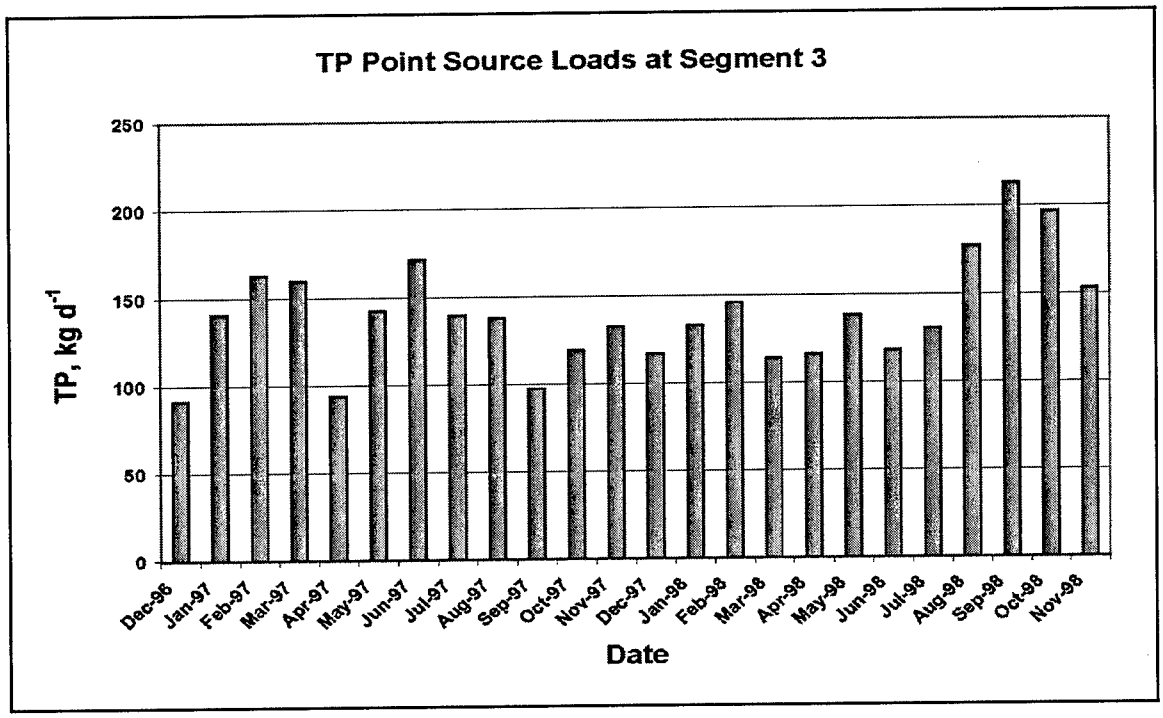

Figure 4-4. Mean monthly TP PS loads into Segment 3, 1996-1998

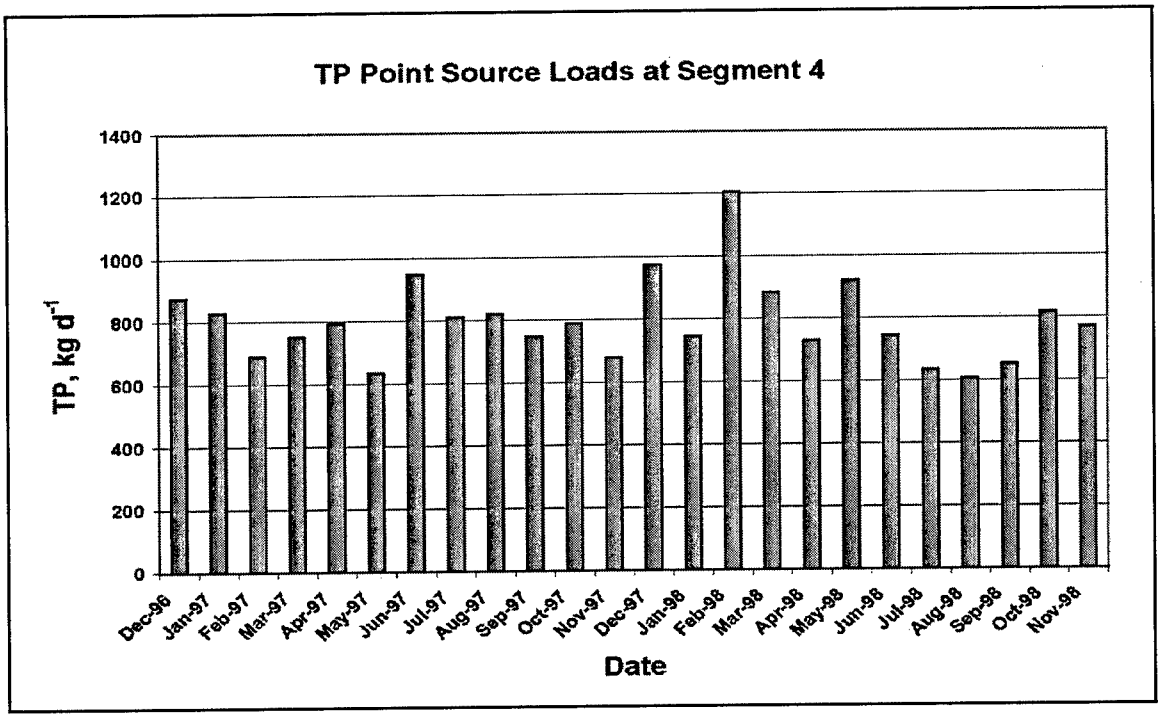

Figure 4-5. Mean monthly TP PS loads into Segment 4, 1996-1998

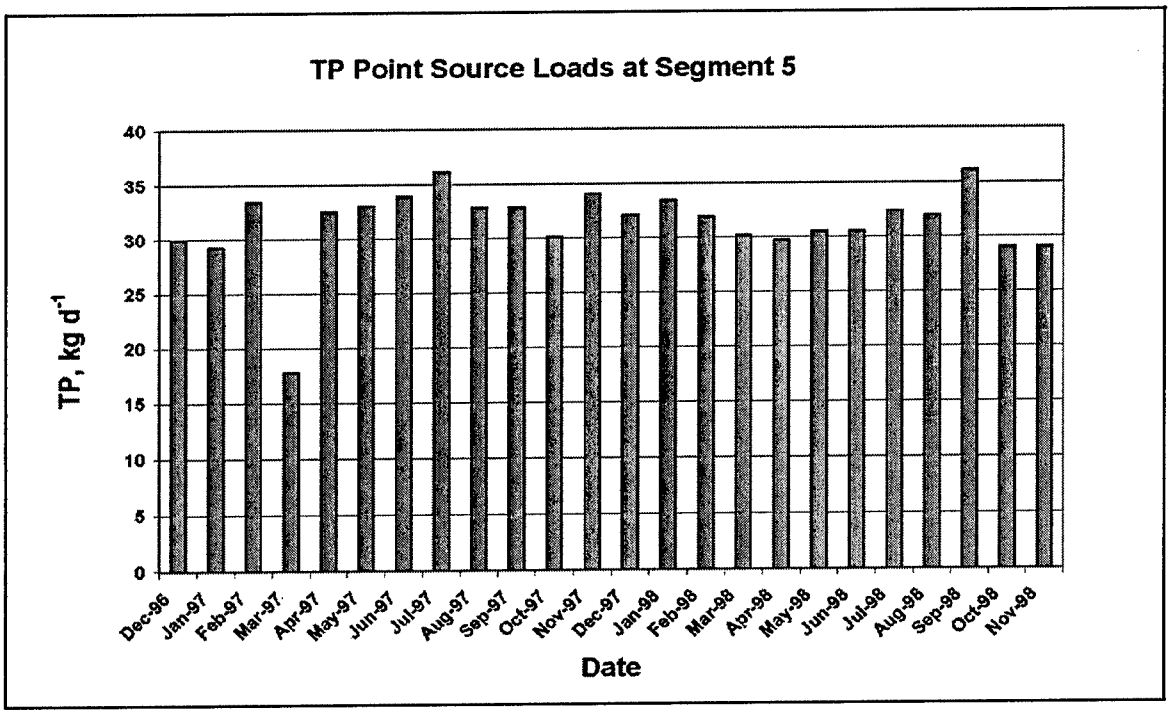

Figure 4-6. Mean monthly TP PS loads into Segment 5, 1996-1998

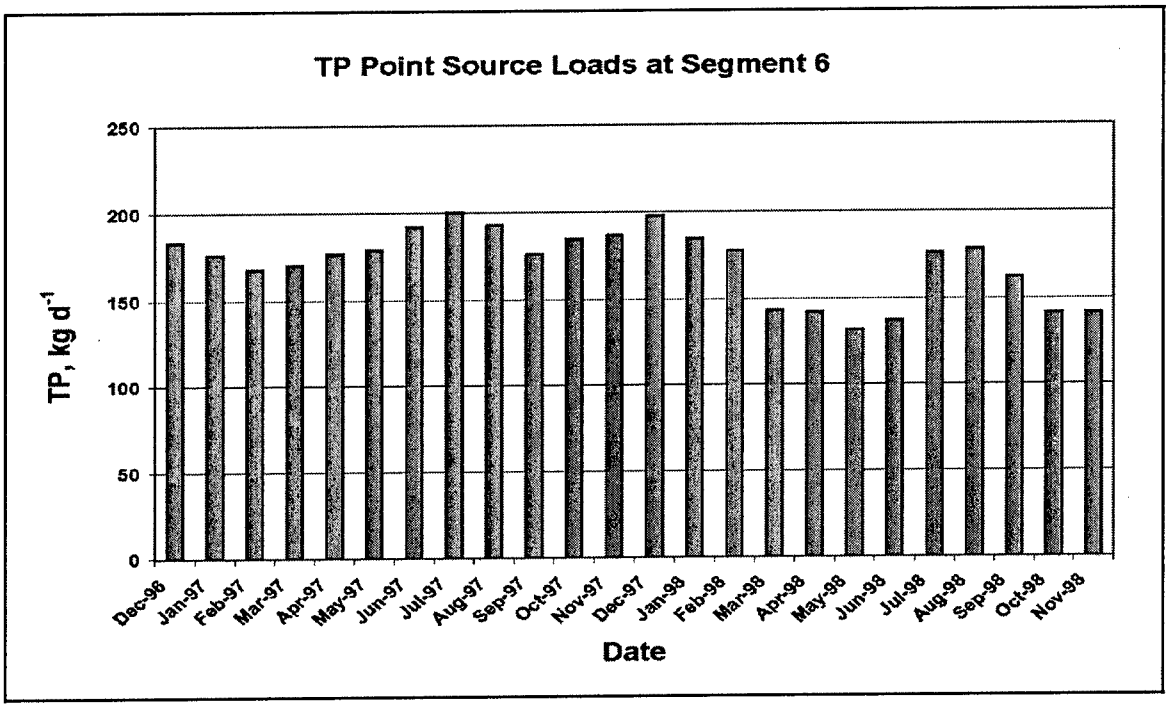

Figure 4-7. Mean monthly TP PS loads into Segment 6, 1996-1998

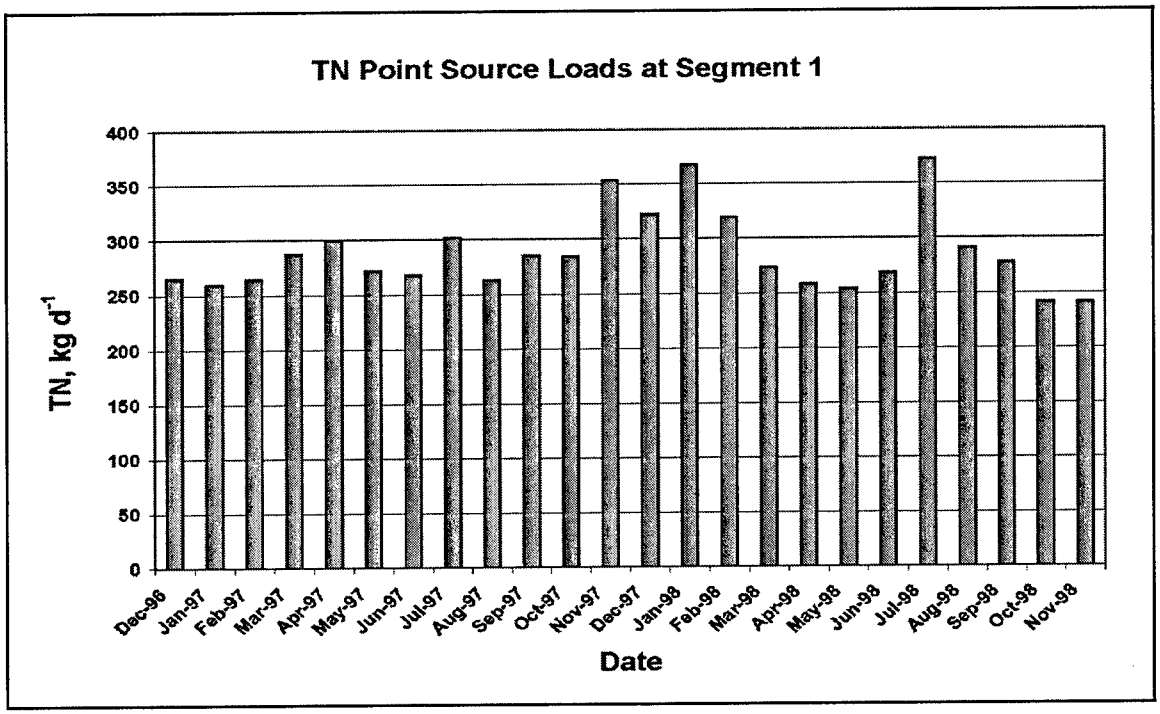

Figure 4-8. Mean monthly TN PS loads into Segment 1, 1996-1998

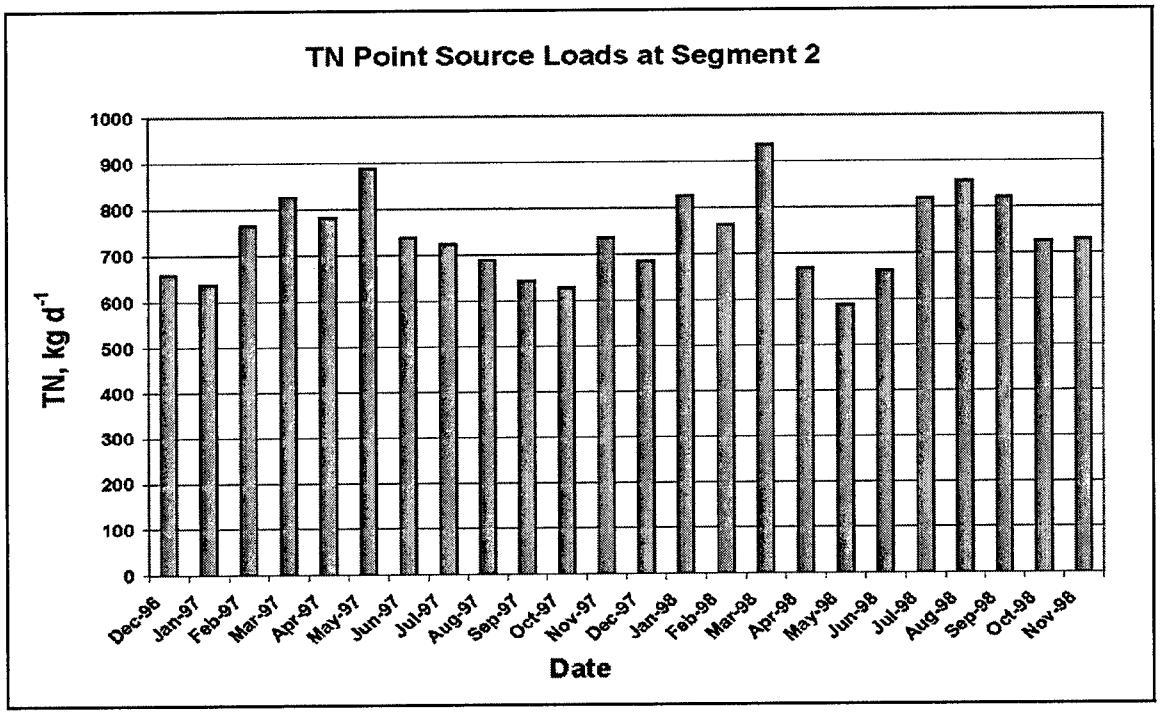

Figure 4-9. Mean monthly TN PS loads into Segment 2, 1996-1998

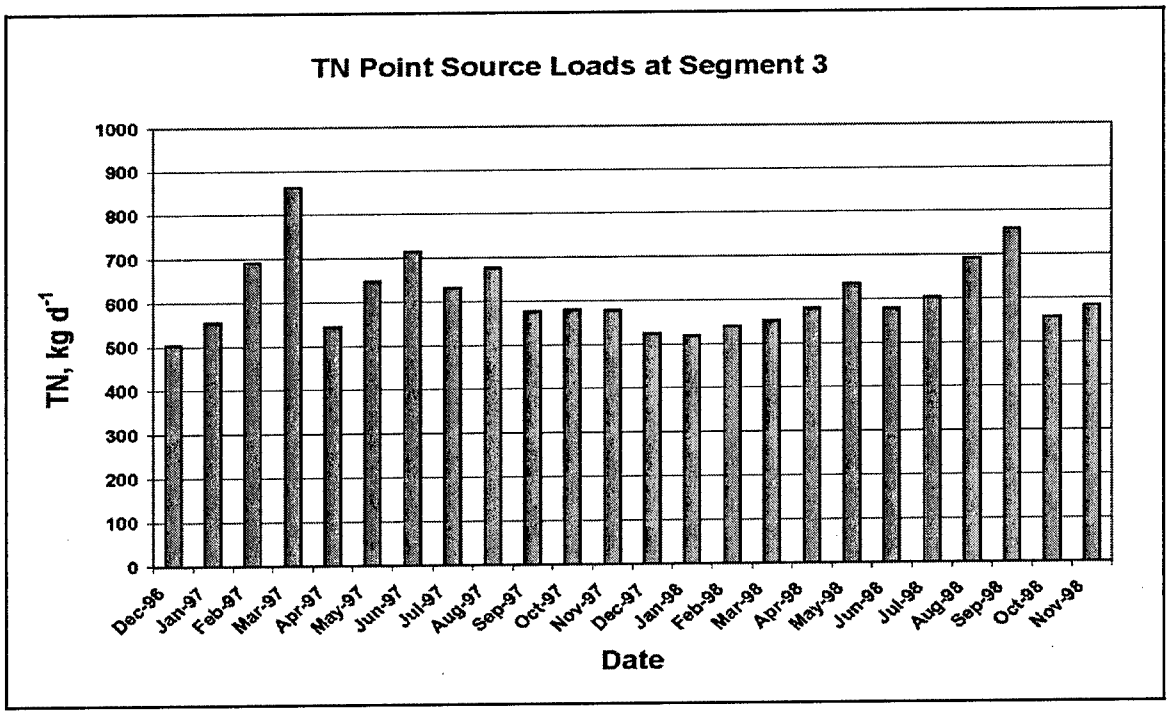

Figure 4-10. Mean monthly TN PS loads into Segment 3, 1996-1998

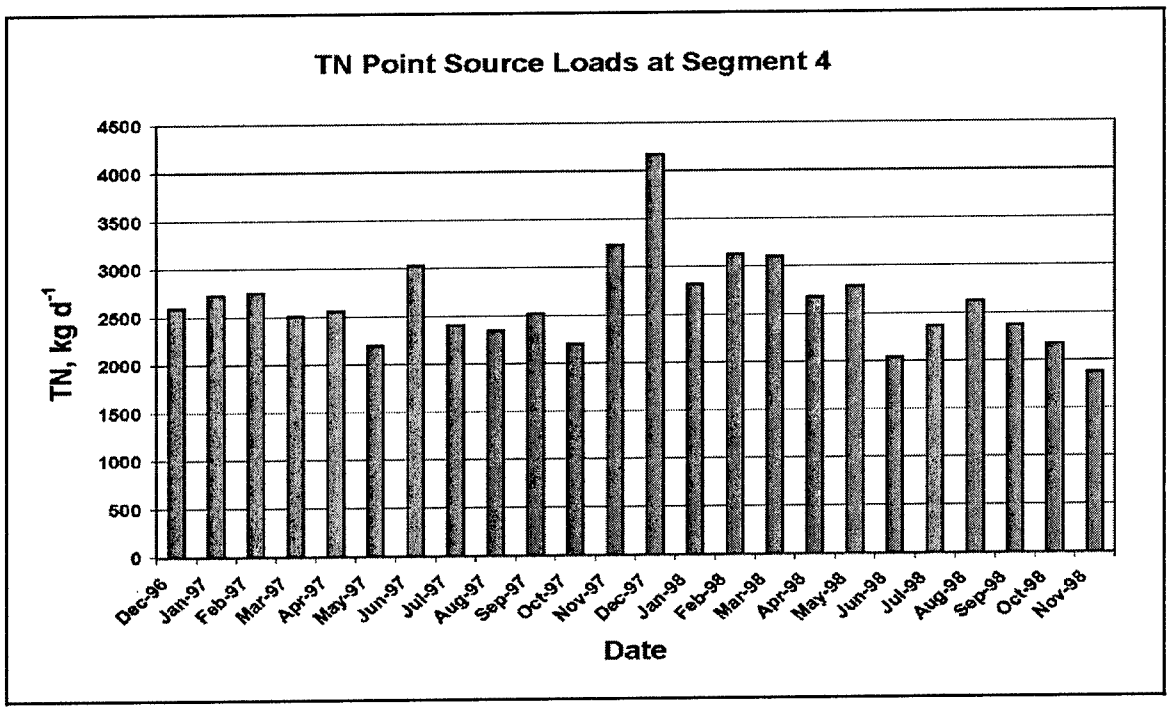

Figure 4-11. Mean monthly TN PS loads into Segment 4, 1996-1998

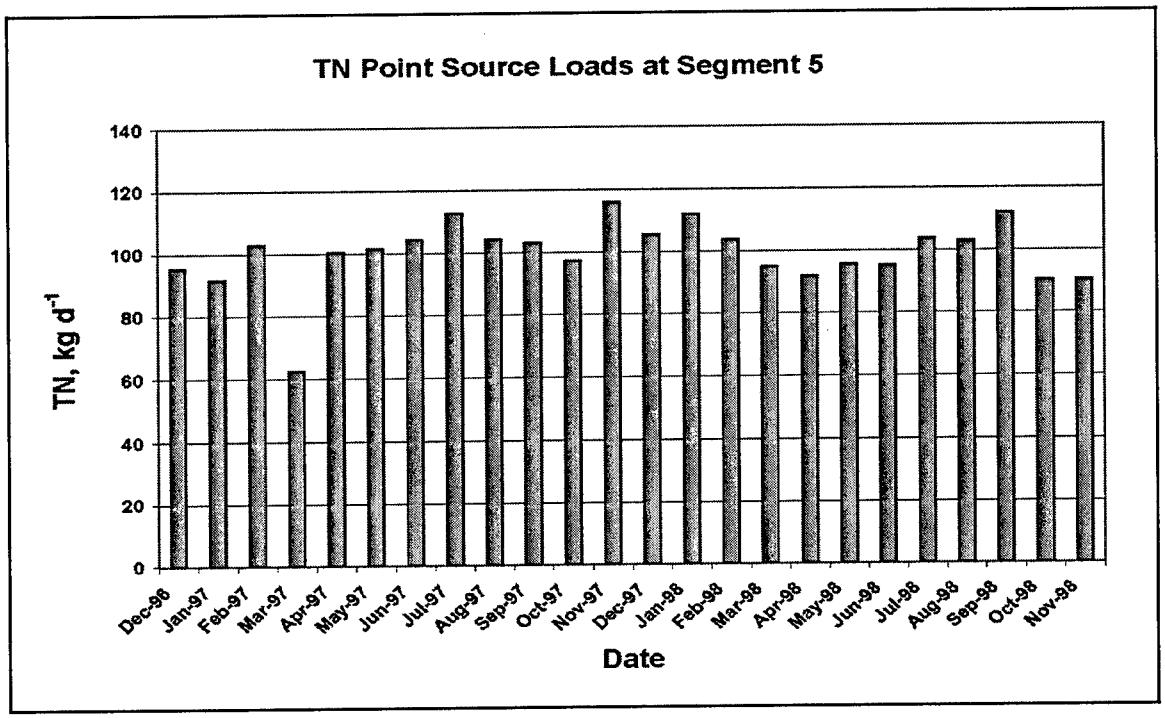

Figure 4-12. Mean monthly TN PS loads into Segment 5, 1996-1998

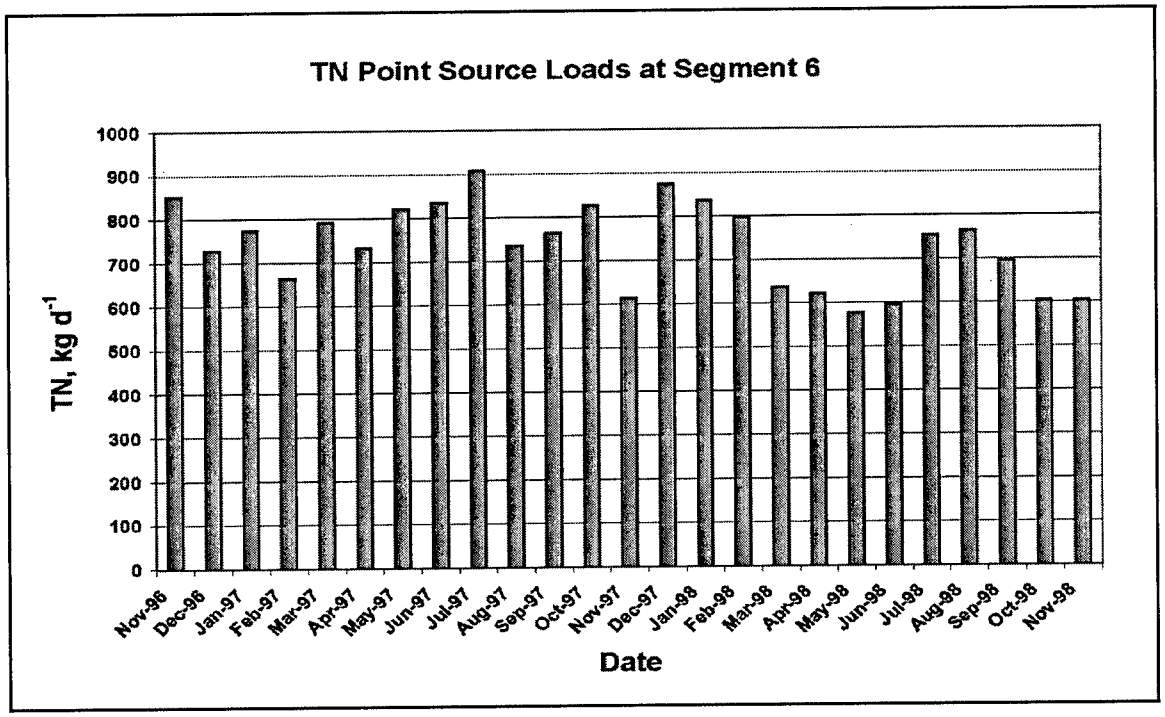

Figure 4-13. Mean monthly TN PS loads into Segment 6, 1996-1998

The data provided by the SJWMD varied from monthly to daily between the point-source dischargers. Two input files were developed for each year of simulation, one for the monthly and one for the daily updated discharges (PS1_96B.NPT, PS1_97B.NPT, PS2_96B.NPT and PS2_97.NPT). The computed total loadings were subdivided into loadings to each of the vertical layers at the specified locations based upon the fraction of layer thickness for each of the six layers in the sigma grid.

Flows and constituent concentrations were provided by the SJRWMD for each of the dischargers listed in Table 4-3. Loads were computed as the product of the flow and specified concentrations for each state variable simulated (Table 4-4). Where only total data were provided and ICM required partitioning among dissolved and particulate fractions, the totals were partitioned using the fractions listed in Table 4-4.

Table 4-4
Point-Source Concentration Data Provided by the SJRWMD With Partitioning Fractions for Corresponding Water Quality Variables

Variable Number	Variable Name	Data Name	Fraction
1	Temperature	none	NA
2	Salinity	none	NA
3	Fixed Suspended Solids	Total Suspended Solids	1.0
4	Algae Type 1	none	NA
5	Algae Type 2	none	NA
6	Algae Type 3	none	NA
7	Zooplankton Type 1	not simulated	NA
8	Zooplankton Type 2	not simulated	NA
9	Labile DOC	Labile TOC	0.9
10	Refractory DOC	Refractory TOC	0.9
11	Labile POC	Labile TOC	0.1
12	Refractory POC	Refractory TOC	0.1
13	Ammonium	Total NH3	1.0
14	Nitrate	(NOx) NO2+NO3	1.0
15	Urea	Not simulated	NA
16	Labile DON	Labile TON	0.9
17	Refractory DON	Refractory TON	0.9
18	Labile PON	Labile TON	0.1
19	Refractory PON	Refractory TON	0.1
20	Total Phosphate	PO4 (Orthophosphate)	1.0

(Continued)

Table 4-4 (Concluded)			
Variable Number	Variable Name	Data Name	Fraction
21	Labile DOP	Labile, Non-ortho P	0.9
22	Refractory DOP	Refract. Non-ortho P	0.9
23	Labile POP	Labile, Non-ortho P	0.1
24	Refractory POP	Refract. Non-ortho P	0.1
25	Particulate Inorganic P	Not simulated	NA
26	COD	none	NA
27	DO	none	NA
28	Particulate Si	none	NA
29	Dissolved Si	none	NA
30	Intternal P1	none	NA
31	Internal P2	none	NA
32	Internal P3	none	NA

Non-point source loads

Data were provided by the SJRWMD for the 63 non-point sources listed in Table 4-5. Also listed in Table 4-4 are the I and J grid coordinates and the surface cell number in the ICM model grid corresponding to the loading location. As previously discussed for point source monthly loads of Total P and N, Total P and N NPS monthly loads were summed for each of the six river segments (Figure 4-1) and are presented in Figures 4-14 through 4-25. As noted in Figures 4-14 through 4-19, segments 3 through 6 received the majority of the Total P loads (average between 500 to 600 kg/day) while the Total P loads to the other segments were small in comparison (<120 kg/day). Similar to Total P loads, most of the Total N loads came into segments 3 through 6 on average approximately 2,500 kg/day as shown in Figures 4-22 through 4-25, while loads to the most downstream segments were on average around 200 kg/day (Figures 4-20 and 4-21).

All loading data varied daily. Two input files were developed for the non-point source loads; for the 2 years of simulation (NPS_96B.NPT and NPS_97B.NPT). The specified loadings were subdivided into loadings to each of the vertical layers at the specified locations based upon the fraction of layer thickness for each of the six layers in the sigma grid.

Constituent loads were provided by the SJRWMD for each of the discharge locations listed in Table 4-5. The loads were provided in units varying from milligrams per day to kilograms per day and were converted to ICM input units of kilograms per day. Where only total data were provided and ICM required partitioning among dissolved and particulate fractions, the totals were partitioned using the fractions listed in Table 4-4. The constituents provided by the

Table 4-5
Non-point Loading Sources Included In Model Simulations

WQ ID	Sub-basin Name	I Coordinate	J Coordinate	ICM Surficial Cell No.
2	Mill Branch	182	31	1216
3	Rice Creek	171	20	134
4	Dog Branch	162	27	1015
5	Mason Branch	158	20	126
6	Deep Creek	154	29	1152
7	Moccasin Branch	153	29	1151
8	McCullough Creek	152	28	1096
9	Cedar Creek	148	20	122
10	Tocoi Creek	145	29	1149
11	Clarkes Creek	140	20	121
12	Sixmile Creek	133	30	1187
13	Orange Grove Branch	125	28	1078
14	Governors Creek	122	20	119
15	Black Creek	118	19	92
16	Cunningham Creek	113	30	1185
17	Swimming Pen Creek	114	18	77
18	Drs Lake West	112	16	45
19	Lucy Branch	110	16	43
20	Drs Lake East	109	18	72
21	Ortega River	92	12	27
22	Cedar River	79	12	14
24	Trout River	46	2	1
25	Broward River	29	11	10
26	Dunn Creek	15	31	1189
27	Gin House Creek	43	54	1584
28	Pottsburg Creek	61	29	1124
31	Julington Creek	110	31	1215
32	Moccasin Creek	170	20	133
33	Unnamed Creek	144	21	195
34	Kendall Creek	127	28	1080
35	Kentucky Branch	117	26	841
36	Peters Branch	112	22	264
37	Durbin Creek	110	31	1215

(Continued)

Table 4-5 (Concluded)

WQ ID	Sub-basin Name	I Coordinate	J Coordinate	ICM Surficial Cell No.
38	Flora Branch	110	31	1215
39	Cormorant Creek	110	31	1215
40	Unnamed Creek	83	30	1181
41	Christopher Branch	94	29	1139
42	New Rose Creek	91	29	1138
43	Craig Creek	80	32	1230
44	Miller Creek	64	27	934
45	Unnamed Creek	41	33	1244
46	Unnamed Creek	41	36	1283
47	New Castle Creek	41	38	1306
48	Jones Creek	43	52	1540
49	Cow Head Creek	43	53	1562
50	Unnamed Creek	31	67	1777
51	Mt Pleasant Creek	35	76	1842
52	Drummond Creek	37	24	452
53	Moncrief Creek	46	15	37
54	Ribault River	46	12	13
55	Block House Creek	46	8	7
56	West Branch	46	5	4
57	Hogan Creek	68	24	483
58	Long Branch	50	23	338
59	McCoy Creek	74	24	489
60	Big Fishweir Creek	84	17	51
61	Williamson Creek	80	12	15
62	Butcher Pen Creek	84	12	19
63	Fishing Creek	86	12	21
64	Unnamed Creek	99	20	114
65	Orange Park Slough	105	22	257
66	Goodbys Creek	97	29	1142
67	Deep Bottom Creek	101	28	1065

SJRWMD and fractions for partitioning to ICM state variables were identical to those used for the PS with the exception of ammonia and nitrate. For the NPS, only total inorganic nitrogen loadings were provided, which were partitioned assuming that 0.75 of the loading was nitrate-nitrogen.

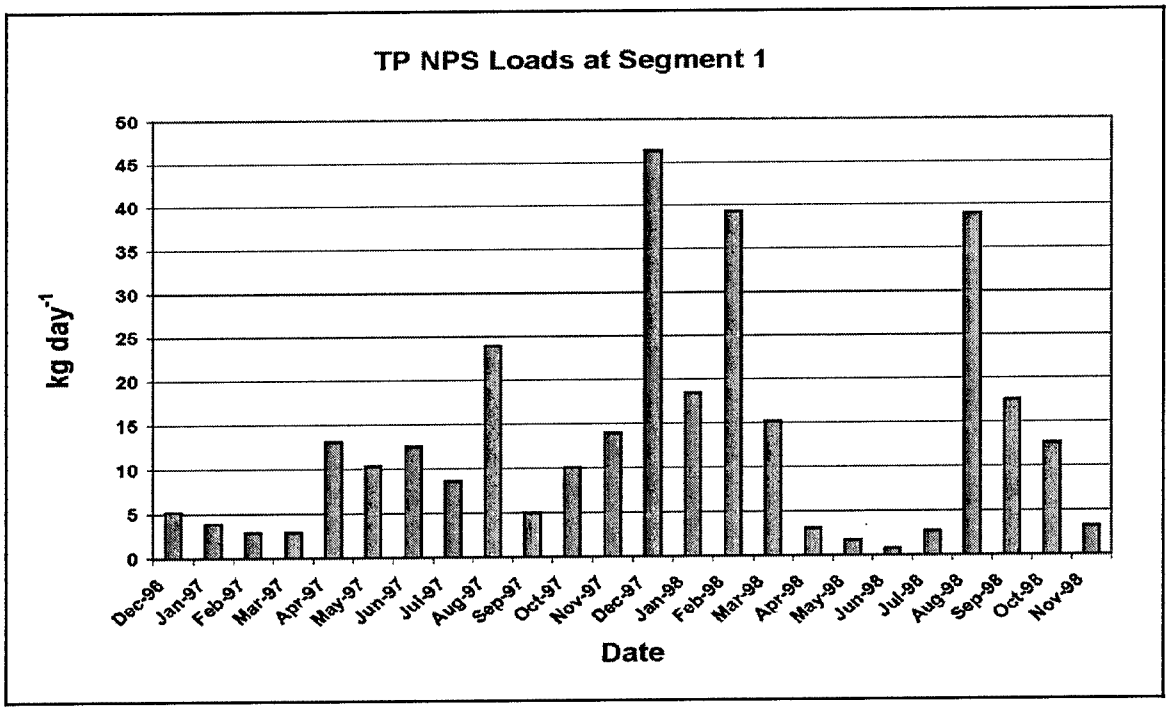

Figure 4-14. Mean monthly TP NPS loads into Segment 1, 1996-1998

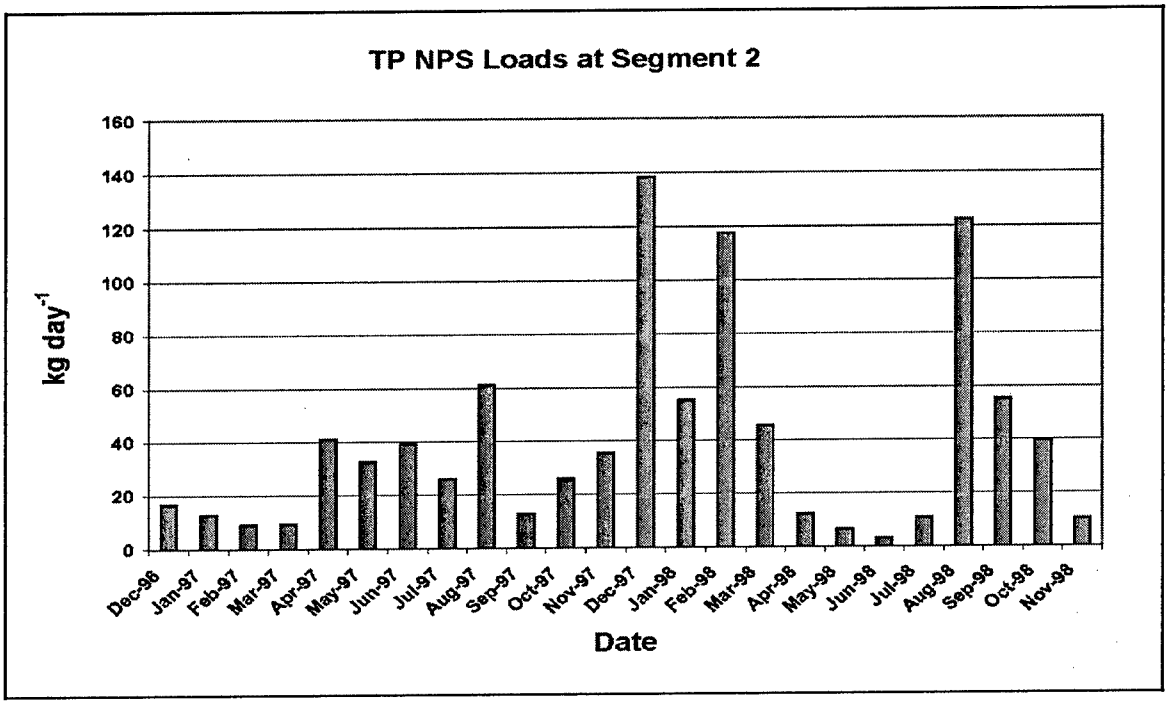

Figure 4-15. Mean monthly TP loads into Segment 2, 1996-1998

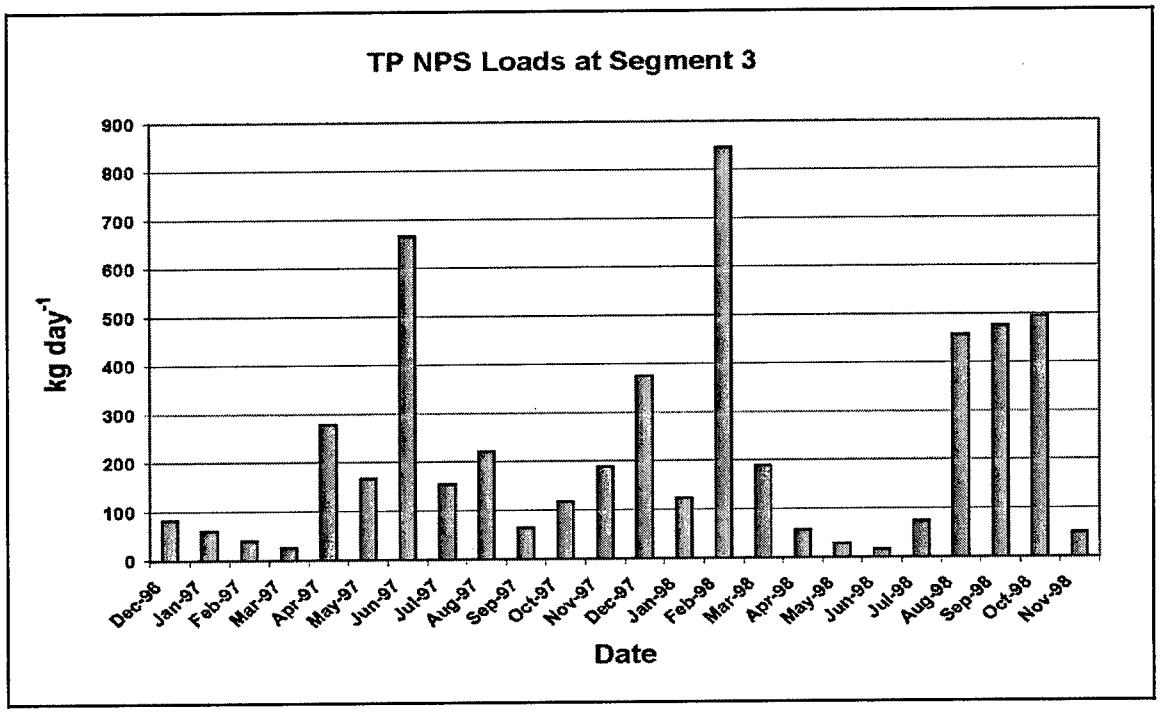

Figure 4-16. Mean monthly TP NPS loads into Segment 3, 1996-1998

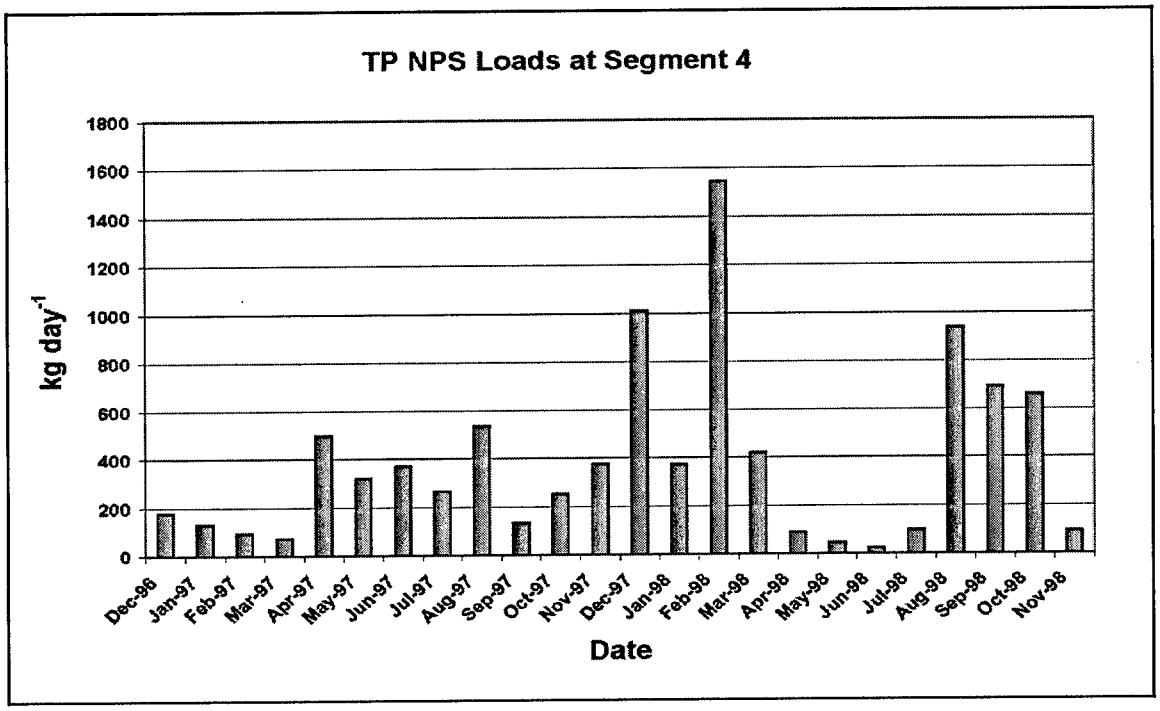

Figure 4-17. Mean monthly TP NPS loads into Segment 4, 1996-1998

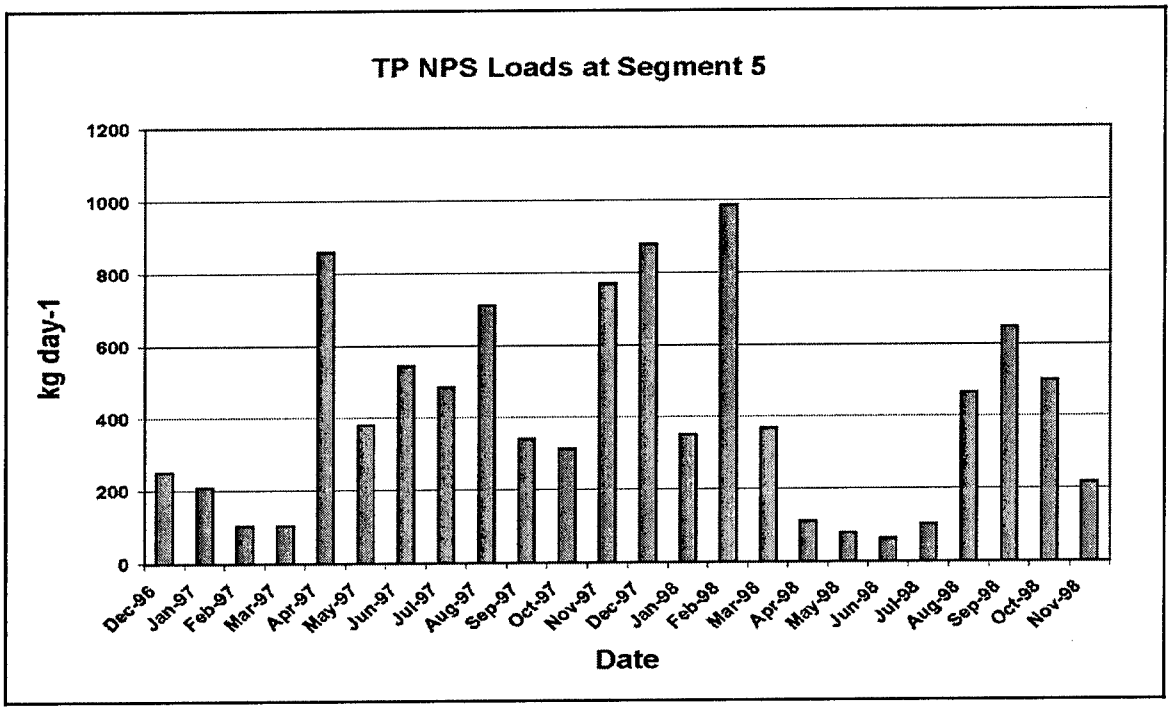

Figure 4-18. Mean monthly TP NPS loads into Segment 5, 1996-1998

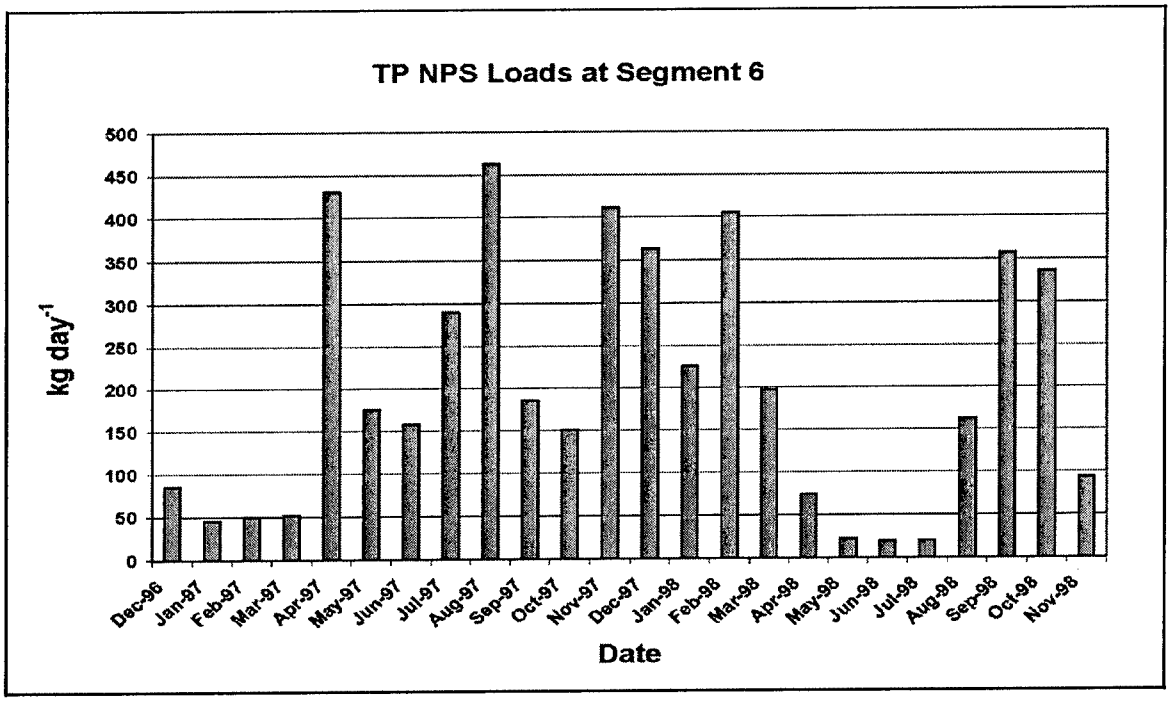

Figure 4-19. Mean monthly TP NPS loads into Segment 6, 1996-1998

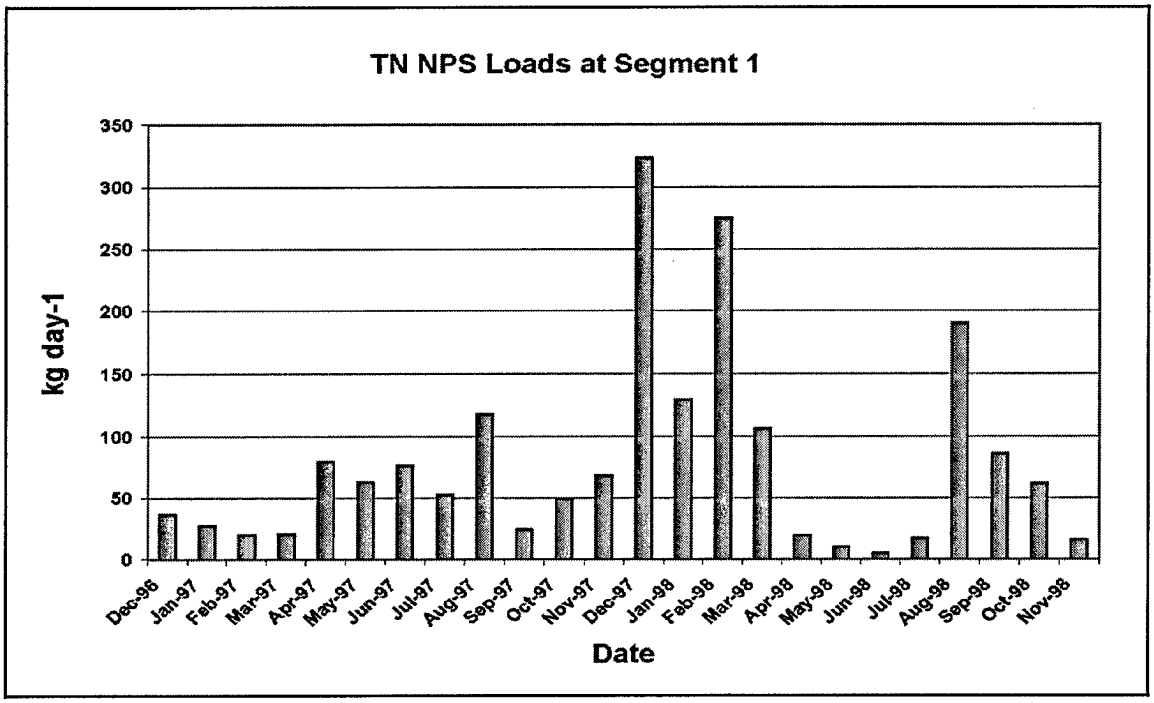

Figure 4-20. Mean monthly TN NPS loads into Segment 1, 1996-1998

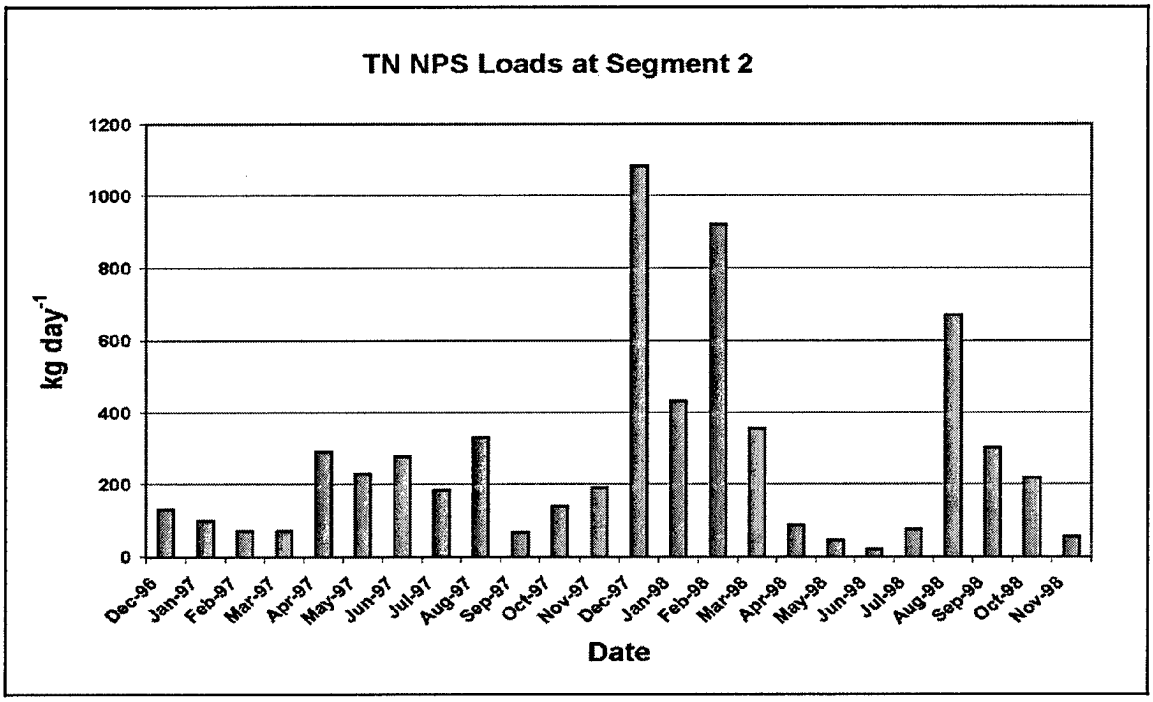

Figure 4-21. Mean monthly TN NPS loads into Segment 2, 1996-1998

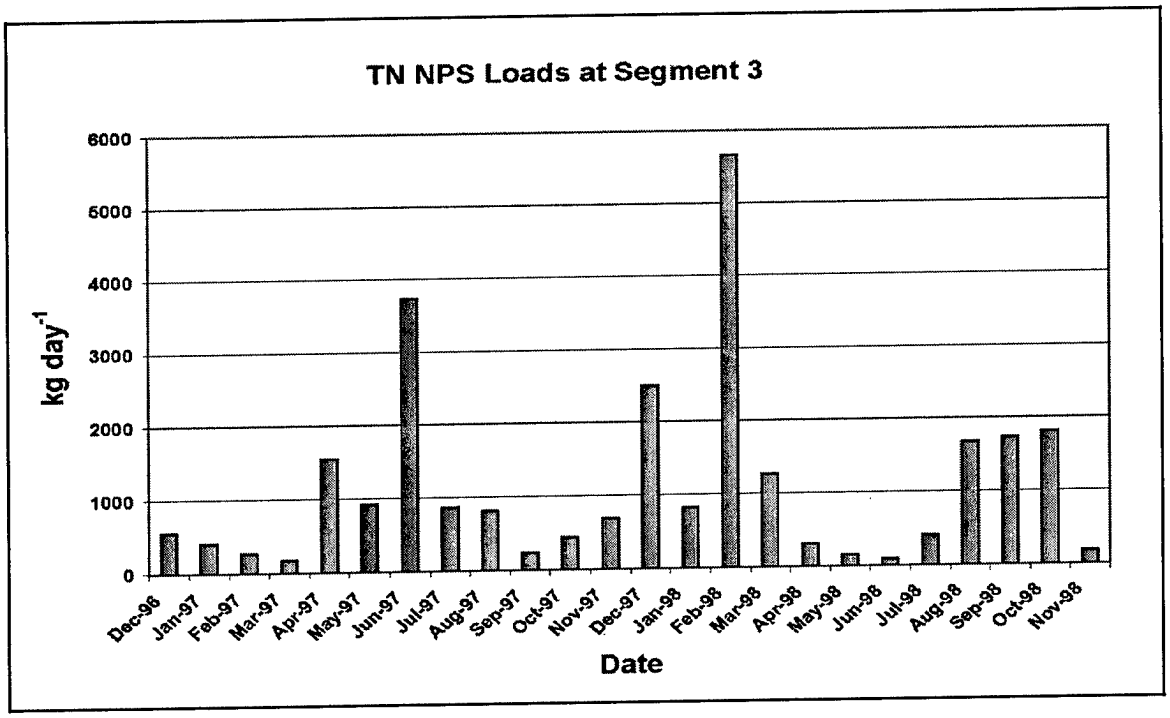

Figure 4-22. Mean monthly TN NPS loads into Segment 3, 1996-1998

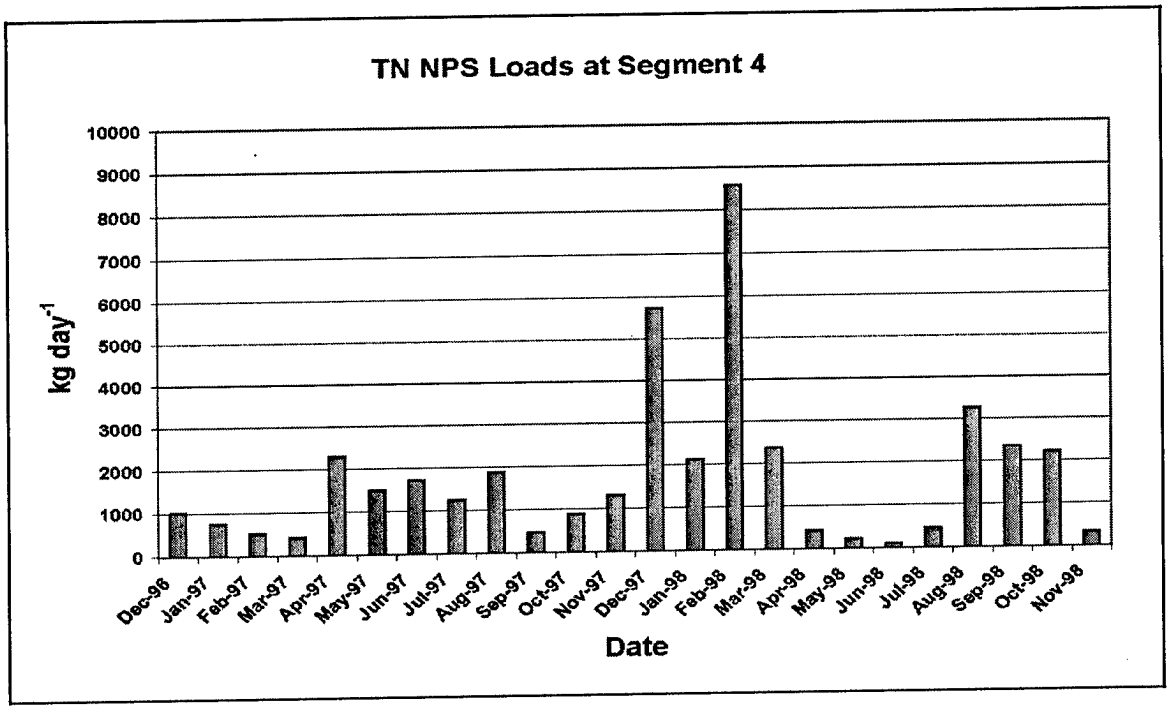

Figure 4-23. Mean monthly TN NPS loads into Segment 4, 1996-1998

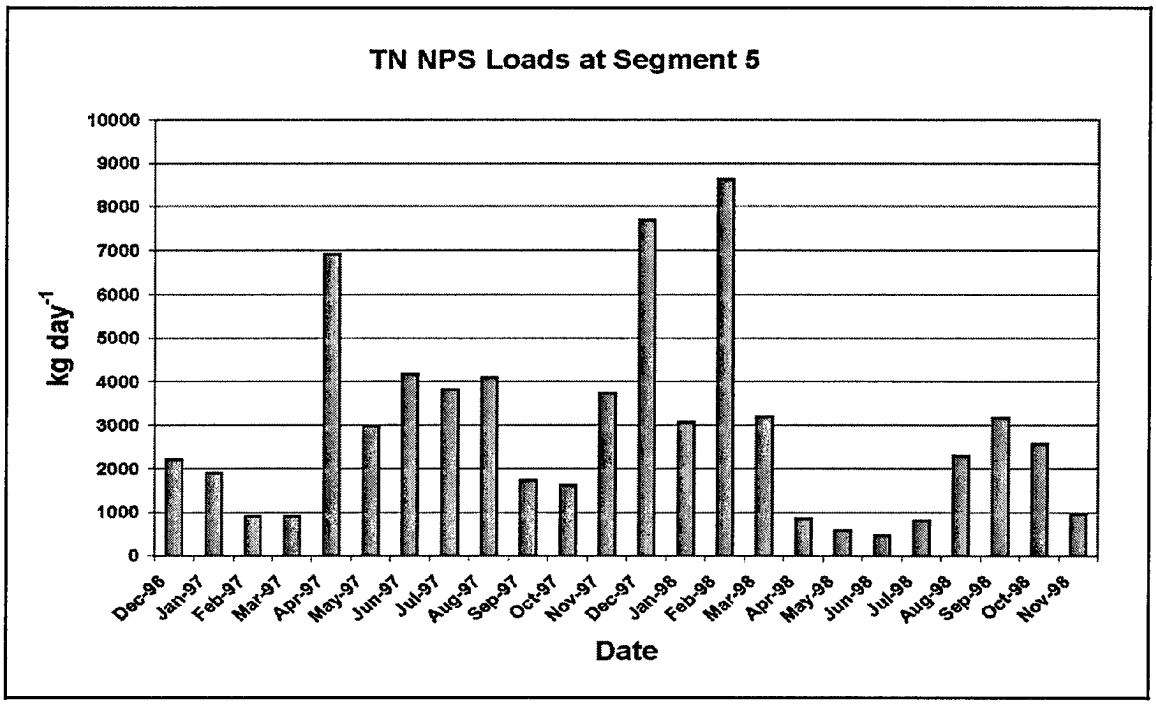

Figure 4-24. Mean monthly TN NPS loads into Segment 5, 1996-1998

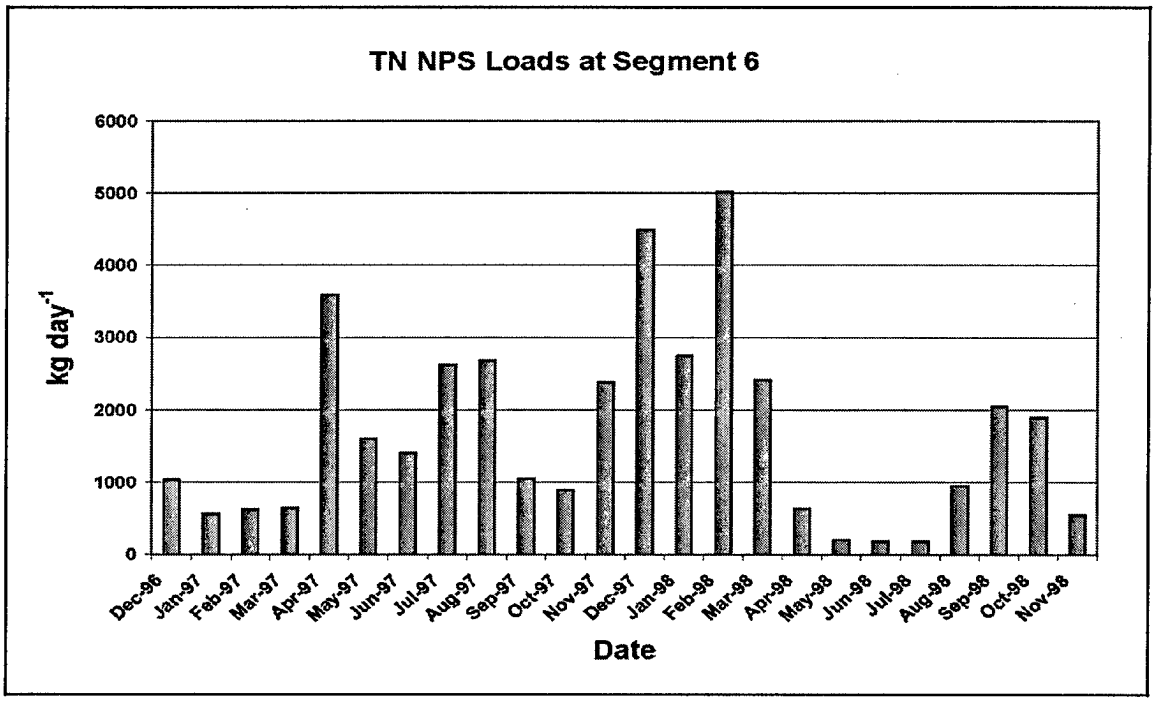

Figure 4-25. Mean monthly TN NPS loads into Segment 6, 1996-1998

Determination of labile and refractory organic carbon and organic nutrient loads

The approach to partitioning labile and refractory organic carbon and nutrients described below was extracted from a report by Hendrickson et al. (2002). Refer to the report for details on the procedure.

Organic carbon. To partition labile and refractory organic carbon, tributary runoff and point source effluent water quality monitoring data collected between 1993 to 1999 within the lower St. Johns River basin were compiled to create a data base of biological oxygen demand (BOD), nutrients, and organic carbon. Station description and number of events sampled are included in Hendrickson et. al (2002). Stations were included in the analysis if the sample constituent suite included carbonaceous biological oxygen demand (CBOD), total organic carbon, total phosphorus, orthophosphate, total ammonia and total nitrate+nitrite nitrogen. In all, 789 samples were available for 28 surface water stations and 22 point sources.

Total organic carbon (TOC) within a sample was considered to be a combination of labile total organic carbon (LTOC) and refractory total organic carbon (RTOC), the proportions of which are determinable through the simultaneous expression of their rates of decomposition, as indicated by oxygen consumption in the $CBOD_5$ test. Using the rates of decomposition of the first-order decay model of 0.075 day^{-1} for labile substrates, and 0.001 day^{-1} for refractory, a pair of equations for the simultaneous solution of labile and refractory portions can be set up in the form (Chapra 1997):

$$C_t = C_{o-r}(1 - e^{-(0.001)*5}) + C_{o-l}(1 - e^{-(0.075)*5}) \tag{4-1}$$

Solving the equation for organic carbon, at time = 5 days, the sum of the carbon consumed was considered = $CBOD_5/2.67$, while at $t = \infty$, C_t = TOC = RTOC + LTOC. The resulting paired equation was simplified for computation to the following:

$$LTOC = (CBOD_5 * 74.906 - TOC)/61.54 \tag{4-2}$$

and

$$RTOC = TOC - LTOC \tag{4-3}$$

In calculations, two of the 88 point source samples and six of the 702 tributary samples had $CBOD_5$ values that indicated decay rates less than 0.001 day^{-1}; conversely, 3 point source samples in the data set exhibited $CBOD_5$ values that, when converted to TOC, exceeded the TOC at the maximum decomposition rate of 0.075 day^{-1}. These values were omitted from subsequent calculations.

Organic nutrients. To determine labile and refractory organic nitrogen and phosphorus in tributary runoff and point source effluents, the relationships between labile organic C content and organic C:N and C:P ratios were examined

to partition organic nitrogen (TON = TKN – NH_4) and non-orthophosphate P (TNOP = TP – PO_4) into these respective pools. Organic C:N and C:P ratios for the tributary and point source data set were plotted against percent LTOC [(LTOC/TOC)*100] to determine if a relationship existed between proportional nutrient content and lability. One data point omitted from this analysis was from stream runoff draining a large dairy and intensive pasture lands in which the organic C:P was 4225:1. Figures in Hendrickson et. al (2002) suggest a significant partitioning of carbon-to-nutrient ratios based upon their content of LTOC, with high LTOC samples exhibiting low organic C:N and C:P ratios.

To determine the organic C:N and C:P for hypothetical, purely labile or refractory substrates, the data set was subdivided into samples with %LTOC less than or equal to 15, and those with %LTOC equal to or greater than 25. Linear regressions using the mean carbon-to-nutrient ratio within 5 percentage-point classes were computed, and the regression equation used to extrapolate the organic C:N and C:P when the %LTOC = 0% and when %LTOC = 100%. This yielded an organic mass (OM) C:N ratio of 33.6 for a completely refractory substrate, and a ratio of 3.6 for a completely labile substrate. In the case of non-orthophosphate phosphorous, the OM C:P ratios obtained were 662.9 for refractory OM and 22.4 for labile.

To constrain predictions of labile and refractory organic nutrients by the computed analytical laboratory fractions (eg., TON = TKN-NH_4; TNOP = TP-PO_4), and to utilize original measured values and already computed watershed model loads, organic C:N and C:P ratios were used to partition existing TON and TNOP concentrations into labile and refractory fractions, rather than developing separate specific land use loading rates. TON was partitioned by establishing a proportional relationship of the form:

$$\mathrm{LTON} = \left\{ \frac{\dfrac{[\mathrm{LTOC}]}{(\mathrm{TOC}*3.6)}}{\dfrac{\mathrm{RTOC}}{(\mathrm{TOC}*33.6)} + \dfrac{\mathrm{LTOC}}{(\mathrm{TOC}*3.6)}} \right\} * \mathrm{TON} \qquad (4\text{-}4)$$

Following this calculation, RTON could be calculated by difference with the relationship

$$\mathrm{RTON} = \mathrm{TON} - \mathrm{LTON} \qquad (4\text{-}5)$$

or with the complementary partitioning equation of the form

$$\mathrm{RTON} = \left\{ \frac{\dfrac{\mathrm{RTOC}}{(\mathrm{TOC}*33.6)}}{\left[\dfrac{\mathrm{RTOC}}{\mathrm{TOC}*336} + \dfrac{\mathrm{LTOC}}{(\mathrm{TOC}*3.6)}\right]} \right\} * \mathrm{TON} \qquad (4\text{-}6)$$

Similarly, TNOP was partitioned with the relationship

$$RTON = \left\{ \frac{\left[\frac{LTNOP}{(TOC * 22.4)} \right]}{\left[\frac{RTNOP}{(TOC * 662.9)} + \frac{LTNOP}{(TOC * 22.4)} \right]} \right\} * TNOP \qquad (4\text{-}7)$$

The concentrations of labile and refractory organic nitrogen, phosphorus, and carbon calculated using this methodology, for the 22 tributary surface water stations, and domestic waste and industrial waste point sources are listed in Hendrikson et al. (2002).

Atmospheric loads

Atmospheric loads to the water surface were treated as a distinctive nutrient source. Atmospheric loads to the watershed were merged with other distributed loads and were not distinguished. Information on atmospheric loads was provided by the sponsor. Monthly wet loads of ammonium and nitrate, dry loads of ammonium and nitrate, and loads of phosphorus were provided for 23 sites. These were averaged into spatially uniform monthly values. No loads were provided for organic nitrogen although these can be substantial (Peierls and Paerl 1997). The nitrogen loads were increased by 20 percent to account for organic nitrogen, and then split the total into 25 percent ammonium, 60 percent nitrate, and 15 percent dissolved organic nitrogen. The amount of organic nitrogen and the fractions were based on atmospheric loads used in the Chesapeake Bay model (Cerco et al. 2002). Loads were input to the model as areal quantities (Table 4-6). These were multiplied internally by cell surface area to produce mass loading to each surface cell in the computational grid. Summaries of the mass loads are presented in Chapter 10.

References

Cerco, C., Linker, L., Sweeney, J., Shenk, G., and Butt, A. (2002). "Nutrient and solids controls in Virginia's Chesapeake Bay tributaries," *Journal of Water Resources Planning and Management*, 128(3), 179-189.

Chapra, S. (1997). *Surface Water Quality Modeling*. McGraw Hill, New York.

Hendrickson, J., Trahan, N., Stecker, E., and Ying, O. (2002). "TMDL and PLRG Modeling of the Lower St. Johns River Technical Report Series, Volume 1: Calculation of the External Load." (Draft). St. Johns River Water Management District, Palatka, FL.

Peierls, B., and Paerl, H. (1997). "Bioavailability of atmospheric organic nitrogen deposition to coastal phytoplankton," *Limnology and Oceanography*, 42(8), 1819-1823.

Table 4-6
Atmospheric Loads to St. Johns River

Year	Month	Ammonium, mg m^{-2} d^{-1}	Nitrate, mg m^{-2} d^{-1}	DON, mg m^{-2} d^{-1}	Phosphate, mg m^{-2} d^{-1}
1996	12	0.38	0.912	0.228	0.007
1997	1	0.268	0.643	0.161	0.005
1997	2	0.254	0.61	0.153	0.018
1997	3	0.407	0.978	0.244	0.019
1997	4	0.741	1.777	0.444	0.017
1997	5	0.474	1.137	0.284	0.016
1997	6	0.898	2.155	0.539	0.035
1997	7	0.647	1.552	0.388	0.019
1997	8	0.53	1.273	0.318	0.03
1997	9	0.429	1.03	0.257	0.011
1997	10	0.448	1.075	0.269	0.022
1997	11	0.475	1.14	0.285	0.035
1997	12	0.696	1.67	0.418	0.018
1998	1	0.381	0.914	0.229	0.008
1998	2	0.629	1.51	0.378	0.146
1998	3	0.404	0.97	0.243	0.024
1998	4	0.757	1.816	0.454	0.002
1998	5	0.344	0.825	0.206	0.004
1998	6	0.586	1.405	0.351	0.008
1998	7	0.808	1.94	0.485	0.022
1998	8	0.9	2.161	0.54	0.039
1998	9	1.25	2.999	0.75	0.022
1998	10	0.354	0.849	0.212	0.005
1998	11	0.508	1.22	0.305	0.02

5 Water Quality Model Formulation

Introduction

CE-QUAL-ICM was designed to be a flexible, widely-applicable eutrophication model. The initial application of the model was to Chesapeake Bay (Cerco and Cole 1994). Subsequent applications included the Delaware Inland Bays (Cerco et al. 1994), Newark Bay (Cerco and Bunch 1997), the San Juan Estuary (Bunch et al. 2000), and Florida Bay (Cerco et al. 2000). Each model application employed a different combination of model features and required addition of system-specific capabilities. This chapter describes general features and site-specific developments of the model as applied to the water column of the St. Johns River.

Conservation of Mass Equation

The foundation of CE-QUAL-ICM is the solution to the 3D mass-conservation equation for a control volume. Control volumes correspond to cells on the model grid. CE-QUAL-ICM solves, for each volume and each state variable, the equation:

$$\frac{\delta\ V_j \cdot C_j}{\delta\ t} = \sum_{k=1}^{n} Q_k \cdot C_k + \sum_{k=1}^{n} A_k \cdot D_k \cdot \frac{\delta\ C}{\delta\ x_k} + \Sigma\ S_j \qquad (5\text{-}1)$$

in which:

V_j = volume of jth control volume (m^3)

C_j = concentration in j^{th} control volume ($g\ m^{-3}$)

t, x = emporal and spatial coordinates

n = number of flow faces attached to j^{th} control volume

Q_k = volumetric flow across flow face k of jth control volume ($m^3\ s^{-1}$)

C_k = concentration in flow across face k ($g\ m^{-3}$)

A_k = area of flow face k (m^2)

D_k = diffusion coefficient at flow face k ($m^2 s^{-1}$)

S_j = xternal loads and kinetic sources and sinks in j^{th} control volume ($g s^{-1}$)

Solution of Equation 5-1 on a digital computer requires specification of parameter values and discretization of the continuous derivatives. The equation is solved using the QUICKEST algorithm (Leonard 1979) in the horizontal plane and a fully implicit central-difference scheme in the vertical direction. The time step, determined by stability requirements, is usually 5 to 15 minutes. The remainder of this chapter is devoted to detailing the kinetics sources and sinks. For notational simplicity, the transport terms are dropped in the reporting of kinetics formulations.

State Variables

CE-QUAL-ICM, as applied to St. Johns River, incorporates 28 state variables in the water column including physical variables, multiple algal groups, and multiple forms of carbon, nitrogen, phosphorus, and silica (Table 5-1). Two zooplankton groups, microzooplankton and mesozooplankton, are available and can be activated when desired.

Table 5-1
Water Quality Model State Variables

Temperature	Salinity
Fixed Solids	Cyanobacteria
Diatoms	Other Phytoplankton
Labile Dissolved Organic Carbon	Refractory Dissolved Organic Carbon
Labile Particulate Organic Carbon	Refractory Particulate Organic Carbon
Ammonium	Nitrate + Nitrite Nitrogen
Labile Dissolved Organic Nitrogen	Refractory Dissolved Organic Nitrogen
Labile Particulate Organic Nitrogen	Refractory Particulate Organic Nitrogen
Total Phosphate	Labile Dissolved Organic Phosphorus
Refractory Dissolved Organic Phosphorus	Labile Particulate Organic Phosphorus
Refractory Particulate Organic Phosphorus	Internal Phosphorus, Algal Group 1
Internal Phosphorus, Algal Group 2	Internal Phosphorus, Algal Group 3
Chemical Oxygen Demand	Dissolved Oxygen
Dissolved Silica	Particulate Biogenic Silica

Algae

Algae are grouped into three model classes: cyanobacteria, diatoms, and others. The grouping is based upon the distinctive characteristics of each class and upon the significant role the characteristics play in the ecosystem. Cyanobacteria, commonly called blue-green algae, are characterized by their abundance (as picoplankton) in saline water and by their bloom-forming characteristics in fresh water. Cyanobacteria are often distinguished as having negligible settling velocity and are subject to low predation pressure.

Cyanobacteria are unique in that some species fix atmospheric nitrogen. Diatoms are distinguished by their requirement for silica as a nutrient to form cell walls. Diatoms are large algae characterized by high settling velocities. Settling of spring diatom blooms to the sediments may be a significant source of carbon for sediment oxygen demand. Algae that do not fall into the preceding two groups are lumped into the heading of other algae. Other algae settle at a rate intermediate between cyanobacteria and diatoms and are subject to greater grazing pressure than cyanobacteria.

Each algal group is quantified as carbonaceous biomass. Carbon-to-chlorophyll ratio may be specified or computed for comparison of computed algal carbon to observed chlorophyll.

Organic carbon

Four organic carbon state variables are considered: labile dissolved, refractory dissolved, labile particulate, and refractory particulate. Labile and refractory distinctions are based upon the time scale of decomposition. Labile organic carbon decomposes on a time scale of days to weeks while refractory organic carbon requires more time. Labile particulate organic carbon decomposes rapidly in the water column or the sediments. Refractory particulate organic carbon decomposes slowly, primarily in the sediments, and may contribute to sediment oxygen demand years after deposition.

Phosphorus

As with carbon, organic phosphorus in the water column is considered in four states: labile dissolved, refractory dissolved, labile particulate, and refractory particulate. A single mineral form, total phosphate, is considered. Total phosphate exists as two states within the model ecosystem: dissolved phosphate and phosphate sorbed to inorganic solids. Phosphorus incorporated in the cells of each algal group is also computed as a state variable. Computation of internal phosphorus provides for variable algal composition and allows luxury phosphorus uptake.

Nitrogen

Nitrogen is first divided into organic and mineral fractions. Organic nitrogen state variables are: labile dissolved, refractory dissolved, labile particulate, and refractory particulate. Two mineral nitrogen forms are considered: ammonium and nitrate. Both are utilized to fulfill algal nutrient requirements, although ammonium is preferred from thermodynamic considerations. The primary reason for distinguishing the two is that ammonium is oxidized by nitrifying bacteria into nitrate. This oxidation can be a significant sink of oxygen in the water column and sediments. An intermediate in the complete oxidation of ammonium, nitrite, also exists. Nitrite concentrations are often much less than nitrate and, for modeling purposes, nitrite is combined with nitrate; therefore, the nitrate state variable actually represents the sum of nitrate plus nitrite.

Silica

Silica is divided into two state variables: dissolved silica and particulate biogenic silica. Dissolved silica is available for utilization by diatoms. Particulate biogenic silica cannot be utilized. In the model, particulate biogenic silica is produced through diatom mortality. Particulate biogenic silica undergoes dissolution to available silica or else settles to the bottom sediments.

Chemical oxygen demand

Chemical oxygen demand is the concentration of reduced substances that are oxidizable by inorganic means. The primary component of chemical oxygen demand is sulfide released from sediments. Oxidation of sulfide to sulfate may remove substantial quantities of dissolved oxygen from the water column.

Dissolved oxygen

Dissolved oxygen is required for the existence of higher life forms. Oxygen availability determines the distribution of organisms and the flows of energy and nutrients in an ecosystem. Dissolved oxygen is a central component of the water-quality model.

Salinity

Salinity is a conservative tracer that provides verification of the transport component of the model and facilitates examination of conservation of mass. Salinity also influences the DO saturation concentration and may be used in the determination of kinetics constants that differ in saline and fresh water.

Temperature

Temperature is a primary determinant of the rate of biochemical reactions. Reaction rates increase as a function of temperature, although extreme temperatures may result in the mortality of organisms and a decrease in kinetics rates.

Fixed solids

Fixed solids are the mineral fraction of total suspended solids. The solids contribute to light attenuation and may play a role in sediment-water phosphorus transfer and in buffering water column phosphorus concentration.

Algae

Algae play a central role in the carbon and nutrient cycles comprised by the model ecosystem. Equations governing the three groups are largely the same. Differences among the groups are expressed through the magnitudes of

parameters in the equations. Algal sources and sinks in the conservation equation include production, respiration, predation, and settling. These are expressed as:

$$\frac{\delta}{\delta t} B = \left(G - R - Wa \frac{\delta}{\delta z} \right) B - PR \tag{5-2}$$

in which:

B = algal biomass, expressed as carbon (g C m^{-3})
G = growth (d^{-1})
R = respiration (d^{-1})
Wa = algal settling velocity (m d^{-1})
PR = predation (g C m^{-3} d^{-1})

Production

Production by phytoplankton is determined by the intensity of light, by the availability of nutrients, and by the ambient temperature.

Light

The influence of light on phytoplankton production is represented by a chlorophyll-specific production equation (Jassby and Platt 1976):

$$P^B = Pm^B \frac{I}{\sqrt{I^2 + Ik^2}} \tag{5-3}$$

in which:

P^B = production (g C g^{-1} Chl d^{-1})
Pm^B = production at optimal illumination (g C g^{-1} Chl d^{-1})
I = irradiance (E m^{-2} d^{-1})

Parameter Ik is defined as the irradiance at which the initial slope of the production versus irradiance relationship (Figure 5-1) intersects the value of Pm^B:

$$Ik = \frac{Pm^B}{\alpha} \tag{5-4}$$

in which α is the initial slope of production versus irradiance relationship (g C g^{-1} Chl (E m^{-2})$^{-1}$)

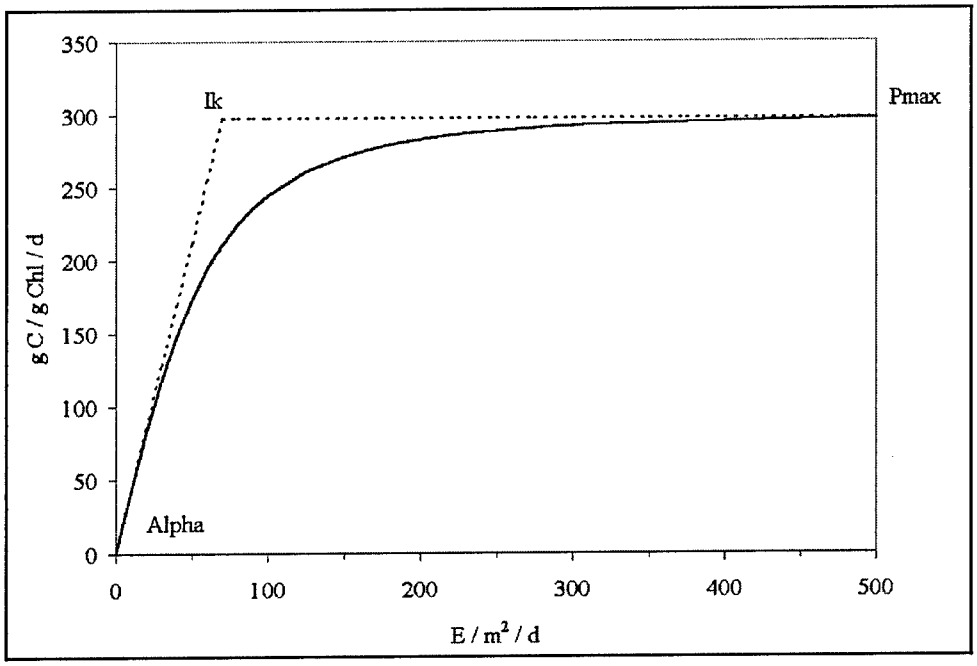

Figure 5-1. Production versus irradiance relationship

Chlorophyll-specific production rate is readily converted to carbon-specific growth rate, for use in Equation 5-2 through division by the carbon-to-chlorophyll ratio:

$$G = \frac{P^B}{CChl} \tag{5-5}$$

in which *CChl* is the carbon-to-chlorophyll ratio (g C g^{-1} chlorophyll *a*).

Carbon-to-chlorophyll ratio

The carbon-to-chlorophyll ratio is determined by an empirical relationship presented by Cloern et al. (1995). They related the chlorophyll-to-carbon ratio to temperature, light, and nutrient limitation:

$$Chl:C = Chl:Cmin + A \cdot e^{B \cdot T} \cdot e^{-C \cdot Itot} \cdot \mu' \tag{5-6}$$

in which:

Chl:Cmin = minimum chlorophyll to carbon ratio (g *Chl* g^{-1} *C*)

Itot = total daily irradiance (E m^{-2})

μ' = nutrient limitation to growth ($0 \leq \mu' \leq 1$)

A, B, C = empirical parameters

The model takes the inverse of Equation 5-6 since carbon-to-chlorophyll ratio is required. Parameters are treated as input variables to be specified for each algal group. (Cloern et al. provided parameter values for coastal diatoms and noted that dinoflagellates have smaller chlorophyll to carbon ratios than diatoms.) A constant carbon-to-chlorophyll ratio can be employed by specifying parameter A as zero.

Examination of the computed ratio, using parameters for coastal diatoms, indicates the carbon-to-chlorophyll ratio takes values from less than 50 to more than 300 (Figures 5-2, 5-3, and 5-4). Light has the greatest influence on the ratio while the effect of temperature is least. The ratio increases as irradiance increases and decreases as a function of temperature. The ratio decreases as nutrients move from severely-limiting to non-limiting conditions. The effect of nutrient limitation on carbon-to-chlorophyll exhibits a strong interaction with irradiance. At low irradiance, the ratio is more sensitive to nutrient limitation than at high irradiance.

Nutrients

Carbon, nitrogen, and phosphorus are the primary nutrients required for algal growth. Diatoms require silica as well. Inorganic carbon is usually available in excess and is not considered in the model.

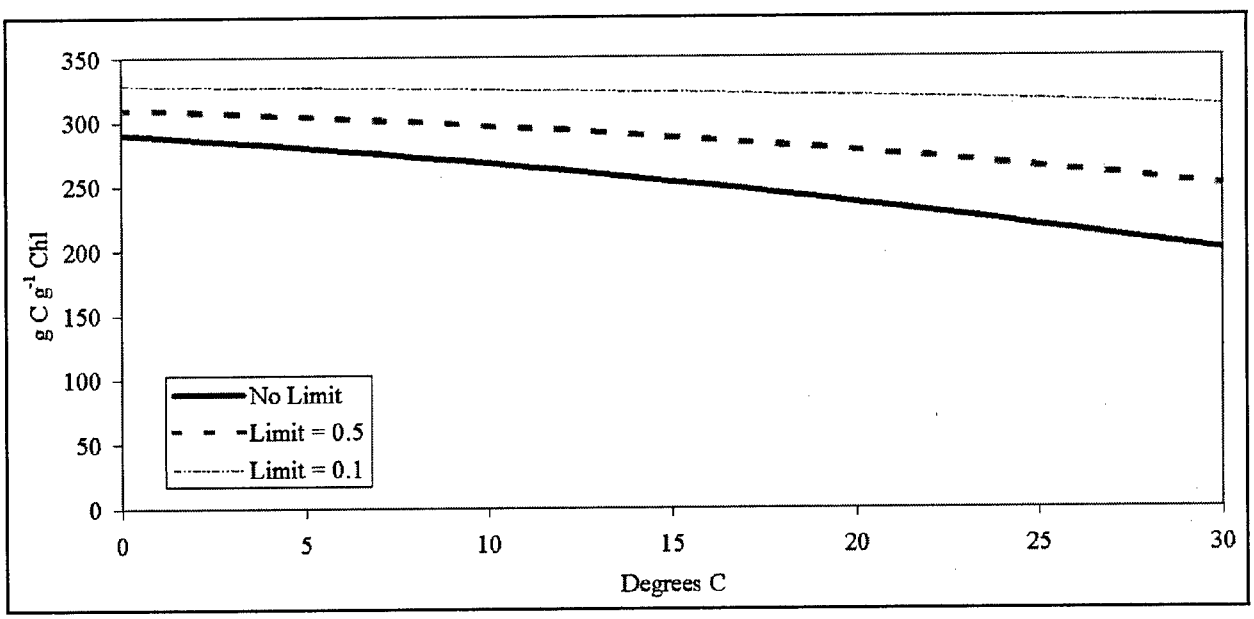

Figure 5-2. Effect of temperature and nutrient limitation on carbon-to-chlorophyll ratio

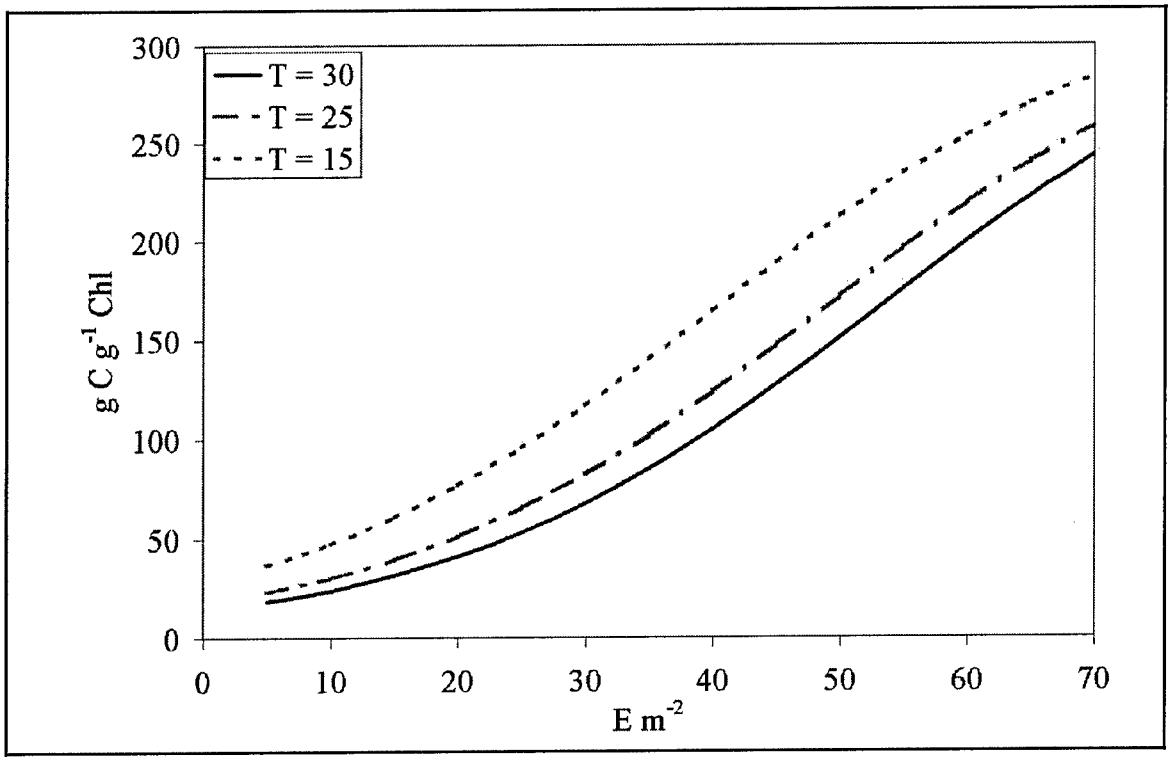

Figure 5-3. Effect of irradiance and temperature on carbon-to-chlorophyll ratio

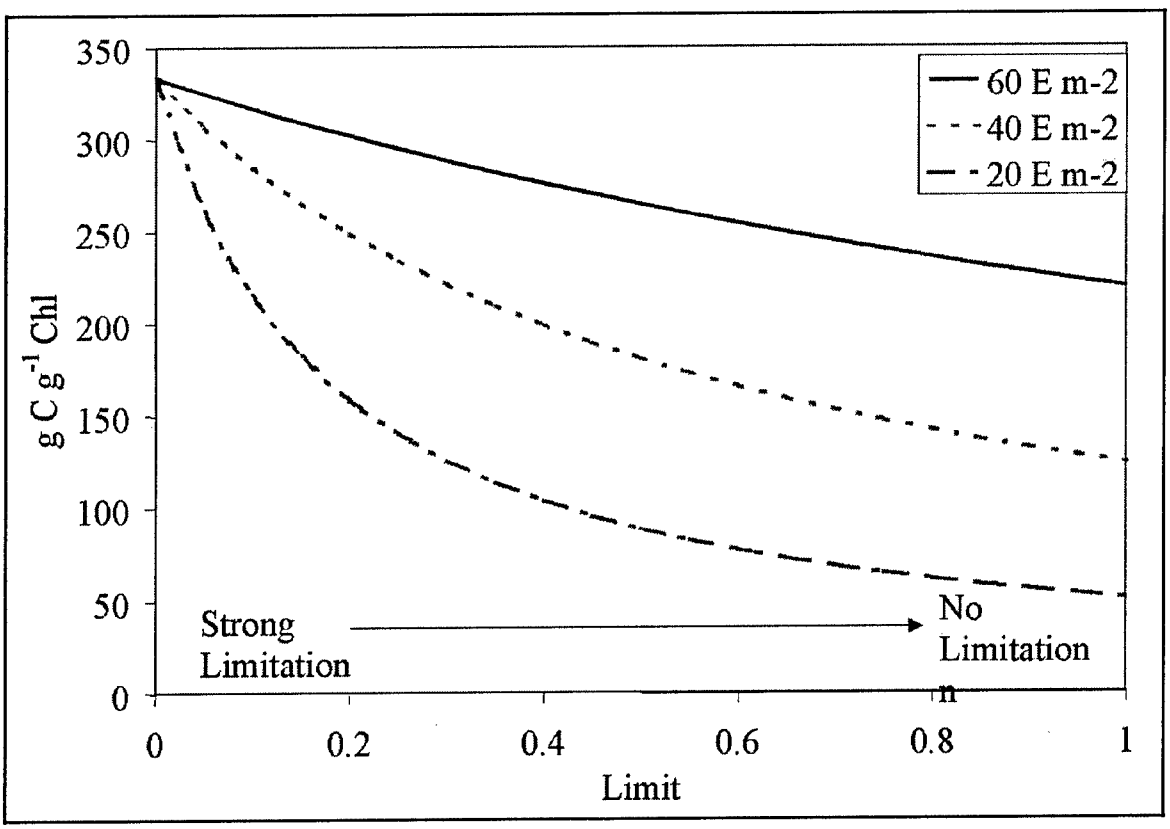

Figure 5-4. Effect of nutrient limitation and irradiance on carbon-to-chlorophyll ratio

Nitrogen and silica. The effects of nitrogen and silica on growth are described by the formulation commonly referred to as "Monod kinetics" (Monod 1949):

$$f(N) = \frac{D}{KHd + D} \tag{5-7}$$

in which:

$f(N)$ = nutrient limitation on algal production ($0 \leq f(N) \leq 1$)
D = concentration of dissolved inorganic nutrient (g m^{-3})
KHd = half-saturation constant for nutrient uptake (g m^{-3})

In the Monod formulation (Figure 5-5) growth is dependent upon nutrient availability at low nutrient concentrations but is independent of nutrients at high concentrations. A key parameter in the formulation is the "half-saturation concentration." Growth rate is half the maximum when available nutrient concentration equals the half-saturation concentration.

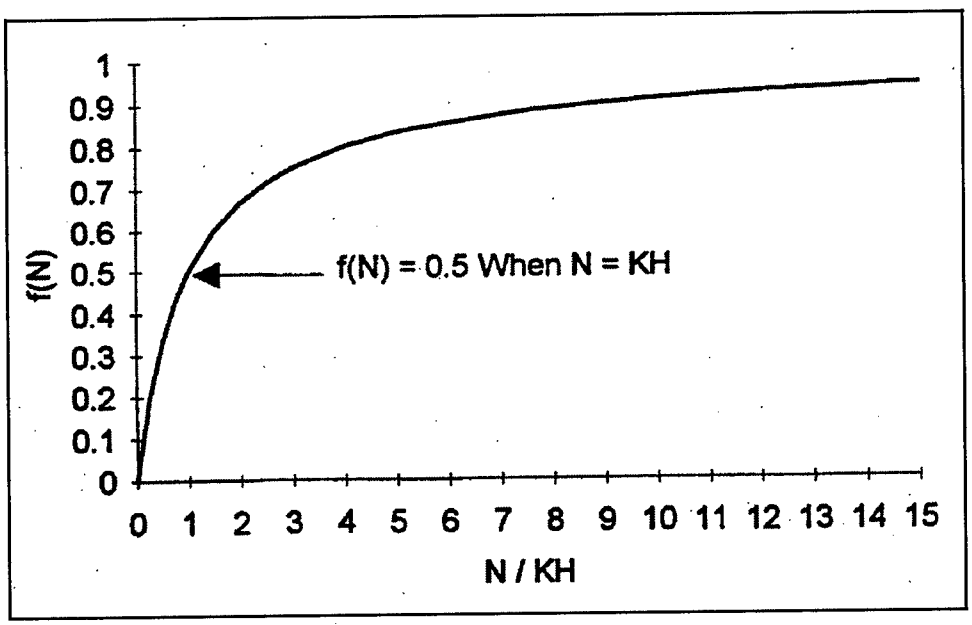

Figure 5-5. Monod formulation for nutrient-limited growth

Phosphorus. The effect of phosphorus on growth is modeled with a formulation commonly known as "Droop kinetics" (Droop 1973). Droop kinetics relate algal growth to the concentration of internal rather than external nutrients. For phosphorus, using terminology employed in the model, the limit is:

$$Plim = \frac{Q - Qo}{Q} \tag{5-8}$$

in which:

$Plim$ = phosphorus limitation on algal production ($0 \leq Plim \leq 1$)

Q = cell quota (g P g^{-1} algal C)

Qo = minimum cell quota (g P g^{-1} algal C)

As noted by Droop, his formula (Figure 5-6) is equivalent to a Monod formulation in which the nutrient concentration is expressed as excess cell quota and the half-saturation concentration is the minimum cell quota:

$$Plim = \frac{Q - Qo}{Qo + (Q - Qo)} \tag{5-9}$$

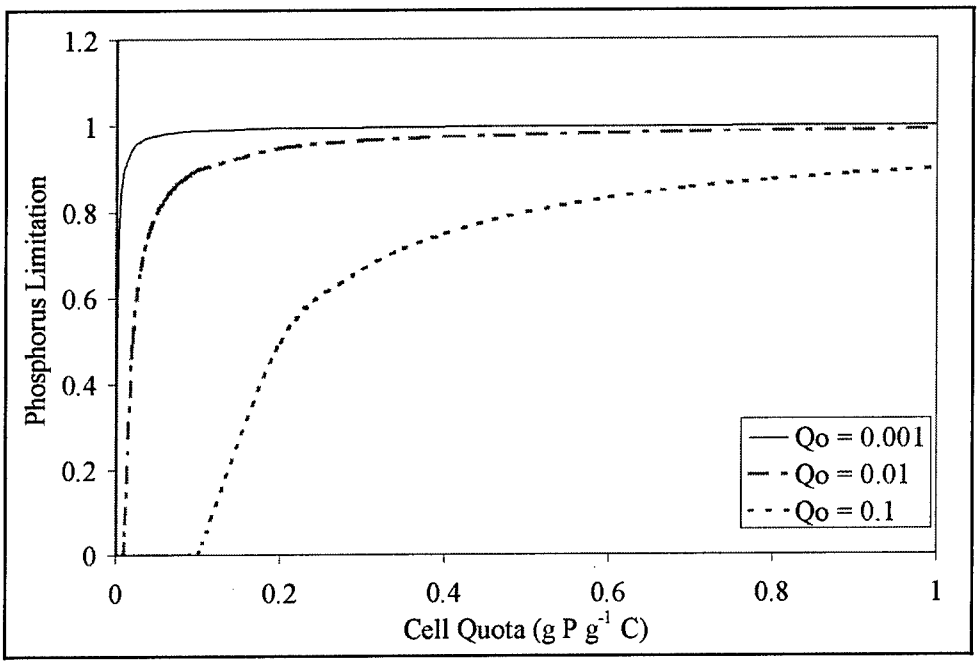

Figure 5-6. Droop formulation for nutrient-limited growth

The original formulation of the Droop model expresses internal nutrients as mass of nutrient per algal cell. The present model quantifies algae as carbon per unit volume, not as discrete cells. The internal phosphorus state variable is also expressed as mass per unit volume. Cell quota is mass of internal phosphorus per unit volume divided by mass of algal carbon per unit volume or mass phosphorus per mass carbon.

Phosphorus is transported from the external pool to the internal pool in accordance with an uptake relationship that is identical to the Monod formula:

$$Pup = Vmax \cdot \frac{PO_4d}{KHp + PO_4d} \tag{5-10}$$

in which:

Pup = phosphorus uptake by algae (g P g^{-1} algal C d^{-1})

$Vmax$ = maximum uptake rate (g P g^{-1} algal C d^{-1})

PO_4d = dissolved portion of total phosphate external to cell (g P m^{-3})

KHp = half saturation concentration for phosphorus uptake (g P m^{-3})

Effect of internal phosphorus calculation. The model was applied to a closed, well-mixed system (Table 5-2) supplied with inorganic nitrogen and light in excess quantities. Phosphorus recycling was eliminated so that only the initial phosphate was available to the algae. The system was simulated for 30 days. Midway through the simulation, a phosphate load equivalent to the initial mass was injected. Three simulations were conducted. The first used the internal phosphorus algorithm. In the second, algal composition was fixed equivalent to the initial cell quota in the internal phosphorus computation (0.025 g P g^{-1} C). In the third, algal composition was fixed equivalent to the minimum cell quota in the internal phosphorus computation (0.007 g P g^{-1} C).

Table 5-2
Properties of Well-Mixed System

Property	Value	Units
Volume	1.0	m^3
Initial phosphate	0.09	g P m^{-3}
Initial internal phosphorus	0.0125	g P m^{-3}
Initial algal biomass	0.5	g C m^{-3}
Growth rate	1.0	d^{-1}
Basal metabolism	0.1	d^{-1}
Photo-respiration	0.1	
KHp	0.01	g P m^{-3}
Phosphorus-to-carbon ratio (fixed composition)	0.007, 0.025	g P g^{-1} C
Qo (variable composition)	0.007	g P g^{-1} C
Vmax	0.01	g P g^{-1} C d^{-1}

Biomass for the fixed-composition calculations took off more rapidly than the internal phosphorus calculation (Figure 5-7). Algae with the high, fixed composition quickly exhausted the available phosphorus (Figure 5-8) and attained peak biomass roughly a third of the other simulations. The effect of the internal phosphorus calculation was to reduce amplitude of biomass fluctuations and delay their occurrence, relative to the computation with minimum, fixed composition (Figure 5-7). Fluctuations in external phosphate were also damped and delayed (Figure 5-8).

Growth of algae with fixed composition stopped abruptly when external phosphorus was exhausted (Figures 5-7 and 5-8). Growth of algae with internal phosphorus continued after external phosphorus was depleted, fueled by the internal pool, and did not cease until internal cell quota reached the minimum (Figures 5-9 and 5-10).

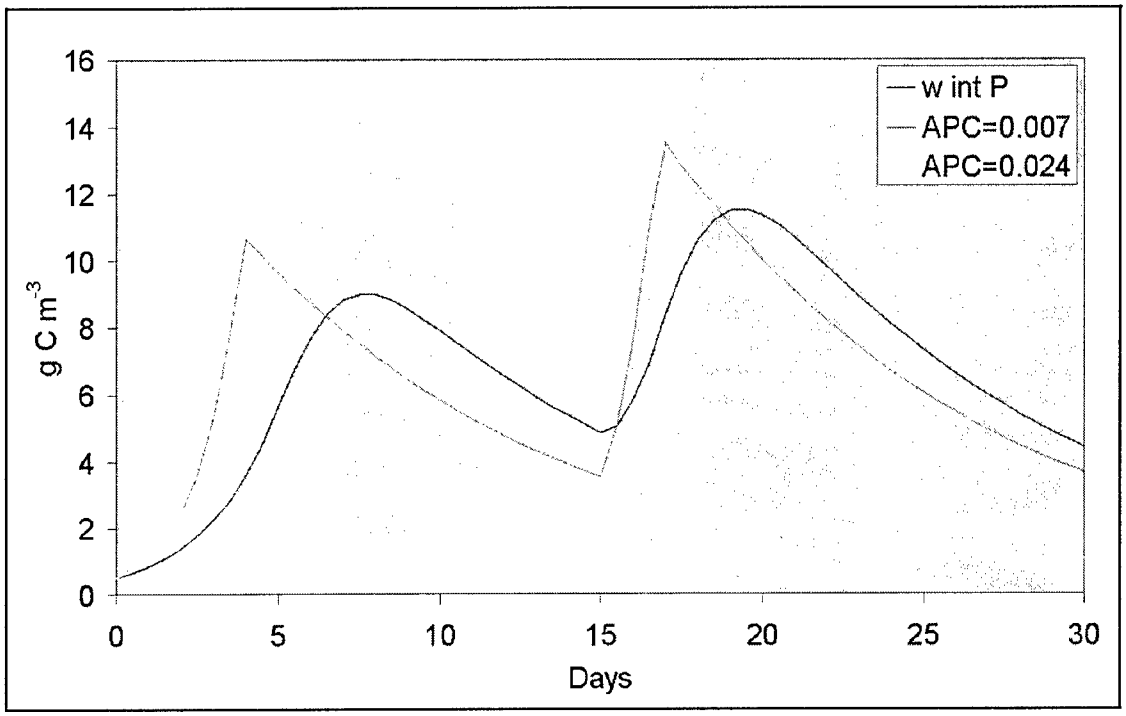

Figure 5-7. Algal biomass with fixed and variable internal phosphorus

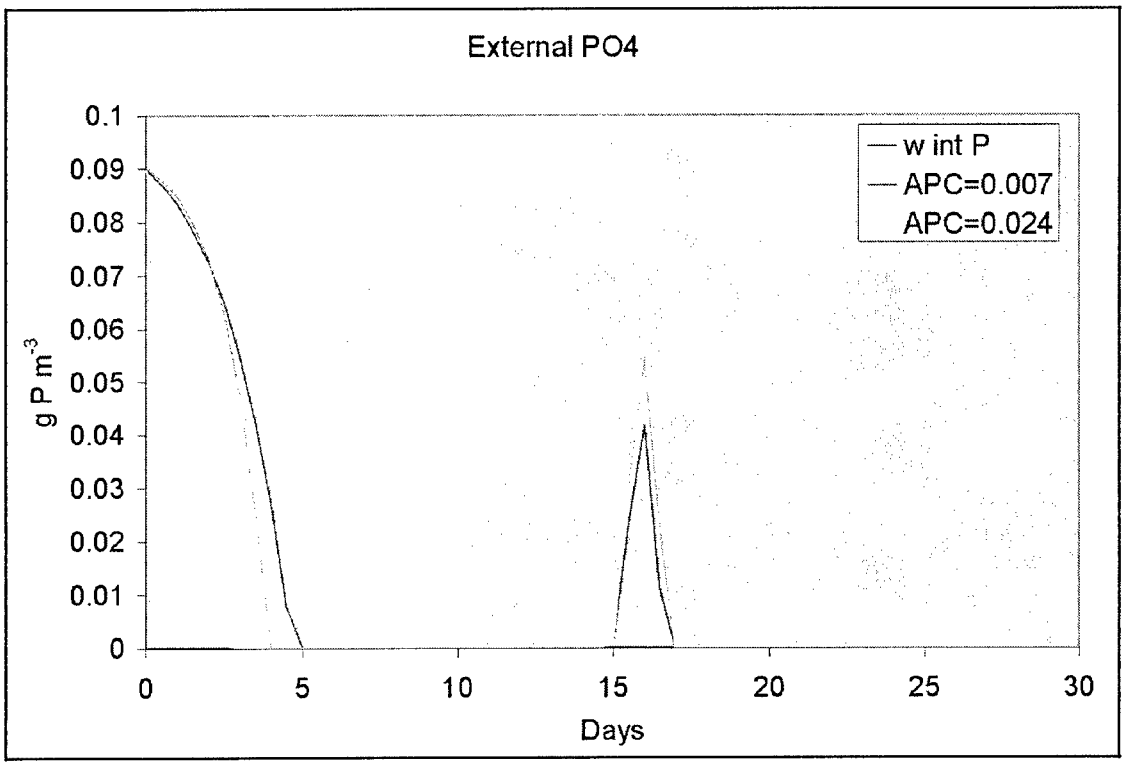

Figure 5-8. Dissolved phosphate with fixed and variable internal phosphorus

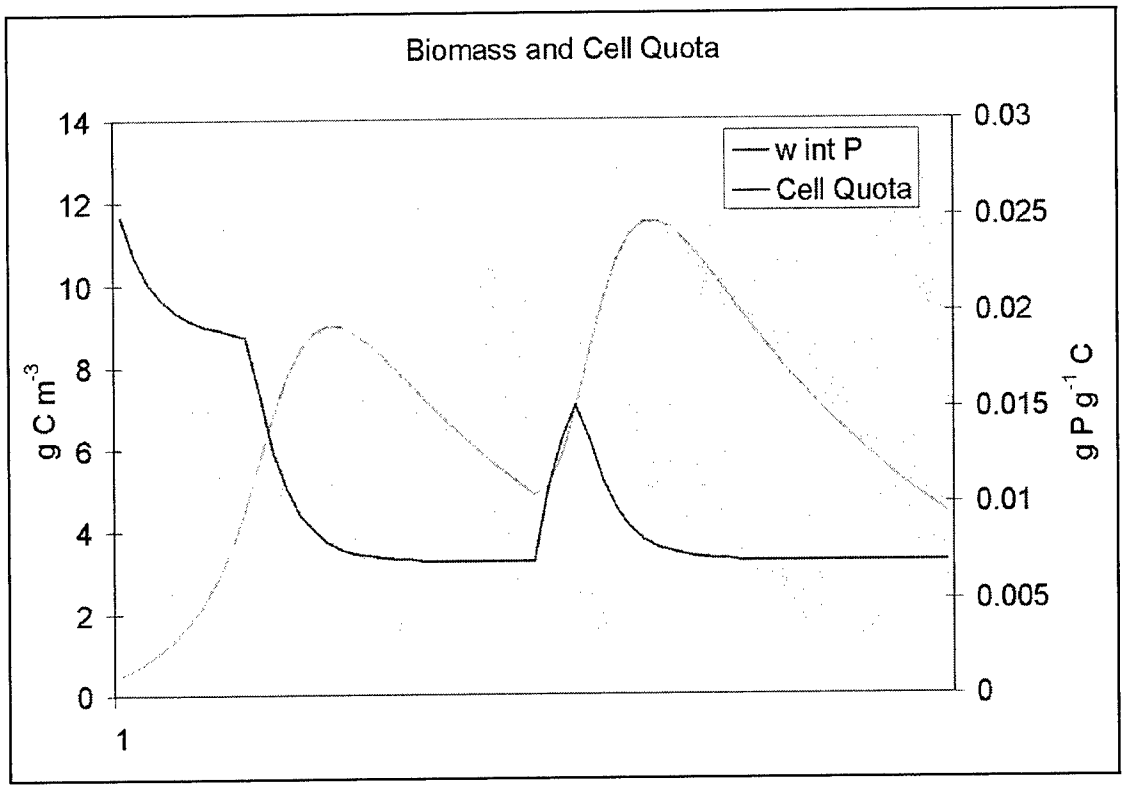

Figure 5-9. Biomass and cell quota for algae with variable internal phosphorus

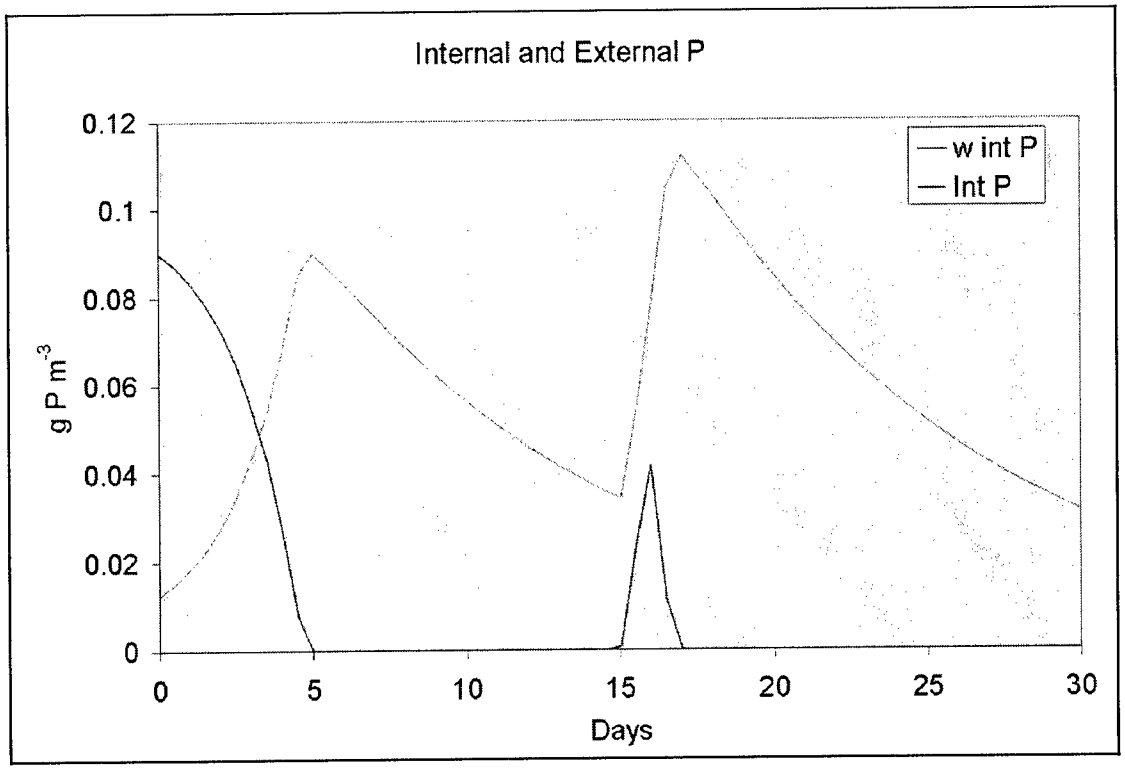

Figure 5-10. Internal and external phosphorus for simulation with variable internal phosphorus

This simulation suggests that application of the internal phosphorus model to a real system will result in damped oscillations in algal biomass and phosphate relative to a model with fixed composition. Peak biomass will not differ substantially, however, from that attained using a model with fixed, minimal phosphorus-to-carbon ratio. The actual impact in a system with multiple, time varying inputs and with recycling is impossible to predict, however, and should be tested in one or more sensitivity runs.

Temperature

Algal production increases as a function of temperature until an optimum temperature or temperature range is reached. Above the optimum, production declines until a temperature lethal to the organisms is attained. Numerous functional representations of temperature effects are available. Inspection of growth versus temperature curves indicates a function similar to a Gaussian probability curve (Figure 5-11) provides a good fit to observations:

$$f(T) = e^{-KTg1 \cdot (T - Topt)^2} \text{ when } T \leq Topt$$

$$= e^{-KTg2 \cdot (Topt - T)^2} \text{ when } T > Topt \qquad (5\text{-}11)$$

in which:

T = temperature (°C)
$Topt$ = optimal temperature for algal growth (°C)
$KTg1$ = effect of temperature below Topt on growth (°C^{-2})
$KTg2$ = effect of temperature above Topt on growth (°C^{-2})

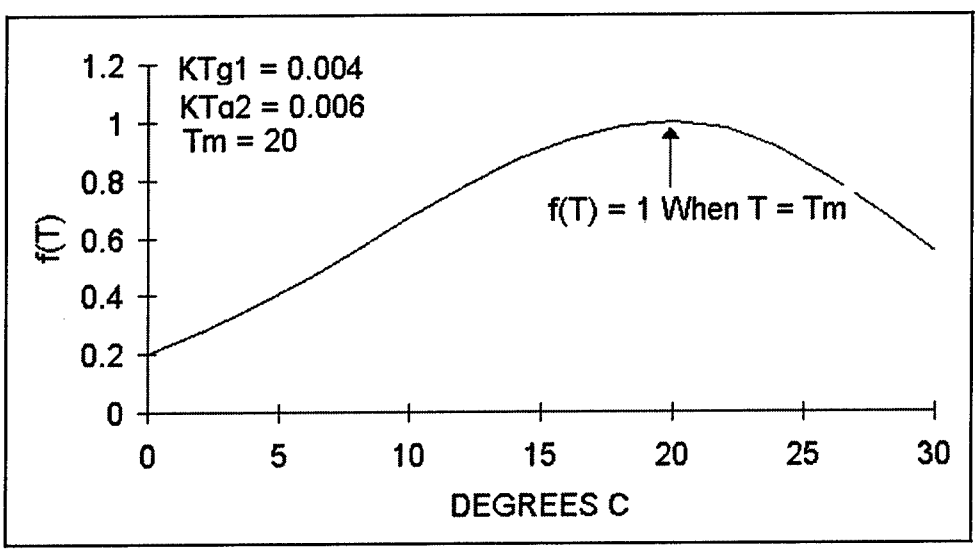

Figure 5-11. Relation of algal production to temperature

Combining effects of light, nutrients, and temperature

A production versus irradiance relationship (Figure 5-12) is constructed for each model cell at each time step. First, Pm^B is determined as a function of ambient temperature and nutrient concentrations:

$$Pm^B = Pmax \cdot f(T) \cdot \tag{5-12}$$

$$minimum\left(\frac{NH_4 + NO_3}{KHn + NH_4 + NO_3}, \frac{Q - Qo}{Q}, \frac{Si}{KHs + Si}\right)$$

in which:

Pm^B = production subject to light and nutrient limitations (g C g^{-1} Chl d^{-1})

$Pmax$ = production at optimal temperature in the absence of light and nutrient limitations (g C g^{-1} Chl d^{-1})

NH_4 = ammonium concentration (g N m^{-3})

NO_3 = nitrate concentration (g N m^{-3})

KHn = half-saturation concentration for nitrogen uptake (g N m^{-3})

Si = dissolved silica concentration (g Si m^{-3})

KHs = half-saturation concentration for silica uptake (g P m^{-3})

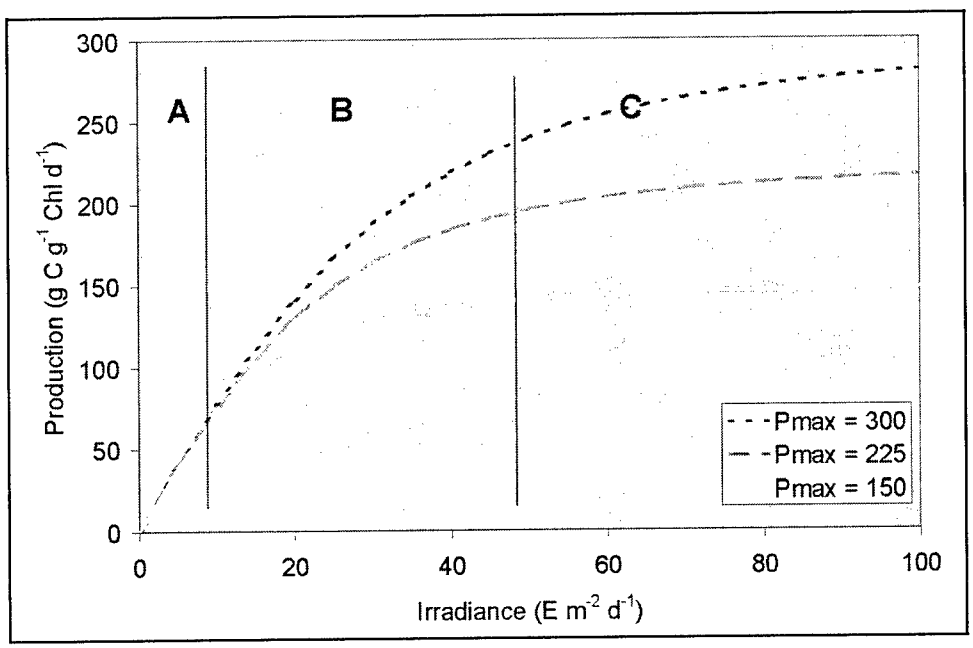

Figure 5-12. Combined effects of light and nutrient limitations. In region A, nutrient limitation has no effect. In region B, light and nutrient limitations exhibit strong interactions. In region C, light exhibits little or no influence on production

Next, parameter *Ik* is derived from Equation 5-4. Finally, production, as a function of temperature, nutrients, and light, is derived from Equation 5-3. The resulting production versus irradiance curve exhibits three regions (Figure 5-12). For $I >> Ik$, the value of the term $I/\sqrt{I^2 + IK^2}$ approaches unity and temperature and nutrients are the primary factors that influence production. For $I << Ik$, production is determined solely by α and irradiance I. In the region where the initial slope of the production versus irradiance curve intercepts the line indicating production at optimal illumination, $I \,.\, Ik$, production is determined by the combined effects of temperature, nutrients, and light.

The model requires, for each phytoplankton group, specification of parameters *Pmax*, α, *Topt*, *KTg*, *KHn*, *KHp*, and (for diatoms) *KHs*. Parameters P^B, Pm^B, and *Ik* are derived. It is assumed that α is constant. Although this assumption is not entirely true, specification of the functional variation of α is beyond the data availability of most model applications.

Irradiance

Irradiance at the water surface is evaluated at each model time step. Instantaneous irradiance is computed by fitting a sin function to daily total irradiance:

$$Io = \frac{\Pi}{2 \cdot FD} \cdot IT \cdot \sin\left(\frac{\Pi \cdot DSSR}{FD}\right) \tag{5-13}$$

in which:

Io = irradiance at water surface (E m^{-2} d^{-1})
FD = fractional daylength ($0 \leq FD \leq 1$)
$DSSR$ = time since sunrise (day)

Io is evaluated only during the interval:

$$\frac{1 - FD}{2} \leq DSM \leq \frac{1 + FD}{2} \tag{5-14}$$

in which *DSM* is the time since midnight (day). Outside the specified interval, *Io* is set to zero.

Respiration

Two forms of respiration are considered in the model: photo-respiration and basal metabolism. Photo-respiration represents the energy expended by carbon fixation and is a fixed fraction of production. In the event of no production (e.g., at night), photo-respiration is zero. Basal metabolism is a continuous energy expenditure to maintain basic life processes. In the model, metabolism is

considered to be an exponentially increasing function (Figure 5-13) of temperature. Total respiration is represented:

$$R = Presp \cdot G + BMr \cdot e^{KTb \cdot (T - Tr)} \tag{5-15}$$

in which:

$Presp$ = photo-respiration ($0 \leq \text{Presp} \leq 1$)
BMr = metabolic rate at reference temperature Tr (d^{-1})
KTb = effect of temperature on metabolism ($°C^{-1}$)
Tr = reference temperature for metabolism (°C).

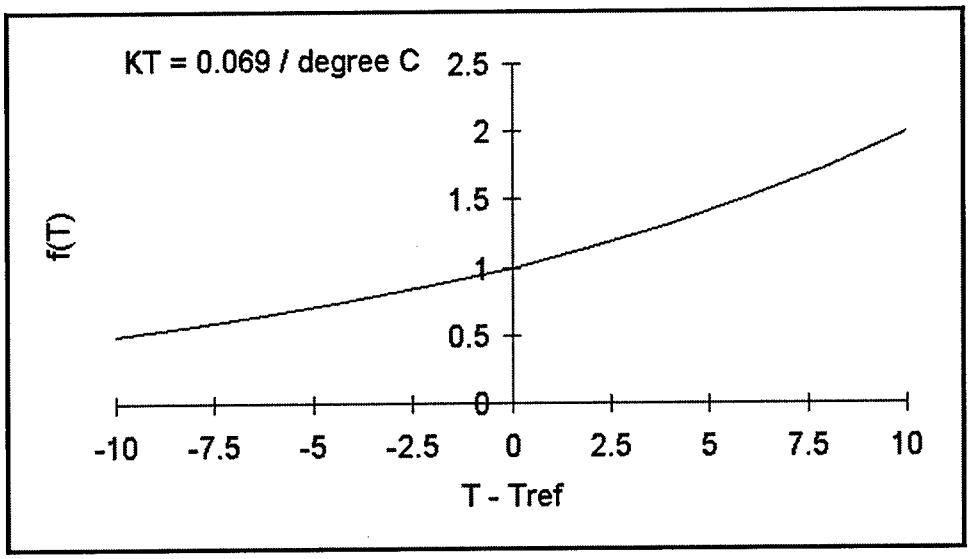

Figure 5-13. Relation of algal metabolism to temperature

Predation

Predation is modeled by assuming zooplankton and other predators clear a specific volume of water per unit biomass:

$$PR = F \cdot B \cdot Z \tag{5-16}$$

in which:

F = filtration rate ($m^3\ g^{-1}$ zooplankton C day^{-1})
Z = zooplankton biomass (g C m^{-3}).

Absent an explicit zooplankton model, specification of the spatial and temporal distribution of the predator population is impossible. One approach is to assume zooplankton biomass is proportional to algal biomass, $Z = \gamma B$, in which case Equation 5-16 can be rewritten:

$$PR = \gamma \cdot F \cdot B^2 \tag{5-17}$$

Since neither γ nor F are known precisely, the logical approach is to combine their product into a single unknown, *Phtl*, determined during the model calibration procedure. Effect of temperature on predation is represented with the same formulation as the effect of temperature on respiration.

Effect of algae on phosphorus

Model phosphorus state variables include total phosphate (dissolved and sorbed), internal phosphorus, labile dissolved organic phosphorus, refractory dissolved organic phosphorus, labile particulate organic phosphorus, and refractory particulate organic phosphorus. Thus, total phosphorus in the model is expressed as:

$$TotP = PO_4t + PIB + LDOP + RDOP + LPOP + RPOP \tag{5-18}$$

in which:

$TotP$ = total phosphorus (g P m^{-3})
PO_4t = total phosphate (g P m^{-3})
PIB = internal phosphorus (g P m^{-3})
$LDOP$ = labile dissolved organic phosphorus (g P m^{-3})
$RDOP$ = refractory dissolved organic phosphorus (g P m^{-3})
$LPOP$ = labile particulate organic phosphorus (g P m^{-3})
$RPOP$ = refractory particulate organic phosphorus (g P m^{-3}).

Algal uptake transfers dissolved phosphate to the internal pool while respiration releases internal phosphorus as dissolved phosphate and organic phosphorus. The division of respired phosphorus into mineral and organic fractions is determined by empirical distribution coefficients. A second set of distribution coefficients determines the fate of algal phosphorus lost through predation.

Effect of algae on nitrogen

Model nitrogen state variables include ammonium, nitrate, labile dissolved organic nitrogen, refractory dissolved organic nitrogen, labile particulate organic nitrogen, and refractory particulate organic nitrogen. The amount of nitrogen incorporated in algal biomass is quantified through a stoichiometric ratio. Thus, total nitrogen in the model is expressed as:

$$TotN = NH_4 + NO_3 + Anc \cdot B + DON + LPON + RPON \tag{5-19}$$

in which:

TotN = total nitrogen (g N m^{-3})

NH_4 = ammonium (g N m^{-3})
NO_3 = nitrate (g N m^{-3})
Anc = lgal nitrogen-to-carbon ratio (g N g^{-1} C)
DON = dissolved organic nitrogen (g N m^{-3})
LPON = labile particulate organic nitrogen (g N m^{-3})
RPON = refractory particulate organic nitrogen (g N m^{-3}).

Algae take up ammonium and nitrate during production and release ammonium and organic nitrogen through respiration. Nitrate is internally reduced to ammonium before synthesis into biomass occurs (Parsons et al. 1984). Trace concentrations of ammonium inhibit nitrate reduction so that, in the presence of ammonium and nitrate, ammonium is utilized first. The "preference" of algae for ammonium is expressed by an empirical function (Thomann and Fitzpatrick 1982) with two limiting values (Figure 5-14). When nitrate is absent, the preference for ammonium is unity. When ammonium is absent, the preference is zero. In the presence of ammonium and nitrate, the preference depends on the abundance of both forms relative to the half-saturation constant for nitrogen uptake. When both ammonium and nitrate are abundant, the preference for ammonium approaches unity. When ammonium is scarce but nitrate is abundant, the preference decreases in magnitude and a significant fraction of algal nitrogen requirement comes from nitrate.

As with phosphorus, the fate of algal nitrogen released by respiration and predation is represented by distribution coefficients.

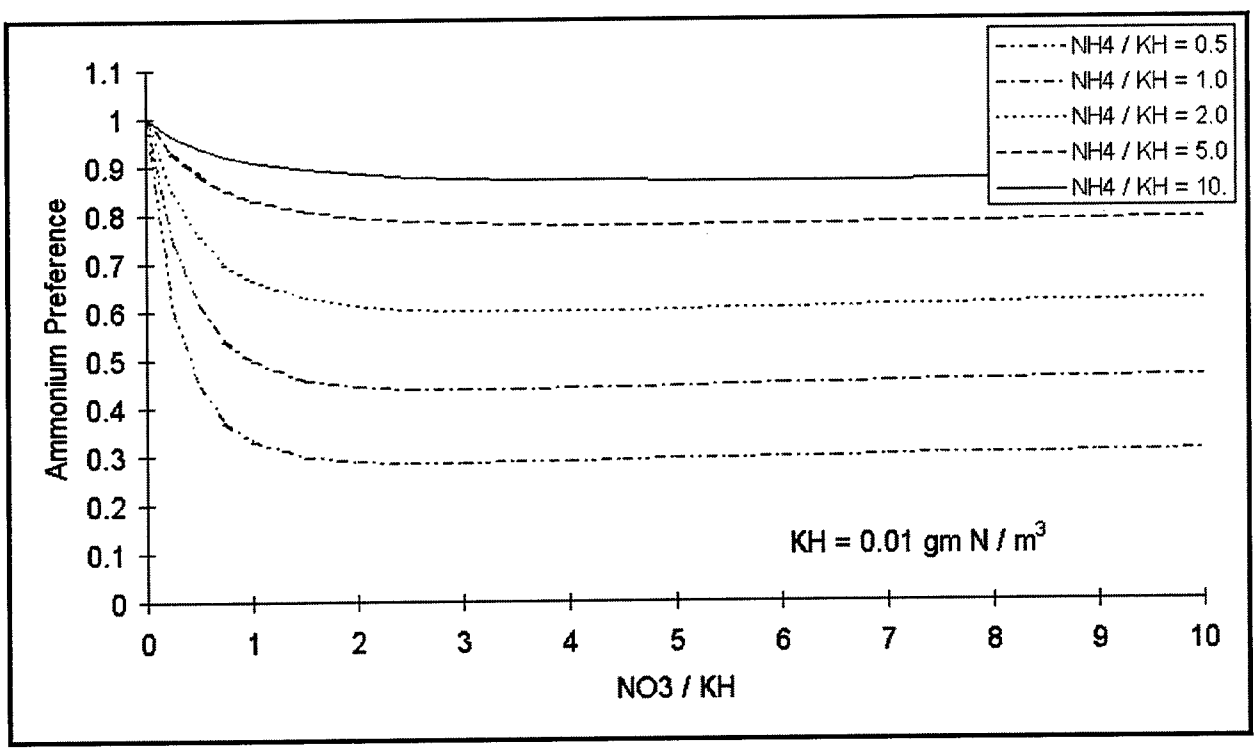

Figure 5-14. Algal ammonium preference

Organic Carbon

Organic carbon undergoes innumerable transformations in the water column. The model carbon cycle (Figure 5-15) consists of the following elements:

- Phytoplankton production
- Phytoplankton exudation
- Predation on phytoplankton
- Dissolution of particulate carbon
- Heterotrophic respiration
- Photo-oxidation
- Coagulation
- Settling and resuspension.

Algal production is the primary carbon source although carbon also enters the system through external loading. Predation on algae releases particulate and dissolved organic carbon to the water column. A fraction of the particulate organic carbon undergoes first-order dissolution to dissolved organic carbon. Dissolved organic carbon produced by phytoplankton exudation, by predation, and by dissolution is respired at a first-order rate to inorganic carbon. Light-mediated reactions convert dissolved organic carbon to inorganic form (photo-oxidation) and induce coagulation to particulate organic carbon. Particulate organic carbon that does not undergo dissolution settles to the bottom sediments.

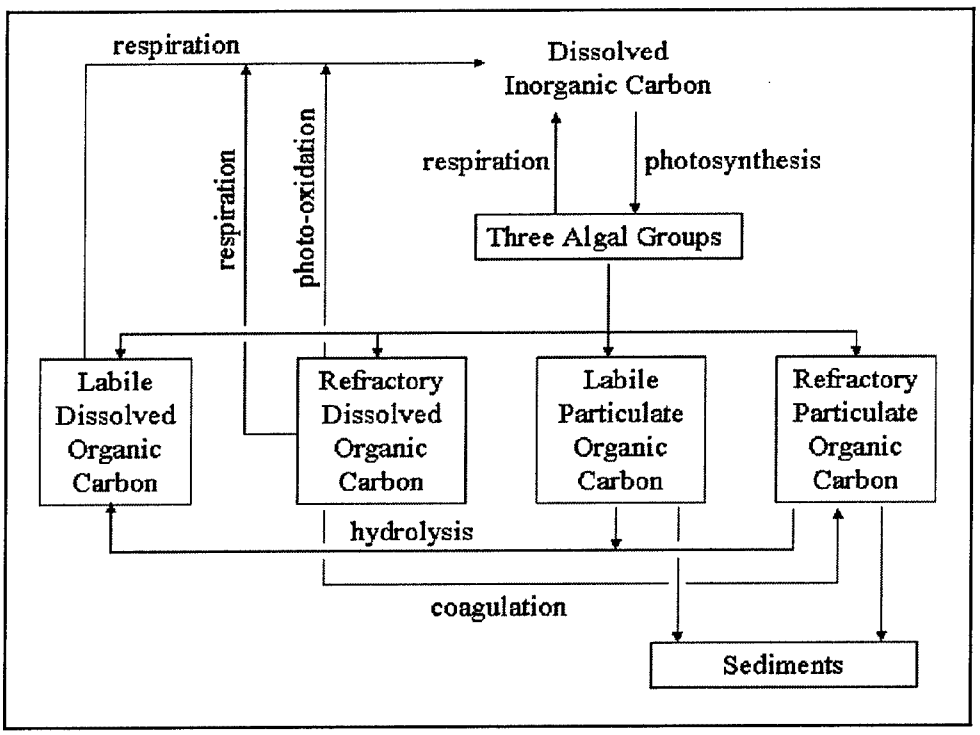

Figure 5-15. Model carbon cycle

Labile dissolved organic carbon

The complete representation of labile dissolved organic carbon sources and sinks in the model ecosystem is:

$$\frac{\delta}{\delta t} LDOC = FCLDP \cdot PR + Klpoc \cdot LPOC + Krpoc \cdot RPOC - Kldoc \cdot LDOC + \frac{BENLDOC}{\Delta z} + \frac{SAVLDOC}{\Delta z} \tag{5-20}$$

in which:

$LDOC$ = labile dissolved organic carbon (g m^{-3})
$LPOC$ = labile particulate organic carbon (g m^{-3})
$RPOC$ = refractory particulate organic carbon (g m^{-3})
$FCLDP$ = fraction of predation on algae released as $LDOC$ ($0 < FCLDP < 1$)
$Klpoc$ = dissolution rate of $LPOC$ (d^{-1})
$Krpoc$ = dissolution rate of $RPOC$ (d^{-1})
Kldoc = respiration rate of $LDOC$ (d^{-1})
$BENLDOC$ = release of DOC from sediments and benthic algae (g C m^{-2} d^{-1})
$SAVLDOC$ = release of DOC from seagrass (g C m^{-2} d^{-1})
Δz = model layer thickness (m).

The fate of refractory particulate organic carbon that is converted to dissolved form is uncertain. Potentially, both labile and refractory dissolved carbon may be produced. The model formulation assumes that all dissolved carbon produced by bacterial hydrolysis is labile whatever the source. The nature of refractory particulate organic carbon is reflected in very low hydrolysis rates rather than in the end product of the dissolution process.

Refractory dissolved organic carbon

Processes that influence refractory dissolved organic carbon are analogous to those for the labile dissolved fraction. In addition, refractory dissolved organic carbon is subject to photoreactions (oxidation and coagulation). The complete representation of refractory dissolved organic carbon sources and sinks in the model ecosystem is:

$$\frac{\delta}{\delta t} RDOC = FCRDP \cdot PR - Krdoc \cdot RDOC - Iavg \cdot Krclit \cdot RDOC + \frac{BENRDOC}{\Delta z} + \frac{SAVRDOC}{\Delta z} \tag{5-21}$$

in which:

$RDOC$ = refractory dissolved organic carbon (g m^{-3})

$FCRDP$ = fraction of predation on algae released as $RDOC$ ($0 < FCRDP < 1$)

$Krdoc$ = respiration rate of $RDOC$ (d^{-1})

$Iavg$ = irradiance averaged over thickness of model cell (E m^{-2} d^{-1})

$Krclit$ = photoreaction rate (E m^{-2})$^{-1}$

$BENRDOC$ = release of $RDOC$ from sediments and benthic algae (g C m^{-2} d^{-1})

$SAVRDOC$ = release of $RDOC$ from seagrass (g C m^{-2} d^{-1}).

The photoreactions that affect dissolved organic matter are complex. As a first approach, it is assumed here that the reaction rate is linearly proportional to ambient light and to dissolved organic carbon. Investigation in one southeast river (Gao and Zepp 1998) indicates that photo-oxidation of dissolved organic carbon consumes oxygen and produces dissolved inorganic carbon in rough stoichiometric proportions. The same investigation illustrates the existence of an iron-mediated reaction that results in coagulation of dissolved organic carbon into particulate form. Iron is not considered in the model. An input parameter, *Fcoag*, determines the fraction of the photoreacted dissolved organic carbon that coagulates. The remainder is oxidized to mineral form with concurrent consumption of dissolved oxygen.

Labile particulate organic carbon

The complete representation of labile particulate organic carbon sources and sinks in the model ecosystem is:

$$\frac{\delta}{\delta t} LPOC = FCLPP \cdot PR - Klpoc \cdot LPOC - Wl \cdot \frac{\delta}{\delta z} LPOC + \frac{BENLPOC}{\Delta z} + \frac{SAVLPOC}{\Delta z} \tag{5-22}$$

in which:

$FCLPP$ = fraction of predation on algae released as $LPOC$ ($0 < FCLPP < 1$)

Wl = settling velocity of labile particles (m d^{-1})

$BENLPOC$ = resuspension of $LPOC$ from sediments (g C m^{-2} d^{-1})

$SAVLPOC$ = release of $LPOC$ from seagrass (g C m^{-2} d^{-1}).

Refractory particulate organic carbon

The complete representation of refractory particulate organic carbon sources and sinks in the model ecosystem is:

$$\frac{\delta}{\delta t} RPOC =$$

$$FCRPP \cdot PR - Krpoc \cdot RPOC + Fcoag \cdot Iavg \cdot Krclit \cdot RDOC \qquad (5\text{-}23)$$

$$-Wr \cdot \frac{\delta}{\delta z} RPOC + \frac{BENRPOC}{\Delta z} + \frac{SAVRPOC}{\Delta z}$$

in which:

$FCRPP$ = fraction of predation on algae released as $RPOC$ ($0 < FCRP < 1$)
$Fcoag$ = fraction of photo-oxidized $RDOC$ that coagulates ($0 < Fcoag < 1$)
Wr = settling velocity of refractory particles (m d^{-1})
$BENRPOC$ = resuspension of $RPOC$ from sediments (g C m^{-2} d^{-1})
$SAVRPOC$ = release of $RPOC$ from seagrass (g C m^{-2} d^{-1}).

Phosphorus

The model phosphorus cycle (Figure 5-16) includes the following processes:

- Algal uptake and respiration
- Predation
- Hydrolysis of particulate organic phosphorus
- Mineralization of dissolved organic phosphorus
- Settling
- Exchange with inorganic solids.

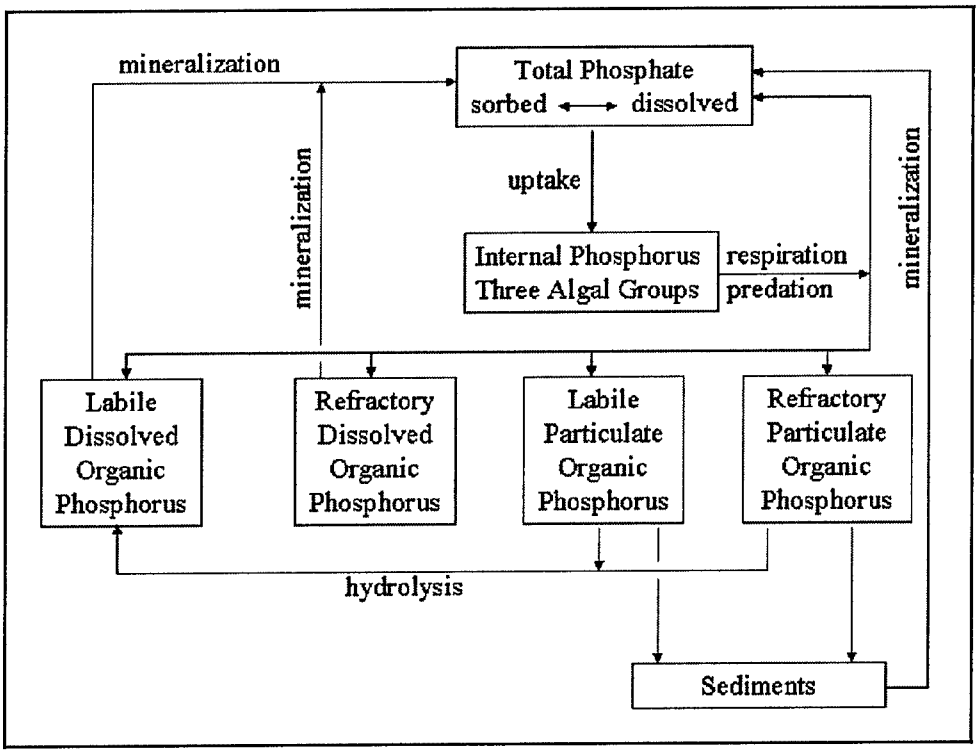

Figure 5-16. Model phosphorus cycle

External loads provide the ultimate source of phosphorus to the system. Dissolved phosphate is taken up by algae to sustain growth and released as phosphate and organic phosphorus through respiration and predation. A portion of the particulate organic phosphorus hydrolyzes to dissolved organic phosphorus. The balance settles to the sediments. Dissolved organic phosphorus is mineralized to phosphate. A portion of the phosphate sorbs to inorganic solids and settles to the sediments. Within the sediments, particulate phosphorus is mineralized and recycled to the water column as dissolved phosphate.

Hydrolysis and mineralization

Within the model, hydrolysis is defined as the process by which particulate organic substances are converted to dissolved organic form. Mineralization is defined as the process by which dissolved organic substances are converted to dissolved inorganic form. Conversion of particulate organic phosphorus to phosphate proceeds through the sequence of hydrolysis and mineralization. Direct mineralization of particulate organic phosphorus does not occur. Analogous to the reasoning applied to dissolved organic carbon, it is assumed hydrolysis of both labile and refractory particulate organic phosphorus produces labile dissolved organic phosphorus. Mineralization of both labile and refractory dissolved organic phosphorus produces phosphate.

Mineralization of organic phosphorus is mediated by the release of nucleotidase and phosphatase enzymes by bacteria (Ammerman and Azam 1985; Chrost and Overbeck 1987) and algae (Matavulj and Flint 1987; Chrost and Overbeck 1987; Boni et al. 1989). Since the algae themselves release the enzyme

and since bacterial abundance is related to algal biomass, the rate of labile organic phosphorus mineralization is related, in the model, to algal biomass. A most remarkable property of the enzyme process is that alkaline phosphatase activity is inversely proportional to ambient phosphate concentration (Chrost and Overbeck 1987; Boni et al. 1989). Put in different terms, when phosphate is scarce, algae stimulate production of an enzyme that mineralizes organic phosphorus to phosphate. This phenomenon is simulated by relating mineralization to the algal phosphorus nutrient limitation. Mineralization is highest when algae are strongly phosphorus limited and is least when no limitation occurs.

The expression for mineralization rate is:

$$Kldop = Kldp + \frac{KHp}{KHp + PO_4d} \cdot Kdpalg \cdot B \qquad (5\text{-}24)$$

in which:

$Kldop$ = mineralization rate of labile dissolved organic phosphorus (d^{-1})
$Kldp$ = minimum mineralization rate (d^{-1})
KHp = half-saturation concentration for algal phosphorus uptake (g P m^{-3})
PO_4d = dissolved phosphate (g P m^{-3})
$Kdpalg$ = constant that relates mineralization to algal biomass (m^3 g^{-1} C d^{-1}).

Potential effects of algal biomass and nutrient limitation on the mineralization rate are shown in Figure 5-17 When nutrient concentration greatly exceeds the half-saturation concentration for algal uptake, the rate roughly equals the minimum. Algal biomass has little influence. As nutrient becomes scarce relative to the half-saturation concentration, the rate increases. The magnitude of increase depends on algal biomass. Factor of two to three increases are feasible.

An exponential function (Figure 5-13) relates mineralization and hydrolysis rates to temperature.

The total phosphate system

The model phosphate state variable is defined as the sum of dissolved and sorbed phosphate:

$$PO_4t = PO_4d + PO_4p \qquad (5\text{-}25)$$

in which:

PO_4t = total phosphate (g P m^{-3})
PO_4d = dissolved phosphate (g P m^{-3})
PO_4p = particulate (sorbed) phosphate (g P m^{-3})

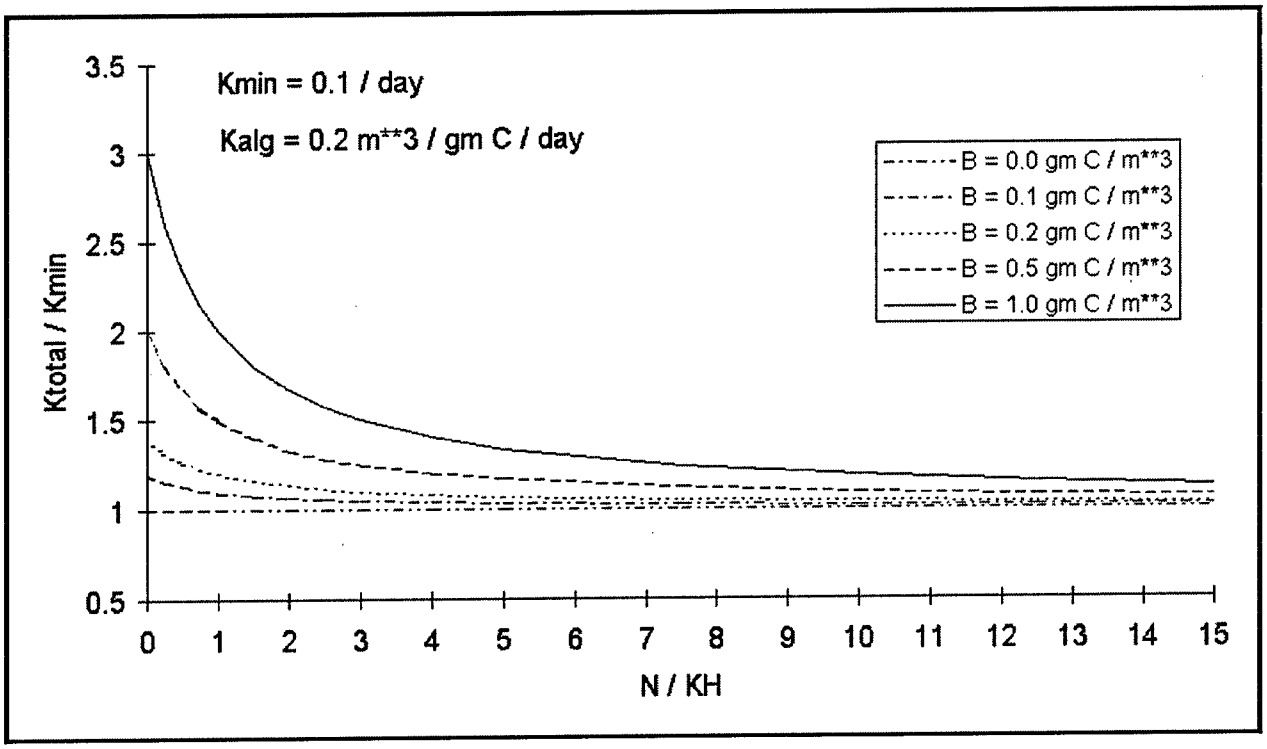

Figure 5-17. Effect of algal biomass and nutrient concentration on phosphorus mineralization

Particulate and dissolved fractions of total phosphate are determined by equilibrium partitioning:

$$PO_4d = \frac{1}{1 + Kadpo4 \cdot ISS} \cdot PO_4t \qquad (5\text{-}26)$$

and

$$PO_4p = \frac{Kadpo4 \cdot ISS}{1 + Kadpo4 \cdot ISS} \cdot PO_4t \qquad (5\text{-}27)$$

in which:

$Kadpo4$ = partition coefficient ($m^3\ g^{-1}$)

ISS = inorganic (fixed) solids concentration ($g\ m^{-3}$)

Total phosphate

The mass-balance equation for the total phosphate state variable is:

$$\frac{\delta}{\delta t} PO_4t = Kldop \cdot LDOP + Krdop \cdot RDOP$$

$$- Vmax \cdot \frac{PO_4d}{Khp + PO_4d} \cdot B + R \cdot B \cdot FPI \cdot Qo + PR \cdot FPIP \cdot Q \qquad (5\text{-}28)$$

$$- Wss \quad \frac{\delta}{\delta z} PO_4p + \frac{BENPO4}{\Delta z} + \frac{SAVPO4}{\Delta z}$$

in which:

$LDOP$ = labile dissolved organic phosphorus (g P m^{-3})

$RDOP$ = refractory dissolved organic phosphorus (g P m^{-3})

$Krdop$ = hydrolysis rate of refractory dissolved organic phosphorus (d^{-1})

FPI = fraction of algal respiration released as total phosphate ($0 \leq FPI \leq 1$)

$FPIP$ = fraction of predation released as total phosphate ($0 \leq FPIP \leq 1$)

$Wiss$ = solids settling rate (m d^{-1})

$BENPO4$ = sum (diagenesis + benthic algae) of sediment water phosphorus transfer (g P m^{-2} d^{-1})

$SAVPO4$ = phosphate release from seagrass (g P m^{-2} d^{-1})

It is assumed that respiration releases phosphorus from the pool represented by the minimum cell quota. Since predators consume entire phytoplankton, predation releases phosphorus from the entire cell quota. The settling term represents the settling of particulate phosphate sorbed to particles.

Internal phosphorus

Internal phosphorus is quantified as mass per unit volume and is subject to the same transport processes as the other state variables. Internal phosphorus is created through algal uptake and depleted by respiration and predation. Algal settling removes associated internal phosphorus. The kinetics portion of the mass-balance equation is:

$$\frac{\delta}{\delta t} PIB = Vmax \cdot \frac{PO_4d}{Khp + PO_4d} \cdot B - R \cdot B \cdot Qo$$

$$- PR \cdot Q - Wa \quad \frac{\delta}{\delta z} PIB \qquad (5\text{-}29)$$

in which PIB is the internal phosphorus concentration (g P m^{-3}).

Labile dissolved organic phosphorus

$$\frac{\delta}{\delta t} LDOP = R \cdot B \cdot FPLD \cdot Qo + PR \cdot FPLDP \cdot Q + Klpop \cdot LPOP + Krpop \cdot RPOP - Kldop \cdot LDOP + \frac{BENLDOP}{\Delta z} + \frac{SAVLDOP}{\Delta z} \tag{5-30}$$

in which:

$FPLD$ = fraction of algal respiration released as $LDOP$ ($0 < FPLD < 1$)
$FPLDP$ = fraction of predation on algae released as $LDOP$ ($0 < FPLDP < 1$)
$LPOP$ = labile particulate organic phosphorus (g P m^{-3})
$RPOP$ = refractory particulate organic phosphorus (g P m^{-3})
$Klpop$ = hydrolysis rate of $LPOP$ (d^{-1})
$Krpop$ = hydrolysis rate of $RPOP$ (d^{-1})
$BENLDOP$ = release of $LDOP$ from sediments and benthic algae (g P m^{-2} d^{-1})
$SAVLDOP$ = release of $LDOP$ from seagrass (g P m^{-2} d^{-1})

Refractory dissolved organic phosphorus

$$\frac{\delta}{\delta t} RDOP = R \cdot B \cdot FPRD \cdot Qo + PR \cdot FPRDP \cdot Q - Krdop \cdot RDOP + \frac{BENLDOP}{\Delta z} + \frac{SAVLDOP}{\Delta z} \tag{5-31}$$

in which:

FPRD = fraction of algal respiration released as RDOP ($0 < FPRD < 1$)
FPRDP = fraction of predation on algae released as RDOP ($0 < FPRDP < 1$)
BENLDOP = release of RDOP from sediments and benthic algae (g P m^{-2} d^{-1})
SAVLDOP = release of RDOP from seagrass (g P m^{-2} d^{-1})

Labile particulate organic phosphorus

$$\frac{\delta}{\delta t} LPOP = R \cdot B \cdot FPLP \cdot Qo + PR \cdot FPLPP \cdot Q - Klpop \cdot LPOP - Wl \cdot \frac{\delta}{\delta z} LPOP + \frac{BENLPOP}{\Delta z} + \frac{SAVLPOP}{\Delta z} \tag{5-32}$$

in which:

$FPLP$ = fraction of algal respiration released as $LPOP$ ($0 < FPLP < 1$)

$FPLPP$ = fraction of predation on algae released as $LPOP$ ($0 < FPLPP < 1$)

$BENLPOP$ = resuspension of LPOP from sediments (g P m^{-2} d^{-1})

$SAVLPOP$ = release of $LPOP$ from seagrass (g P m^{-2} d^{-1})

Refractory particulate organic phosphorus

$$\frac{\delta}{\delta t} RPOP = R \cdot B \cdot FPRP \cdot Qo + PR \cdot FPRPP \cdot Q - Krpop \cdot RPOP - Wr \cdot \frac{\delta}{\delta z} RPOP + \frac{BENRPOP}{\Delta z} + \frac{SAVRPOP}{\Delta z} \quad (5\text{-}33)$$

in which:

FPRP = fraction of algal respiration released as RPOP ($0 < FPRP < 1$)

FPRPP = fraction of predation on algae released as RPOP ($0 < FPRPP < 1$)

BENRPOP = resuspension of RPOP from sediments (g P m^{-2} d^{-1})

SAVRPOP = release of RPOP from seagrass (g P m^{-2} d^{-1})

Nitrogen

The model nitrogen cycle (Figure 5-18) includes the following processes:

- Algal production and respiration
- Predation
- Hydrolysis of particulate organic nitrogen
- Mineralization of dissolved organic nitrogen
- Settling
- Nitrification.

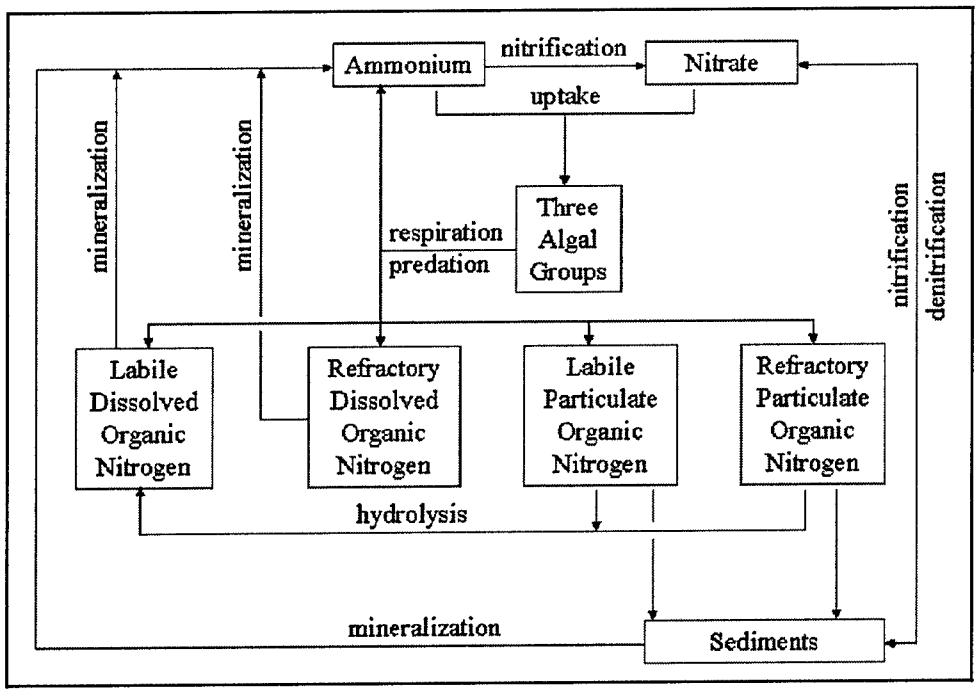

Figure 5-18. Model nitrogen cycle

External loads provide the ultimate source of nitrogen to the system. Inorganic nitrogen is incorporated by algae during growth and released as ammonium and organic nitrogen through respiration and predation. A portion of the particulate organic nitrogen hydrolyzes to dissolved organic nitrogen. The balance settles to the sediments. Dissolved organic nitrogen is mineralized to ammonium. In an oxygenated water column, a fraction of the ammonium is subsequently oxidized to nitrate through the nitrification process. Particulate nitrogen that settles to the sediments is mineralized and recycled to the water column, primarily as ammonium. Nitrate moves in both directions across the sediment-water interface, depending on relative concentrations in the water column and sediment interstices.

Analogous to the reasoning applied to carbon and phosphorus, it is assumed that hydrolysis of both labile and refractory particulate organic nitrogen produces labile dissolved organic nitrogen. Mineralization of both labile and refractory dissolved organic nitrogen produces ammonium.

Nitrification

Nitrification is a process mediated by specialized groups of autotrophic bacteria that obtain energy through the oxidation of ammonium to nitrite and oxidation of nitrite to nitrate. A simplified expression for complete nitrification (Tchobanoglous and Schroeder 1987) is:

$$NH_4^+ + O_2 --> NO_3^- + H_2O + 2H^+ \qquad (5\text{-}34)$$

The simplified stoichiometry indicates that two moles of oxygen are required to nitrify one mole of ammonium into nitrate. The simplified equation is not strictly true, however. Cell synthesis by nitrifying bacteria is accomplished by the fixation of carbon dioxide so that less than two moles of oxygen are consumed per mole ammonium utilized (Wezernak and Gannon 1968).

The kinetics of complete nitrification are modeled as a function of available ammonium, dissolved oxygen, and temperature:

$$NT = \frac{DO}{KHont + DO} \cdot \frac{NH_4}{KHnnt + NH_4} \cdot f(T) \cdot NTm \qquad (5\text{-}35)$$

in which:

NT = nitrification rate (g N m^{-3} d^{-1})

$KHont$ = half-saturation constant of dissolved oxygen required for nitrification (g O_2 m^{-3})

$KHnnt$ = half-saturation constant of NH_4 required for nitrification (g N m^{-3})

NTm = maximum nitrification rate at optimal temperature (g N m^{-3} day^{-1})

The kinetics formulation (Figure 5-19) incorporates the products of two "Monod" functions. The first function diminishes nitrification at low DO concentration. The second function expresses the influence of ammonium concentration on nitrification. When ammonium concentration is low relative to *KHnnt*, nitrification is proportional to ammonium concentration. For *NH4* << KHnnt, the reaction is approximately first-order. (The first-order decay constant ≈ *NTm/KHnnt.*) When ammonium concentration is large relative to *KHnnt*, nitrification approaches a maximum rate. This formulation is based on a concept proposed by Tuffey et al. (1974). Nitrifying bacteria adhere to benthic or suspended sediments. When ammonium is scarce, vacant surfaces suitable for nitrifying bacteria exist. As ammonium concentration increases, bacterial biomass increases, vacant surfaces are occupied, and the rate of nitrification increases. The bacterial population attains maximum density when all surfaces suitable for bacteria are occupied. At this point, nitrification proceeds at a maximum rate independent of additional increase in ammonium concentration.

The optimal temperature for nitrification may be less than peak temperatures that occur in coastal waters. To allow for a decrease in nitrification at superoptimal temperature, the effect of temperature on nitrification is modeled in the Gaussian form of Equation 5-11.

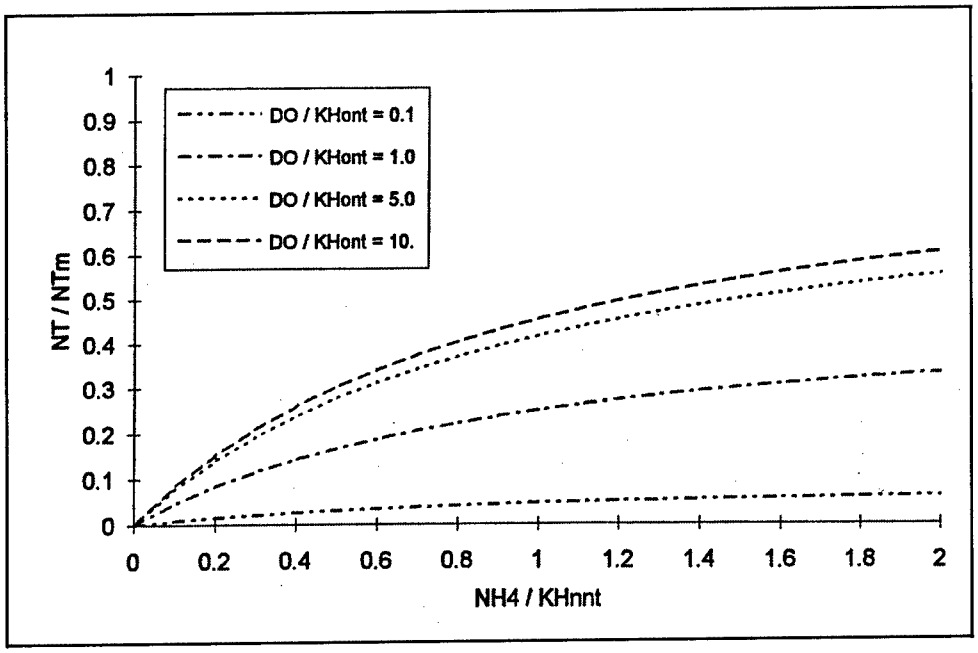

Figure 5-19. Effect of DO and ammonium on nitrification rate

Nitrogen mass balance equations

The mass-balance equation for nitrogen state variables are written by summing all previously described sources and sinks:

Ammonium

$$\frac{\delta}{\delta t} NH_4 = Anc \cdot [(BM \cdot FNI - PN \cdot P) \cdot B + PR \cdot FNIP]$$
$$+ Kldon \cdot LDON + Krdon \cdot RDON - NT + \frac{BENNH4}{\Delta z} \qquad (5\text{-}36)$$
$$+ \frac{SAVNH4}{\Delta z}$$

in which:

$LDON$ = labile dissolved organic nitrogen (g N m^{-3})
$RDON$ = refractory dissolved organic nitrogen (g N m^{-3})
FNI = fraction of algal respiration released as $NH4$ ($0 \leq FNI \leq 1$)
PN = algal ammonium preference ($0 \leq PN \leq 1$)
$FNIP$ = fraction of predation released as NH4 ($0 \leq FNIP \leq 1$)
$BENNH4$ = release of ammonium from sediments and benthic algae (g N m^{-2} d^{-1})
$SAVNH4$ = release of ammonium from seagrass (g N m^{-2} d^{-1}).

Nitrate

$$\frac{\delta}{\delta t} NO_3 = -Anc \cdot (1-PN) \cdot P \cdot B + NT + \frac{BENNO3}{\Delta z} - \frac{SAVNO3}{\Delta z} \tag{5-37}$$

in which:

BENNO3 = release of nitrate from sediments and benthic algae (g N m^{-2} d^{-1})
SAVNO3 = nitrate uptake by seagrass (g N m^{-2} d^{-1}).

Labile dissolved organic nitrogen

$$\frac{\delta}{\delta t} LDON = Anc \cdot (BM \cdot B \cdot FNLD + PR \cdot FNLDP) + Klpon \cdot LPON + Krpon \cdot RPON - Kldon \cdot LDON + \frac{BENLDON}{\Delta z} + \frac{SAVLDON}{\Delta z} \tag{5-38}$$

in which:

LPON = labile particulate organic nitrogen (g P m^{-3})
RPON = refractory particulate organic nitrogen (g P m^{-3})
FNLD = fraction of algal respiration released as *LDON* ($0 < FNLD < 1$)
FNLDP = fraction of predation on algae released as *LDON* ($0 < FNLDP < 1$)
Klpon = hydrolysis rate of *LPON* (d^{-1})
Krpon = hydrolysis rate of *RPON* (d^{-1})
Kldon = mineralization rate of *LDON* (d^{-1})
BENLDON = release of *LDON* from sediments and benthic algae (g P m^{-2} d^{-1})
SAVLDON = release of *LDON* from seagrass (g P m^{-2} d^{-1}).

Refractory dissolved organic nitrogen

$$\frac{\delta}{\delta t} RDON = Anc \cdot (BM \cdot B \cdot FNRD + PR \cdot FNRDP) - Krdon \cdot RDON + \frac{BENRDON}{\Delta z} + \frac{SAVRDON}{\Delta z} \tag{5-39}$$

in which:

FNRD = fraction of algal respiration released as *RDON* ($0 < FNRD < 1$)

$FNRDP$ = fraction of predation on algae released as $RDON$ ($0 < FNRDP < 1$)

$Kldon$ = mineralization rate of $RDON$ (d^{-1})

$BENRDON$ = release of $RDON$ from sediments and benthic algae (g P m^{-2} d^{-1})

$SAVRDON$ = release of $RDON$ from seagrass (g P m^{-2} d^{-1}).

Labile particulate organic nitrogen

$$\frac{\delta}{\delta t} LPON = Anc \cdot (BM \cdot B \cdot FNLP + PR \cdot FNLPP) - Klpon \cdot LPON - Wl \cdot \frac{\delta}{\delta z} LPON + \frac{BENLPON}{\Delta z} + \frac{SAVLPON}{\Delta z} \tag{5-40}$$

in which:

$FNLP$ = fraction of algal respiration released as $LPON$ ($0 < FNLP < 1$)

$FNLPP$ = fraction of predation on algae released as $LPON$ ($0 < FNLPP < 1$)

$BENLPON$ = resuspension of $LPON$ from sediments (g N m^{-2} d^{-1})

$SAVLPON$ = release of $LPON$ from seagrass (g N m^{-2} d^{-1})

Refractory particulate organic nitrogen

$$\frac{\delta}{\delta t} RPON = Anc \cdot (BM \cdot B \cdot FNRP + PR \cdot FNRPP) - Krpon \cdot RPON - Wr \cdot \frac{\delta}{\delta z} RPON + \frac{BENRPON}{\Delta z} + \frac{SAVRPON}{\Delta z} \tag{5-41}$$

in which:

$FNRP$ = fraction of algal respiration released as $RPON$ ($0 < FNR < 1$)

$FNRPP$ = fraction of predation on algae released as $RPON$ ($0 < FNRP < 1$)

$BENRPON$ = resuspension of $RPON$ from sediments (g N m^{-2} d^{-1})

$SAVRPON$ = release of $RPON$ from seagrass (g N m^{-2} d^{-1}).

Silica

The model incorporates two siliceous state variables, dissolved silica and particulate biogenic silica. The silica cycle (Figure 5-20) is a simple one in which diatoms take up available silica and recycle available and particulate biogenic silica through the actions of respiration and predation. Particulate silica dissolves in the water column or settles to the bottom. A portion of the settled

particulate biogenic silica dissolves within the sediments and returns to the water column. Sources and sinks represented are:

- Diatom production and respiration
- Predation
- Dissolution of particulate to dissolved silica
- Settling

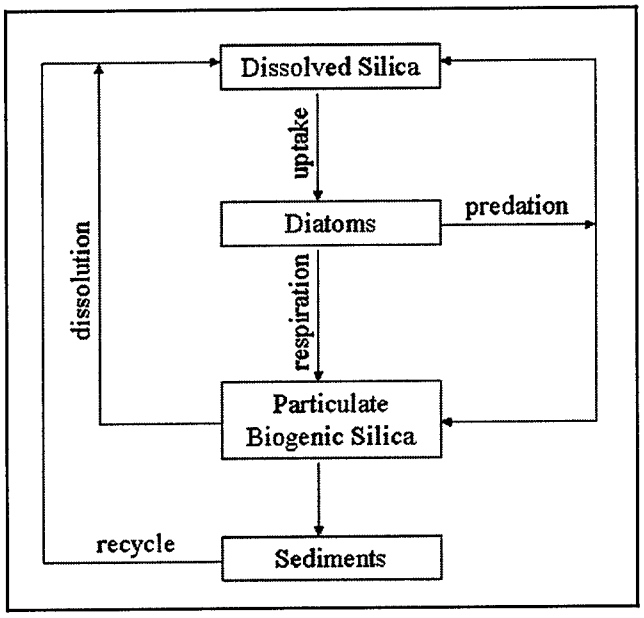

Figure 5-20. Model silica cycle

Dissolved silica. The kinetics equation for dissolved silicia is:

$$\frac{\delta}{\delta t} SA = Asc \cdot (-P \cdot B + FSAP \cdot PR) + Kpbs \cdot PBS + \frac{BENSA}{\Delta z} \qquad (5\text{-}42)$$

in which:

SA = dissolved silica (g Si m^{-3})
Asc = algal silica-to-carbon ratio (g Si g^{-1} C)
$FSAP$ = fraction of predation released as dissolved silica ($0 < FSAP < 1$)
PBS = particulate biogenic silica (g Si m^{-3})
$Kpbs$ = particulate biogenic silica dissolution rate (d^{-1})
$BENSA$ = release of SA from sediments (g Si m^{-2} d^{-1}).

The model allows a silica-to-carbon ratio to be defined for each algal group. This flexibility provides for the definition of groups consisting of mixtures of diatoms and other phytoplankton.

Particulate biogenic silica. The kinetics equation for particulate biogenic silica is:

$$\frac{\delta}{\delta t} PBS = Asc \cdot [R \cdot B - (1 - Fsap) \cdot PR] - Kpbs \cdot PBS - Wpbs \frac{\delta}{\delta z} PBS \tag{5-43}$$

in which *Wpbs* is the settling velocity of particulate biogenic silica (m d^{-1}).

Chemical Oxygen Demand

Chemical oxygen demand is the concentration of reduced substances that are oxidizable through inorganic means. The source of chemical oxygen demand in saline water is sulfide released from sediments. A cycle occurs in which sulfate is reduced to sulfide in the sediments and reoxidized to sulfate in the water column. In freshwater, methane is released to the water column by the sediment model. Both sulfide and methane are quantified in units of oxygen demand and are treated with the same kinetics formulation:

$$\frac{\delta}{\delta t} COD = -\frac{DO}{KHocod + DO} \cdot Kcod \cdot COD \tag{5-44}$$

in which:

COD = chemical oxygen demand concentration (g oxygen-equivalents m^{-3})

KHocod = half-saturation concentration of DO required for exertion of chemical oxygen demand (g O_2 m^{-3})

Kcod = oxidation rate of chemical oxygen demand (d^{-1}).

An exponential function (Figure 5-13) describes the effect of temperature on exertion of chemical oxygen demand.

Dissolved Oxygen

Sources and sinks of DO in the water column (Figure 5-21) include:

- Algal photosynthesis
- Atmospheric reaeration
- Algal respiration
- Heterotrophic respiration
- Nitrification
- Chemical oxygen demand
- Photo-oxidation

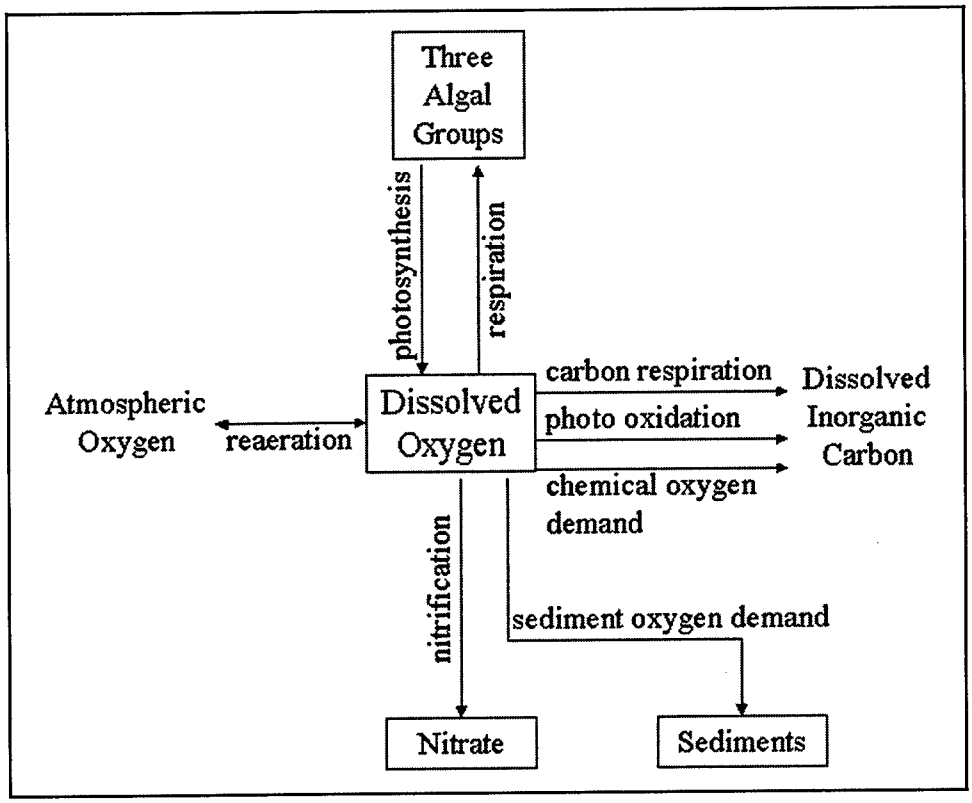

Figure 5-21. DO sources and sinks

Reaeration

The reaeration rate is proportional to the DO deficit in model segments that from the air-water interface:

$$\frac{\delta}{\delta t} DO = \frac{Kr}{\Delta z} \cdot (DOs - DO) \tag{5-45}$$

in which:

DO = dissolved oxygen concentration (g O^2 m^{-3})

Kr = reaeration coefficient (m d^{-1})

DOs = dissolved oxygen saturation concentration (g O_2 m^{-3}).

In freeflowing streams, the reaeration coefficient depends largely on turbulence generated by bottom shear stress (O'Connor and Dobbins 1958). In lakes and coastal waters, however, wind effects may dominate the reaeration process (O'Connor 1983). The model employs a relationship for wind-driven gas exchange (Hartman and Hammond 1985):

$$Kr = 0.157 \cdot Rv \cdot Wms^{1.5} \tag{5-46}$$

in which:

$R\nu$ = ratio of kinematic viscosity of pure water at 20 °C to kinematic viscosity of water at specified temperature and salinity

Wms = wind speed measured at 10 m above water surface (m s^{-1}).

An empirical function that fits (Figure 5-22) tabulated values of $R\nu$ is:

$$R\nu = 0.54 + 0.0233 \cdot T - 0.0020 \cdot S \tag{5-47}$$

in which S is salinity (ppt).

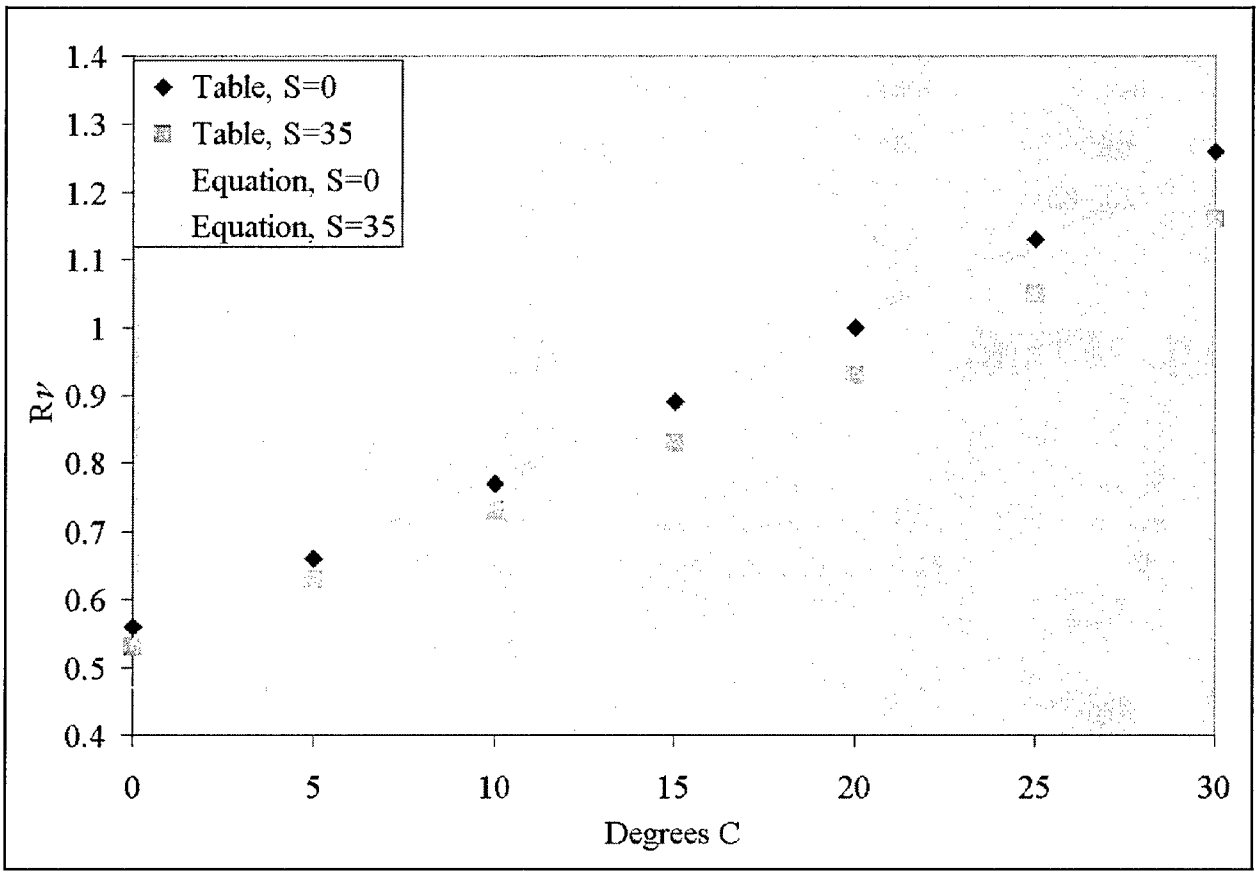

Figure 5-22. Computed and tabulated values of Rν

Saturation DO concentration diminishes as temperature and salinity increase. An empirical formula that describes these effects (Genet et al. 1974) is:

$$DOs = 14.5532 - 0.38217 \cdot T + 0.0054258 \cdot T^2 - CL \cdot (1.665 _ 10^{-4} - 5.866 _ 10^{-6} \cdot T + 9.796 _ 10^{-8} \cdot T^2) \tag{5-48}$$

in which:

CL = chloride concentration (= salinity/1.80655)

T = temperature (°C).

Mass balance equation for DO

$$\frac{\delta}{\delta t} DO = Aocr \cdot (P - R) \cdot B - Aont \cdot NT$$

$$- Aocr \cdot (Kldoc \cdot LDOC + Krdoc \cdot RDOC)$$

$$- Aocr \cdot (1 - Fcoag) \cdot Iavg \cdot Krclit \cdot RDOC \qquad (5\text{-}49)$$

$$- Kcod \cdot COD + \frac{Kr}{\Delta z} \cdot (DOs - DO) + \frac{BENDO}{\Delta z} + \frac{SAVDO}{\Delta z}$$

in which:

$Aocr$ = oxygen-to-carbon mass ratio in production, respiration, and photo-oxidation (= 2.67 g O_2 g^{-1} C)

$Aont$ = oxygen consumed per mass ammonium nitrified (= 4.33 g O_2 g^{-1} N)

$BENDO$ = sediment oxygen flux (g DO m^{-2} d^{-1})

$SAVDO$ = seagrass dissolved oxygen production (g DO m^{-2} d^{-1}).

Temperature

Computation of temperature uses a conservation of internal energy equation that is analogous to the conservation of mass equation. For practical purposes, the internal energy equation can be written as a conservation of temperature equation. The only source or sink of temperature considered is exchange with the atmosphere. Atmospheric exchange is considered proportional to the temperature difference between the water surface and a theoretical equilibrium temperature (Edinger et al. 1974):

$$\frac{\delta}{\delta t} T = \frac{KT}{\rho \cdot Cp \cdot H} \cdot (Te - T) \qquad (5\text{-}50)$$

in which:

T = water temperature (°C)

Te = equilibrium temperature (°C)

KT = Heat exchange coefficient (watt m^{-2} $°C^{-1}$)

Cp = specific heat of water (4,200 watt s kg^{-1} $^{o}C^{-1}$)

ρ = density of water (1,000 kg m^{-3}).

Inorganic (Fixed) Solids

The only internal sources and sinks of fixed solids are resuspension and settling. To account for resuspension dynamically requires a sediment transport model linked to the hydrodynamic model. In the absence of such a model, resuspension is considered in a long-term, average sense. Net settling to the bottom sediments is specified less than settling through the water column. The difference between settling through the water and settling into the sediments is the quantity resuspended:

$$\frac{\delta}{\delta t} ISS = -Wiss \cdot \frac{\delta}{\delta z} ISS + (Wiss - Wissnet) \frac{ISS}{\Delta z} \tag{5-51}$$

in which:

ISS = fixed solids concentration (g m^{-3})

$Wiss$ = solids settling velocity (m d^{-1})

$Wissnet$ = net settling to sediments (m d^{-1})

Resuspension is represented by the term involving *Wissnet* and is evaluated in the bottom cell of the water column only.

Light attenuation

Fixed solids are one component of light attenuation, which is computed:

$$Kess = Keb + Kevss \cdot VSS + Keiss \cdot ISS + Kedoc \cdot RDOC \tag{5-52}$$

in which:

$Kess$ = diffuse light attenuation (m^{-1})

Keb = background light attenuation (m^{-1})

$Kevss$ = attenuation coefficient for volatile solids (m^2 g^{-1})

VSS = volatile solids concentration (g m^{-3})

$Keiss$ = attenuation coefficient for fixed solids (m^2 g^{-1})

$Kedoc$ = attenuation coefficient for refractory dissolved organic carbon (m^2 g^{-1})

Volatile solids are computed from the sum of algal biomass and particulate organic carbon. These state variables, as carbon, are converted to solids using a ratio 2.5 g solids g^{-1} C (assuming organic matter is composed of carbon, hydrogen, and oxygen in the atomic ratio 1:2:1). Attenuation by phytoplankton chlorophyll is taken into account in the parameter that relates attenuation to volatile solids.

Salinity

Salinity is modeled by the conservation of mass equation with no internal sources or sinks.

Parameter Values

Model parameter evaluation is a recursive process. Parameters are selected from a range of feasible values, tested in the model, and adjusted until satisfactory agreement between predicted and observed variables is obtained. Ideally, the range of feasible values is determined by observation or experiment. For some parameters, however, no observations are available. Then, the feasible range is determined by parameter values employed in similar models or by the judgment of the modeler. For the St. Johns River, an initial parameter set was adapted from the Chesapeake Bay study (Cerco and Cole 1994), the most extensive model application to date. Parameter values were adjusted, where appropriate, for the subtropical environment. Subsequent adjustment was performed to improve agreement between model and observations. A complete set of parameter values is provided in Table 5-3.

Table 5-3
Parameters in Kinetics Equations

Symbol	Definition	Value	Units
AANOX	ratio of anoxic to oxic respiration	0.5	$0 \leq AANOX \leq 1$
ANC	nitrogen-to-carbon ratio of algae	0.135 (diatoms), 0.175 (other)	$g\ N\ g^{-1}\ C$
AOCR	dissolved oxygen-to-carbon ratio in respiration	2.67	$g\ O_2\ g^{-1}\ C$
AONT	mass DO consumed per mass ammonium nitrified	4.33	$g\ O_2\ g^{-1}\ N$
Qo	minimum cell quota	0.004 (blue greens), 0.005 (other)	$g\ P\ g^{-1}\ C$
Vmax	maximum uptake rate	0.006 (diatoms), 0.0033 (cyan), 0.0044 (greens)	$g\ P\ g^{-1}\ C$
Areaer	empirical constant in reaeration equation	0.08	
ASC	algal silica-to-carbon ratio	0.0 (cyan), 0.8 (diatom), 0.0 (green)	$g\ Si\ g^{-1}\ C$
BMr	basal metabolic rate of algae at reference temperature Tr	0.05 (cyan), 0.05 (diatom), 0.05 (green)	d^{-1}
FCLDP	fraction of labile dissolved carbon produced by predation	0.1	$0 \leq FCLDP \leq 1$
FCRDP	fraction of refractory dissolved carbon produced by predation	0.2	$0 \leq FCRDP \leq 1$
FCLPP	fraction of labile particulate carbon produced by predation	0.5	$0 \leq FCLPP \leq 1$

(Sheet 1 of 4)

Table 5-3 (Continued)

Symbol	Definition	Value	Units
FCRPP	fraction of refractory particulate carbon produced by predation	0.2	$0 \leq FCRPP \leq 1$
FNI	fraction of inorganic nitrogen produced by algal metabolism	0.55	$0 \leq FNI \leq 1$
FNIP	fraction of inorganic nitrogen produced by predation	0.4	$0 \leq FNIP \leq 1$
FNLD	fraction of labile dissolved organic nitrogen produced by algal metabolism	0.18	$0 \leq FNLD \leq 1$
FNLDP	fraction of labile dissolved organic nitrogen produced by predation	0.18	$0 \leq FNLDP \leq 1$
FNRD	fraction of refractory dissolved organic nitrogen produced by algal metabolism	0.02	$0 \leq FNRD \leq 1$
FNRDP	fraction of labile dissolved organic nitrogen produced by predation	0.2	$0 \leq FNRDP \leq 1$
FNLP	fraction of labile particulate organic nitrogen produced by algal metabolism	0.2	$0 \leq FNLP \leq 1$
FNLPP	fraction of labile particulate organic nitrogen produced by predation	0.3	$0 \leq FNLPP \leq 1$
FNRP	fraction of refractory particulate organic nitrogen produced by algal metabolism	0.05	$0 \leq FNRP \leq 1$
FNRPP	fraction of refractory particulate organic nitrogen produced by predation	0.1	$0 \leq FNRPP \leq 1$
FPLD	fraction of labile dissolved organic phosphorus produced by algal metabolism	0.2	$0 \leq FPLD \leq 1$
FPLDP	fraction of labile dissolved organic phosphorus produced by predation	0.36	$0 \leq FPLDP \leq 1$
FPRD	fraction of refractory dissolved organic phosphorus produced by algal metabolism	0.02	$0 \leq FPRD \leq 1$
FPRDP	fraction of refractory dissolved organic phosphorus produced by predation	0.04	$0 \leq FPRDP \leq 1$
FPI	fraction of dissolved inorganic phosphorus produced by algal metabolism	0.75	$0 \leq FPI \leq 1$
FPIP	fraction of dissolved inorganic phosphorus produced by predation	0.5	$0 \leq FPIP \leq 1$
FPLP	fraction of labile particulate organic phosphorus produced by algal metabolism	0.2	$0 \leq FPLP \leq 1$
FPLPP	fraction of labile particulate organic phosphorus produced by predation	0.07	$0 \leq FPLPP \leq 1$
FPRP	fraction of refractory particulate organic phosphorus produced by algal metabolism	0.05	$0 \leq FPRP \leq 1$
FPRPP	fraction of refractory particulate phosphorus produced by predation	0.03	$0 \leq FPRPP \leq 1$
FSAP	fraction of dissolved silica produced by predation	0.3	$0 \leq FSAP \leq 1$
Kadpo4	partition coefficient	0.0	$m^3\ g^{-1}$
Kcod	oxidation rate of chemical oxygen demand	20	d^{-1}
Kdpalg	constant that relates mineralization rate to algal biomass	0.2	$m^3\ g^{-1}\ C\ d^{-1}$
KHn	half-saturation concentration for nitrogen uptake by algae	0.02 (cyan), 0.03 (diatoms), 0.025 (greens)	$g\ N\ m^{-3}$

(Sheet 2 of 4)

Table 5-3 (Continued)

Symbol	Definition	Value	Units
KHndn	half-saturation concentration of nitrate required for denitrification	0.1	g N m^{-3}
KHnnt	half-saturation concentration of NH_4 required for nitrification	1.0	g N m^{-3}
KHocod	half-saturation concentration of dissolved oxygen required for exertion of COD	0.5	g O_2 m^{-3}
KHodoc	half-saturation concentration of dissolved oxygen required for oxic respiration	0.5	g O_2 m^{-3}
KHont	half-saturation concentration of dissolved oxygen required for nitrification	1.0	g O_2 m^{-3}
KHp	half-saturation concentration for phosphorus uptake by algae	0.00075 (cyan), 0.003 (diatoms), 0.001 (greens)	g P m^{-3}
KHs	half-saturation concentration for silica uptake by algae	0.0 (cyan), 0.03 (diatom), 0.01 (green)	g Si m^{-3}
KHst	salinity at which algal mortality is half maximum value	2.0 (cyan), 2.0 (diatom), 35.0 (green)	ppt
Klpoc	labile particulate organic carbon dissolution rate	0.075	d^{-1}
Kldoc	labile dissolved organic carbon dissolution rate	0.05	d^{-1}
Klpon	labile particulate organic nitrogen hydrolysis rate	0.0375	d^{-1}
Kldon	labile dissolved organic nitrogen hydrolysis rate	0.025	d^{-1}
Klpop	labile particulate organic phosphorus hydrolysis rate	0.075	d^{-1}
Kldop	labile dissolved organic phosphorus hydrolysis rate	0.1	d^{-1}
Krpoc	refractory particulate organic carbon dissolution rate	0.0025	d^{-1}
Krdoc	refractory dissolved organic carbon dissolution rate	0.0025	d^{-1}
Krpon	refractory particulate organic nitrogen hydrolysis rate	0.0025	d^{-1}
Krdon	refractory dissolved organic nitrogen hydrolysis rate	0.0025	d^{-1}
Krpop	refractory particulate organic phosphorus hydrolysis rate	0.005	d^{-1}
Krdop	refractory dissolved organic phosphorus hydrolysis rate	0.01	d^{-1}
Kpbs	biogenic silica dissolution rate	0.03	d^{-1}
KTb	effect of temperature on basal metabolism of algae	0.032	$°C^{-1}$
KTcod	effect of temperature on exertion of chemical oxygen demand	0.041	d^{-1}
KTg1	effect of temperature below Tm on growth of algae	0.007 (cyan), 0.006 (diatom), 0.004 (green)	$°C^{-2}$
KTg2	effect of temperature above Tm on growth of algae	0.004 (cyan), 0.000 (diatom)," 0.010 (green)	$°C^{-2}$
KThdr	effect of temperature on hydrolysis rates	0.092	$°C^{-1}$
KTmnl	effect of temperature on mineralization rates	0.092	$°C^{-1}$
KTnt1	effect of temperature below Tmnt on nitrification	0.0045	$°C^{-2}$
KTnt2	effect of temperature above Tmnt on nitrification	0.0045	$°C^{-2}$
KTsua	effect of temperature on biogenic silica dissolution	0.092	$°C^{-1}$
Krclit	photoreaction rate	0.0	$(Em^{-2})^{-1}$
Fcoag	fraction of dissolved organic carbon coagulated	0.0	$0 \leq Fcoag \bullet 1$

(Sheet 3 of 4)

Table 5-3 (Concluded)

Symbol	Definition	Value	Units
NTm	maximum nitrification rate at optimal temperature	0.1 to 0.5	g N m^{-3} d^{-1}
Phtl	predation rate on algae	0.05 (cyan), 1.0 (diatom), 1.0 (green)	m^3 g^{-1} C d^{-1}
Pm^B	maximum photosynthetic rate	200 (cyan), 350 (diatom), 200 (green)	g C g^{-1} Chl d^{-1}
Presp	photo-respiration fraction	0.25	$0 \leq$ Presp ≤ 1
STF	salinity toxicity factor	0.2 (cyan), 0.1 (others)	d^{-1}
Topt	optimal temperature for growth of algae	35 (cyan), 25 (diatom), 35 (green)	°C
Tmnt	optimal temperature for nitrification	30	°C
Tr	reference temperature for metabolism	20	°C
Trhdr	reference temperature for hydrolysis	20	°C
Trmnl	reference temperature for mineralization	20	°C
Trsua	reference temperature for biogenic silica dissolution	20	°C
Wa	algal settling rate	0.0 (cyan), 0.1 (other)	m d^{-1}
Wl	settling velocity of labile particles	0.25	m d^{-1}
Wr	settling velocity of refractory particles	0.25	m d^{-1}
Wiss	settling velocity of fixed solids	0.75	m d^{-1}
Wpbs	settling velocity of biogenic silica	0.25	m d^{-1}
Keb	background light attenuation	0.03	m^{-1}
Kevss	attenuation coefficient for volatile solids	0.06	m^2 g^{-1}
Keiss	attenuation coefficient for fixed solids	0.08	m^2 g^{-1}
Kedoc	attenuation coefficient for refractory dissolved organic carbon	0.15	m^2 g^{-1}
α	initial slope of production vs. irradiance relationship	3.15 (cyan), 8.0 (other)	g C g^{-1} Chl $(E\ m^{-2})^{-1}$

(Sheet 4 of 4)

References

Ammerman, J., and Azam, F. (1985). "Bacterial 5'-nucleodase in aquatic ecosystems: a novel mechanism of phosphorus regeneration," *Science* 227, 1338-1340.

Boni, L., Carpene, E., Wynne, D., and Reti, M. (1989). "Alkaline phosphatase activity in *Protogonyaulax Tamarensis," Journal of Plankton Research* 11, 879-885.

Bunch, B., Cerco, C., Dortch, M., Johnson, B., and Kim, K. (2000). "Hydrodynamic and water quality model study of San Juan Bay and Estuary," ERDC TR-00-1, U.S. Army Engineer Research and Development Center, Vicksburg, MS.

Cerco, C., and Cole, T. (1994). "Three-dimensional eutrophication model of Chesapeake Bay," Technical Report EL-94-4, U.S. Army Engineer Waterways Experiment Station, Vicksburg, MS.

Cerco, C., Bunch, B., Cialone, M., and Wang, H. (1994). "Hydrodynamic and eutrophication model study of Indian River and Rehoboth Bay, Delaware," Technical Report EL-94-5, U.S. Army Engineer Waterways Experiment Station, Vicksburg, MS.

Cerco, C., and Bunch, B. (1997). "Passaic River tunnel diversion model study; Report 5, Water quality modeling," Technical Report HL-96-2, U.S. Army Engineer Waterways Experiment Station, Vicksburg, MS.

Cerco, C., Bunch, B., Teeter, A., and Dortch, M. (2000). "Water quality model of Florida Bay," ERDC/EL TR-00-10, U.S. Army Engineer Research and Development Center, Vicksburg, MS.

Chrost, R., and Overbeck, J. (1987). "Kinetics of alkaline phosphatase activity and phosphorus availability for phytoplankton and bacterioplankton in Lake Plubsee (north German eutrophic lake)," *Microbial Ecology* 13, 229-248.

Cloern, J., Grenz, C., and Vidergar-Lucas, L. (1995). "An empirical model of the phytoplankton chlorophyll:carbon ratio - The conversion factor between productivity and growth rate," *Limnology and Oceanography* 40(7), 1313-1321.

Droop, M. (1973). "Some thoughts on nutrient limitation in algae," *Journal of Phycology* 9, 264-272.

Edinger, J., Brady, D., and Geyer, J. (1974). "Heat exchange and transport in the environment," Report 14, Department of Geography and Environmental Engineering, Johns Hopkins University, Baltimore, MD.

Gao, H., and Zepp, R. (1998). "Factors influencing photoreactions of dissolved organic matter in a coastal river of the southeastern United States," *Environmental Science and Technology* 32, 2940-2946.

Genet, L., Smith, D., and Sonnen, M. (1974). "Computer program documentation for the Dynamic Estuary Model," U.S. Environmental Protection Agency, Systems Development Branch, Washington, D.C.

Hartman, B., and Hammond, D. (1985). "Gas exchange in San Francisco Bay," *Hydrobiologia* 129, 59-68.

Jassby, A., and Platt, T. (1976). "Mathematical formulation of the relationship between photosynthesis and light for phytoplankton," *Limnology and Oceanography* 21, 540-547.

Leonard, B. (1979). "A stable and accurate convection modelling procedure based on quadratic upstream interpolation," *Computer Methods in Applied Mechanics and Engineering* 19, 59-98.

Matavulj, M., and Flint, K. (1987). "A model for acid and alkaline phosphatase activity in a small pond," *Microbial Ecology* 13, 141-158.

Monod, J. (1949). "The growth of bacterial cultures," *Annual Review of Microbiology* 3, 371-394.

O'Connor, D., and Dobbins, W. (1958). "Mechanisms of reaeration in natural streams," *Transactions of the American Society of Civil Engineers* 123, 641-666.

O'Connor, D. (1983). "Wind effects on gas-liquid transfer coefficients," *Journal of the Environmental Engineering Division* 190, 731-752.

Parsons, T., Takahashi, M., and Hargrave, B. (1984). *Biological oceanographic processes*. 3rd ed., Pergamon Press, Oxford.

Thomann, R., and Fitzpatrick, J. (1982). "Calibration and verification of a mathematical model of the eutrophication of the Potomac Estuary," HydroQual Inc., Mahwah, NJ.

Tchobanoglous, G., and Schroeder, E. (1987). *Water quality,* Addison Wesley, Reading, MA.

Tuffey, T., Hunter, J., and Matulewich, V. (1974). "Zones of nitrification," *Water Resources Bulletin* 10, 555-564.

Wezernak, C., and Gannon, J. (1968). "Evaluation of nitrification in streams," *Journal of the Sanitary Engineering Division* 94(SA5), 883-895.

6 Water Column Calibration Results

The Calibration Period

The SJRWMD chose 1 December 1996 to 30 November 1998 as the calibration period. Calibration is an iterative process; consequently, more than 50 model runs were made in the effort to calibrate the model. In each run, model parameters or other factors were adjusted until an adequate fit between observations and model results was obtained. Calibration was considered complete when no substantial improvement in calibration status resulted from additional adjustments. Final model parameters were presented in Chapter 5 (Table 5-3).

Hydrodynamics for the 2-year calibration period were obtained from an EFDC application by the SJRWMD. The sources and update periods of the forcing functions used to drive the hydrodynamics for the simulation period are discussed in Sucsy and Morris (2002).

Wind speed during the 2-year simulation period exhibited a minor seasonal variability displayed as a rough sinusoidal pattern with higher wind speeds occurring in the winter months and lower wind speeds occurring in the late summer months (Figure 6-1). The windiest 3-month period usually occurred from February-April and the calmest from July-September, with a 24 percent difference between the two periods (Suscy and Morris 2002). Wind patterns showed deviations during the simulation period. For instance, wind speeds during summer 1997 (especially in July) were higher on the average than what had occurred in summer 1996. Moreover, winter speeds during the winter months in 1997 were of a greater magnitude than what had occurred during the winter of the previous year.

Suscy and Morris (2002) examined wind directions by creating cumulative wind-run plots for east and north components of the observed wind vector. During the simulation period for the St. Johns River, the east-west wind component showed relatively low seasonal variability, the wind-run plot indicating a long period of nearly zero net east-west wind movement (July 1996-November 1997). Predominate west winds occurred from November 1997 to August 1998. In contrast, according to Suscy and Morris (2002), the north-south wind component showed a definite seasonal variability with north winds

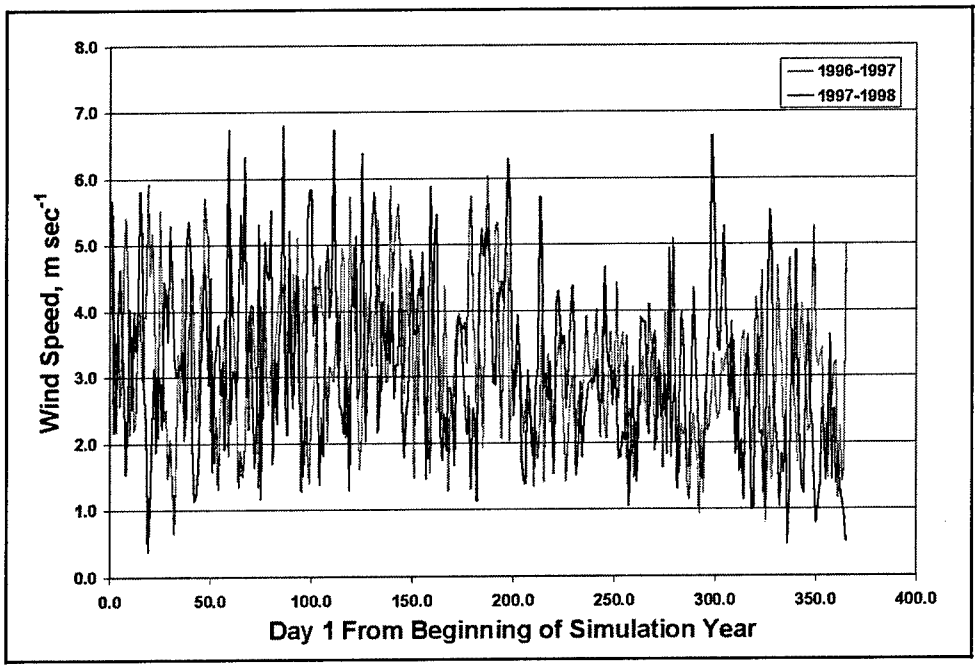

Figure 6-1. Wind speed for both simulation years

predominating in early fall (September-October) to early winter (December-January) and south winds predominating in early spring (February-March) to late summer (September-October).

TP and TN loads during the simulation period were separated into two source types - point (PS) and non-point source (NPS) (refer to Chapter 4). Magnitudes of TP from PS loads showed small variations from month to month for each segment (Figure 4-1), but magnitudes of loads for the six river segments ranged from a low of 85 to 1,200 kg/day. Average TP PS load values were approximately 100 kg/day for all segments except segment 4, which received the highest average loads of 1,000 kg/day. TP loads from NPSs showed the greatest deviations in loading magnitudes from month to month for each river segment. Segments 1, 2, and 4 showed similar peak TP loads during August and December 1997, and February and August 1998 (Figures 4-14, 4-15, and 4-17) while segments 3, 5, and 6 showed peak TP loads during these months as well as April and November 1997 (Figures 4-16, 4-18, and 4-19). NPS peak loads did not follow the convention of the wet season (June-October) entirely. The winter of 1997-1998 was an exceptionally wet period (Sucsy and Morris 2002) resulting in the notably higher loads.

Similar to TP loadings, TN PS and NPS loads showed similar loading patterns. Magnitudes of TN PS loads showed small variations from month to month for each segment, but values of loads per segment ranged from a low of 65 to 4,100 kg/day. While most segments received similar TP PS loads, average TN PS loads varied from 100 kg/day for segment 5, to 250 kg/day for segment 1, to 700 kg/day for segments 2 and 6, and to 2,750 kg/day for segment 4. Comparable to TP NPS loads, TN NPS loads showed the most variations in magnitude from month to month for each river segment. Segments 1, 2, and 4 showed similar peak TN loads especially during December 1997 through March

1998 and August 1998 (Figures 4-20, 4-21, and 4-23) while segments 3, 5, and 6 showed peak TN loads during these months as well as late spring/early summer 1997 (Figures 4-22, 4-24, and 4-25). As just discussed for TP NPS peak loads, TN NPS peak loads did not follow the convention of the wet season entirely either. With the 1997-1998 winter being abnormally wet, TN NPS loads peaked during this period.

Presentation Formats

CE-QUAL-ICM calibration performance was evaluated by comparing model output with observed data. Numerous methods were used to present and analyze model results. Three forms of graphical comparison were used: time-series plots (Figures 6-2 through 6-4), monthly longitudinal plots (Figure 6-5), and percent cumulative frequency plots (Figure 6-6). In addition, four statistics, mean error (ME), absolute mean error (AME), root mean square error (RMSE), and relative error (RE) were calculated to further evaluate model performance.

Statistics

The RMSE is an indicator of the deviation between predicted water quality values and observed values. A value of zero would indicate no variation between the observed and predicted. The ME indicates on average how the model is doing. For example, a positive ME indicates predictions are less than observed and a negative ME indicates predictions exceed observed. A value of zero for ME would also indicate complete agreement between predicted and observed. The AME indicates the how model reproduces data on average. An AME of 0.5 °C means that the computed temperatures are, on average, within ± 0.5 °C of the observed temperatures. Lastly, the RE is the ratio of the AME to the mean of observations expressed as a percent. The RE is the best statistic to use to make comparisons of model performance between other study results since it has been normalized. Each statistic was calculated for all data where observed data were available; data were not distinguished by layer, thus in essence getting the overall model performance. The equations for each statistic are presented below:

$$ME = \frac{\sum (O - P)}{n} \tag{6-1}$$

in which:

O = observation

P = model prediction

n = number of observations,

$$AME = \frac{\sum | O - P |}{n}, \tag{6-2}$$

$$RMSE = \sqrt{\frac{\sum (O-P)**2}{n}}, \tag{6-3}$$

and

$$RE = \frac{\sum |O-P|}{\sum O} \cdot 100. \tag{6-4}$$

Tables 6-1 through 6-4 present the value for each statistic for a particular water quality constituent of the LSJR results.

Graphical plots

Three graphical plot types will be used to evaluate model performance. Beginning with Time-series plots, comparison of time-specific model output (12:00 P.M.) and observed data demonstrate model performance over time and provide indications of interactions between modeled parameters. From the model output, constituent concentrations were selected that corresponded to the day and location at which the observed data were collected. Time-series plots were generated for stations shown in Figure 1-1. Only results at three stations (Fulton Point, Piney Point, and Picolota) are presented here (Figures 6-2 though 6-4). Results for all other stations are available from the first author on CD-ROM.

Monthly longitudinal plots synopsize overall model performance along the longitudinal profile of the river. Monthly averaged concentrations were output for all cells. Comparisons were made between observed data and a monthly averaged computed value that corresponds to the location and month the data were collected. Results for longitudinal profiles were presented during a month critical to water quality (i.e., August). The remaining monthly longitudinal plots are provided on a CD-ROM. A point to consider when viewing the longitudinal comparisons is that comparison of monthly averaged constituent concentrations to time-specific observed values will make the computed values appear not as robust as the observed (missed peak and low values). This gives the appearance that the model is over- or under-predicting observed data. For example, if the observed value were collected during an extreme event but the average does not show it, this may be interpreted as poor model performance.

The third and final graphical form used to evaluate model performance is the cumulative distribution plot. The percent cumulative distribution plots (Figure 6-6) show how concentration distribution of the predicted values compare with observed data (i.e., does CE-QUAL-ICM capture the range of low to high concentrations for a particular variable).

Table 6-1
Combined Water Quality Statistics for All Stations

	ME (%)	AME (%)	RMSE (%)	RE (%)	Number of Observations
Alg1	-0.0995	0.2263	0.3989	79.1301	176
Alg2	0.0563	0.1536	0.2238	70.8107	176
Alg3	-0.0107	0.0442	0.0626	77.8866	176
Chl a	-1.2406	6.3779	10.5498	49.2799	398
DIN	0.0015	0.0769	0.1058	62.0053	381
DIP	0.0018	0.0167	0.0215	45.8258	433
DOC	0.8384	2.2858	3.4526	17.9821	382
DO	0.0404	0.6721	1.001	9.321	438
DS	-0.7666	0.8887	1.2086	86.1118	308
KESS	0.3127	0.48	0.6267	15.6112	44
NH3	-0.0218	0.0313	0.0385	149.156	397
NO2+NO3	0.0271	0.0729	0.1029	66.6979	433
SALT	-0.2367	2.0944	3.9605	27.6057	4164
TEMP	0.023	0.8098	1.0413	3.4565	450
TN	0.1727	0.3448	0.5029	29.0253	452
TOC	-0.1723	2.3612	3.2976	18.1437	394
TP	0.0113	0.0263	0.0361	26.9685	451
TSS	10.7921	13.1717	21.863	60.3667	446

Table 6-2
Combined Water Quality Statistics for All Stations – 1996-1997

	ME (%)	AME (%)	RMSE (%)	RE (%)	Number of Observations
Alg1	-0.0643	0.237	0.3941	70.7428	82
Alg2	0.0423	0.148	0.2069	69.229	82
Alg3	-0.0009	0.0469	0.0704	68.9381	82
Chl a	-1.9296	6.9826	10.9265	52.0002	184
DIN	-0.0189	0.0764	0.1026	92.119	175
DIP	0.0026	0.0165	0.0205	46.671	193
DOC	0.9236	2.1227	3.6434	17.5127	171
DO	-0.0289	0.6684	0.9541	9.1931	202
DS	-0.7695	0.9797	1.2819	78.3678	94
KESS	0.0788	0.3328	0.4769	13.2055	14
NH3	-0.0113	0.029	0.0372	100.4467	185
NO2+NO3	-0.0046	0.0669	0.0903	108.6081	196
SALT	-0.4415	2.26	3.8114	24.8191	2256
TEMP	0.0879	0.8611	1.1164	3.751	205
TN	0.1806	0.3199	0.3925	28.0026	206
TOC	-0.1107	2.1584	3.2556	17.5618	180
TP	0.0082	0.0251	0.0341	25.8909	205
TSS	3.6428	8.0825	11.1412	57.2114	200

Table 6-3
Combined Water Quality Statistics for all Stations – 1997-1998

	ME (%)	AME (%)	RMSE (%)	RE (%)	Number of Observatons
Alg1	-0.1303	0.2169	0.403	89.2141	94
Alg2	0.0685	0.1584	0.2376	72.1536	94
Alg3	-0.0192	0.0417	0.055	89.2484	94
Chl a	-0.6482	5.858	10.2147	46.7722	214
DIN	0.0189	0.0774	0.1085	48.6618	206
DIP	0.0012	0.0168	0.0222	45.1771	240
DOC	0.7694	2.4179	3.2899	18.3316	211
DO	0.0997	0.6751	1.0395	9.4321	236
DS	-0.7653	0.8487	1.175	90.6542	214
KESS	0.4218	0.5487	0.6855	16.4599	30
NH3	-0.0309	0.0332	0.0395	236.5711	212
NO2+NO3	0.0532	0.0778	0.1122	52.3278	237
SALT	0.0093	1.8895	4.1061	32.6088	1908
TEMP	-0.0312	0.7669	0.9742	3.219	245
TN	0.1662	0.3657	0.5794	29.8233	246
TOC	-0.2242	2.5318	3.3324	18.5853	214
TP	0.014	0.0274	0.0377	27.8538	246
TSS	16.6047	17.3093	27.6711	61.6577	246

Table 6-4
Statistics for All Water Quality Constituents at Each Station

Station Name	Water Quality Constituent	ME (%)	AME (%)	RMSE (%)	RE (%)	Number of Observations
Picolata	DIN	0.0126	0.0596	0.091	64.8078	45
Racey Point	DIN	-0.011	0.0557	0.0906	87.2722	41
Palatka	DIN	-0.0091	0.0365	0.0543	55.6701	46
Fulton Point	DIN	-0.0261	0.0716	0.0877	74.8024	98
Talleyrand	DIN	0.0098	0.1061	0.1356	50.2256	93
Piney Point	DIN	0.0006	0.0875	0.1151	71.5169	35
Mandarin Point	DIN	0.1093	0.1184	0.1464	64.8747	23
Picolata	NO2+NO3	0.0352	0.0464	0.079	63.4202	46
Racey Point	NO2+NO3	0.011	0.0325	0.057	71.7185	42
Palatka	NO2+NO3	0.0098	0.0256	0.0393	56.8372	47
Fulton Point	NO2+NO3	-0.0087	0.0628	0.0783	75.2032	109
Talleyrand	NO2+NO3	0.0442	0.1112	0.1392	60.8322	118
Piney Point	NO2+NO3	0.0433	0.0846	0.1116	74.1125	48
Mandarin Point	NO2+NO3	0.123	0.1232	0.1526	74.8556	23
Picolata	ALG1	-0.1692	0.3871	0.5425	88.2033	23
Racey Point	ALG1	-0.0489	0.2827	0.4139	41.6959	24
Palatka	ALG1	0.0016	0.3146	0.4391	41.708	23

(Sheet 1 of 4)

Table 6-4 (Continued)

Station Name	Water Quality Constituent	ME (%)	AME (%)	RMSE (%)	RE (%)	Number of Observations
Fulton Point	ALG1	0.0042	0.0044	0.0055	79.4255	29
Talleyrand	ALG1	-0.0089	0.0529	0.1003	155.2768	32
Piney Point	ALG1	-0.1552	0.1869	0.3142	191.2262	22
Mandarin Point	ALG1	-0.3874	0.4767	0.6657	341.5012	23
Picolata	ALG2	0.1115	0.1384	0.1917	55.5985	23
Racey Point	ALG2	0.1772	0.1921	0.2683	54.8697	24
Palatka	ALG2	0.0638	0.1241	0.1916	46.5092	23
Fulton Point	ALG2	0.0052	0.122	0.1678	78.6965	29
Talleyrand	ALG2	-0.0375	0.1446	0.2078	119.6059	32
Piney Point	ALG2	0.0622	0.1912	0.3053	85.8067	22
Mandarin Point	ALG2	0.0565	0.1742	0.2237	86.4256	23
Picolata	ALG3	0.0238	0.033	0.0546	42.6788	23
Racey Point	ALG3	0.0255	0.0368	0.05	38.7159	24
Palatka	ALG3	0.0104	0.0306	0.0459	33.9283	23
Fulton Point	ALG3	-0.0281	0.0637	0.0949	161.9991	29
Talleyrand	ALG3	-0.0594	0.0594	0.0675	291.735	32
Piney Point	ALG3	-0.0342	0.0399	0.0493	128.0452	22
Mandarin Point	ALG3	0.0083	0.0347	0.0479	58.442	23
Picolata	CHL	0.7964	10.2998	16.1976	42.9803	47
Racey Point	CHL	-1.256	11.855	15.2619	43.3187	48
Palatka	CHL	-3.1248	10.0343	13.1694	37.0068	48
Fulton Point	CHL	0.4147	1.867	2.3249	48.5684	94
Talleyrand	CHL	-0.1672	3.4841	5.7725	74.1422	98
Piney Point	CHL	-2.6275	5.2398	7.9957	62.3889	40
Mandarin Point	CHL	-10.3654	12.0479	16.3246	110.0647	23
Picolata	DIP	0.007	0.0115	0.016	47.3804	47
Racey Point	DIP	-0.0098	0.0152	0.019	102.9034	48
Palatka	DIP	-0.0069	0.0096	0.0147	100.029	48
Fulton Point	DIP	-0.0064	0.0193	0.0243	60.3248	104
Talleyrand	DIP	0.0052	0.0183	0.0233	30.9496	116
Piney Point	DIP	0.0171	0.0174	0.0214	36.0368	47
Mandarin Point	DIP	0.023	0.023	0.0255	55.1421	23
Picolata	DO	0.2885	0.8394	1.2849	10.649	45
Racey Point	DO	0.6593	1.058	1.4002	12.8434	47
Palatka	DO	0.1425	0.8154	1.0875	11.1094	46
Fulton Point	DO	-0.3074	0.5708	0.6724	8.5958	115
Talleyrand	DO	-0.0675	0.5782	1.0202	8.6108	120
Piney Point	DO	0.2837	0.4841	0.697	6.2068	42
Mandarin Point	DO	-0.056	0.6083	0.9502	7.7089	23
Picolata	DOC	1.5017	1.8881	4.697	11.2723	45
Racey Point	DOC	-0.1853	1.5641	1.945	9.4968	46
Palatka	DOC	-0.1345	1.7958	2.8242	11.5876	46
Fulton Point	DOC	0.9638	2.8742	3.8767	45.4394	90
Talleyrand	DOC	0.6989	2.4663	3.2108	20.6033	95

(Sheet 2 of 4)

Table 6-4 (Continued)

Station Name	Water Quality Constituent	ME (%)	AME (%)	RMSE (%)	RE (%)r	Number of Observations
Piney Point	DOC	1.6983	1.9967	2.3821	13.5154	37
Mandarin Point	DOC	2.2362	2.9037	4.5588	17.6493	23
Picolata	DS	-1.0389	1.0821	1.2992	113.5525	47
Racey Point	DS	-0.6847	0.7466	1.0034	60.2834	48
Palatka	DS	0.0447	0.3473	0.5719	21.3923	48
Fulton Point	DS	-0.4637	0.5906	0.8444	115.5002	58
Talleyrand	DS	-1.0993	1.141	1.455	115.8101	63
Piney Point	DS	-1.3824	1.4776	1.7739	155.4876	21
Mandarin Point	DS	-1.3646	1.4425	1.6908	138.1621	23
Picolata	KESS	0.485	0.5523	0.7598	17.6073	16
Racey Point	KESS	0.1942	0.4623	0.5405	15.1037	15
Palatka	KESS	0.2373	0.4115	0.5308	13.6494	13
Picolata	NH3	-0.0216	0.0287	0.0359	142.4267	46
Racey Point	NH3	-0.0222	0.0341	0.0438	200.391	47
Palatka	NH3	-0.0182	0.0245	0.0309	122.493	47
Fulton Point	NH3	-0.013	0.0257	0.0306	145.1112	102
Talleyrand	NH3	-0.0337	0.042	0.048	152.4601	95
Piney Point	NH3	-0.025	0.0334	0.0407	150.451	37
Mandarin Point	NH3	-0.0136	0.0214	0.0277	119.8573	23
	SALT	-6.466	9.0025	10.9468	39.7339	252
	SALT	0.4267	4.3016	5.3153	20.1748	912
	SALT	0.0026	1.9502	2.8475	40.8684	1072
	SALT	0.2568	0.4857	0.9107	45.1763	789
	SALT	0.0433	0.0489	0.064	11.7622	1139
Picolata	TEMP	0.2171	0.6318	0.7981	2.6992	46
Racey Point	TEMP	0.3144	0.7238	0.9681	3.0729	48
Palatka	TEMP	0.2172	0.7544	0.912	3.1847	47
Fulton Point	TEMP	-0.1272	1.0899	1.4032	4.7195	115
Talleyrand	TEMP	-0.0719	0.7783	0.9417	3.2911	121
Piney Point	TEMP	-0.0745	0.6728	0.8079	2.8887	50
Mandarin Point	TEMP	0.0931	0.5216	0.5988	2.2198	23
Picolata	TN	0.1663	0.3908	0.4906	27.7724	47
Racey Point	TN	0.0232	0.3182	0.3904	22.5363	48
Palatka	TN	-0.055	0.2468	0.3723	18.1996	48
Fulton Point	TN	0.2062	0.3196	0.4112	38.1332	115
Talleyrand	TN	0.2693	0.3892	0.6838	31.5464	121
Piney Point	TN	0.2358	0.3457	0.4093	27.1943	50
Mandarin Point	TN	0.1611	0.4016	0.449	32.1285	23
Picolata	TOC	0.1187	1.8056	3.2328	10.5937	46
Racey Point	TOC	-1.7091	2.1316	2.6132	12.3417	46
Palatka	TOC	-2.5264	2.8262	3.3912	17.509	47
Fulton Point	TOC	0.4948	2.7208	3.7633	41.2941	94
Talleyrand	TOC	0.2048	2.4265	3.0636	19.8457	98

(Sheet 3 of 4)

Table 6-4 (Concluded)

Station Name	Water Quality Constituent	ME (%)	AME (%)	RMSE (%)	RE (%)	Number of Observations
Piney Point	TOC	0.6661	1.484	1.9221	10.1454	40
Mandarin Point	TOC	1.3379	2.7595	4.8906	16.3706	23
Picolata	TP	0.0072	0.0213	0.0272	25.7402	47
Racey Point	TP	-0.0027	0.0198	0.0266	24.6371	48
Palatka	TP	-0.0057	0.0197	0.0269	31.1412	48
Fulton Point	TP	0.0134	0.0287	0.0386	29.5916	115
Talleyrand	TP	0.0181	0.0313	0.0441	25.5435	120
Piney Point	TP	0.0232	0.0279	0.0353	25.9022	50
Mandarin Point	TP	0.013	0.0231	0.0276	26.2696	23
Picolata	TSS	6.0358	6.6736	8.2961	56.5151	47
Racey Point	TSS	4.7167	5.6751	8.1873	44.2213	48
Palatka	TSS	-0.3208	2.8995	3.7672	26.4846	48
Fulton Point	TSS	17.3264	22.7931	33.5352	61.4843	112
Talleyrand	TSS	14.7414	16.3968	24.0571	66.8684	119
Piney Point	TSS	10.1084	10.2071	14.2746	68.4664	49
Mandarin Point	TSS	5.5877	6.3108	7.3411	61.8974	23

(Sheet 4 of 4)

Temperature

Time-series plots for three stations are presented in Figures 6-2 through 6-4. Figures indicate good comparison between observed and predicted results. CE-QUAL-ICM captured the cooler early summer temperatures in 1997 as compared to temperatures during the same time period in 1998. This is also noted by the RE statistic for temperature in Table 6-1 (e.g., RE approximately 3.5 percent). Having an RE similar or slightly better than REs reported for other studies (Table 6-5) signifies good model performance for this constituent.

Salinity

Ocean boundary conditions for salinity varied from 35-36 parts per thousand (ppt) from top to bottom year round. Ocean boundary conditions had greater influence on stations in the most downstream reaches as seen in Figures 6-2 through 6-4. Boundary conditions for 63 tributary or point sources were also included with concentrations ranging from approximately 0.03 to 0.4 ppt. Buffalo Bluff was treated as a separate boundary file with salinity concentrations of roughly 0.55 ppt developed from two stations presented in Sucsy and Morris (2002). Salinity time-series plots show good comparison to observed data with predictions at Bar Pilot bottom layer showing the greatest difference between observed and predicted data. The model captured the wide variability of salinity in the upstream direction, especially between Dames Point and Buckman Bridge stations, and between Buckman Bridge and Shands Bridge stations.

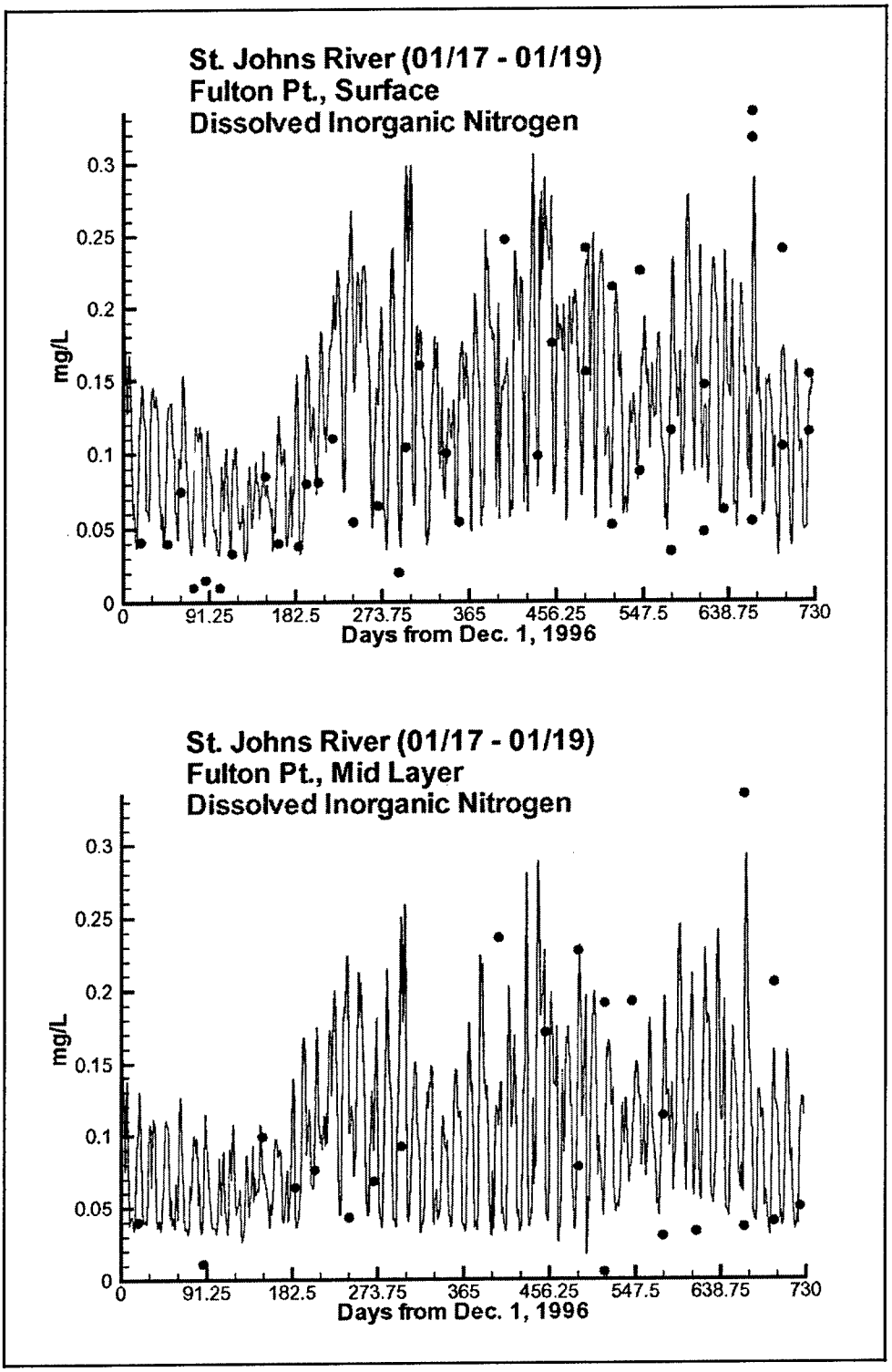

Figure 6-2. Time-series plots at Fulton Point for top, middle, and bottom layers for all water quality constituents (Sheet 1 of 20)

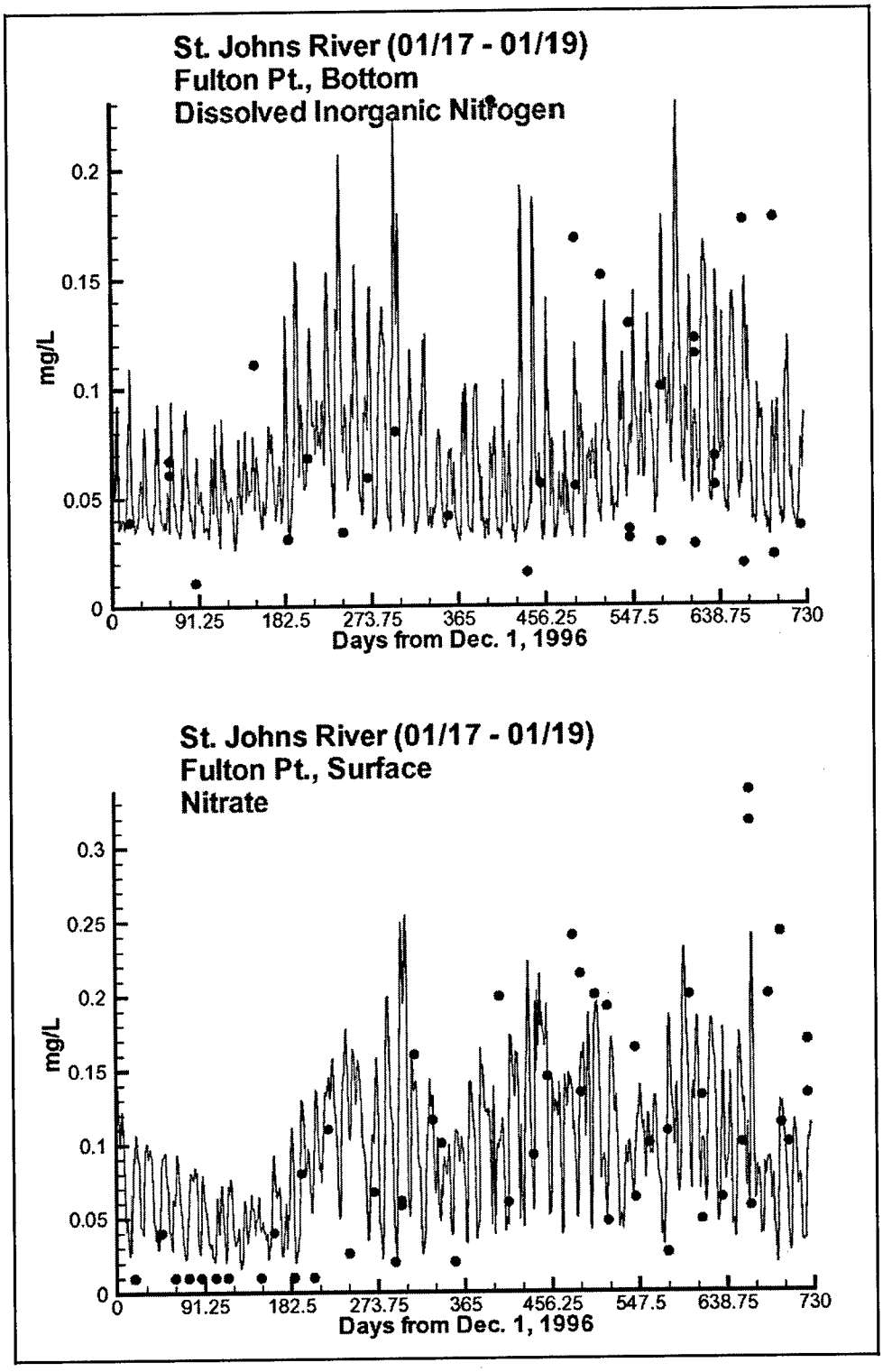

Figure 6-2. (Sheet 2 of 20)

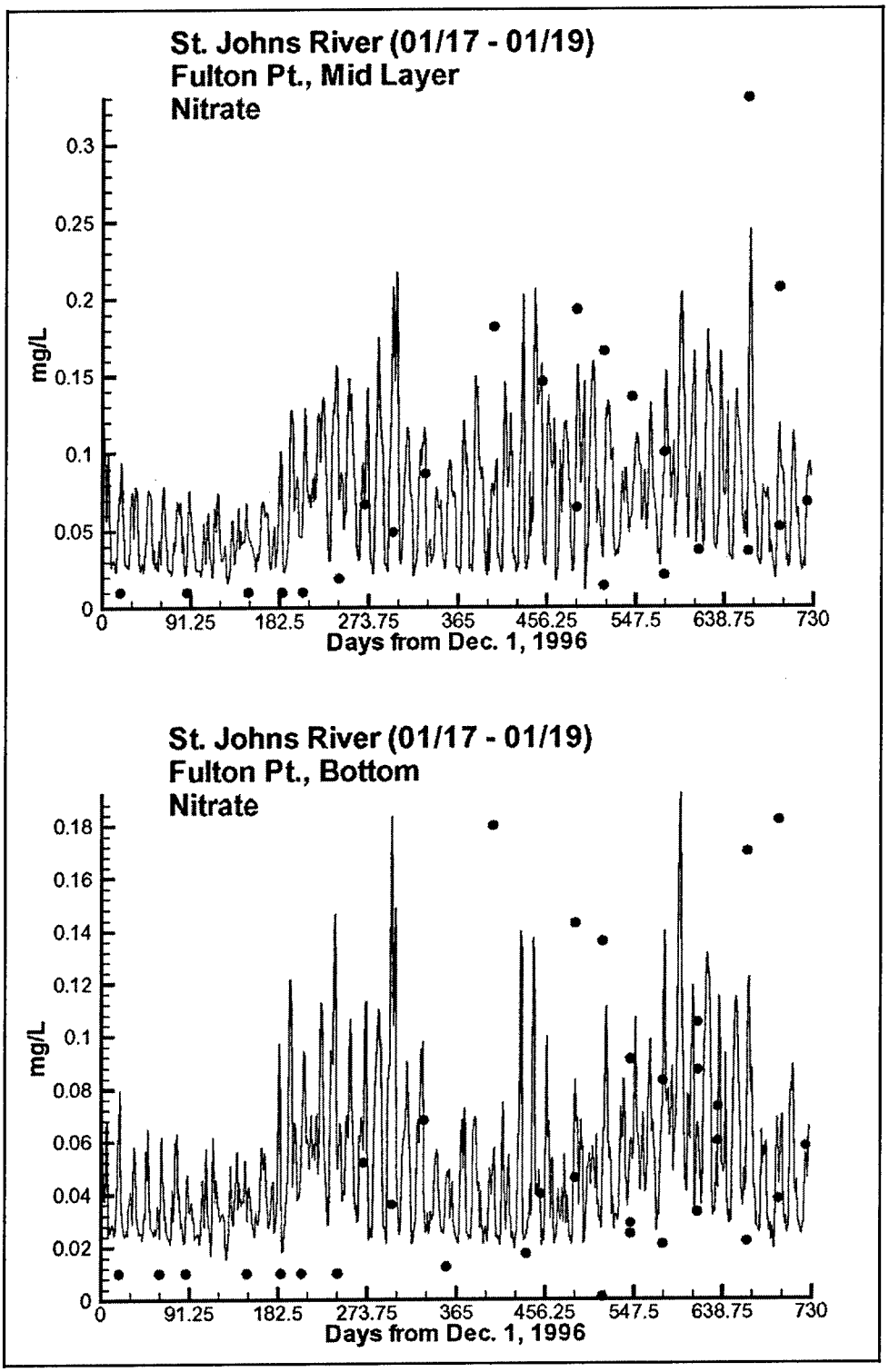

Figure 6-2. (Sheet 3 of 20)

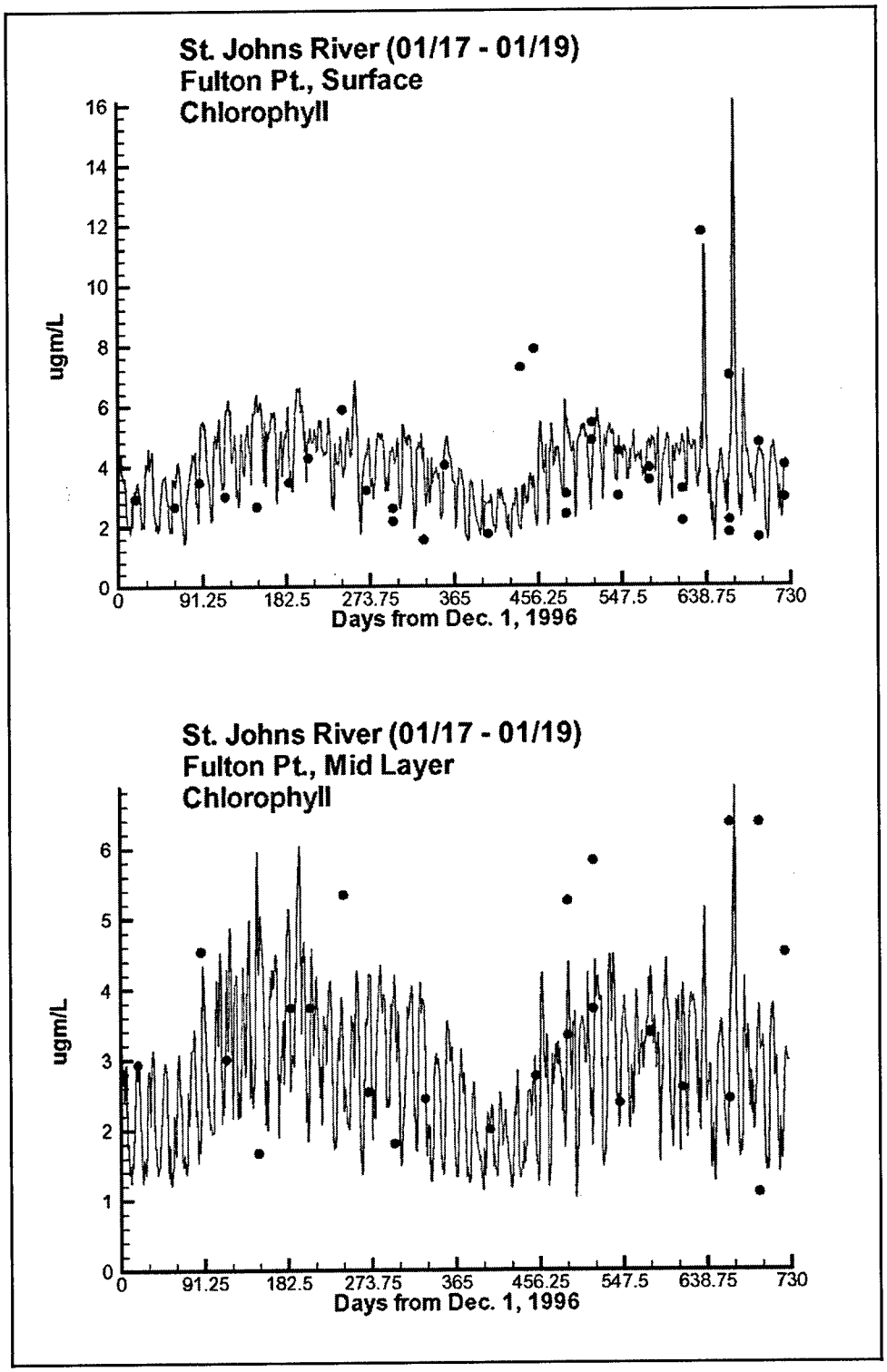

Figure 6-2. (Sheet 4 of 20)

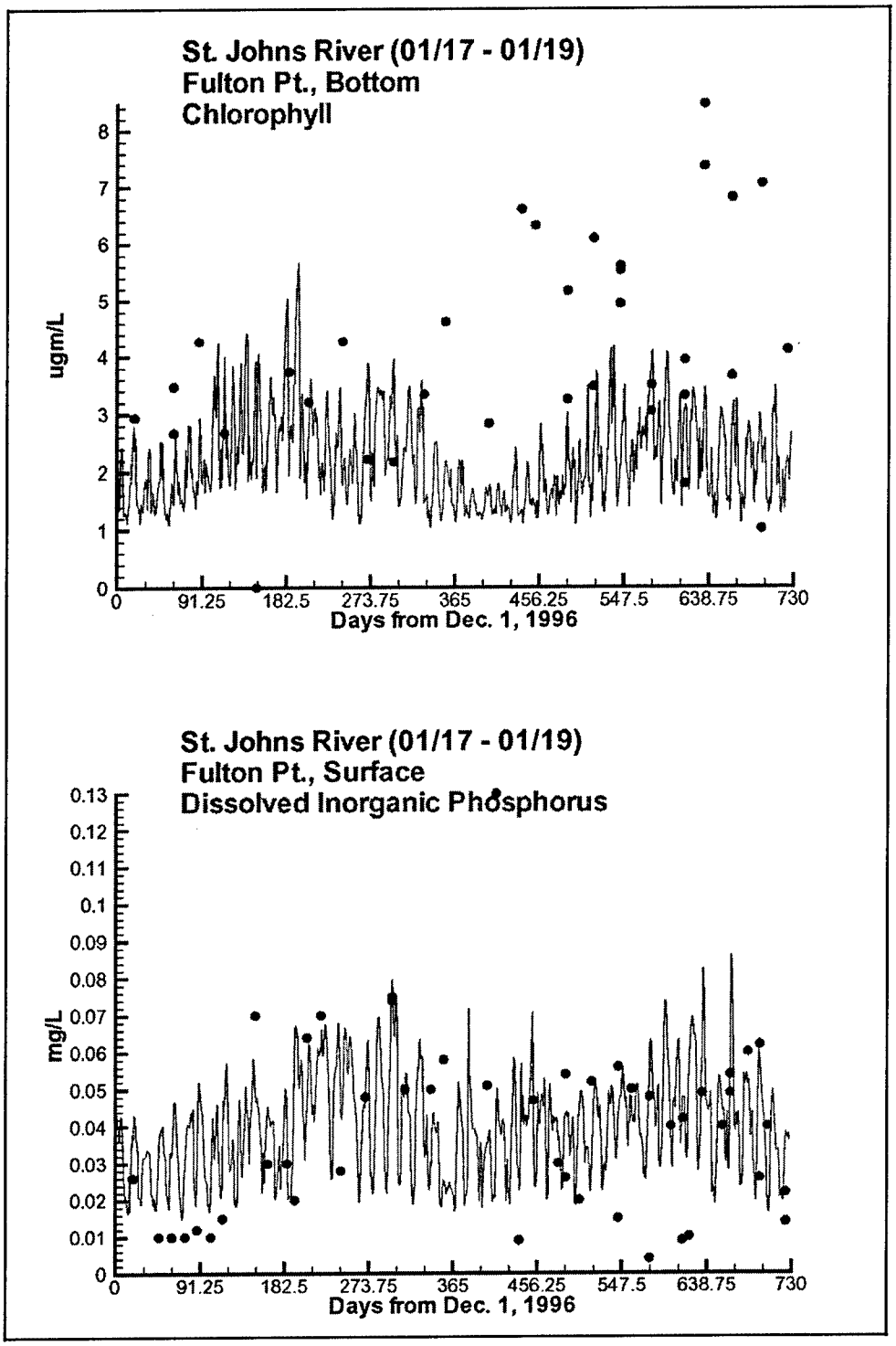

Figure 6-2. (Sheet 5 of 20)

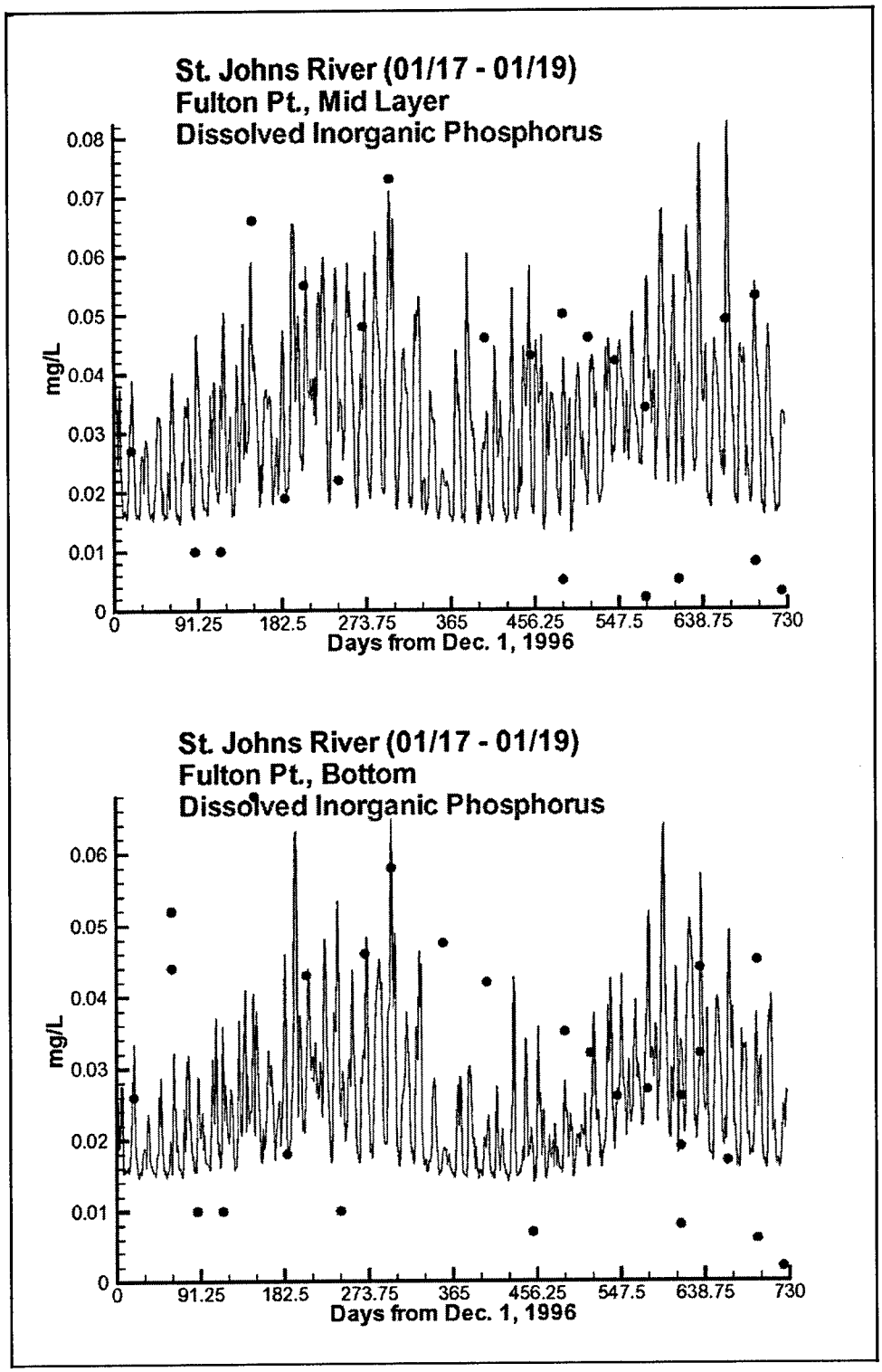

Figure 6-2. (Sheet 6 of 20)

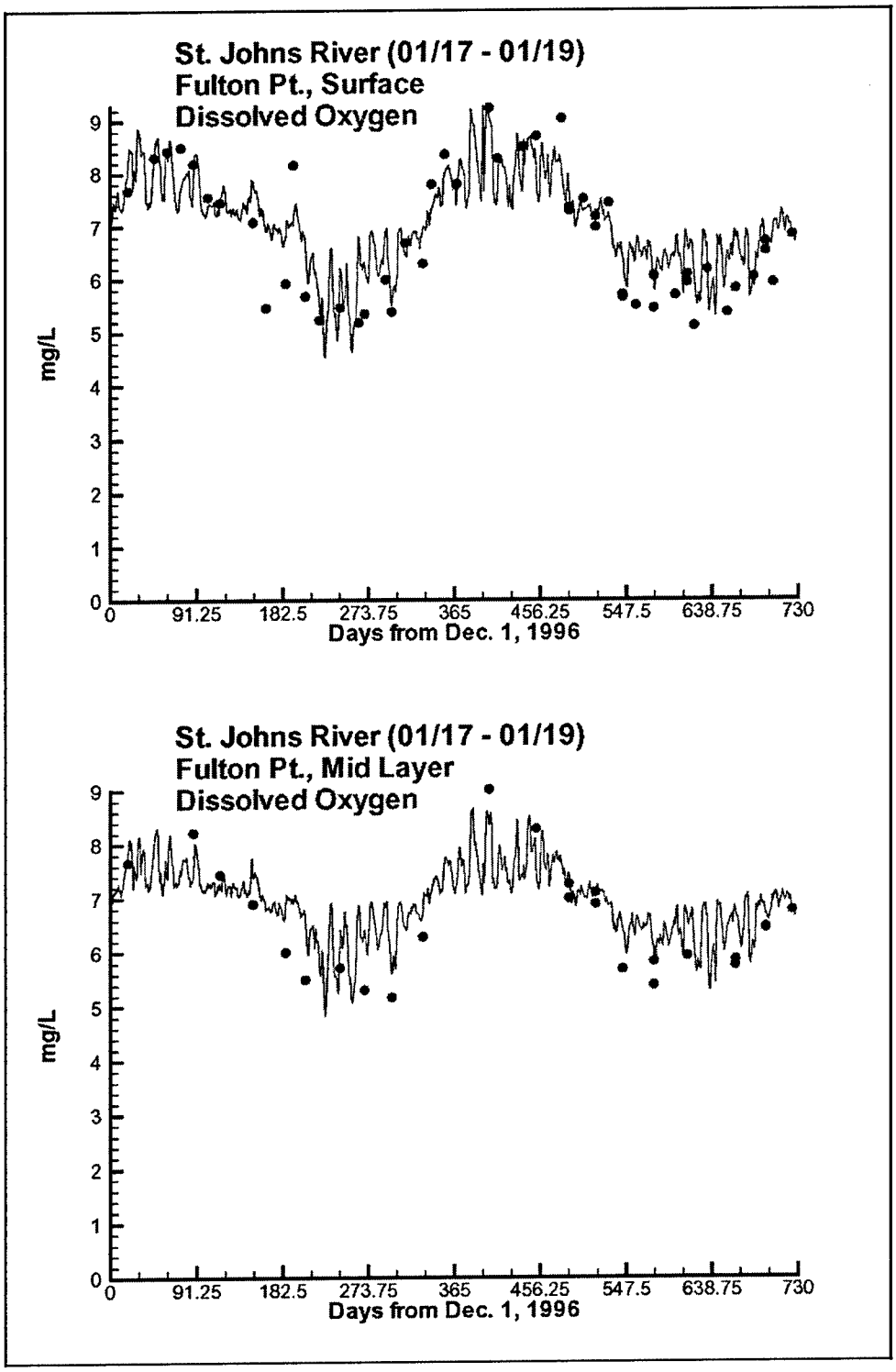

Figure 6-2. (Sheet 7 of 20)

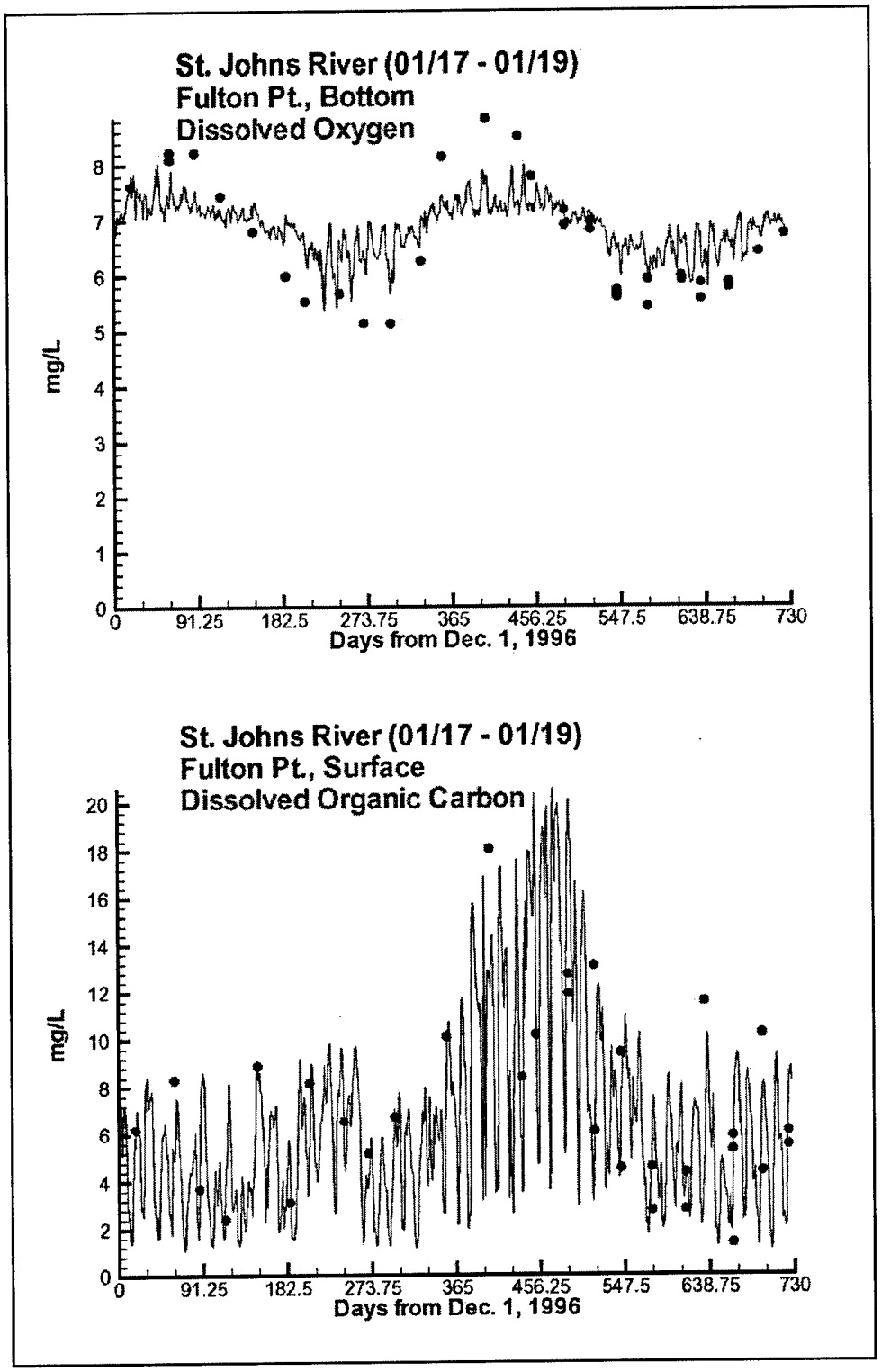

Figure 6-2. (Sheet 8 of 20)

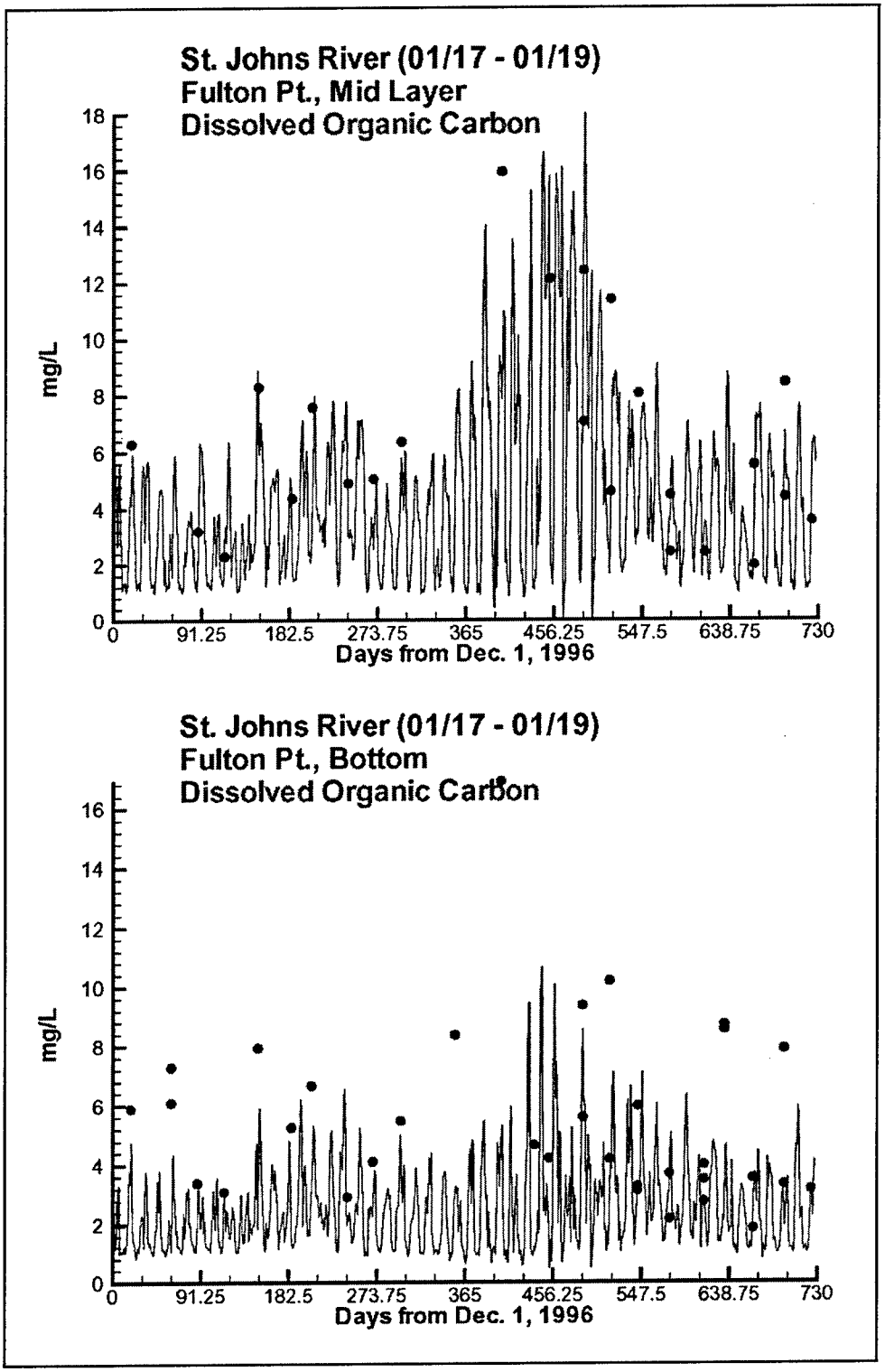

Figure 6-2. (Sheet 9 of 20)

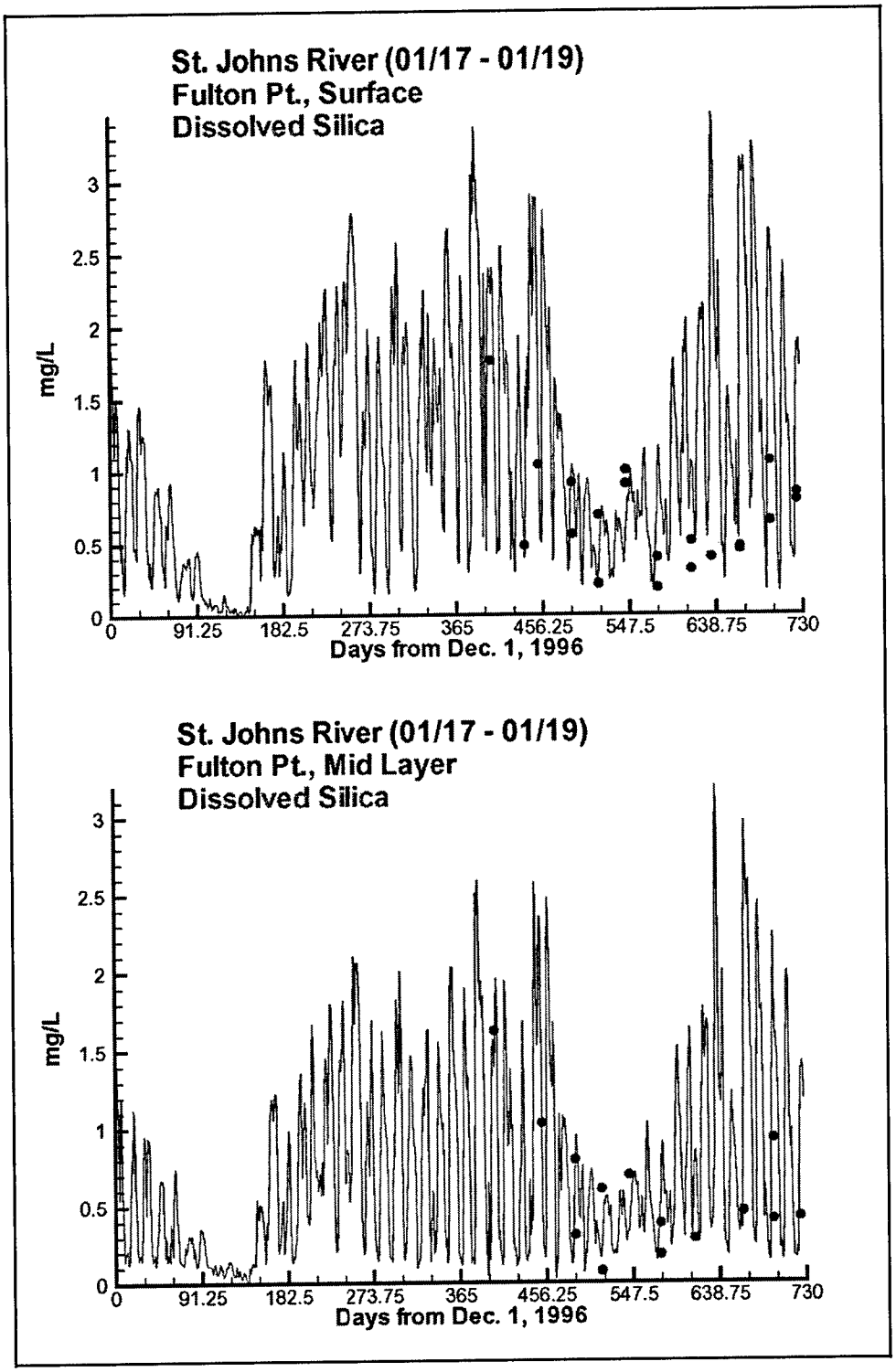

Figure 6-2. (Sheet 10 of 20)

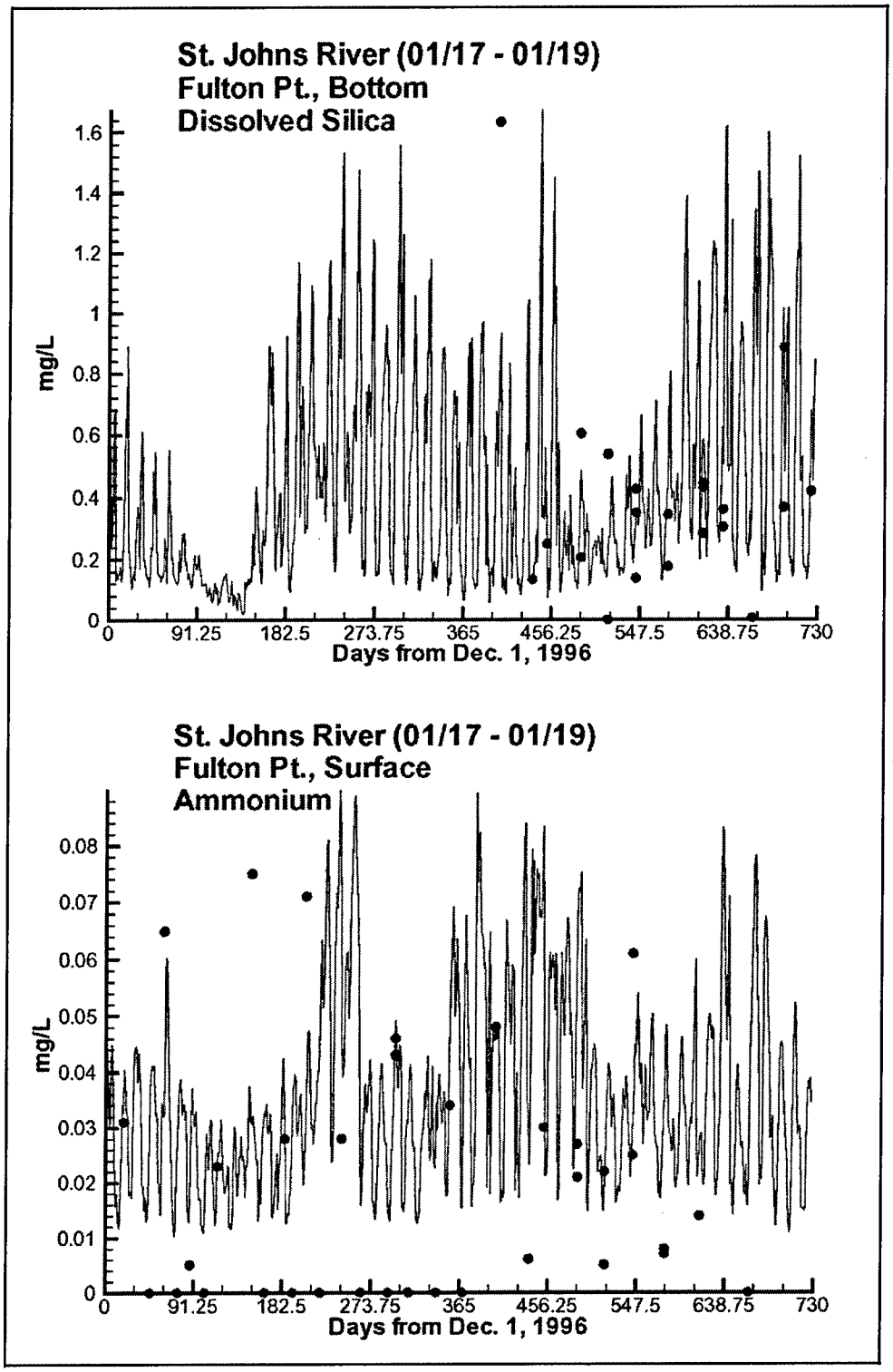

Figure 6-2. (Sheet 11 of 20)

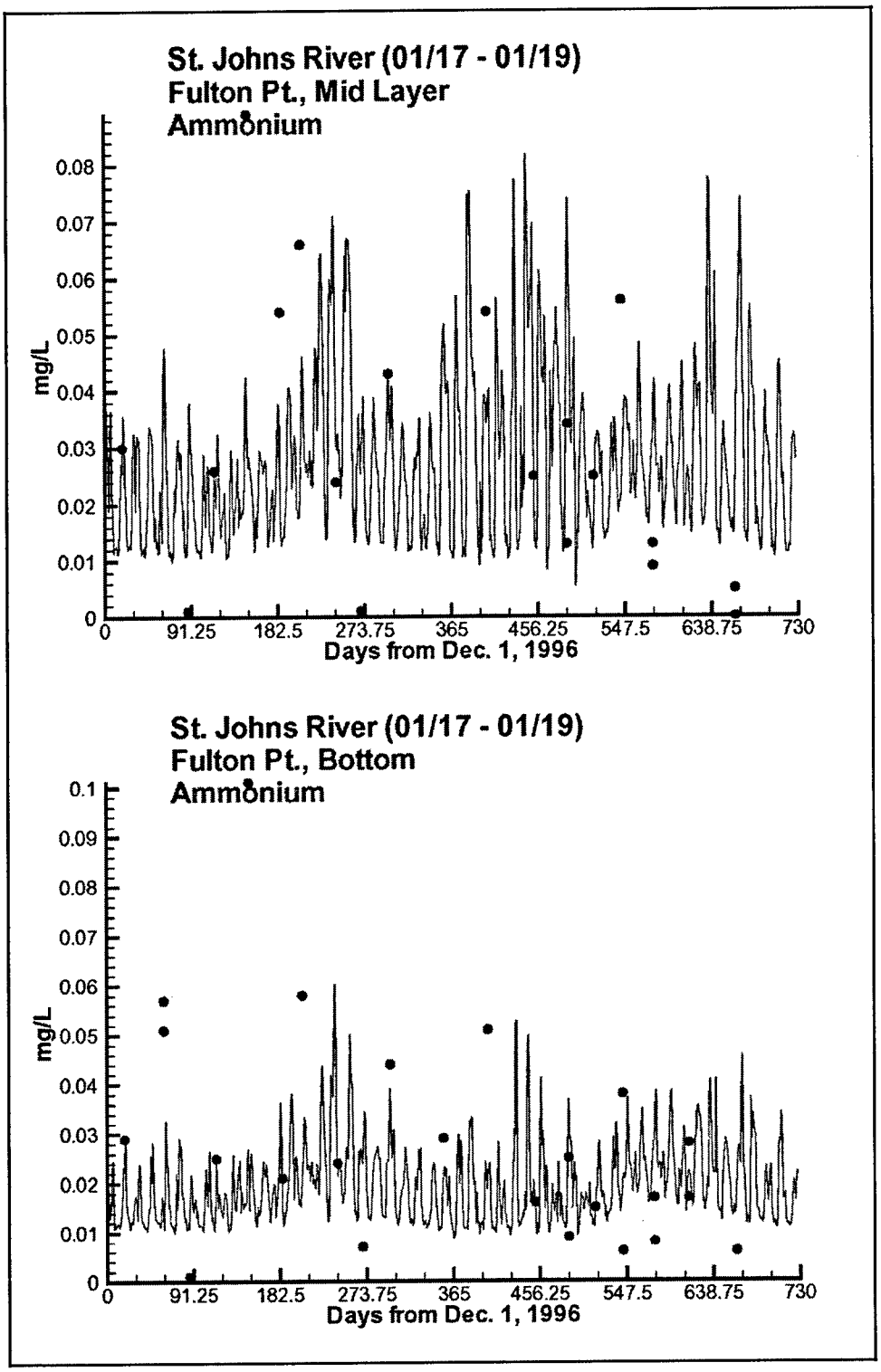

Figure 6-2. (Sheet 12 of 20)

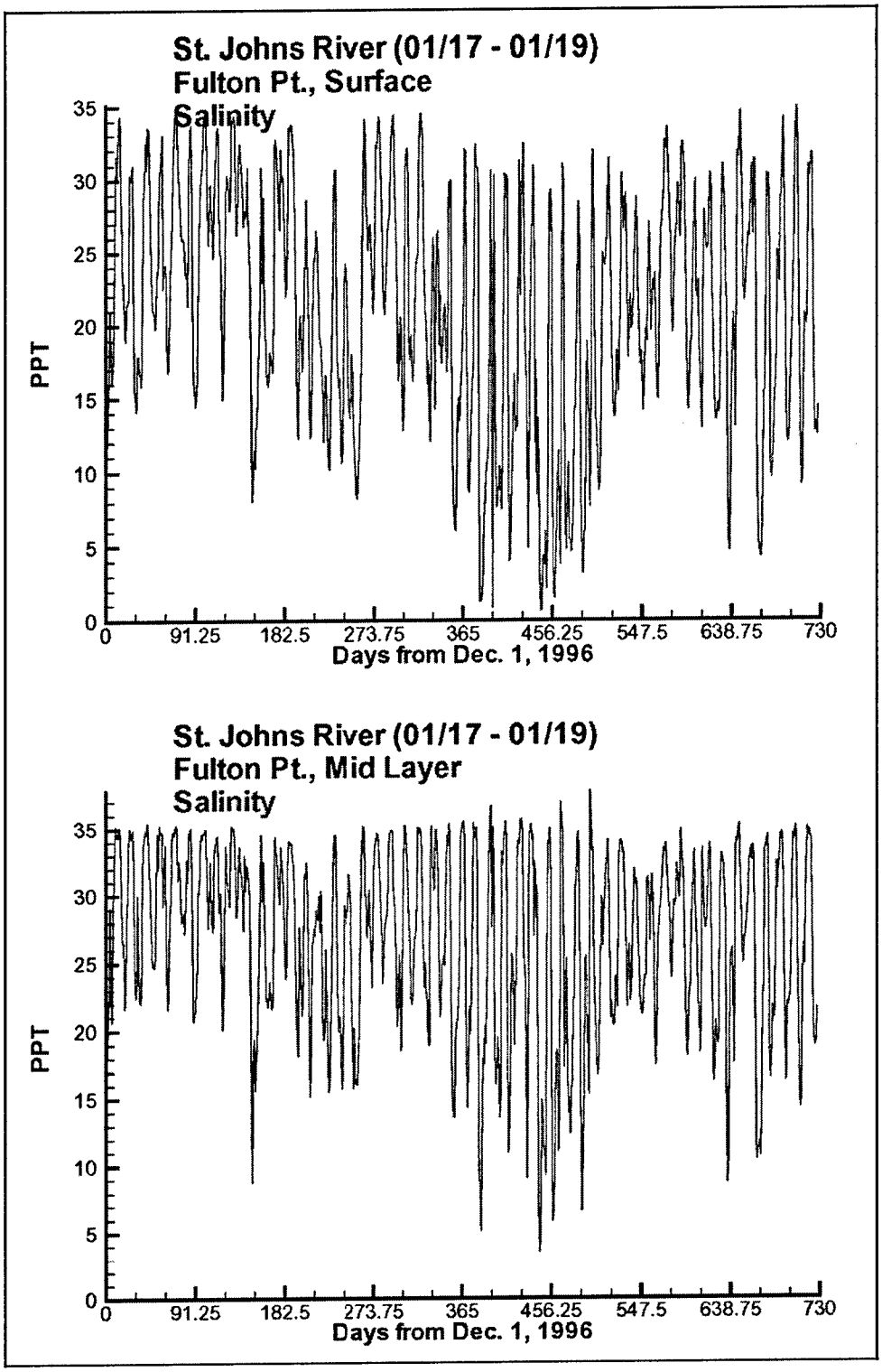

Figure 6-2. (Sheet 13 of 20)

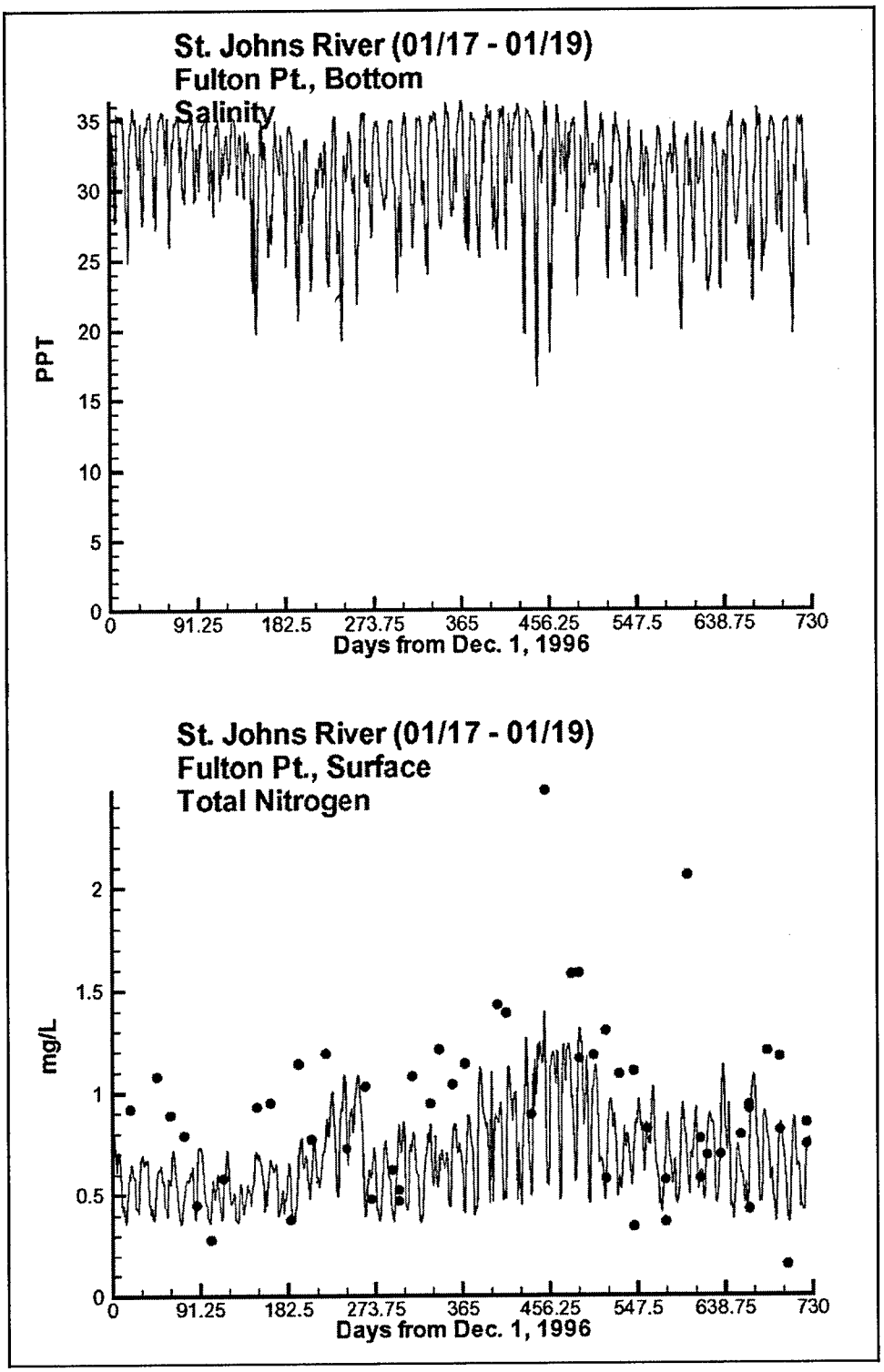

Figure 6-2. (Sheet 14 of 20)

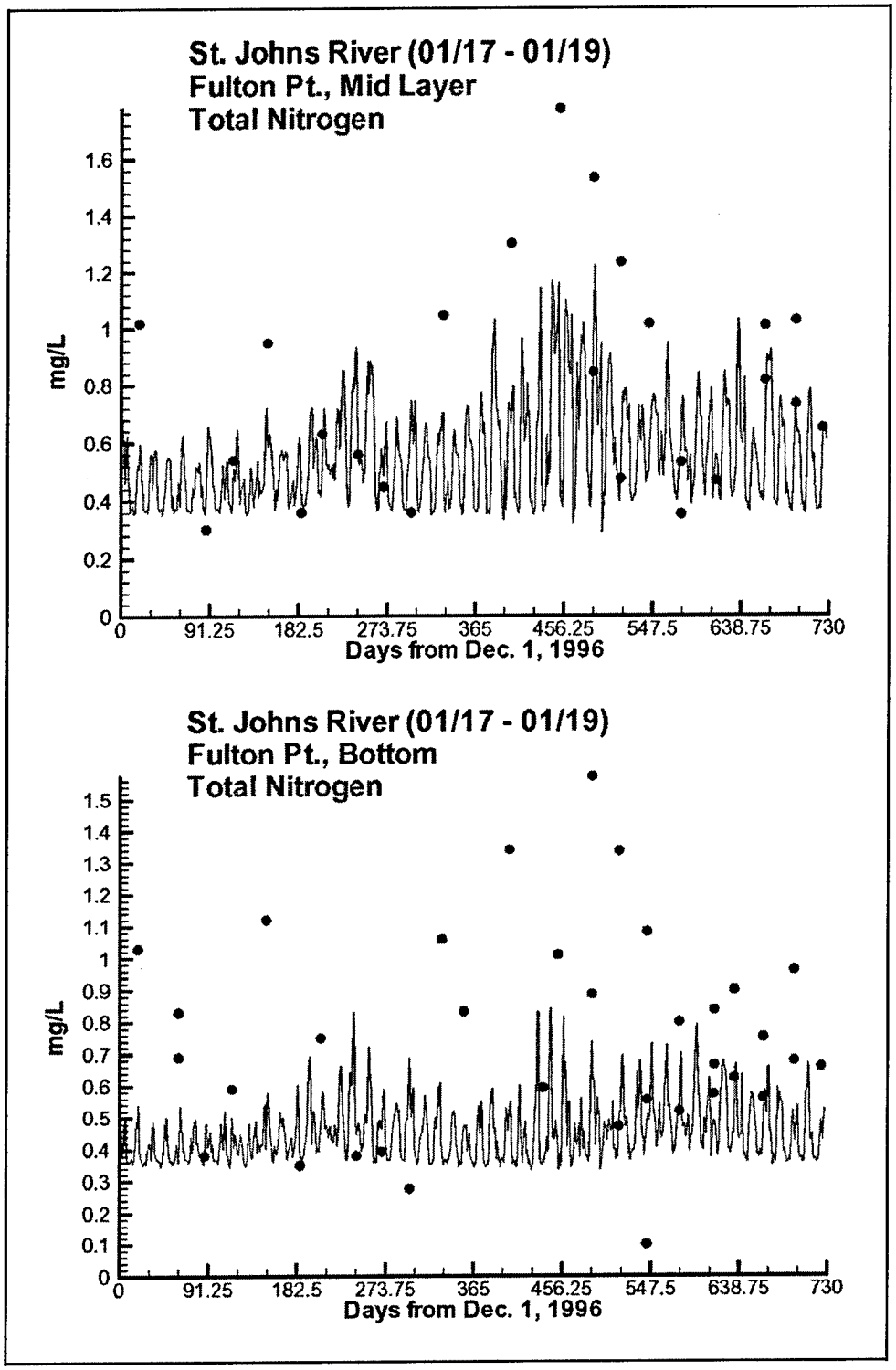

Figure 6-2. (Sheet 15 of 20)

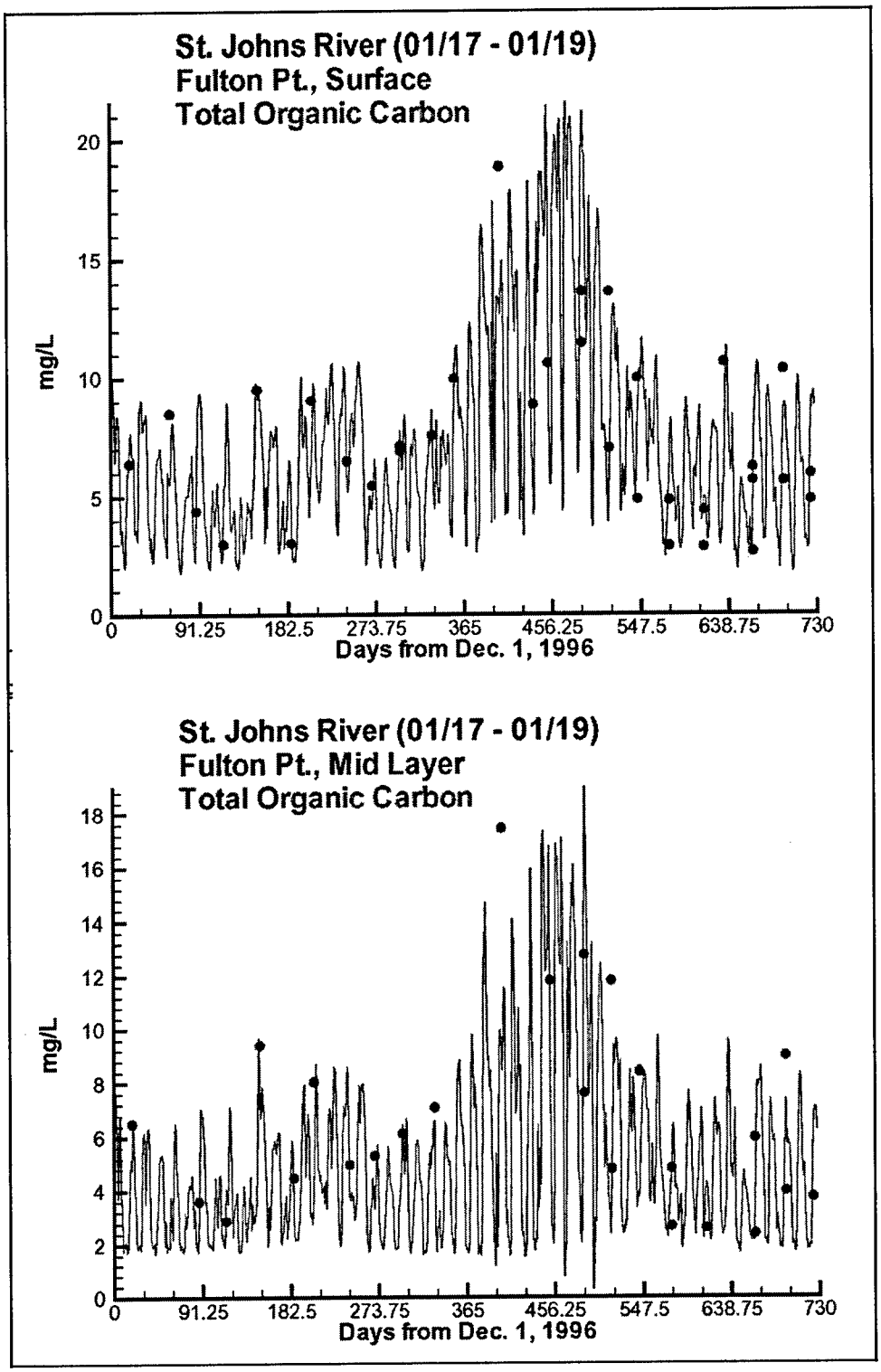

Figure 6-2. (Sheet 16 of 20)

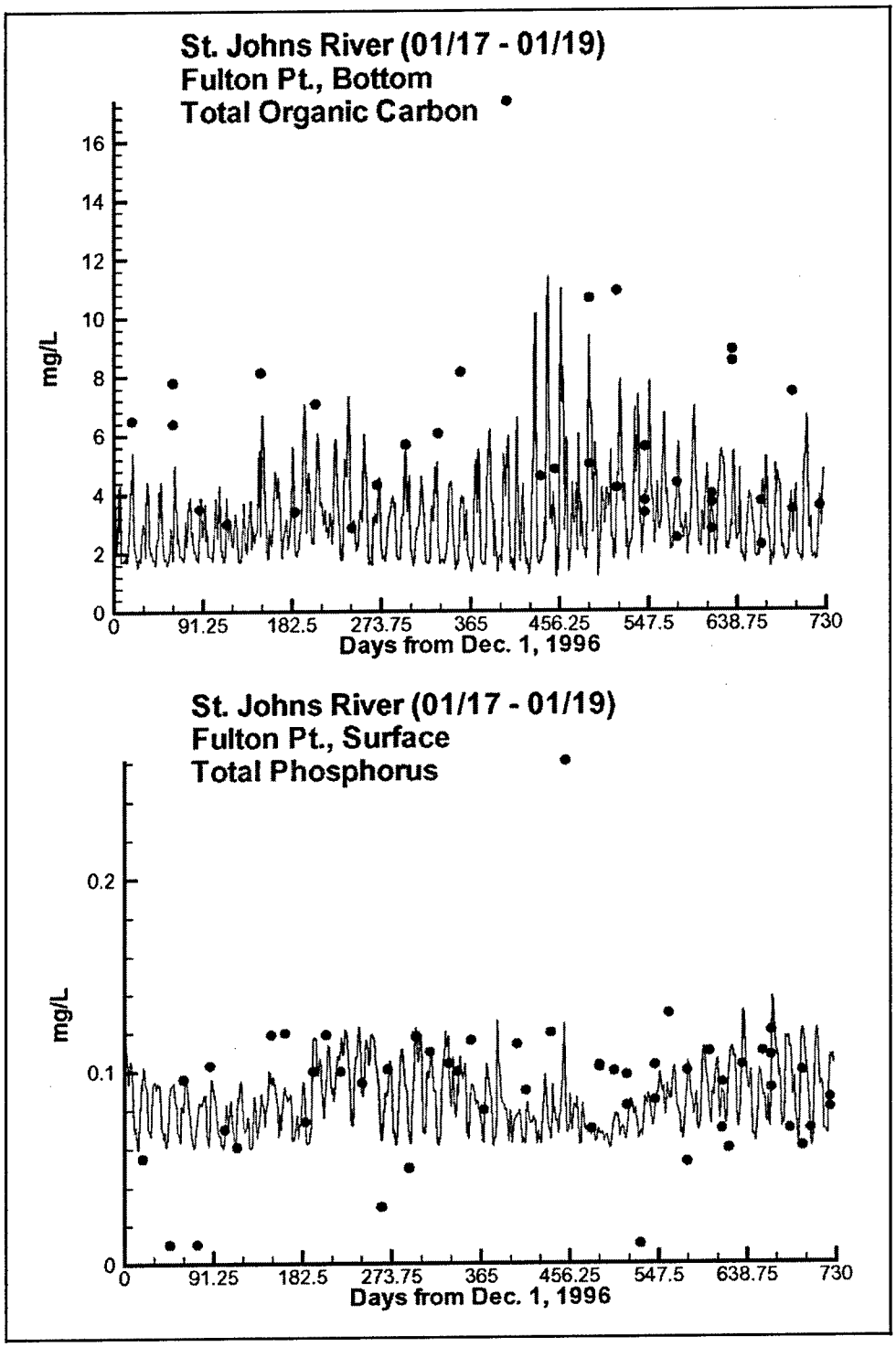

Figure 6-2. (Sheet 17 of 20)

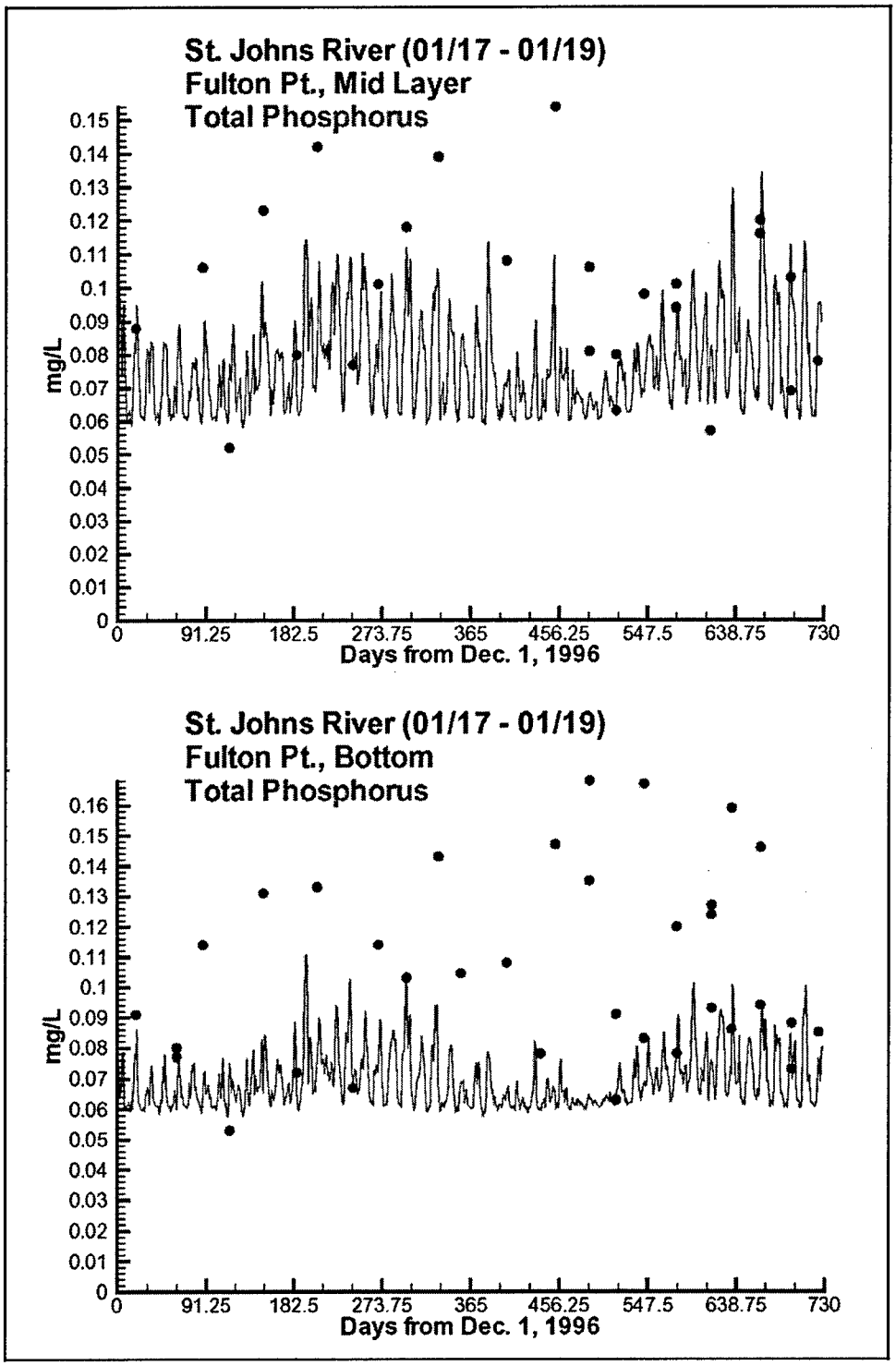

Figure 6-2. (Sheet 18 of 20)

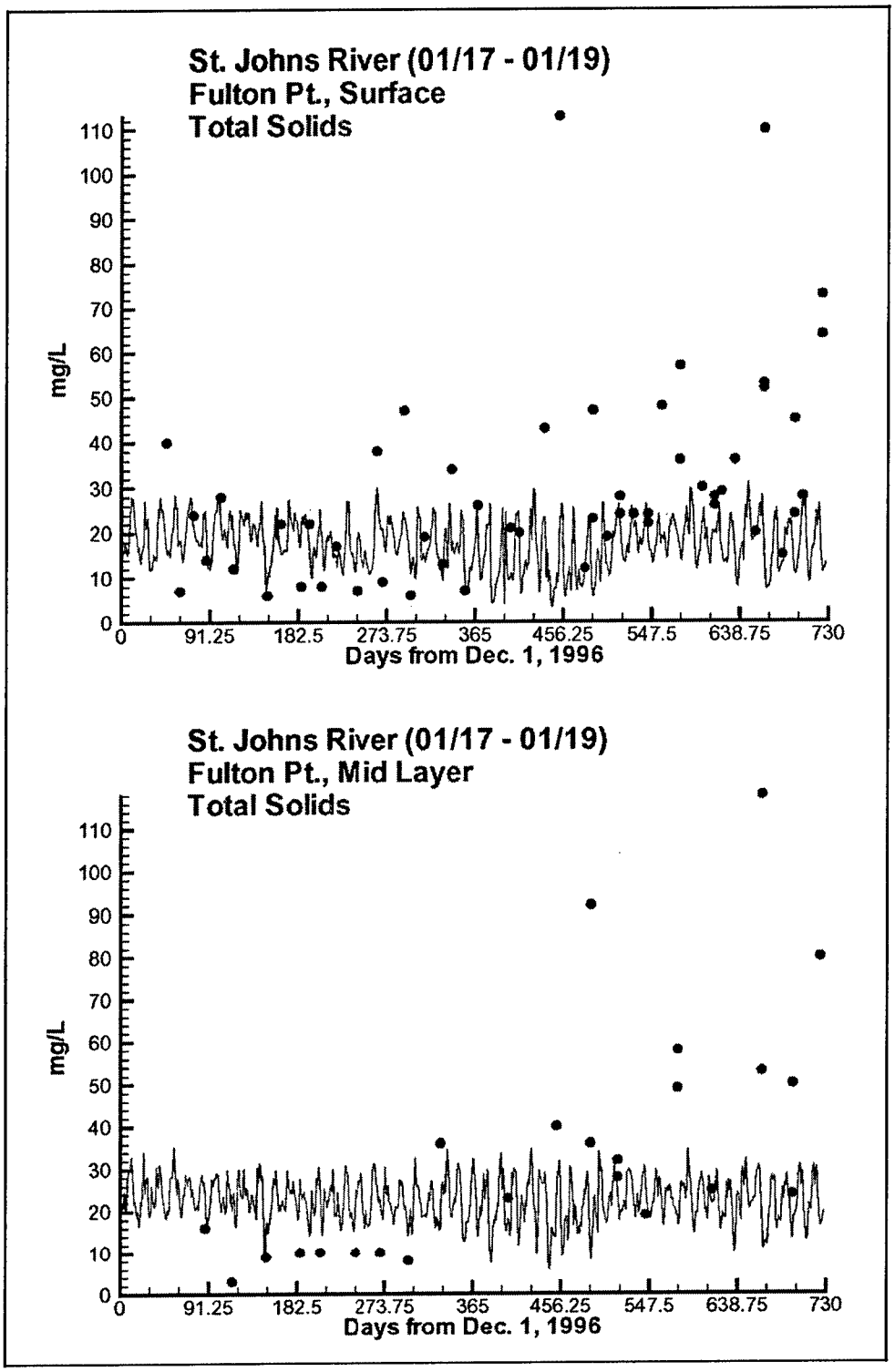

Figure 6-2. (Sheet 19 of 20)

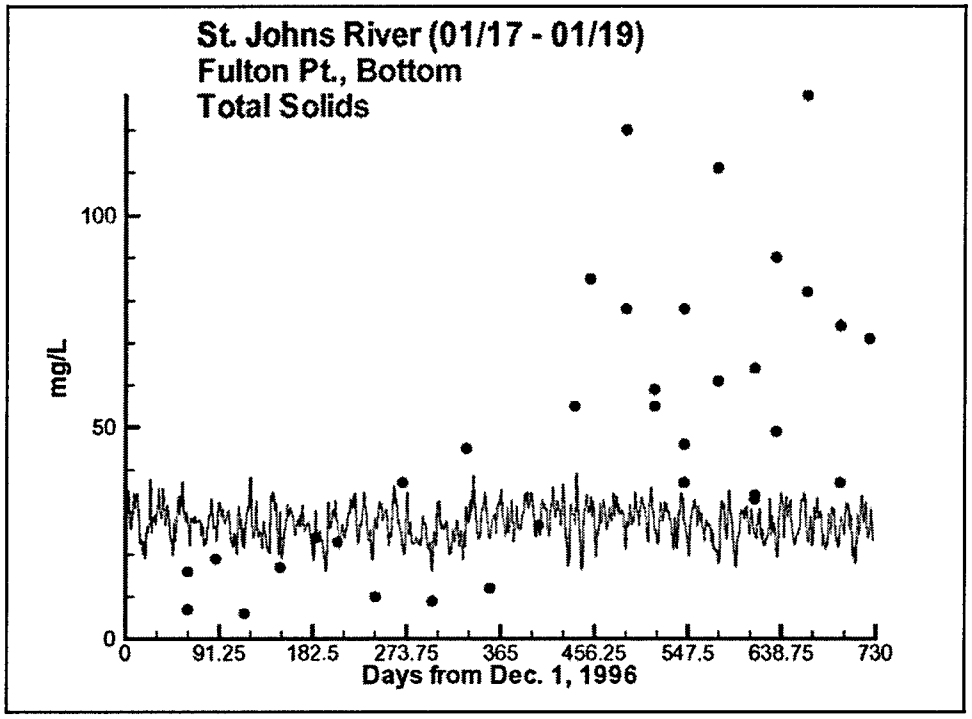

Figure 6-2. (Sheet 20 of 20)

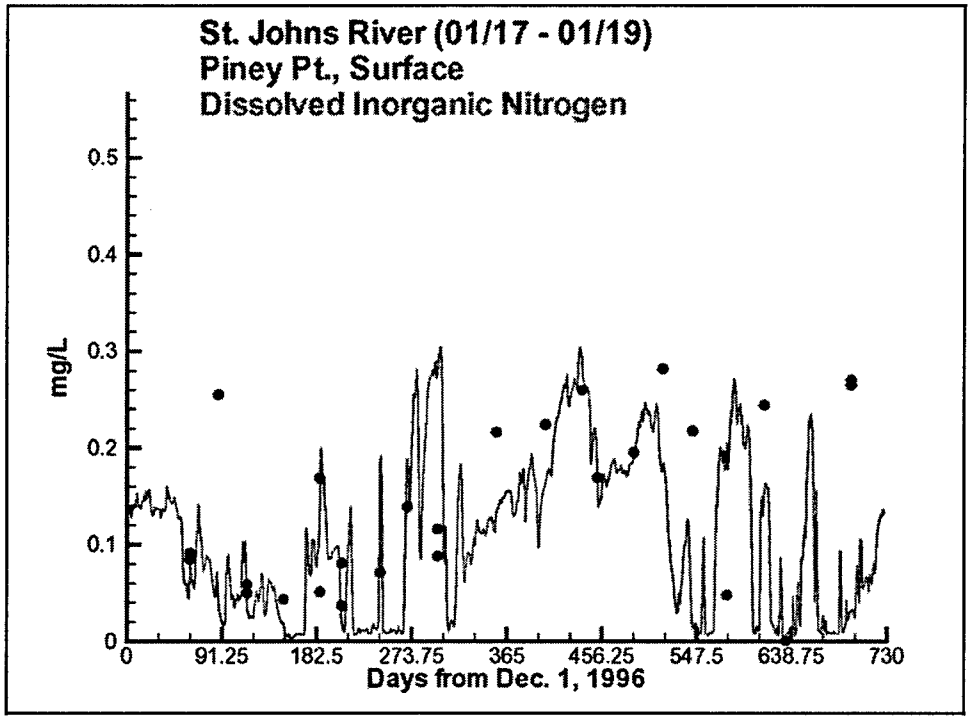

Figure 6-3. Time-series plots at Piney Point for top and middle layers for all water quality constituents (Sheet 1 of 14)

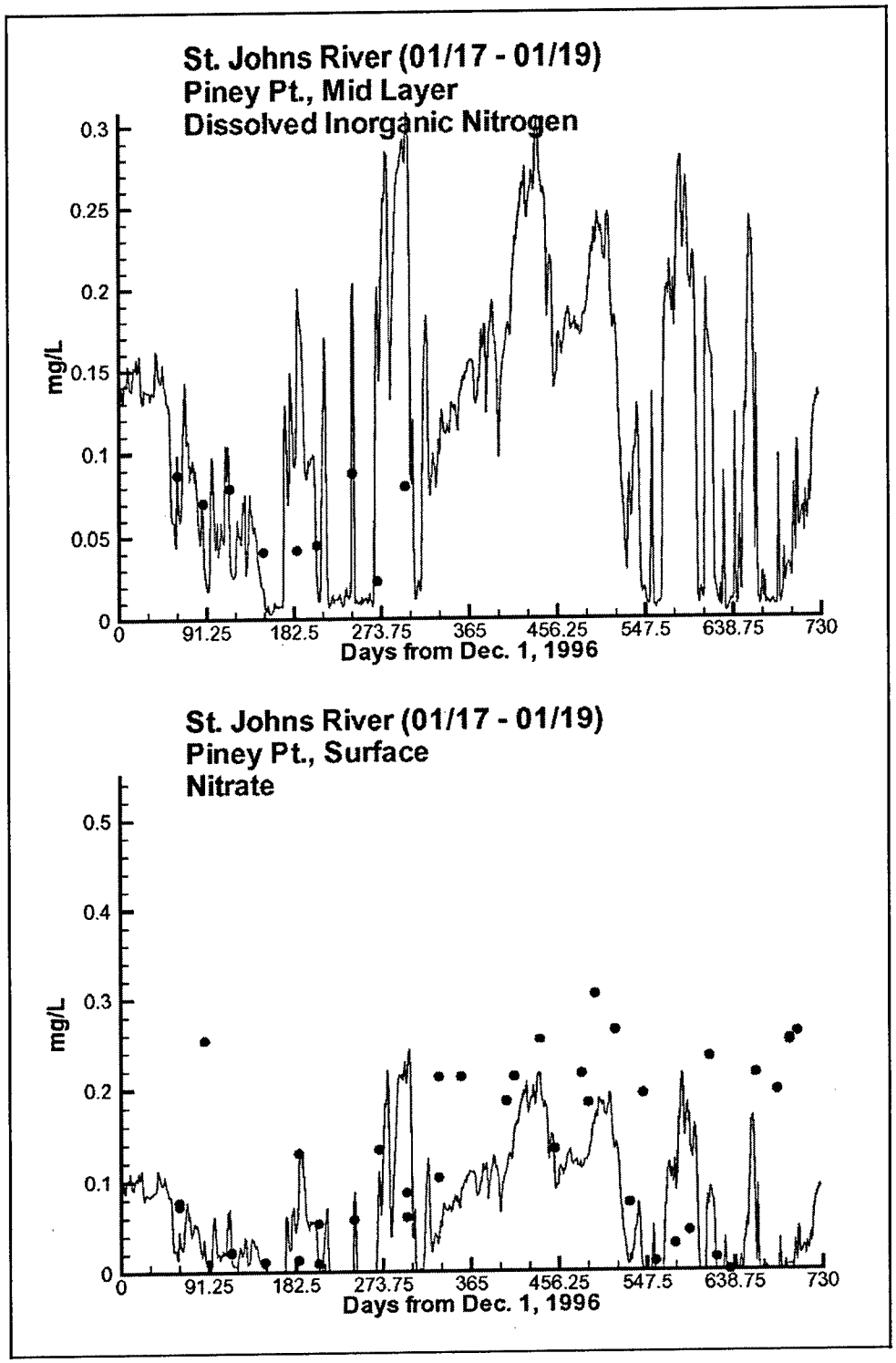

Figure 6-3. (Sheet 2 of 14)

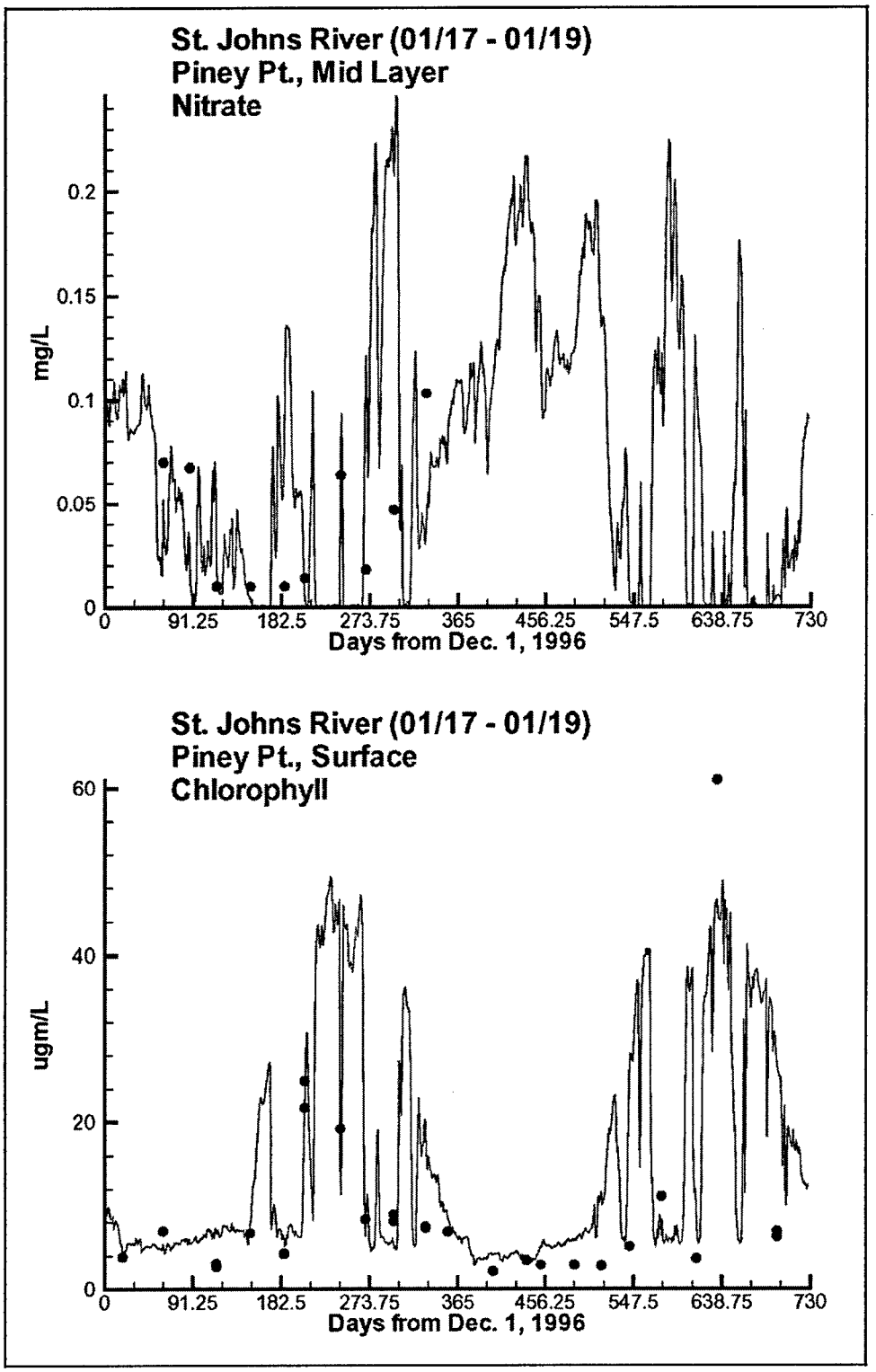

Figure 6-3. (Sheet 3 of 14)

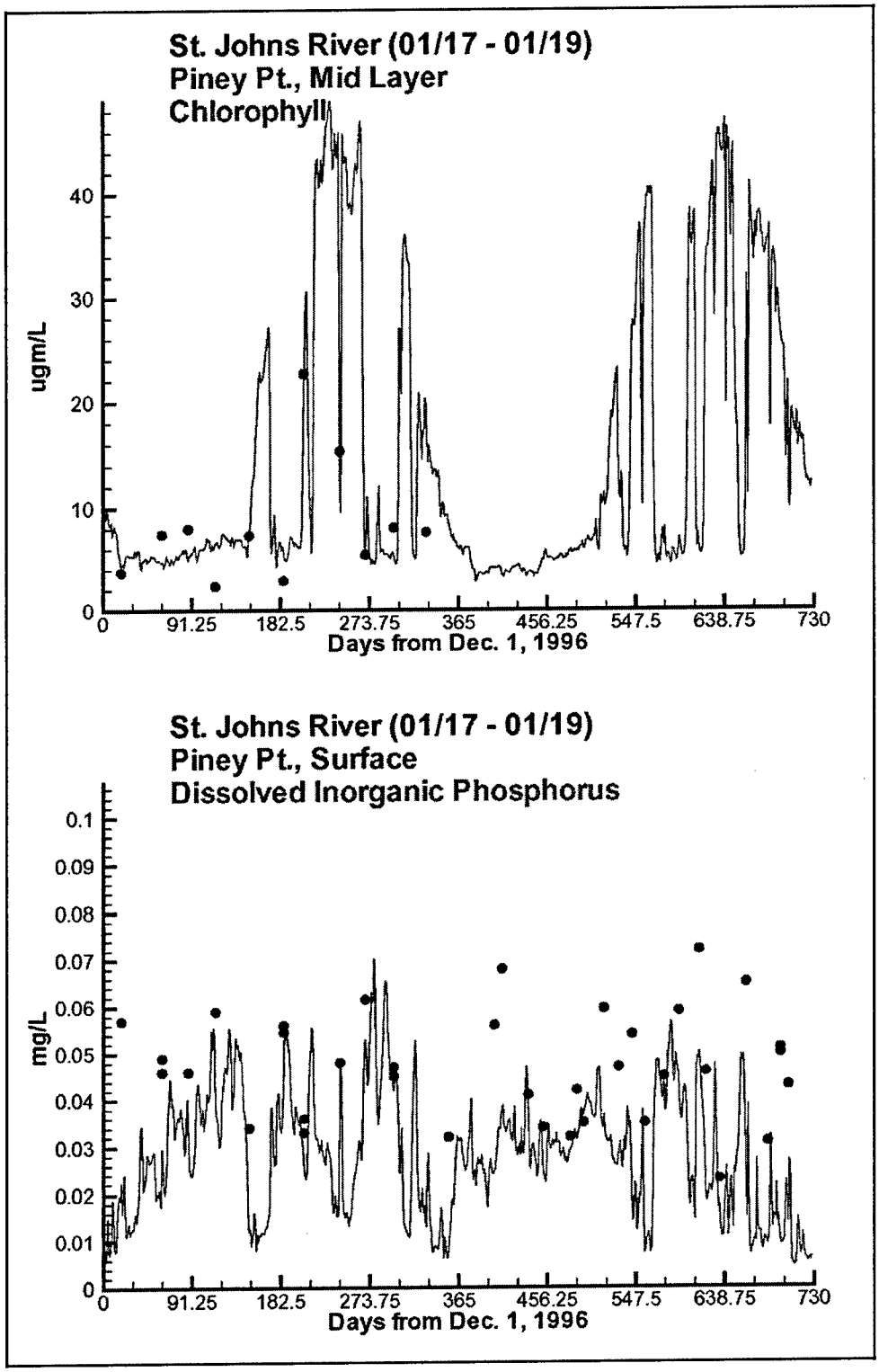

Figure 6-3. (Sheet 4 of 14)

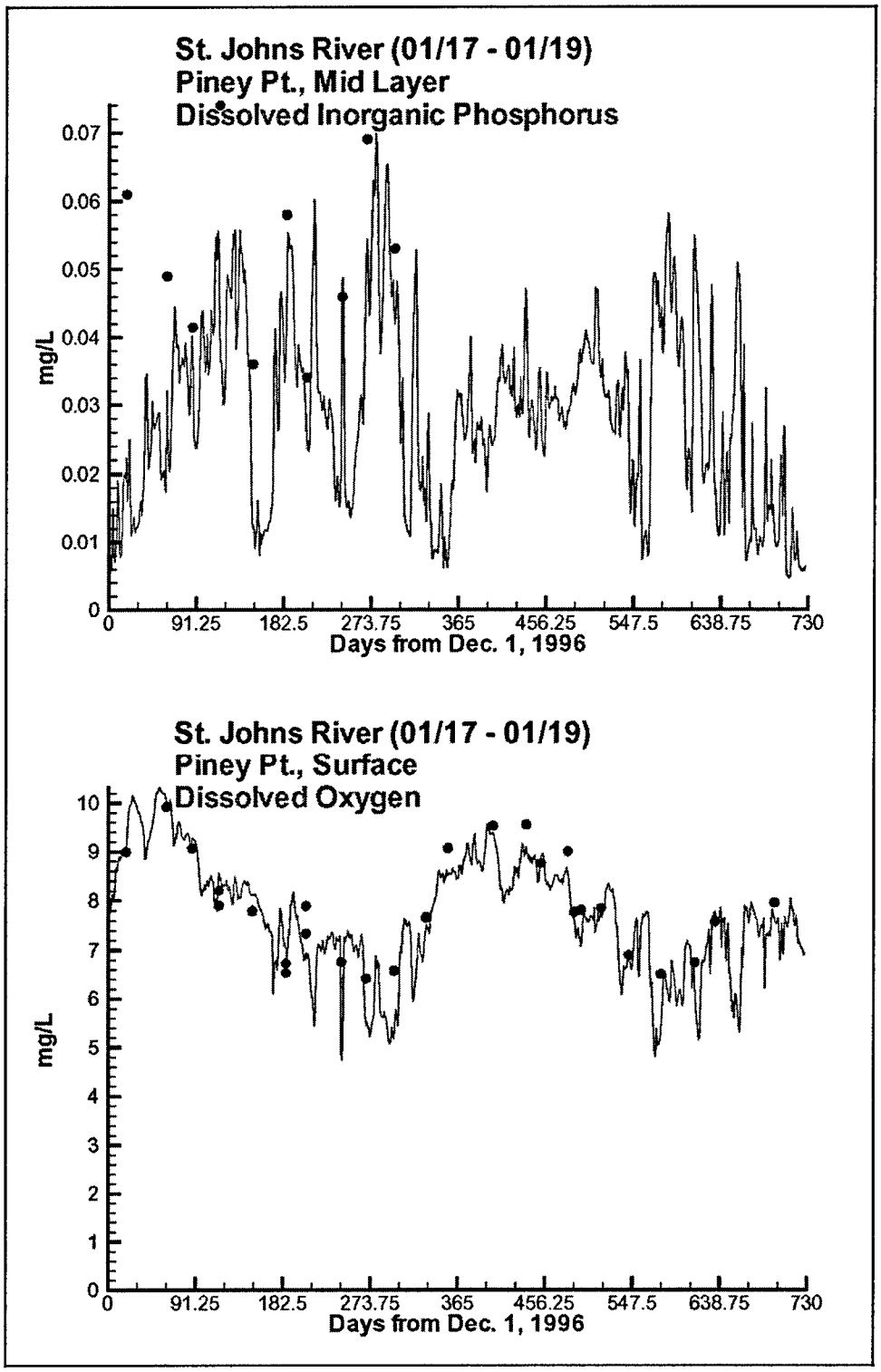

Figure 6-3. (Sheet 5 of 14)

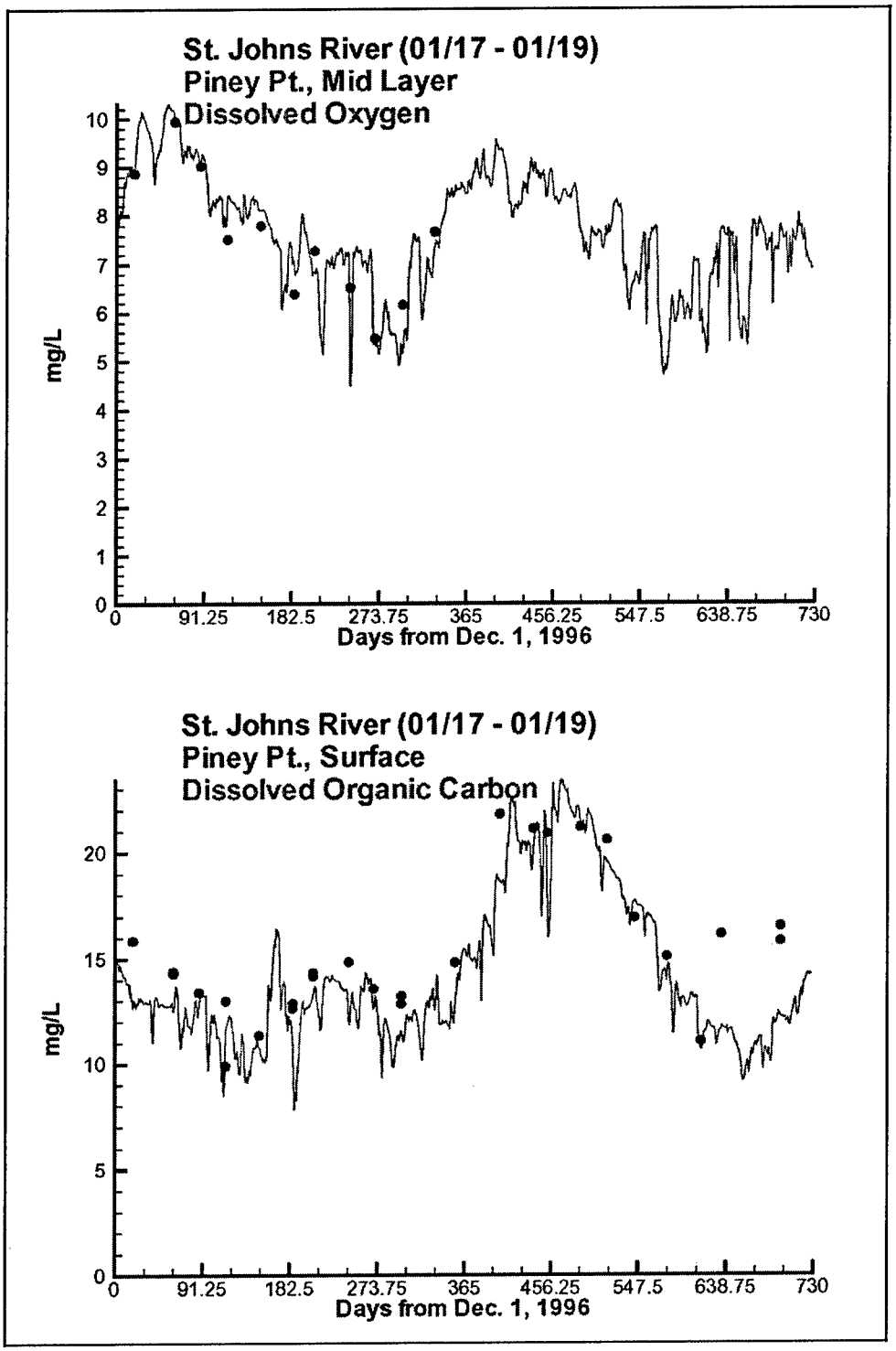

Figure 6-3. (Sheet 6 of 14)

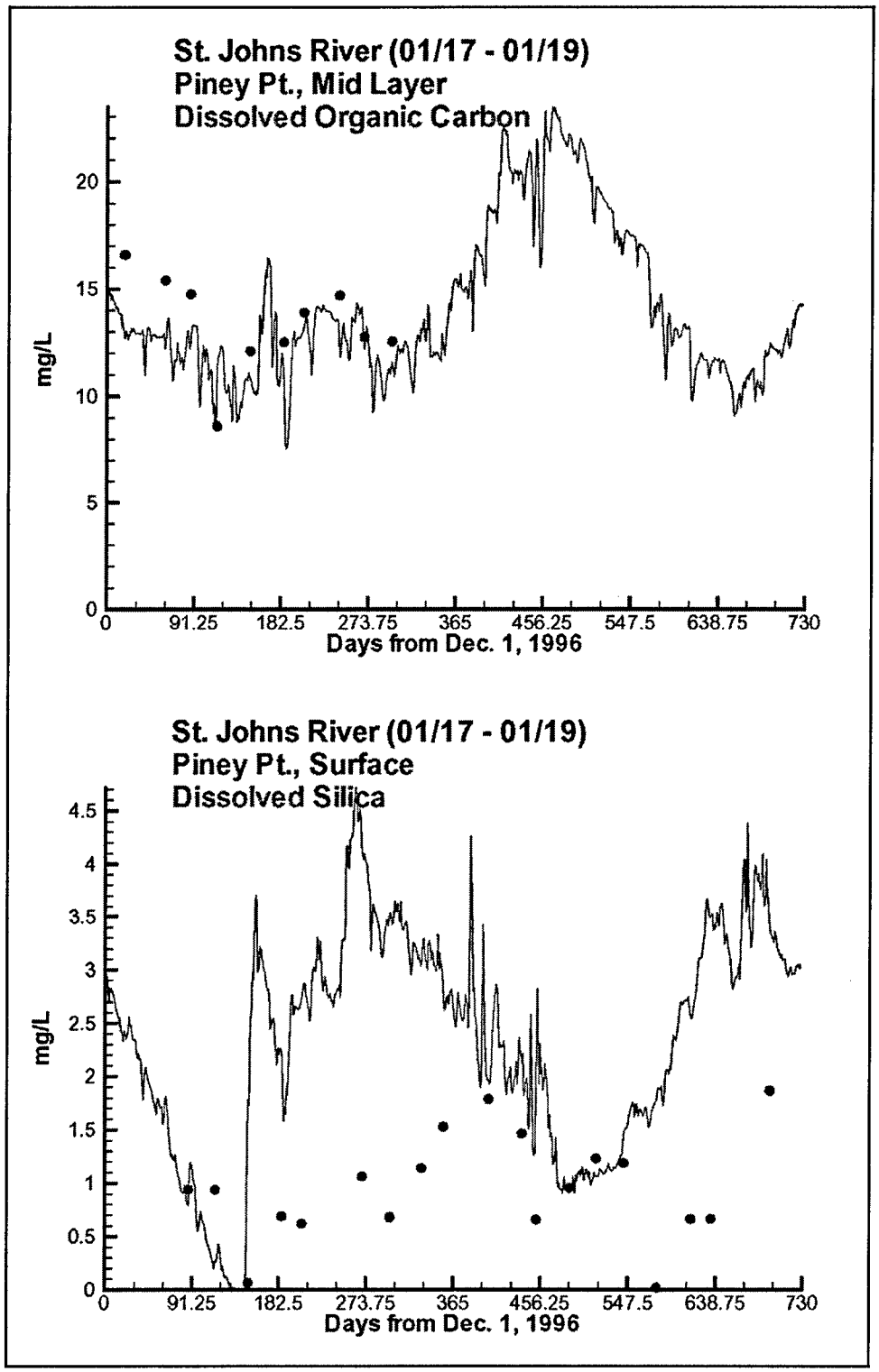

Figure 6-3. (Sheet 7 of 14)

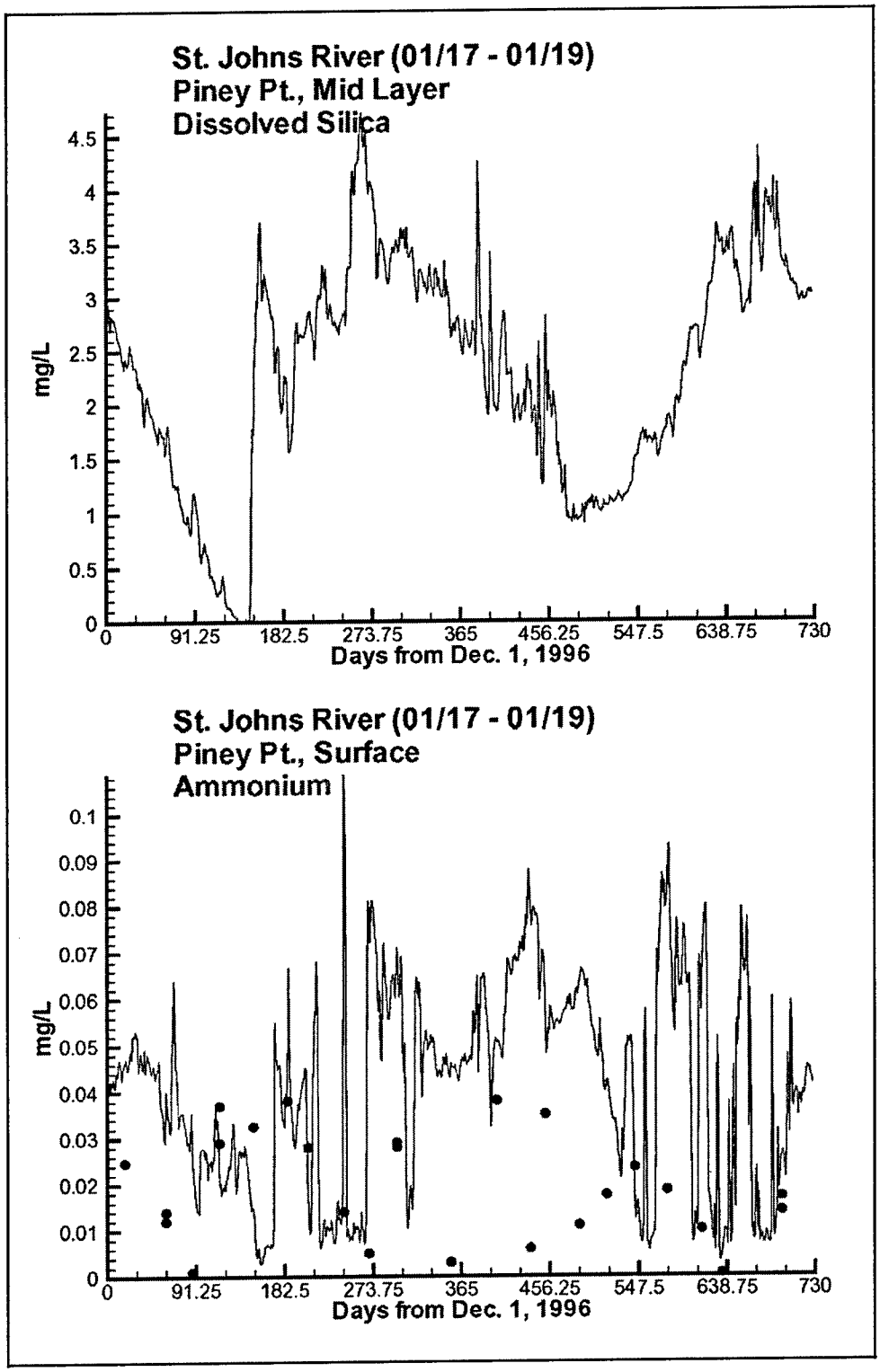

Figure 6-3. (Sheet 8 of 14)

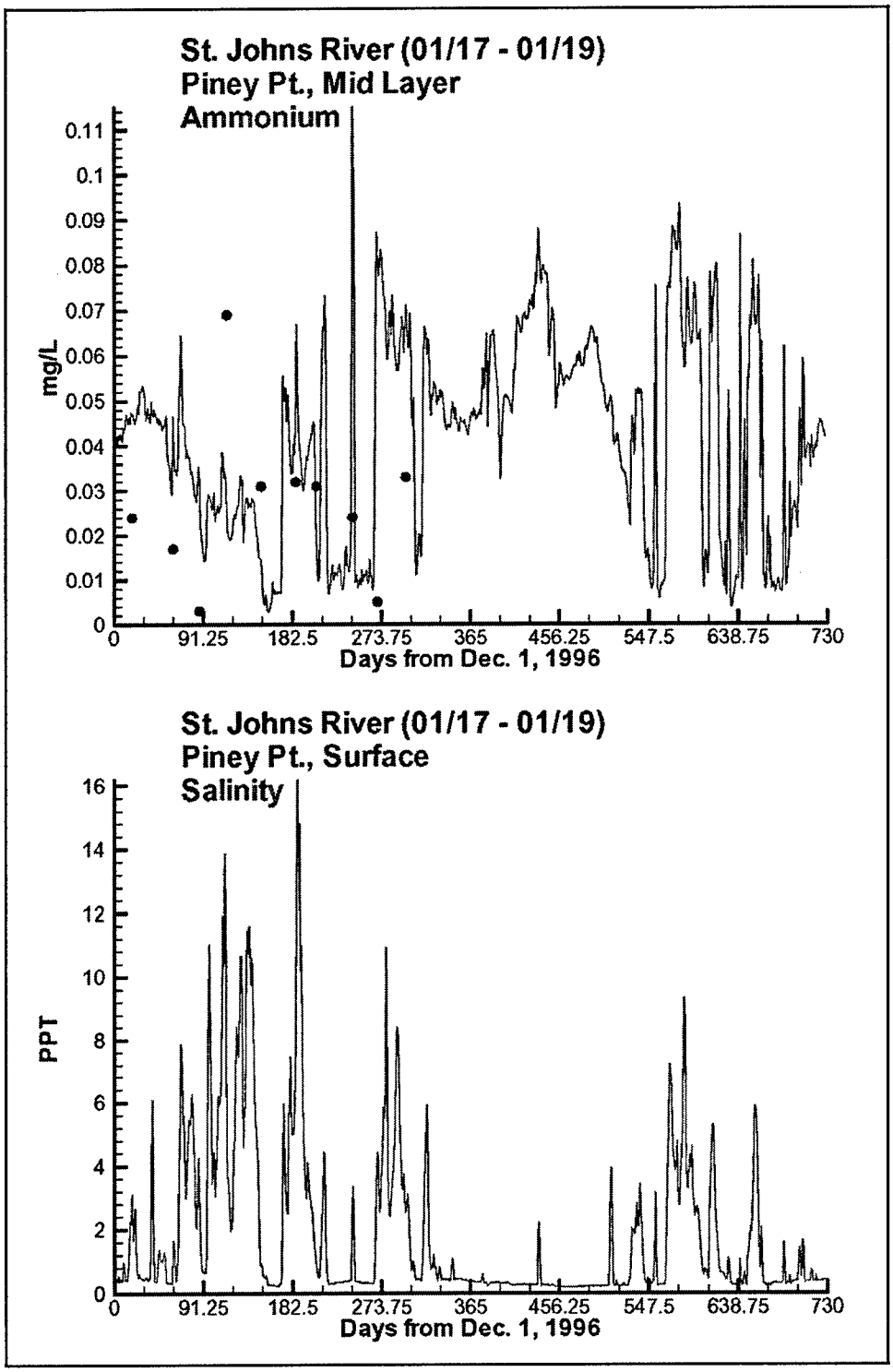

Figure 6-3. (Sheet 9 of 14)

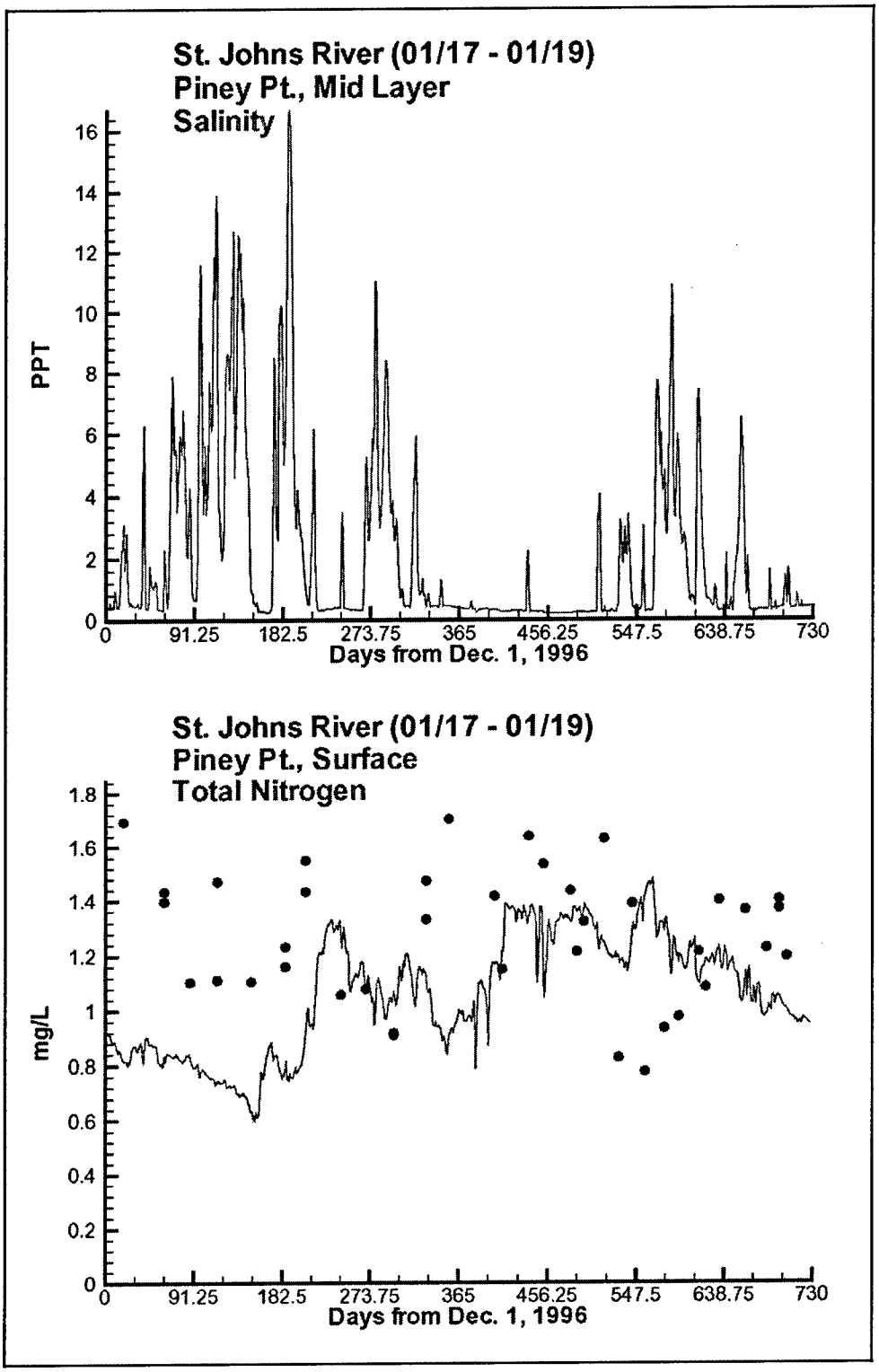

Figure 6-3. (Sheet 10 of 14)

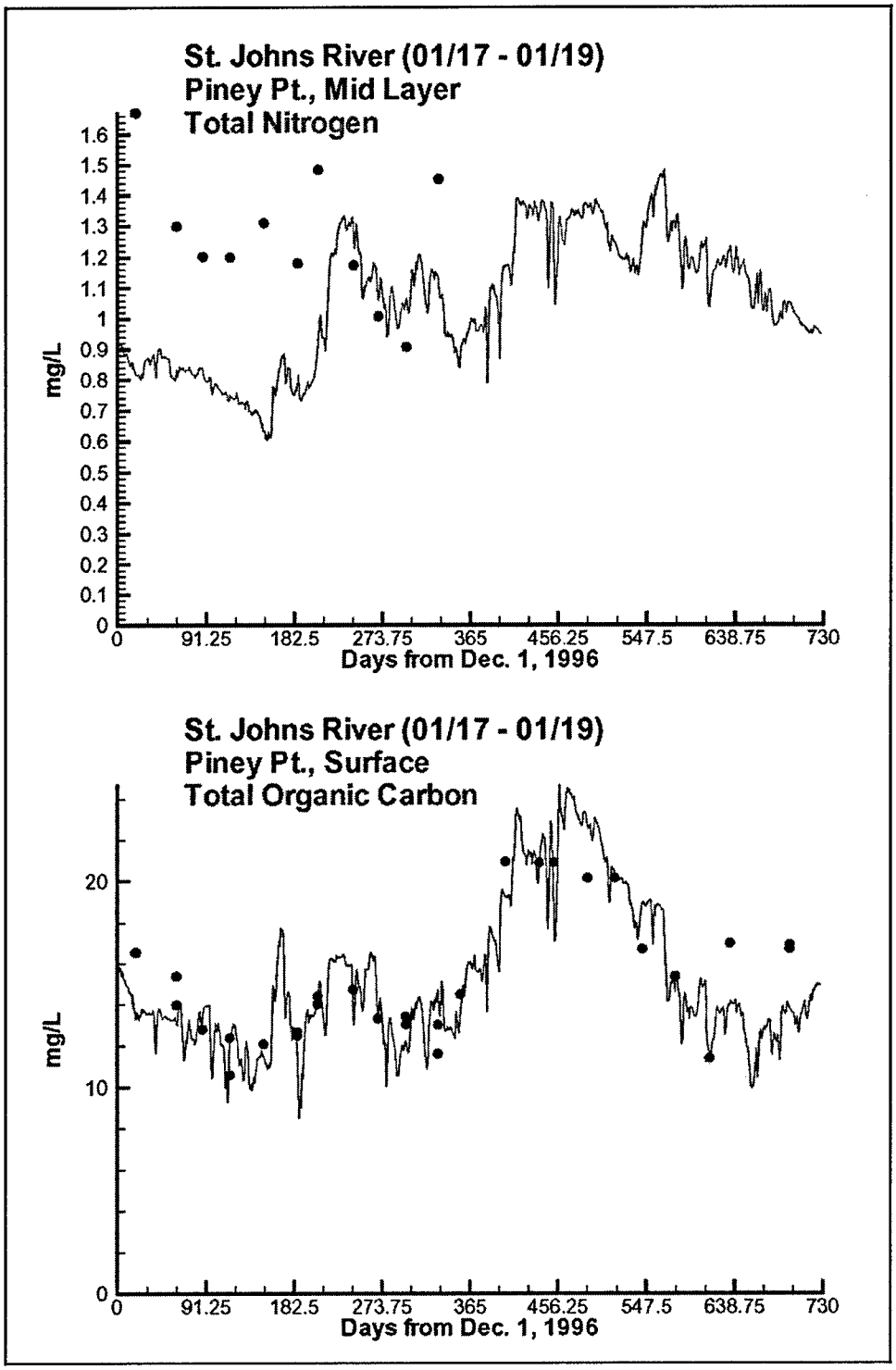

Figure 6-3. (Sheet 11 of 14)

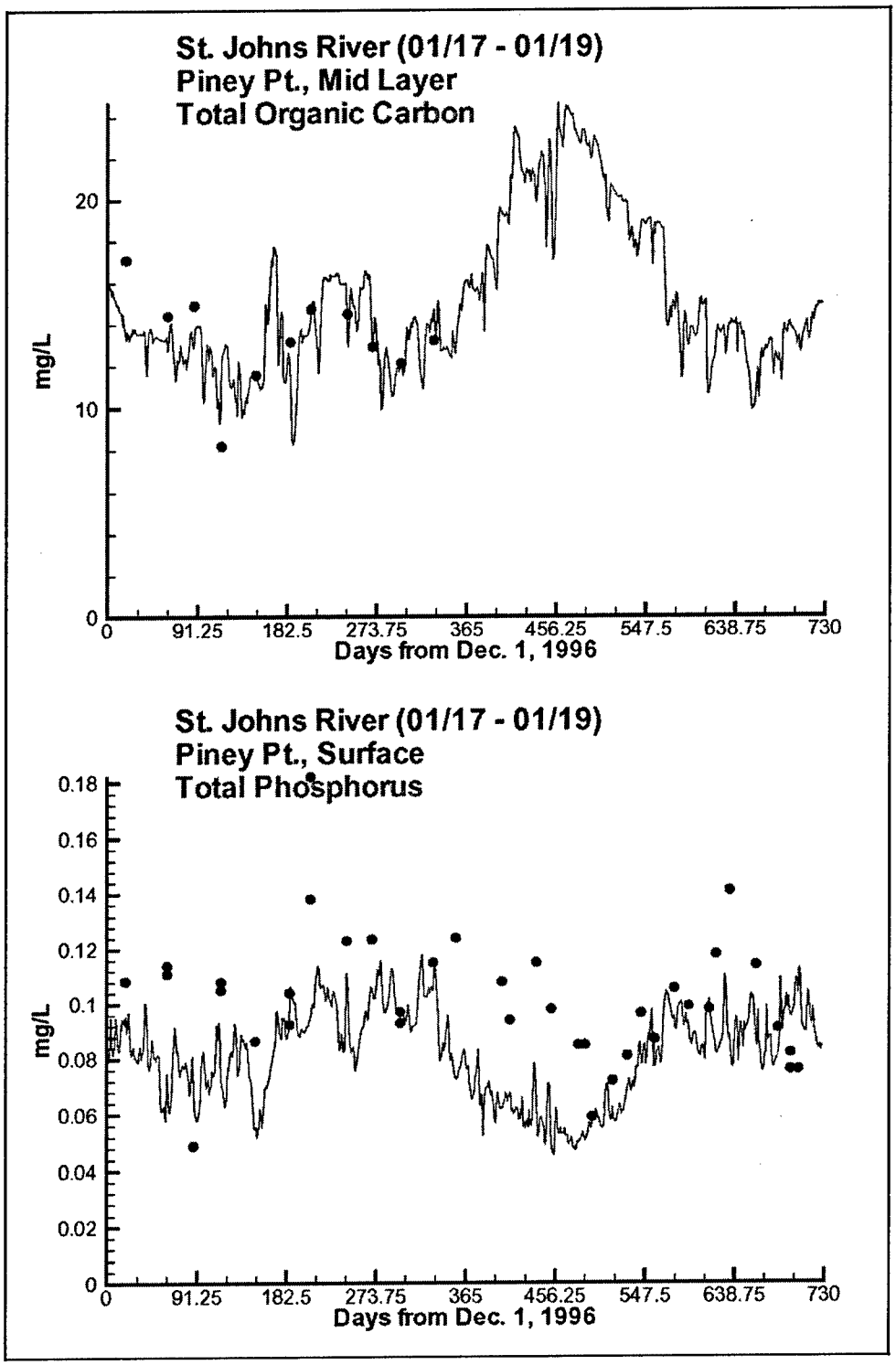

Figure 6-3. (Sheet 12 of 14)

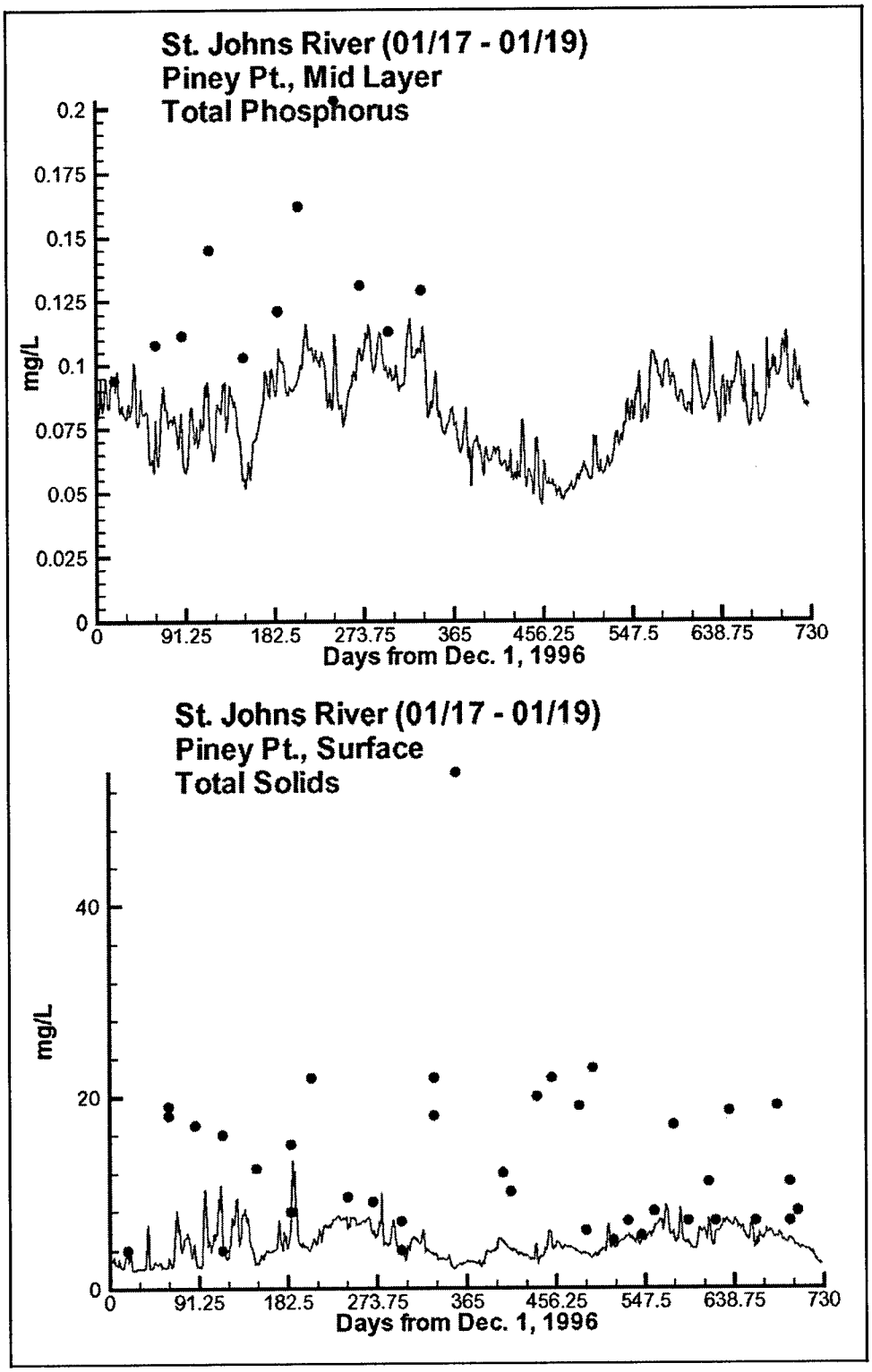

Figure 6-3. (Sheet 13 of 14)

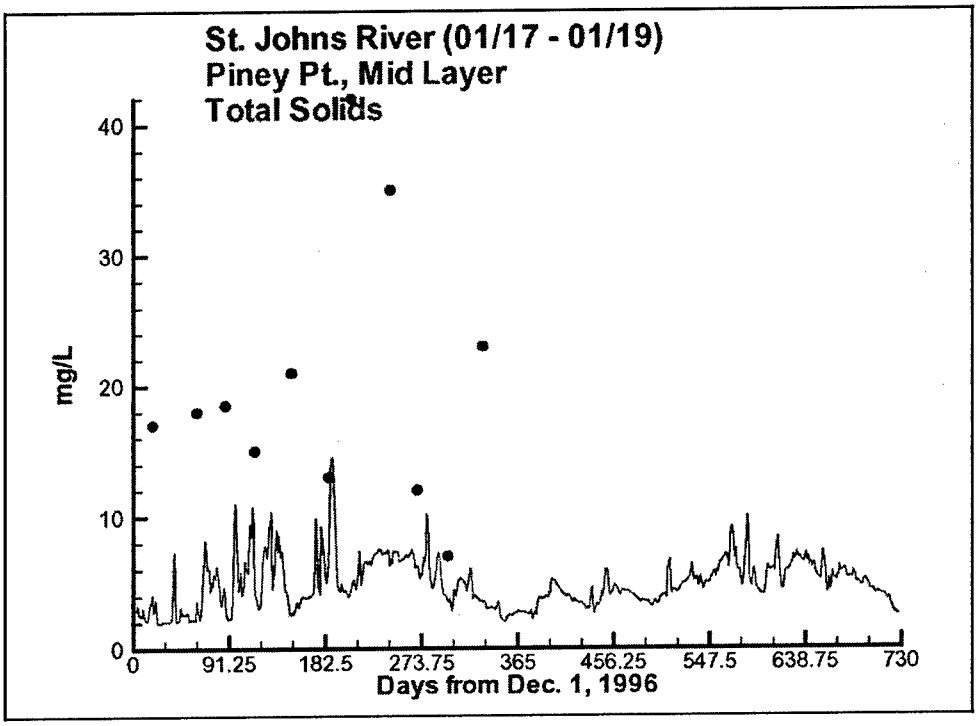

Figure 6-3. (Sheet 14 of 14)

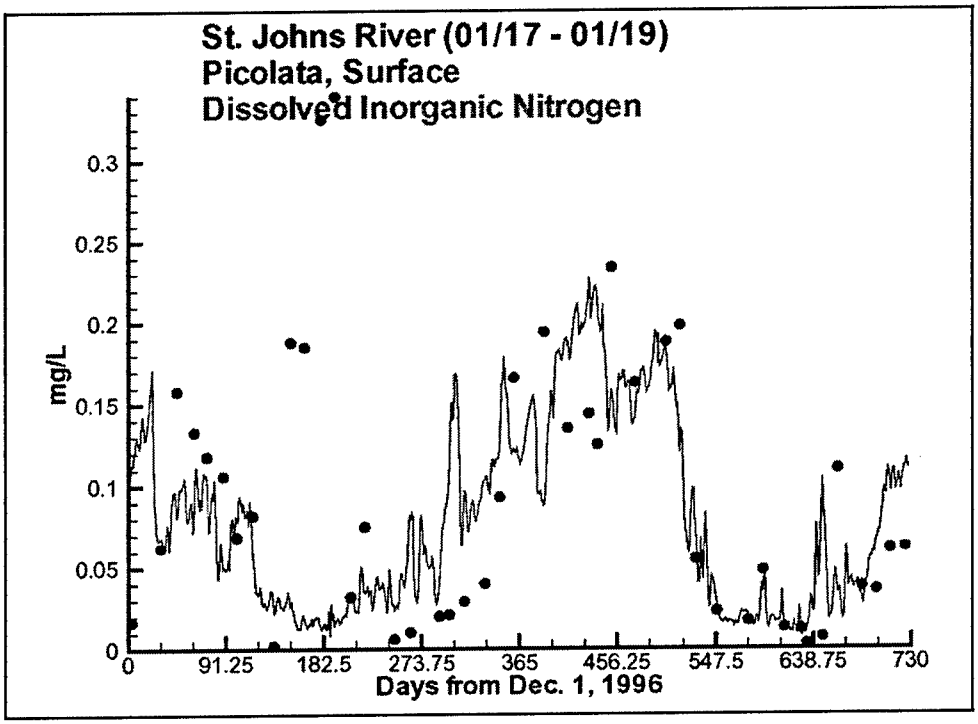

Figure 6-4. Time-series plots at Picolata for top layer for all water quality constituents (Sheet 1 of 7)

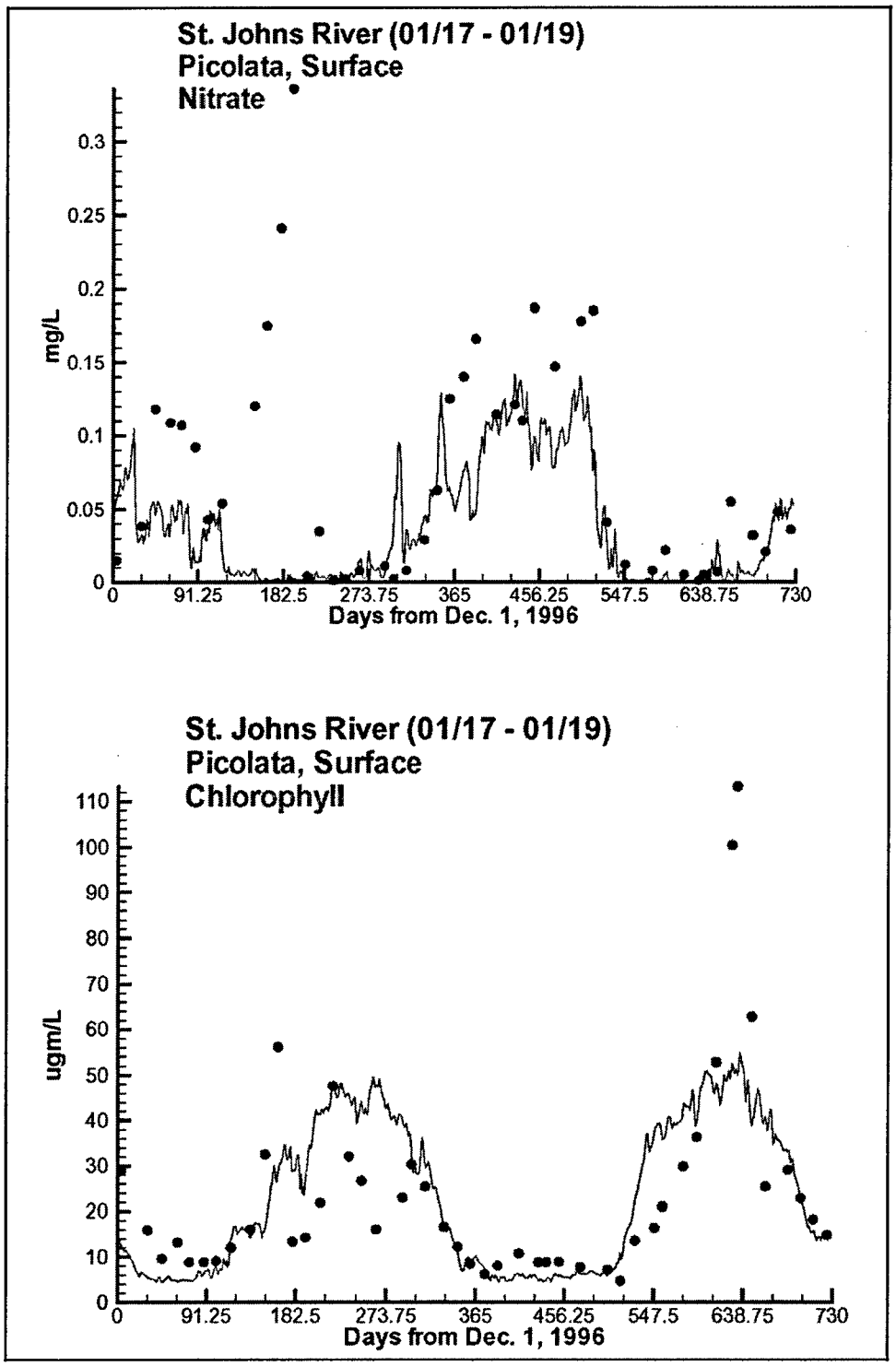

Figure 6-4. (Sheet 2 of 7)

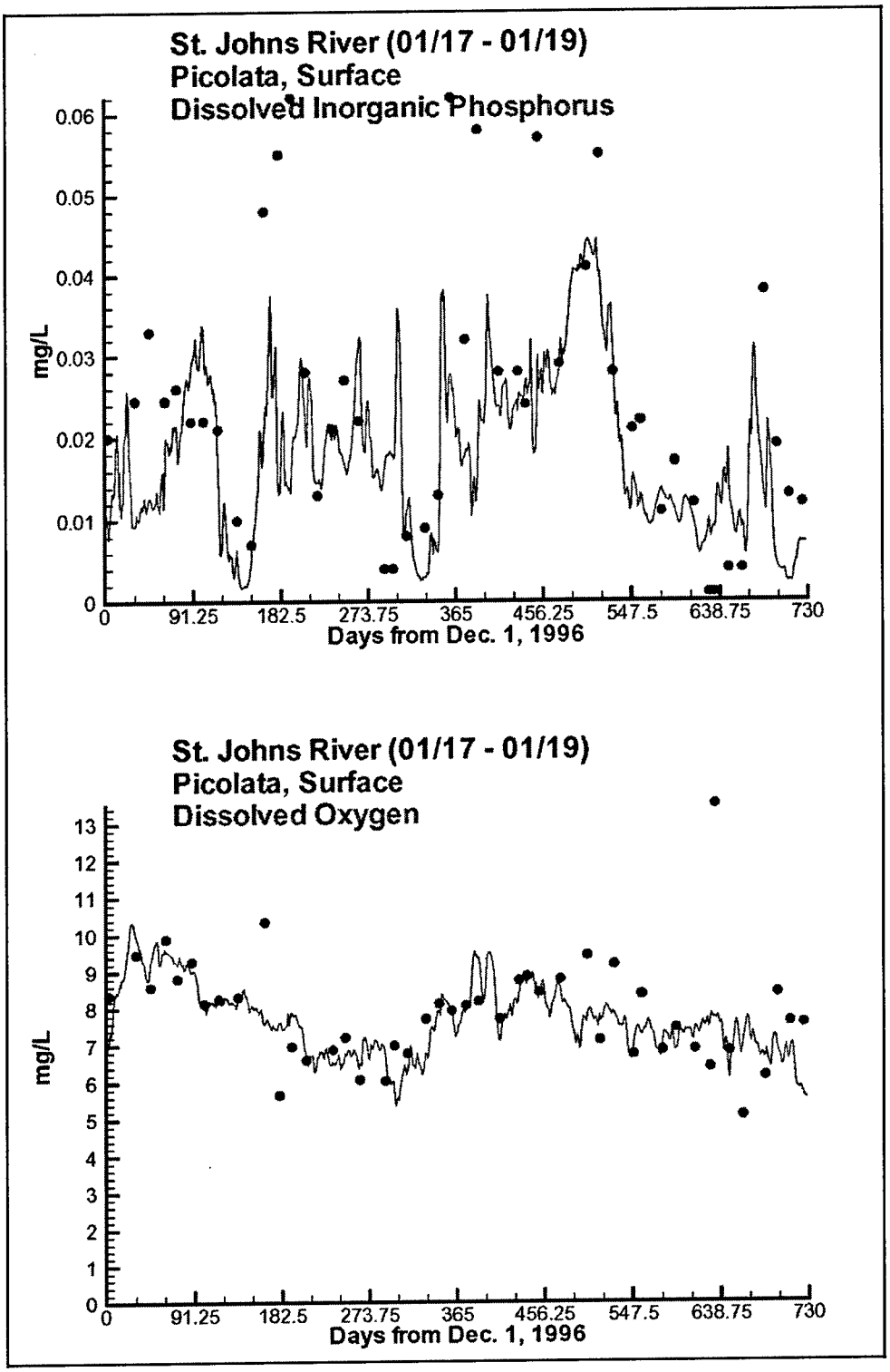

Figure 6-4. (Sheet 3 of 7)

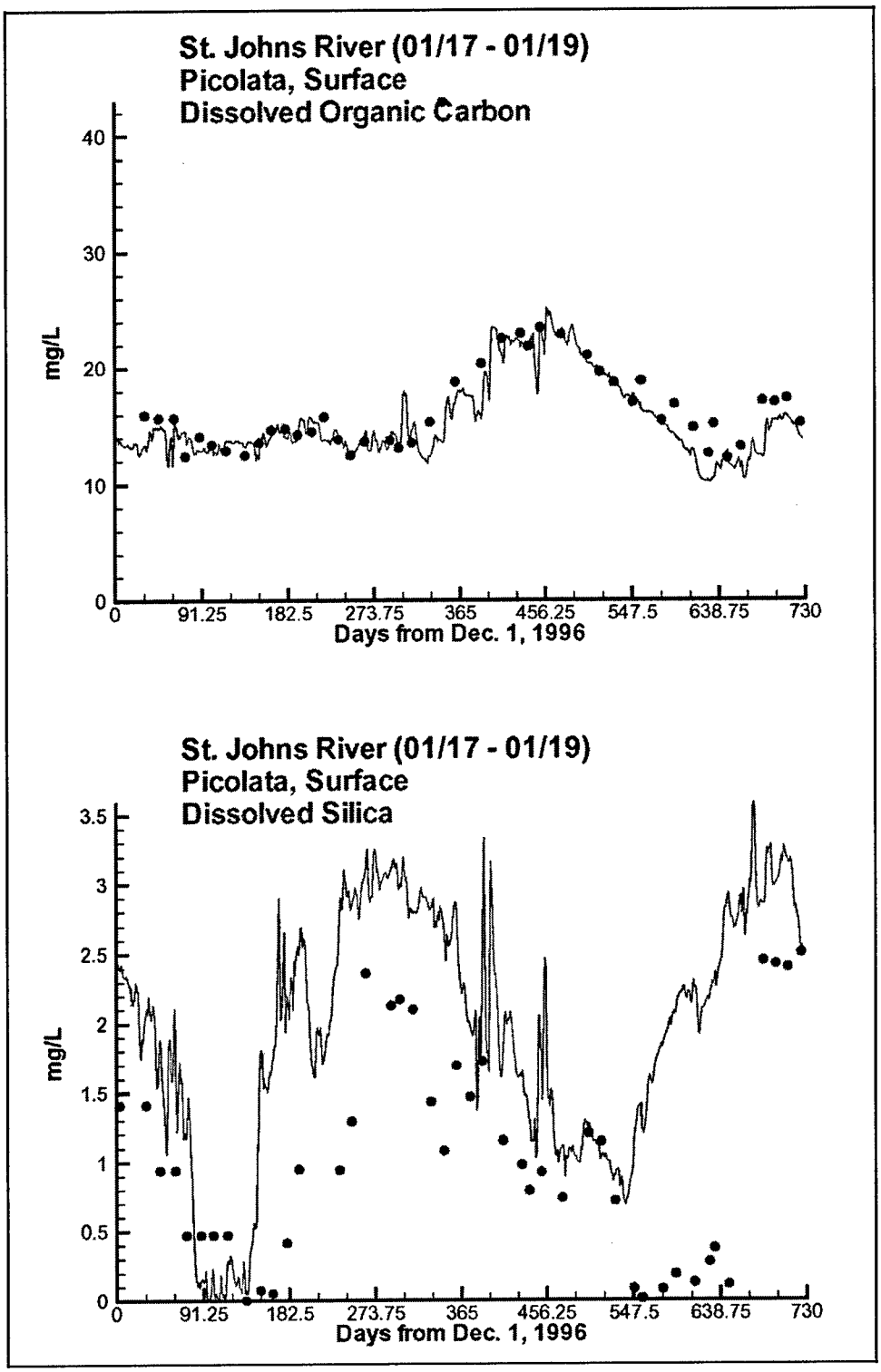

Figure 6-4. (Sheet 4 of 7)

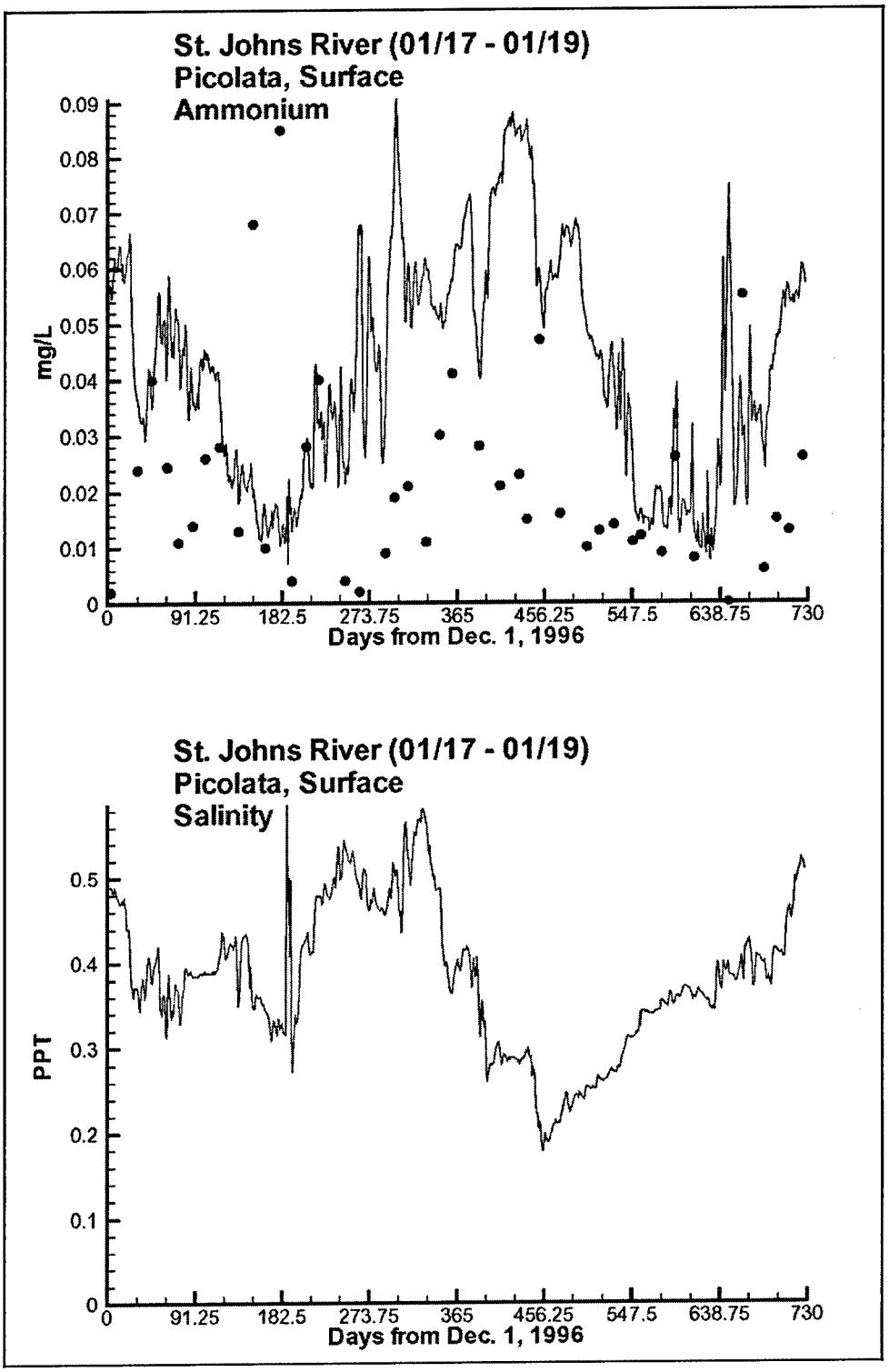

Figure 6-4. (Sheet 5 of 7)

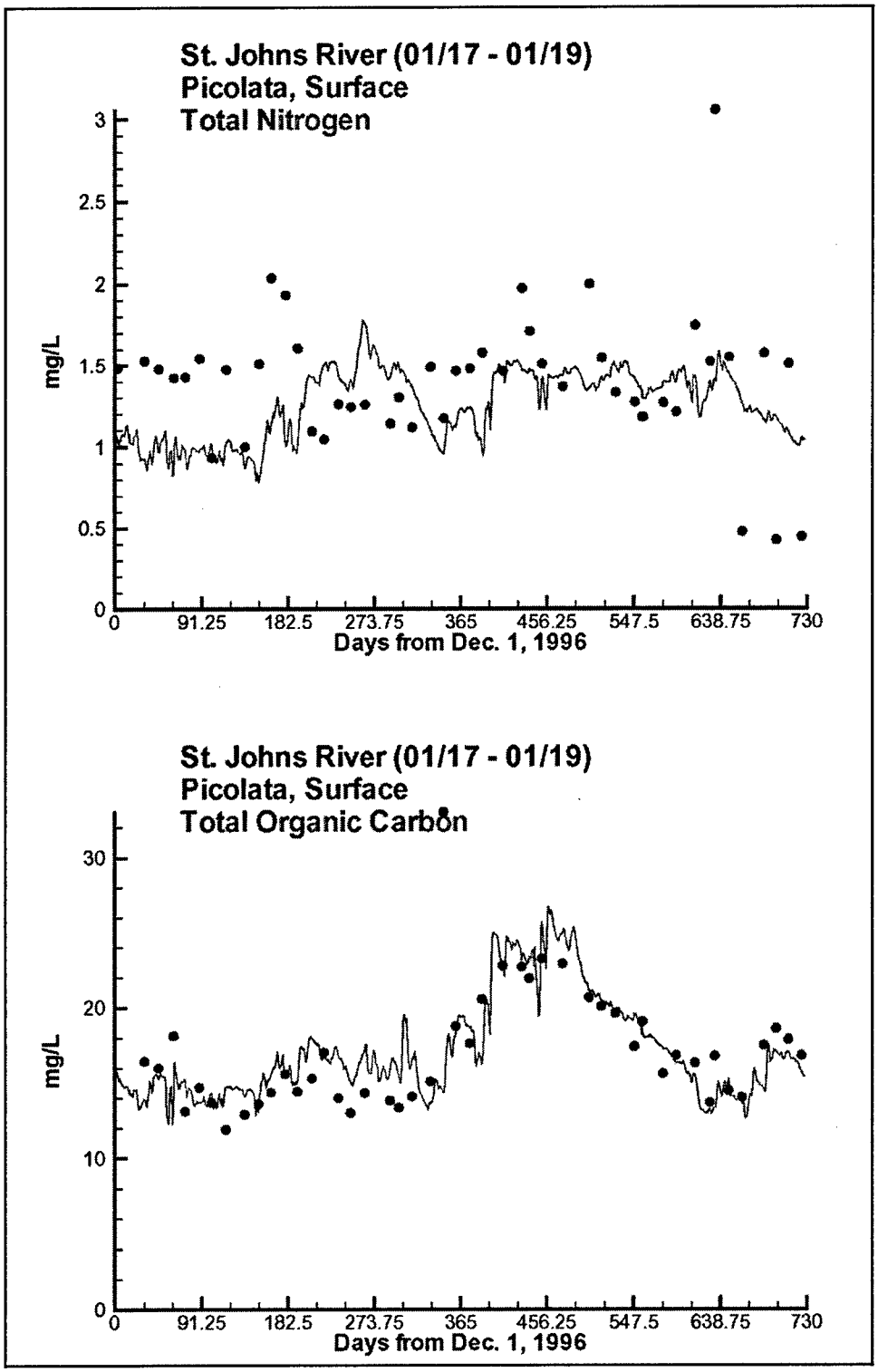

Figure 6-4. (Sheet 6 of 7)

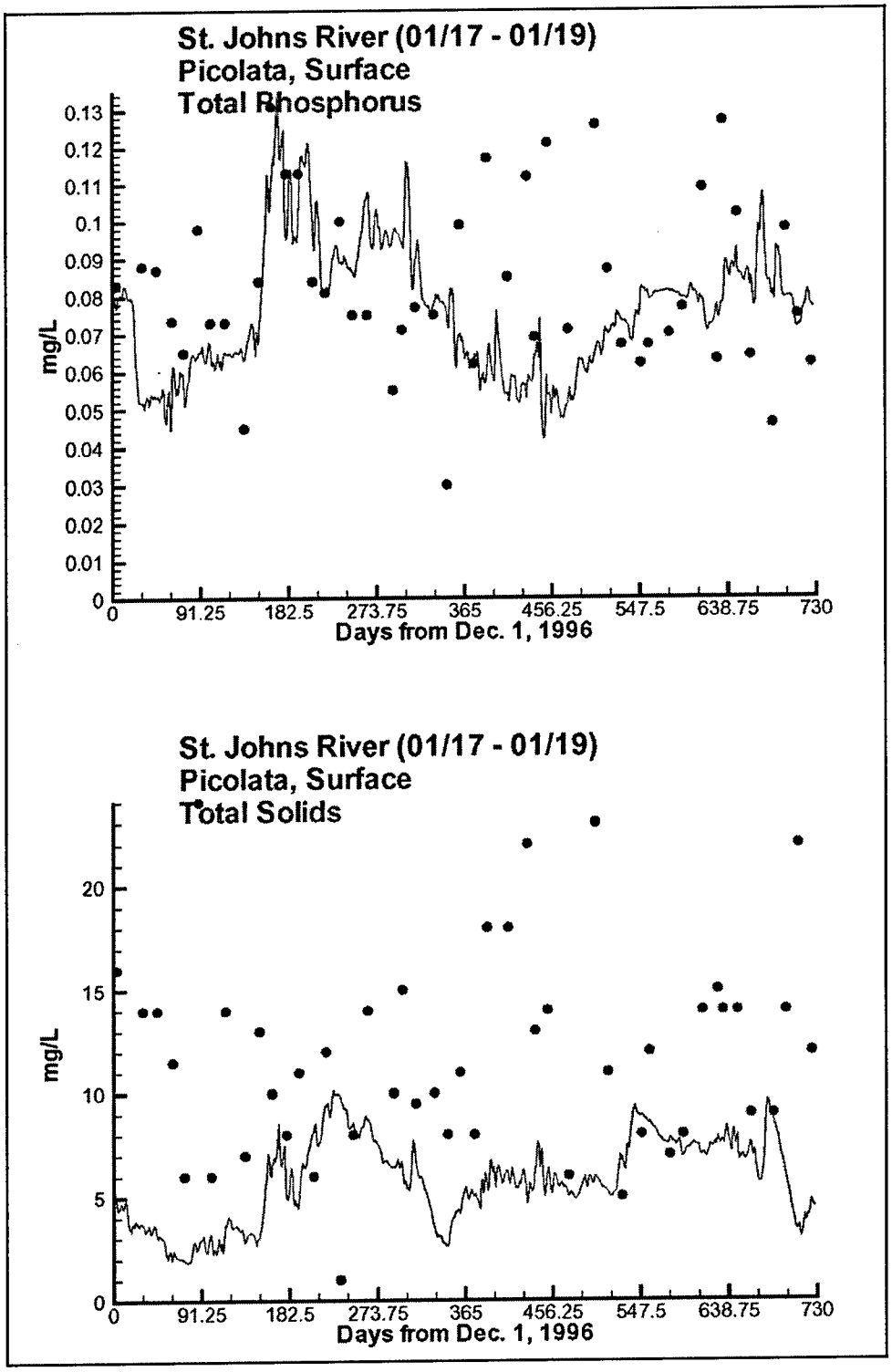

Figure 6-4. (Sheet 7 of 7)

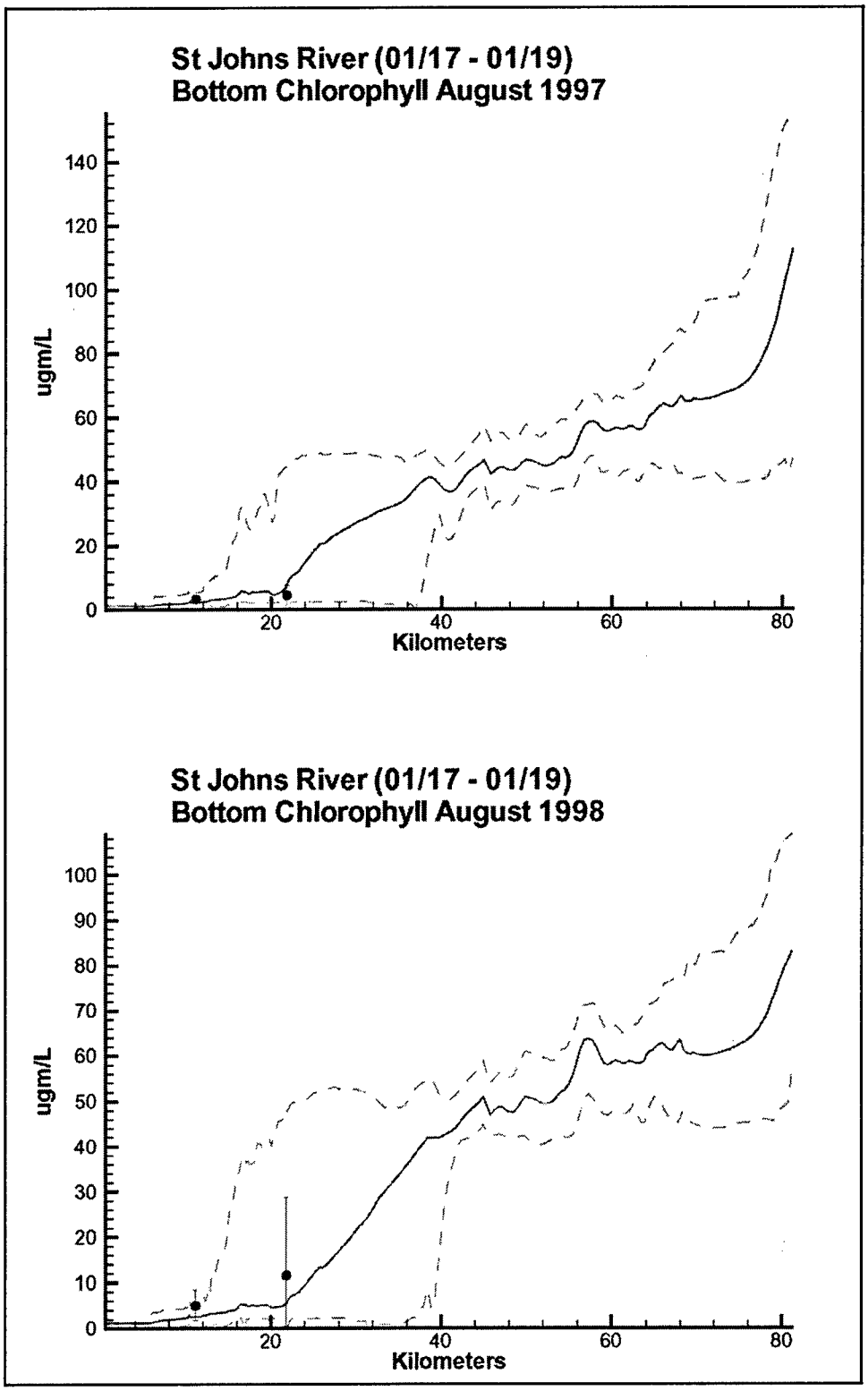

Figure 6-5. Longitudinal water quality results for August 1997 and 1998 (Sheet 1 of 15)

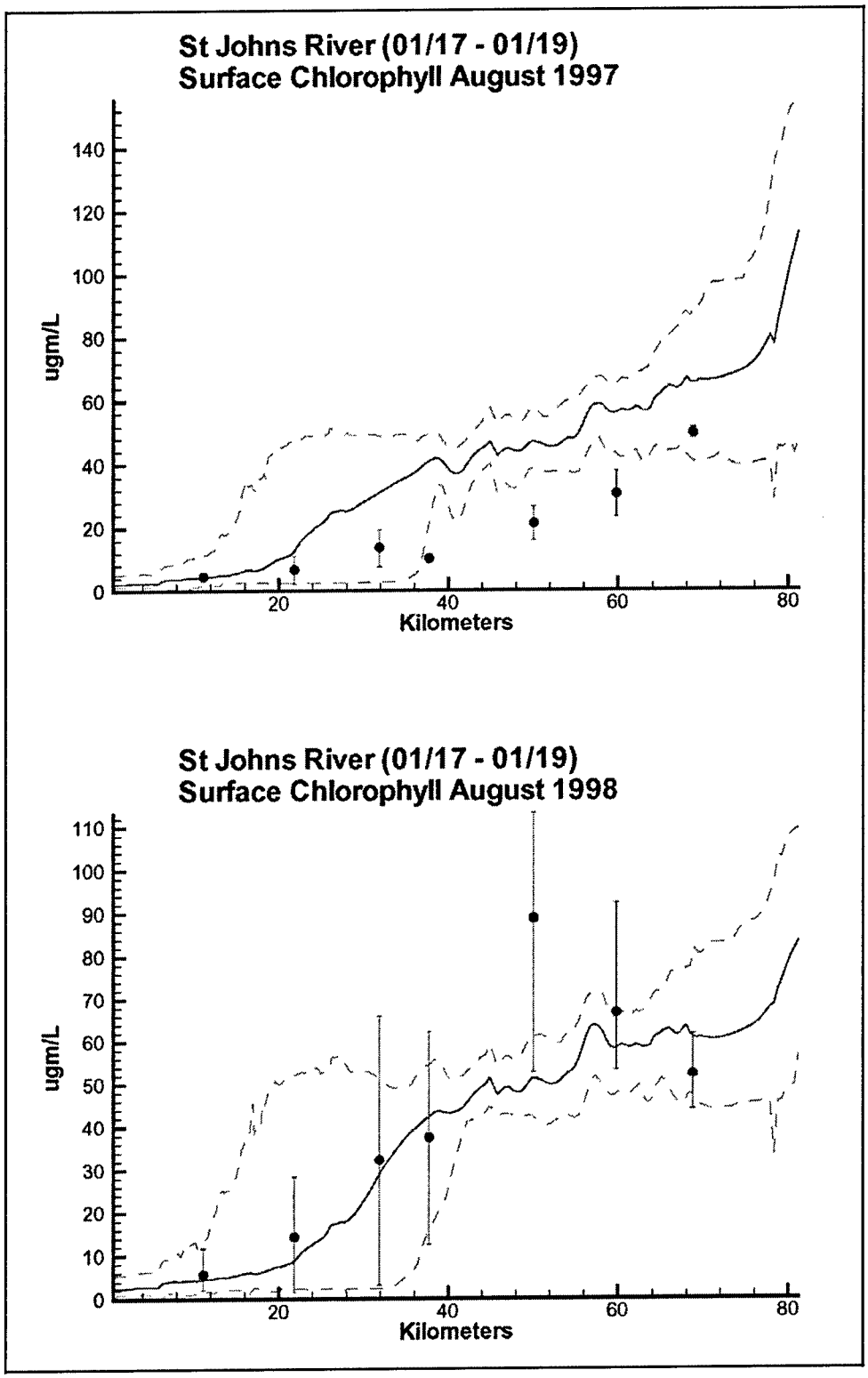

Figure 6-5. (Sheet 2 of 15)

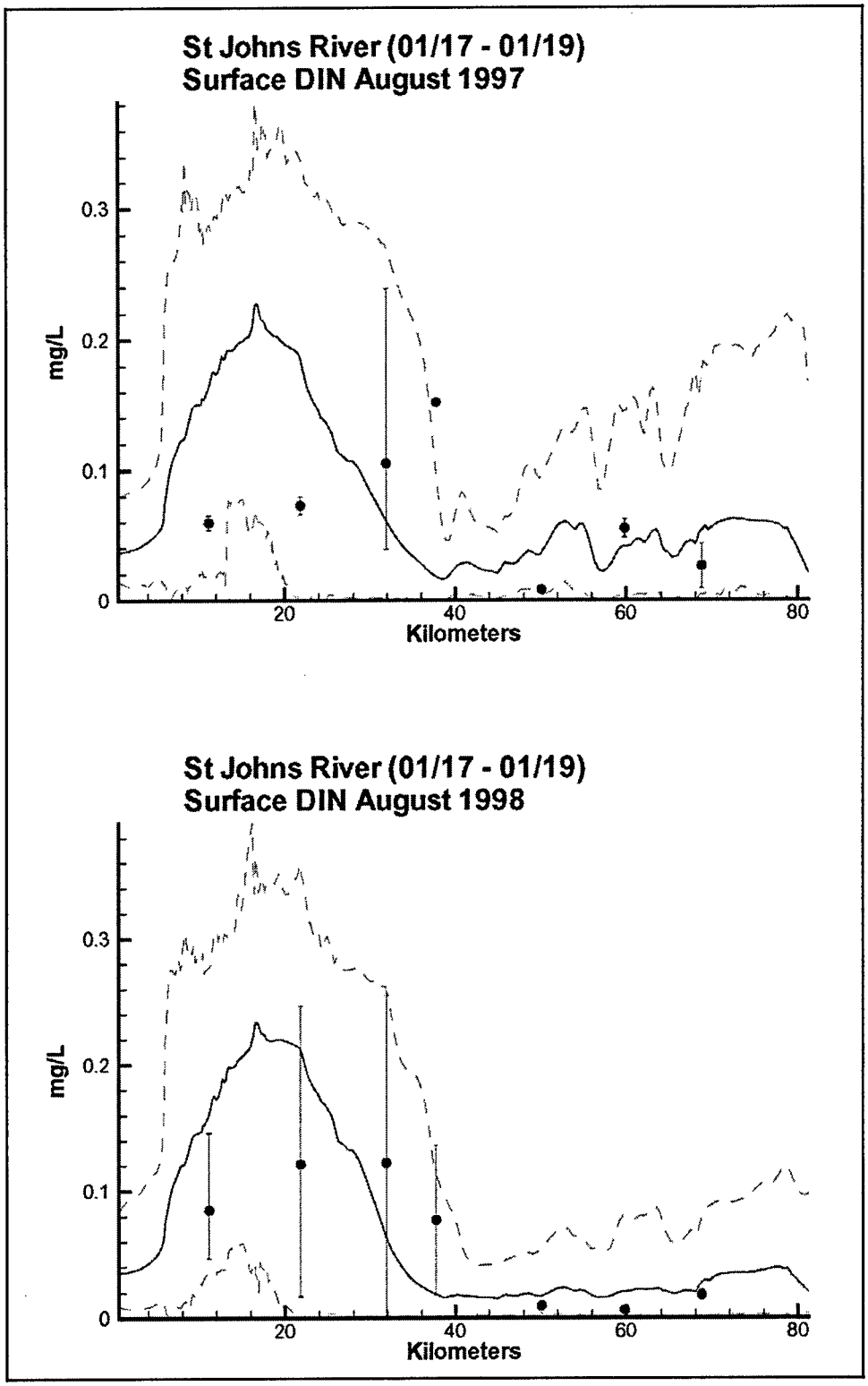

Figure 6-5. (Sheet 3 of 15)

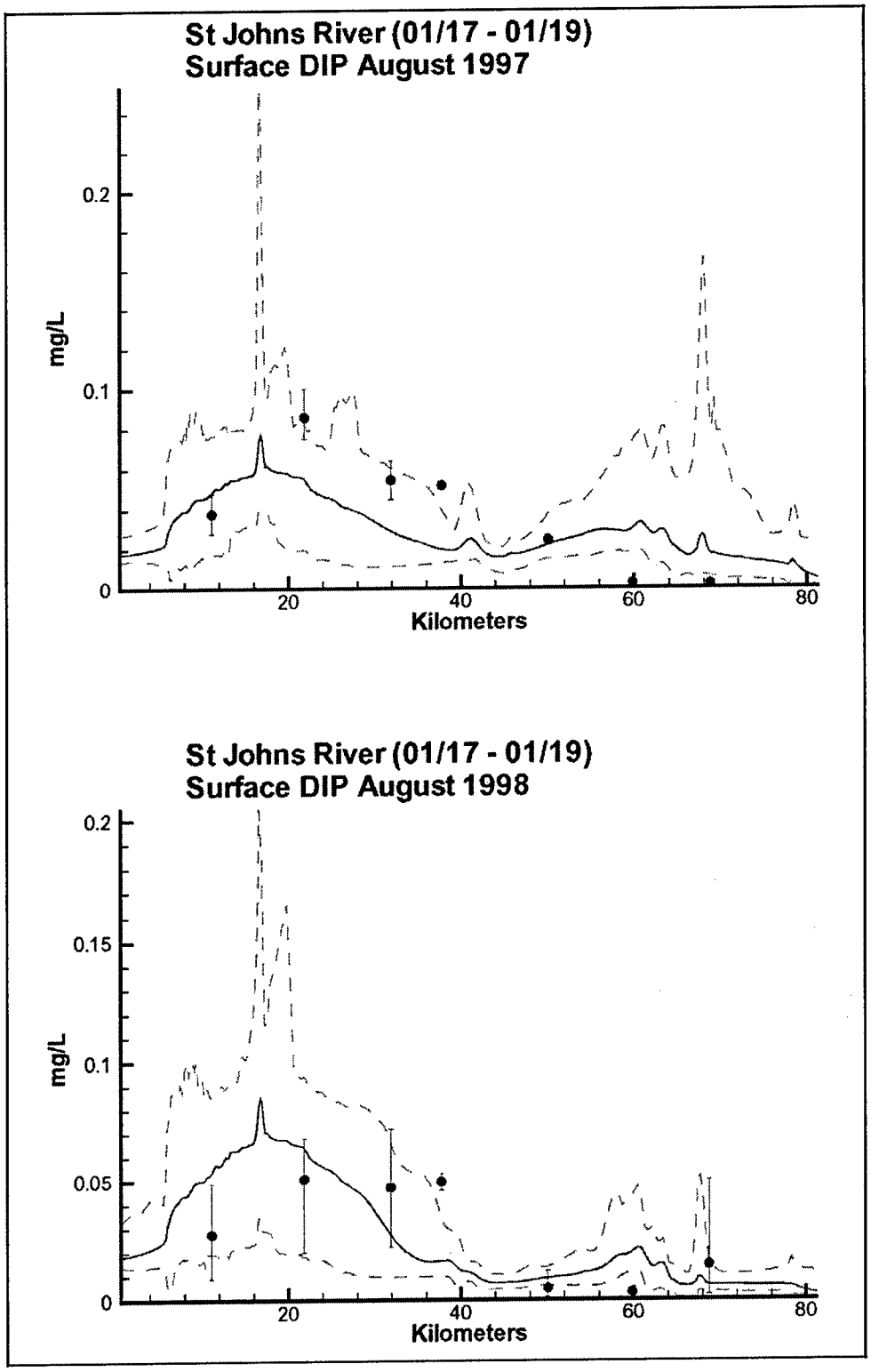

Figure 6-5. (Sheet 4 of 15)

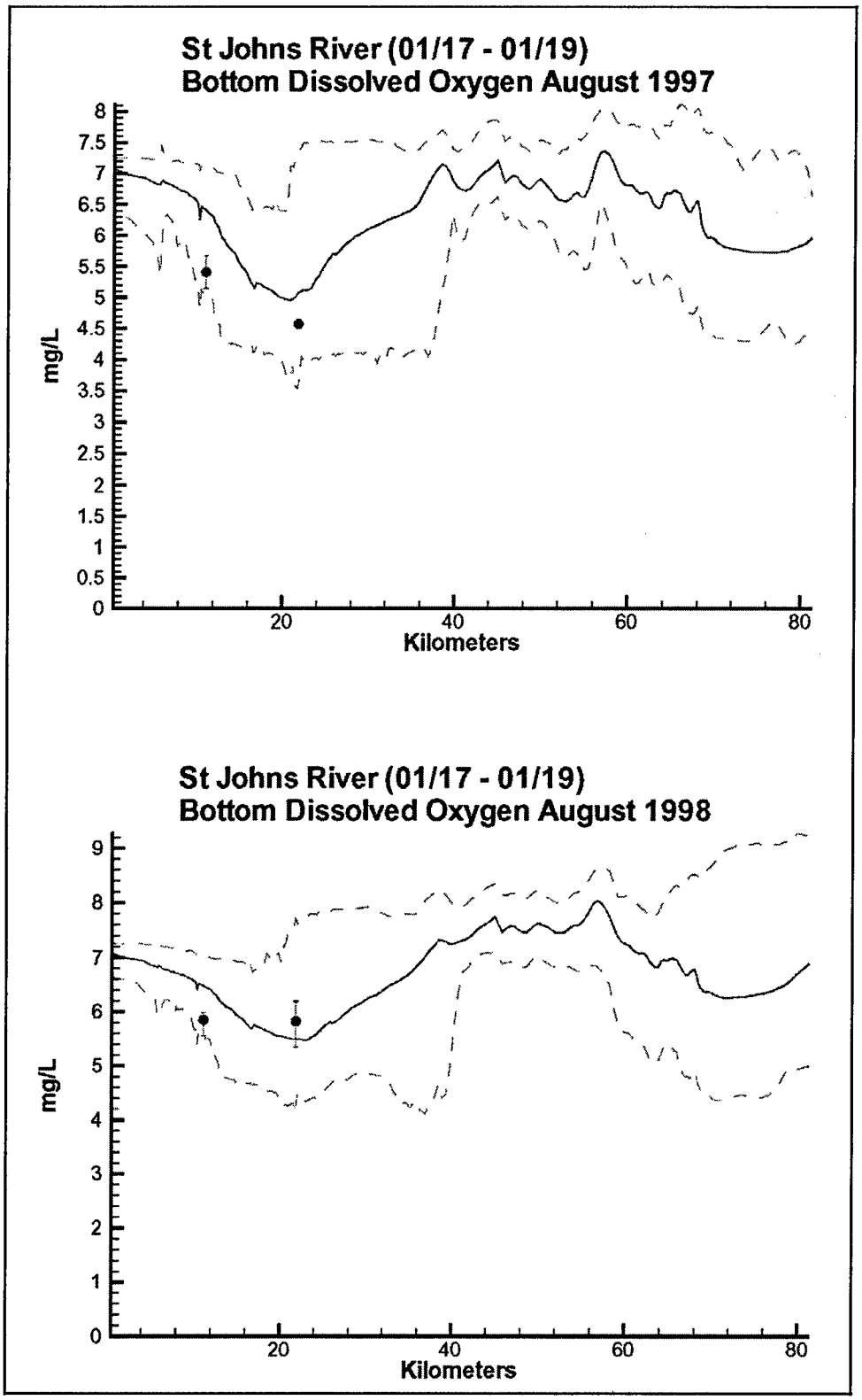

Figure 6-5. (Sheet 5 of 15)

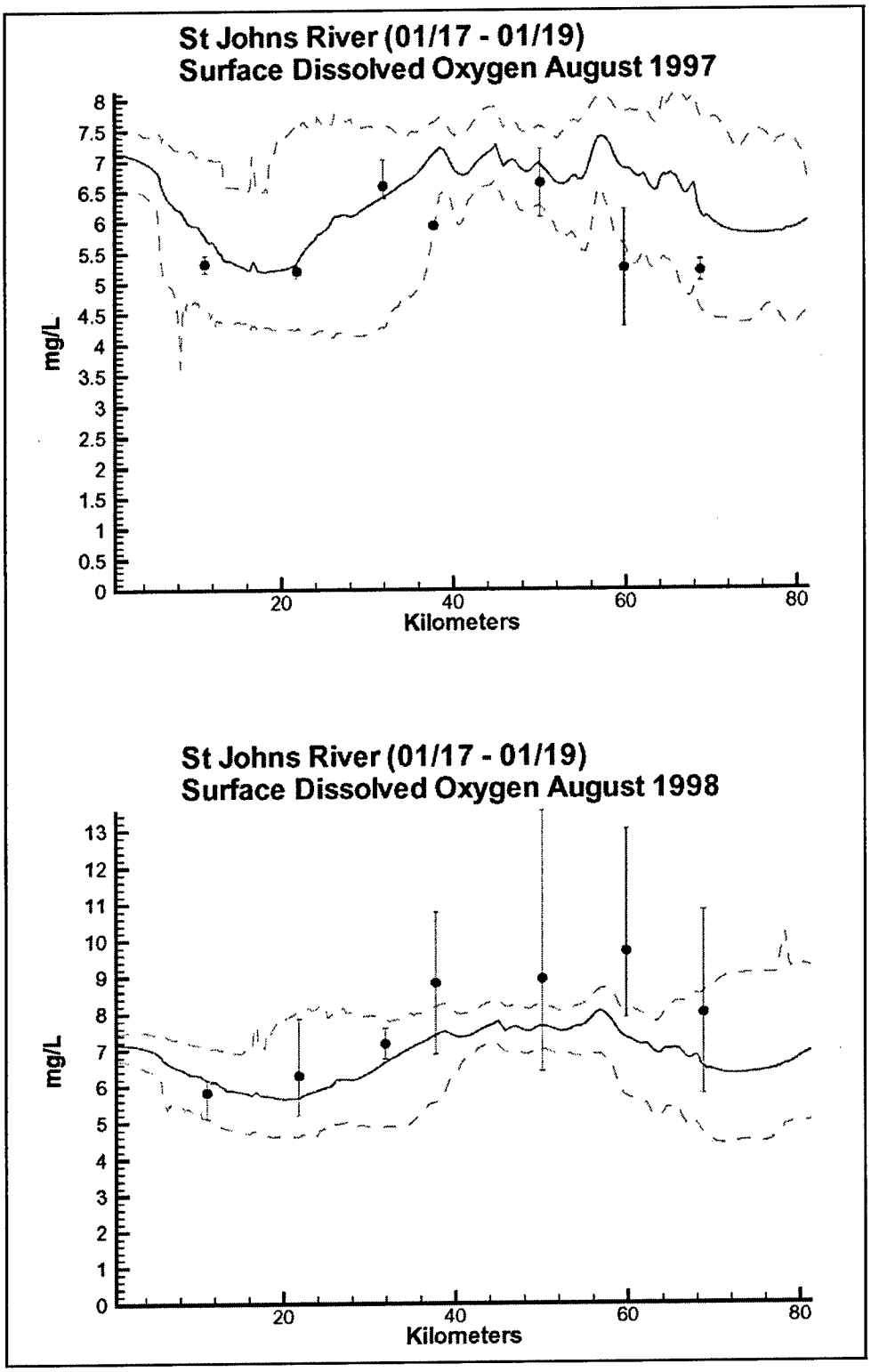

Figure 6-5. (Sheet 6 of 15)

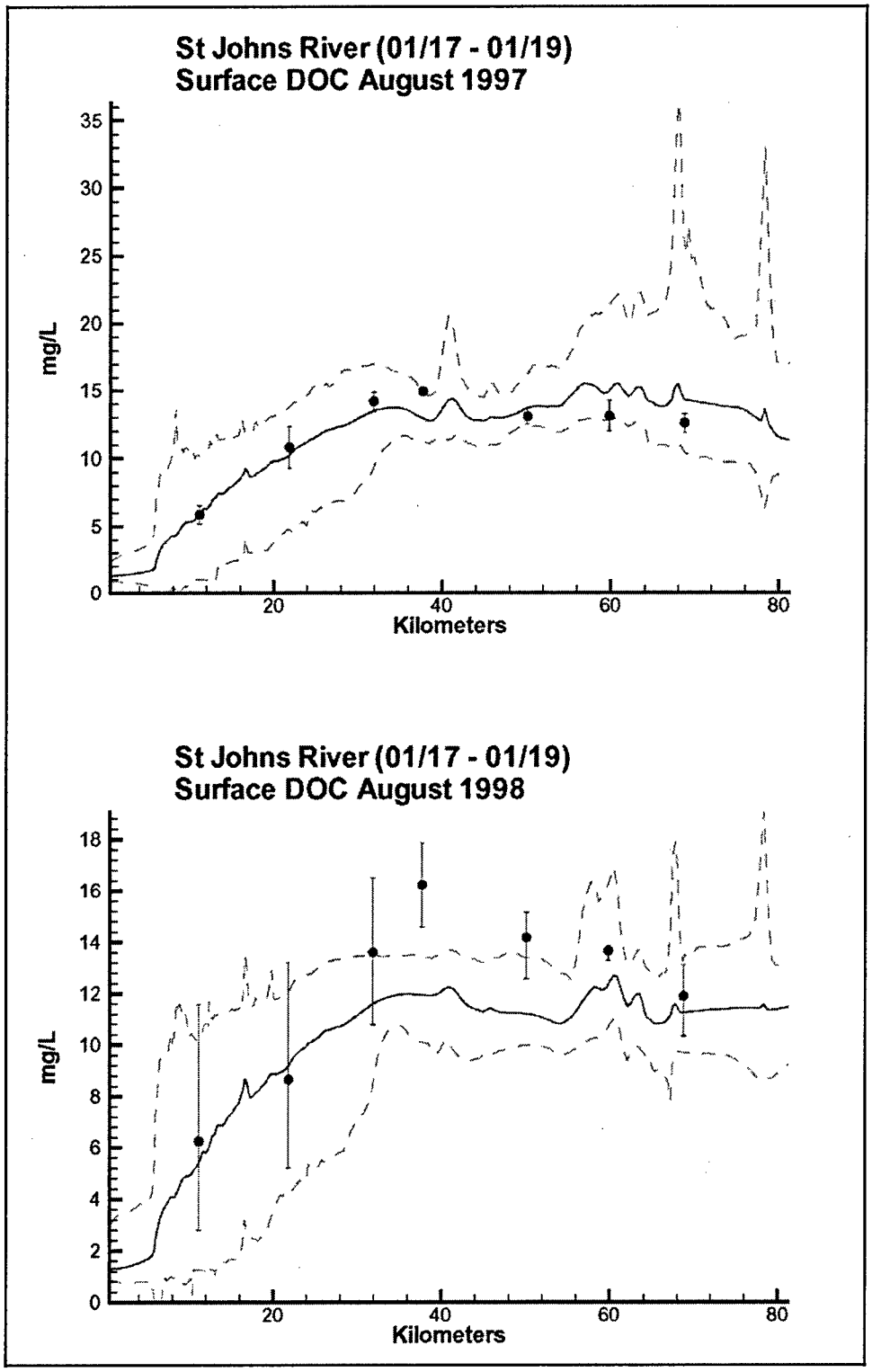

Figure 6-5. (Sheet 7 of 15)

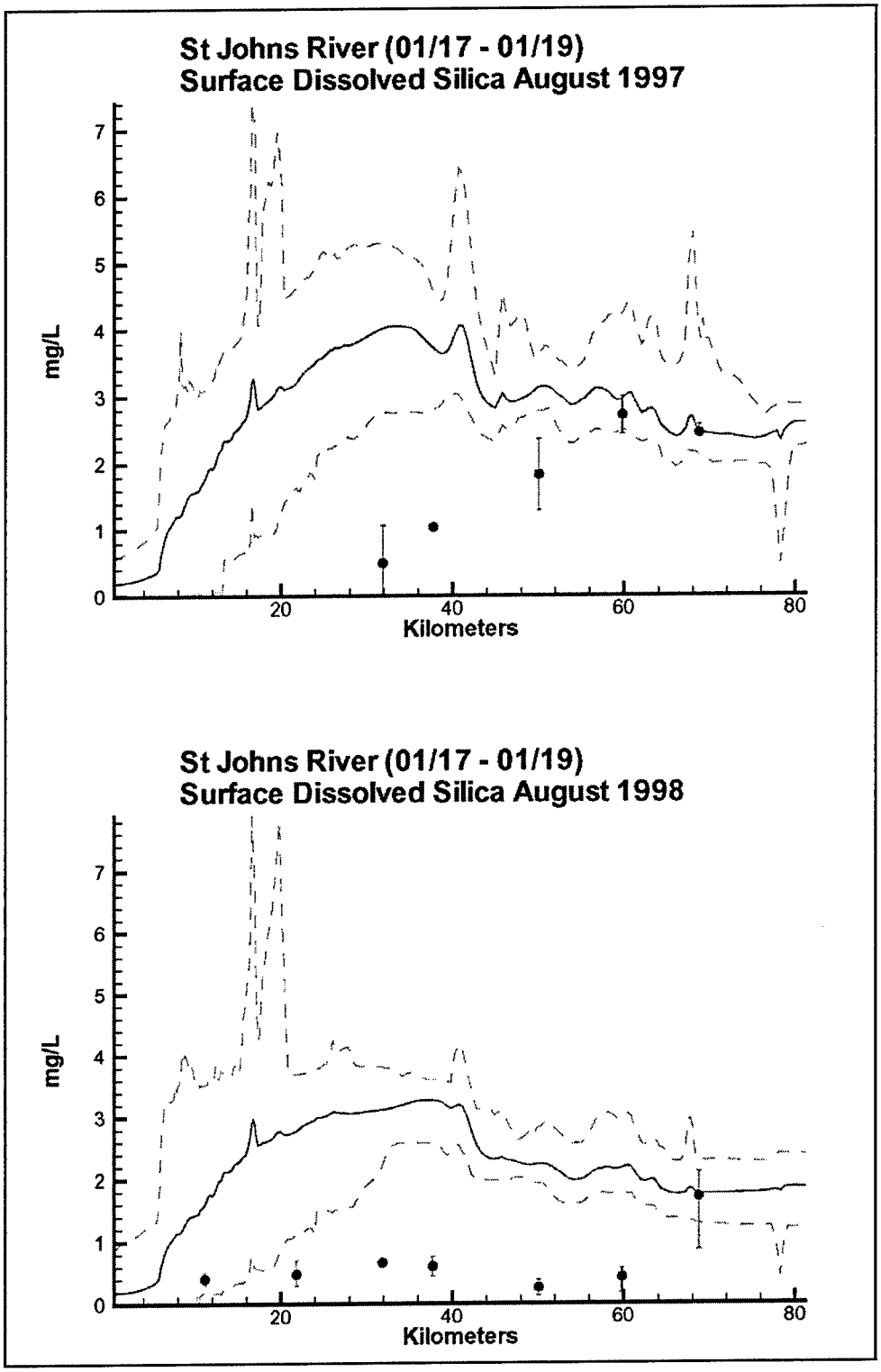

Figure 6-5. (Sheet 8 of 15)

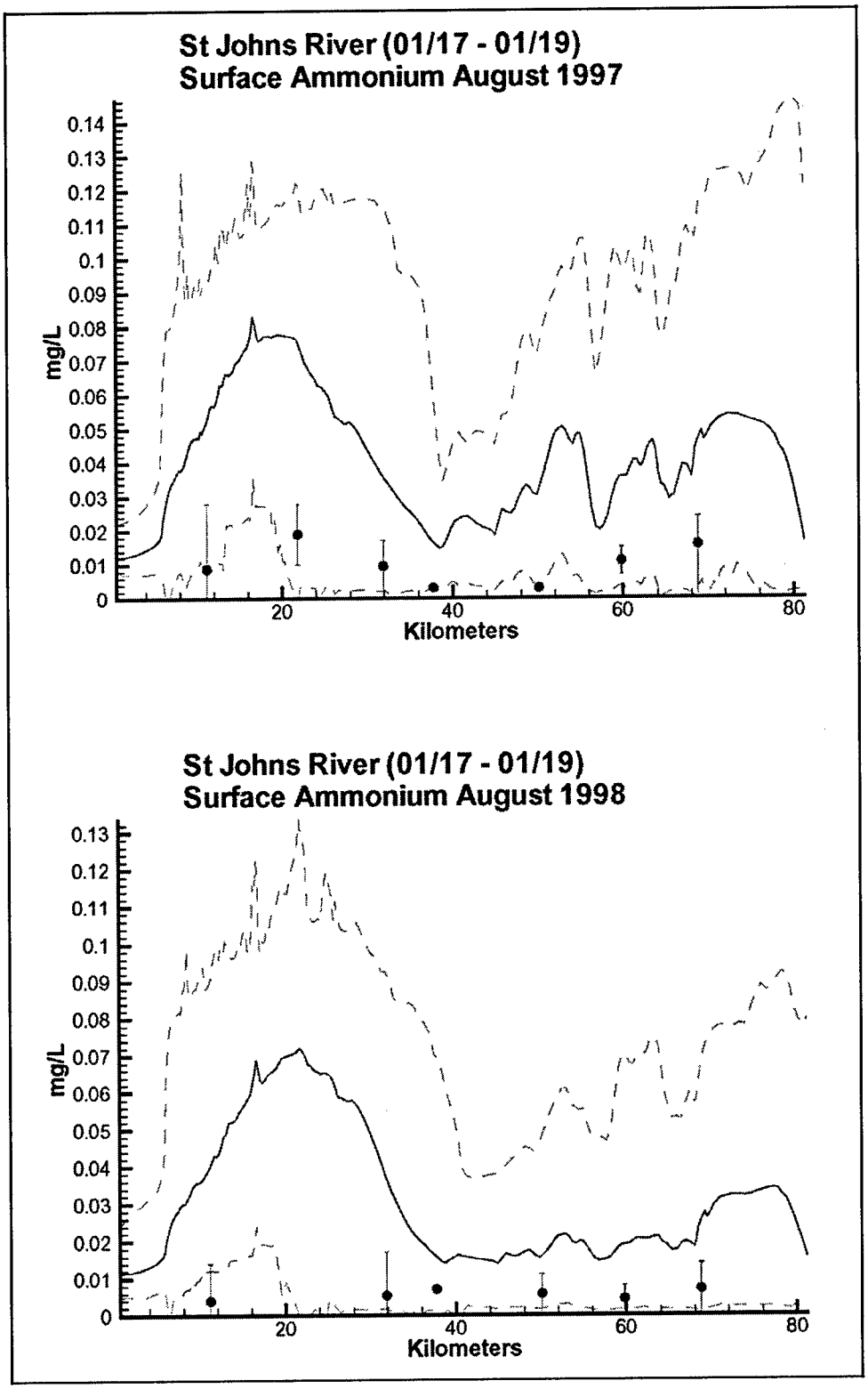

Figure 6-5. (Sheet 9 of 15)

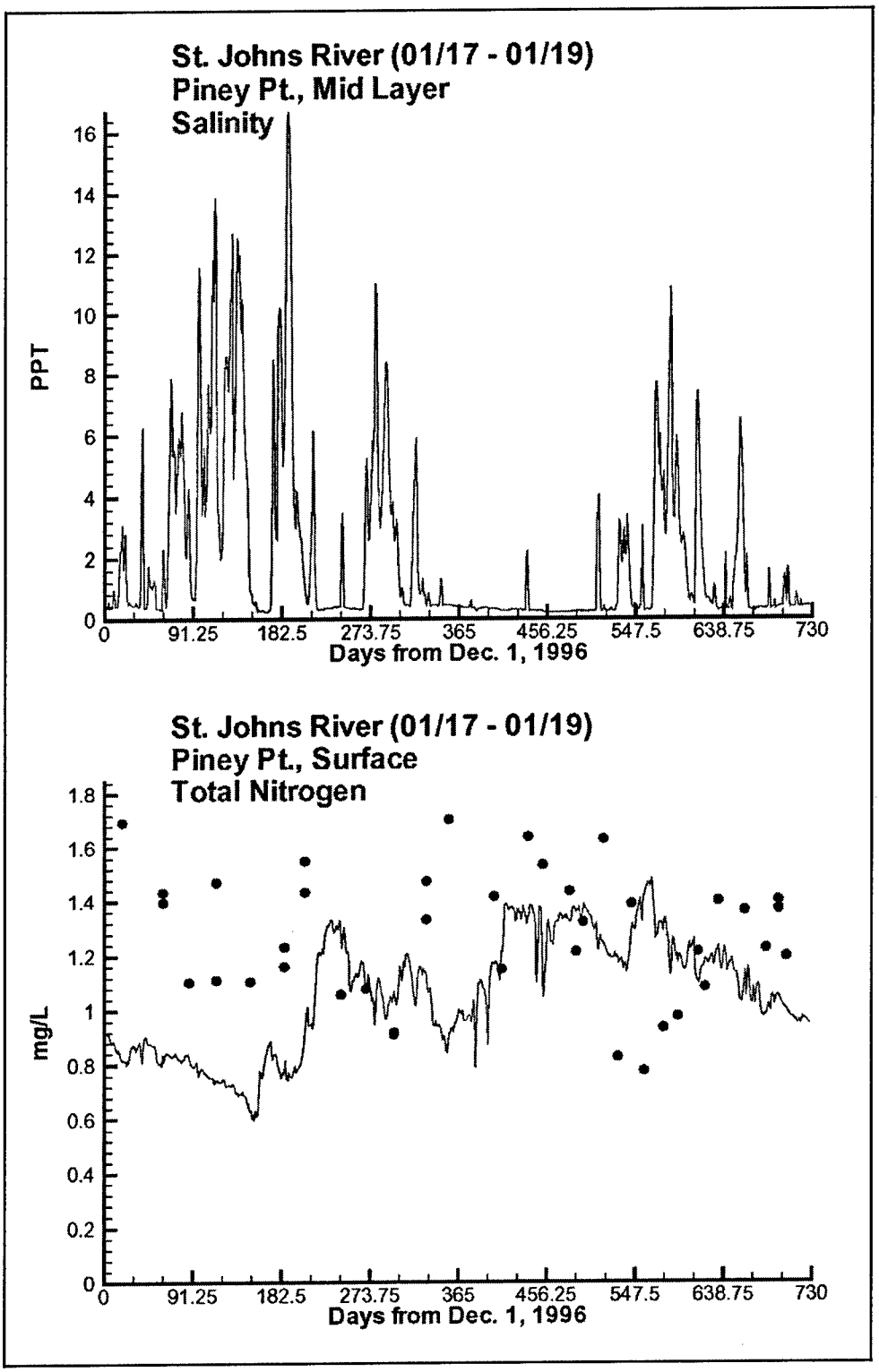

Figure 6-5. (Sheet 10 of 15)

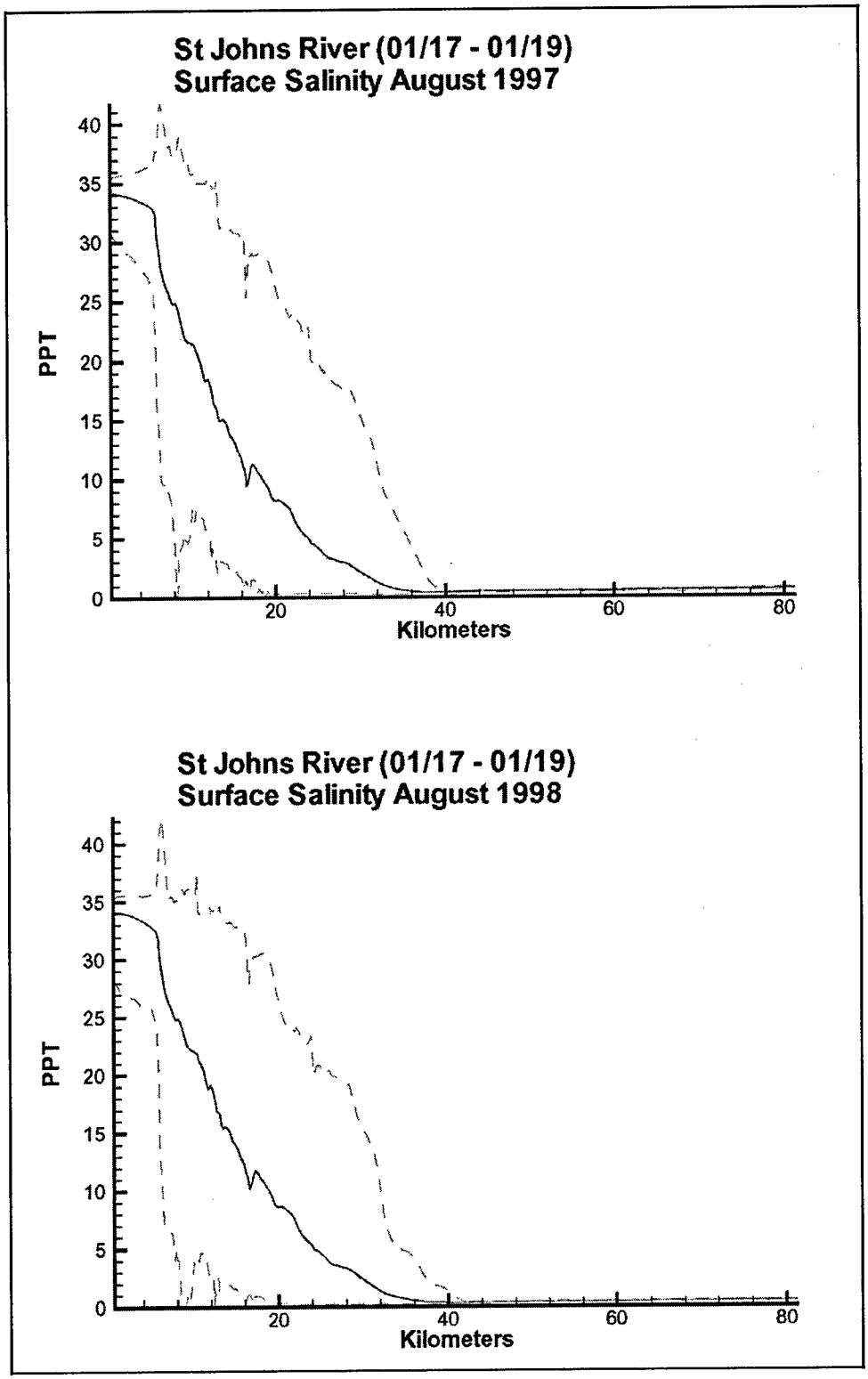

Figure 6-5. (Sheet 11 of 15)

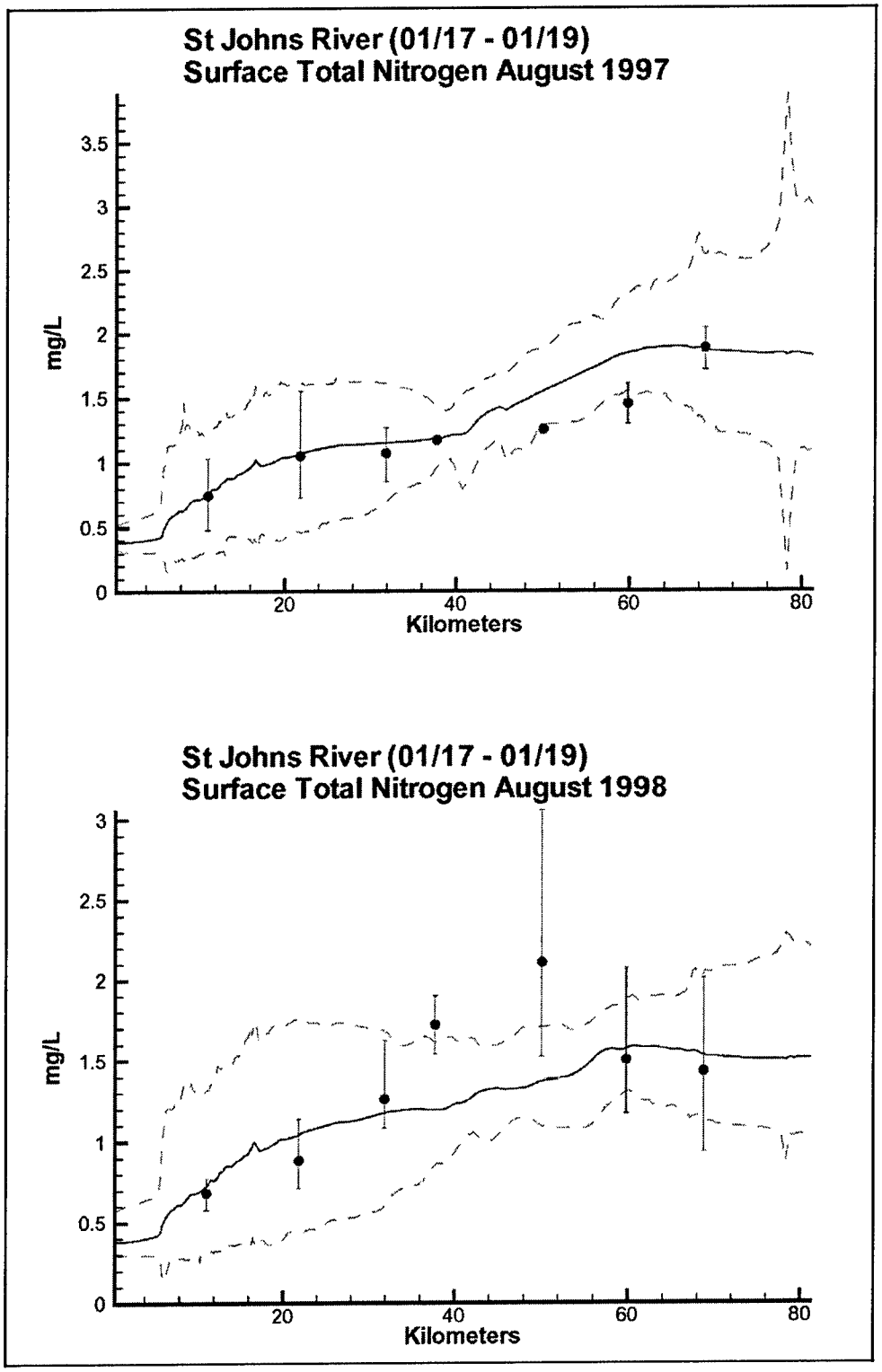

Figure 6-5. (Sheet 12 of 15)

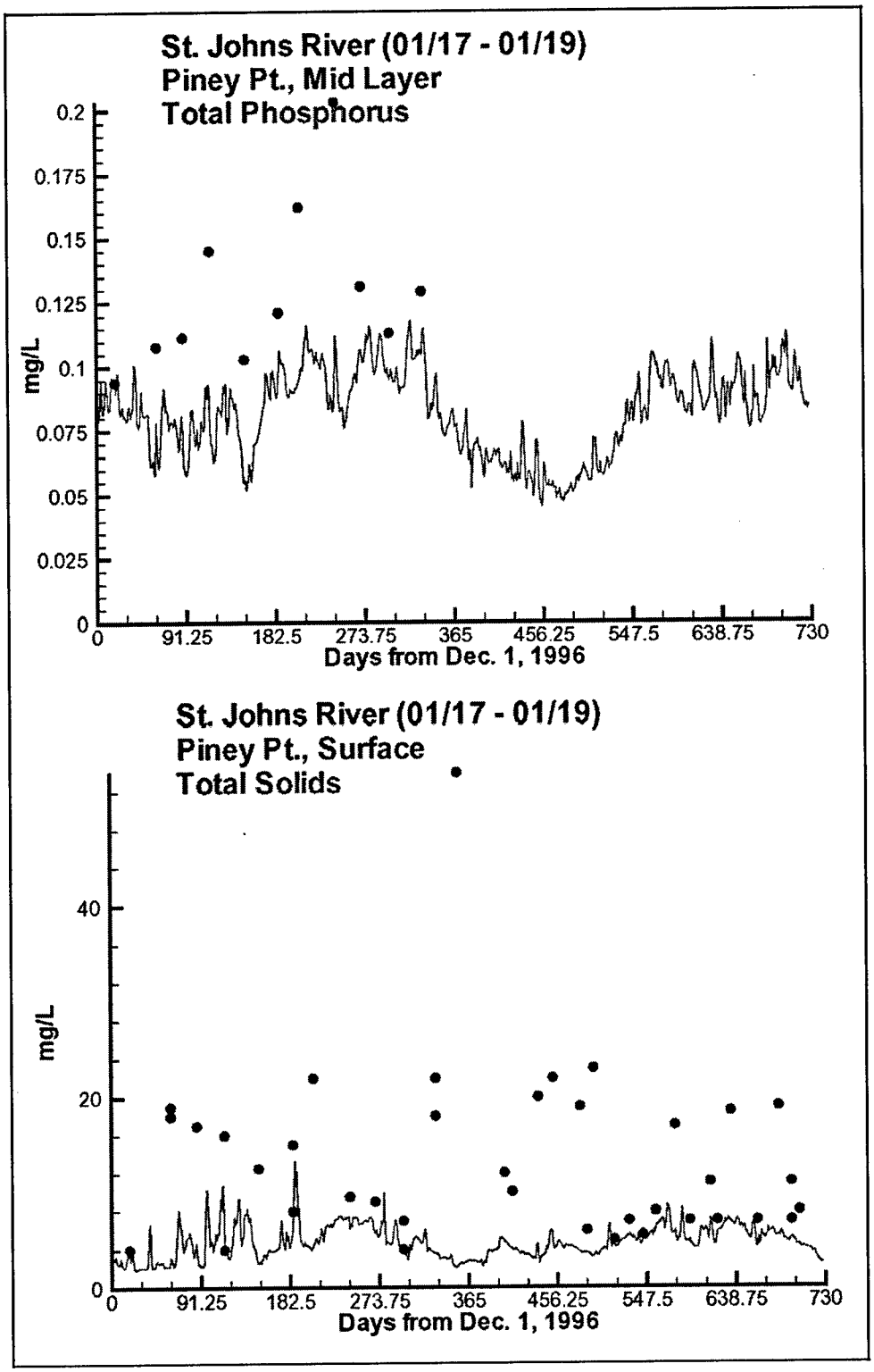

Figure 6-5. (Sheet 13 of 15)

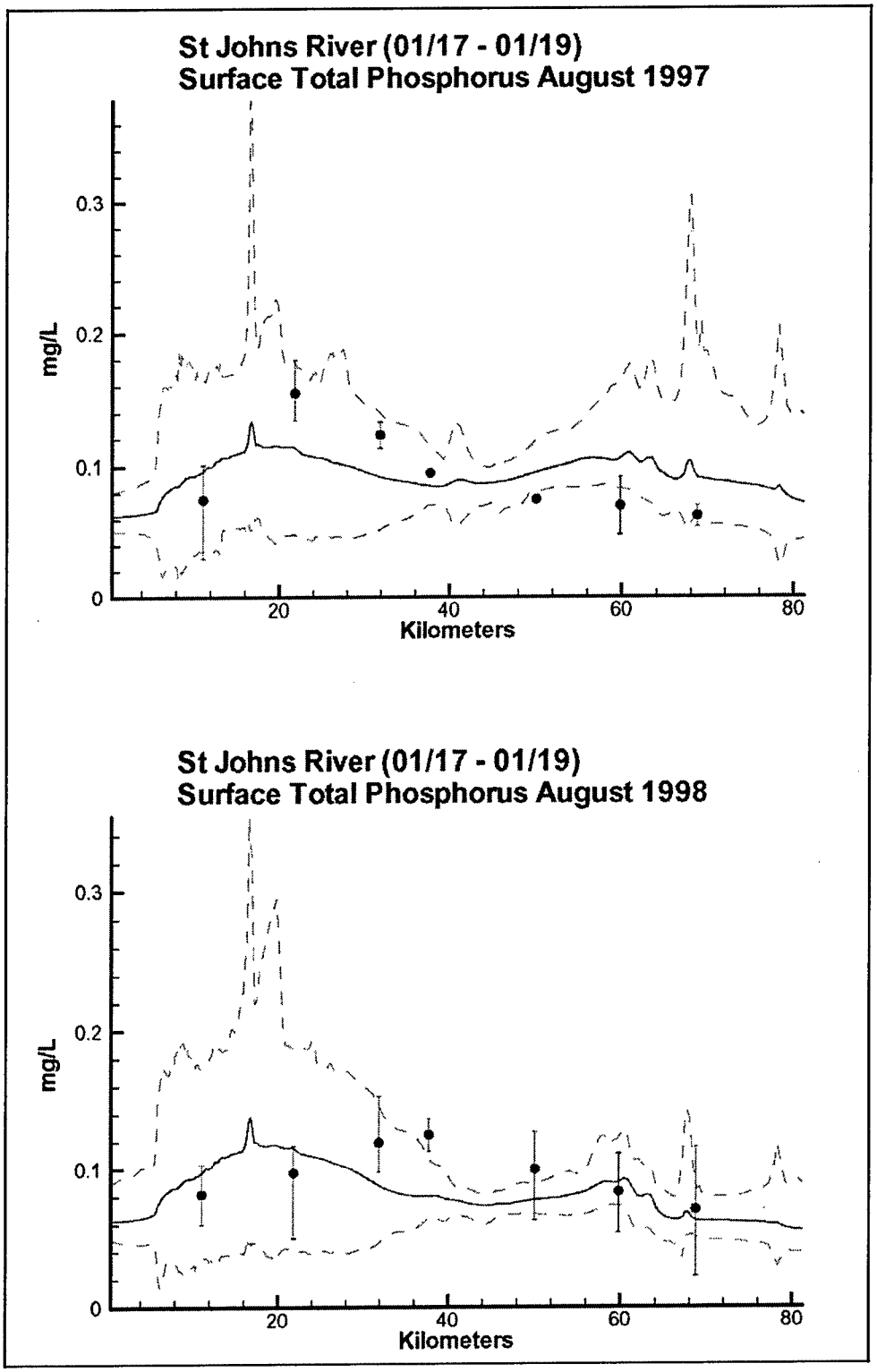

Figure 6-5. (Sheet 14 of 15)

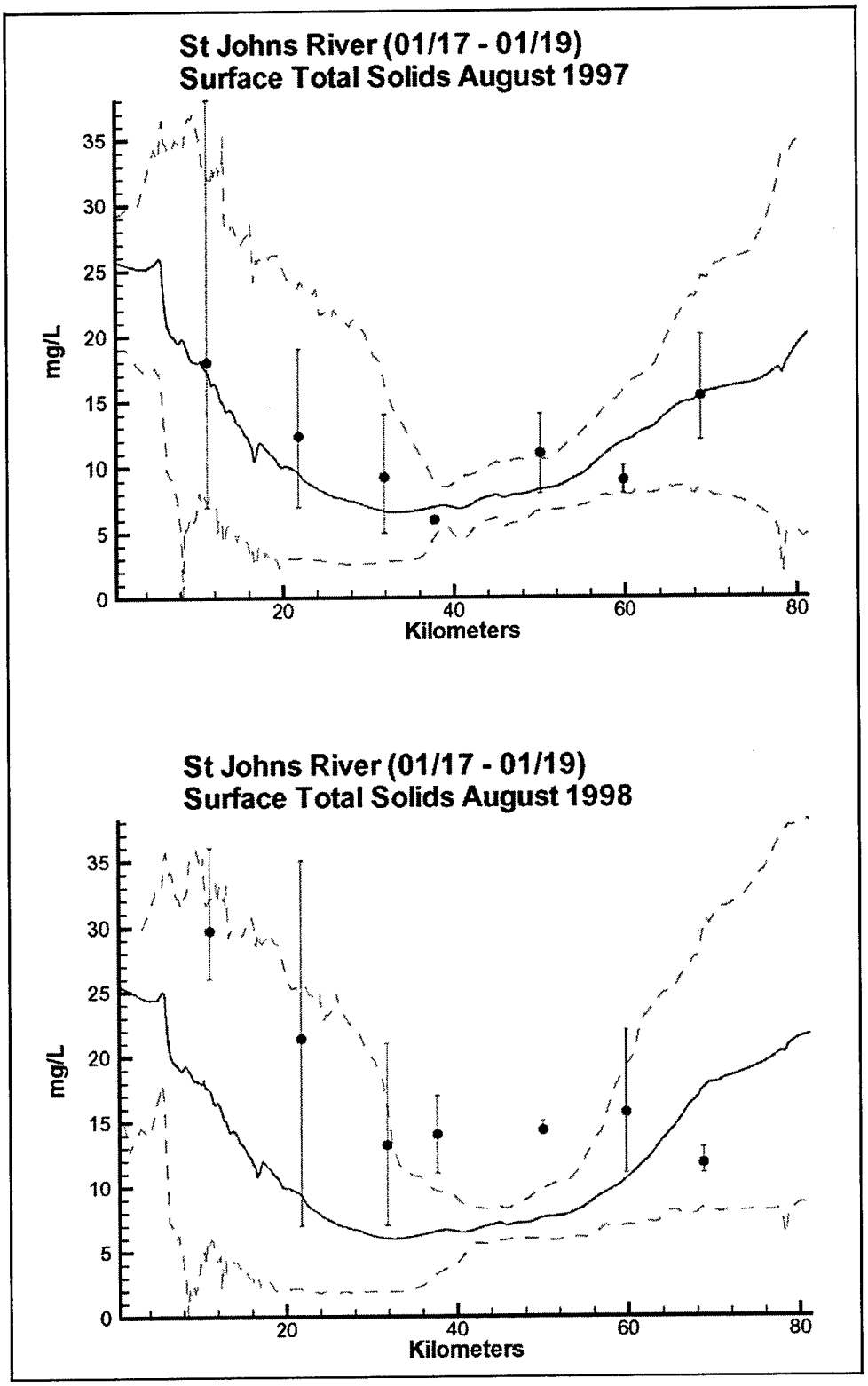

Figure 6-5. (Sheet 15 of 15)

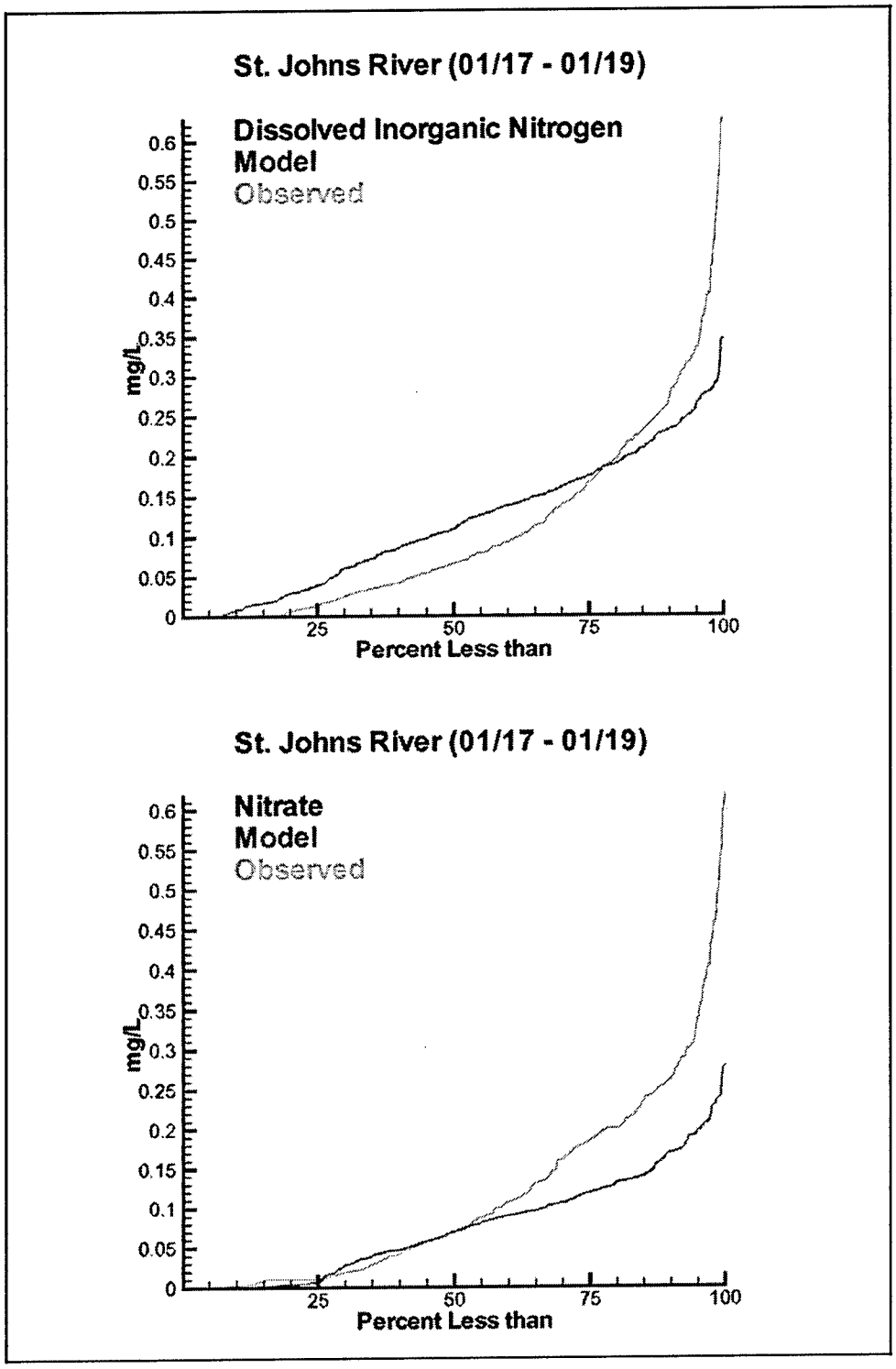

Figure 6-6. Cumulative distribution results for all water quality constituents (Sheet 1 of 8)

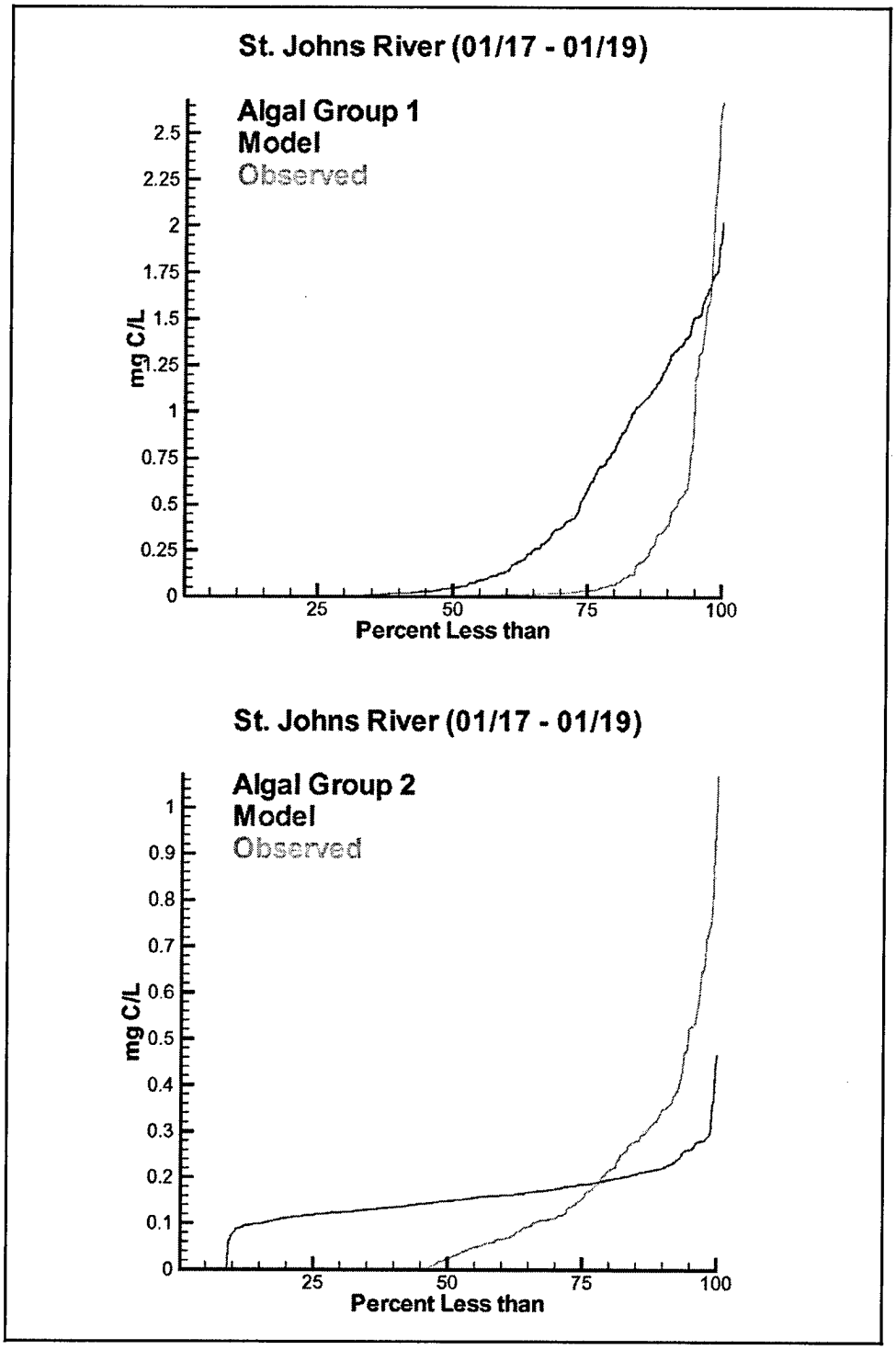

Figure 6-6. (Sheet 2 of 8)

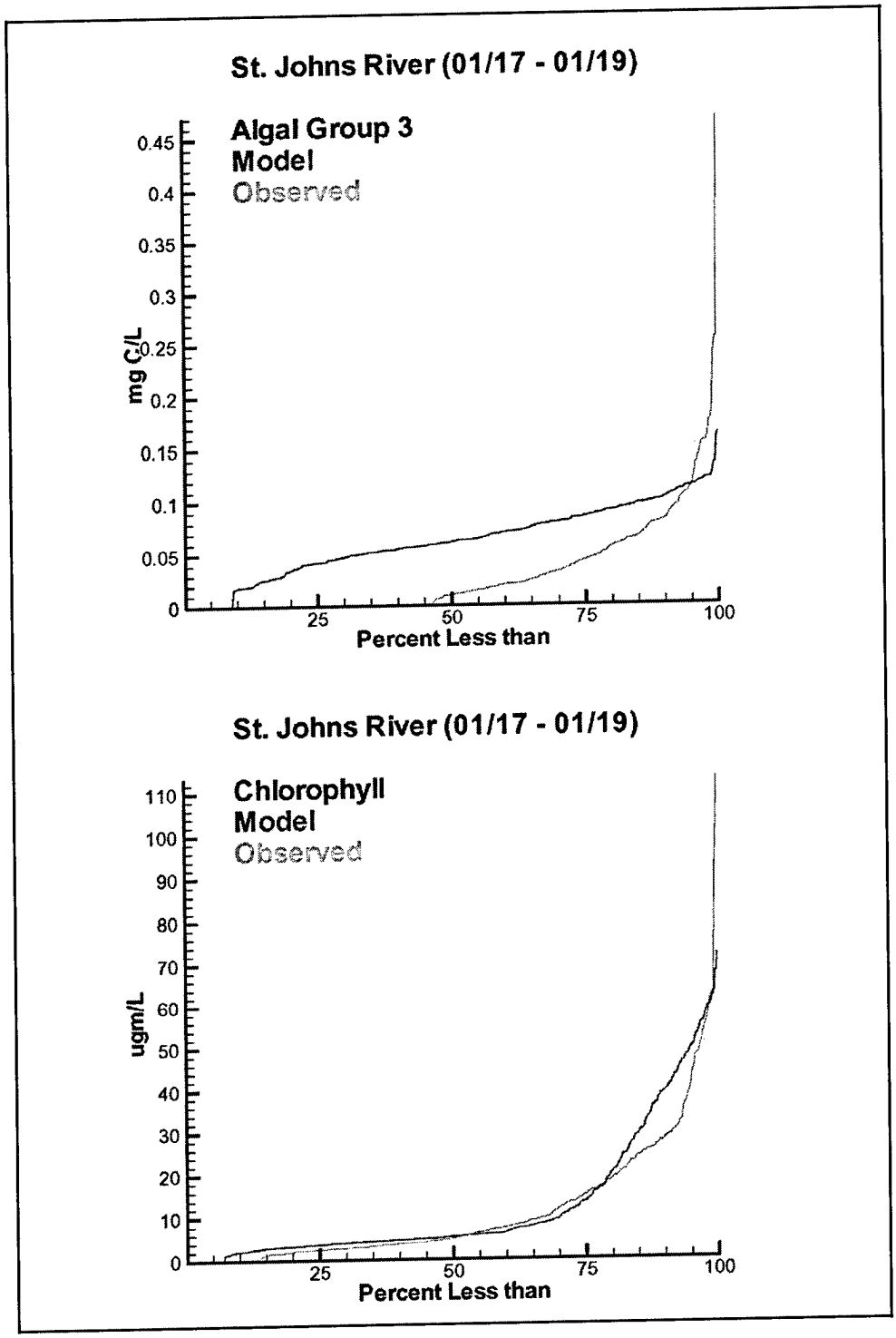

Figure 6-6. (Sheet 3 of 8)

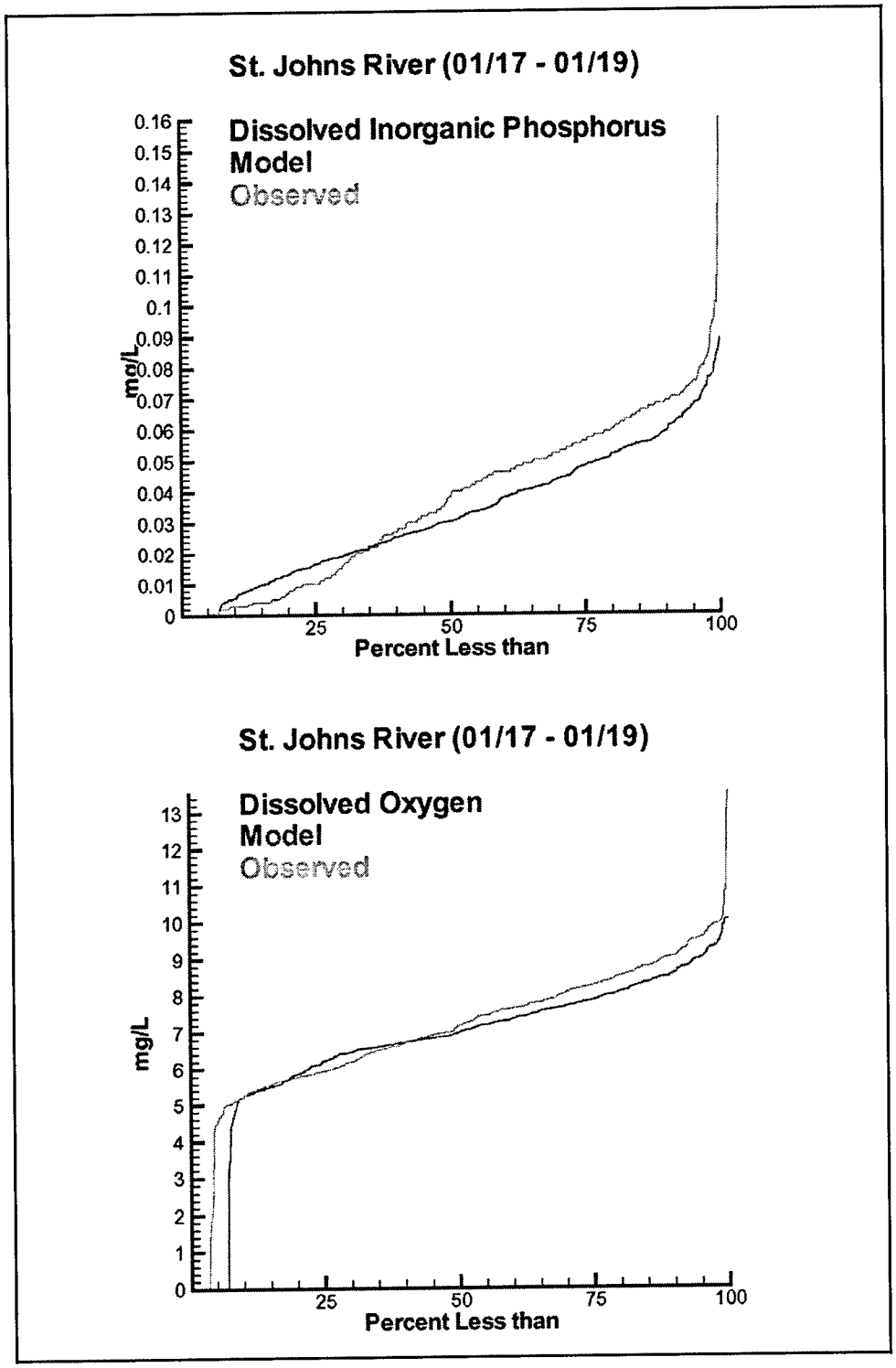

Figure 6-6. (Sheet 4 of 8)

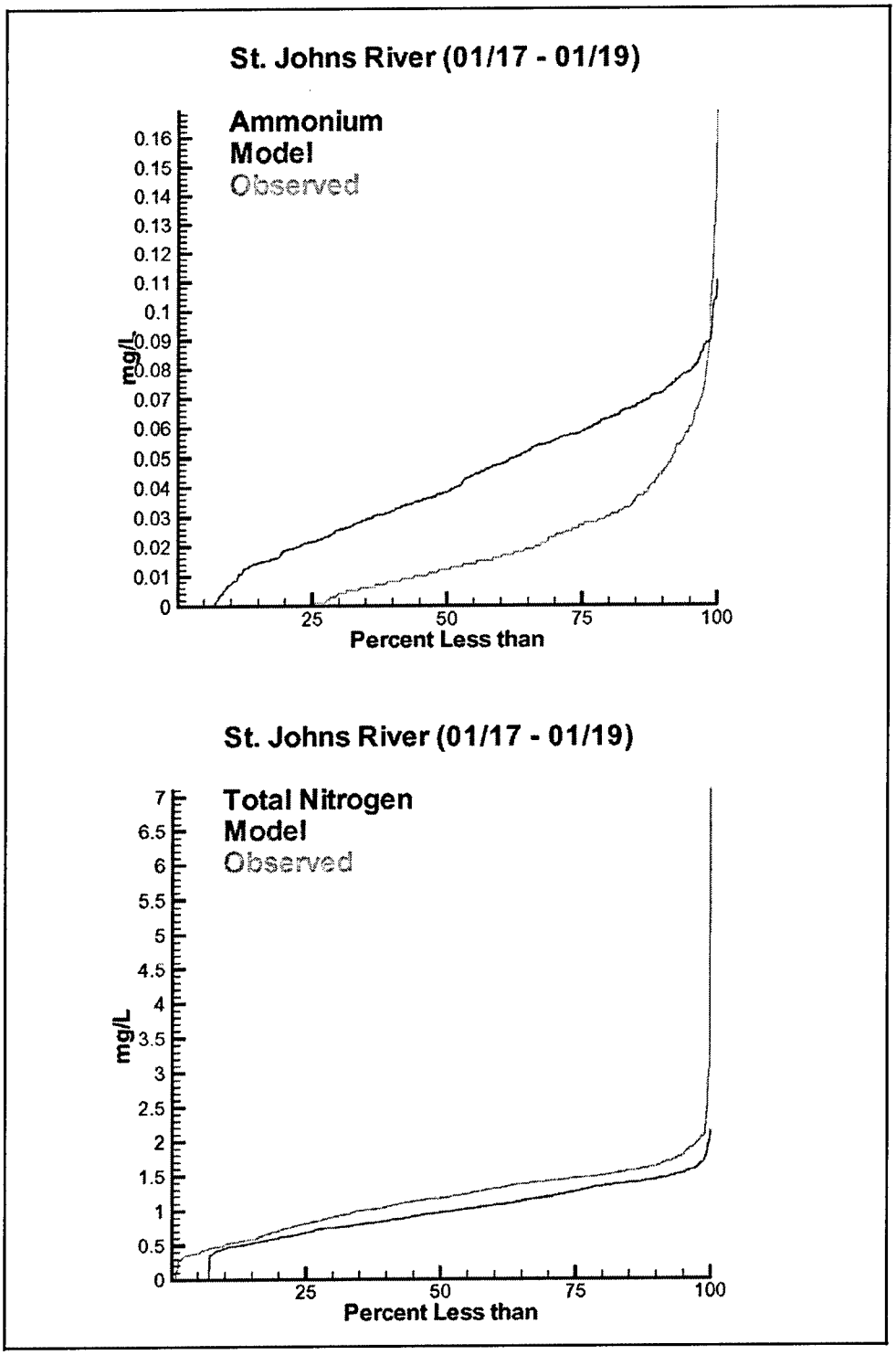

Figure 6-6. (Sheet 5 of 8)

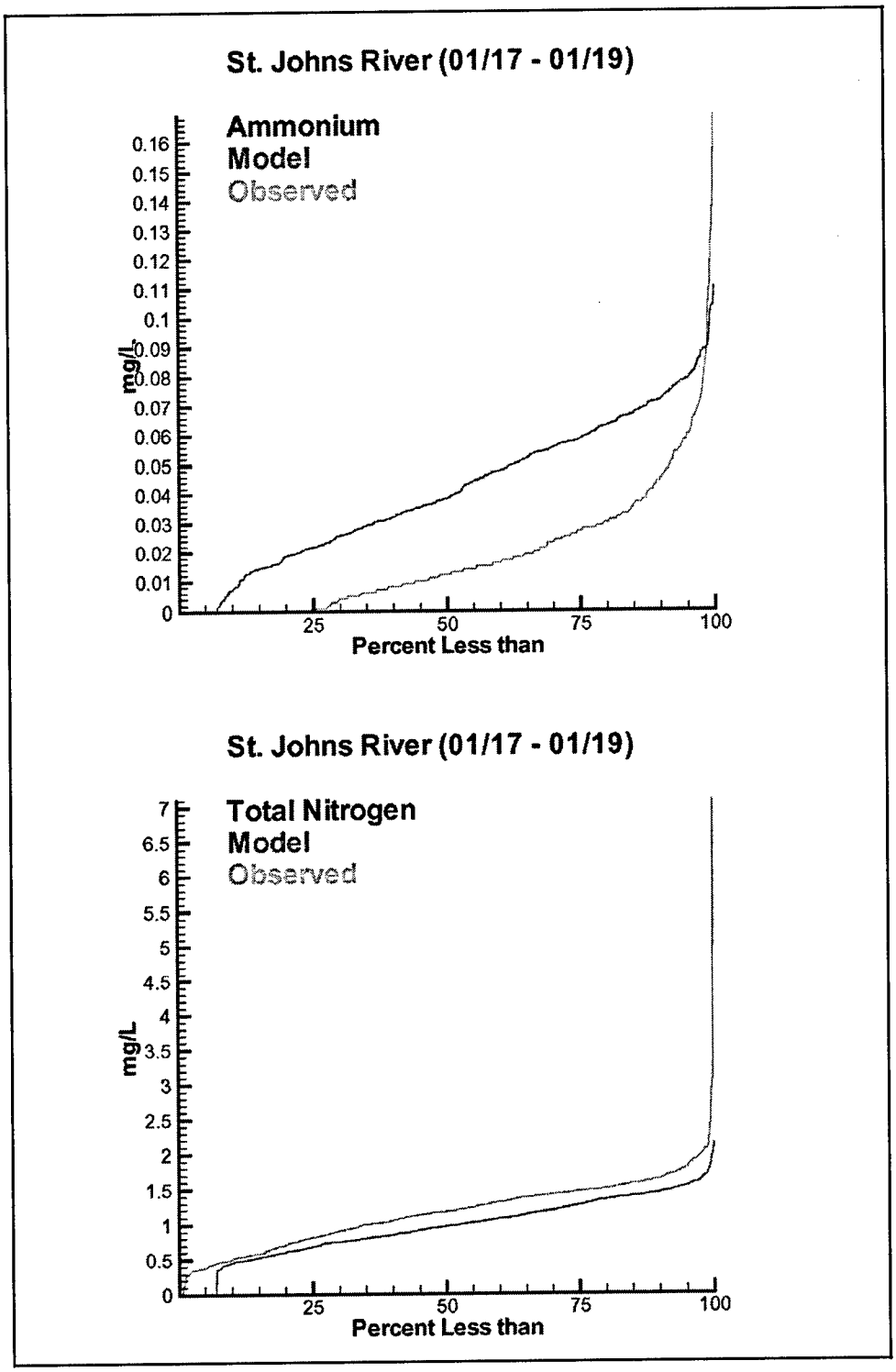

Figure 6-6. (Sheet 6 of 8)

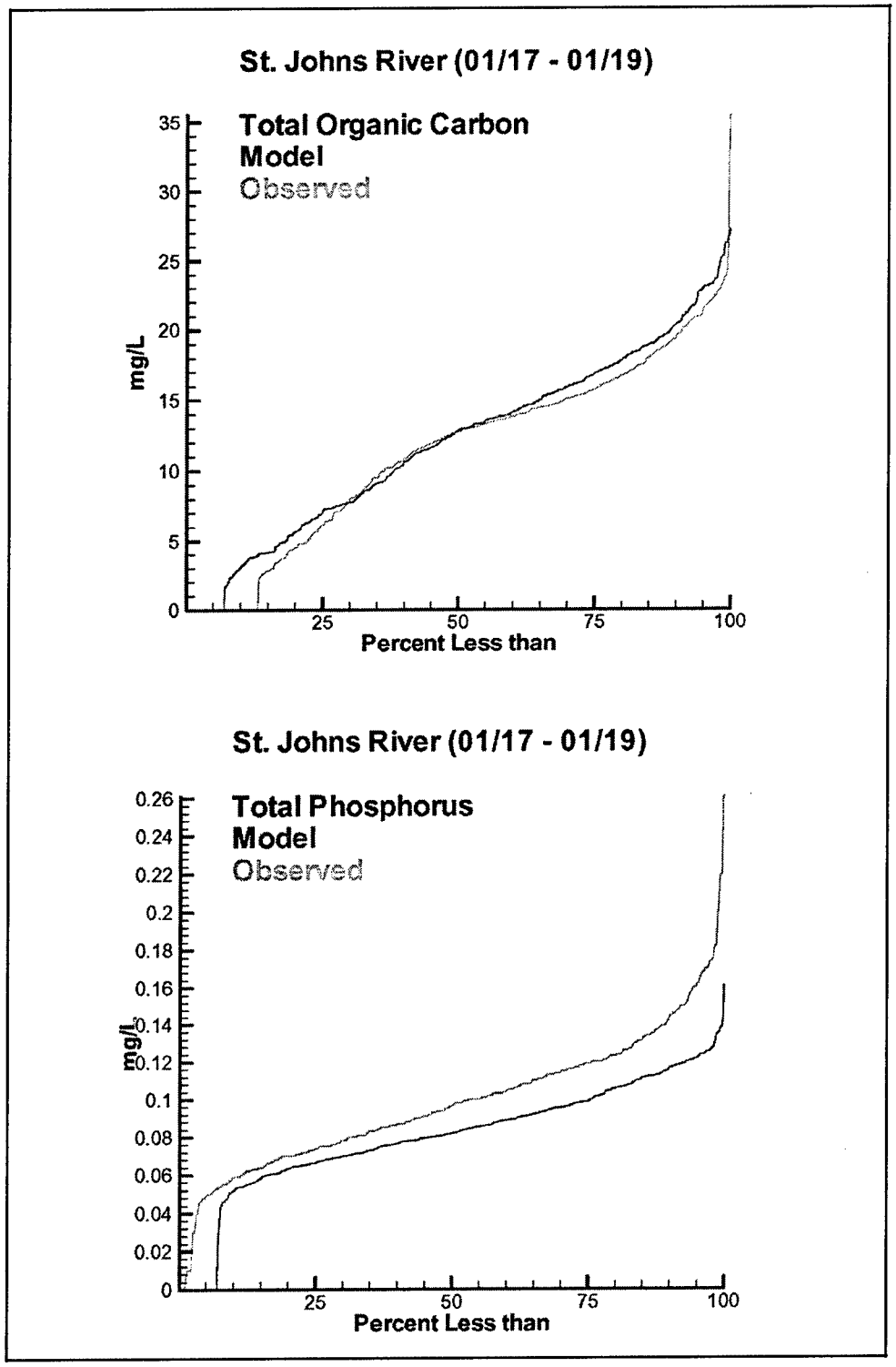

Figure 6-6. (Sheet 7 of 8)

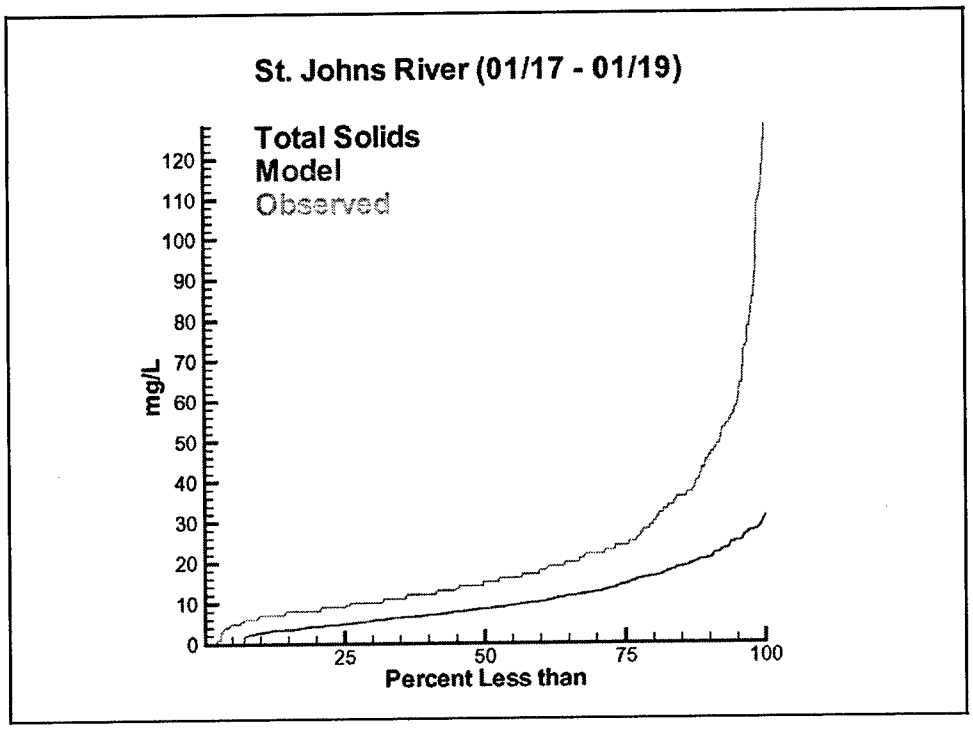

Figure 6-6. (Sheet 8 of 8)

Table 6-5
Comparison of Water Quality Relative Error (%) Statistics at Five CE-QUAL-ICM Study Sites

	LSJR RE (%)	Lake Washington RE (%)	Mainstem Bay – Chesapeake Bay RE (%)	Florida Bay RE (%)	San Juan Bay RE (%)
Chl a	49.3	16.3	58.34	72.0	60.8
DO	9.3	6.3	35.7	7.7	39.8
SALT	27.6	N/A	11.85	4.7	12.9
TEMP	3.5	7.6	N/A	5.3	3.3
TN	29.0	5.1	24.33	38.9	70.1
TP	26.9	8.6	37.64	31.3	58.3
DIP	45.8	N/A	N/A	212.7	82.3
TOC	18.1	N/A	N/A	39.0	40.7
TSS	60.4	N/A	N/A	139.6	78.0

Statistically CE-QUAL-ICM is performing adequately with an ME of -0.2367 and an RMSE of 3.9605, indicating a slight overprediction of salinity. If model performance for each individual station is examined (Table 6-4), stations farthest upstream from the ocean boundary show better comparisons to observed data. Influences at these stations are mostly from tributary boundary conditions. The RE for the combined statistic for all stations is around 27 percent, which is 7 percent higher than what was reported in Sucsy and Morris (2002). It is thought that the difference in RE between reports is due to how RE

was calculated. Sucsy and Morris looked at the median RE of tidally averaged salinity, and RE in this report was calculated from daily salinity output at 12:00 PM and daily averaged observed salinity data. Comparison of the RE for LSJR to other studies shows a higher value for LSJR. As already mentioned, the greatest differences occur at the Bar Pilot station (closest to the ocean boundary) where CE-QUAL-ICM failed to predict the variation in salinity concentrations in the bottom layer.

Chlorophyll

Higher observed chlorophyll values occurred in the study area's most upstream reaches, corresponding to an absence of salinity. CE-QUAL-ICM has captured this trend as shown in time series and longitudinal plots (Figures 6-2 through 6-5). As demonstrated in the time-series figures, CE-QUAL-ICM has also reproduced the seasonality of increased chlorophyll values during the summers of each year modeled. Statistically CE-QUAL-ICM's model performance is more than adequate for chlorophyll with an RE of 49.38 percent. This value is comparable or better to other studies reported in Table 6-5. Comparison of the RE for each year modeled shows that the 1997-1998 year is slightly better than the 1996-1997 year (i.e., 47 percent as compared to 52 percent, respectively). This may suggest that nutrients or conditions required for algal growth are being computed more realistically for the 1997-1998 year. Statistics presented for individual stations (Table 6-4) indicated that computed values compared better to observed data at stations closest to the boundaries (i.e., Palatka RE approximately 40 percent and Fulton Point RE approximately 48 percent) than at the mid-reach stations.

The cumulative distribution plot (Figure 6-6) demonstrates that CE-QUAL-ICM has a propensity to overpredict chlorophyll. This is also affirmed by an ME value of -1.2406. From the cumulative distribution plot, discrepancies between observed and predicted chlorophyll values occurred most often for chlorophyll values greater than 20 μg/L. Above this value, CE-QUAL-ICM has a tendency to overpredict concentrations.

Spatially, chlorophyll values showed similar trends during August for both simulation years (Figures 6-5). As would be expected, these plots (and additional longitudinal plots provided on a CD-ROM) illustrate how chlorophyll values increased in the upstream direction whether during cool or warm months. Higher chlorophyll values occurred during summer months and could get as high as 90 μg/L (Figure 6-5).

Ammonia and Nitrate

Initially, ammonia and nitrate were examined separately. Observed ammonia concentrations were usually an order of magnitude less than nitrate concentrations. There are three distinct peaks of high ammonia and nitrate values, with the highest occurring between days 273 and 547 from the start of the simulation. Ammonia and nitrate time series (Figures 6-2 through 6-4) show CE-QUAL-ICM is able to reproduce this trend, although ammonia is usually over-predicted and

nitrate underpredicted. As noted from the cumulative distribution plot (Figure 6-6), ammonia values for all concentration ranges were on the whole being over-predicted. On the other hand, nitrate values below 0.1 mg/L were accurately predicted while values above this level were underpredicted (Figure 6-6).

After consideration of the arbitrary division of dissolved inorganic nitrogen (DIN) loads (ammonia split 25 percent and nitrate split 75 percent) and the difficulty of computing reasonable results for ammonia and nitrate individually, ammonia and nitrate values were combined for the computed and observed values to arrive at computed and observed DIN values. For the remainder of this report, reference to ammonia and nitrate will be as DIN. Times series of DIN implied that combining the two variables produced more accurate comparisons (Figures 6-2 through 6-4). This accuracy is also demonstrated in the improved statistic of DIN as compared to statistics for ammonia or nitrate. The RE for DIN-combined statistics for all stations was approximately 48 percent. When the RE statistics are compared by year modeled (Tables 6-2 and 6-3), the 1996-1997 year has a much higher RE than the 1997-1998 year and is 92 percent compared to 48 percent, respectively. This difference could suggest problems in loads or boundary conditions for the first year modeled. Also, problems computing DIN in the first year may be influenced by chlorophyll values (see chlorophyll discussion above). Comparison of the RE for individual stations shows the RE varies from station to station about 20 percent, with no discernable pattern.

The cumulative distribution plots (Figure 6-6) indicate that CE-QUAL-ICM has a tendency to overpredict DIN for concentrations below 0.17 mg/L, which occur about 75 percent of the time. For values greater than this, CE-QUAL-ICM usually underpredicts.

Spatially, CE-QUAL-ICM does reasonably well in predicting DIN longitudinally. Most of the major disparities occur at stations in the middle of the study reach (i.e., Piney Point, Mandarin Point, and Racey Point). These stations are where much of the PS and NPS loads are entering the study area. During August 1997 and August 1998, summer months critical to water quality, CE-QUAL-ICM is able for the most part to reproduce the trend of higher DIN values at the downstream stations and lower values at the upstream stations (Figure 6-5). Longitudinal plots of DIN for other months of the simulation period are provided on the CD-ROM.

Total Nitrogen (TN)

TN appears to be dominated by the organic phase when compared to DIN. This observation is based on most of the TN values being around 1.0 mg/L or greater while DIN values are usually less than 0.3 mg/L. Hendrickson and Konwinski (1998) reported similar trends in magnitudes of observed data for TN and DIN. Hendrickson et al. (2002) stated that much of the organic nutrients were associated with anthropogenic nutrient enrichment as well as terrestrially derived, colored humic, and nonhumic substances that come primarily from vascular plants. Recently, although it is not clear what form TN is in, loads to the LSJR have been attributed to PS discharge, with most nutrient portions being bioavailable (Hendrickson et al. 2002).

All stations presented in the time-series plots (Figures 6-2 through 6-4) show a similar range of TN predictions with an overall RE of 29 percent (Table 6-1). CE-QUAL-ICM does a commendable job in representing the dominance of the organic form over the mineral form. With the RE value reported, it is comparable to published values from other studies (Table 6-5). From comparison of the RE statistics for each year modeled, there is very little difference in RE value between years (Tables 6-2 and 6-3). Comparison of the RE for individual stations indicates that the greatest RE values occur from the stations closest to the ocean boundary upstream to Mandarin Point. This may indicate problems with how loads or boundary conditions were set in these reaches. From the cumulative distribution plot (Figure 6-6), the CE-QUAL-ICM consistently underpredicts TN slightly at all concentrations.

Spatially, CE-QUAL-ICM does reasonably well in predicting TN longitudinally. As with DIN values, most of the major disparities occur at the stations in the middle of the study reach (i.e., Piney Point, Mandarin Point, and Racey Point), again implying errors in load or boundary estimates. During August 1997 and August 1998, months critical for water quality, CE-QUAL-ICM does a very good job of reproducing the trend of TN values increasing in the upstream direction (Figure 6-4). Longitudinal plots of TN for other months of the simulation period are provided on the CD-ROM.

Dissolved Inorganic Phosphate

Figures 6-2 through 6-4 show that the range of DIP values is similar at all stations presented. The magnitudes of DIP values are about one-third the value of DIN. The figures show that CE-QUAL-ICM does reasonably well at computing higher concentrations of DIP but consistently overpredicts the lower values. This is also indicated in the cumulative distribution plot (Figure 6-5); CE-QUAL-ICM consistently overpredicts concentrations less than 0.02 mg/L and underpredicts values greater than this. Statistics demonstrate good model performance with the RE at approximately 45 percent for the combined statistics for all stations (Table 6-1). That is comparable to or better than other study results presented in Table 6-5, implying better model performance for LSJR. Comparison of the RE statistics by year modeled illustrates that there is very little difference in model performance between years (Tables 6-2 and 6-3). When the REs for individual stations are compared, the greatest RE values occur at the stations closest to the boundary locations in the grid (i.e., Palatka and the ocean). At Palatka, the high RE reflects the low observed DIP concentration in the denominator of the error formula. Near the ocean, the RE reflects the difficulty in assigning open-mouth boundary conditions.

The CE-QUAL-ICM was reasonably able to spatially reproduce the DIP increase then decrease longitudinally through the study reach during the warm months of August 1997 and August 1998. At the most upstream stations for both years, the CE-QUAL-ICM was slightly overpredicting DIP. Longitudinal plots of DIP for other months of the simulation period are provided on the CD-ROM.

Total Phosphorus (TP)

TP values for the simulation period have similar magnitudes to DIN values, and approximately half of TP appears to be in the organic form. Time-series plots presented in Figures 6-2 through 6-4 show that the magnitude of observed TP values is in the same range at all stations, as was also noted for DIP above. The figures indicate two periods of increasing/decreasing TP concentrations, which CE-QUAL-ICM appears to be capturing. The RE for the combined statistics for all stations (Table 6-1) is approximately 27 percent. This RE value is better than or comparable to what has been reported for other studies (Table 6-5). When RE statistics are compared by year, the RE value is only slightly better for the first year indicating that CE-QUAL-ICM performs about the same for both years. The RE is distributed roughly uniformly among stations with no distinct trends.

As indicated in Figure 6-6, CE-QUAL-ICM consistently underpredicts TP concentrations at all levels. This trend is also demonstrated with an ME value of 0.014 mg/L.

Spatially, CE-QUAL-ICM is able to predict trends in TP values, which were similar to trends seen in DIP values during the critical months of August 1997 and August 1998. CE-QUAL-ICM reproduced reasonably well the increase then decrease of TP values longitudinally throughout the study reach. Like DIP values at the most upstream stations, CE-QUAL-ICM was slightly overpredicting TP. Longitudinal plots of TP for other months of the simulation period are provided on the CD-ROM.

TOC and DOC

As pointed out by Cole (1995), DOC is extremely important when addressing eutrophication-related issues in the LSJR. DOC affects light penetration in the freshwater reaches of the LSJR, limiting productivity and making it imperative that DOC loading be accurately estimated. The TOC of the LSJR system is composed of approximately 10 percent LTOC (Hendrickson et al. 2002). To address this concern, the model was modified to handle labile and refractory classes of TOC and DOC. Comparing observed values of TOC and DOC shows that most of the TOC is in the dissolved form. For this reason, the rest of this section discusses only DOC.

Figures 6-2 through 6-4 contain time series of computed versus observed data for DOC. From the figures, it can be seen that CE-QUAL-ICM is reproducing the variability in DOC values, especially the increase from early to late winter in 1997-1998. The model appears to be performing very well with the RE of DOC and TOC for the combined station statistics at approximately 18 percent (Table 6-1). Comparison of this value to reported values of RE in other studies demonstrates that CE-QUAL-ICM performs better at LSJR for this constituent. With the capability of being able to model different classes of TOC and DOC, model performance has been improved. When RE statistics are compared by year, RE values are very similar, indicating CE-QUAL-ICM performs about the same for both years. Individual station statistics shows that the station closest to

the ocean boundary, Fulton Point, has the highest RE of all stations (approximately 45 percent). Problems at boundary stations have been seen for other constituents discussed previously.

The cumulative distribution plot (Figure 6-6) shows that, for concentrations less than 8 mg/L, CE-QUAL-ICM slightly overpredicts DOC values (Figure 6-6). For greater values, CE-QUAL-ICM does an adequate job accurately predicting DOC values. This tendency is also verified with the ME of -0.17 mg/L.

Spatially, CE-QUAL-ICM was able to reproduce DOC values longitudinally during the critical months of August 1997 and August 1998. CE-QUAL-ICM was able to reproduce the trend of increased DOC concentrations from the ocean boundary to the middle of the study reach, then a leveling off of concentration magnitudes in the upstream direction (Figure 6-5). Longitudinal plots of DOC and TOC for other months of the simulation period are provided on the CD-ROM.

Dissolved Oxygen

Times-series plots shown in Figures 6-2 through 6-4 demonstrate that CE-QUAL-ICM has the ability to reproduce trends in seasonal DO variation (i.e., higher DO values during winter months and lower values during summer months). Influence in saturation concentrations (a function of salinity and temperature) can also be seen when comparisons are made between the lower DO values found close to the ocean boundary and the higher values found in the freshwater regions. The greatest differences are most noticeable for time-series plots showing bottom level DO results (e.g., Fulton Point or Piney Point). The RE value for LSJR was 9.3 percent. When compared to the RE value of other studies (Table 6-6), model performance is comparable to most other sites except for Chesapeake Bay's Mainstem and San Juan Bay. CE-QUAL-ICM appears to be doing better, but this is not actually the case, since only bottom DO values were used in computing the RE statistics at Mainstem and San Juan Bays. At LSJR ,all levels of DO values were used in computing the RE statistics. If only bottom DO values were used in calculating the RE at LSJR, a comparable RE would probably be obtained. When RE statistics are compared by year, RE values are very similar, indicating CE-QUAL-ICM performs about the same for both years. Like other constituents previously discussed, the individual station statistics show the greatest RE (as well as increases in other statistics) occurs at the upstream stations closest to the boundary.

The DO cumulative distribution plot (Figure 6-6) demonstrates that CE-QUAL-ICM is capturing DO values at all concentration ranges with a slight underprediction in the higher values (>7mg/L). This trend is also implied by an ME of 0.04 mg/L.

Spatially observed data for August 1997 and August 1998 show similar behavior trends in DO (Figure 6-4), a dip in DO concentrations in the downstream stations then increase to mid-stations followed by a decrease toward the most upstream station. A noted difference in the 2 years is that, during August 1998, DO values beginning at stations mid-LSJR to most of the upstream

stations are higher than those observed in August 1997. This difference is probably the result of higher observed chlorophyll values, thus more DO being produced. The model does not capture this. Longitudinal plots of DO for other months of the simulation period are provided on the CD-ROM.

Total Suspended Solids (TSS)

Observed TSS concentrations are highest at the most downstream station (Figure 6-2), and decrease in the upstream direction (Figure 6-4). Time-series plots all show computed TSS is underpredicted at all stations (Figure 6-2 through 6-4). It is not clear why underprediction occurs since settling is set to a low rate. Problems in computing TSS may be caused by not having PS and NPS loads correctly estimated. The RE of TSS for the combined station statistics is 60 percent (Table 6-1). When the RE statistics are compared by year, the RE value during the 1996-1997 year is slightly better than for the 1997-1998 year (i.e., 57 percent as compared to 61 percent, respectively). This indicates that CE-QUAL-ICM performs better during the first year of simulation for this variable, possibly because loads are set more accurately. Comparing individual station statistics shows the highest RE values occur from about mid-study reach in the downstream direction where much of the loads enter.

From the cumulative distribution plot, TSS is being underpredicted by CE-QUAL-ICM at all concentration levels (Figure 6-6). The ME for the combined statistics also indicates that TSS is on average approximately 10 mg/L lower than observed. If you look at ME for TSS for each year modeled, the model does better at predicting TSS in 1996-1997 (ME = 3.64 mg/L) than in 1997-1998 (ME = 16.6 mg/L).

Spatially observed data for August 1997 and August 1998 show similar behavior trends longitudinally in TSS (Figure 6-5), higher concentrations of TSS at the downstream stations, then a decrease to middle stations followed by an increase toward the most upstream station. CE-QUAL-ICM reproduces this trend better longitudinally in August 1997 than in August 1998 (Figure 6-5). This affirms the previous discussion about comparison of the RE statistic for each year modeled.

References

Cole, T. M. (1995). "Review of water quality monitoring and recommendations for water quality modeling of the Lower St. Johns River," Miscellaneous Paper EL-95-3, U.S. Army Engineer Waterways Experiment Station, Vicksburg, MS.

Hendrickson, J. C., and Konwinski, J. (1998). "Seasonal nutrient import-export budgets for the Lower St. Johns River, Florida." Final report under Contract No. WM598, Florida Department of Environmental Protection. Tallahassee, FL. 109 pp.

Hendrickson, J., Trahan, N., Stecker, E., and Ying, O. (2002). "TMDL and PLRG modeling of the Lower St. Johns River Technical Report Series,

Volume 1: Calculation of the external load." (Draft). St. Johns River Water Management District, Palatka, FL.

Sucsy, P. V., and Morris, F. W. (2002). "Calibration of a three-dimensional circulation and mixing model of the Lower St. Johns River." (Draft Technical Memorandum). St. Johns River Water Management District, Palatka, FL.

7 Modeling Processes at the Sediment-Water Interface

Introduction

The predictive benthic sediment model applied to the St. Johns River was first developed for use in Chesapeake Bay (DiToro and Fitzpatrick 1993). Management of the bay required a model with two fundamental capabilities:

- Predict effects of management actions on sediment-water exchange processes, and
- Predict time scale for alterations in sediment-water exchange processes.

The model (Figure 7-1, Table 7-1) is driven by net settling of organic matter from the water column to the sediments. In the sediments, the model simulates the diagenesis (decay) of the organic matter. Diagenesis produces oxygen

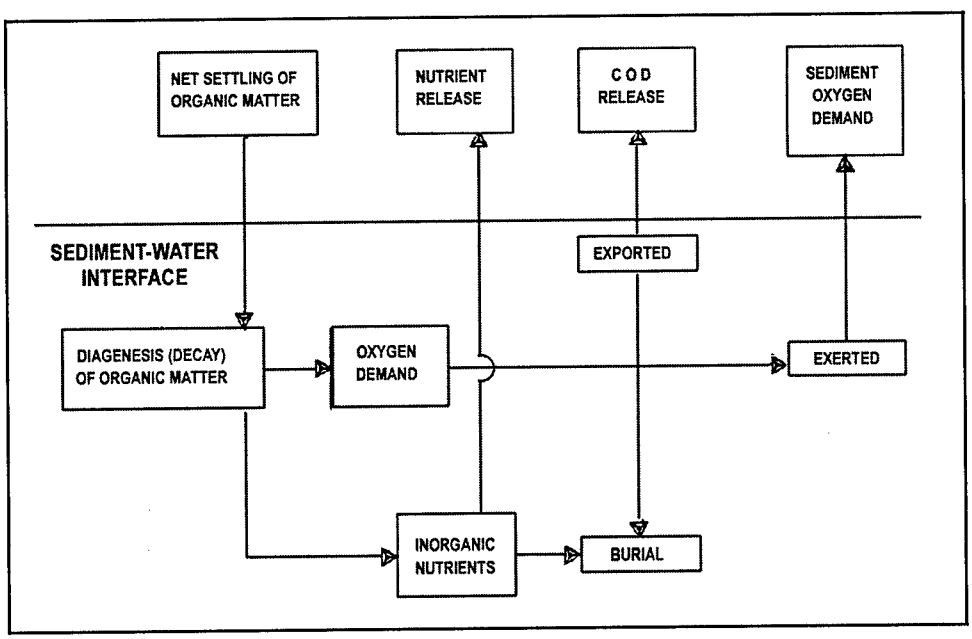

Figure 7-1. Sediment model schematic

Table 7-1
Sediment Model State Variables and Fluxes

State Variable	Sediment-Water Flux
Temperature	
Particulate Organic Carbon	Sediment Oxygen Demand
Sulfide/Methane	Release of Chemical Oxygen Demand
Particulate Organic Nitrogen	
Ammonium	Ammonium Flux
Nitrate	Nitrate Flux
Particulate Organic Phosphorus	
Phosphate	Phosphate Flux
Particulate Biogenic Silica	
Available Silica	Silica Flux

demand and inorganic nutrients. Oxygen demand, as sulfide (in saltwater) or methane (in freshwater), takes three paths out of the sediments: export to the water column as chemical oxygen demand, oxidation at the sediment-water interface as sediment oxygen demand, or burial to deep, inactive sediments. Inorganic nutrients produced by diagenesis take two paths out of the sediments: release to the water column, or burial to deep, inactive sediments.

The formulation of the diagenesis model is too extensive to repeat here. Complete model documentation was provided by DiToro and Fitzpatrick (1993). More accessible documentation may be found in DiToro (2001). Details of the sediment model, required to understand the coupling of the sediment submodel to the model of the water column, are provided in this chapter.

Coupling With the Sediment Diagenesis Model

Benthic sediments are represented as two layers with a total depth of 10 cm (Figure 7-2). The upper layer, in contact with the water column, may be oxic or anoxic depending on DO concentration in the water. The lower layer is permanently anoxic. The thickness of the upper layer is determined by the penetration of oxygen into the sediments. At its maximum thickness, the oxic layer depth is only a small fraction of the total.

The sediment model consists of three basic processes. The first is deposition of particulate organic matter from the water column to the sediments. Due to the negligible thickness of the upper layer, deposition proceeds from the water column directly to the lower, anoxic layer. Within the lower layer, organic matter is subject to the second basic process, diagenesis. The third basic process is flux of substances produced by diagenesis to the upper sediment layer, to the water column, and to deep, inactive sediments. The flux portion of the model is the most complex. Computation of flux requires consideration of reactions in both sediment layers, of partitioning between particulate and dissolved fractions

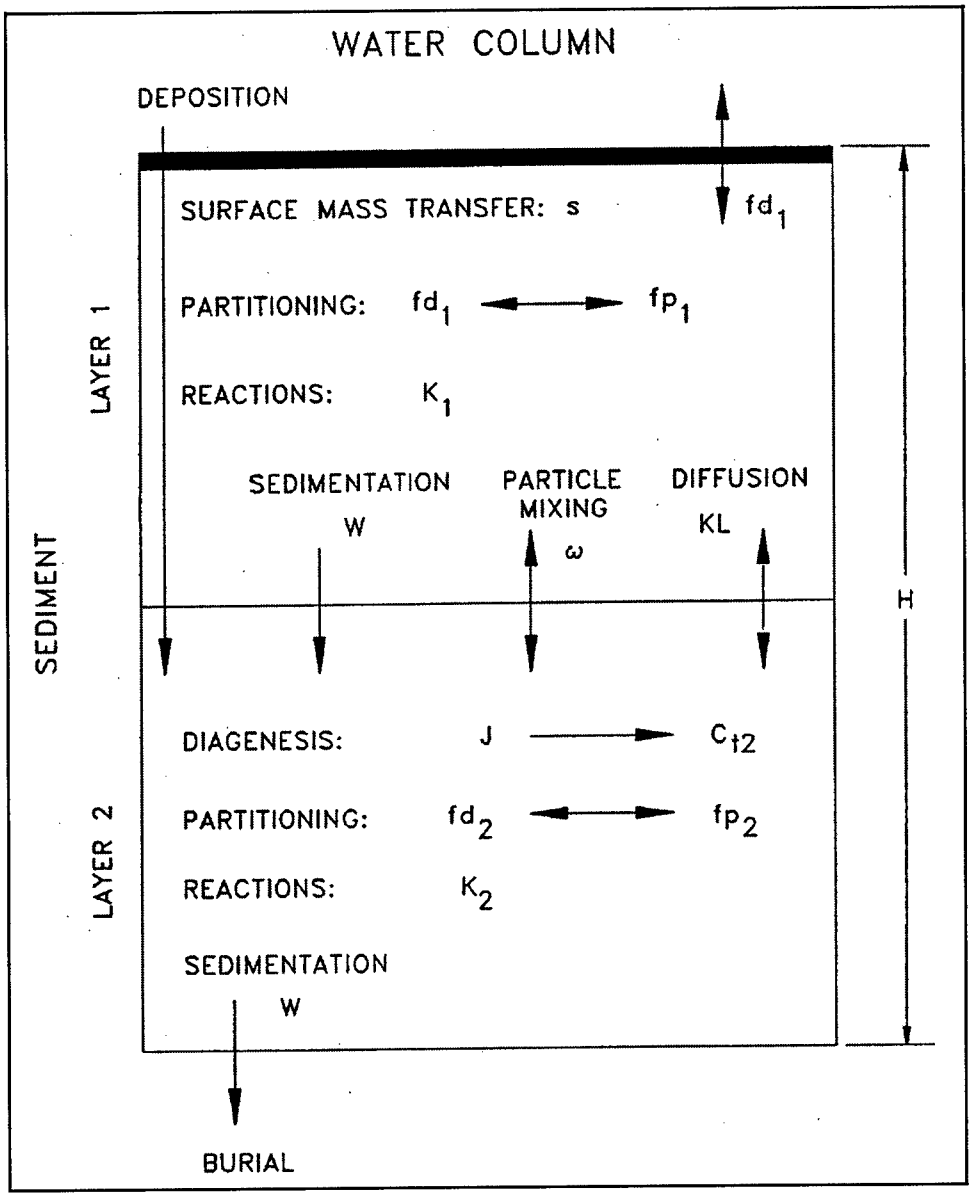

Figure 7-2. Sediment model elevation

in both layers, of sedimentation from the upper to lower layer and from the lower layer to deep inactive sediments, of particle mixing between layers, of diffusion between layers, and of mass transfer between the upper layer and the water column.

The water quality and sediment models interact on a time scale equal to the integration time step of the water quality model. After each integration, predicted particle deposition, temperature, nutrient and DO concentrations are passed from the water quality model to the sediment model. The sediment model computes sediment-water fluxes of dissolved nutrients and oxygen based on predicted diagenesis and concentrations in the sediments and water. The computed sediment-water fluxes are incorporated by the water quality model into appropriate mass balances and kinetic reactions.

Deposition

Deposition is one process that couples the model of the water column with the model of the sediments. Consequently, deposition is represented in both the sediment and water-column models. In the water column, deposition is represented with a modification of the mass-balance equation applied only to cells that interface the sediments:

$$\frac{\delta C}{\delta t} = [transport] + [kinetics] + \frac{WS}{\Delta z} \cdot C_{up} - \frac{W_{net}}{\Delta z} \cdot C \qquad (7\text{-}1)$$

in which:

C = concentration of particulate constituent in cell above sediments (g m^{-3})
WS = settling velocity in water column (m d^{-1})
C_{up} = constituent concentration two cells above sediments (g m^{-3})
W_{net} = net settling to sediments (m d^{-1})
Δz = cell thickness (m)

Net settling to the sediments may be less than or equal to settling in the water column. Sediment resuspension is implied when settling to the sediments is less than settling through the water column.

Diagenesis

Organic matter in the sediments is divided into three G classes or fractions, in accordance with principles established by Westrich and Berner (1984). Division into G classes accounts for differential decay rates of organic matter fractions. The $G1$ (labile) fraction has a half-life of 20 days. The $G2$ (refractory) fraction has a half-life of 1 year. The $G3$ (inert) fraction undergoes no significant decay before burial into deep, inactive sediments. Each G class has its own mass-conservation equation:

$$H \cdot \frac{\delta Gi}{\delta t} = W_{net} \cdot f_i \cdot C - W \cdot Gi - H \cdot K_i \cdot Gi \cdot \theta_i^{(T-20)} \qquad (7\text{-}2)$$

in which:

H = total thickness of sediment layer (m)
Gi = concentration of organic matter in G class i (g m^{-3})
f_i = fraction of deposited organic matter assigned to G class i
W = burial rate (m d^{-1})
K_i = decay rate of G class i (d^{-1})
θ_i = constant that expresses effect of temperature on decay of G class i

Since the $G3$ class is inert, $K_3 = 0$.

Sediment-water flux

The exchange of dissolved substances between the sediments and water column is driven by the concentration difference between the surface sediment layer and the overlying water. Flux may be in either direction across the sediment-water interface, depending on concentration gradient. Sediment-water flux is computed within the diagenesis model as the product of concentration difference and an internally-computed mass-transfer coefficient. In the water column, sediment-water exchange of dissolved substances is represented with a modification of the mass-balance equation applied only to cells that interface with bottom sediments:

$$\frac{\delta C}{\delta t} = [transport] + [kinetics] + \frac{BENFLX}{\Delta z} \tag{7-3}$$

in which *BENFLX* is the sediment-water flux of dissolved substance (g m^{-2} d^{-1}).

By convention, positive fluxes are from sediment to water. Negative fluxes, including sediment oxygen demand, are from water to sediments.

Field and Laboratory Program

A program of field and laboratory analyses, aimed at quantifying sediment-water interactions in the St. Johns River, was conducted by personnel from the University of Florida. Numerous observations were conducted, not all of which were germane to the present model effort and domain. Relevant portions of the program included measures of sediment-water fluxes, measures of bulk sediment properties, and measures of interstitial water concentrations.

Sediment-water fluxes

Measures of sediment-water fluxes of oxygen, ammonium, and phosphate were conducted via laboratory incubation of intact cores. Cores were collected in June and October 2001 from four locations (Figure 7-3). Triplicate cores were incubated under aerobic (all substances) and anaerobic conditions (nutrients only). Blank nutrient columns, containing water only, were run for two locations during the October sampling. Cores for sediment oxygen demand analyses were incubated from 12 to 24 hours at approximately 20 °C. Sampling interval varied with more intensive measures of DO concentration early in the incubation. Cores for nutrient analyses were incubated for 5 days. Sampling interval varied with samples collected more frequently early in the incubation.

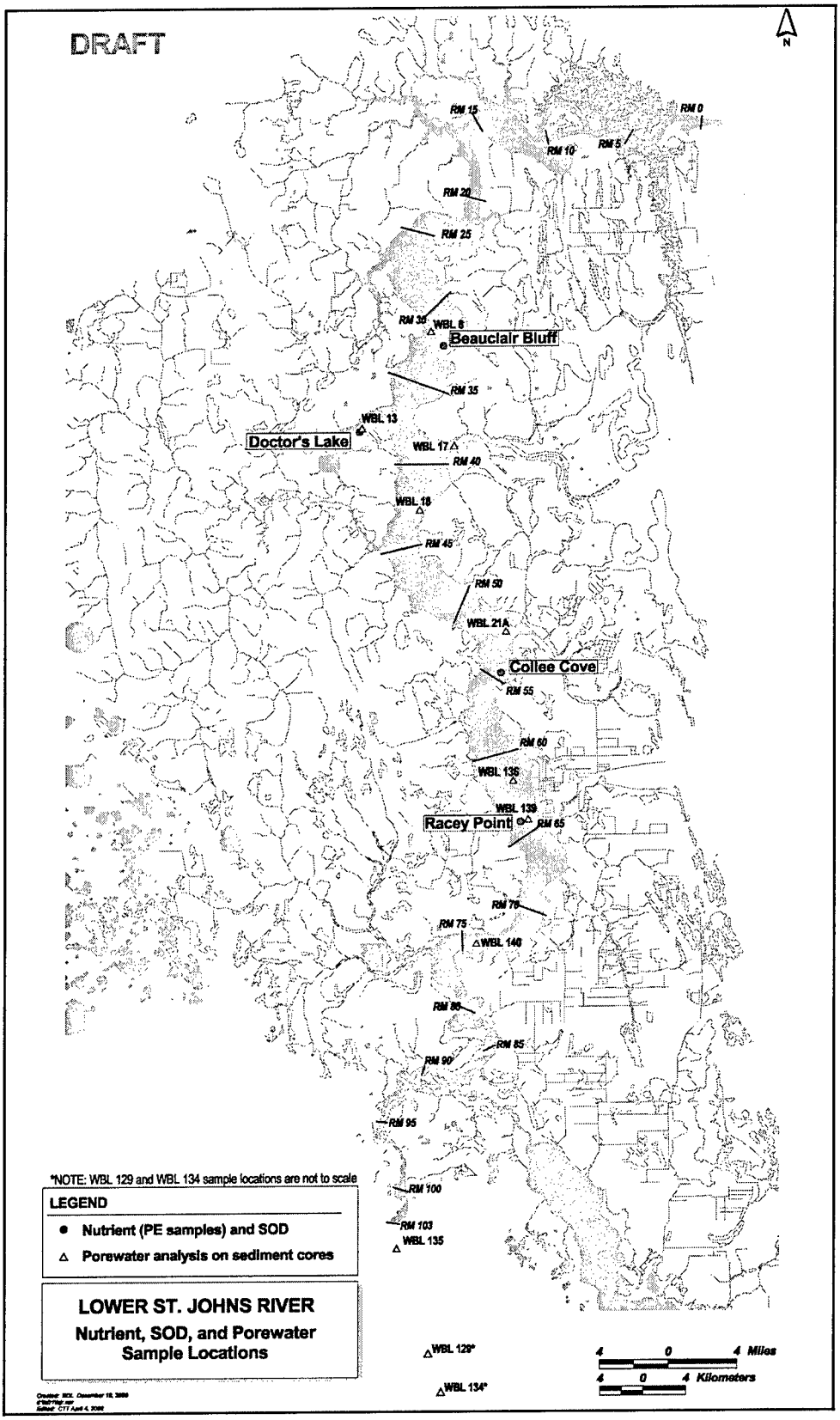

Figure 7-3. Location of sediment-water flux and interstitial water measurements

Bulk sediment properties

Analyses of bulk sediment properties were conducted at 31 locations within the model domain. Analyses were conducted on the upper 10 cm of sediment, consistent with the layer thickness of the diagenesis model. Properties analyzed included dry density, wet density, total carbon, total nitrogen, total phosphorus, and HCL-extractable phosphorus.

Interstitial water

Sediment peepers were used for in-situ sampling of interstitial water at the four locations selected for measurement of sediment-water fluxes. Water collected in the peepers was analyzed for ammonium, nitrate, and phosphate. Interstitial water was removed from intact cores collected at eight locations within the model domain. These samples were analyzed for sulfide and silica as well as ammonium, nitrate, and phosphate.

Data Analyses

Sediment-water fluxes

Sediment-water oxygen and nutrient fluxes are measured by sampling the water overlying sediment cores. Fluxes are inferred from concentration changes in the water. Simultaneous sampling of a control or blank column, containing water only, is advisable to identify concentration changes due to processes in the water or between the water and column walls. Apparent fluxes in the blank column are then subtracted from the fluxes measured in the columns containing both sediment and water.

The time series of DO in water overlying the sediment cores showed a two-phase behavior. A very rapid decline was followed by a slower, more linear decrease. This behavior is frequently seen in flux measurements and is usually attributed to disturbance of the sediment-water interface and, perhaps, sediment resuspension. The first 2 hours of data were eliminated to allow time for initial disturbances to settle. Linear regression was used to fit a line to the remaining DO observations in each core. The slope of this line, g O_2 m^{-3} d^{-1}, multiplied by the depth of water, 0.15 m, resulted in sediment oxygen demand, g O_2 m^{-2} d^{-1}. From 5 to 12 samples were in each regression. Strength of individual relationships, quantified as R^2, varied from essentially zero to unity. Median R^2, over all regressions, was 0.88. No blank column was run, so the measured demand (Table 7-2) is a combination of demand from the sediments and overlying water.

A similar process was followed to quantify the sediment-water nutrient fluxes. Observations from the first 2 hours were dropped to eliminate initial disturbances. The sample collected after 5 days was often aberrant, so this

Table 7-2
Summary of Sediment-Water Fluxes

		Aerobic NH4 Flux, mg m^{-2} d^{-1}		Anoxic NH4 Flux, mg m^{-2} d^{-1}		Aerobic PO4 Flux, mg m^{-2} d^{-1}		SOD, g m^{-2} d^{-1}	
		Mean	Standard Dev.	Mean	Standard Dev.	Mean	Standard Dev.	Mean	Standard Dev.
June	Beauclair*	-1.08	0.10	23.37	0.95	1.13	0.102	-0.27	0.024
June	Doctor Lk*	-14.46	1.51	13.83	0.85	0.85	0.135	-0.24	0.062
June	Collee Cv*	-0.35	0.09	28.03	0.55	0.95	0.044	-0.21	0.022
June	Racey Pt*	0.71	0.52	27.37	0.68	2.11	0.035	-0.36	0.155
October	Beauclair*	-8.33	1.28	53.37	2.71	0.75	0.107	-0.11	0.000
October	Doctor Lk*	-11.59	0.61	102.93	7.29	1.63	0.035	-0.26	0.040
October	Collee Cv*	-38.46	0.33	37.37	1.65	-0.25	0.038	-0.21	0.030
October	Racey Pt*	0.46	1.50	15.80	1.47	0.78	0.059	-0.37	0.137
October	Doctor Lk (water)	-0.41	0.08	11.07	0.54	-1.97	0.015		
October	Racey Pt (water)	0.00	0.04	11.53	0.60	-1.49	0.023		

* Corrected for activity in water.

sample was dropped as well. Consequently, regressions were based on four to six samples collected over a 2-day period. The value of R^2 again ranged from near-zero to unity. Median R^2 was 0.61 for the aerobic phosphorus measures, 0.66 for the aerobic ammonium measures, and 0.95 for the anaerobic ammonium measures. Measures in blank columns were available from two locations in the October sampling. These were used to correct the apparent fluxes in all cores from the June and October samplings (Table 7-2).

The St. Johns River does not exhibit bottom-water anoxia. Therefore, the aerobic nutrient fluxes are the best reflection of in-situ sediment-water nutrient exchanges. The anoxic nitrogen fluxes are valuable, however, as indicators of "diagenesis flux" (DiToro 2001). Diagenesis flux is the amount of ammonium produced by decay of organic matter in the sediments. The diagenetic ammonium flux is attenuated by nitrification in the aerobic sediment layer. Nitrate produced by nitrification is subsequently reduced to gaseous nitrogen by denitrification in anoxic microzones (Jenkins and Kemp 1984). Consequently, ammonium released to overlying water, under aerobic conditions, is much less than the amount produced through diagenesis. Sediment nitrification in the St. Johns River apparently proceeds at such a rate that ammonium is often stripped from the water column (Table 7-2).

Sediment oxygen demand observed in this study, ≈0.1 to 0.4 g m^{-2} d^{-1} is low relative to other systems in which we have worked. In Chesapeake Bay, for example, the vast preponderance of sediment oxygen demand observations exceed 0.5 g m^{-2} d^{-1} (DiToro 2001) while in the St. Johns, none of the observations achieve this level.

Sediment phosphorus release is also small, consistent with the aerobic conditions of the overlying waters. Significant sediment phosphorus release usually occurs under anoxic conditions when iron oxides in surficial sediments, which adsorb phosphate and prevent its release under oxic conditions, are reduced to soluble form allowing free diffusion of phosphate to overlying water. The sediment-water phosphate fluxes in the St. Johns are, in fact, indeterminate. Phosphorus uptake in the blank columns was large relative to phosphate flux in the columns containing sediment. Subtraction of the blank flux from the sediment-water fluxes resulted in small net release from sediments to water. Due to the limited number of blank observations and the classic problem of obtaining a small difference via subtraction of two large numbers, we believe the best statement about sediment-water phosphate flux in the St. Johns is that it is so small it cannot be reliably measured.

Interstitial water

Concentrations in interstitial water were reported based on volume of interstitial water. Concentrations in the sediment model are computed based on bulk sediment volume. For comparison with the model, observed concentrations were converted to a bulk basis through multiplication by porosity (≈0.9).

Bulk sediment properties

Bulk sediment properties were reported based on weight (e.g., g kg^{-1}). Concentrations in the sediment model are computed based on bulk sediment volume. For comparison with the model, observed concentrations were converted to a bulk basis via the relationship:

$$Cb = Cw \cdot (1 - \phi) \cdot \rho \tag{7-4}$$

in which:

Cb = bulk concentration (g m^{-3})

Cw = weight-based concentration (g g^{-1})

ϕ = porosity

ρ = solids density (1.64 g m^{-3})

Solids density was derived from bulk density and moisture content analyses provided by the original investigators.

Parameter Specification

Coupling with the sediment model requires specification of net settling rates, of the G splits of organic matter, and of burial rates.

Net settling rates

Net settling for inorganic solids was specified as 0.075 m d^{-1}, 10 percent of the value in the water column. This specification indicates 90 percent of the solids that initially settle to the bottom are resuspended. Net settling of organic matter was specified identical to settling in the water column: 0.25 m d^{-1} for labile and refractory detritus and 0.1 m d^{-1} for diatoms and green algae. Zero net settling was specified for the buoyant cyanobacteria. Specifications in this study indicate no resuspension occurs for organic matter.

Assignment to *G* classes

Upon deposition in the sediments, state variables representing particulate organic matter in the water quality model required conversion into sediment model state variables (Table 7-3). The water quality model considered two classes of particulate organic matter: labile and refractory. The sediment model was based on three classes of organic particles: labile (G1), refractory (G2), and inert (G3). Labile particles from the water quality model were transferred directly into the G1 class in the sediment model. Refractory particles from the water quality model had to be split into G2 and G3 fractions upon entering the sediments. Algae settling directly to the sediments also required routing into sediment model state variables. Initial guidance for the splits was obtained from the most recent Chesapeake Bay model calibration (Cerco and Noel 2003). Subsequently, the fraction of refractory carbon routed to the G3 class was increased to reflect the large sediment carbon concentrations observed in the St. Johns River.

Table 7-3
Routing Organic Particles Into Sediment Classes

WQM Variable	Carbon			Nitrogen			Phosphorus		
	% G1	% G2	% G3	% G1	% G2	% G3	% G1	% G2	% G3
Labile Particles	100			100			100		
Refractory Particles		60	40		86	14		73	27
Algae	60	20	20	65	30	5	65	25	10

Burial rates

Lead-210 sedimentation rates were provided from 20 cores collected in 8 locations. Burial rates ranged from 0.19 to 3.88 cm yr^{-1} with two-thirds of the data in the range 0.4 to 1.2 cm yr^{-1}. A range of options existed for employment of this data. At one extreme, the observed rates could be employed at measurement locations and the rates elsewhere obtained by interpolation/ extrapolation. At the other extreme, a single value could be used everywhere. A compromise would be to explore the data for trends that could be represented in the model. The data were too sparse for meaningful extrapolation of

individual observations and spatial patterns were difficult to distinguish. This study uses the median value, 0.9 cm yr^{-1}, throughout.

Sediment model parameters

With one exception, all parameters within the diagenesis model are exactly as derived for the original model application (DiToro and Fitzpatrick 1993). The model bulk solids density was reduced from 0.5 kg L^{-1} (Chesapeake Bay) to 0.3 kg L^{-1}, based on data supplied by the original investigators.

Model Results

The field program was conducted during 2001, while the model application period was December 1996 through November 1998. For comparison with the observations, model results in the cells corresponding to sample locations were averaged over June and October of the computed years.

Sediment-water fluxes

Computed and observed diagenesis flux show remarkable agreement, with values centered in the range of 20 to 40 mg N m^{-2} d^{-1} (Figure 7-4). The close agreement indicates the model is correctly computing the rate of organic matter decomposition in the sediments. Both observations and model indicate that little or none of the diagenesis flux escapes to the water column (Figure 7-5). Observations suggest sediments strip ammonium from the water column, while the model computes ≈15 percent of the diagenetically produced ammonium escapes the sediments. In view of the uncertainties in the observations, uncertainties associated with comparisons of different years, and the small magnitude of the fluxes, it is concluded that the model adequately represents sediment-water ammonium flux.

Both observations and model indicate low rates of sediment oxygen demand (Figure 7-6), although the modeled rate exceeds the observed. The most likely reason for the computed excess is the difference between incubation temperature and in-situ temperature. Laboratory measures were conducted at ≈20 °C, while computations were based on in-situ temperatures of 22.5 °C (June) and 30 °C (October). Commonly used temperature corrections indicate laboratory oxygen demand should be increased by 12 percent to correct for June temperatures and by 62 percent to correct for October temperatures. Some small downward adjustments in computed sediment oxygen demand might still be made and could be readily accomplished by various parameter adjustments. Potential downward adjustments will cause associated declines in computed diagenesis flux, however, which is presently well-represented. The present model calibration is a compromise that provides good representation of diagenesis flux and sediment oxygen demand but not perfect representation of either.

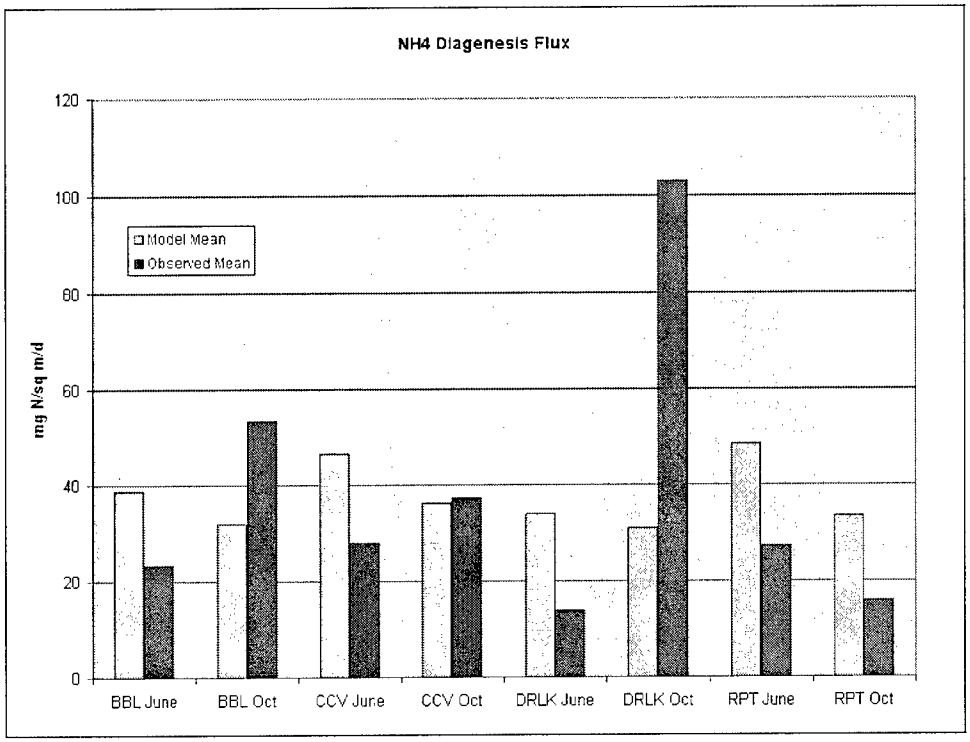

Figure 7-4. Computed and observed sediment diagenesis flux

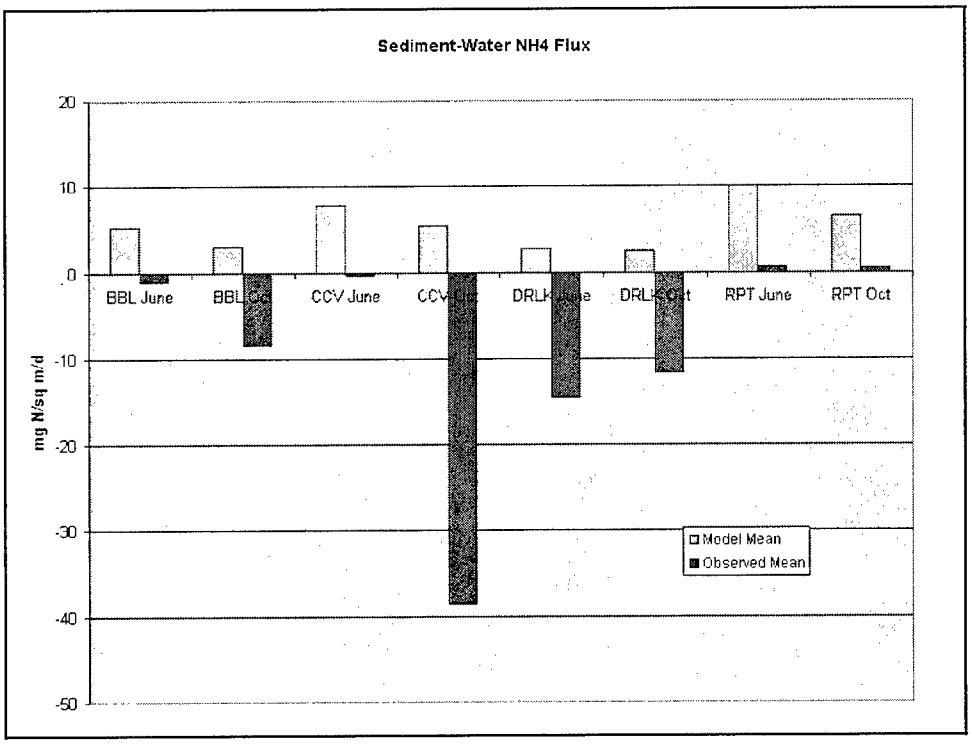

Figure 7-5. Computed and observed sediment-water ammonium flux

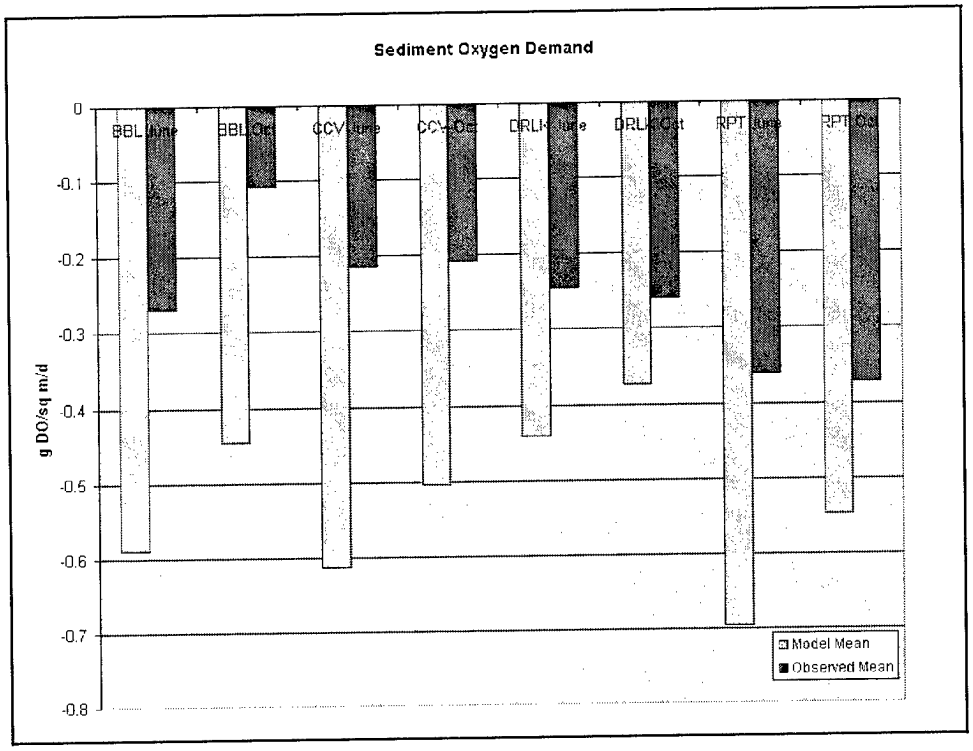

Figure 7-6. Computed and observed sediment oxygen demand

Observations indicate small sediment phosphate releases, but they are, as previously noted, too small to effectively determine. Modeled releases are also small, ≈ 1 mg P m^{-2} d^{-1} (Figure 7-7). It is concluded that the model well represents observed sediment-water phosphate flux, especially in view of uncertainties in the observations, uncertainties associated with comparisons of different years, and the small magnitude of the fluxes.

Interstitial water

The primary goal of the sediment model is to provide accurate computations of sediment-water fluxes. Comparison of other computed and observed properties provides an indication that processes within the sediment model, which lead to fluxes, are operating correctly. Matching computed and observed properties is not a goal in itself.

Computed interstitial ammonium concentration is perhaps half the observed concentration (Figure 7-8). The computed concentration can be raised by changing the ammonium partition coefficient in the model. This change would produce increased sediment ammonium release, which is already on the high side (Figure 7-5). In view of the numerous uncertainties associated with the measures and with conversion of measures into equivalent model quantities, a factor-of-two agreement between modeled and observed concentration is believed to be reasonable.

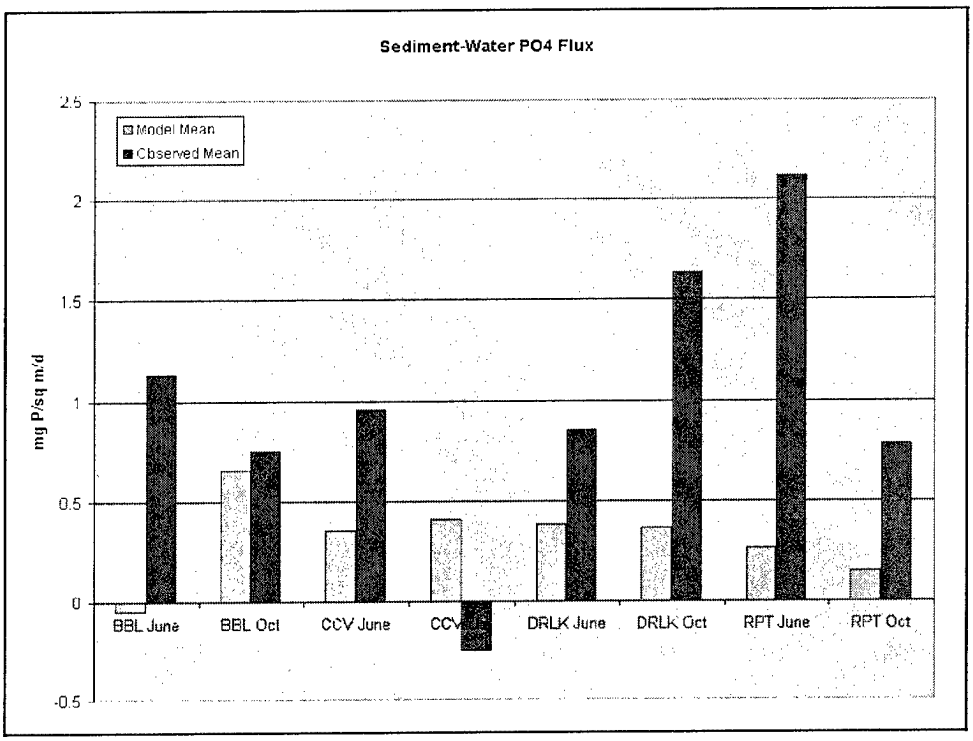

Figure 7-7. Computed and observed sediment phosphate flux

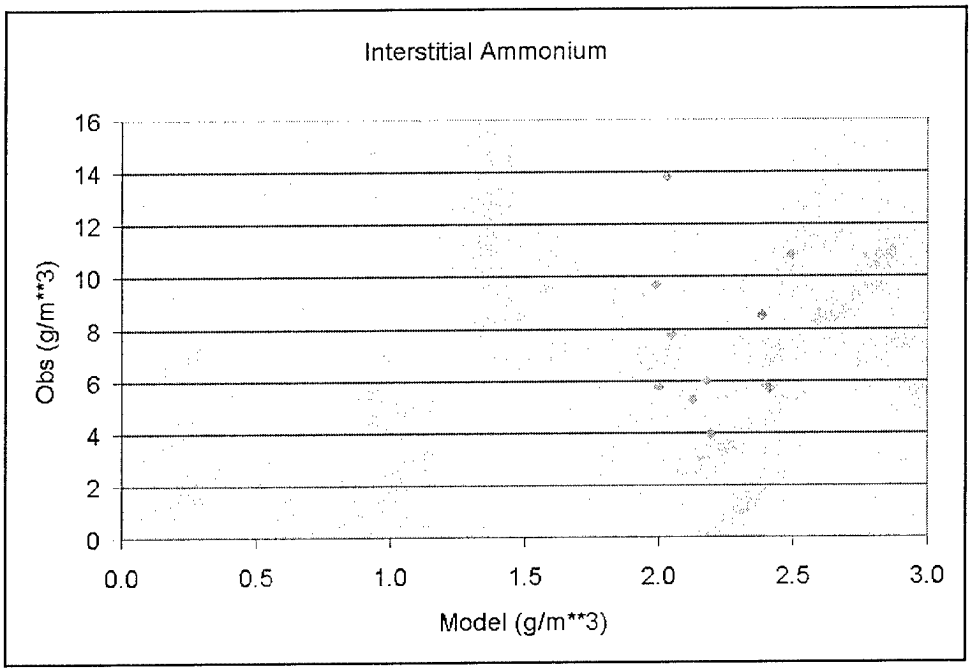

Figure 7-8. Observed versus computed interstitial ammonium concentration

Although a few elevated concentrations are present in the observations, the preponderance of observed and computed nitrate concentrations are low (Figure 7-9). These low concentrations indicate sediment nitrate is rapidly reduced to gaseous nitrogen by the denitrification process.

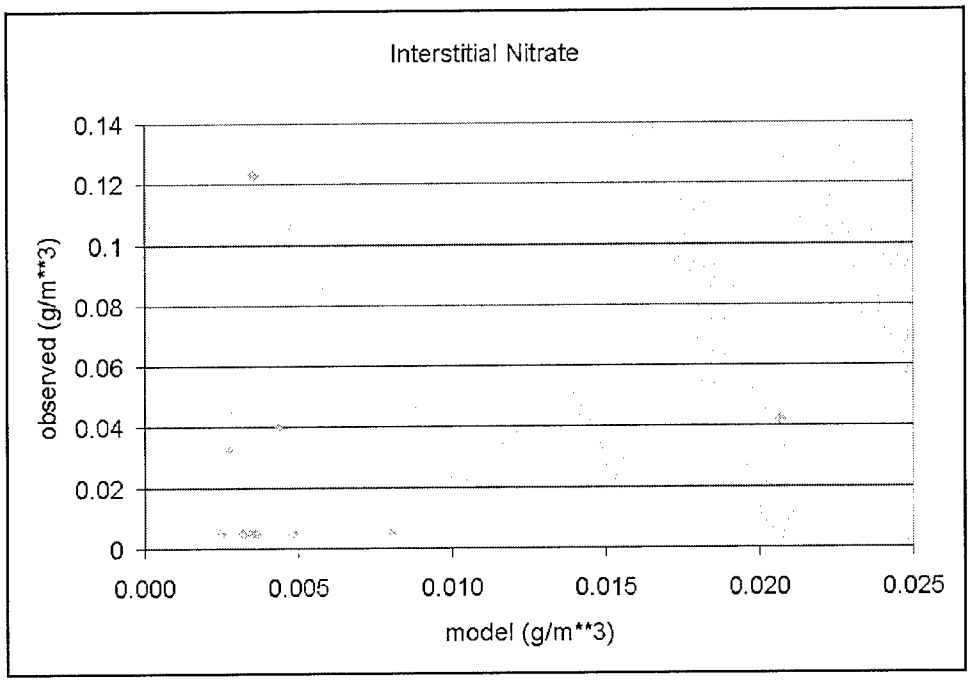

Figure 7-9. Observed versus computed interstitial nitrate concentration

Computed interstitial phosphate agrees well with observed (Figure 7-10). Both observed and computed concentrations are ≈2 g P m^{-3}. Computed interstitial sulfide, a component in the computation of sediment oxygen demand, is a bit larger, on average, than observed although there is a good deal of scatter in both computations and observations (Figure 7-11). As with other substances, the agreement is believed to be good in view of uncertainties in data analysis and conversion. Computed and observed interstitial silica show excellent agreement centered around 15 g Si m^{-3} (Figure 7-12). Since no silica flux measures were collected, this agreement is the best indication that the computed sediment-water silica fluxes are correct.

Bulk concentrations

Computed sediment nitrogen (Figure 7-13) and carbon (Figure 7-14) are an order of magnitude less than observed. Although computed sediment inorganic phosphorus agrees well with observed (Figure 7-15), computed TP is about half the observed TP (Figure 7-16). These discrepancies are too large to attribute to uncertainties in data and model. An interesting question is how the bulk concentrations can be off by a large amount but the computed fluxes can be well represented. The answer is that the preponderance of sediment organic matter is inert G3 material. This material has been described as the "ashes" of the

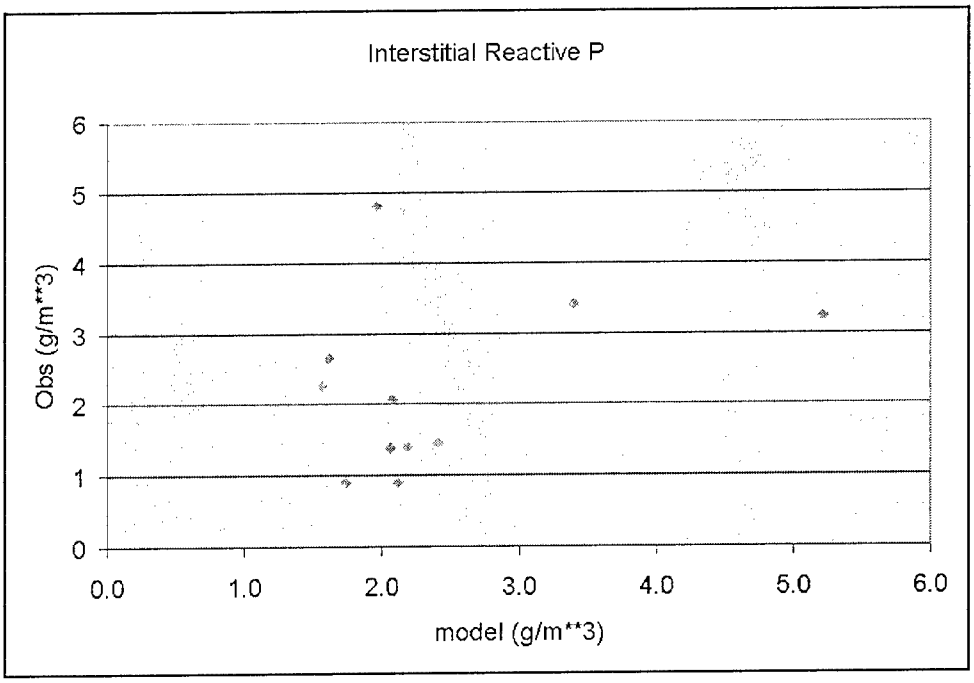

Figure 7-10. Observed versus computed interstitial phosphate concentration

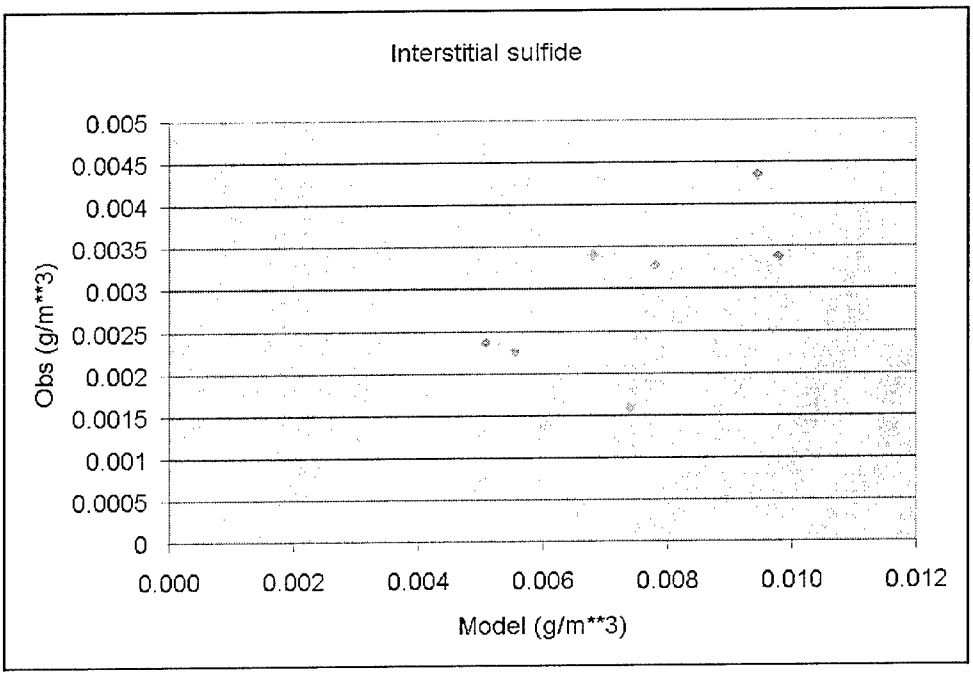

Figure 7-11. Observed versus computed interstitial sulfide concentration

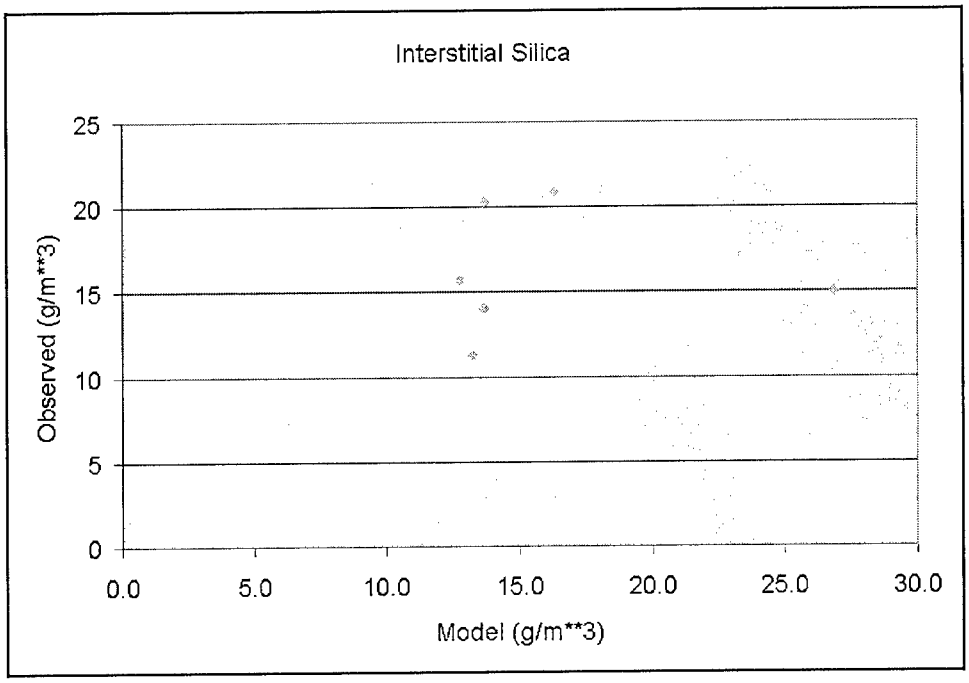

Figure 7-12. Observed versus computed interstitial silica concentration

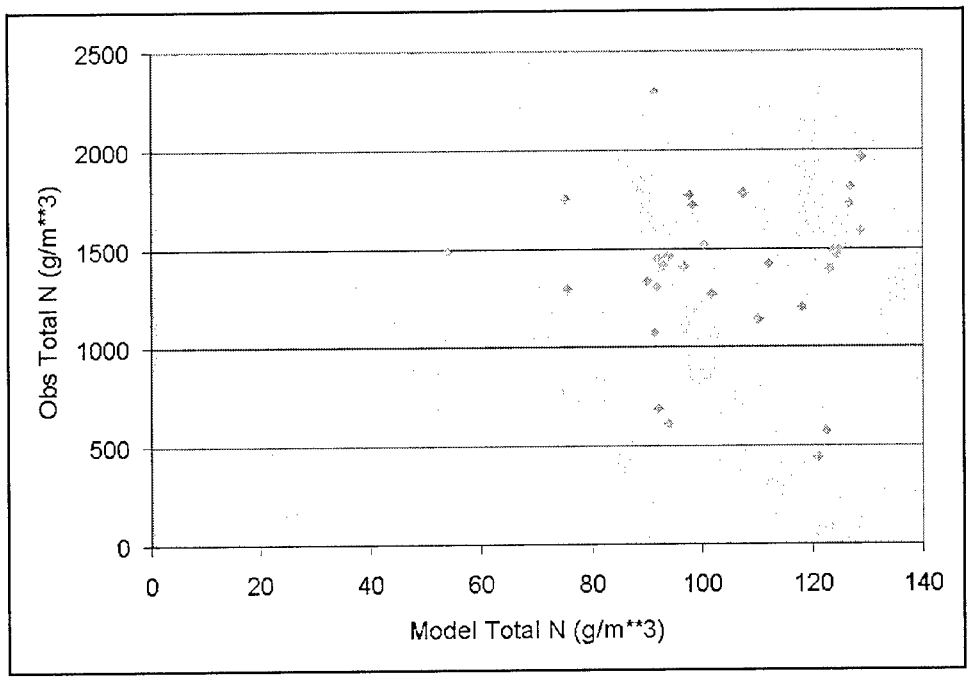

Figure 7-13. Observed versus computed sediment bulk nitrogen concentration

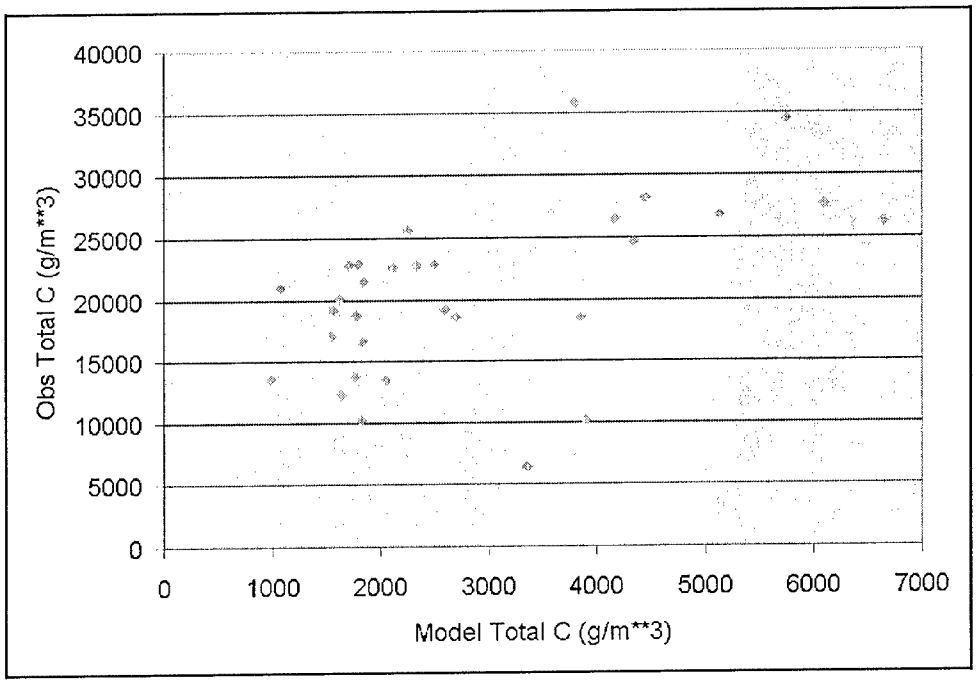

Figure 7-14. Observed versus computed sediment bulk organic carbon concentration

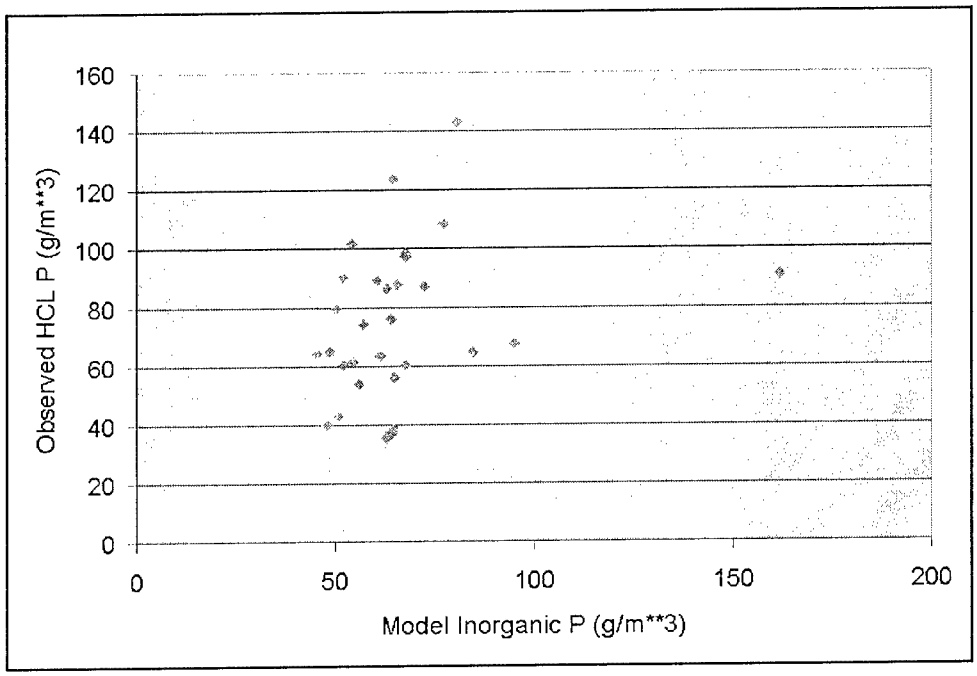

Figure 7-15. Observed versus computed sediment bulk inorganic phosphorus concentration

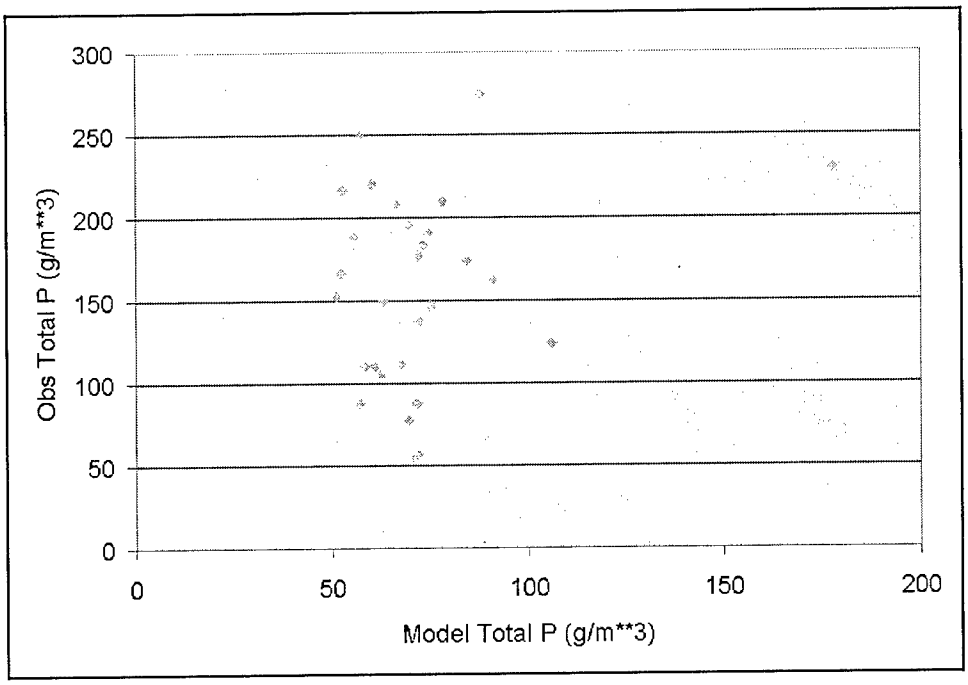

Figure 7-16. Observed versus computed sediment bulk phosphorus concentration

diagenesis process. Since the material is inert, its concentration has no impact on computed fluxes. The concentration of G3 organic matter can be increased by increasing deposition, by decreasing burial, or by increasing the fraction assigned to the G3 class upon deposition. The observed bulk concentrations indicate some adjustments in processes and rates are appropriate, but these will have little or no effect on sediment-water fluxes.

One process that might account for the large concentration of inert sediment organic matter is flocculation and settling of dissolved organic matter in the water column. Some initial analyses of sensitivity to flocculation were performed, but incorporation of the process proved beyond the scope of the present model effort.

References

Cerco, C., and Noel, M. (2003). "The 2002 Chesapeake Bay eutrophication model," ERDC Technical Report (Draft), U.S. Army Engineer Research and Development Center, Vicksburg, MS.

DiToro, D., and Fitzpatrick, J. (1993). "Chesapeake Bay sediment flux model," Contract Report EL-93-2, U.S. Army Engineer Waterways Experiment Station, Vicksburg, MS.

DiToro, D. (2001). *Sediment Flux Modeling*, John Wiley and Sons, New York.

Jenkins, M., and Kemp, W. (1984). "The coupling of nitrification and denitrification in two estuarine sediments," *Limnology and Oceanography* 29(3), 609-619.

Westrich, J., and Berner, R. (1984). "The role of sedimentary organic matter in bacterial sulfate reduction: The G model tested," *Limnology and Oceanography* 29, 236-249.

8 Analysis of Water Column Kinetics

Introduction

This study added several new features to the conventional CE-QUAL-ICM kinetics. These included Droop kinetics, nitrogen fixation, and the split of dissolved organic matter into labile and refractory fractions. This chapter presents initial analysis of the influence of these improvements and also provides the opportunity for comparison of computed and observed phytoplankton primary production and water column respiration.

Droop Kinetics

Representations of the effect of nutrients on phytoplankton growth can be divided into two classes. The first class represents growth as a function of nutrient concentration external to the cell. The second represents growth as a function of nutrients internal to the cell. The formulation and implications of growth based on internal nutrients were reported 30 years ago by Droop (1973). Droop's work was based on three postulates:

- Nutrient uptake depends on external nutrient concentration
- Growth depends on internal nutrient concentration
- At steady state, nutrient uptake must equal the product of growth rate and internal nutrient concentration

DiToro (1980) compared the effects of phytoplankton growth kinetics based on external and internal nutrient concentrations. For realistic cases, he found the growth rates computed by the two formulations were indistinguishable. Formulations based on internal nutrients did, however, provide substantial variation in algal composition relative to the constant composition used in formulations based on external nutrients.

DiToro cited one study (Bierman 1976) that considered internal nutrients in the calculation of algal growth. No additional studies that consider internal nutrients were identified. The formulation commonly known as "Droop kinetics" seems to have fallen by the wayside. Concern over the role of luxury phosphorus uptake in the propagation of the spring algal bloom caused the sponsor to request the consideration of internal nutrients in the present study. While Droop

considered multiple internal nutrients and their interactions, this study is limited to phosphorus. Nutrient limitations due to nitrogen and silica were modeled with conventional relationships based on external nutrient concentrations. Our consideration of phosphorus alone was motivated by the sponsor's concern and by our own experience. Multiple Chesapeake Bay models have used different phosphorus stoichiometry between spring and summer algal groups. In contrast, nitrogen composition requires little or no difference. Experience such as that reflected in DiToro's analyses shows that theoretical variations in algal phosphorus content exceed by an order of magnitude theoretical variations in nitrogen and silica content.

Initial parameter evaluation

As formulated here, the Droop kinetics require evaluation of three parameters for each of the three algal groups. The parameters are:

- *V*max, the maximum rate of algal nutrient uptake (g *P* g^{-1} algal *C* d^{-1})
- *Qo*, the minimum cell quota (g *P* g^{-1} algal *C*)
- *KHp*, the half-saturation concentration for phosphorus uptake (g *P* m^{-3}).

Guidance for evaluation of these parameters is minimal, no doubt due to the lack of this model's employment. DiToro reported cell-based values (attributed to Rhee 1973) for *Scenedesmus*. The reported values can be converted to our model units using cell carbon of 1.5×10^{-6} μmol C/cell (Rhee and Gotham 1981):

- *V*max = 0.2 g *P* g^{-1} algal *C* d^{-1}
- *Qo* = 0.003 g *P* g^{-1} algal *C*
- *KHp* = 0.02 g *P* m^{-3}.

The value for *Qo* corresponds to an algal carbon-to-phosphorus ratio of 333:1, which is enormous relative to the commonly accepted Redfield ratio of 40:1 (Redfield et al. 1966). The original Chesapeake Bay application (Cerco and Cole 1994) used a carbon-to-phosphorus ratio of 127:1 for phosphorus-limited phytoplankton. This ratio corresponds to a cell quota of 0.008 g *P* g^{-1} algal *C*, which is presumed to be close to the minimum since it represents stringently phosphorus-limited conditions. It appears the order-of-magnitude range for *Qo* is 10^{-3} to 10^{-2} g *P* g^{-1} algal *C*.

*V*max can be estimated by noting that, at steady state, phosphorus uptake must equal the algal growth rate. Maximum specific algal growth rate, averaged over a day, is ≈2 d-1. Using the Redfield ratio for cell quota results in:

$$V\max = \frac{2}{day} \cdot \frac{gP}{40gC} = \frac{0.05gP}{gCday} \tag{8-1}$$

It appears *V*max is in the order of magnitude 10^{-1} g *P* g^{-1} algal *C* d^{-1}.

Great care must be taken to distinguish the half-saturation concentration for phosphorus uptake from the half-saturation concentration for algal growth

(DiToro 1980). Taft et al. (1975) reported half-saturation concentration for short-term phosphorus uptake by estuarine algae in the range of 0.003 to 0.053 g P m^{-3}. It appears the order-of-magnitude range for KHp is 10^{-3} to 10^{-2} g P m^{-3}.

Analysis of cell quota

Although the parameters in the Droop kinetics could be approximately evaluated, there was no insight into the response of the model to variations in these parameters. In particular, insight was lacking into how to tune the model to bring results into calibration. An analytical investigation of computation of cell quota was conducted to guide the calibration process.

At steady state, algal growth must equal respiration:

$$G = G\max \cdot \left[1 - \frac{Qo}{Q}\right] = r \tag{8-2}$$

in which:

G = specific growth rate (d^{-1})
Gmax = maximum specific growth rate (d^{-1})
Q = cell quota (g P g^{-1} C)
Qo = minimum cell quota (g P g^{-1} C)
r = specific respiration rate (d^{-1}).

At steady state also, nutrient uptake must equal nutrient release:

$$V\max \cdot \frac{S}{KHp + S} = r \cdot Qo \tag{8-3}$$

in which:

Vmax = maximum nutrient uptake rate (g P g^{-1} C d^{-1})
S = external nutrient concentration (g P m^{-3})
KHp = half saturation concentration for nutrient uptake (g P m^{-3}).

Equations 8-2 and 8-3 can be rearranged to solve for Qo and then equated to each other. The result is:

$$Q \cdot \left[1 - \frac{r}{G\max}\right] = \frac{V\max}{r} \cdot \frac{S}{KHp + S} \tag{8-4}$$

which can be rearranged to yield:

$$Q = \frac{V\max}{r} \cdot \frac{S}{KHp + S} \Big/ \left[1 - \frac{r}{G\max}\right] \tag{8-5}$$

Equation 8-5 yields two insights. First, cell quota is directly proportional to the maximum nutrient uptake rate. Second, minimum cell quota does not appear. This insight is remarkable. Apparently, specification of minimum cell quota does not impact cell quota at all.

The effect of substrate concentration on cell quota can be examined at two extremes. First, note that respiration is much less than the maximum growth rate so that $r/G\max << 1$, and the denominator of Equation 8-5 approaches unity. Then examine conditions of nutrients in great excess, $S >> KHp$. In that case:

$$Q \approx \frac{V\max}{r} \tag{8-6}$$

Cell quota is linearly proportional to the maximum nutrient uptake rate and inversely proportional to the respiration rate.

The opposite extreme is extreme scarcity of nutrients, $S << KHp$. In that case:

$$Q \approx \frac{V\max}{r} \cdot \frac{S}{KHp} \tag{8-7}$$

When nutrients are scarce, cell quota is linearly proportional to external nutrient concentration and inversely proportional to half-saturation concentration for nutrient uptake.

The minimum cell quota can be approached but never attained. The degree to which the minimum can be approached is determined by the ratio of respiration to maximum growth rate. This result is obtained by rearranging Equation 8-2 to yield:

$$Q = Qo \Big/ \left[1 - \frac{r}{G\max}\right] \tag{8-8}$$

Although the ratio r/Gmax is small, it is non-zero. Increasing the respiration rate relative to growth moves the realizable cell quota away from the minimum. Increasing the growth rate relative to respiration moves the realizable cell quota towards the minimum.

Model parameter values

Following initial evaluation, model parameter values were evaluated through a recursive calibration process. Calibration was determined by visual comparison of computed and observed substrate concentrations and algal biomass, and by evaluation of computed cell quotas. Final values of minimum cell quotas and half-saturation concentrations were in the expected range. The maximum uptake rate was considerably lower than the values expected based on published quantities and on order-of-magnitude scaling.

Sensitivity analyses

Sensitivity analyses, conducted during model development (Chapter 5), indicated the following characteristics of Droop kinetics:

- Oscillations in algal biomass and in dissolved phosphate are damped, relative to a model with fixed algal stoichiometry
- Peak biomass does not differ substantially from a model with fixed, minimal phosphorus-to-carbon ratio.

The sensitivity analyses were conducted on a reduced simplified system. It was noted that analyses should be repeated on a system with multiple, time-varying inputs and with complete nutrient kinetics. The enormous effort involved in model set-up, calibration, and execution precluded comparison of Droop kinetics with a second model using fixed algal composition. It was reasoned that a model based on fixed composition could be approximated by reducing the range of computed composition. An attempt was made to reduce the range by increasing minimum cell quota and by reducing maximum nutrient uptake velocity. Minimum cell quota was doubled over the calibration value (Table 8-1). Calibration values were restored and uptake velocity was halved in a subsequent run.

Table 8-1
Parameters in Droop Kinetics

Algal Group	Vmax, g P g^{-1} algal C d^{-1}	Qo, g P g^{-1} algal C	KHp, g P m^{-3}
cyanobacteria	0.006	0.005	0.00075
diatoms	0.0033	0.005	0.003
other	0.0044	0.004	0.001

Results are presented at two locations: Racey Point (near the upstream end of the system) and Talleyrand (near the lower end). Nitrogen is calculated to be the predominant limiting nutrient at Racey Point except during late winter and early spring when phosphorus is predominant (Figure 8-1). Phosphorus is calculated to be the predominant limiting nutrient at Talleyrand (Figure 8-2). Cell quota and nutrient limitations, calculated individually for each algal group, are presented here as mean values, weighted by the biomass of each algal group.

Increasing the minimum cell quota had little effect on the computed cell quota (Figures 8-3, 8-4). This behavior is consistent with the analytical study

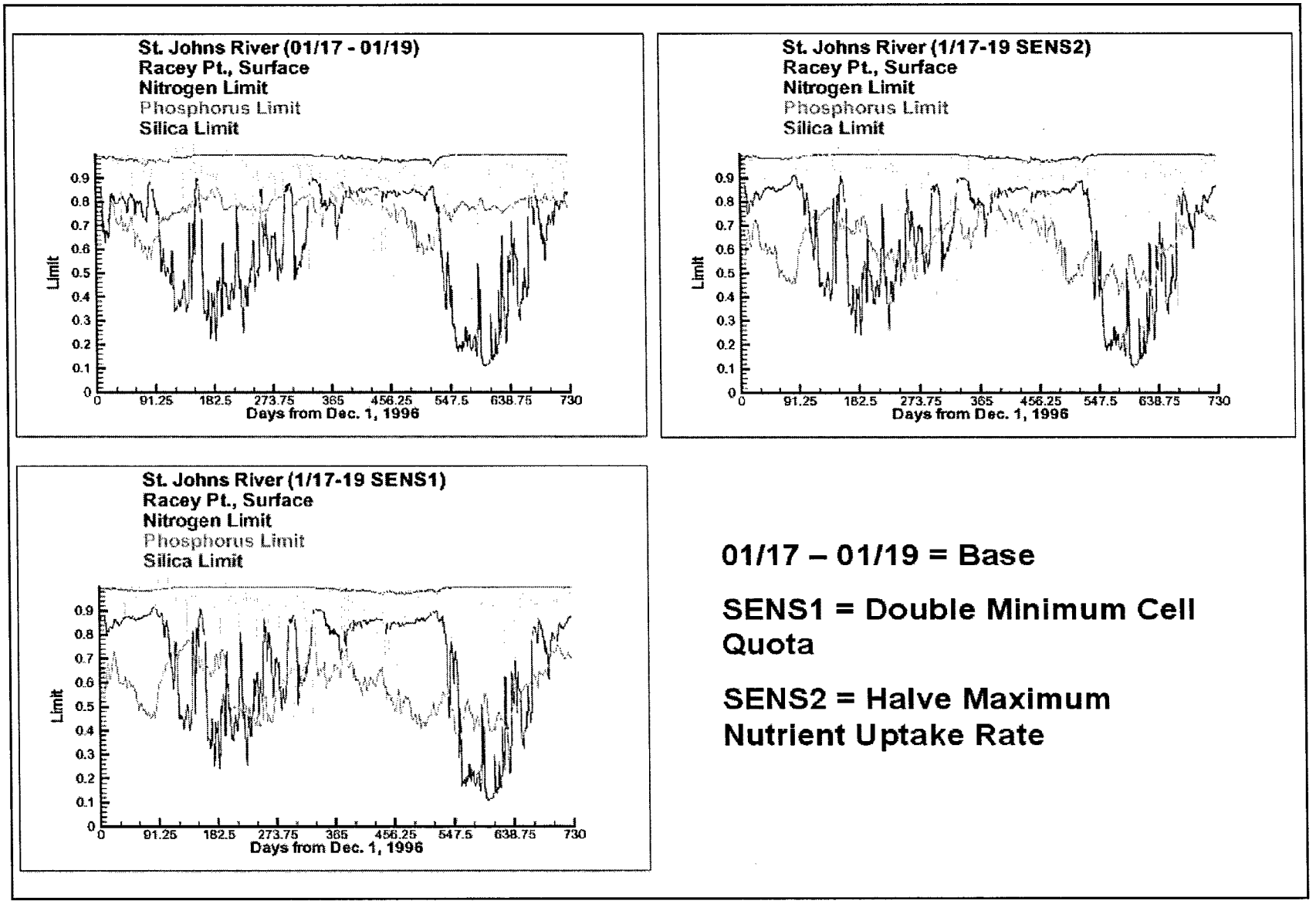

Figure 8-1. Computed limits to algal production at Racey Point

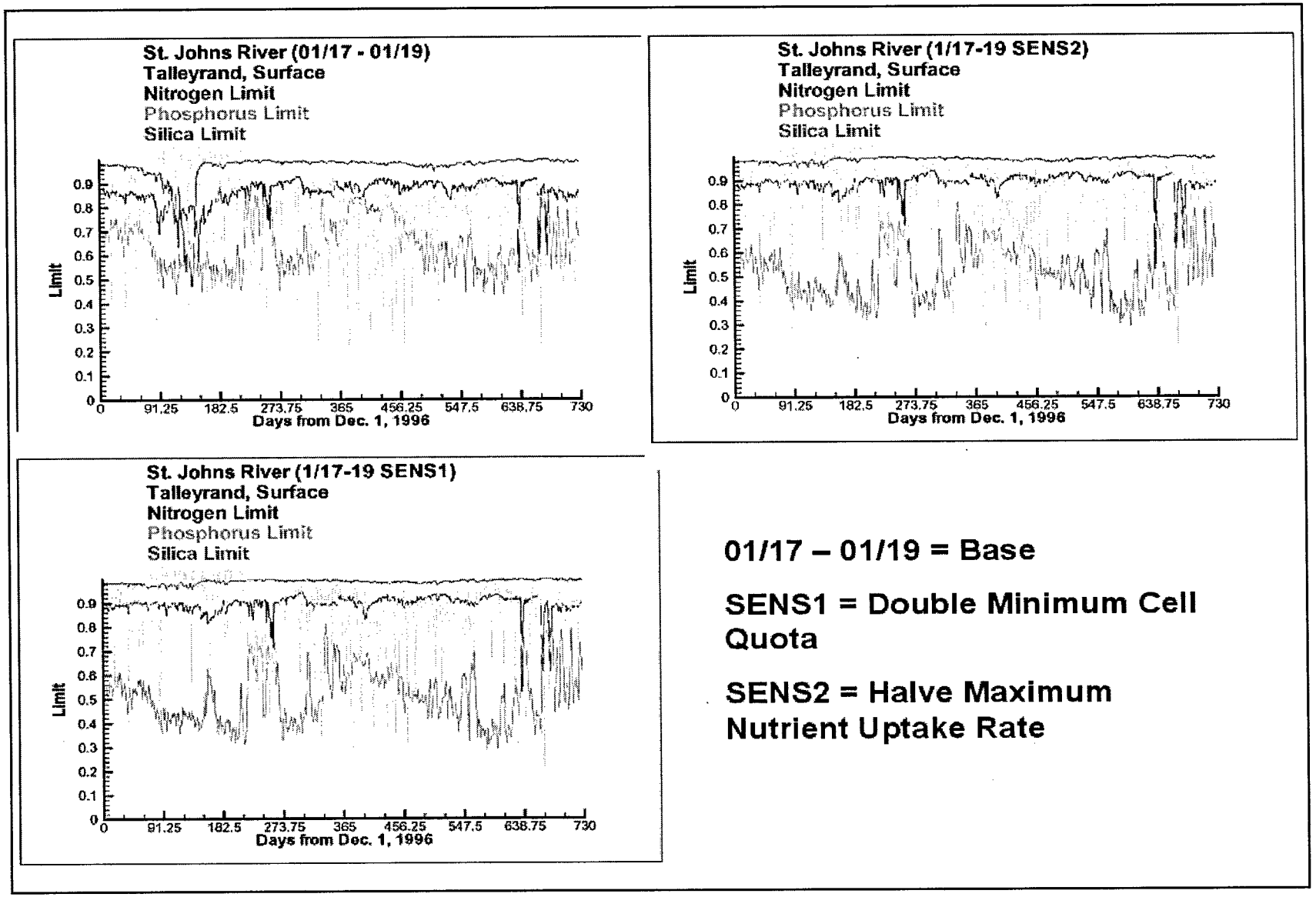

Figure 8-2. Computed limits to algal production at Talleyrand

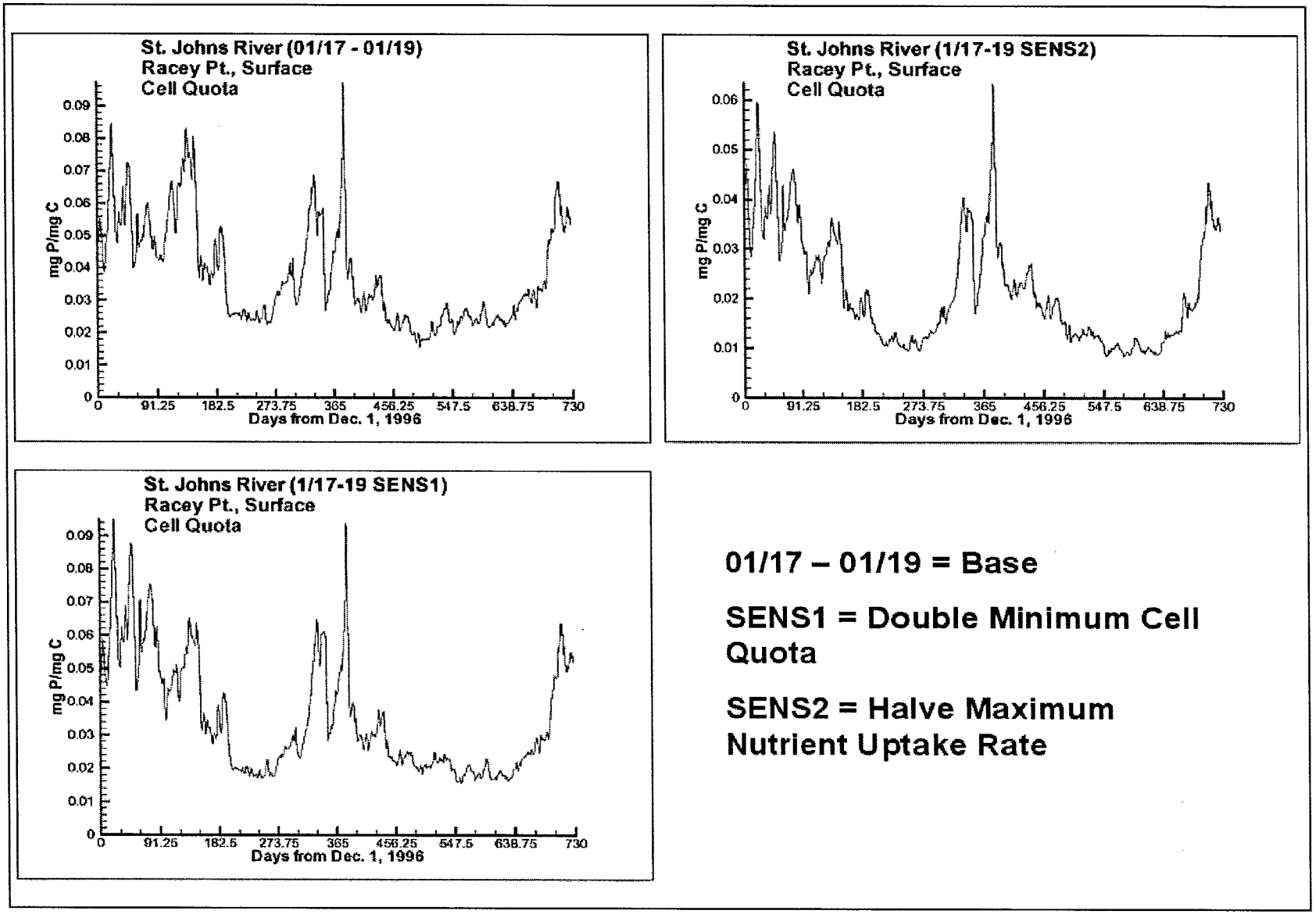

Figure 8-3. Computed cell quota at Racey Point

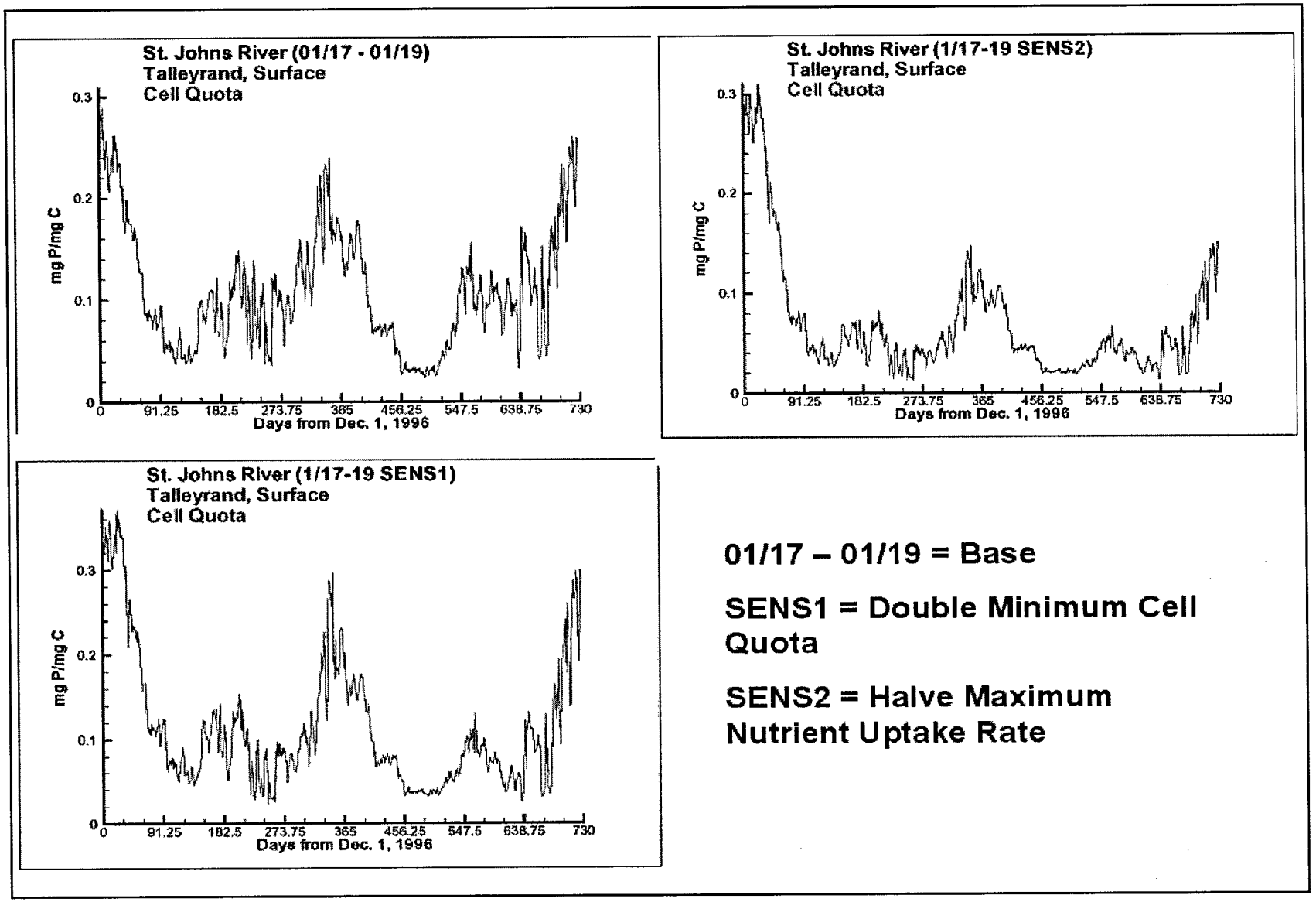

Figure 8-4. Computed cell quota at Talleyrand

(Equation 8-5), which indicated that specification of the minimum cell quota does not influence the computed quota. Reducing the maximum nutrient uptake rate reduced the cell quota by one-third to one-half (Figures 8-3, 8-4). This behavior is consistent with the analytical study (Equation 8-5), which indicated that cell quota is linearly proportional to maximum nutrient uptake rate.

Increasing the minimum cell quota increased phosphorus limitation on growth at both locations (Figures 8-1, 8-2). This behavior can be readily interpreted by noting the role of minimum cell quota in computed nutrient limitation:

$$G = G\max \cdot \left[1 - \frac{Qo}{Q} \right] \tag{8-9}$$

Likewise, decreasing the maximum nutrient uptake rate also increased phosphorus limitation on growth (Figures 8-1, 8-2). This behavior can also be interpreted in light of Equation 8-9. Instead of diminished growth brought about by increased Qo, however, diminished growth is induced by a reduction in cell quota, Q (Figures 8-3 and 8-4, Equation 8-5).

At Racey Point, computed chlorophyll was largely unaffected by changes in either minimum cell quota or maximum nutrient uptake rate (Figure 8-5). Close inspection indicates some small, transient differences between model runs but, for practical purposes, chlorophyll was unchanged. Certainly the agreement between computed and observed chlorophyll was unaffected by the parameter variations. To a large extent, this behavior can be attributed to the predominant nitrogen limitation at this location, but chlorophyll is not substantially altered during the periods of phosphorus limitation either. At Talleyrand, computed chlorophyll was reduced through much of the application period (Figure 8-6). This behavior can be readily interpreted as the reaction to increased phosphorus limitation in a predominantly phosphorus-limited region. The peak algal blooms were not truncated, however. These blooms were composed of cyanobacteria that predominated upstream in a largely nitrogen-limited region. Cyanobacteria were apparently transported into the lower estuary where they rapidly perished due to salinity-induced mortality. Since their presence was due to transport rather than production, they were unaffected by parameter changes that induced phosphorus limitation.

At Racey Point, increasing the minimum cell quota had minimum influence on dissolved phosphate concentration (Figure 8-7). To the extent a change was noticeable, dissolved phosphate increased. A large increase in dissolved phosphate accompanied the reduction in nutrient uptake rate, behavior that is readily understood. Close inspection indicates the increases were primarily during the periods when nitrogen was the limiting nutrient. At Talleyrand, dissolved phosphate increased in response to the parameter changes but not to the extent apparent at Racey Point (Figure 8-8). The behaviors at the two locations indicate that external phosphate is sensitive to specification of nutrient uptake velocity when phosphorus is not the limiting nutrient but is less sensitive when phosphorus is limiting.

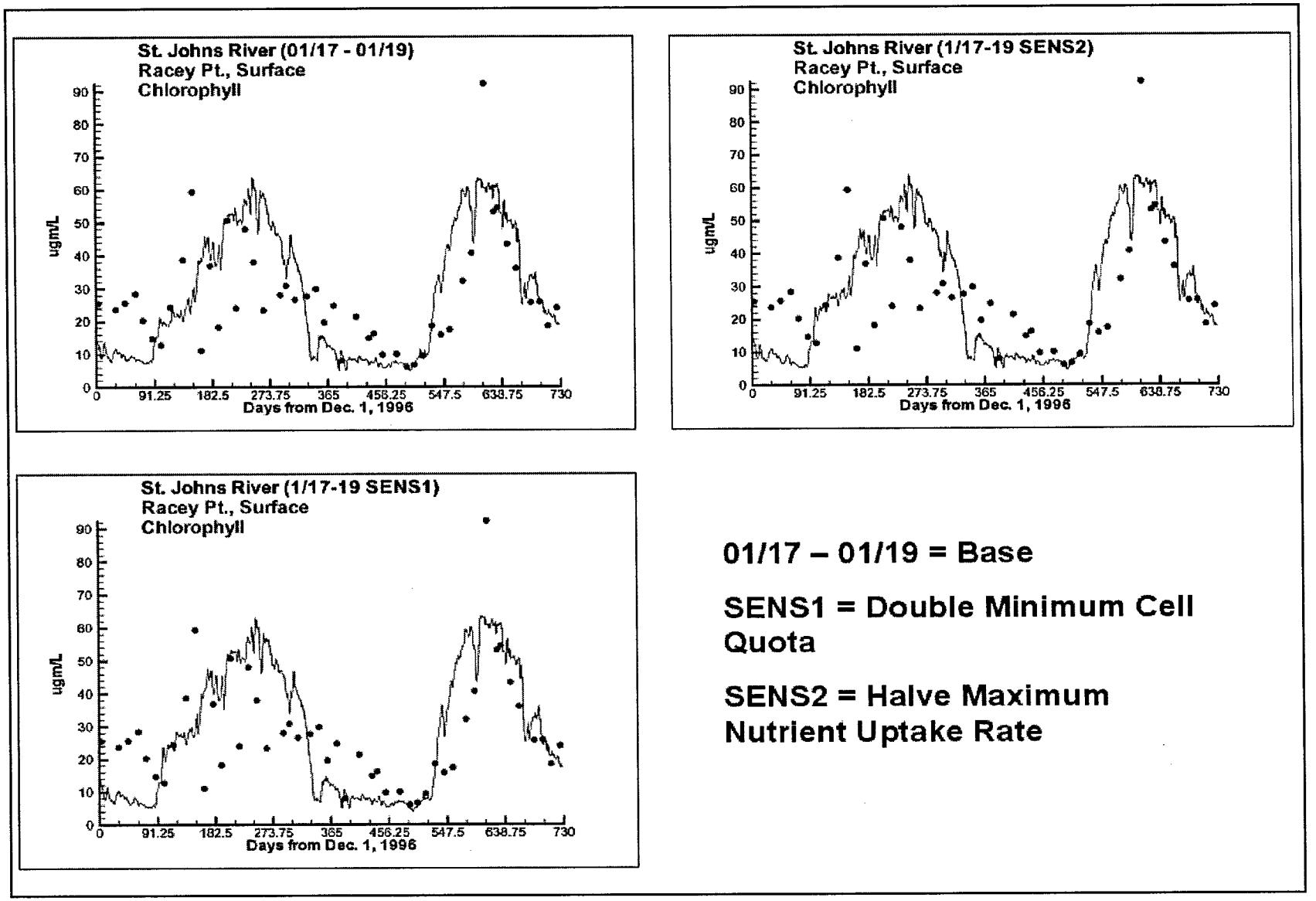

Figure 8-5. Computed and observed chlorophyll at Racey Point

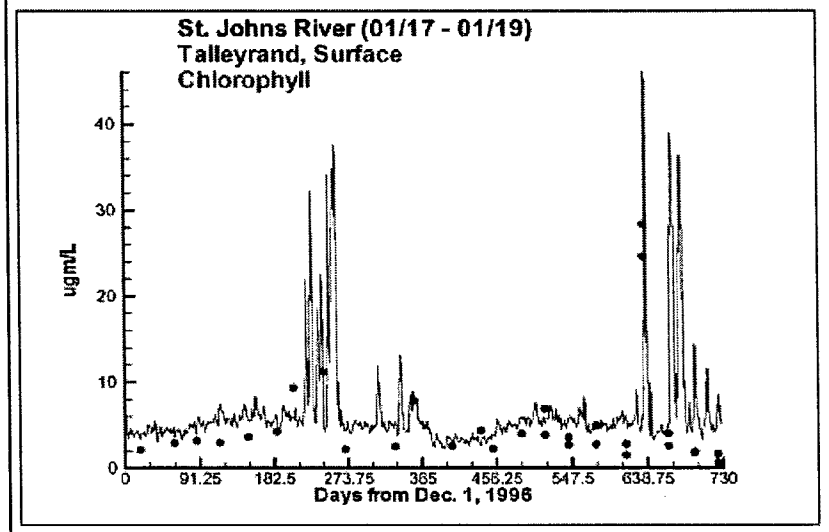

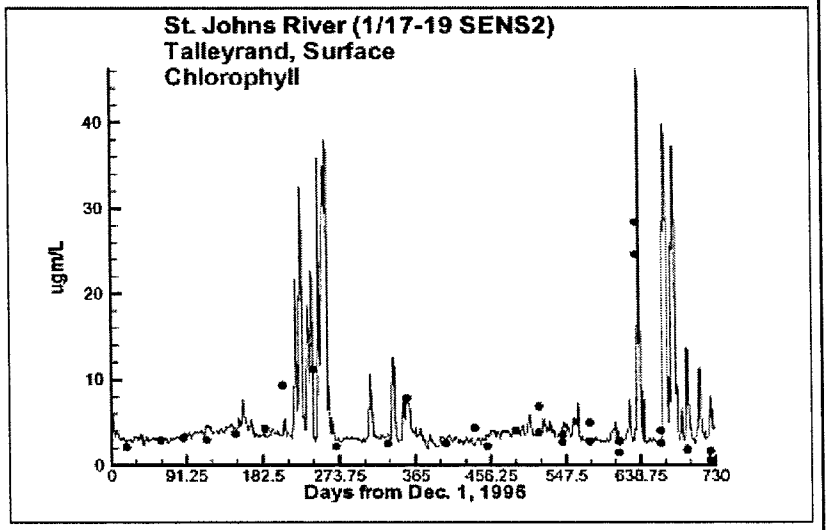

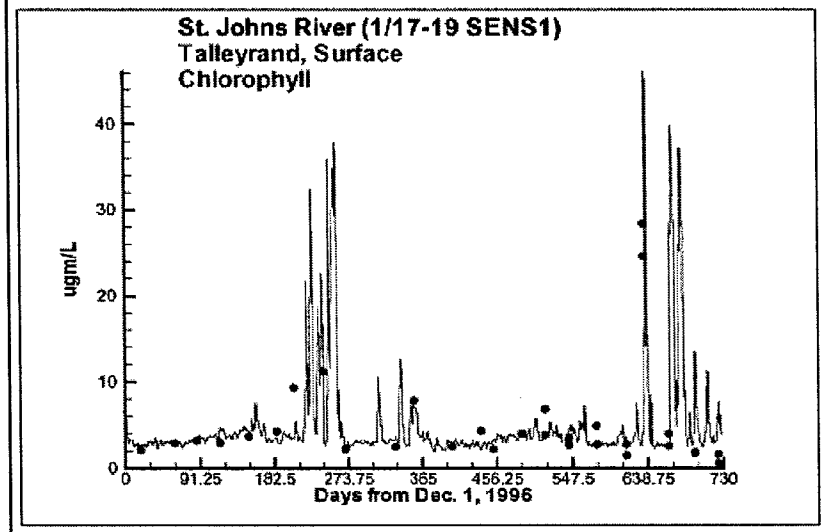

01/17 – 01/19 = Base

SENS1 = Double Minimum Cell Quota

SENS2 = Halve Maximum Nutrient Uptake Rate

Figure 8-6. Computed and observed chlorophyll at Talleyrand

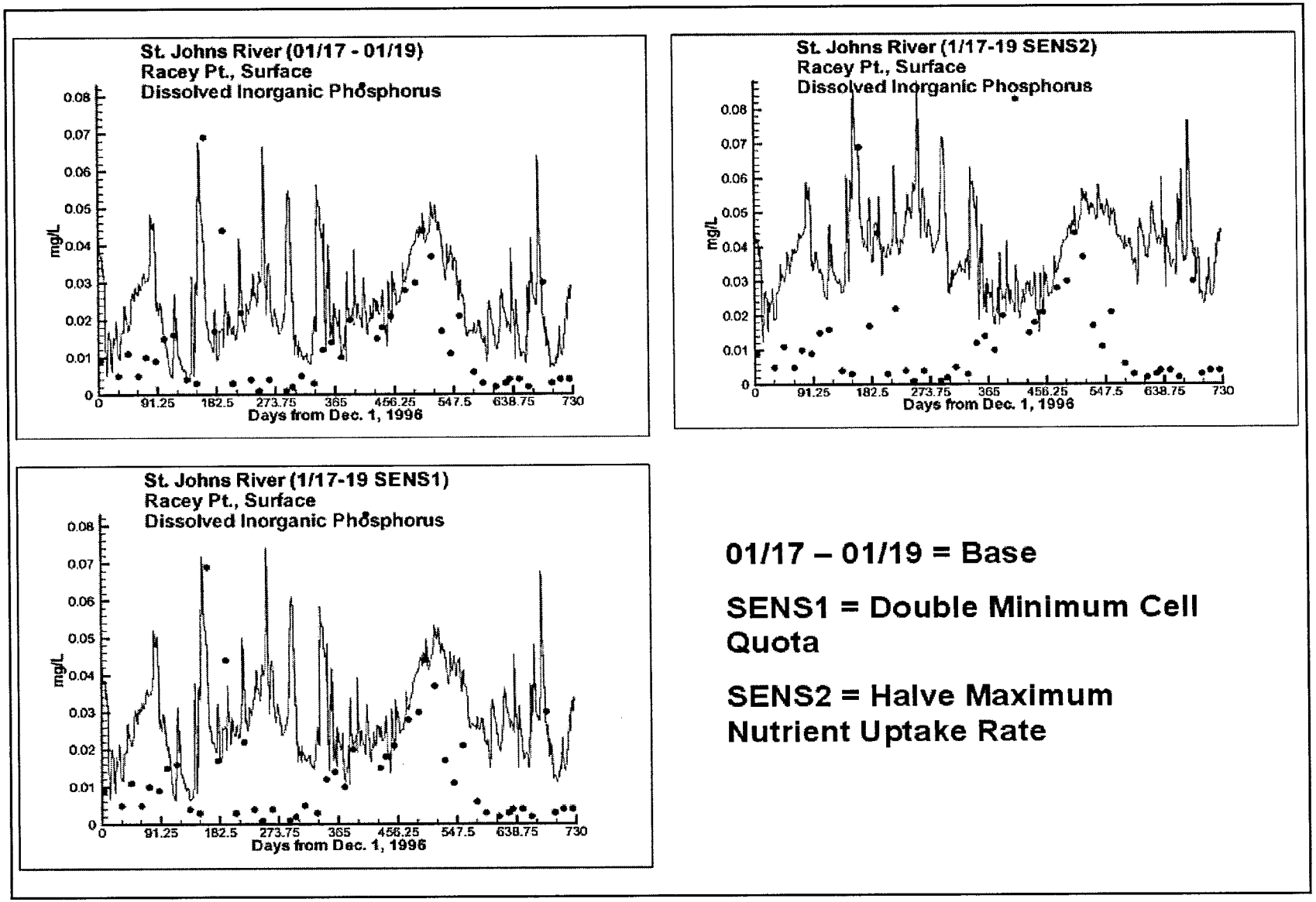

Figure 8-7. Computed and observed DIP at Racey Point

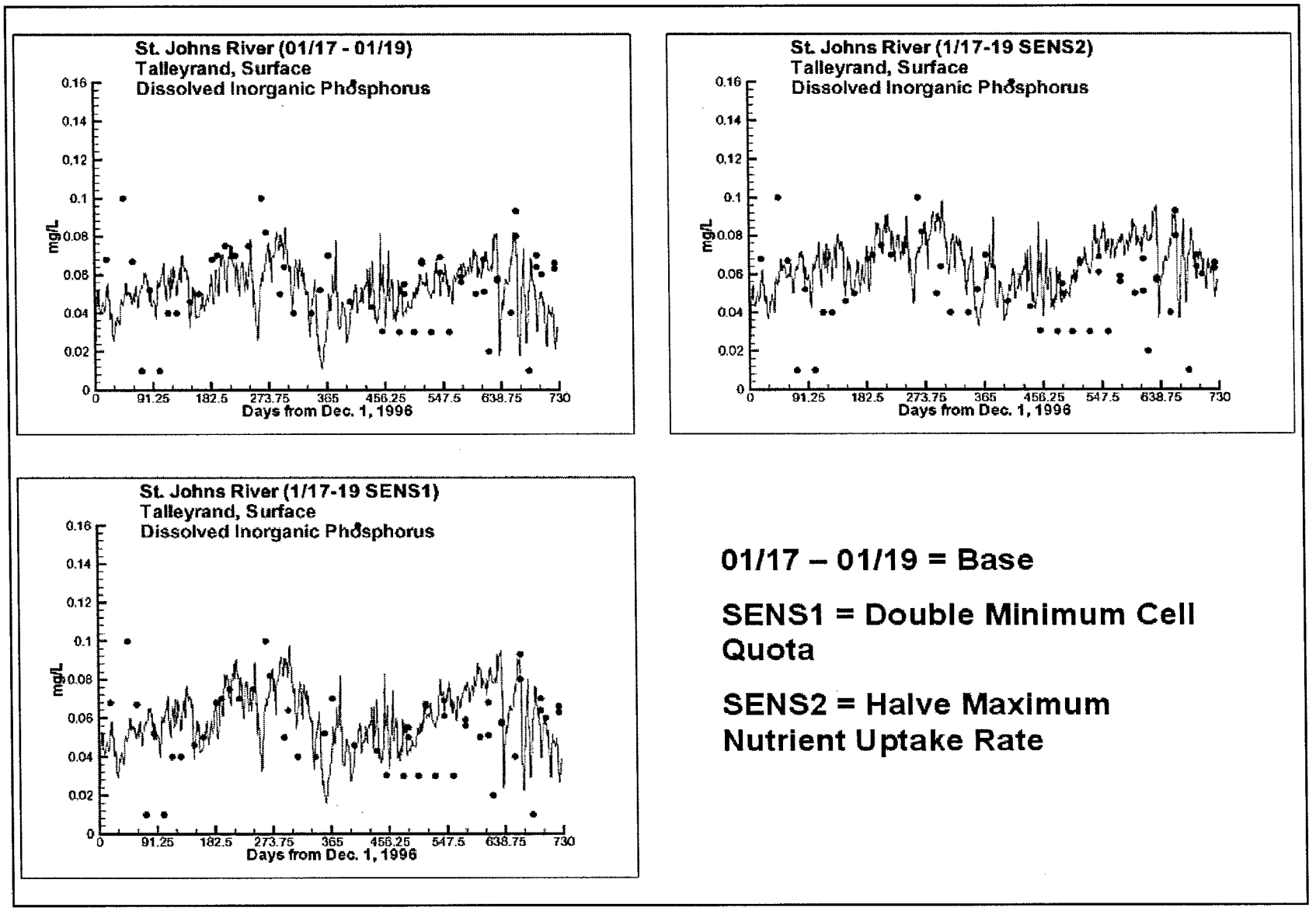

Figure 8-8. Computed and observed DIP at Talleyrand

While comparison of the Droop model with a realistic model based on fixed algal composition was not possible, these sensitivity runs allow inferences to be made regarding the Droop model. Changes in parameter values had little influence on computed chlorophyll. In particular, peak chlorophyll concentrations were unaffected. This finding is consistent with earlier sensitivity runs on the reduced system and with DiToro's 1980 findings. It is concluded that employment of a Droop model to improve computed chlorophyll concentration is unnecessary. Droop model parameters exerted a major influence on dissolved phosphate concentration. Luxury uptake, in excess of algal requirements, was computed when nitrogen was limiting. Several other CE-QUAL-ICM applications are plagued with excessive phosphate concentration (Cerco 2000). Specification of a minimum phosphorus composition, necessary to compute chlorophyll correctly during phosphorus limitation, results in excessive phosphorus concentration at times and locations where phosphorus is not limiting. Use of Droop kinetics appears to offer a remedy to this problem. Ironically then, Droop kinetics present a mechanism for regulating computed nutrient concentrations rather than computed chlorophyll concentrations.

Nitrogen Fixation

Nitrogen fixation is the microbial-mediated conversion of gaseous nitrogen to ammonium. Nitrogen fixation may be conducted by heterotrophic bacteria or by autotrophic cyanobacteria (blue-green algae). Not all cyanobacteria are nitrogen fixers. In the St. Johns River, the genera *Cylindrospermopsis* and *Anabaena* fix nitrogen while *Microcystis* does not. Intuition suggests the nitrogen fixers should be dominant under strongly nitrogen-limited conditions when their ability to utilize gaseous nitrogen gives them a competitive advantage over organisms limited to the use of ammonium and nitrate. In reality, a host of factors influences the presence of nitrogen fixers, and prediction of their occurrence is problematic.

Concern for the role of nitrogen fixation in supporting algal blooms led the sponsor to adopt a two-pronged approach. Field programs were initiated to investigate cyanobacteria physiology and to measure nitrogen fixation rates (Paerl et al. 2002, Phlips 2002). Incorporation of nitrogen fixation was planned as a later addition to the model. Difficulty in calibrating the model absent nitrogen fixation led to accelerating the incorporation of the process into the present model.

Observations

Measures of nitrogen fixation were obtained from the original investigator (Phlips 2002). Measures were conducted in light and dark at 15 stations at monthly intervals from January through October 2000. The investigator also provided observations of conventional water quality parameters collected concurrently with the nitrogen fixation measures. The two data bases were merged and purged of observations outside of the model domain, partial records, and a few questionable measures. Nitrogen fixation was measured by an acetylene reduction method and reported as ng ethylene L^{-1} h^{-1}. From tables in the Phlips report, the conversion ng ethylene L^{-1} h^{-1} * 0.33 = ng N_2 L^{-1} h^{-1} was

derived. Subsequent units conversions resulted in a data base of light and dark nitrogen fixation, as mg N m^{-3} d^{-1}, and concurrent water temperature, salinity, chlorophyll, dissolved inorganic nitrogen, and additional parameters. Roughly 10 records were available from each of 11 stations.

Model formulation

Incorporation of nitrogen fixation in the model required two considerations. The first was relaxation of the nitrogen limitation to blue-green algal growth. The second was incorporation of nitrogen fixed into the total nitrogen budget. Inspection of the observations indicated significant relationships between nitrogen fixation and temperature (Figure 8-9), salinity (Figure 8-10), and dissolved inorganic nitrogen (Figure 8-11). One approach would have been to develop a function that related nitrogen fixation to these parameters. Relationships were already in place, however, that related cyanobacteria production and mortality to salinity and temperature. Creation of a new relationship for nitrogen fixation would have been redundant and, possibly, in conflict with the existing relationships. The approach taken in this study concentrated on the relationship of nitrogen fixation to dissolved inorganic nitrogen. The salinity and temperature relationships were left to the existing formulations.

Our revised nutrient limitation required specification of the fraction of nitrogen fixers in the blue-green algal population and specification of a new half-saturation coefficient:

$$N\lim = \frac{DIN}{KHn + DIN} \cdot \left[1 - Fnfix\right] + \frac{DIN + KHnfix}{DIN + KHn + KHnfix} \cdot Fnfix \qquad (8\text{-}10)$$

in which:

$N\lim$ = nitrogen limitation ($0 \leq N\lim \leq 1$)
DIN = dissolved inorganic nitrogen (g N m^{-3})
KHn = half-saturation concentration for nitrogen uptake (g N m^{-3})
$KHnfix$ = half-saturation concentration for nitrogen fixation (g N m^{-3})
$Fnfix$ = fraction of nitrogen fixers in blue-green algal population ($0 \leq Fnfix \leq 1$).

Parameter *KHnfix* is a parameter that relaxes the nitrogen limit for a portion of the population (Figure 8-12). As *KHnfix* increases, the limitation is reduced. The influence of *KHnfix* is greater at low nitrogen concentrations and diminishes at higher concentrations.

Computed nitrogen fixation takes place only when nitrogen is the most limiting of the potential limits (nitrogen, phosphorus, light) to algal production. Total nitrogen is incremented by first removing from the dissolved inorganic nitrogen pool the amount of nitrogen calculated by conventional limitation:

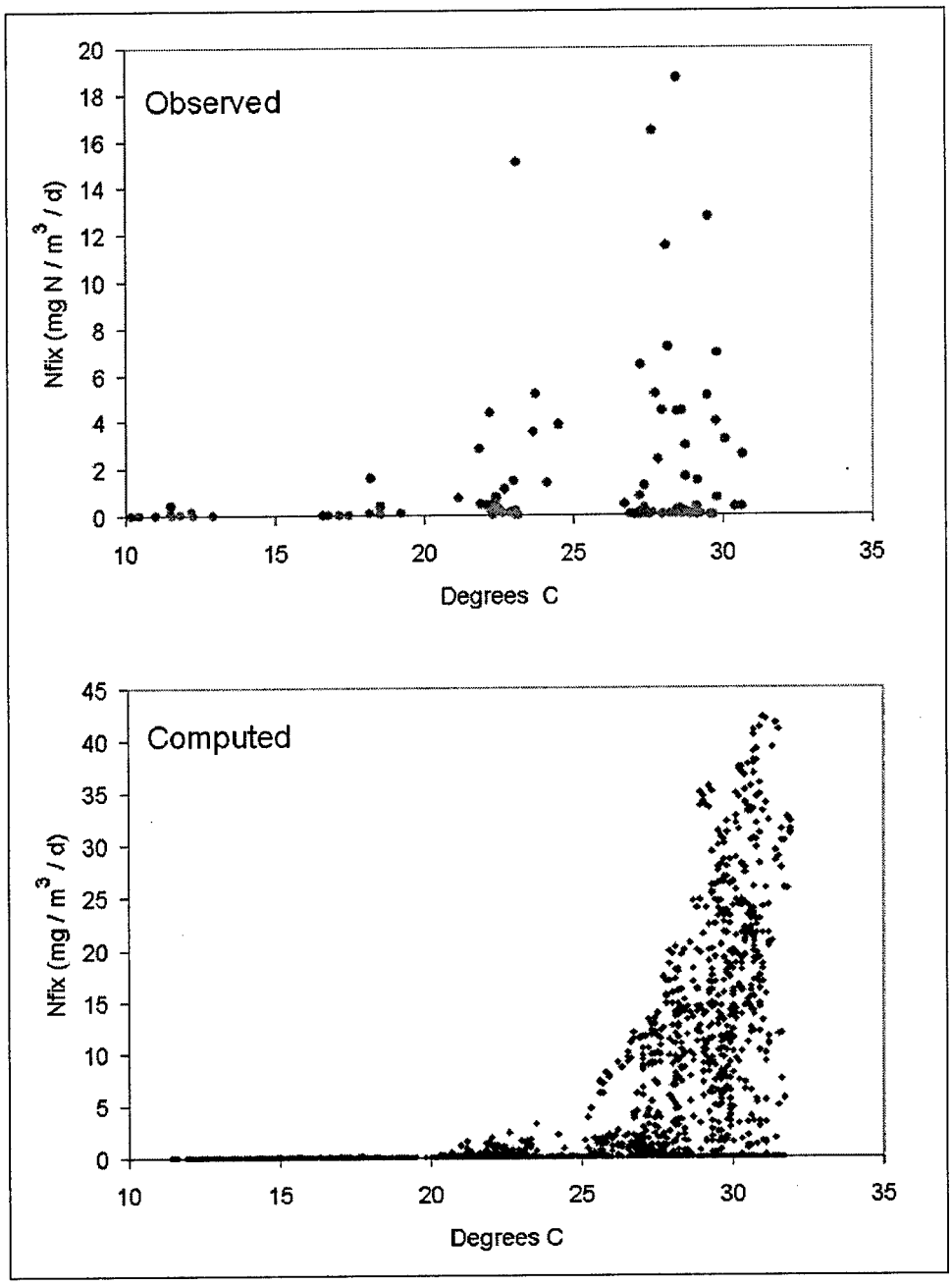

Figure 8-9. Computed and observed relationship between temperature and nitrogen fixation

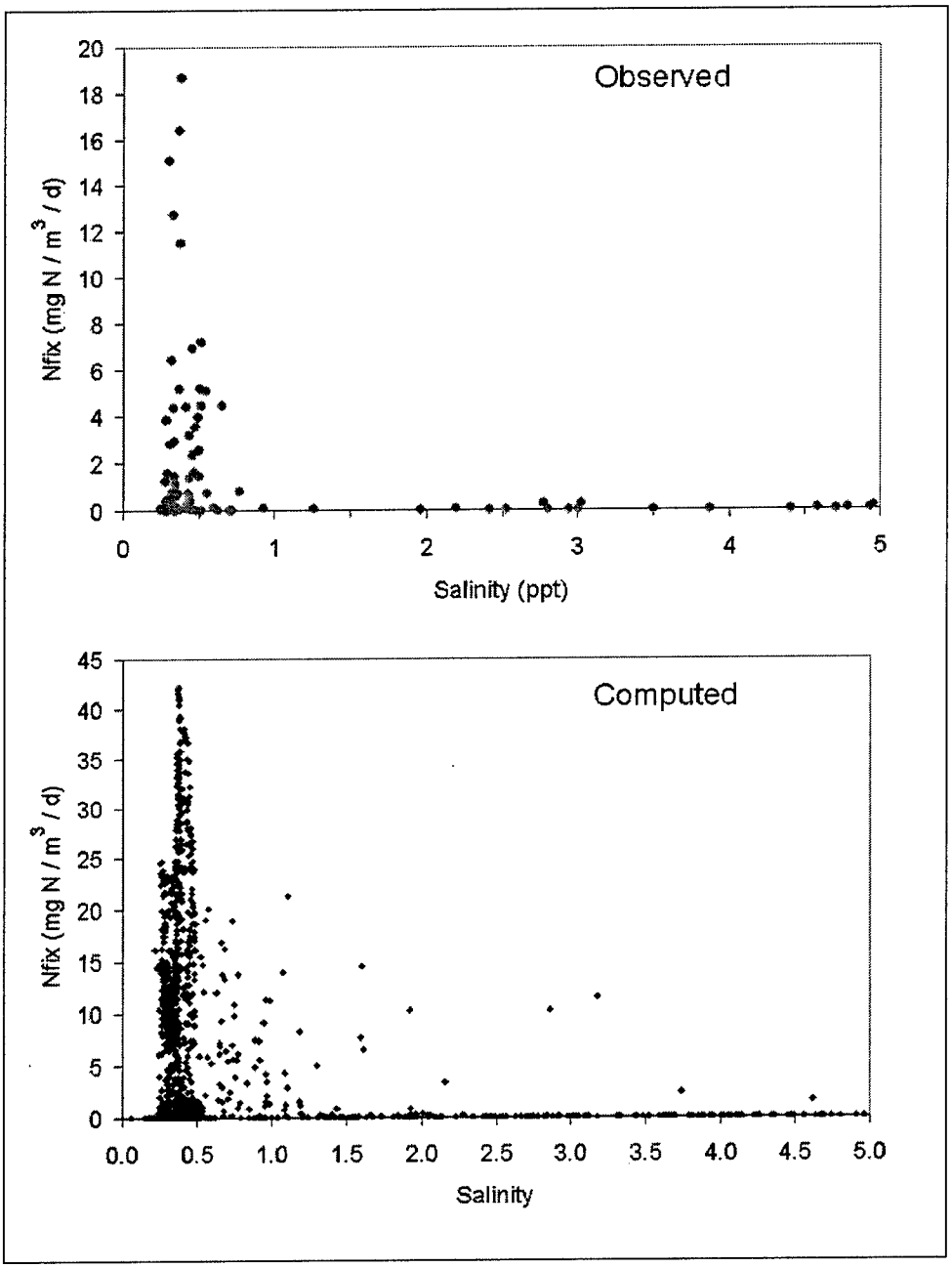

Figure 8-10. Computed and observed relationship between salinity and nitrogen fixation

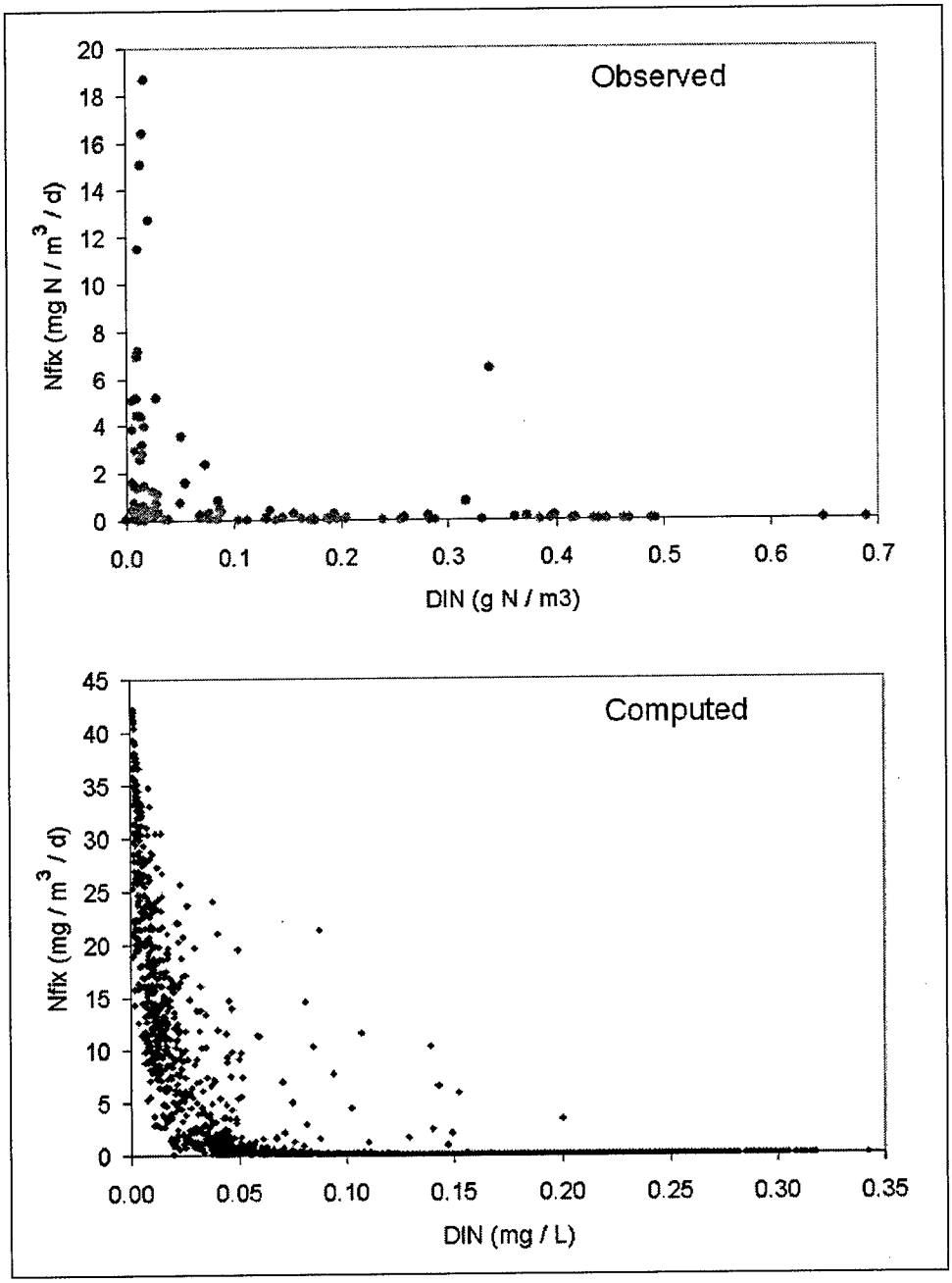

Figure 8-11. Computed and observed relationship between DIN and nitrogen fixation

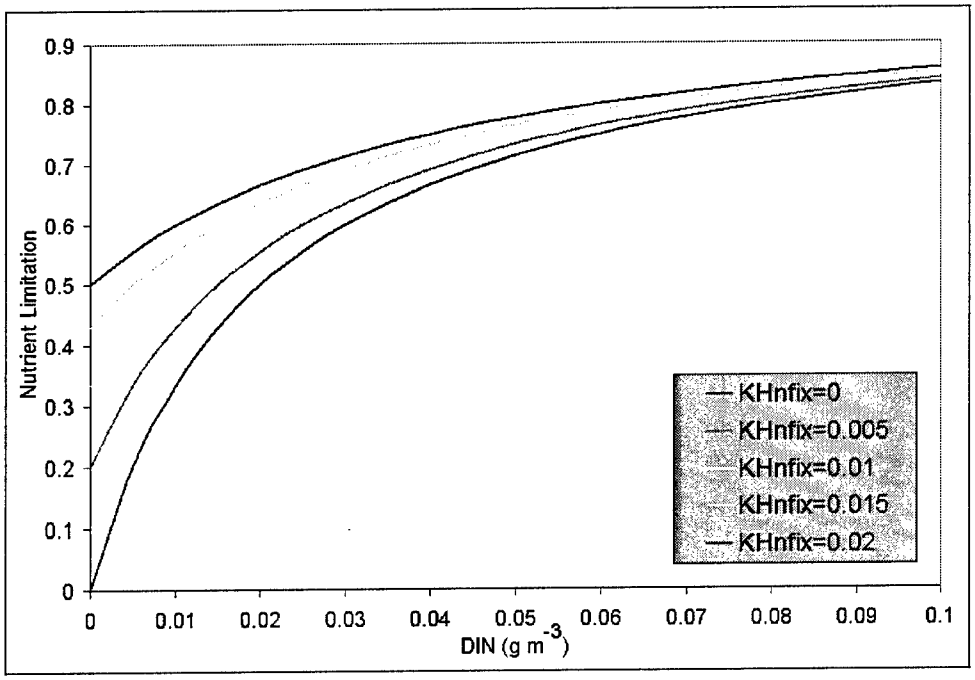

Figure 8-12. Effect of parameter KHnfix on nitrogen limitation computed for KHn = 0.02 g N m^{-3}

$$DINup = \frac{DIN}{KHn + DIN} \cdot G \cdot B1 \cdot Anc \tag{8-11}$$

in which:

$DINup$ = uptake of dissolved inorganic nitrogen by cyanobacteria (g N m^{-3} d^{-1})

G = maximum specific growth rate without nutrient limitation (d^{-1})

$B1$ = cyanobacteria biomass (g C m^{-3})

Anc = cyanobacteria nitrogen-to-carbon ratio (g N g^{-1} C)

Algal biomass is next incremented by the amount calculated using the nutrient limitation with nitrogen fixation:

$$\frac{\delta B1}{\delta t} = N\lim \cdot G \cdot B1 \tag{8-12}$$

The amount of nitrogen fixed is the difference between nitrogen uptake and increase in nitrogenous algal biomass:

$$Nfix = \left[\frac{DIN + KHnfix}{DIN + KHn + KHnfix} - \frac{DIN}{DIN + KHn} \right] \cdot Fnfix \cdot G \cdot B1 \cdot Anc \tag{8-13}$$

in which $Nfix$ is the amount of nitrogen fixed (g N m^{-3} d^{-1}).

Model results

Computed nitrogen fixation was extracted from the model on a daily-average basis at six locations corresponding to sampling sites. For comparison with the model, observations conducted in light and dark were averaged into a single daily value. Parameters *KHnfix* and *Fnfix* were evaluated visually primarily through comparison of computed and observed nitrogen fixation rates and their relation to temperature, salinity, and dissolved inorganic nitrogen. Final parameter values were *KHnfix* = 0.01 g N m^{-3} and *Fnfix* = 0.175.

Temperature. Observations (Figure 8-9) indicate significant nitrogen fixing activity does not occur below 20 °C. Thereafter, activity increases in a rough exponential relationship to temperature. The model replicates well the temperature relationship apparent in the observations. Maximum computed nitrogen fixation rates are about double the maximum observed rates. This discrepancy can be attributed to the comparison of the model population from 1997-1998 to the observed samples from 2000. Aside from potential differences in rates between the computed and observed years, the complete computational set of over 2,000 daily rates should show greater range than the sampled set of roughly 100 observations.

Salinity. Virtually no nitrogen fixation was observed when salinity exceeded 1 ppt; the preponderance of nitrogen fixation occurred when salinity was less than 0.5 ppt (Figure 8-10). The model provided excellent representation of the observed dependence of nitrogen fixation on salinity.

Dissolved inorganic nitrogen. Nitrogen fixation was not observed when dissolved inorganic nitrogen exceeded 0.1 g N m^{-3} (Figure 8-11). The rate was greatly enhanced when dissolved inorganic nitrogen was less than 0.05 g N m^{-3}. Computed nitrogen fixation was largely cut off when dissolved inorganic nitrogen exceeded ≈0.05 g N m^{-3}. Below this concentration, computed nitrogen fixation increased in inverse proportion to dissolved inorganic nitrogen concentration. The model behavior well replicated the observed relationship between dissolved inorganic nitrogen and nitrogen fixation.

Chlorophyll. Observations indicated a loose relationship between chlorophyll and nitrogen fixation (Figure 8-13). Clearly, nitrogen fixation increased as chlorophyll increased. Highest fixation rates were observed when chlorophyll exceeded 40 mg m^{-3}, although significant nitrogen fixation occurred at lower chlorophyll concentrations. In one instance, a chlorophyll concentration in excess of 60 mg m^{-3} was accompanied by no nitrogen fixation. The loose relationship between nitrogen fixation and chlorophyll was no doubt due to the fact that chlorophyll concentration represented the entire algal population rather than the population of nitrogen fixers alone. Model computations provided a good representation of observed characteristics. The general increase of nitrogen fixation as a function of chlorophyll was computed, although occasional outliers produced significant nitrogen fixation at low chlorophyll concentrations or else no nitrogen fixation at high chlorophyll concentrations.

Nitrogen fixation was modeled in order to represent chlorophyll (Figure 8-14) and nitrogen (Figure 8-15) concentrations during algal blooms.

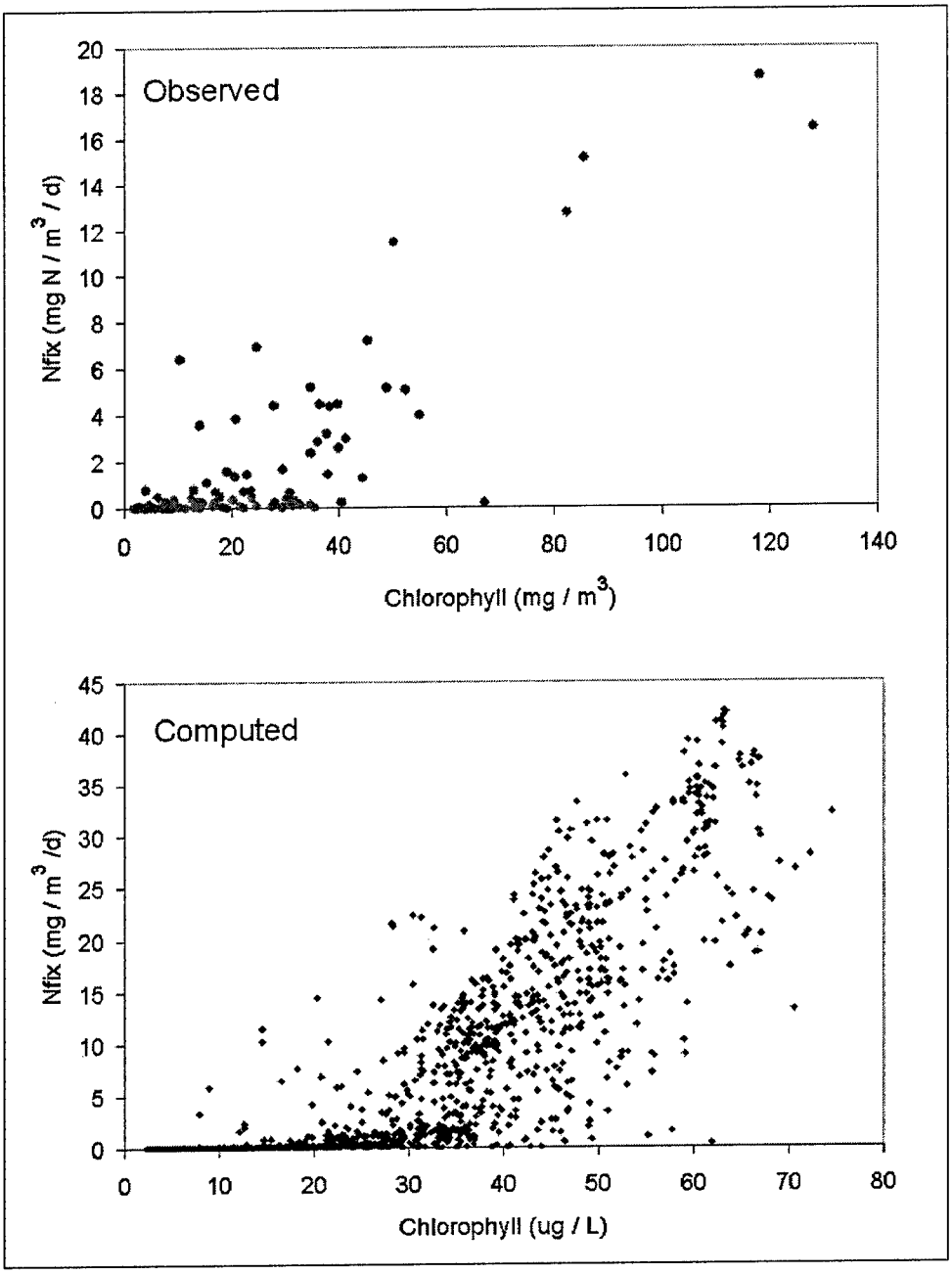

Figure 8-13. Computed and observed relationship between chlorophyll and nitrogen fixation.

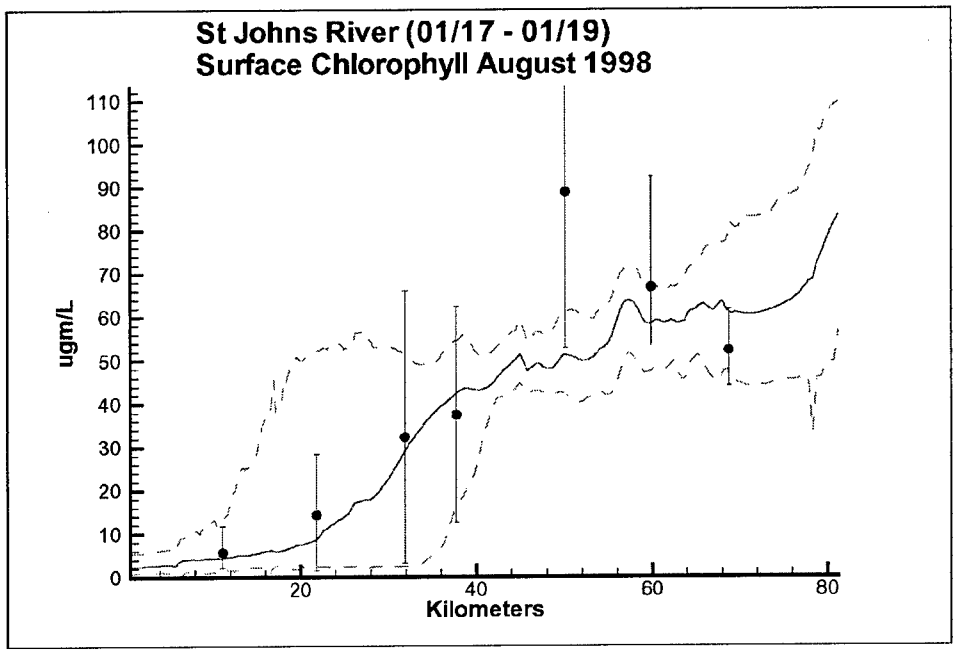

Figure 8-14. Computed and observed chlorophyll concentration, with nitrogen fixation, along river axis, August 1998.

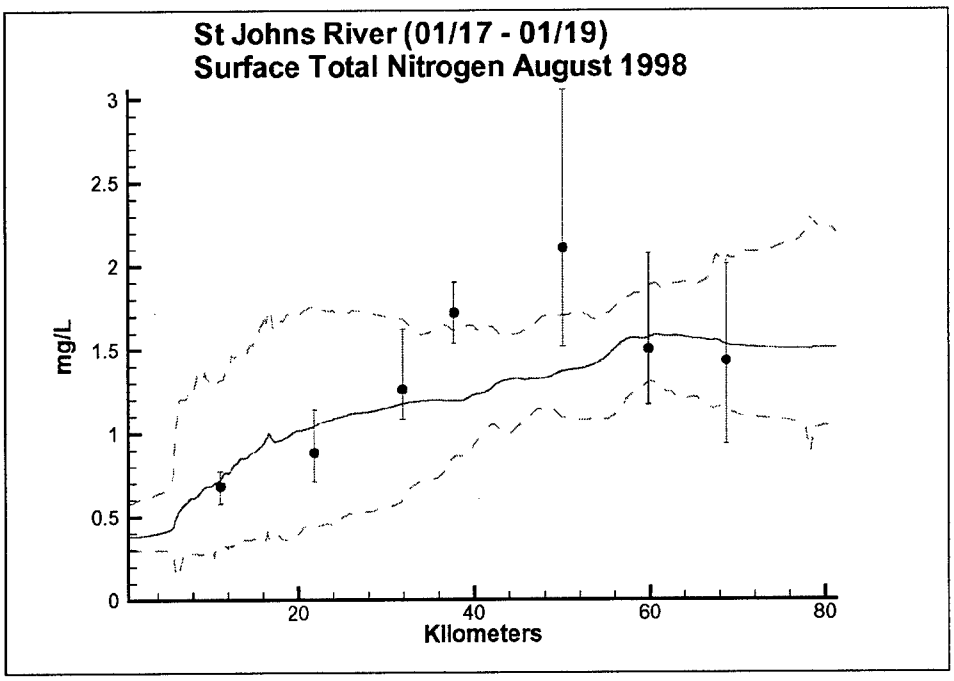

Figure 8-15. Computed and observed total nitrogen concentration, with nitrogen fixation, along river axis, August 1998

A model sensitivity run indicated chlorophyll (Figure 8-16) and total nitrogen (Figure 8-17) observed during the August 1998 bloom could not be replicated without nitrogen fixation. One interesting observation is that salinity (Figure 8-18)

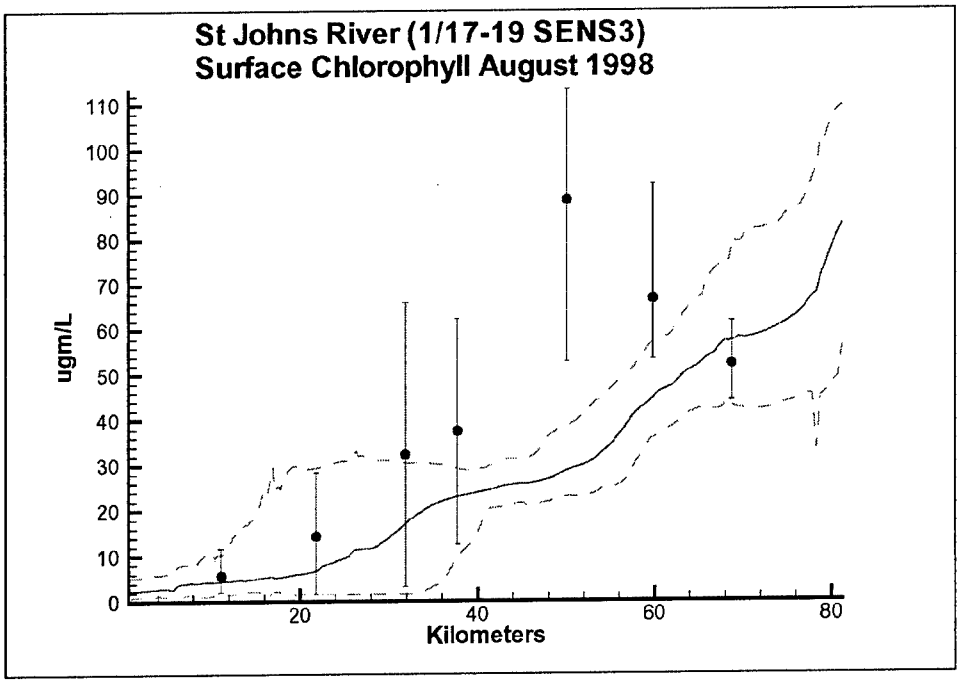

Figure 8-16. Computed and observed chlorophyll concentration, without nitrogen fixation, along river axis, August 1998

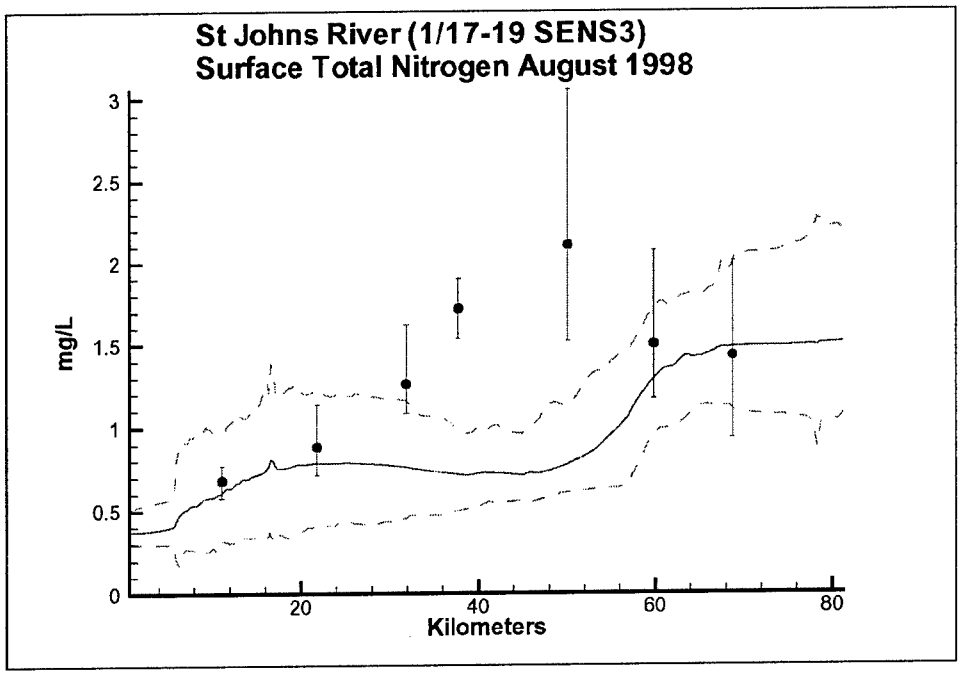

Figure 8-17. Computed and observed total nitrogen concentration, without nitrogen fixation, along river axis, August 1998

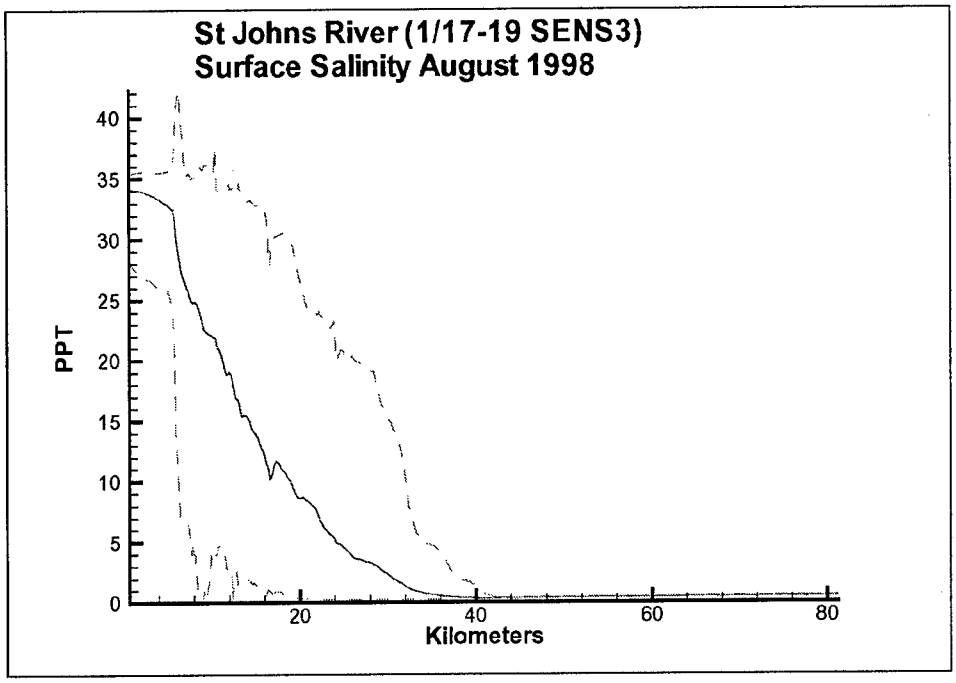

Figure 8-18. Computed salinity along river axis, August 1998

restricted nitrogen fixation to the region of the river above km 40, but chlorophyll and total nitrogen increased downstream. Apparently nitrogen fixed upstream was carried into the lower portion of the river. Chlorophyll was also carried downstream and, perhaps, algal production in the lower river was stimulated by nitrogen fixed upstream.

The modeled nitrogen fixation rates do not completely replicate the August 1998 bloom; higher rates are required. The modeled rates can readily be increased but must be tempered by the requirement to match chlorophyll and total nitrogen at other times. The goal is to optimize model behavior over the 2-year calibration period rather than during one bloom event. The overall effect of nitrogen fixation on the model results is best examined in a quantitative format by using the ME statistic:

$$ME = \frac{\sum (O - P)}{n} \tag{8-14}$$

in which:

ME = mean error
O = observation
P = prediction
n = number of observations

An ME of zero is ideal. Positive ME indicates observations exceed computations, on average. Negative ME indicates computations exceed observations, on average.

Nitrogen fixation increases computed chlorophyll by 0 to 5 mg m^{-3} (Figure 8-19). The greatest effect is in the reach from Mandarin Point to Picolata. The net effect on ME is close to zero. For every station in which nitrogen fixation moves ME towards zero (e.g., Picolata), there is another station in which ME moves away from zero (e.g., Mandarin Point). Nitrogen fixation increases computed total nitrogen by 0.01 to more than 0.1 g N m^{-3} (Figure 8-20). In this case, nitrogen fixation almost always moves ME close to the ideal value of zero.

The nitrogen fixation algorithm is based on a constant fraction, 17.5 percent, of nitrogen fixers in the total cyanobacteria population. No doubt, results could be improved if this fraction were variable. The fraction can readily be varied to match observed nitrogen and chlorophyll but there are no means to specify the fraction in a predictive mode. One approach to predicting the fraction of nitrogen fixers would be to increase the fraction in the presence of nitrogen limitation. But, as has been noted, prediction of the occurrence of nitrogen fixers is not so easy. An algal state variable can also be incorporated that specifically represents nitrogen fixers if sufficient information becomes available to isolate and model this population.

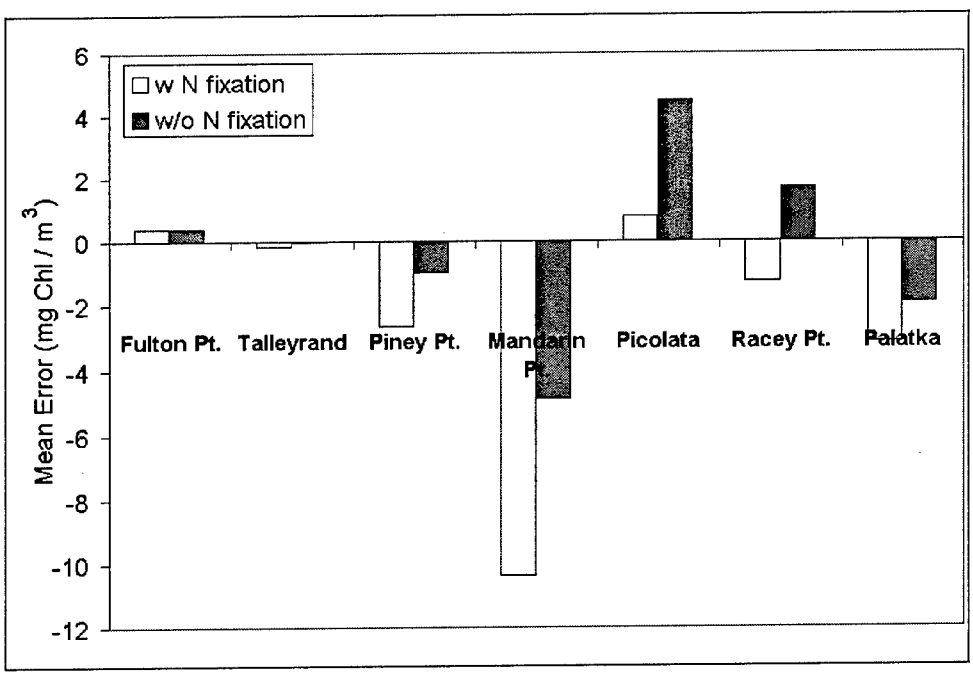

Figure 8-19. Chlorophyll ME with and without nitrogen fixation

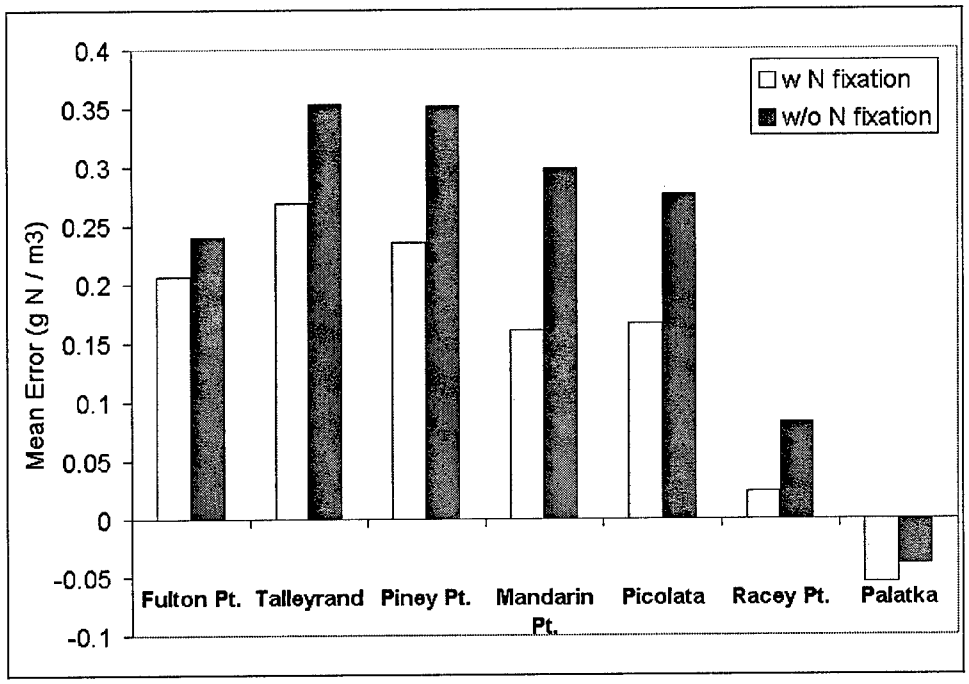

Figure 8-20. Total nitrogen ME with and without nitrogen fixation

Conclusions

It is concluded that:

- The CE-QUAL-ICM model captures apparent relationships between observed nitrogen fixation and temperature, salinity, dissolved inorganic nitrogen, and chlorophyll
- Nitrogen fixation is required to match observed chlorophyll and total nitrogen during algal blooms
- The major effect of computed nitrogen fixation is improvement of overall computed total nitrogen. Little or no effect on overall computed chlorophyll is apparent.
- Improved representation of nitrogen fixation and its effects requires improved information about the temporal and spatial distribution of the nitrogen fixing population.

Labile and Refractory Dissolved Organic Matter

A novel approach in the St. Johns River study was the partitioning of dissolved organic matter into labile and refractory components. These fractions were represented as distinct model state variables: labile dissolved organic carbon (DOC), refractory DOC, labile DO nitrogen, refractory DO nitrogen, labile DO phosphorus, and refractory DO phosphorus. Previous applications of the CE-QUAL-ICM model (e.g., Cerco and Cole 1994) split particulate organic matter into labile and refractory fractions but represented dissolved organic carbon and nutrients as homogenous components.

The split of particulate organic matter was driven by the need to partition organic matter for the sediment diagenesis model (DiToro and Fitzpatrick 1993). Although the existence of components of various lability within the dissolved pools was recognized, no explicit need to partition dissolved organic matter was apparent. Within the St. Johns River, the obvious difference between dissolved organic matter entering the system as "blackwater" from upstream wetlands and dissolved organic matter entering the system from algal decomposition indicated these components should be individually represented in the model. The humic material in blackwater was considered to be highly refractory, while fresh organic matter recycled from phytoplankton was expected to be more labile. The split of dissolved organic matter also presented the opportunity to apportion point-source loads and, perhaps, to provide more detailed information on the effects of point-source controls on eutrophication.

Splitting the loads

Guidance on defining and partitioning particulate organic matter was provided by the G model (Westrich and Berner 1984). Experiments on oxic decomposition of phytoplankton found that 50 percent of the organic matter decomposed in 70 days (first-order decay rate 0.066 d^{-1}), 16 percent decomposed over 600 days (first order decay rate 0.004 d^{-1}) and the remainder was nonreactive. For modeling purposes, the fraction that decomposed on a time scale of 2 months was defined as labile, while the remaining material, which decomposed on a time scale of 2 years or more, was defined as refractory.

The Westrich and Berner experiments were conducted over a period of 2 years. Incubations of this duration conducted on organic matter collected from multiple sources are impractical. A simpler, less time-consuming method of partitioning must be found. A method based on BOD analyses was derived by the sponsor and used to partition loads to the St. Johns River (Hendrickson 2002). Decay rates for labile and refractory material, taken from an earlier application of the CE-QUAL-ICM model, were used to apportion 5-day biochemical oxygen demand into labile and refractory contributions. Stoichiometry was used to convert oxygen consumed into equivalent labile and refractory fractions of total organic carbon (TOC). Nutrients were partitioned using distinct mass ratios for labile and refractory components. These were C:N = 3.6 for labile organic nitrogen, C:N = 33.6 for refractory organic nitrogen, C:P = 22.4 for labile organic phosphorus, and C:P = 663 for refractory organic phosphorus.

Using this approach, organic carbon runoff into the St. Johns River was determined to be largely refractory. Organic nitrogen in runoff was split roughly evenly into labile and refractory components. Organic phosphorus runoff was predominantly labile. Exact proportions varied, however, as a function of land use and other factors. Proportions of labile and refractory DOC and DON computed in the water column followed the partitioning of the loads (Figures 8-21, 8-22). Concentrations of refractory DOC were an order of magnitude greater than labile, while labile and refractory DON were about evenly split. Computed concentrations of labile and refractory DOP were also evenly split (Figure 8-23) although the labile fraction predominated in the loads. A simple explanation is that the labile load was rapidly converted to dissolved inorganic phosphorus leaving a larger fraction of the refractory material behind.

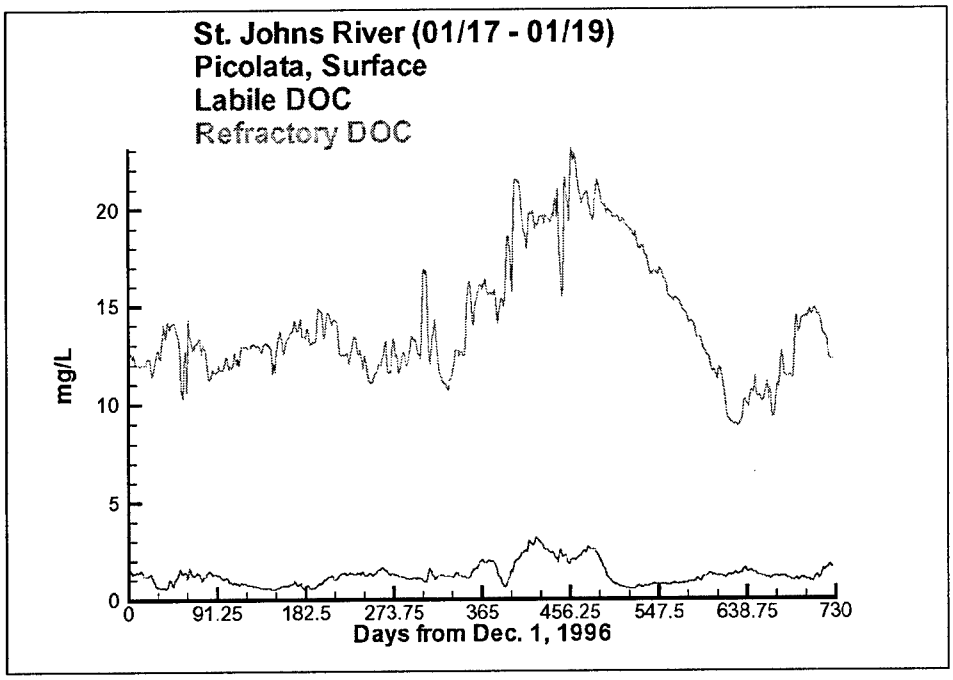

Figure 8-21. Computed labile and refractory DOC at Picolata

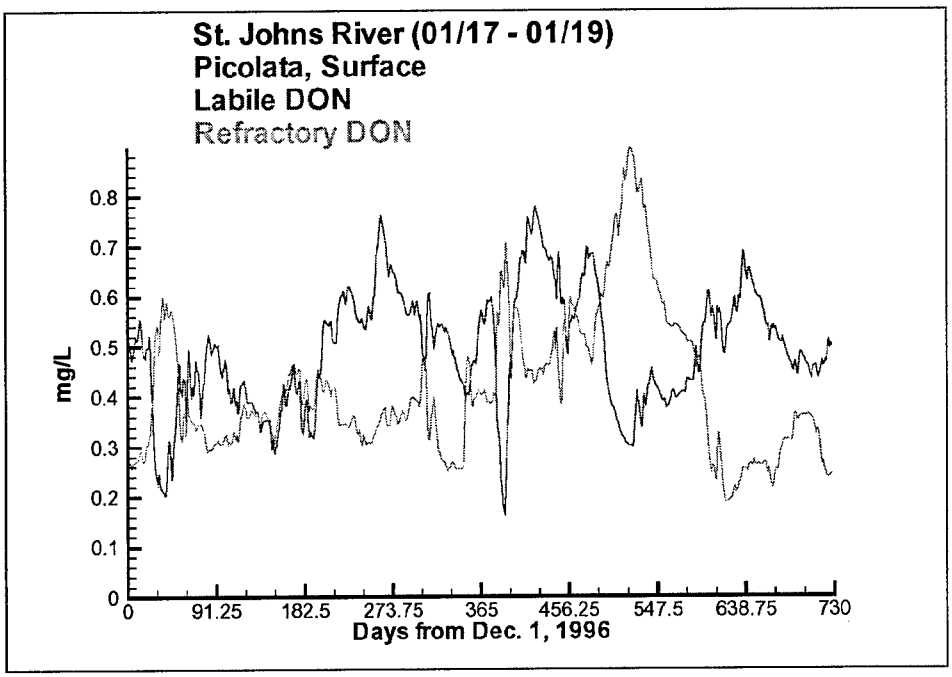

Figure 8-22. Computed labile and refractory DON at Picolata

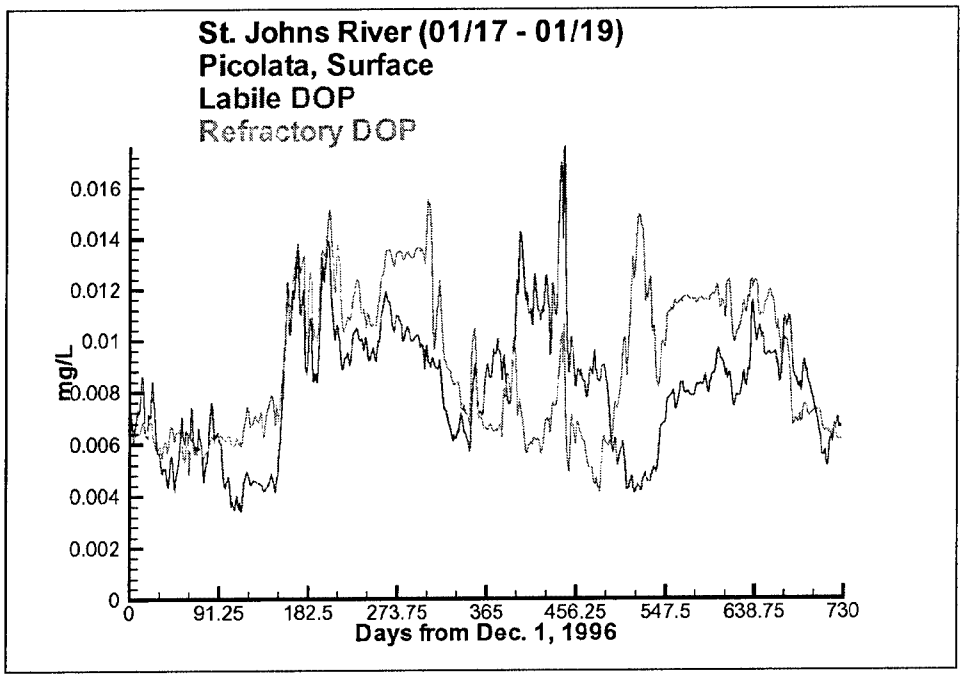

Figure 8-23. Computed labile and refractory DOP at Picolata

Sensitivity analyses

Since the division of dissolved organic matter into labile and refractory portions was a new addition to the model, it was decided to examine the effects of the addition. The calibrated model was contrasted with three sensitivity runs (Table 8-2). In the first run, SENS4, all dissolved organic matter was considered labile. In the second, SENS5, all dissolved organic matter was considered refractory. In the third, SENS6, an average decay rate was used for all DO matter. DOC observations were available for the St. Johns River. Sensitivity analyses focused on this state variable as well as DO, since oxygen consumption is largely the result of carbon oxidation. Observations were not available for dissolved organic nutrients. Sensitivity analyses focused on inorganic nutrient forms, since these are produced in the model through mineralization of dissolved organic nutrients, and on chlorophyll, since phytoplankton production is supported by inorganic nutrients. Results were examined as time-series comparisons with observations and as cumulative plots of computed and observed properties.

Table 8-2
Dissolved Organic Matter Mineralization Rates

	Labile, d^{-1}	Refractory, d^{-1}	Average, d^{-1}
St. Johns River			
Carbon	0.05	0.0025	0.011
Nitrogen	0.025	0.0025	0.008
Phosphorus	0.10	0.01	0.032
Chesapeake Bay (Cerco and Noel 2003)			
Carbon			0.011
Nitrogen			0.025
Phosphorus			0.15
Florida Bay (Cerco et al. 2000)			
Carbon			0.01
Nitrogen			0.01
Phosphorus			0.20

Carbon and dissolved oxygen. Time series of comparisons of computed and observed dissolved organic carbon are different but essentially equivalent for the calibration and for the all-refractory run (Figure 8-24). Thereafter, computed DOC declines below the observed rate as the mineralization rate increases through the average and all-labile runs. Careful examination of the cumulative distributions (Figure 8-25) indicates the calibration provides superior calculation of DOC system-wide. The all-refractory run calculates DOC too high while the other sensitivity runs calculate DOC too low.

Time-series comparisons of computed and observed DO are roughly equivalent for the calibration and for the all-refractory run (Figure 8-26). Computations deteriorate as the mineralization rate increases and are obviously incorrect for the all-labile run. The cumulative plots indicate computed DO moves up or down as the mineralization rate decreases or increases (Figure 8-27). At the median, the calibration provides superior results. The all-refractory run matches the upper end of the DO distribution well but is inferior to the calibration for the lower portion of the distribution. The average run underestimates DO throughout the distribution while the all-labile run provides completely unsatisfactory results.

Nitrogen and chlorophyll. Highest dissolved inorganic nitrogen concentrations are computed for the all-labile run and decline thereafter as mineralization rate declines. At Picolata, visual examination indicates the calibration provides superior results (Figure 8-28). The cumulative distribution plots are not as clear (Figure 8-29). In the lower half of the observed distribution, the average run is best, although this run underestimates the upper portion of the distribution. The calibration is high on the lower end and low on the higher end of the observed distribution. In a sense, the calibration may be viewed as superior overall, although the run with average mineralization rate provides better results when nitrogen is potentially a limiting nutrient. Both the average run and the calibration are superior to the all-labile and all-refractory runs.

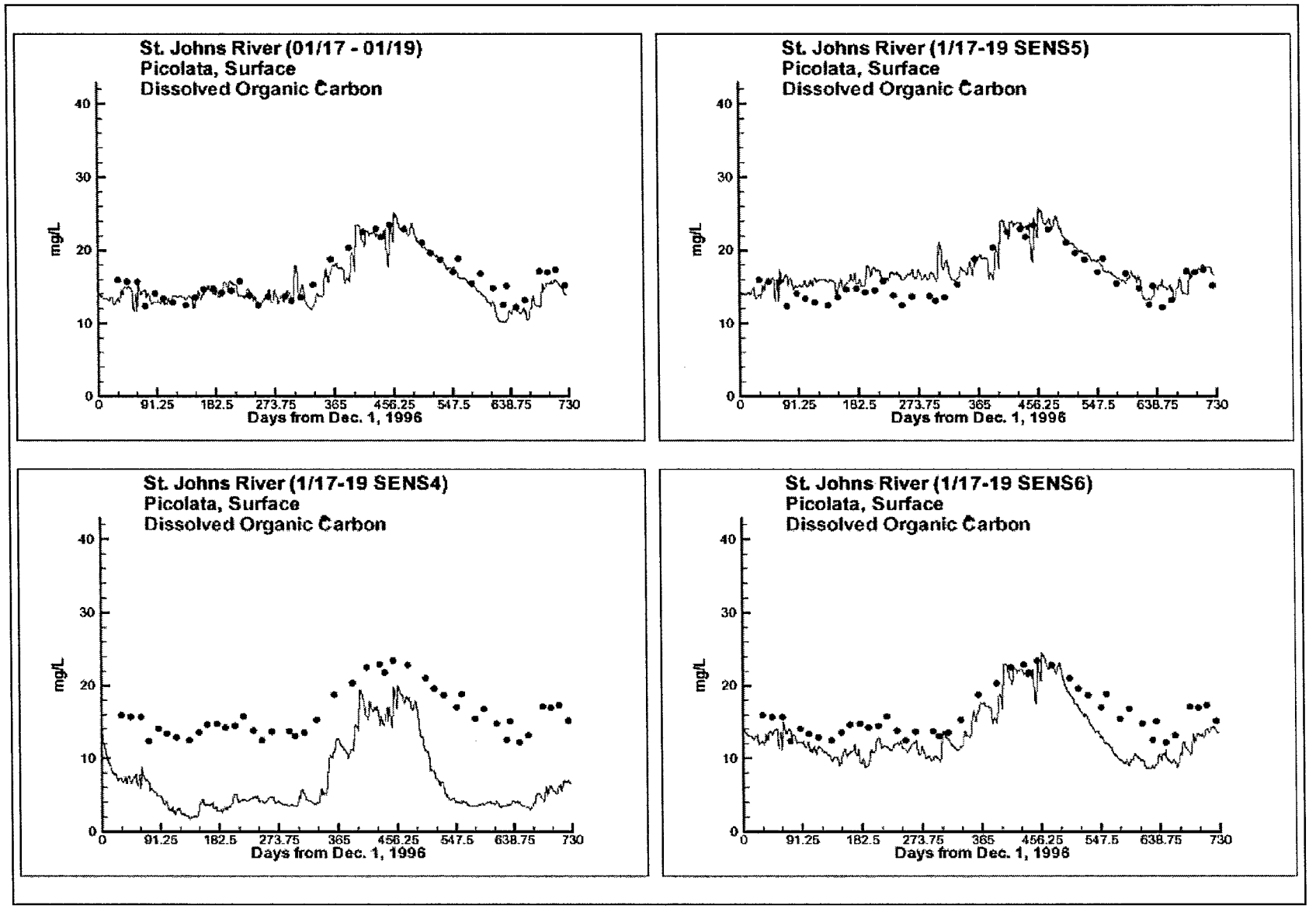

Figure 8-24. Computed and observed DOC at Picolata for calibration (01/10 – 01/19), all labile (SENS4), all refractory (SENS5), and average (SENS6) splits

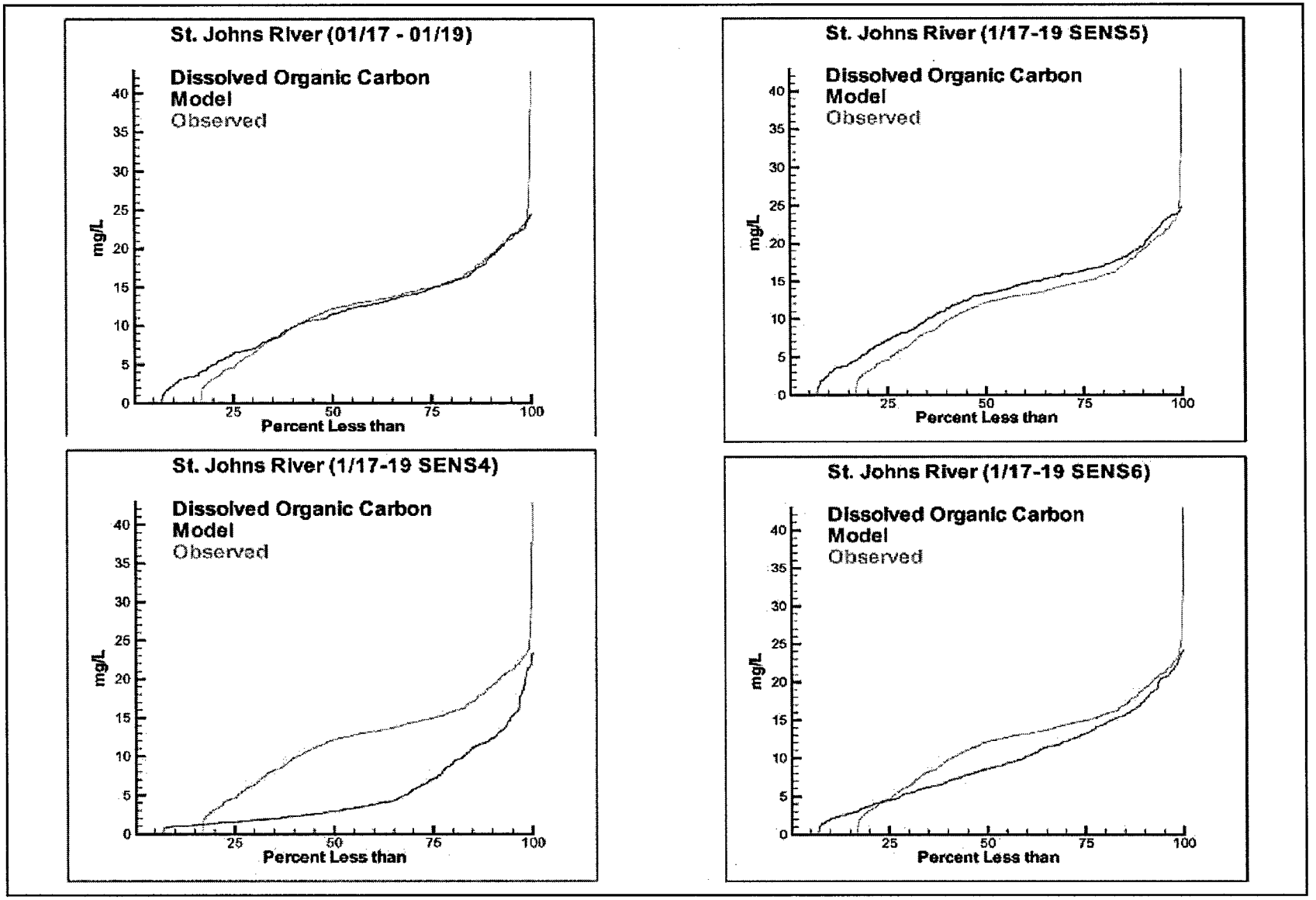

Figure 8-25. System-wide cumulative distributions of computed and observed DOC for calibration (01/10 – 01/19), all labile (SENS4), all refractory (SENS5), and average (SENS6) splits

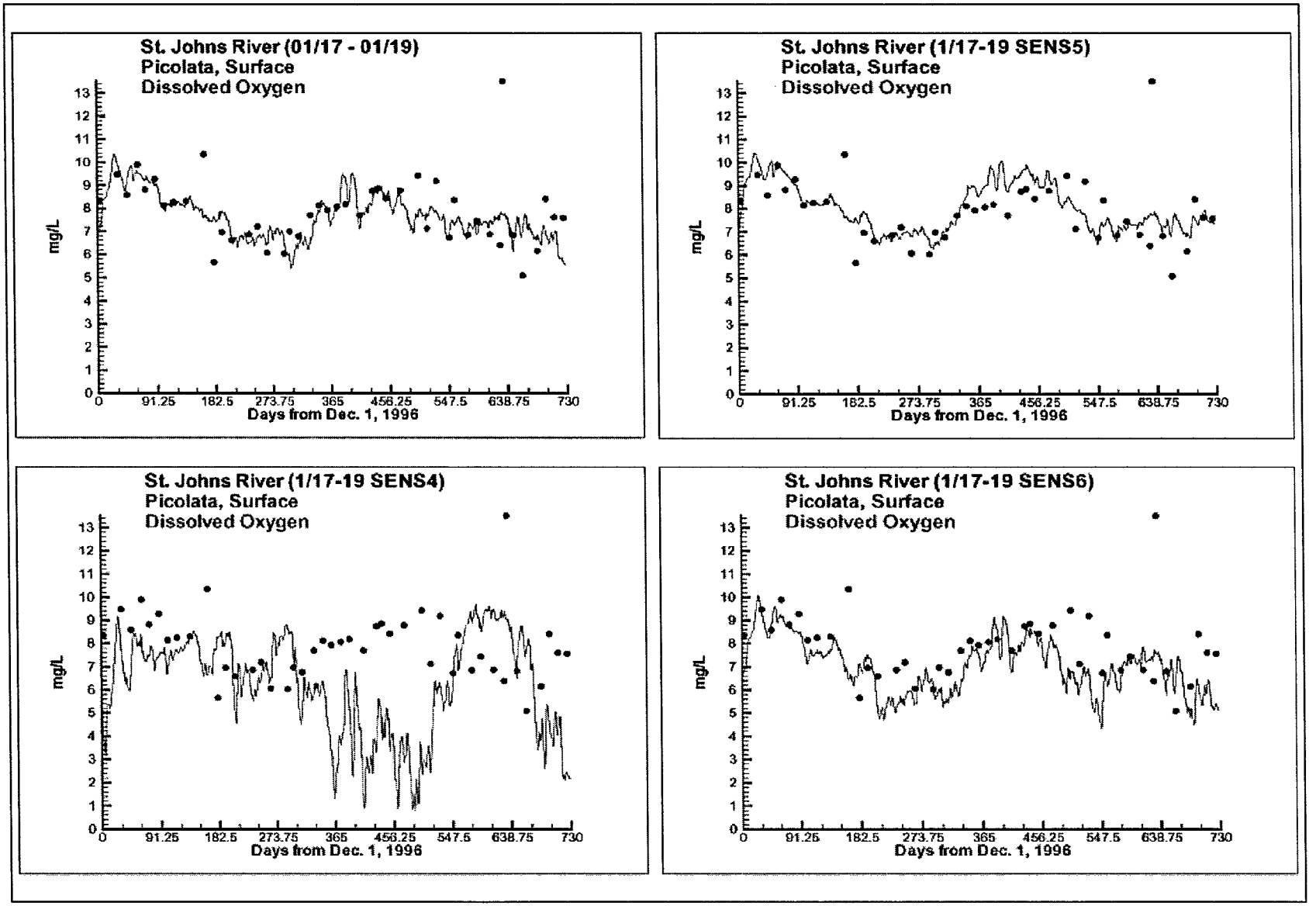

Figure 8-26. Computed and observed DO at Picolata for calibration (01/10 – 01/19), all labile (SENS4), all refractory (SENS5), and average (SENS6) splits.

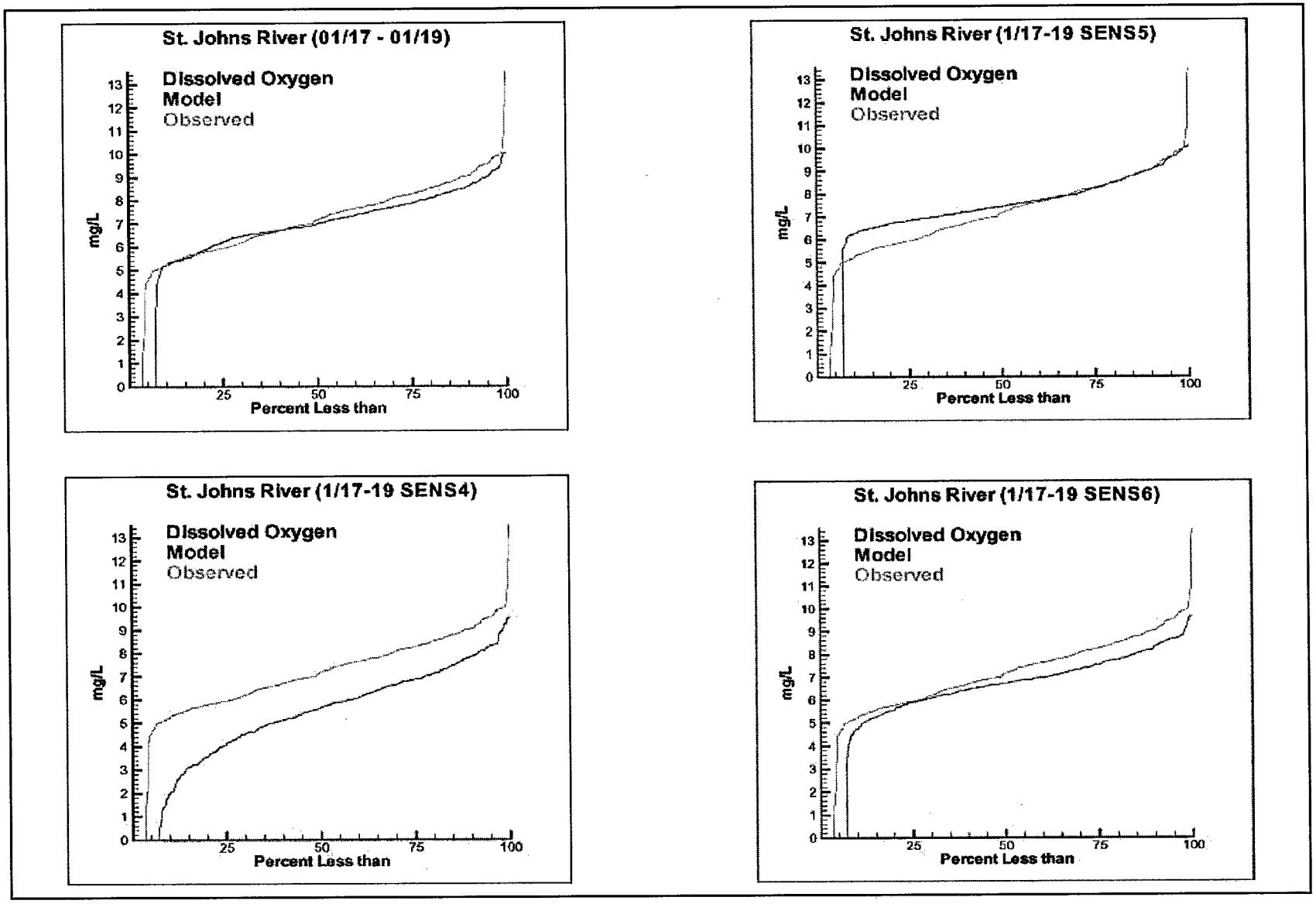

Figure 8-27. System-wide cumulative distributions of computed and observed DO for calibration (01/10 – 01/19), all labile (SENS4), all refractory (SENS5), and average (SENS6) splits.

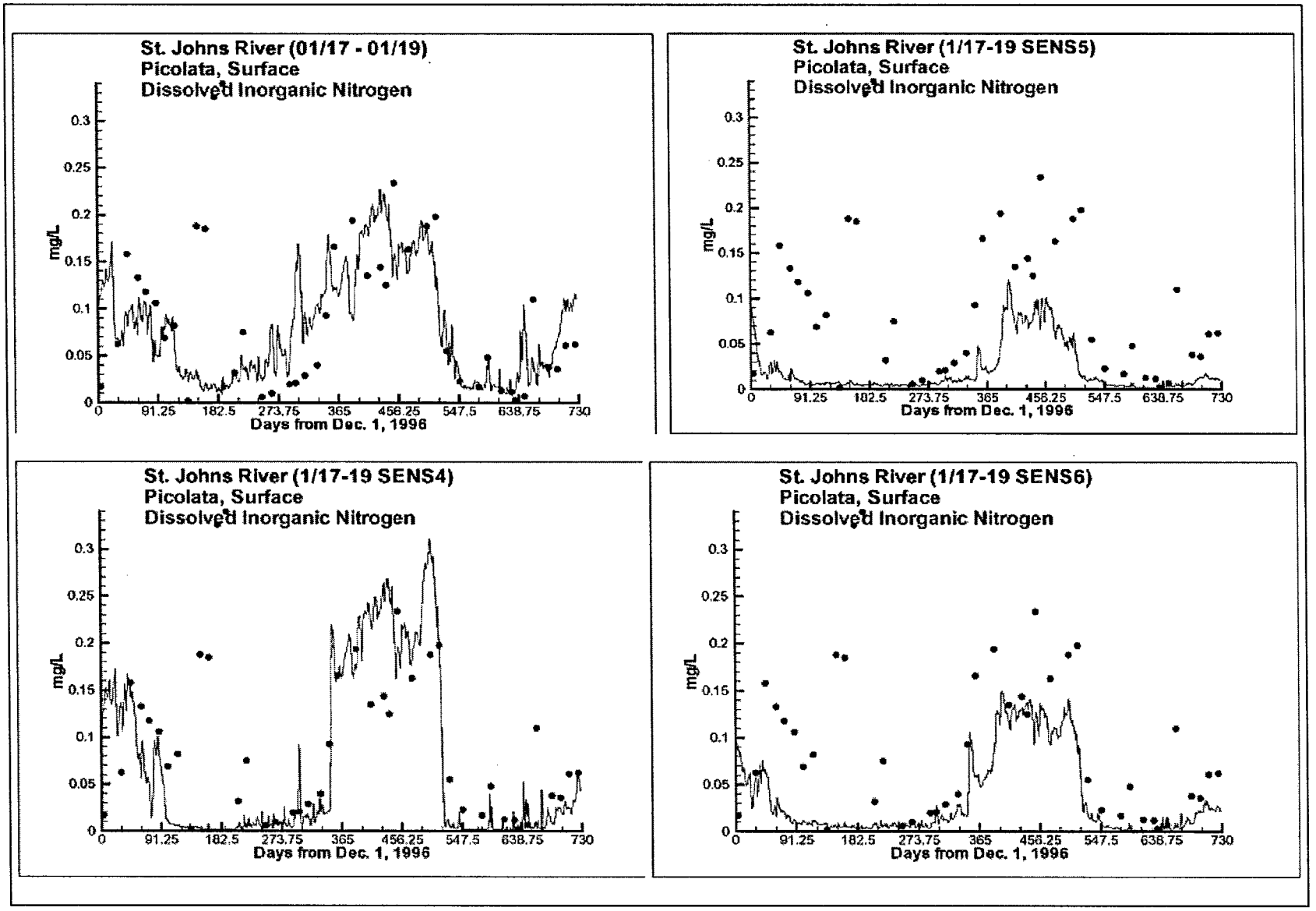

Figure 8-28. Computed and observed DIN at Picolata for calibration (01/10 – 01/19), all labile (SENS4), all refractory (SENS5), and average (SENS6) splits.

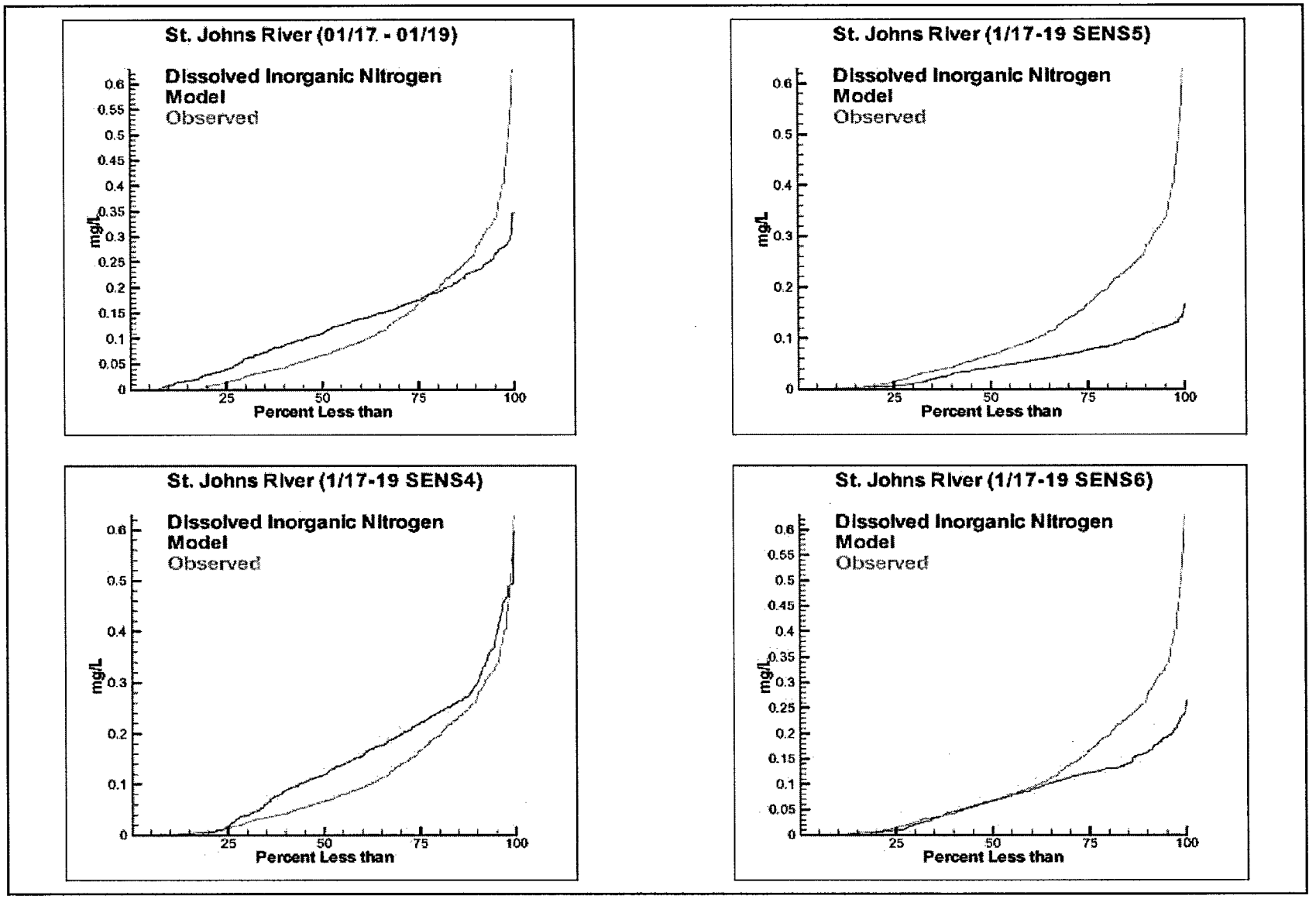

Figure 8-29. System-wide cumulative distributions of computed and observed DIN for calibration (01/10 – 01/19) all labile (SENS4), all refractory (SENS5), and average (SENS6) splits

The chlorophyll time series at Picolata are indistinguishable for the calibration and average runs (Figure 8-30). Computed chlorophyll is on the low side of observed for the all-refractory run and on the high side for the all-labile run. Neither can the calibration and average runs be distinguished in the cumulative plots (Figure 8-31). The all-refractory run is equivalent to the calibration and average runs up to the median observed chlorophyll but underestimates the higher end of the observations. The all-labile run is clearly inferior to all three alternatives.

Phosphorus. The wide range of computed dissolved inorganic phosphorus makes it impossible to select a superior run from the time series at Picolata (Figure 8-32). No dramatic differences are apparent in the cumulative distributions (Figure 8-33), although they can be ranked in order of agreement with the observed distributions, from the all-labile run through the calibration, the average run, and the all-refractory run.

Conclusions

The splitting of dissolved organic matter into labile and dissolved components was most successful for DOC. The split was beneficial from two aspects. First, the calibration was superior to alternatives that considered only one component. Second, the split reflected obvious differences in carbon derived from internal versus external sources.

The benefits of splitting DON and DOP were less apparent. The model results using two components could not be clearly distinguished from alternate runs using only one component. The use of a single, average mineralization rate for nitrogen and a single labile rate for phosphorus provided results as good as or superior to the calibration. These conclusions must be moderated by the fact that no observations of DON or DOP were available for comparison with the model. Also, the impact of the splits on management alternatives involving load controls was not examined.

The justification for splitting DON into two components is based more on reasoning than on results. Organic carbon and nitrogen do not exist as independent entities, although they are modeled as such. Rather, they exist together in a host of organic compounds. The processes mimicked by our first-order mineralization of DOC and DON involve activity of heterotrophic bacteria. Bacteria take up organic compounds containing carbon and nitrogen. Portions of the carbon and nitrogen are incorporated into bacterial biomass. The remainder of the carbon is respired away. Excess nitrogen, if any, is excreted as ammonium. Consequently, it is reasonable to represent organic nitrogen mineralization with a rate close to the rate used for organic carbon mineralization. If DOC is split into two components with different mineralization rates, then it is reasonable to split DON into equivalent components.

The justification for splitting DOP into two components is less clear. The process mimicked by our first-order mineralization of DOP is an enzyme-mediated reaction. Phosphatase enzymes produced by bacteria (Ammerman and Azam 1985; Chrost and Overbeck 1987) and algae (Matavulj and Flint 1987;

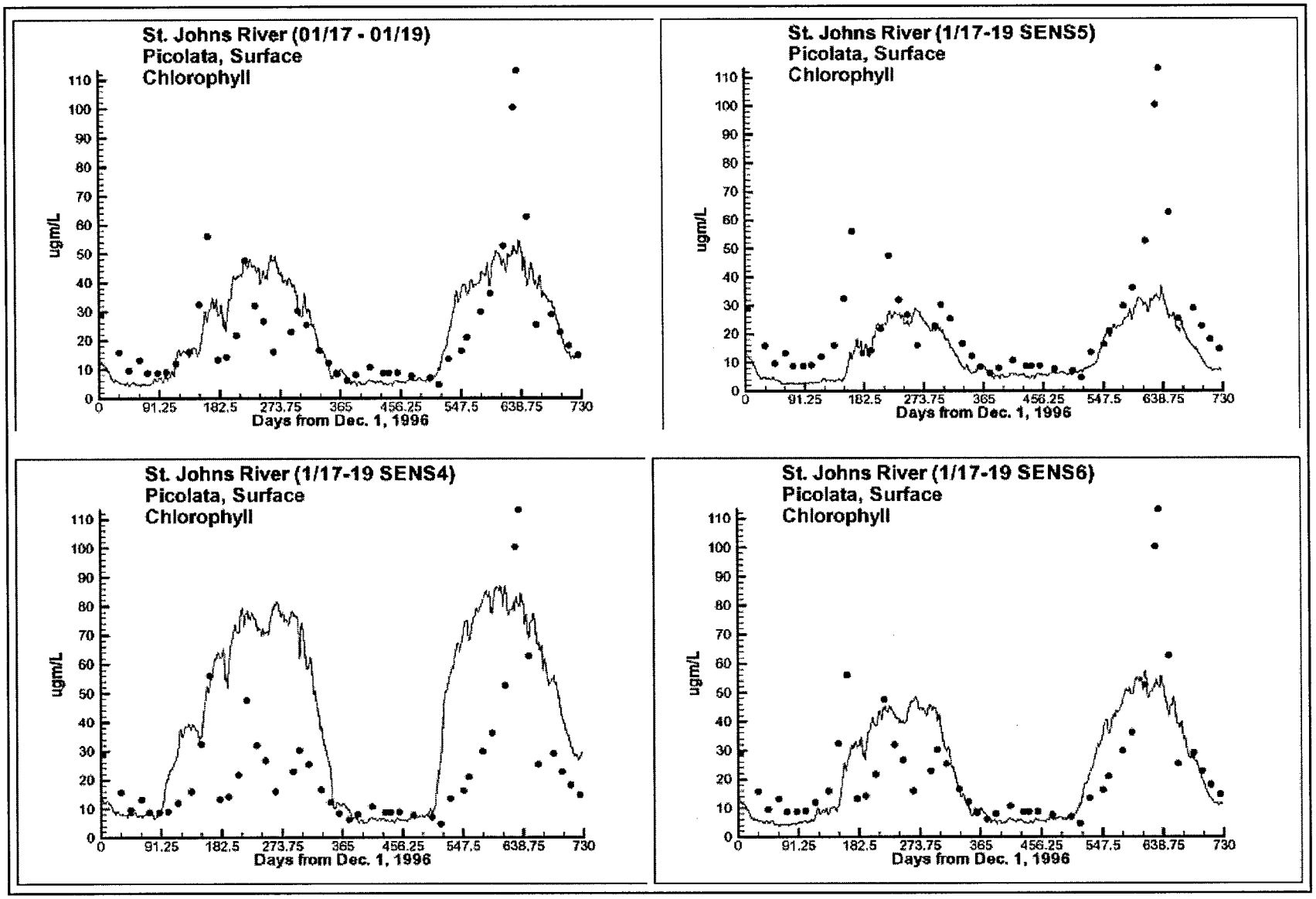

Figure 8-30. Computed and observed chlorophyll at Picolata for calibration (01/10 – 01/19), all labile (SENS4), all refractory (SENS5), and average (SENS6) splits

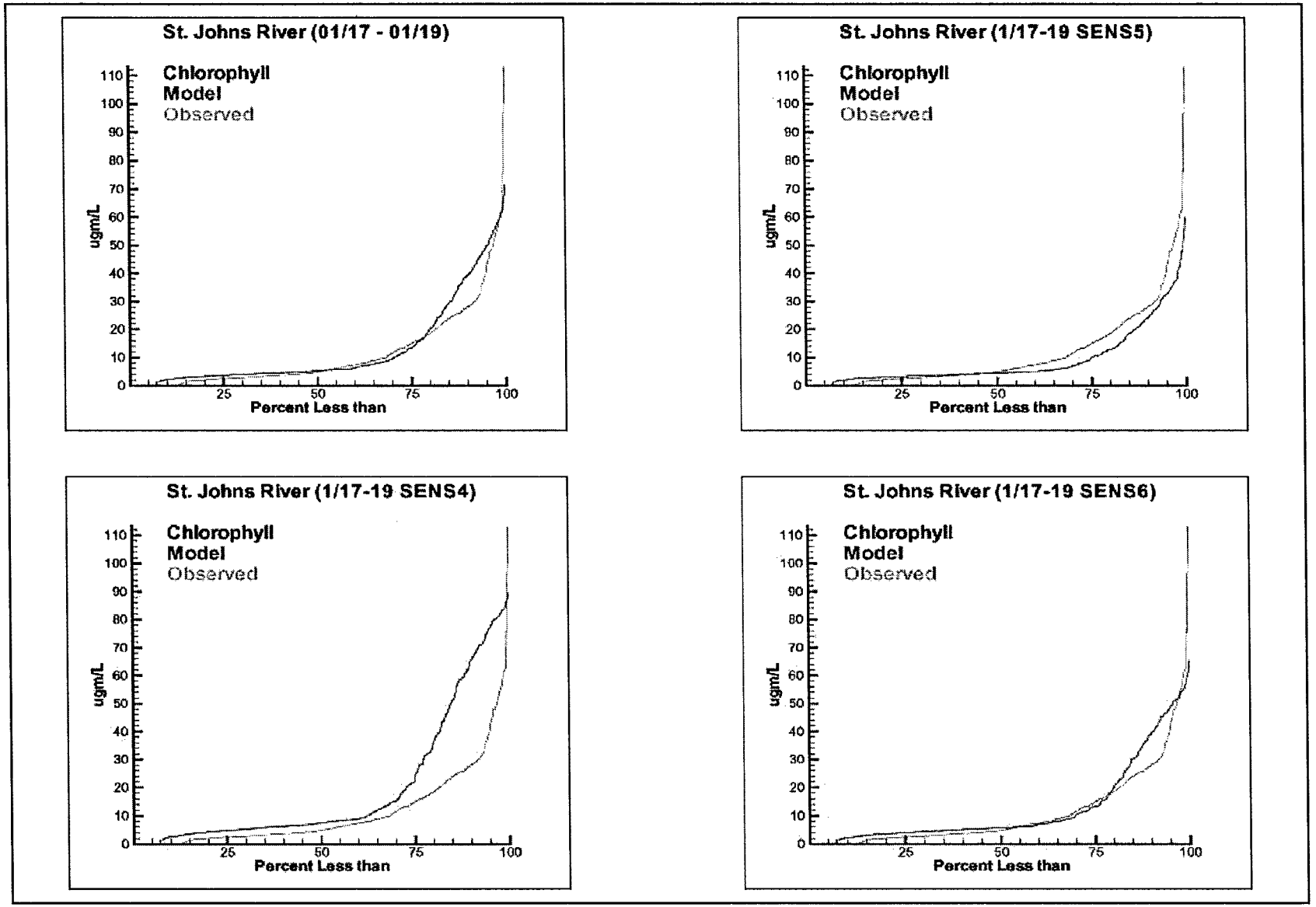

Figure 8-31. System-wide cumulative distributions of computed and observed chlorophyll for calibration (01/10 – 01/19), all labile (SENS4), all refractory (SENS5), and average (SENS6) splits.

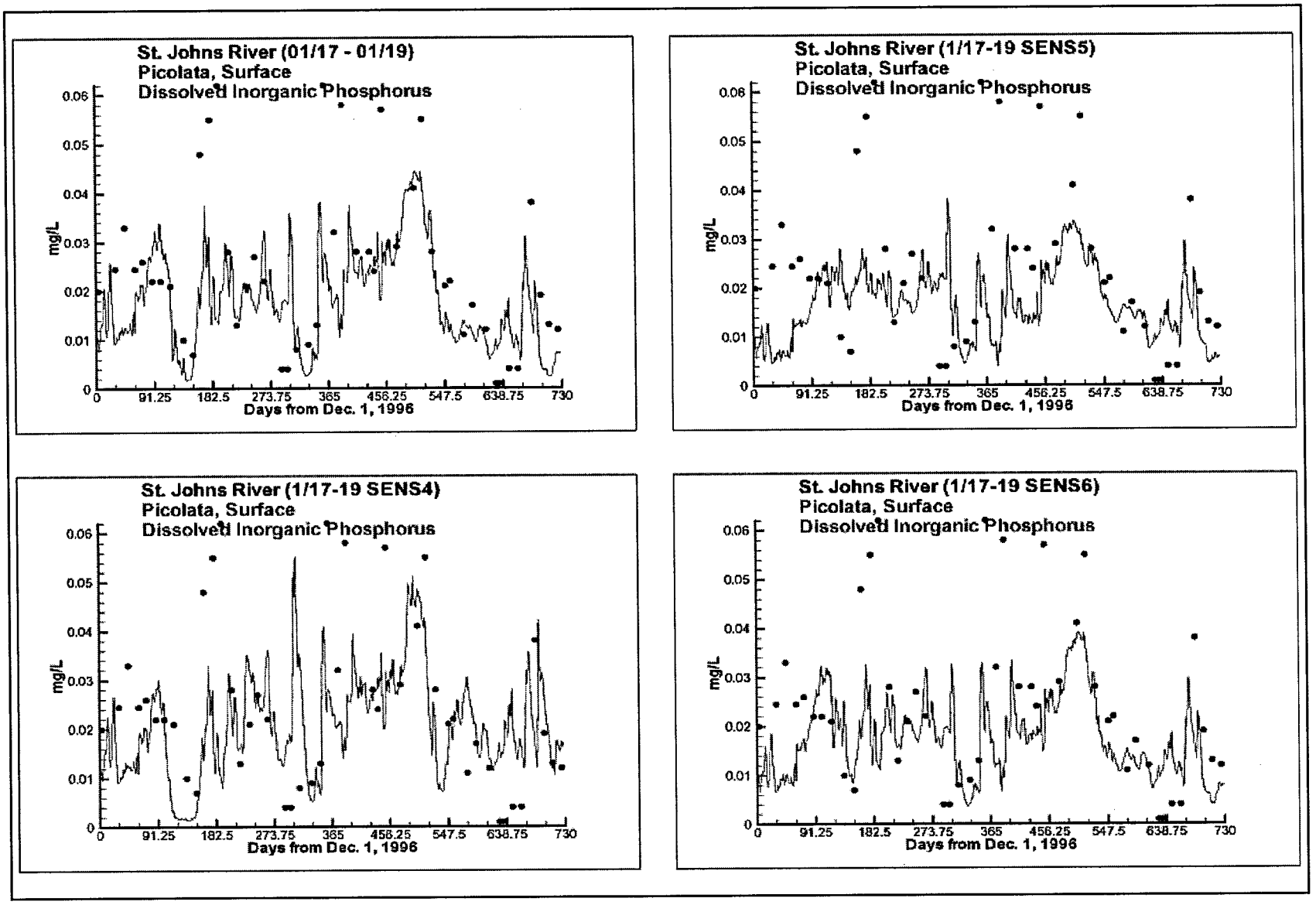

Figure 8-32. Computed and observed DIP at Picolata for calibration (01/10 – 01/19), all labile (SENS4), all refractory (SENS5), and average (SENS6) splits.

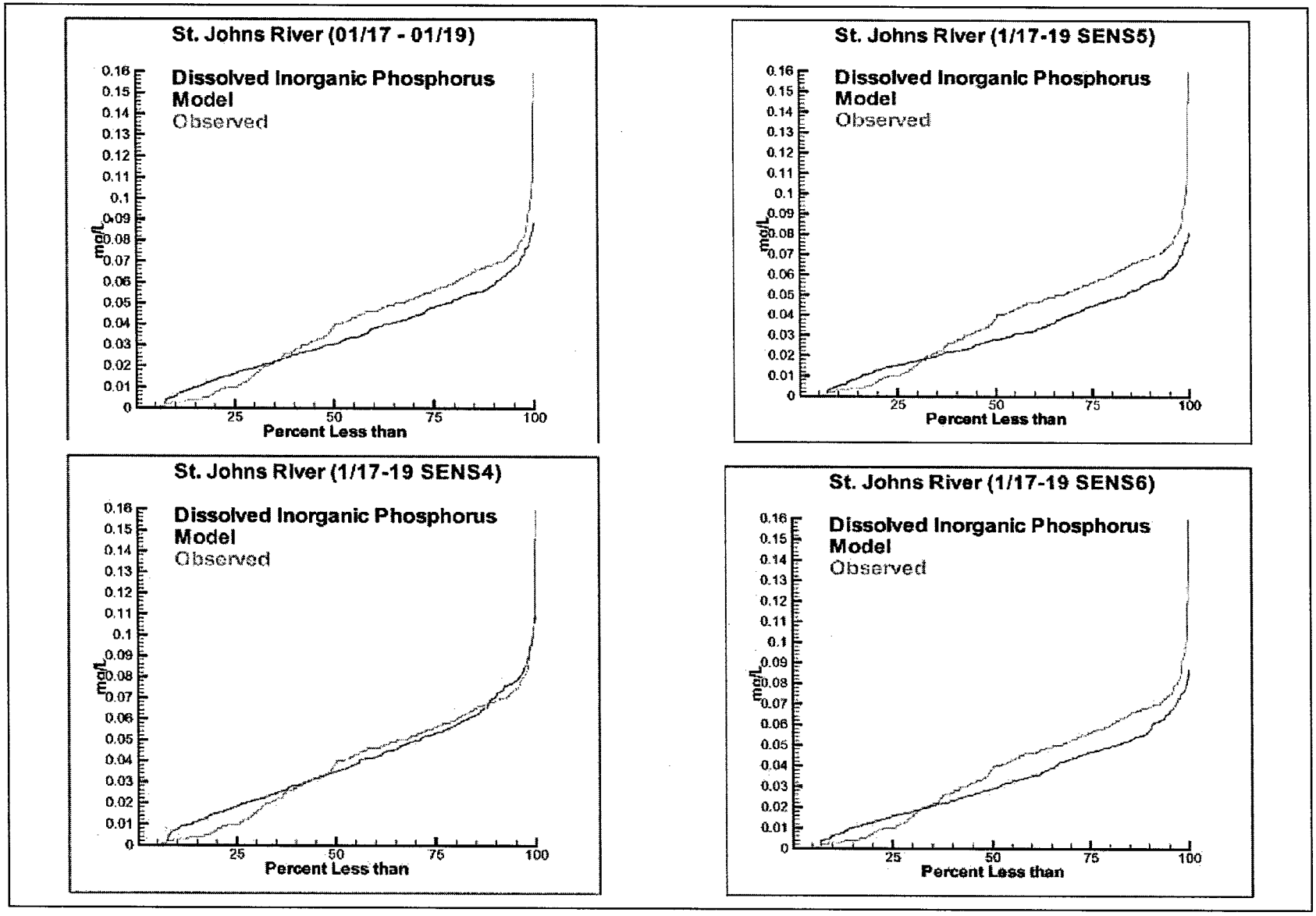

Figure 8-33. System-wide cumulative distributions of computed and observed DIP for calibration (01/10 – 01/19), all labile (SENS4), all refractory (SENS5), and average (SENS6) splits.

Chrost and Overbeck 1987; Boni et al. 1989) convert DOP into phosphate. This process is distinct from heterotrophic carbon utilization and need not proceed at a similar rate. In our models, the first-order mineralization rate for DOP is usually an order-of-magnitude larger than rates for carbon and nitrogen (Table 8-2). The uncertainty in assigning fractions and the absence of distinct model improvements indicate splitting DOP into components is not worthwhile except for consistency with other dissolved organic substances.

Primary Production and Respiration

The data base

Observations were provided from three stations: Federal Point, Picolata, and Mandarin Point. The data base consisted of 25 observations at each station collected August 1994 to August 1996. Observations of interest included Gross Areal Production (GAP), Volumetric Community Respiration (VCR), and Areal Community Respiration (ACR).

Gross areal production was measured via oxygen evolution over a 3-hour period at midday. Oxygen consumed in accompanying dark bottles was added to oxygen evolved to obtain gross production. A photosynthesis quotient of 1.2 was used to convert oxygen production to carbon units. Respiration measured as oxygen consumption was converted to equivalent carbon units using a respiration quotient of unity. Respiration measured on a volumetric basis was integrated over the depth of the water column to obtain respiration on an areal basis.

The observations were collected prior to the modeled period. For comparison with the model, monthly means were computed at each station. The mean was usually taken from of two observations, up to four observations were available for some months. Observations were entirely missing for several other months. Available monthly means were subsequently averaged into annual means.

Comparison with model

Model results at locations corresponding to the observations were averaged into monthly means. Since the production observations were collected at midday, model computations at noon were used. Roughly 60 individual computations (2 months × 30 days) went into each monthly mean. Monthly means were subsequently averaged into annual means.

Observed gross areal production exhibited peak values of roughly 350 mg C m^{-2} hr^{-1} at all stations (Figures 8-34 through 8-36). A strong seasonal trend was exhibited so that production during the winter months was less than 10 percent of the summer peak. The summer production maximum encompassed more months at Federal Point than further downstream so that annual production was greatest at the Federal Point station (Table 8-3). The model production cycle was "flatter" than observed. Peak model production was ≈70 percent of observed while minimum modeled production was two times larger than observed. The temporal behavior of computed production lagged the observations. Observed

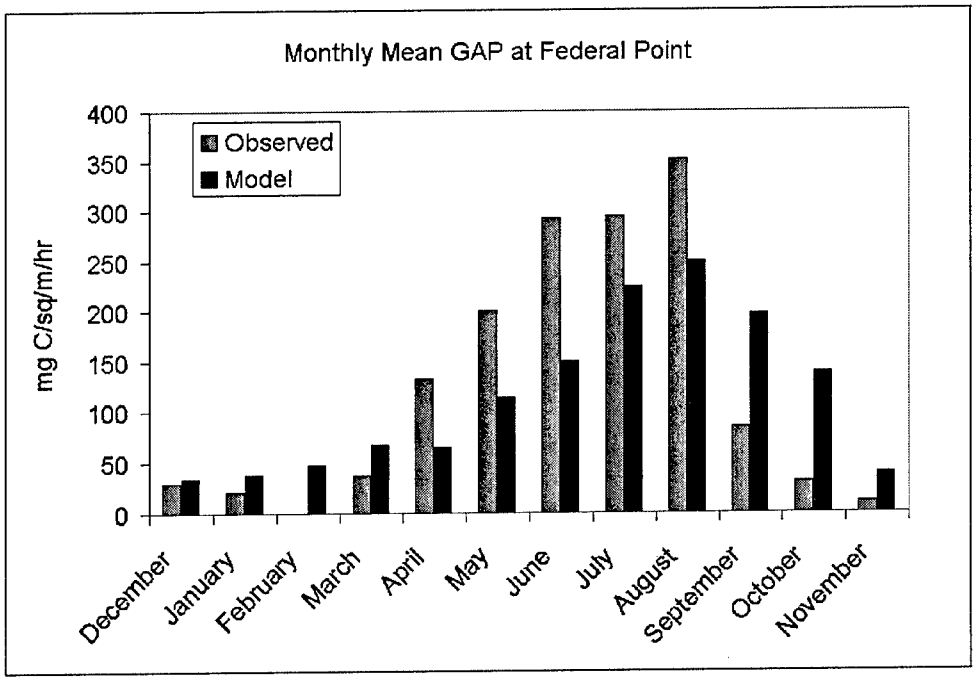

Figure 8-34. Observed and computed monthly mean GAP at Federal Point

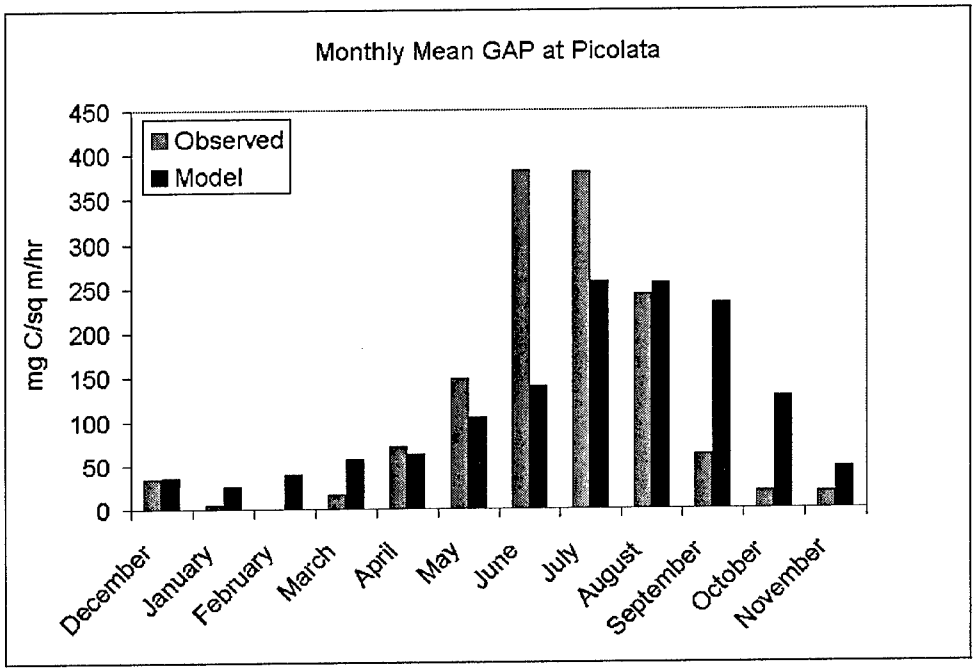

Figure 8-35. Observed and computed monthly mean GAP at Picolata

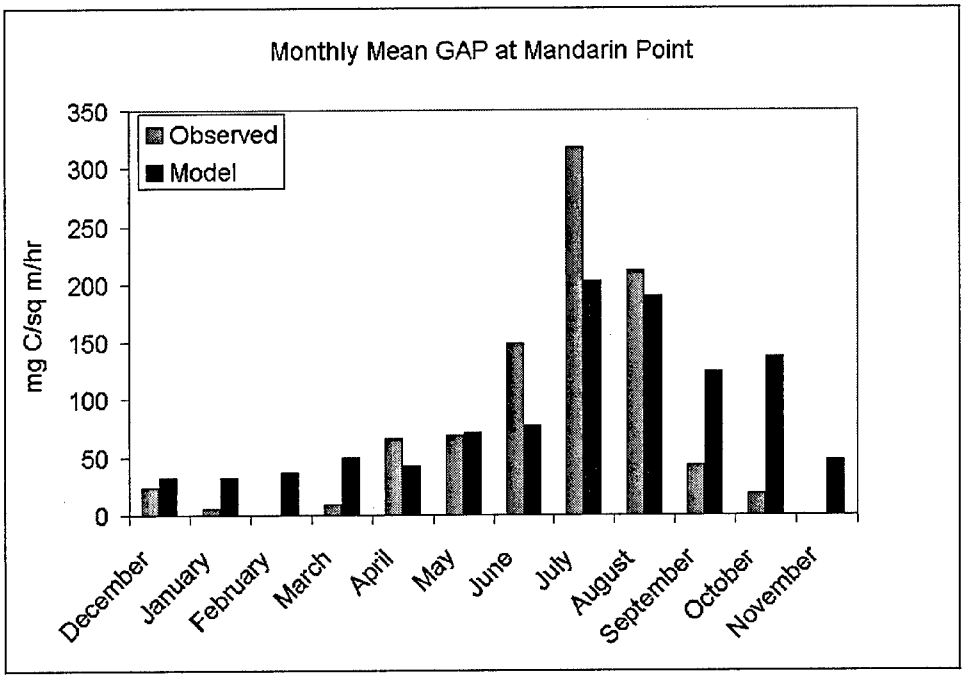

Figure 8-36. Observed and computed monthly mean GAP at Mandarin Point

Table 8-3
Observed and Computed Annual-Average Production and Respiration

	Gross Areal Production, mg C m^{-2} hr^{-1}		Volumetric Carbon Respiration, mg C m^{-3} hr^{-1}	
	Observed	Model	Observed	Model
Federal Pt.	123.8	98.4	24.6	18.5
Picolata	115.0	115.9	15.7	14.4
Mandarin Pt.	98.5	121.1	33.8	16.5

production in spring was undercomputed, while computed production exceed observed in autumn. On an annual-average basis, modeled production exceeded observed at Mandarin Point by ≈25 percent, was nearly perfect at Picolata, and fell ≈25 percent below observed at Federal Point (Table 8-3). In view of the limited number of samples and the absence of temporal correspondence between observations and computations, the differences between computed and observed annual-average production are not considered significant.

Observed volumetric carbon respiration exhibited no seasonal trend (Figures 8-37 through 8-39). Peak values were roughly 50 mg C m^{-3} hr^{-1}. Observations were erratic with multiple questionable values, notably the occurrence of zeroes (as opposed to missing observations), i.e., August 24, 1994, at Picolata. Modeled respiration exhibited seasonality that corresponded with temperature so that peak respiration occurred during the summer months.

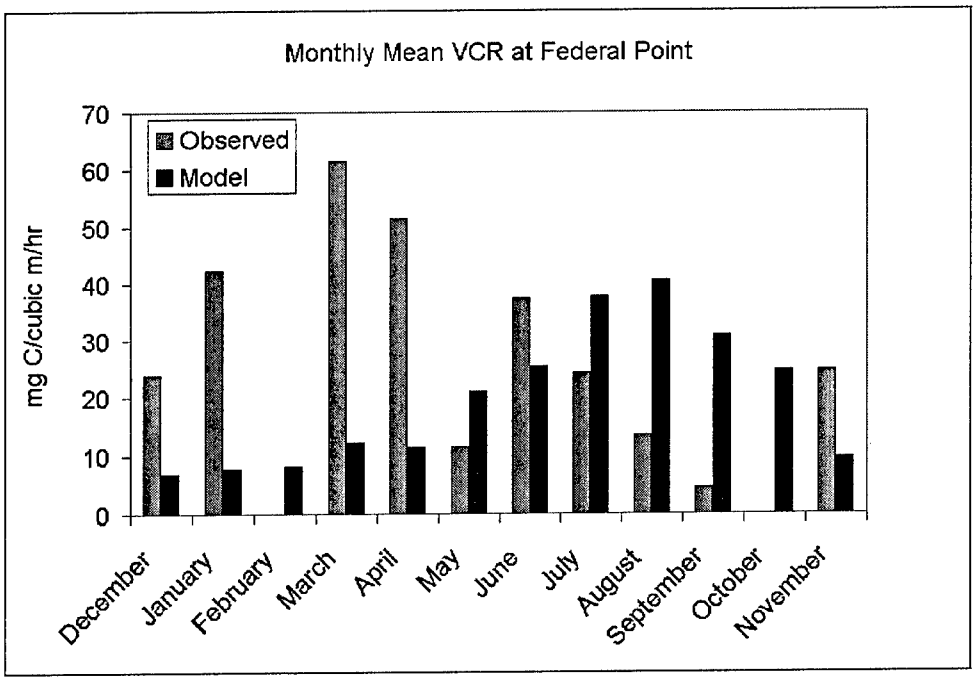

Figure 8-37. Observed and computed monthly mean VCR at Federal Point

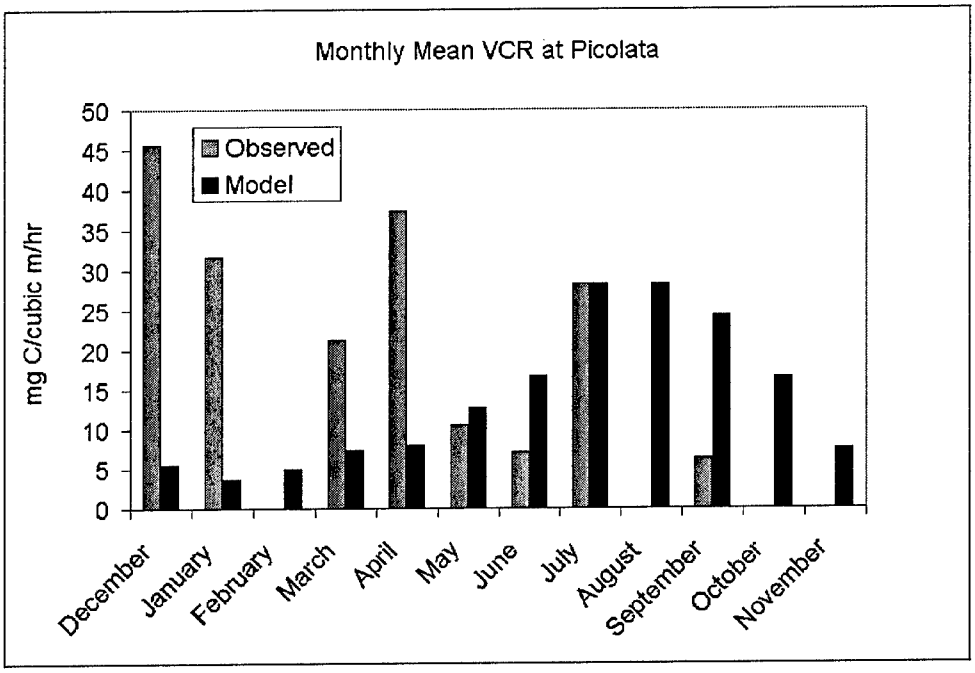

Figure 8-38. Observed and computed monthly mean VCR at Picolata

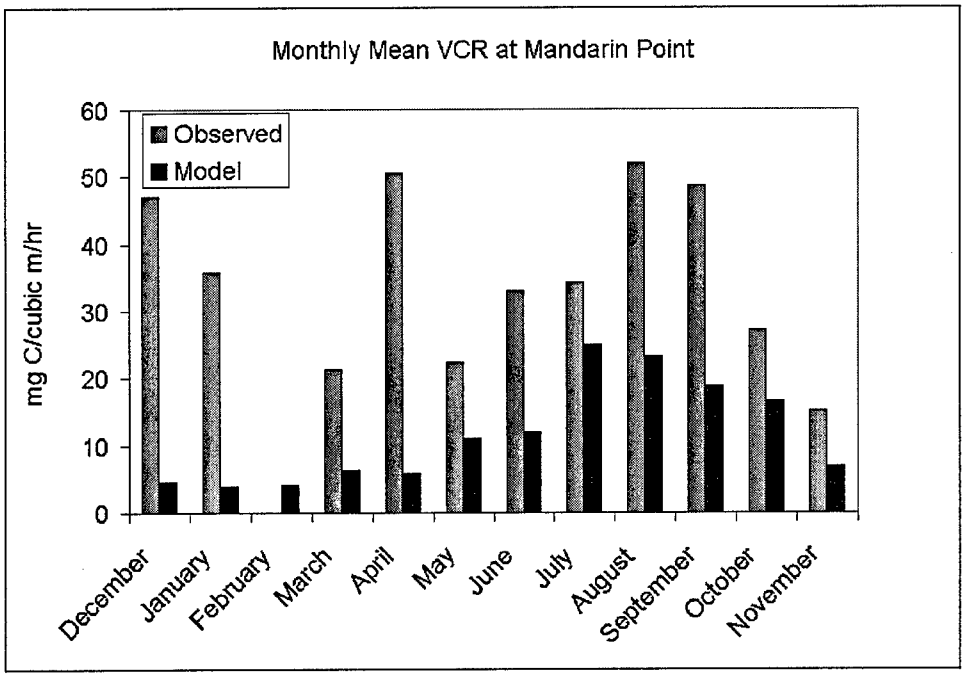

Figure 8-39. Observed and computed monthly mean VCR at Mandarin Point

Magnitude of peak model respiration was roughly half observed. In view of the erratic behavior of the observations, long-term means should be the most reliable representation of respiration. On an annual-average basis, model respiration ranged from half to nearly 100 percent of the observed values (Table 8-3).

Discussion

On an annual-average basis, the model provides good representation of gross areal production. The production-temperature relationships presently applied in the algal component of the model can, perhaps, be revised to enhance seasonality but existing discrepancies between observations and computations must be viewed as minor compared to previous applications of this and other models. Difficulty in simultaneously computing chlorophyll concentration and primary production has been observed in previous CE-QUAL-ICM applications (Cerco 2000) and is a common characteristic of eutrophication models (Brush et al. 2002). The primary production computations in the St. Johns River present a welcome contrast to previous results. Successful computations of both chlorophyll concentration and production in the St. Johns reflect formulations and parameter values adapted from an application specifically intended to reproduce primary production (Cerco and Noel 2004).

Respiration in the model is tightly coupled to temperature and to primary production. Production is temperature-dependent and provides the substrate for heterotrophic respiration (represented as organic carbon mineralization in the model). Both algal and heterotrophic respiration are temperature dependent and enhance the influence of greater substrate availability. The coupling of respiration to production is an entirely reasonable behavior and indicates that internally produced carbon is the primary source of oxidizable substrate.

Observed respiration shows no coupling to temperature or production. In particular, peak respiration often occurs from December to April when production is low. The validity of these measures requires examination. If the respiration measures are valid, they indicate an external source of oxidizable material. To reproduce observed respiration in the model, carbon loads must be re-examined and, perhaps, re-evaluated. Alternately, the present split of loads into labile and refractory fractions may require revision.

References

Ammerman, J., and Azam, F. (1985). "Bacterial 5'-nucleodase in aquatic ecosystems: A novel mechanism of phosphorus regeneration," *Science* 227, 1338-1340.

Bierman, V. (1976). "Mathematical model of the selective enhancement of blue green algae by nutrient enrichment." *Modeling biochemical processes in aquatic ecosystems*. R. Canale ed., Ann Arbor Science, Ann Arbor MI, 1-32.

Boni, L., Carpene, E., Wynne, D., and Reti, M. (1989). "Alkaline phosphatase activity in *Protogonyaulax Tamarensis*," *Journal of Plankton Research*, 11, 879-885.

Brush, M., Brawley, J., Nixon, S., and Kremer, J. (2002). "Modeling phytoplankton production: problems with the Eppley curve and an empirical alternative," *Marine Ecology Progress Series* 238, 31045.

Cerco, C., and Cole, T. (1994). "Three-dimensional eutrophication model of Chesapeake Bay," Technical Report EL-94-4, U.S. Army Engineer Waterways Experiment Station, Vicksburg, MS.

Cerco, C. (2000). "Phytoplankton kinetics in the Chesapeake Bay eutrophication model," *Water Quality and Ecosystem Modeling*," 1, 5-49.

Cerco, C., Bunch, B., Teeter, A., and Dortch, M. (2000). "Water quality model of Florida Bay," Technical Report ERDC/EL TR-00-10, U.S. Army Engineer Research and Development Center, Vicksburg, MS.

Cerco, C., and Noel, M. (2004). "The 2002 Chesapeake Bay eutrophication model," Draft Technical Report, U.S. Army Engineer Research and Development Center, Vicksburg, MS.

Chrost, R., and Overbeck, J. (1987). "Kinetics of alkaline phosphatase activity and phosphorus availability for phytoplankton and bacterioplankton in Lake Plubsee (north German eutrophic lake)," *Microbial Ecology* 13, 229-248.

DiToro, D. (1980). "Applicability of cellular equilibrium and Monod theory to phytoplankton growth kinetics," *Ecological Modelin*, 8, 201-218.

DiToro, D., and Fitzpatrick, J. (1993). "Chesapeake Bay sediment flux model," Contract Report EL-93-2, U.S. Army Engineer Waterways Experiment Station, Vicksburg, MS.

Droop, M. (1973). "Some thoughts on nutrient limitation in algae," *Journal of Phycology* 9, 264-272.

Hendrickson, J. (2002). "Calculation of the external load," TMDL and PLRG modeling of the lower St. Johns River Technical Report Series, Volume 1, St. Johns River Water Management District, Palatka, FL.

Matavulj, M., and Flint, K. (1987). "A model for acid and alkaline phosphatase activity in a small pond," *Microbial Ecology* 13, 141-158.

Paerl, H., Piehler, M., Dyble, J., Moisander, P., Leonard, J., Waggener, A., and Carmichael, W. (2002). "Phytoplankton and zooplankton in the St. Johns River system: Factors affecting community structure and function," progress report prepared for the St. Johns River Water Management District, Palatka, FL.

Phlips, E. (2002). "Biological monitoring of the lower St. Johns River: Temporal and spatial trends in plankton," Final Report Task C, prepared for the St. Johns River Water Management District, Palatka, FL.

Redfield, A., Ketchum, B., and Richards, F. (1966). "The influence of organisms on the composition of sea-water," *The Sea Volume II*, Interscience Publishers, New York, 26-48.

Rhee, G-Y. (1973). "A continuous culture study of phosphate uptake, growth rate and polyphosphates in Scenedesmus spp.," *Journal of Phycology* 9, 495-506.

Rhee, G-Y., and Gotham, I. (1981). "The effect of environmental factors on phytoplankton growth: Light and the interactions of light with nitrate limitation," *Limnology and Oceanography* 26(4), 649-659.

Taft, J., Taylor, W., and McCarthy, J. (1975). "Uptake and release of phosphorus by phytoplankton in the Chesapeake Bay estuary, USA," *Marine Biology* 33, 21-32.

Westrich, J., and Berner, R. (1984). "The role of sedimentary organic matter in bacterial sulfate reduction: The G model tested," *Limnology and Oceanography* 29, 236-249.

9 Light Attenuation

The Data Base

A data base of more than 700 measures of light attenuation was provided by the sponsor. The majority of the observations were collected outside the spatial and temporal domains of the present model application. The data set was reduced to observations collected at eight stations located along the river axis within the model grid:

- Bar Pilot
- Fulton Point
- Talleyrand
- Piney Point
- Mandarin Point
- Picolata
- Racey Point
- Palatka.

The preponderance of observations remained outside the model application period. These observations were retained since they were often the sole characterization of conditions at the sample stations.

The Model

An additive model was applied that considered attenuation from four sources: clear water, inorganic solids, organic solids, and dissolved organic matter. Organic solids were computed as 2.5 times the sum of the model particulate organic carbon state variables. This ratio was based on the assumption that organic matter is composed of carbon, hydrogen, and oxygen in the atomic ratio 1:2:1. DOC was used as a surrogate for dissolved organic matter. The resulting model was:

$$Ke = a_1 + a_2 \cdot ISS + a_3 \cdot VSS + a_4 \cdot DOC \qquad (9\text{-}1)$$

in which:

Ke = coefficient of diffuse light attenuation (m^{-1})

a_1 = attenuation of clear water

a_2 = contribution of inorganic solids to light attenuation ($m^2\ g^{-1}$)

a_3 = contribution of organic solids to light attenuation ($m^2\ g^{-1}$)

a_4 = contribution of dissolved organic carbon to light attenuation ($m^2\ g^{-1}$)

ISS = inorganic (fixed) solids concentration ($g\ m^{-3}$)

VSS = organic (volatile) solids concentration ($g\ m^{-3}$)

DOC = dissolved organic carbon concentration ($g\ m^{-3}$)

Parameters in the model were initially adapted from published values (Pennock 1985; Kirk 1994; Cerco and Noel 2004). Good, consistent guidance was available for the contributions from clear water and solids. Little guidance was available for the contribution from DOC. Initial values were refined through visual fitting of computed and observed attenuation. Final values used in the model were: $a_1 = 0.03\ m^{-1}$; $a_2 = 0.08\ m^2\ g^{-1}$; $a_3 = 0.06\ m^2\ g^{-1}$; and $a_4 = 0.15\ m^2\ g^{-1}$. Light attenuation was computed in every model cell at every time step using computed values of solids and DOC concentrations.

Model Results

Computed and observed results were in very good agreement throughout the greater portion of the river (Figures 9-1 through 9-5). Computations departed from observations near the river mouth (Figures 9-6 through 9-8). Observations indicated a sharp and continuous decline in attenuation downstream of Piney Point while the model computed a flat spatial distribution in which the mouth of the river differed little from the headwaters (Figure 9-9).

Two factors contribute to the discrepancies between computations and observations near the mouth of the river. The first is an apparent overestimation of the parameters that relate attenuation to solids concentration. At the two most downstream stations, Bar Pilot and Fulton Point, the major component of computed attenuation is suspended solids (Figure 9-10). Reduction of computed attenuation into the observed range requires reduction of the solids contribution. Exact matching of the observed mean attenuation at these two stations requires virtual elimination of attenuation by solids. Elimination of solids attenuation is unrealistic.

The second contributor to the discrepancies between computations and observations is the assignment of attenuation to DOC. DOC is used as a surrogate for dissolved, colored organic matter. It is felt that the use of DOC overestimates the contribution of colored material in the lower river. One alternative is that color is bleached out as DOC moves downstream from the headwaters to the mouth. Another alternative, favored by us, recognizes that DOC in the river is a mixture of carbon from multiple sources. Carbon produced

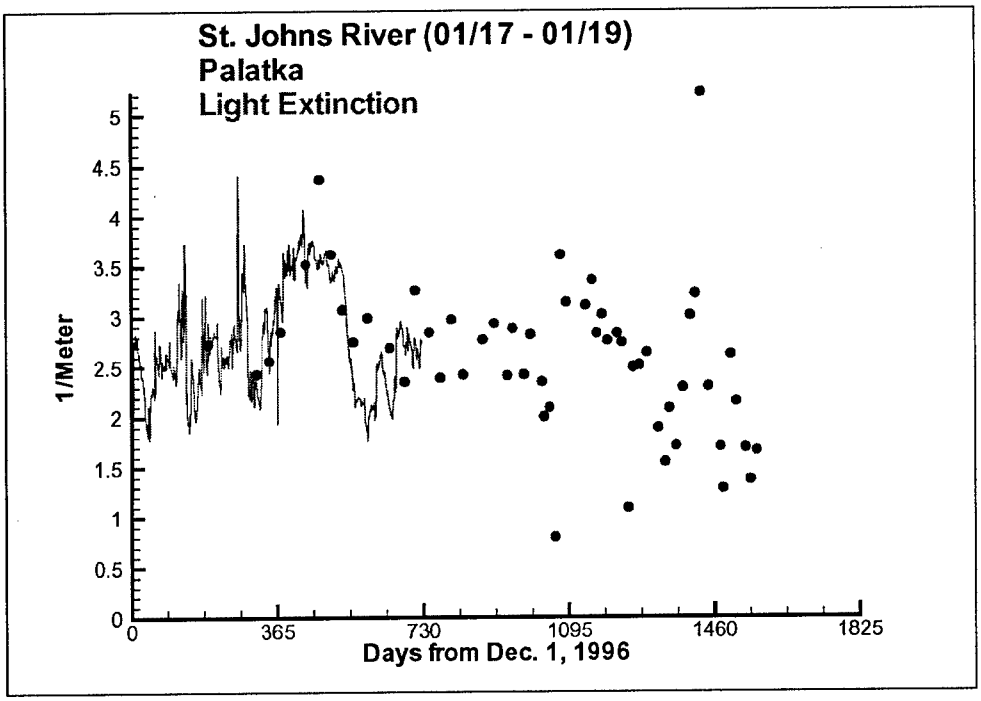

Figure 9-1. Computed and observed light attenuation at Palatka

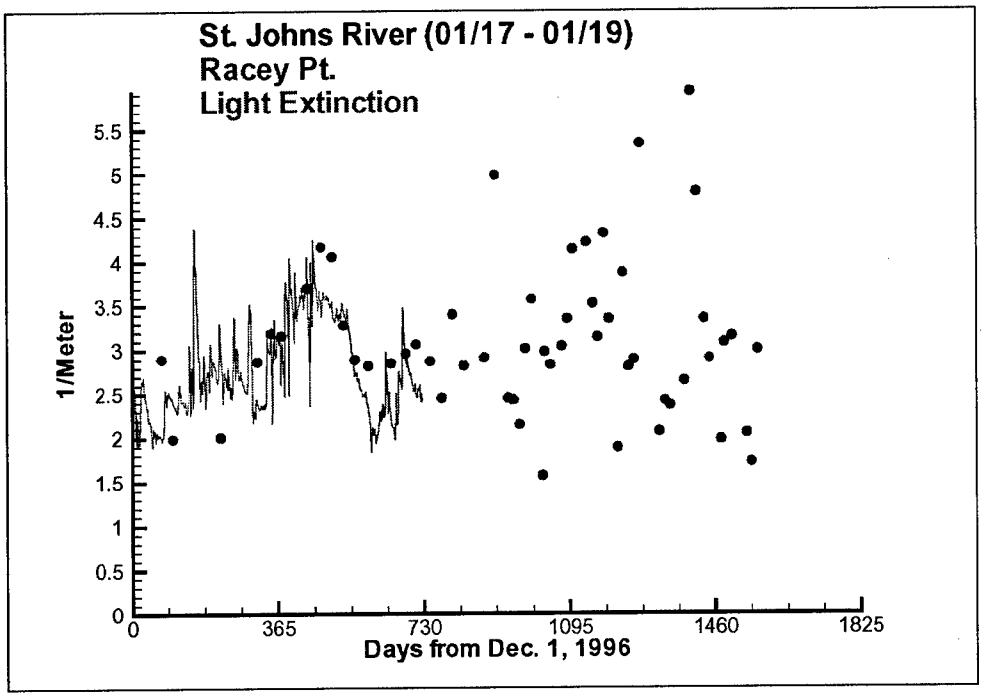

Figure 9-2. Computed and observed light attenuation at Racey Point

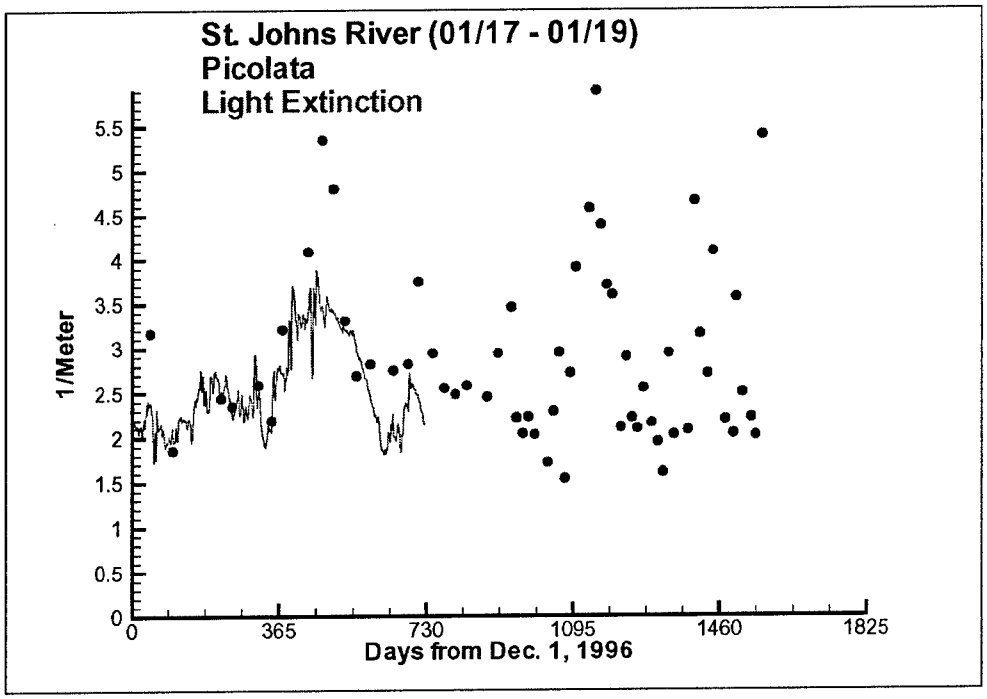

Figure 9-3. Computed and observed light attenuation at Picolata

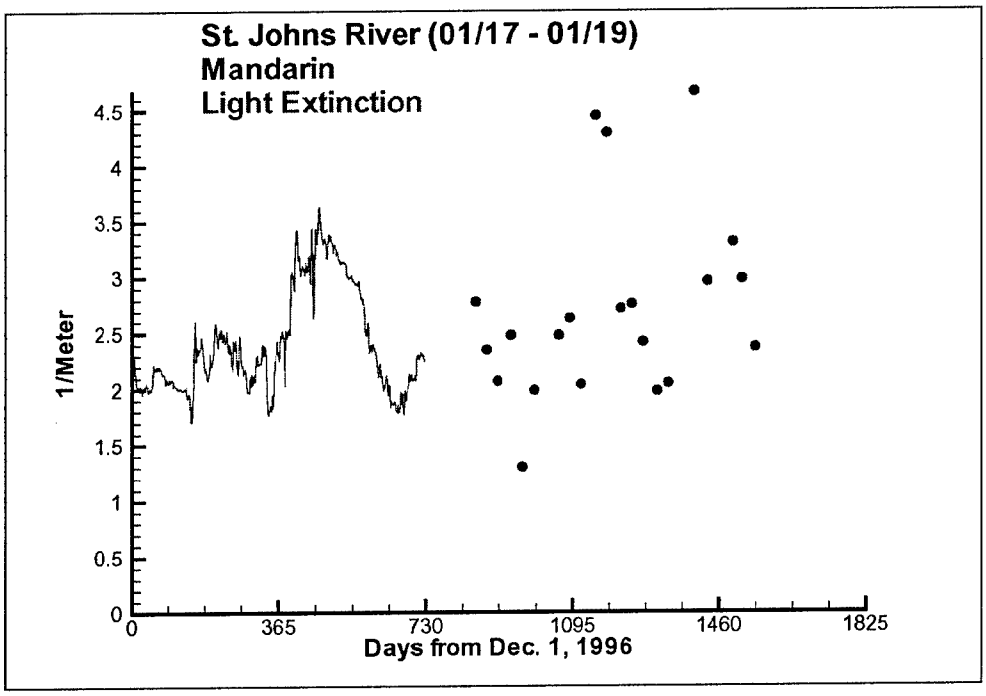

Figure 9-4. Computed and observed light attenuation at Mandarin Point

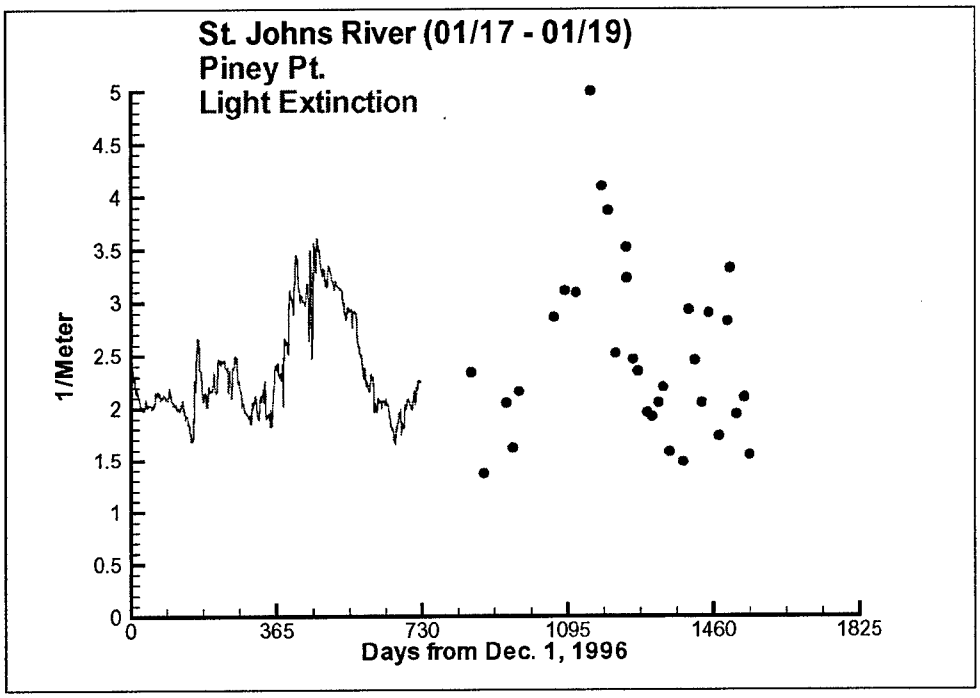

Figure 9-5. Computed and observed light attenuation at Piney Point

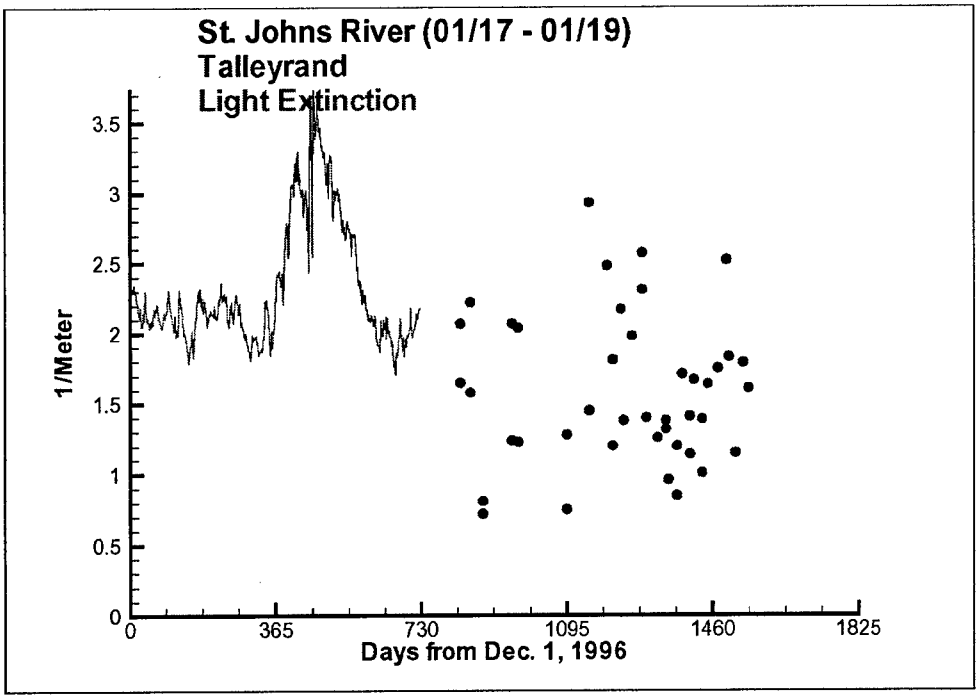

Figure 9-6. Computed and observed light attenuation at Talleyrand

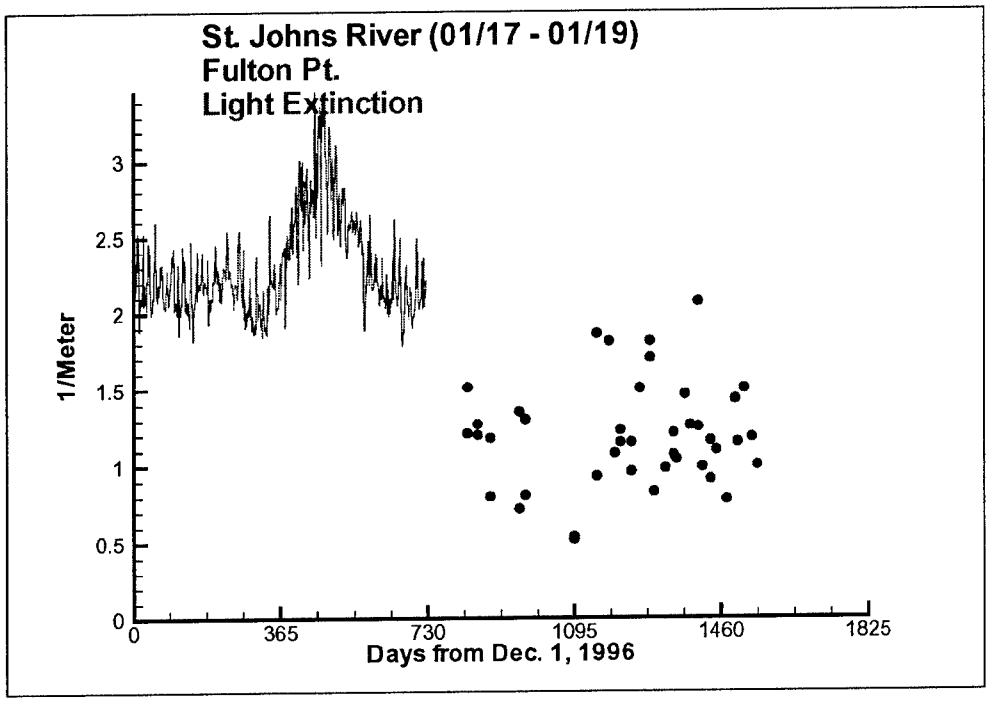

Figure 9-7. Computed and observed light attenuation at Fulton Point

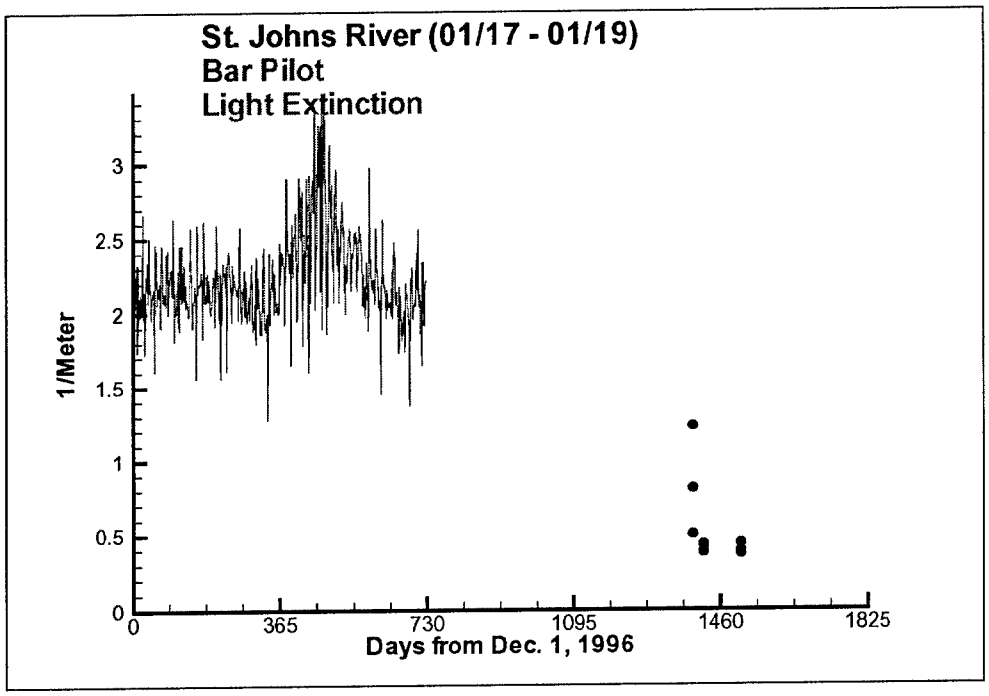

Figure 9-8. Computed and observed light attenuation at Bar Pilot

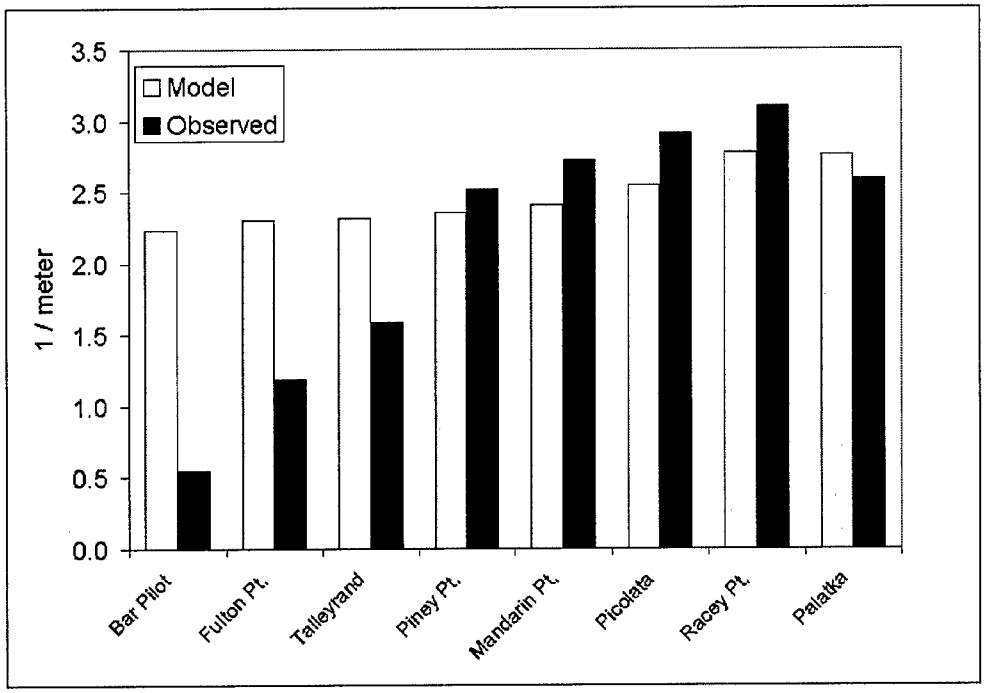

Figure 9-9. Mean computed and observed light attenuation at eight stations

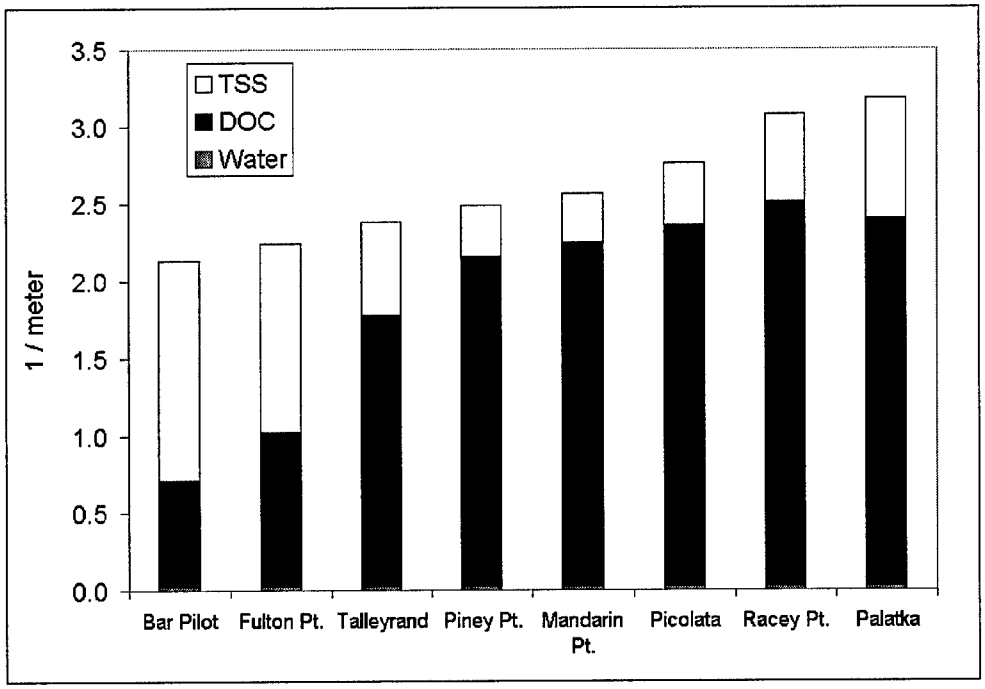

Figure 9-10. Components of modeled light attenuation

in-situ, expressed in the model primarily as labile DOC, is a small fraction of the total. The remaining carbon, expressed in the model primarily as refractory DOC, enters the river oceanic and upland sources.

In the tidal freshwater, the refractory DOC originates largely from upland sources. The oceanic contribution must be zero since salt is absent. As salinity increases downstream, the contribution of oceanic DOC increases. For a moment, assume that refractory DOC is conservative. Near the mouth, where salinity is ≈25 ppt, the contribution from the ocean end member is ≈70 percent of the total refractory DOC pool (obtained by ratio based on oceanic salinity of 35 ppt). Use of a single, constant, parameter value to represent DOC attenuation throughout the system assumes that attenuation by the various pools that total DOC comprises is identical. Yet fresh water is recognized as more highly colored than sea water (Kirk 1994). If attenuation is to be related to DOC, we should lower the value of parameter a_4 near the river mouth should be lowered to recognize that a large portion of the DOC in that vicinity is oceanic and less colored than DOC that originates in the watershed. An empirical relationship could readily be developed based on an observed relationship between attenuation and salinity (Figure 9-11).

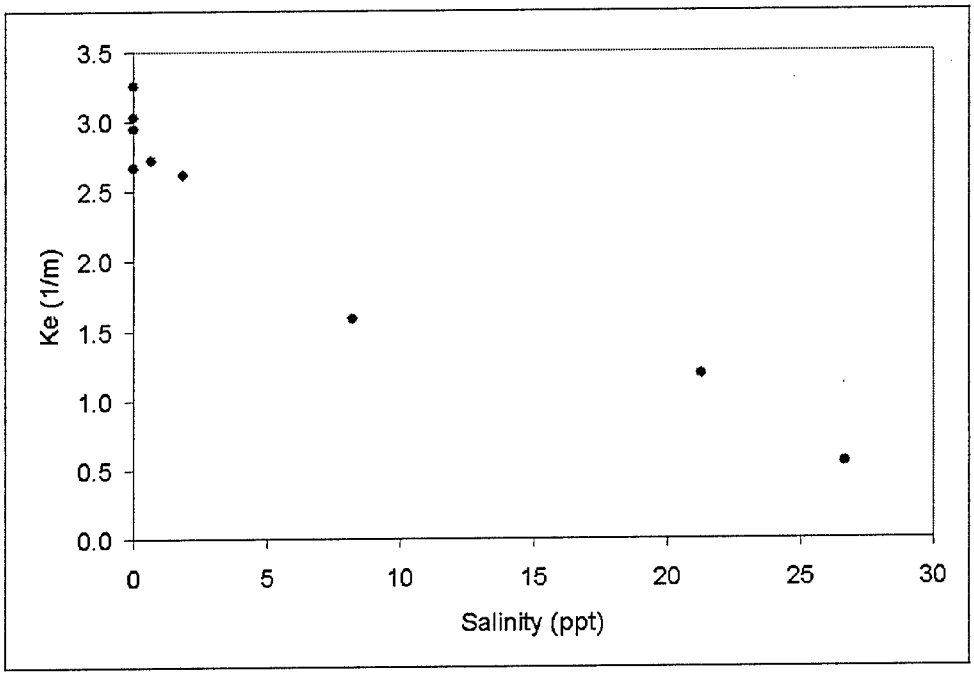

Figure 9-11. Observed mean light attenuation versus salinity at nine stations in the modeled domain

Discussion

Original plans for this phase of the modeling activity called for incorporation of a state-of-the-art optical model (Gallegos 2002) into our own model. As the project progressed, implementation of nitrogen fixation gained priority. Implementation of the advanced optical model is now planned for the next phase

of our modeling activity. We heartily support employment of the advanced technology. Our enthusiasm is based as much on the careful measures of optical properties that accompany the advanced model as on the model formulation. Additive models such as we employed here provide useful approximations for systems in which absorption is the dominant contributor to light attenuation (Kirk 1994). A major problem with additive models is in parameter evaluation through regression, visual fitting, or other methods. Employment of carefully-measured parameters will eliminate a source of uncertainty and contribute to overall improvement in model calibration and predictive power.

References

Cerco, C., and Noel, M. (2004). "Managing for water clarity in Chesapeake Bay," *Journal of Environmental Engineering*, in press.

Gallegos, C. (2002). "Development of an optical water quality model for the lower St. Johns River," Contract #99B144B, Smithsonian Environmental Research Center, Edgewater, MD.

Kirk, J. (1994). *Light and photosynthesis in aquatic ecosystems*. 2nd edition, Cambridge University Press, Cambridge, England.

Pennock, J. (1985). "Chlorophyll distributions in the Delaware Estuary: Regulation by light limitation," *Estuarine, Coastal and Shelf Science* 21, 711-725.

10 Analysis

Limiting Nutrients

The LSJR system has been described as a nitrogen-limited estuary with nitrogen being the primary limiting nutrient to algal growth (Hendrickson and Konwinski 1998). This description is based on observed nutrient ratios and concentrations. Nutrient limits computed by the model are based on the Monod formulation for nutrient uptake (nitrogen, silica) or the Droop formulation (phosphorus). The model limitations range from zero (growth completely inhibited by a specific nutrient) to unity (no growth inhibition by the specified nutrient). Computed limitations largely agree with observations. That is, the model computes strong nitrogen limitation during the growing season (Figure 10-1) at most locations. At times, growth is limited to less than 20 percent of its potential value by nitrogen limitation. Computed nutrient limits

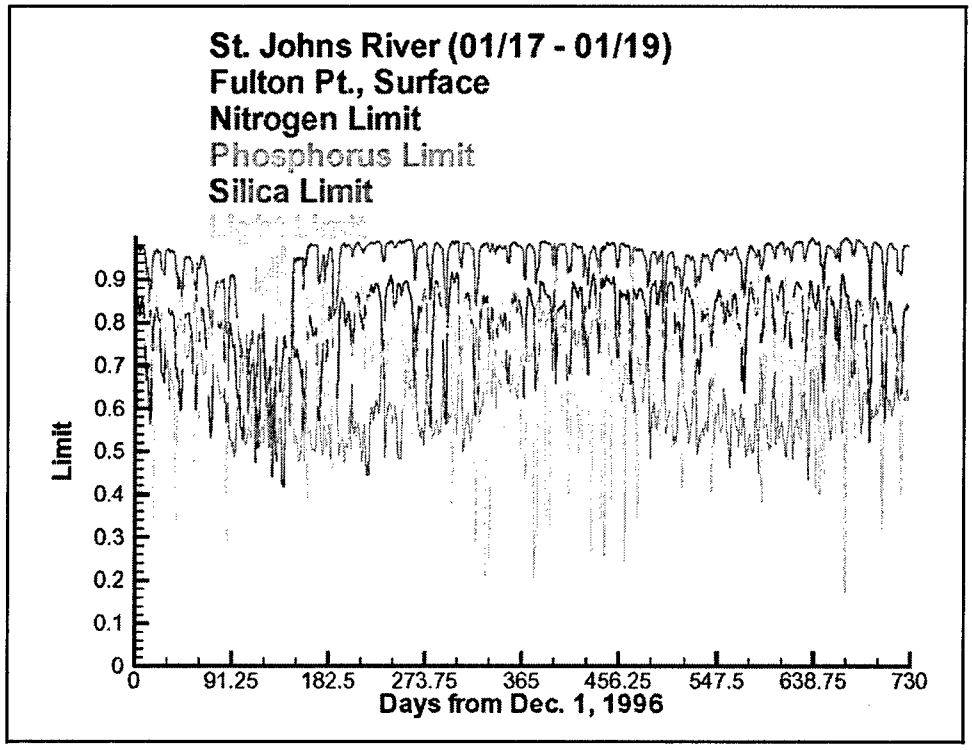

Figure 10-1. Limiting factors of algal growth at seven stations on the St. Johns River (Sheet 1 of 4)

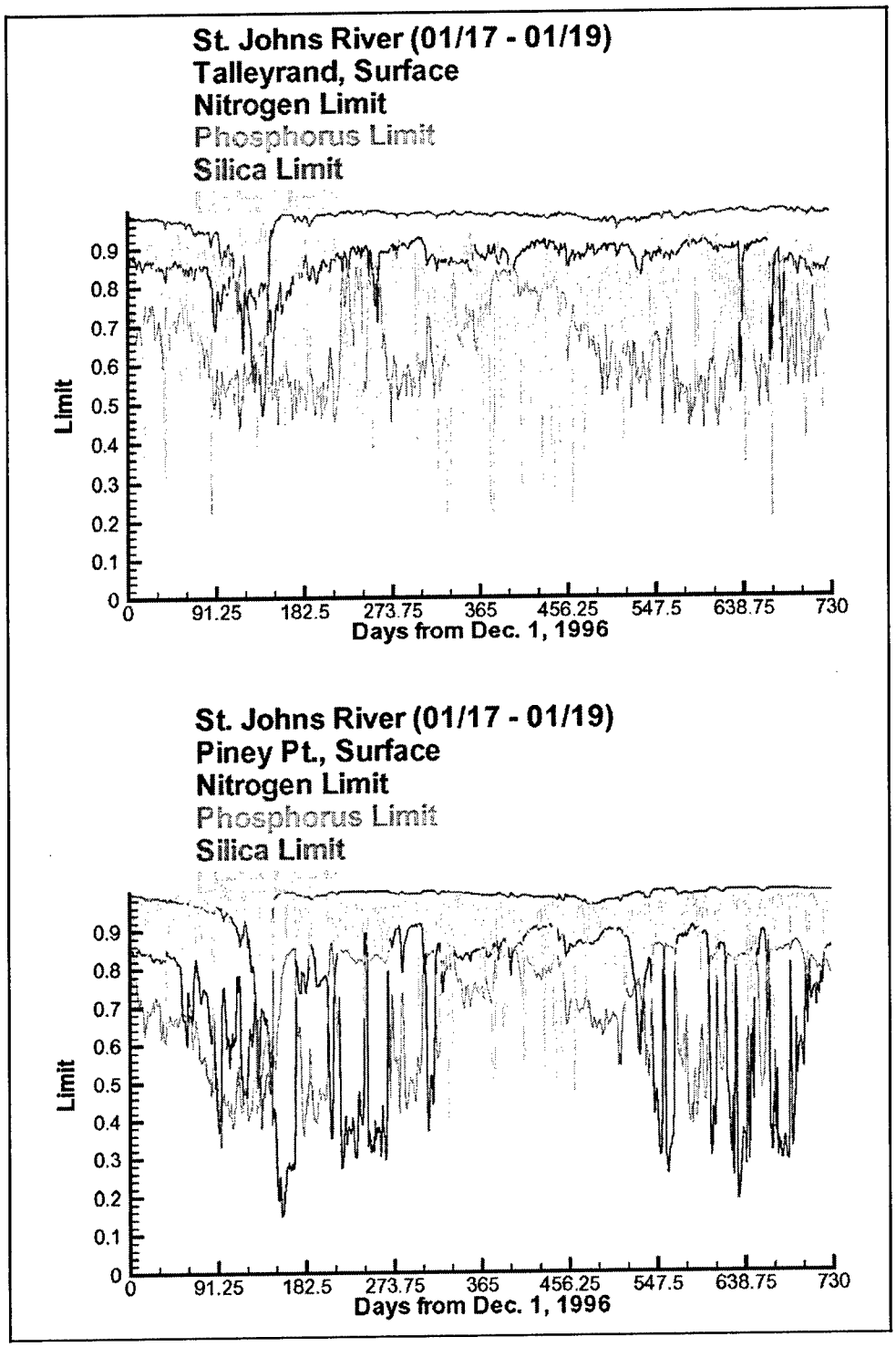

Figure 10-1. (Sheet 2 of 4)

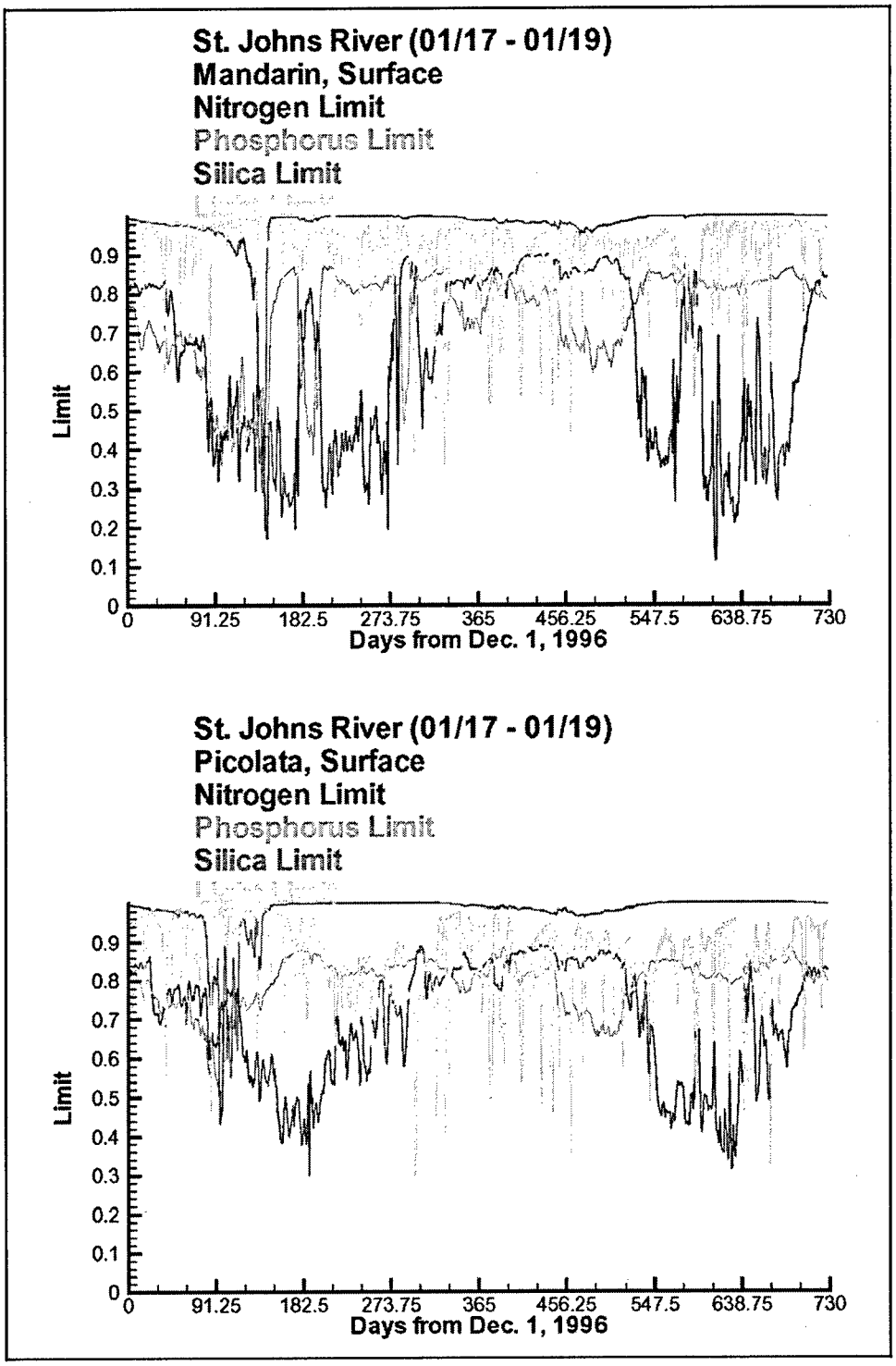

Figure 10-1. (Sheet 3 of 4)

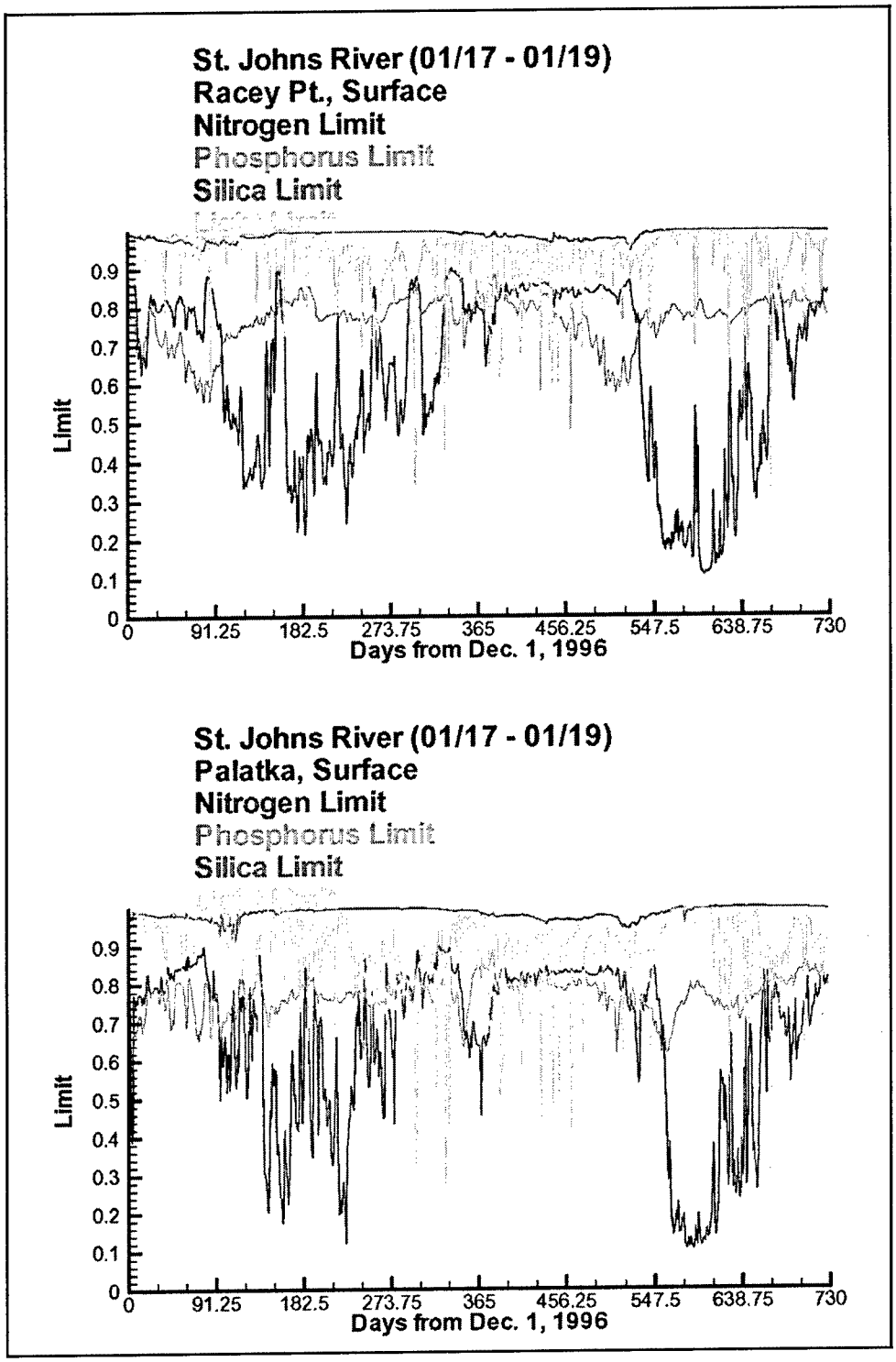

Figure 10-1. (Sheet 4 of 4)

to growth are relaxed near the mouth of the river and indicate primarily phosphorus rather than nitrogen limitation. Examination of computed DIN at Fulton Point indicates computations tend to exceed observations. Consequently the model may underestimate nitrogen limitation at this location relative to phosphorus limitation. In view of the limited spatial extent of the computed phosphorus limitation, and the relative abundance of both nutrients near the river mouth, it is believed that the model is suited for use in examining nutrient control alternatives throughout the river.

Variables With No Observed Data

Several variables were analyzed that did not have observed data associated with them. Table 10-1 lists these variables. In keeping with previous discussions of computed results (see Chapter 6), only results at the Fulton Point, Piney Point, and Picolata stations presented in Figures 10-2 through 10-4 will be shown here. Results at other stations are provided on the CD-ROM.

Table 10-1
Variables With No Observed Data

Algal POC	Algal PON	Algal POP	Labile POC
Refractory POC	Labile PON	Refractory PON	Labile POP
Refractory POP	Labile DOC	Refractory DOC	Labile DON
Refractory DON	Labile DOP	Refractory DOP	

Algal particulate organic matter is proportioned into three forms – algal particulate organic carbon (POC), algal particulate organic nitrogen (PON), and algal particulate organic phosphorus (POP). At each station presented (Figures 10-2 through 10-4), algal POC makes up about 90 percent of the total algal biomass, while the other elements form roughly 6 percent (algal PON) and 4 percent (algal POP) of the total biomass.

If labile and refractory portions of particulate organic matter are considered, concentrations at Fulton Point show different trends for the PON portions but similar trends for POC than what is seen at Piney Point and Picolata. At Fulton Point (Figure 10-2) for the surface and bottom layers, the refractory portion of POC was twice that of the labile portion. This trend is also seen at Piney Point and Picolata (Figures 10-3 and 10-4). The refractory portion of PON at Fulton Point is more than twice the labile portion for the surface layer and more than one order of magnitude higher in the bottom layer. Piney Point and Picolata differ from this trend with 70 percent of the PON in the labile form while 30 percent is in the refractory form.

Internal algal phosphorus can be considered a form of POP. Nearly all of the POP values at Fulton Point are equally split between refractory POP and algal POP. Labile POP at this station makes up a very minor portion (<5 percent) of this variable. At Piney Point and Picolata, POP values are almost all from algal POP. Labile and refractory forms of POP are approximately 1 percent of the total POP value at these stations.

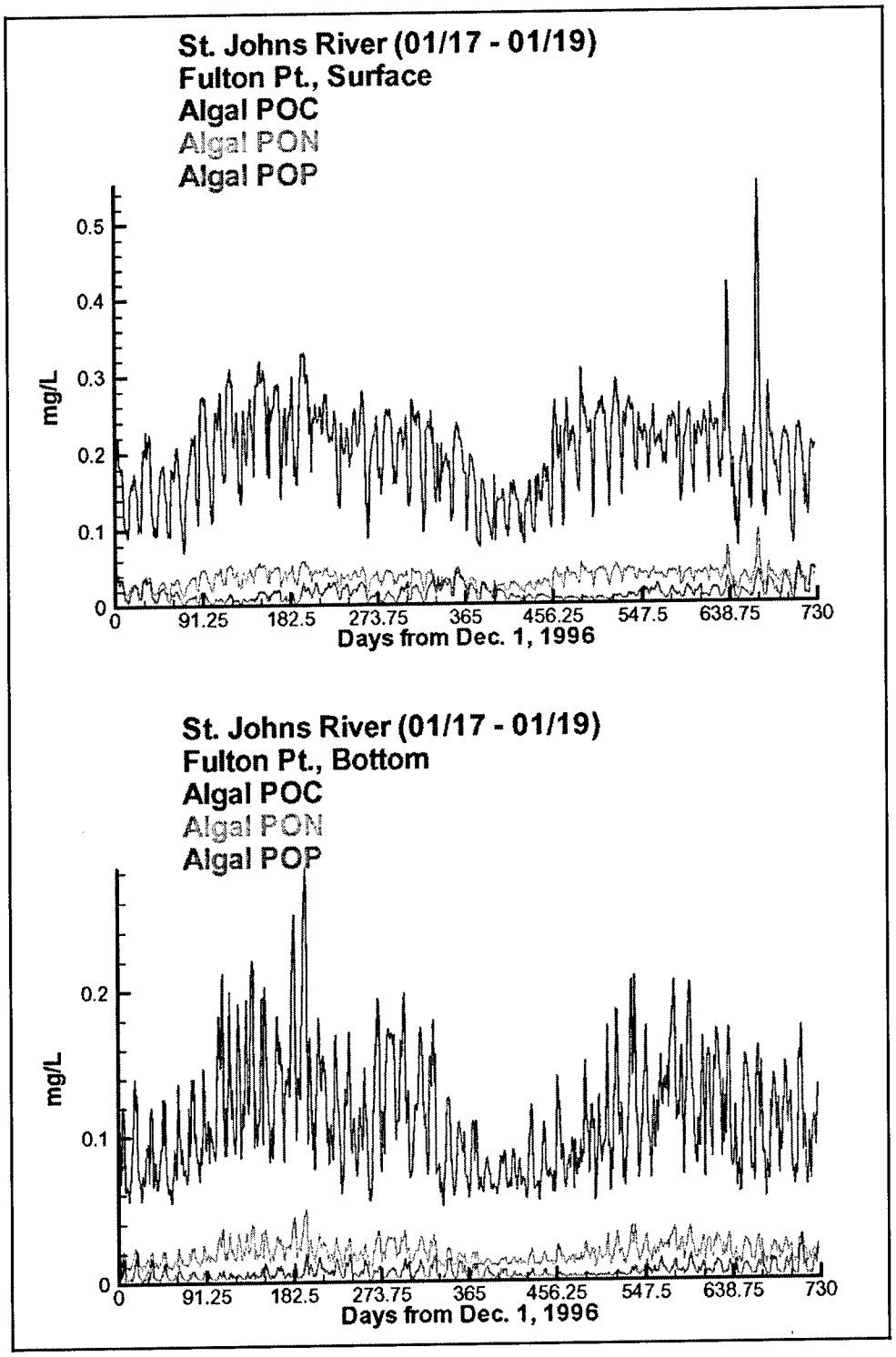

Figure 10-2. Fulton Point computed water quality constituents that have no observed data available (Sheet 1 of 7)

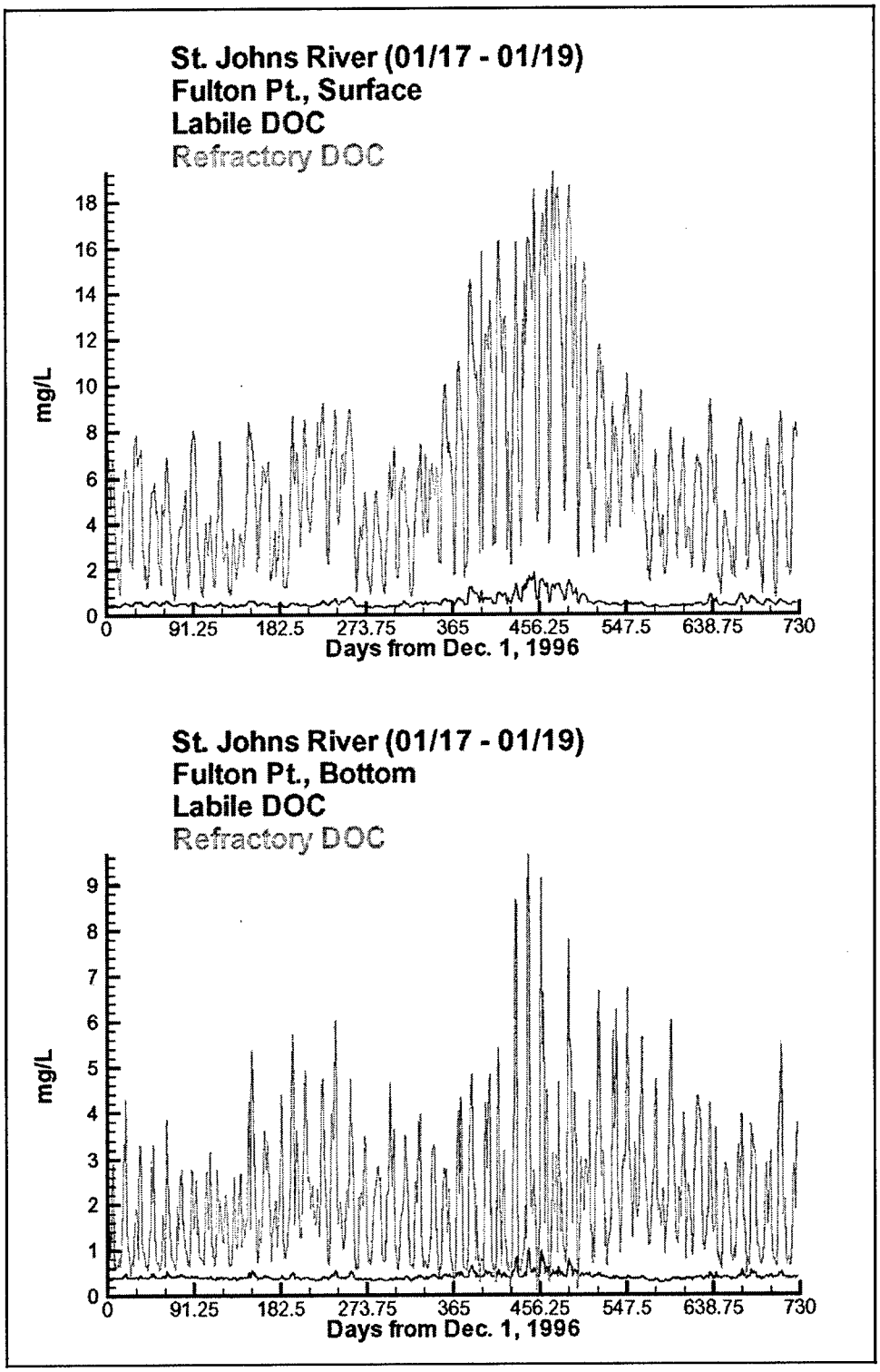

Figure 10-2. (Sheet 2 of 7)

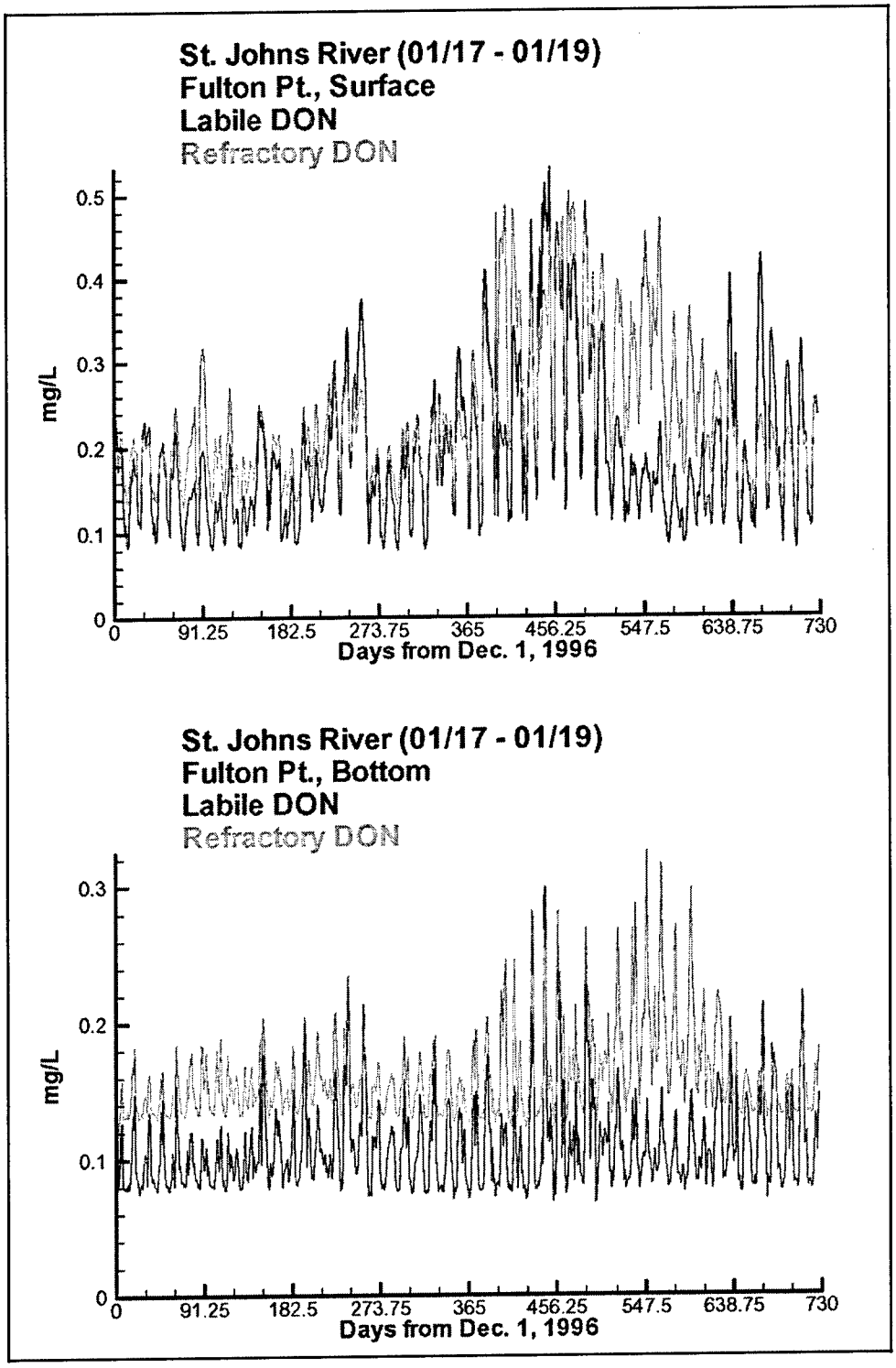

Figure 10-2. (Sheet 3 of 7)

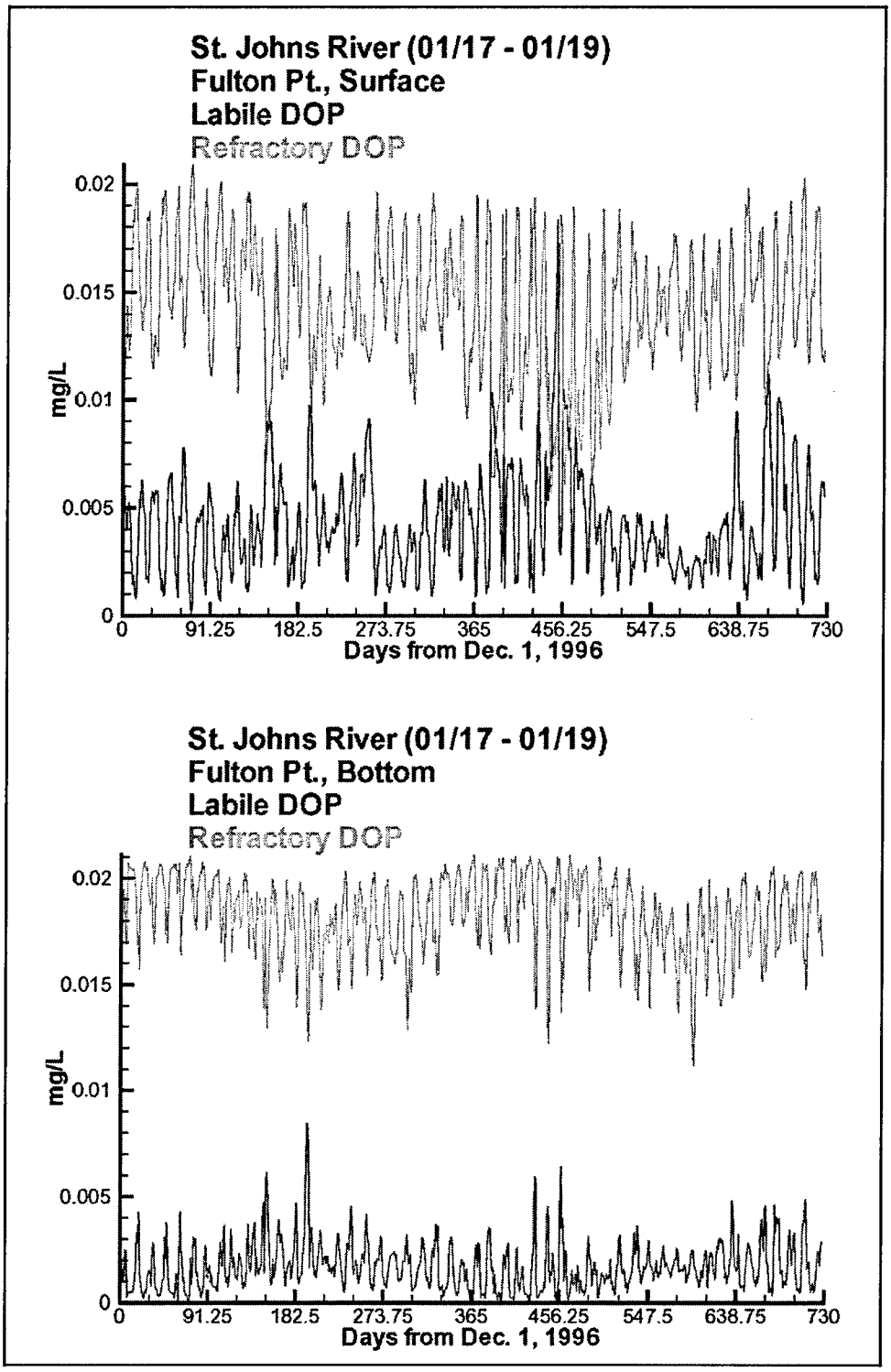

Figure 10-2. (Sheet 4 of 7)

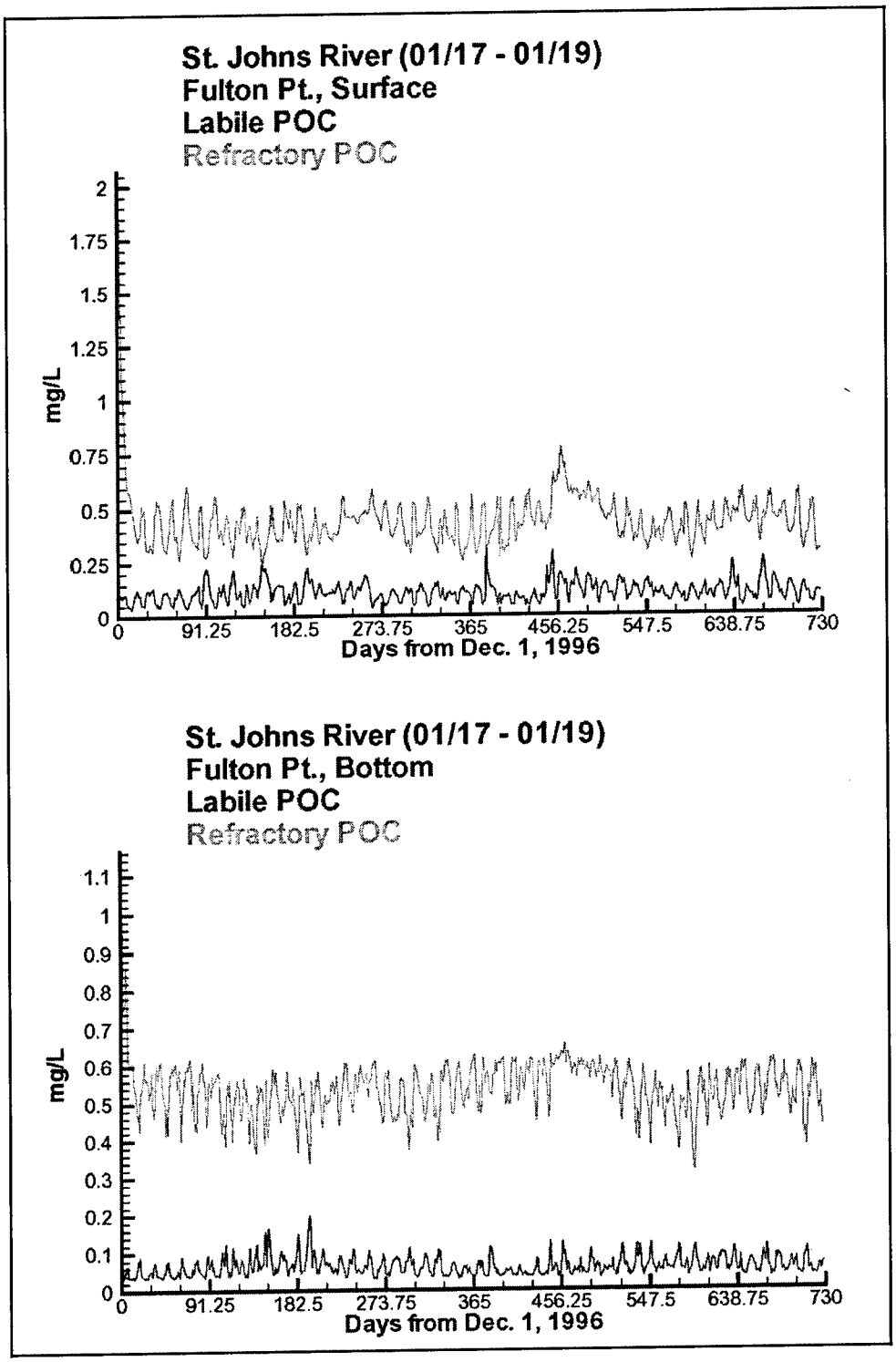

Figure 10-2. (Sheet 5 of 7)

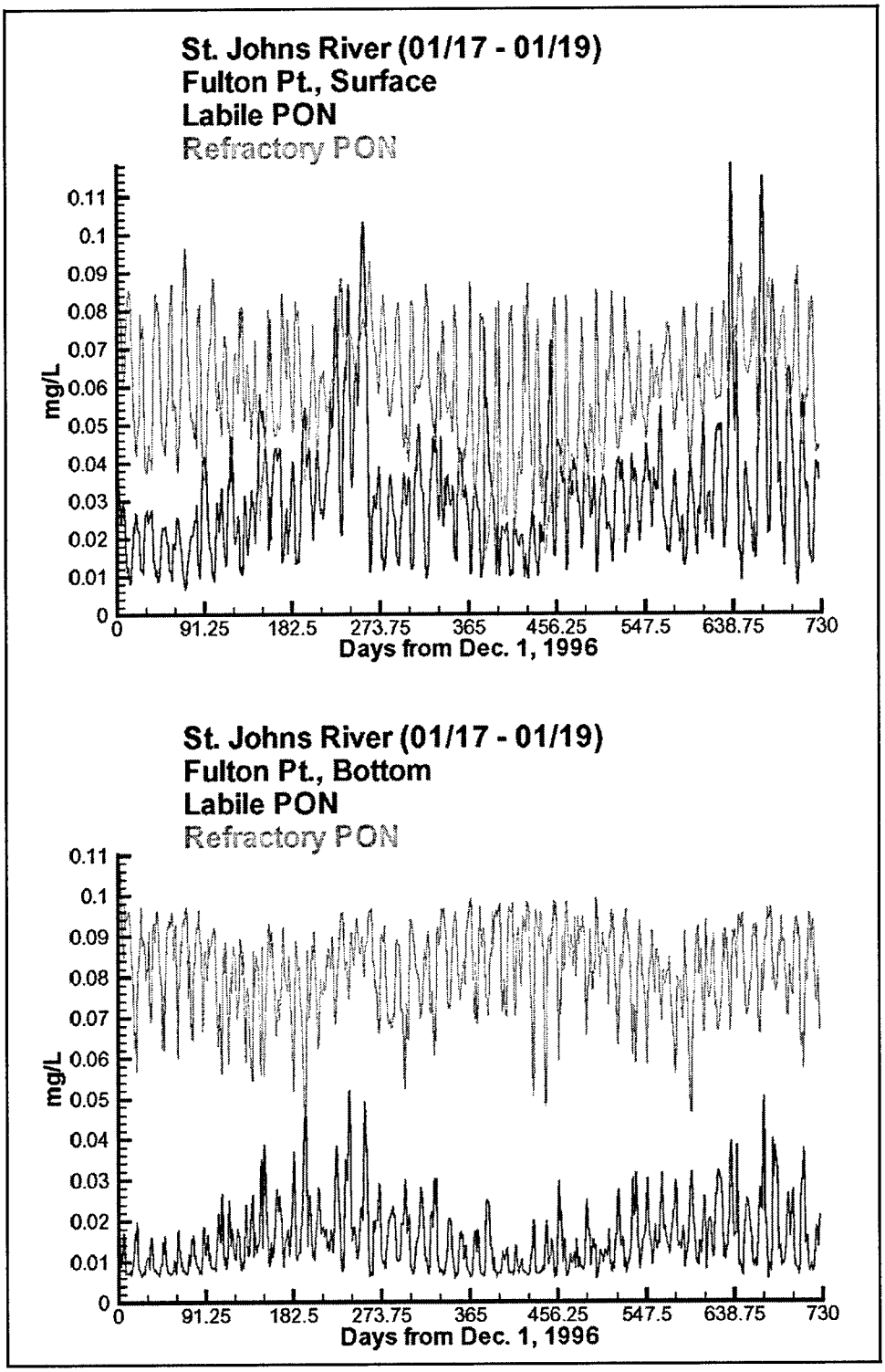

Figure 10-2. (Sheet 6 of 7)

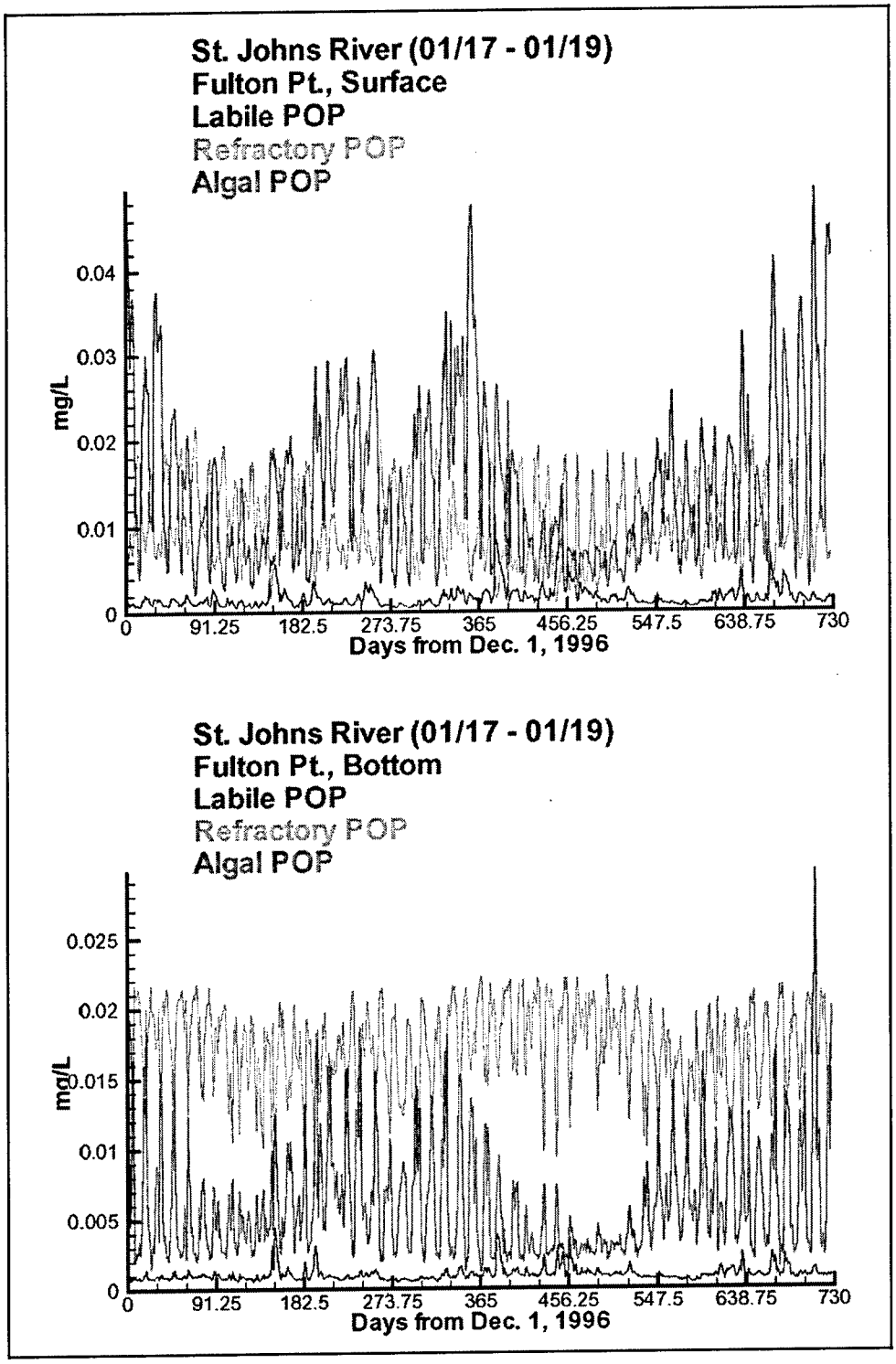

Figure 10-2. (Sheet 7 of 7)

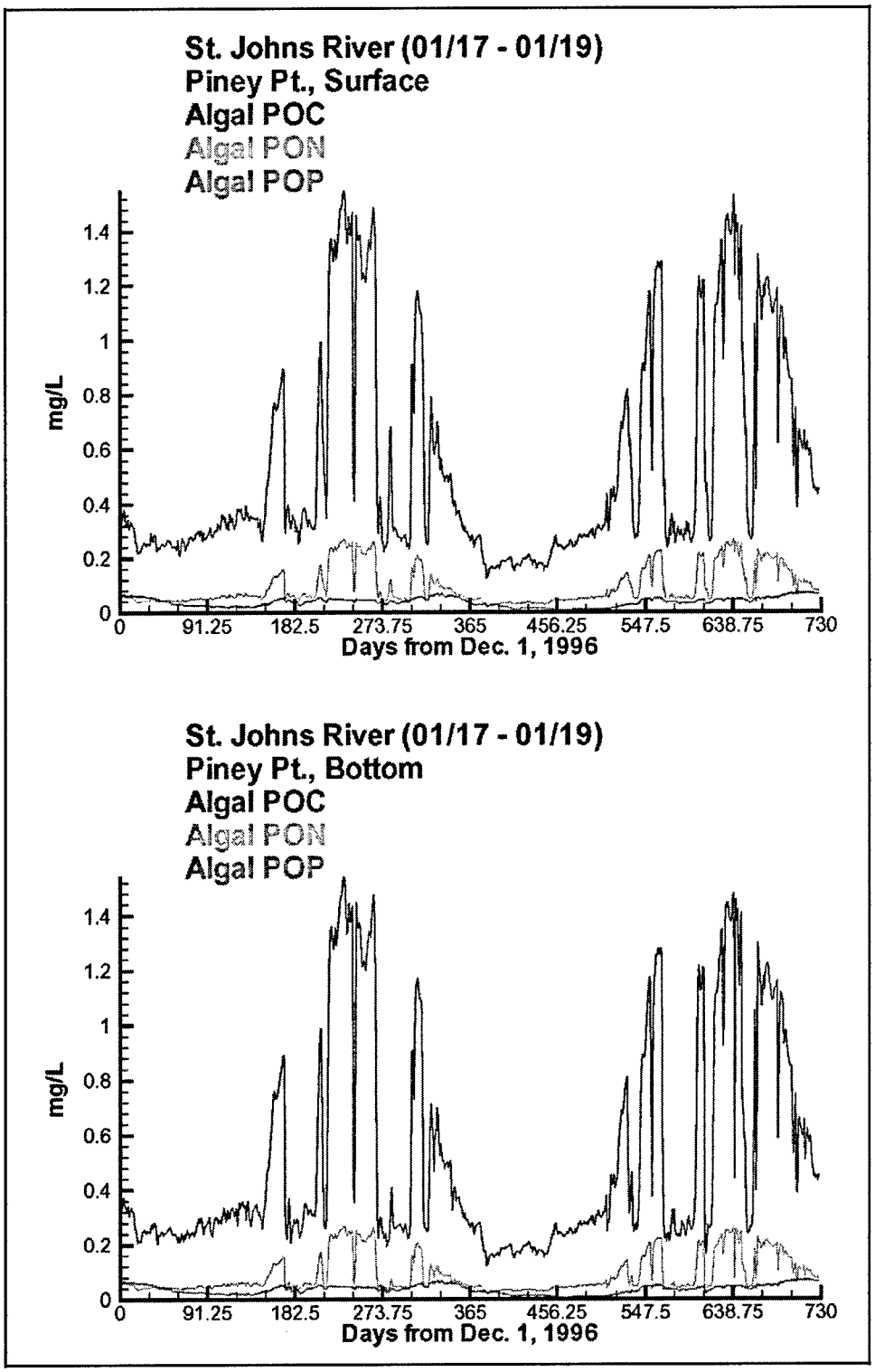

Figure 10-3. Piney Point computed water quality constituents that have no observed data available (Sheet 1 of 7)

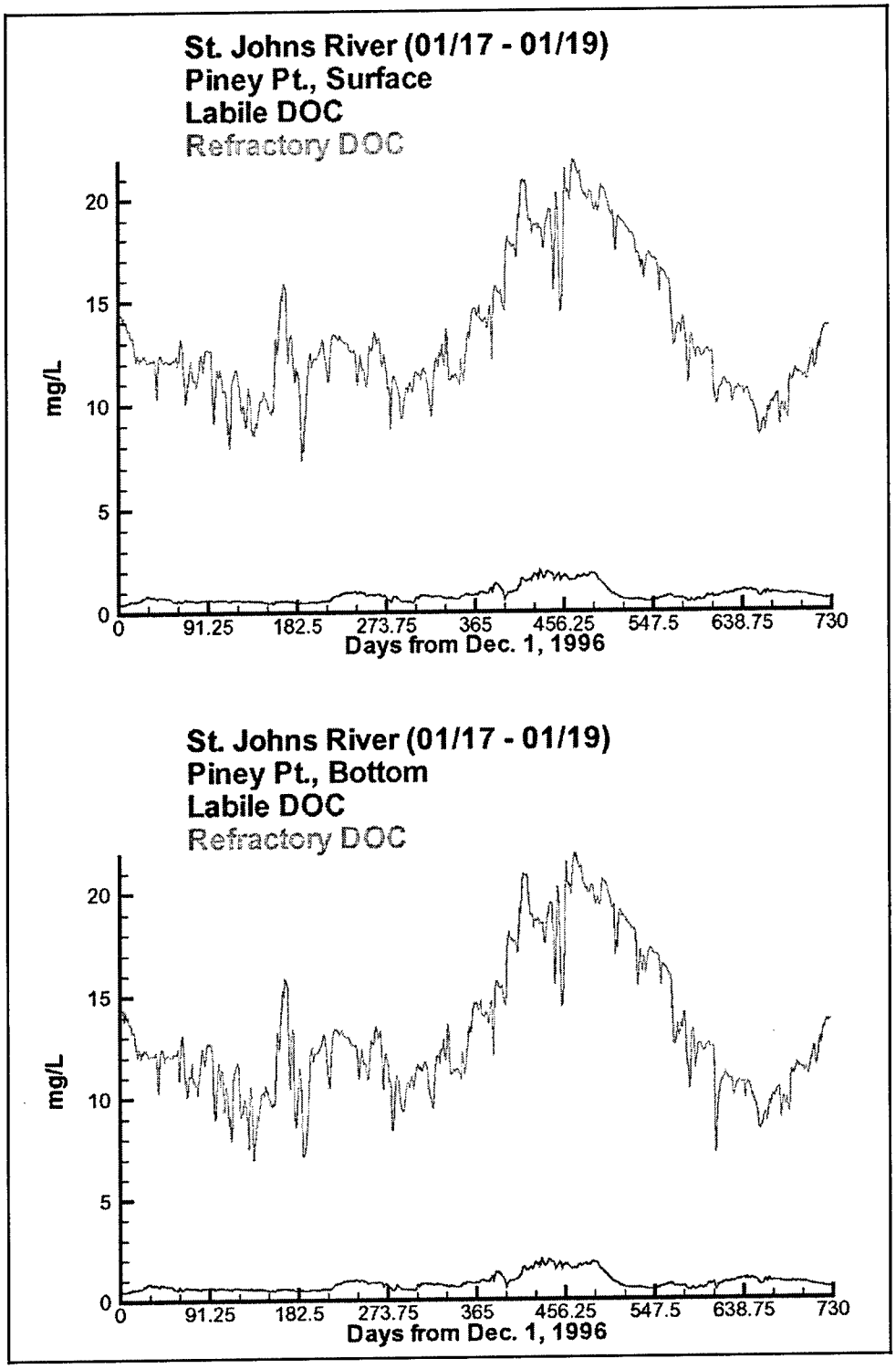

Figure 10-3. (Sheet 2 of 7)

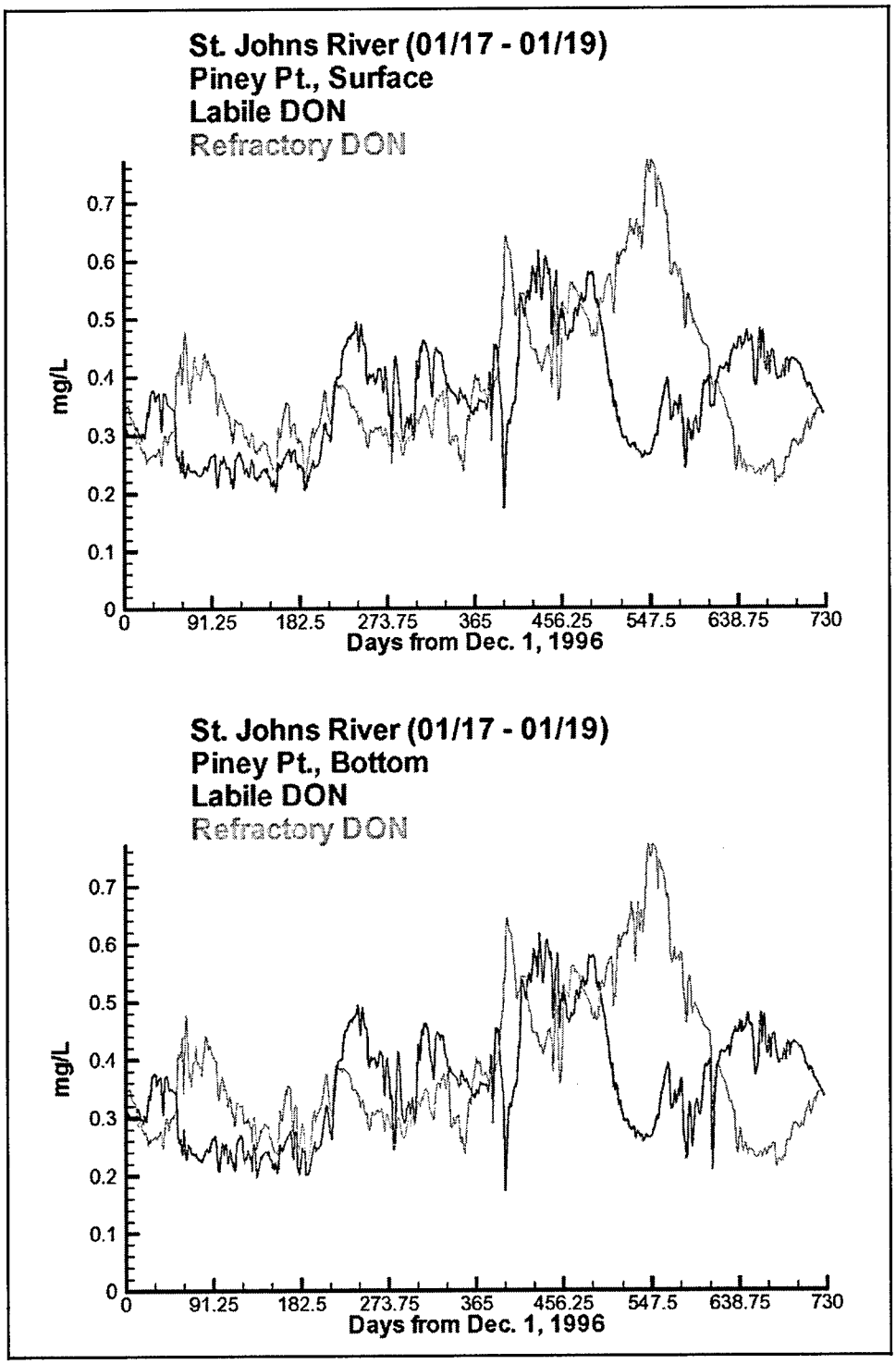

Figure 10-3. (Sheet 3 of 7)

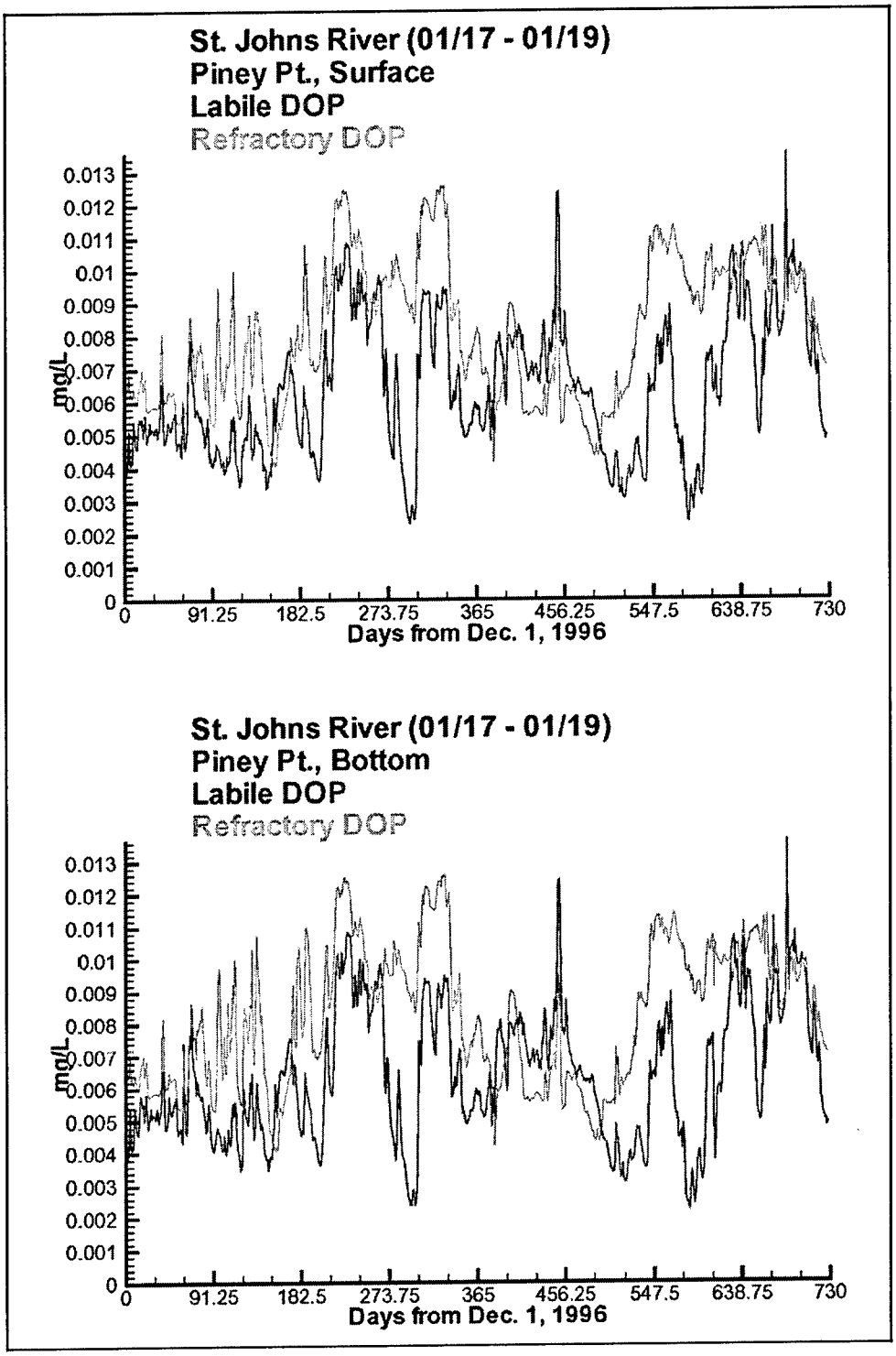

Figure 10-3. (Sheet 4 of 7)

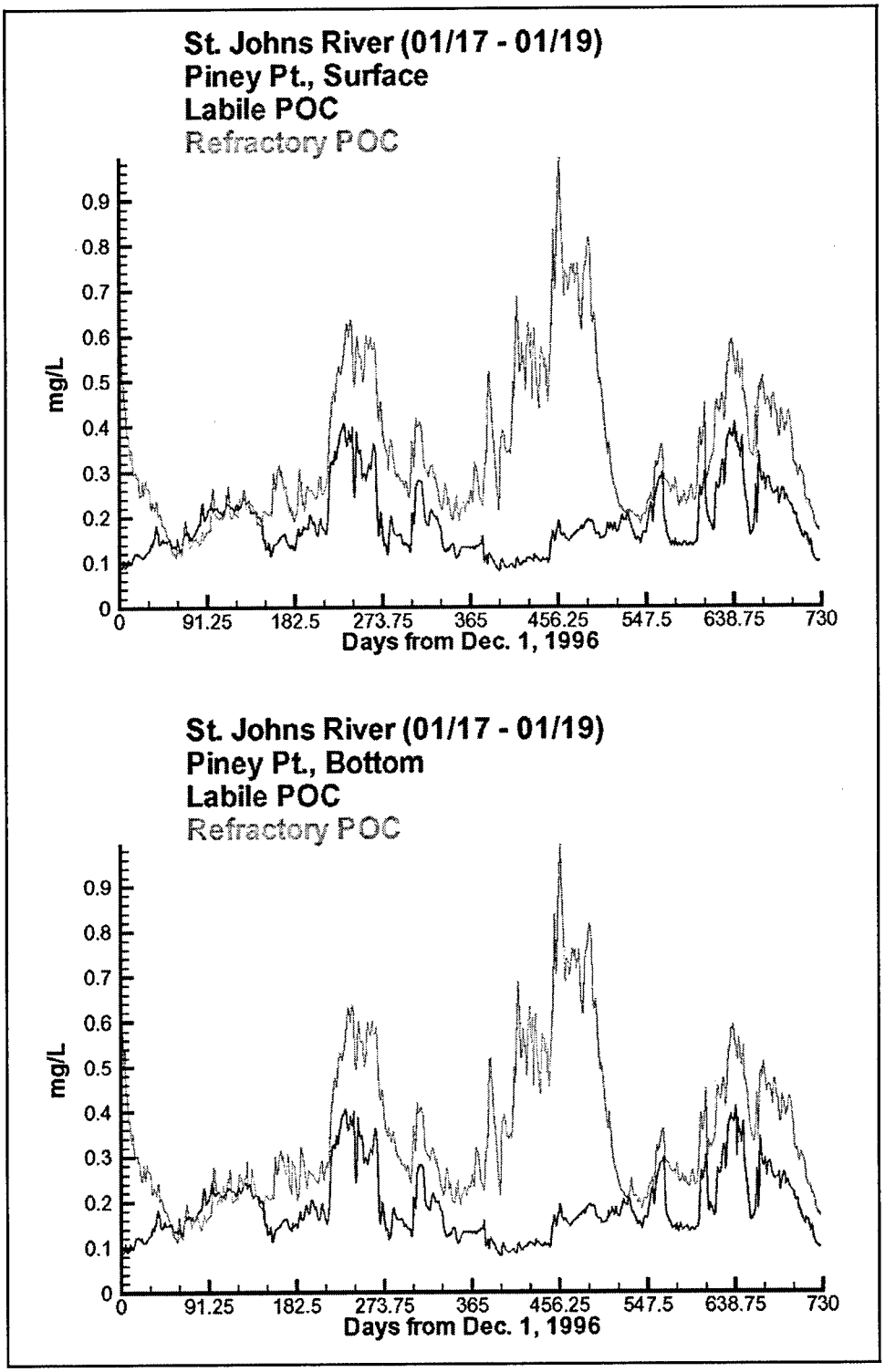

Figure 10-3. (Sheet 5 of 7)

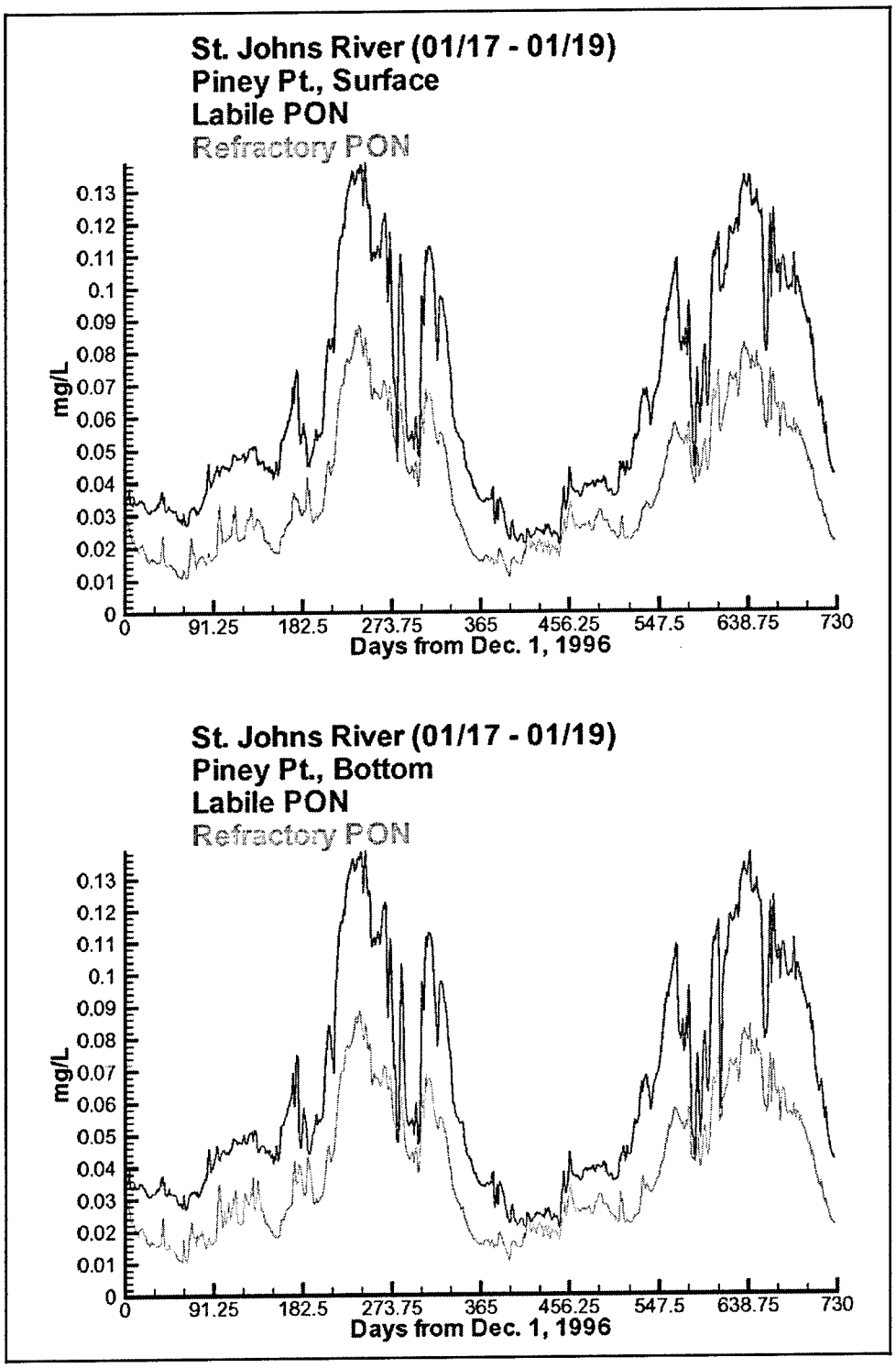

Figure 10-3. (Sheet 6 of 7)

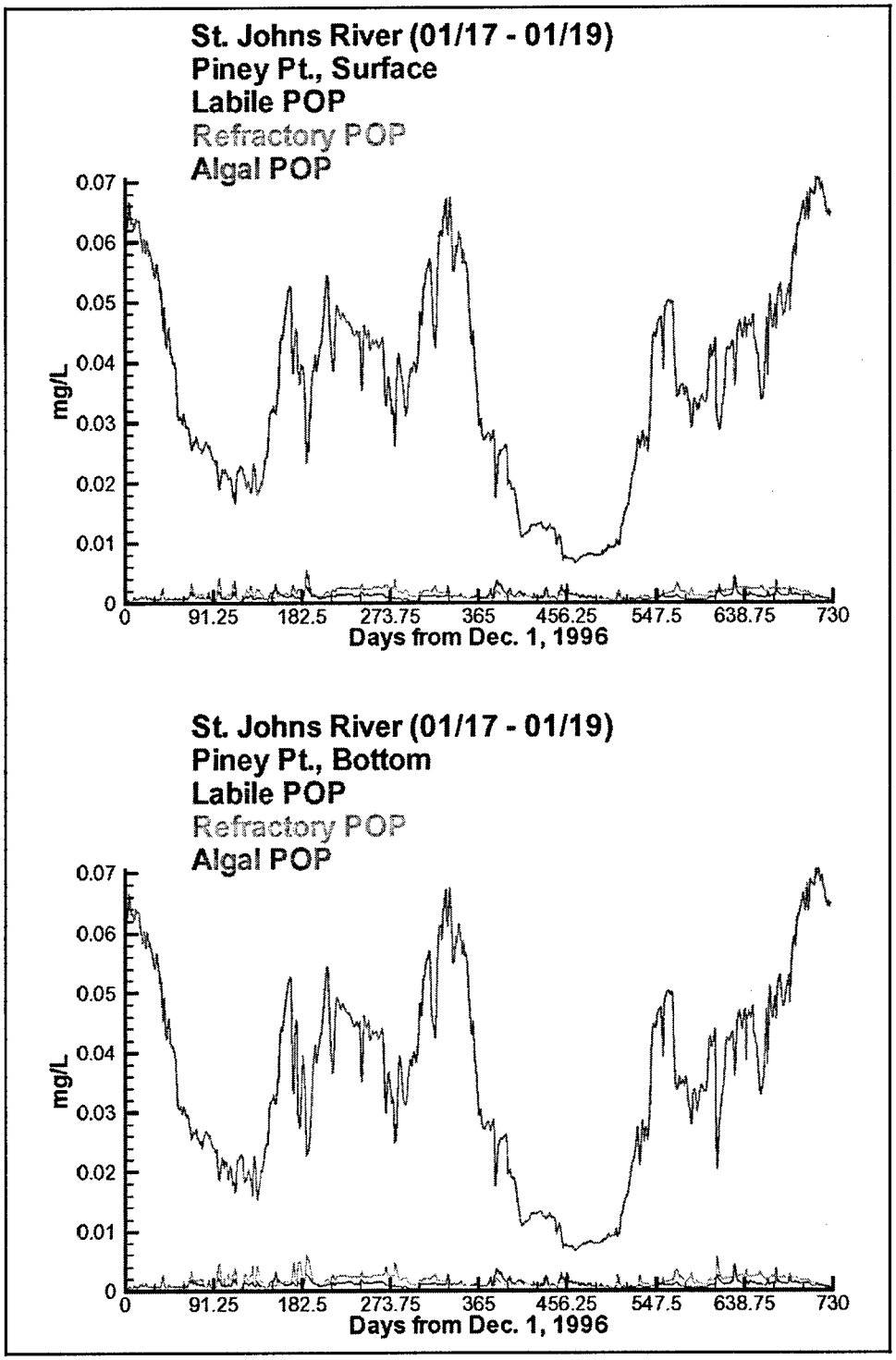

Figure 10-3. (Sheet 7 of 7)

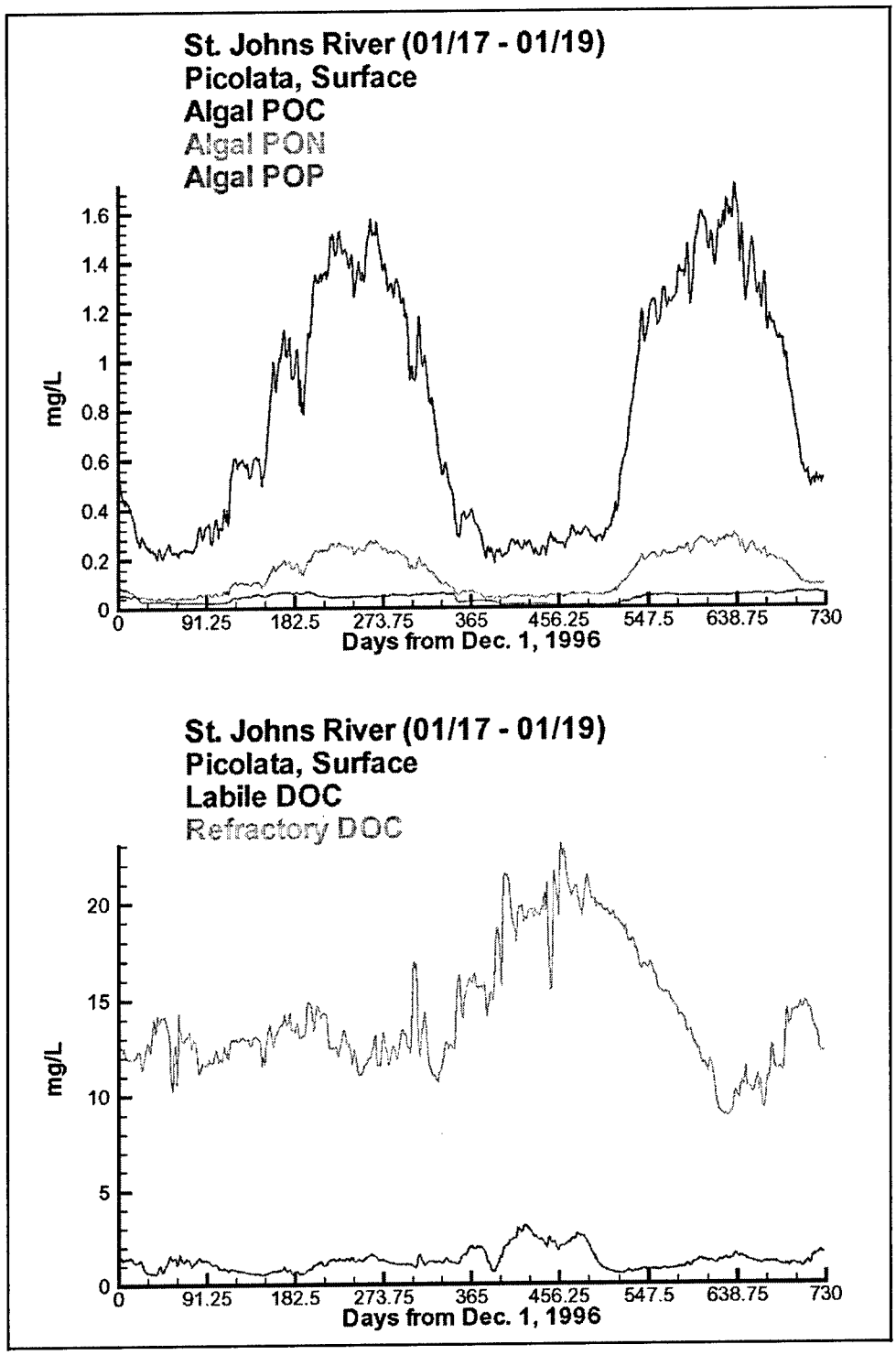

Figure 10-4. Picolata computed water quality constituents that have no observed data available (Sheet 1 of 4)

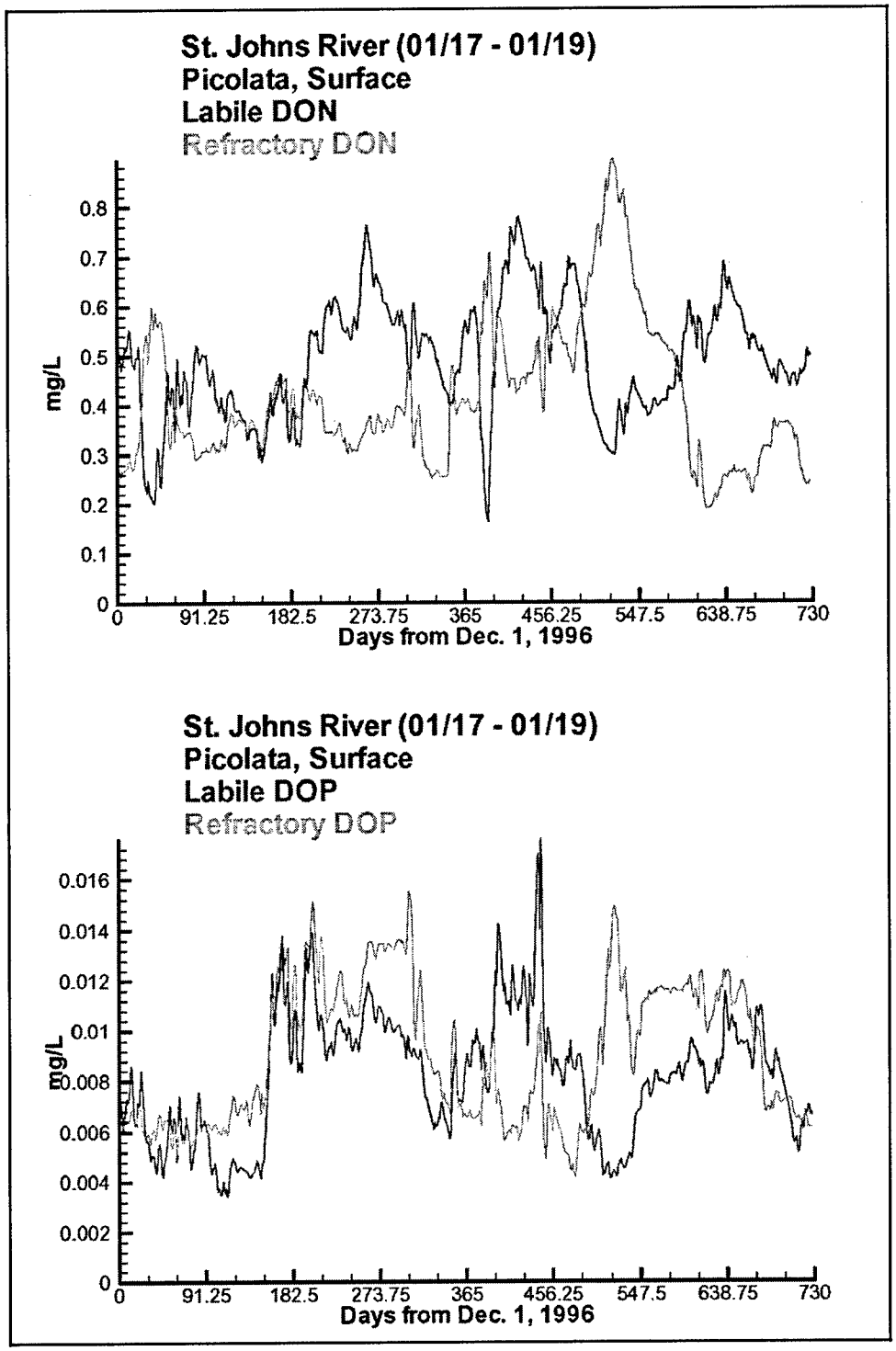

Figure 10-4. (Sheet 2 of 4)

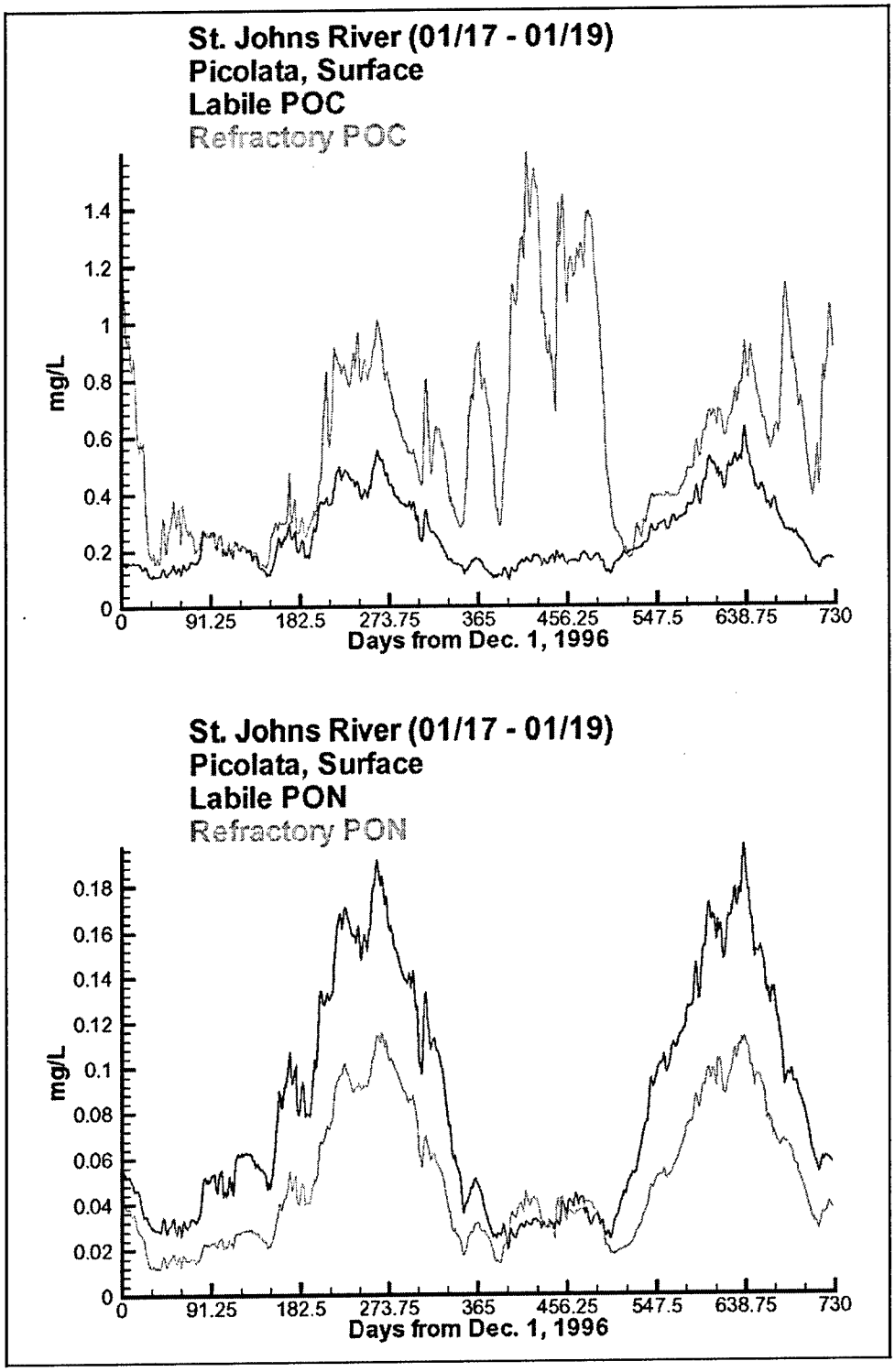

Figure 10-4. (Sheet 3 of 4)

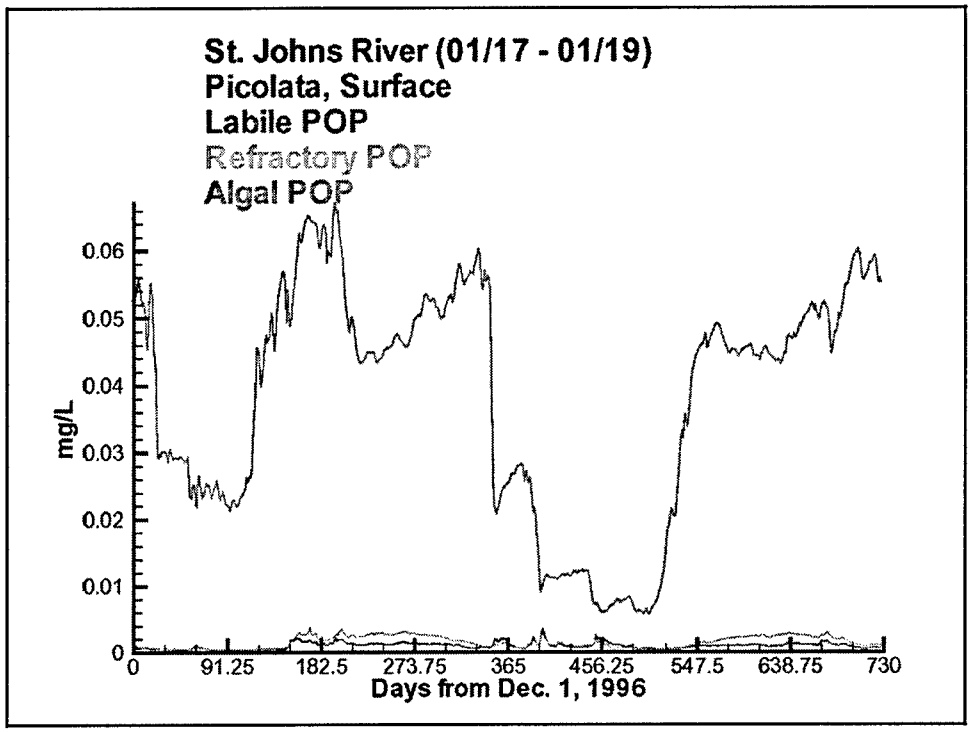

Figure 10-4. (Sheet 4 of 4)

The dissolved forms of organic matter show similar trends at all stations for surface and bottom layers. From comparing DOC at all stations, Figures 10-2 through 10-4 showed higher refractory DOC values than labile (90 percent as compared to 10 percent). Values for DON were about equally split between refractory and labile for all stations except that Fulton Point showed slightly higher bottom refractory DON. Finally, DOP for surface and bottom levels at Piney Point and Picolata were split approximately 55 percent refractory and 45 percent labile, while refractory DOP at Fulton Point was an order of magnitude higher than labile DOP.

Overall, the dominant form of organic matter at the stations discussed previously was refractory DOC. At all stations, the maximum value of refractory DOC computed by CE-QUAL-ICM was approximately 18 mg/L. This computed value was comparable to observed values of DOC reported.

Transport Across Boundaries and Nutrient Budgets

Nutrient budgets were analyzed by computing the mass balance (i.e., transfer of mass to the system and transformation within the system) for the six reach segments of the LSJR (Figure 4-1) for each simulation year. A yearly nutrient budget is composed of many components. Budgets or mass balance for TN and TP were expressed as:

$$Accumulation = Loadings \pm Transport \pm Reactions + \varepsilon \quad (10\text{-}1)$$

in which:

Accumulation = Net change in mass over a year

Loadings = PS, NPS, and Atmospheric loads to the segments

Transport = Mass moved into or out of segments

Reactions = Settling of nutrients, chemical transformation, and sediment releases of nutrients within the segments.

ε = Error term

The error term arises due to round-off error in internal calculations, small discrepancies in loadings summarized external to the model, and other factors.

A major component of the nutrient budget was the transport across segment boundary faces. Monthly averaged output flux information for cells making up the segment boundary faces was used in from CE-QUAL-ICM computing the yearly transport values for TN and TP in and out of segments.

Figures 10-5 and 10-6 present results by year for each segment of the LSJR. Note that transport is plotted separately on a smaller plot within the plotting area showing mass components of the mass balance. Positive terms represent sources to the water column of the region. Expressions in the legend representing components of the mass balance are:

a. TN and TP Epsilon represent error terms for the mass balance equation.

b. NPS represents mass from NPS loads.

c. PS represents mass from PS loads.

d. Particle PNFWS and PPFWS represent the mass of nitrogen and phosphorus, respectively, settling to the sediments.

e. Dissolved BENNH4, BENNO3, and BENPO4 represent the mass of ammonium, nitrate, and phosphate, respectively, released from the sediments.

f. ATM_N and ATM_P represent the mass of atmospheric nitrogen and phosphorus depositing to the segment.

g. NFIX represents the mass of nitrogen from nitrogen fixation added to the segment.

h. Delta represents net accumulation in the region, over the year.

Observations from comparison of TN and TP budgets for both years modeled are:

a. PS, NPS, and atmospheric loads did not show large variability from year to year.

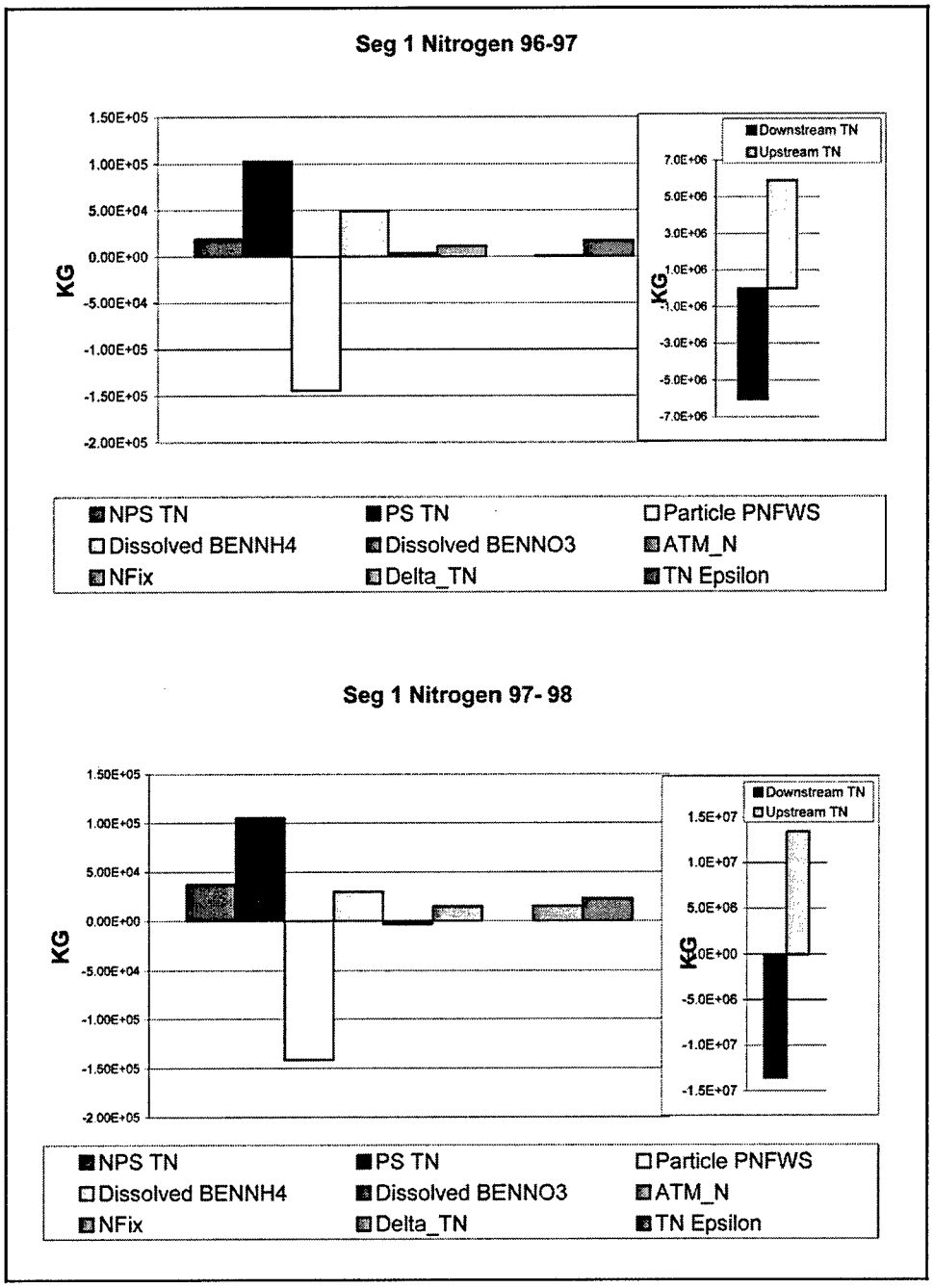

Figure 10-5. TN budget by segments for both simulation years (Sheet 1 of 6)

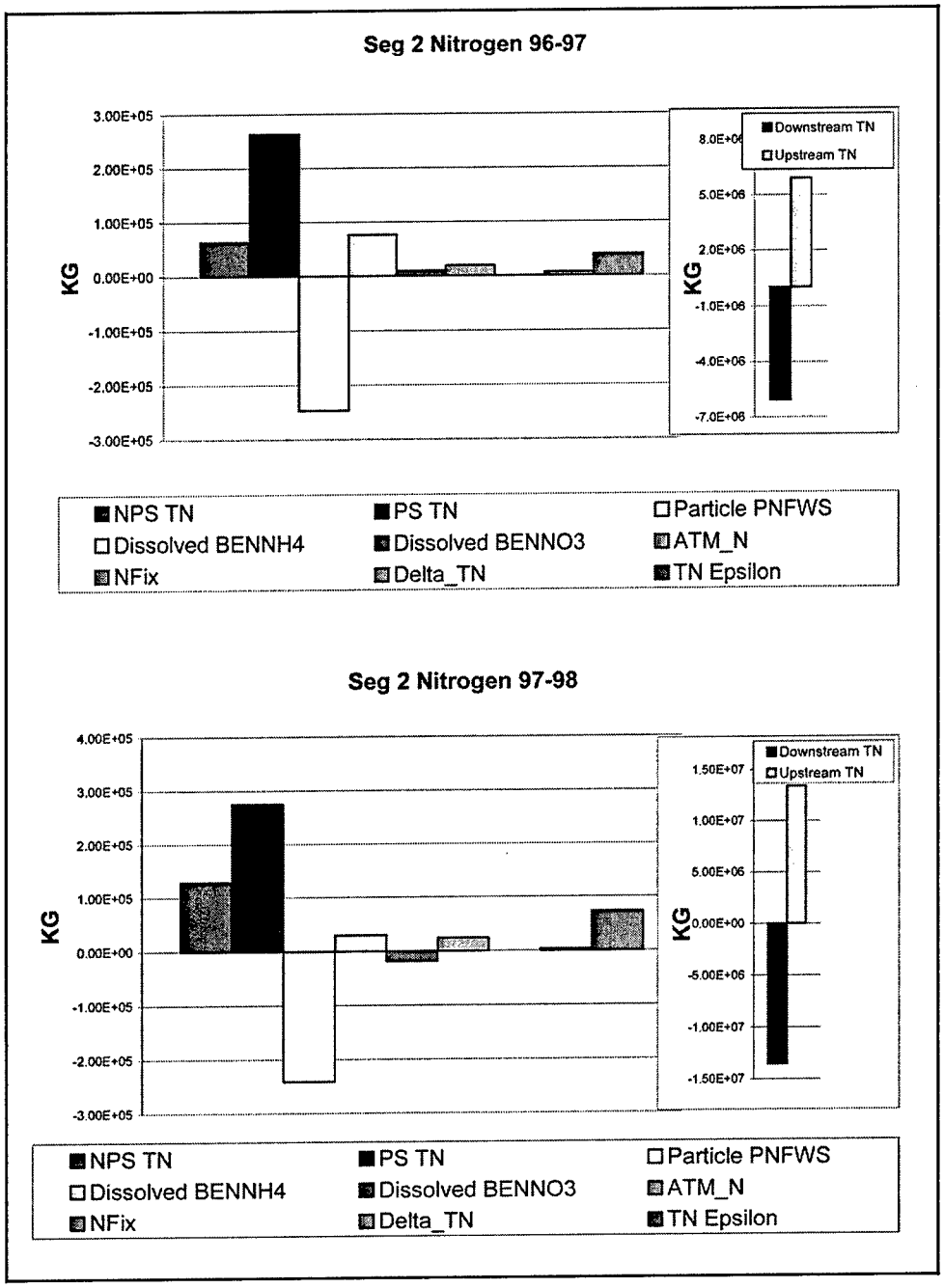

Figure 10-5. (Sheet 2 of 6)

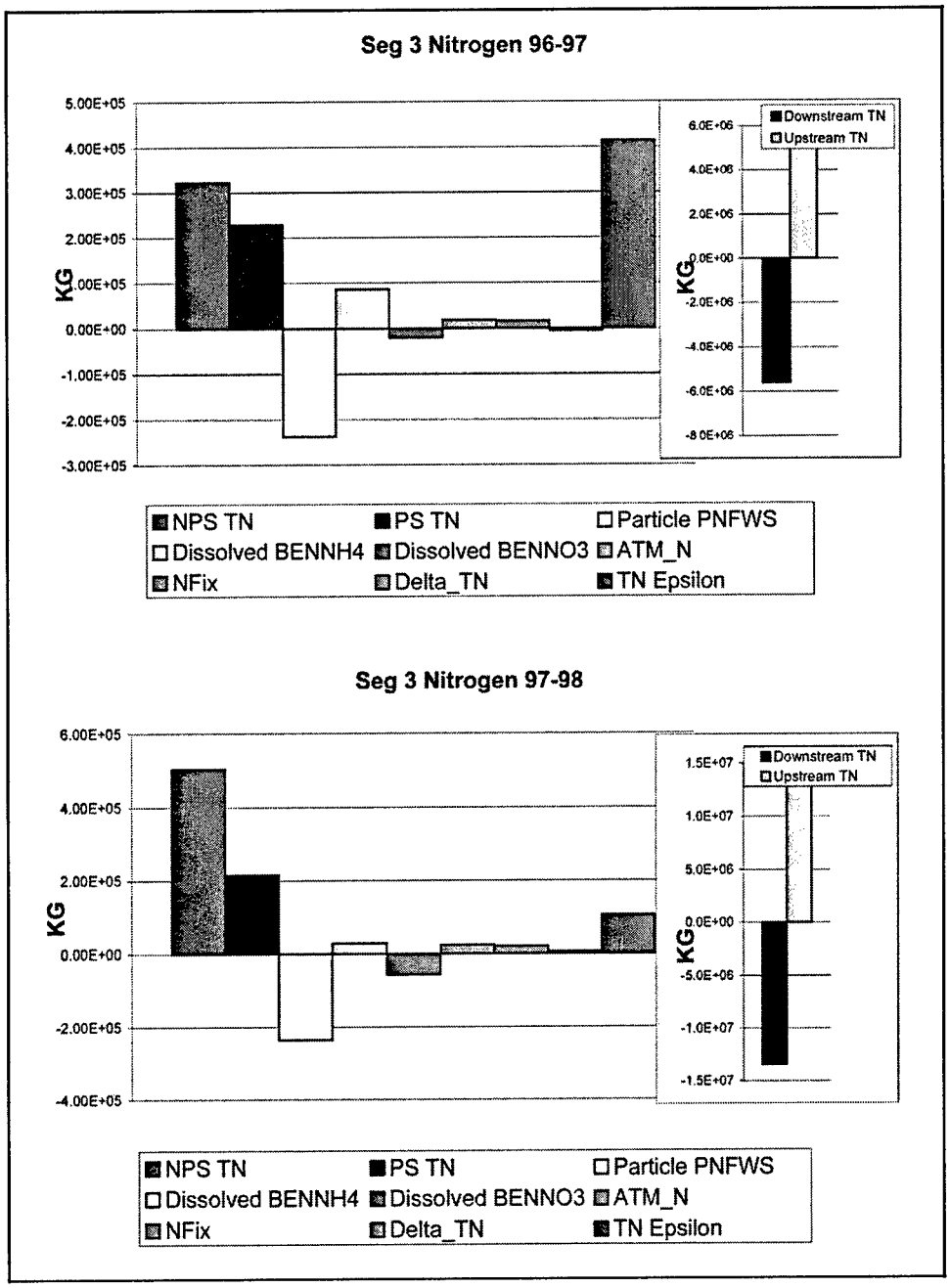

Figure 10-5. (Sheet 3 of 6)

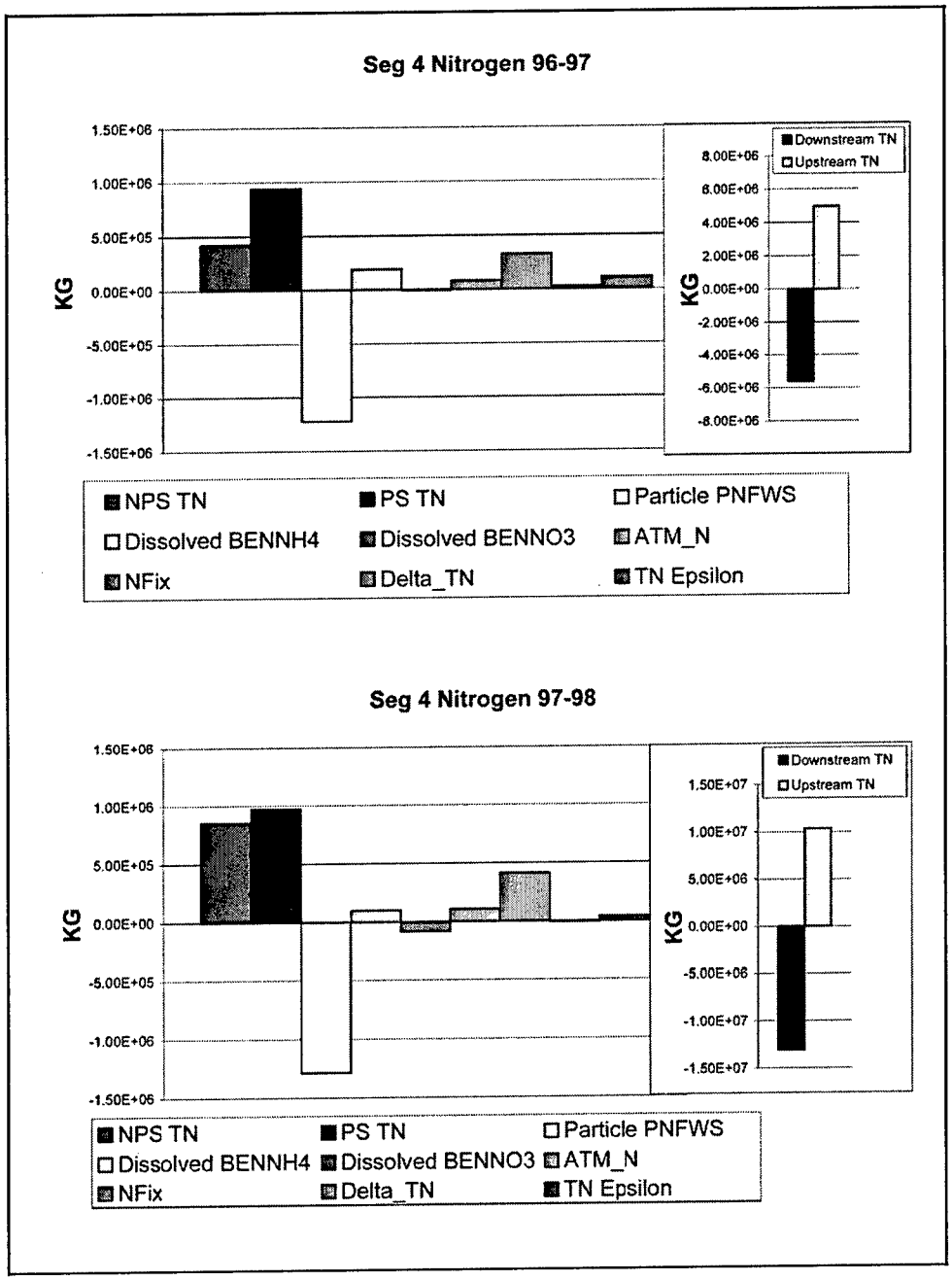

Figure 10-5. (Sheet 4 of 6)

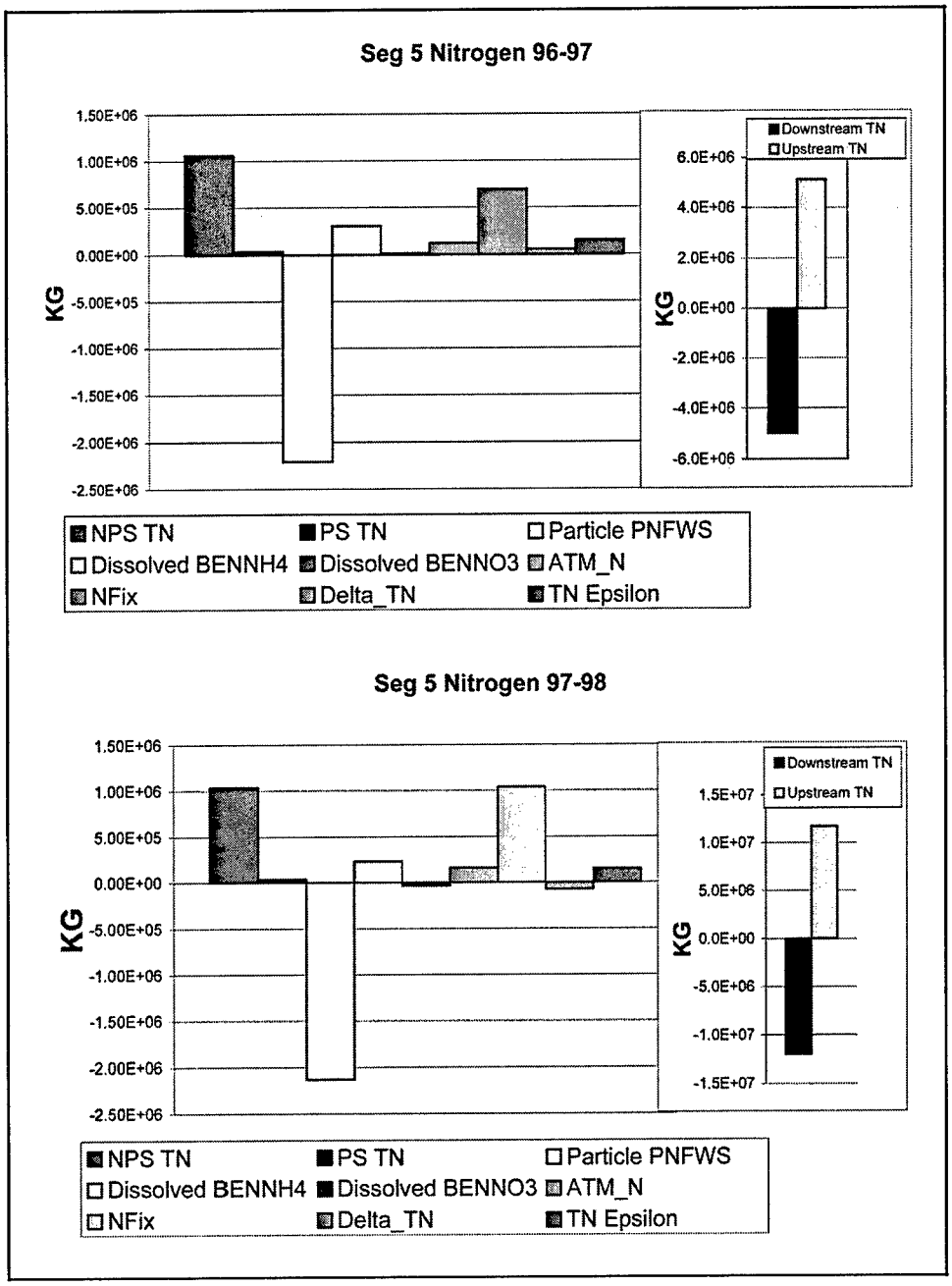

Figure 10-5. (Sheet 5 of 6)

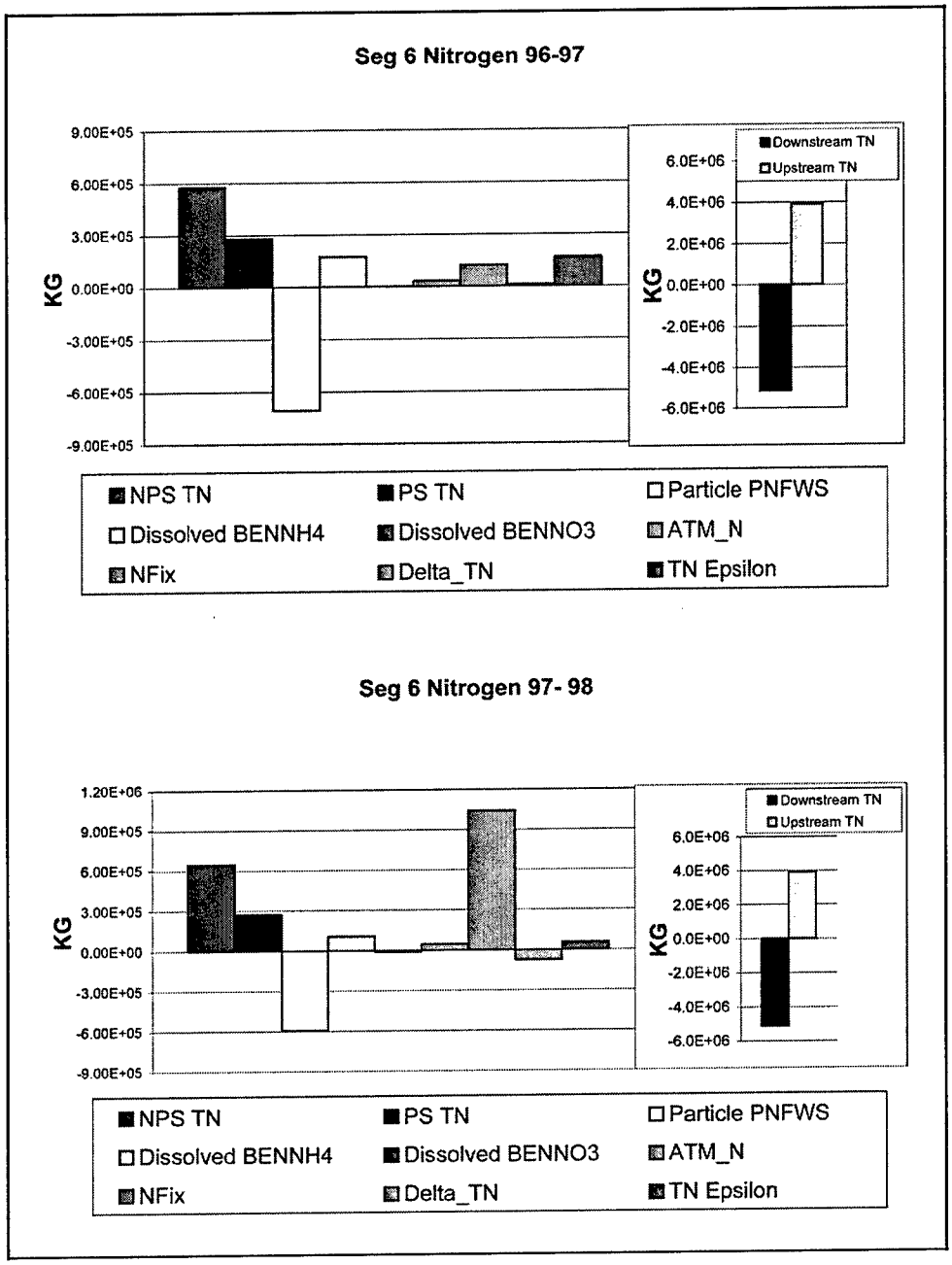

Figure 10-5. (Sheet 6 of 6)

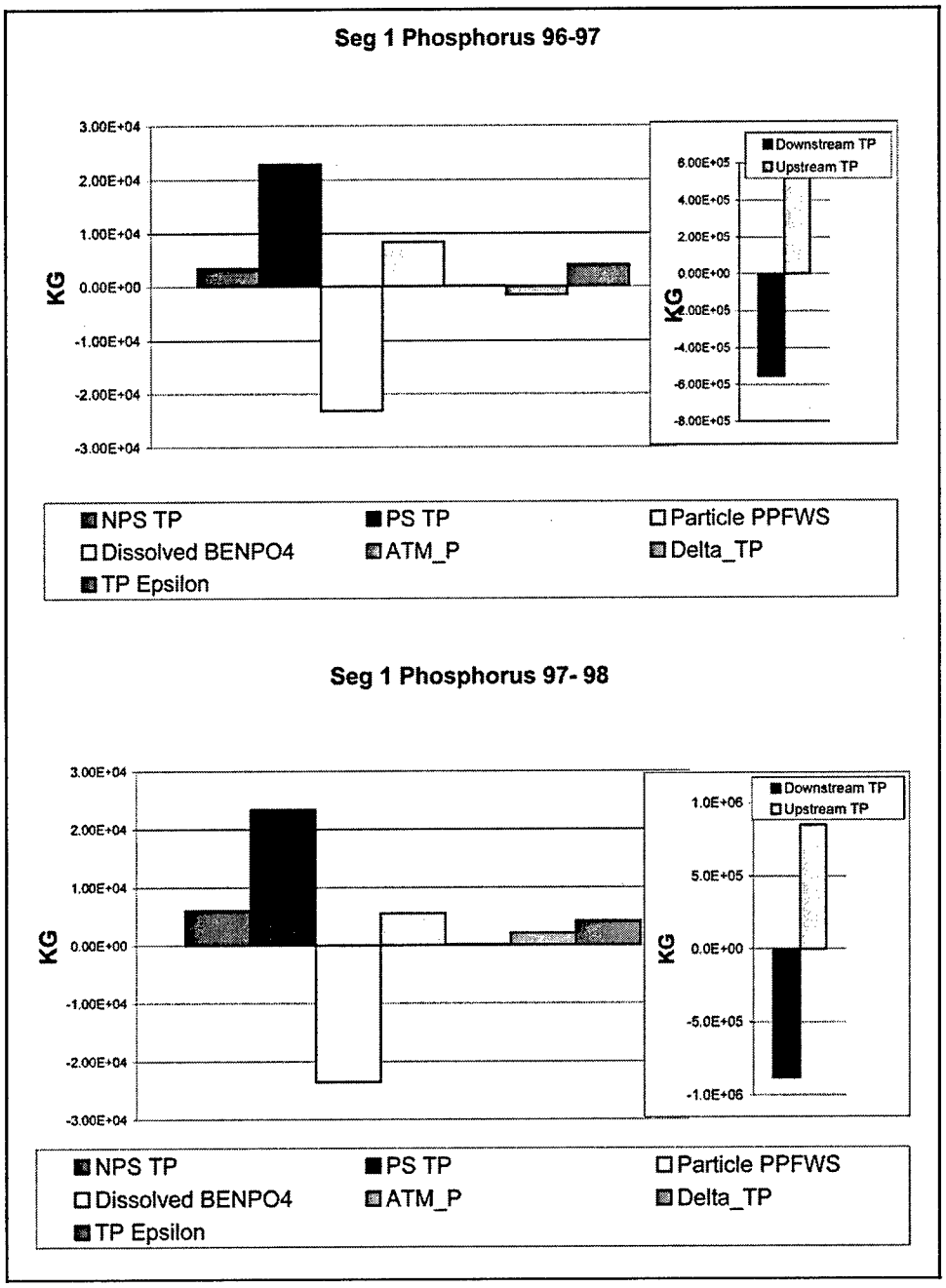

Figure 10-6. TP budget by segments for both simulation years (Sheet 1 of 6)

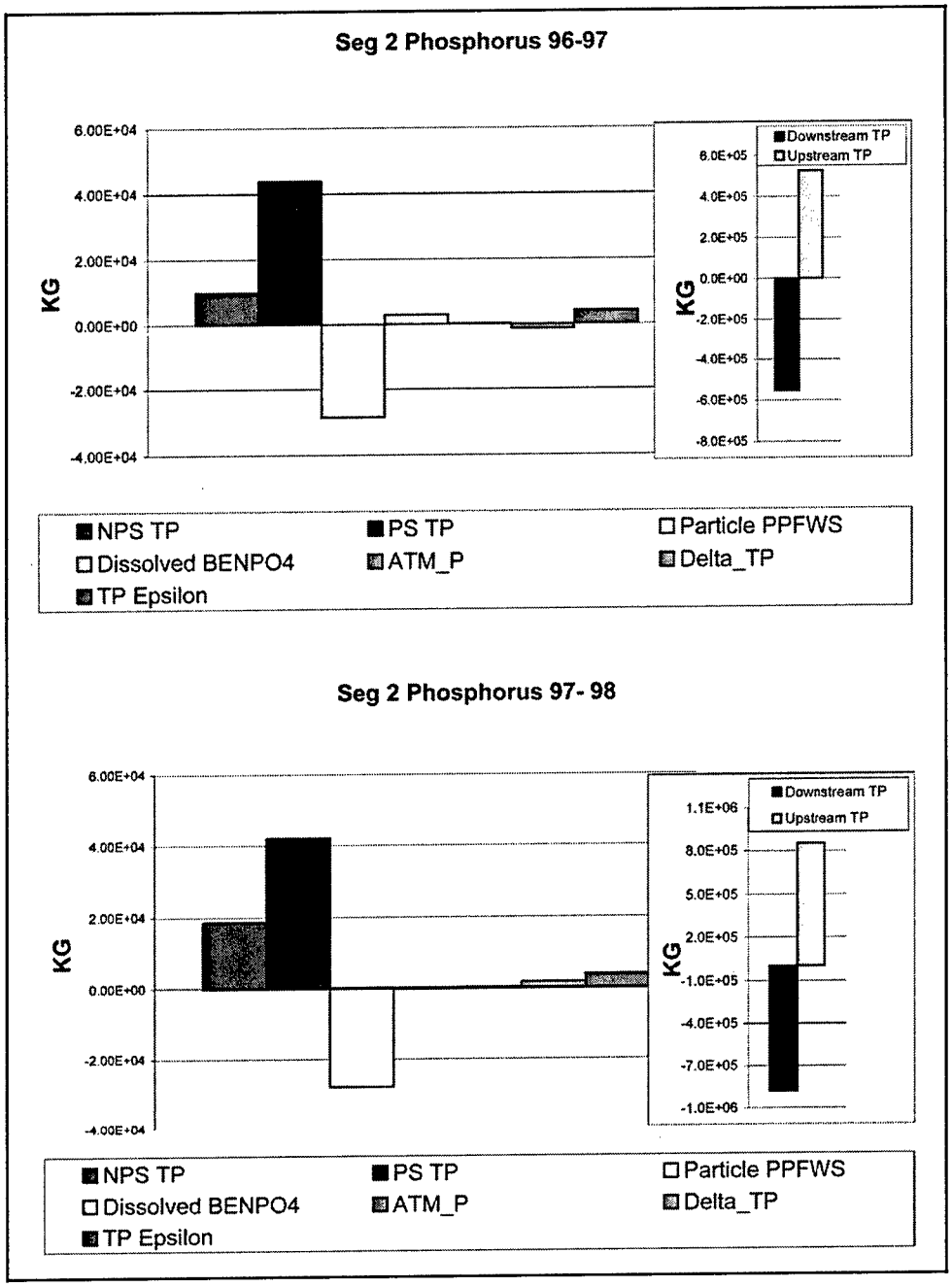

Figure 10-6. (Sheet 2 of 6)

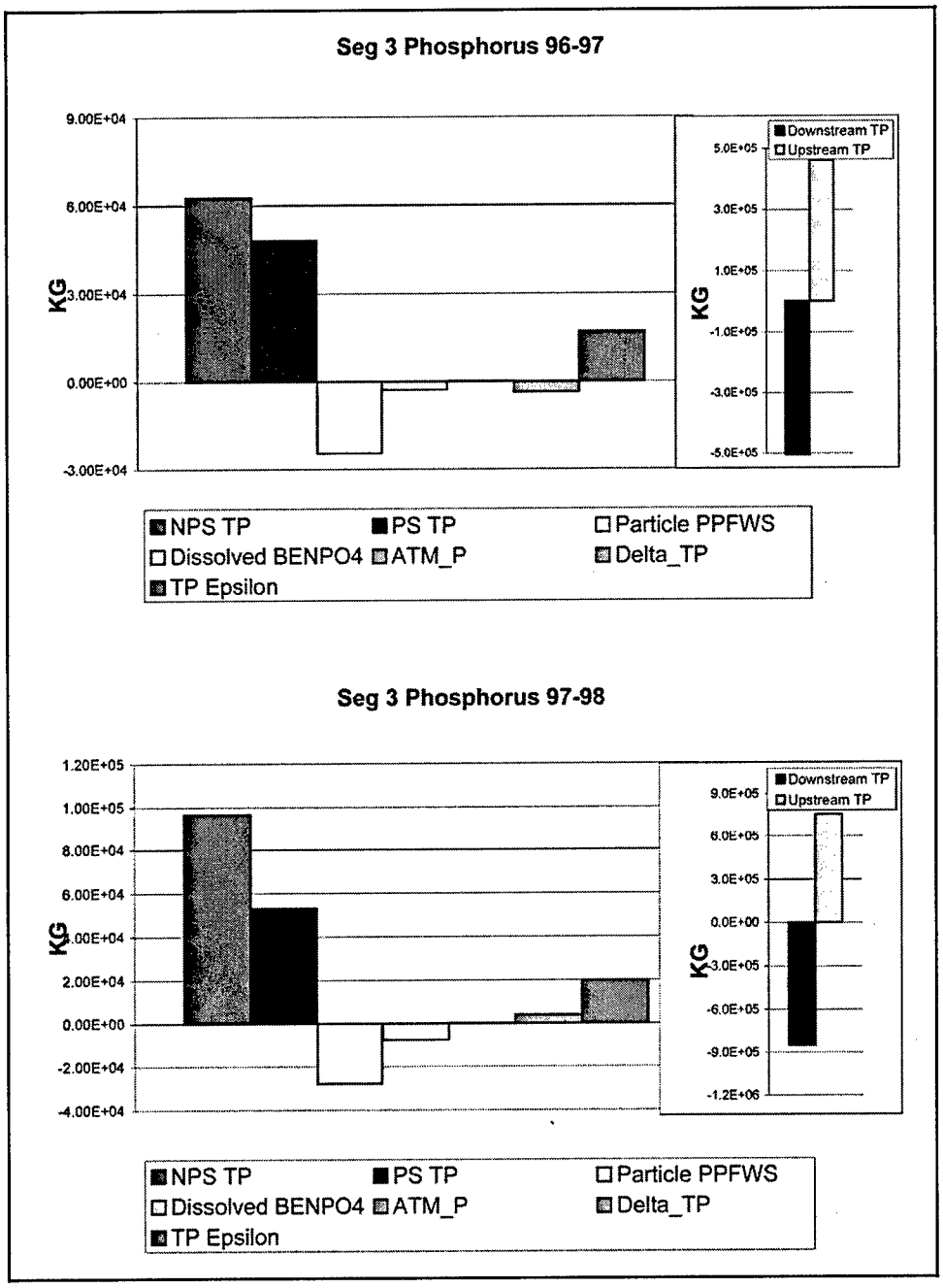

Figure 10-6. (Sheet 3 of 6)

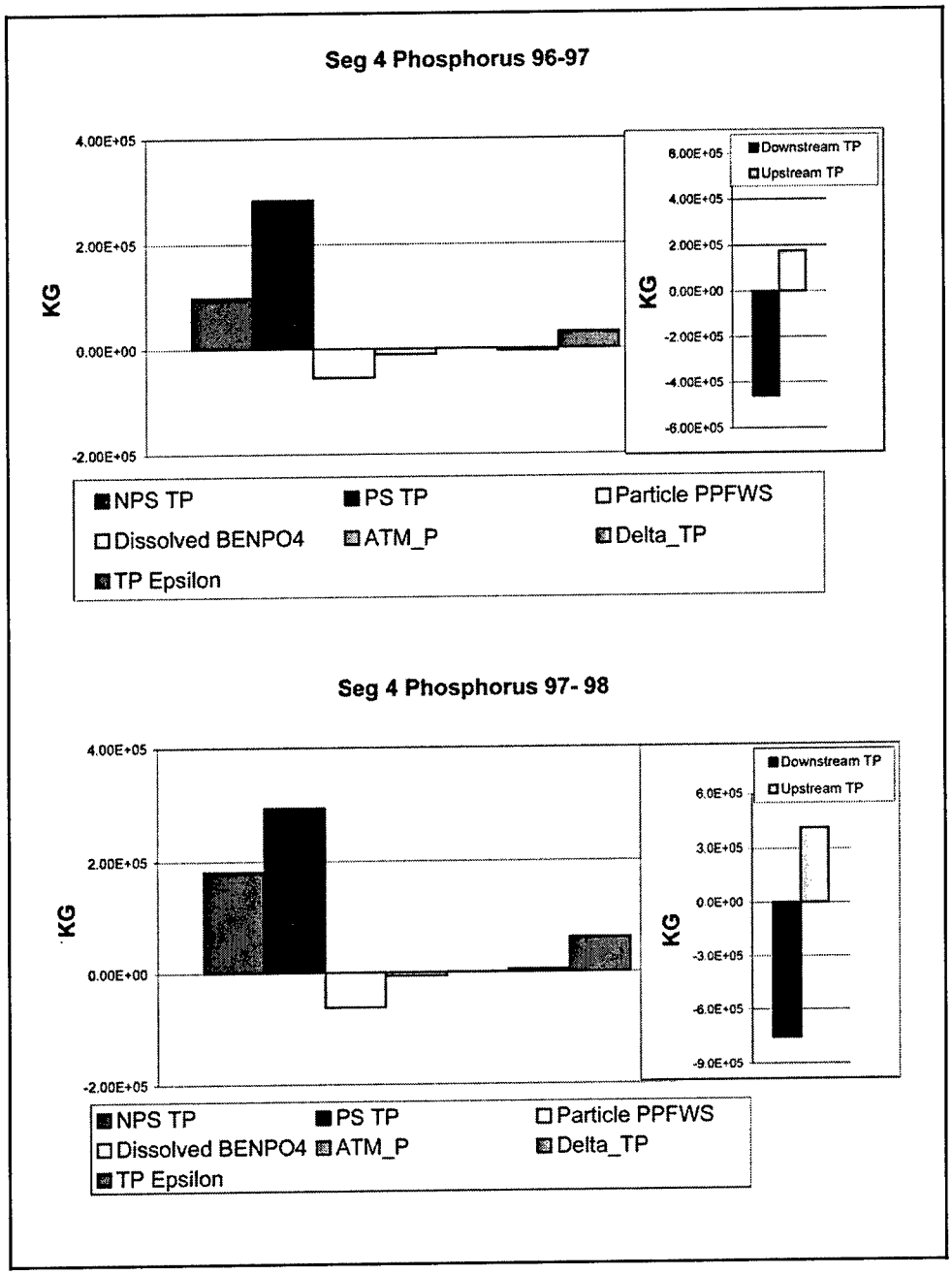

Figure 10-6. (Sheet 4 of 6)

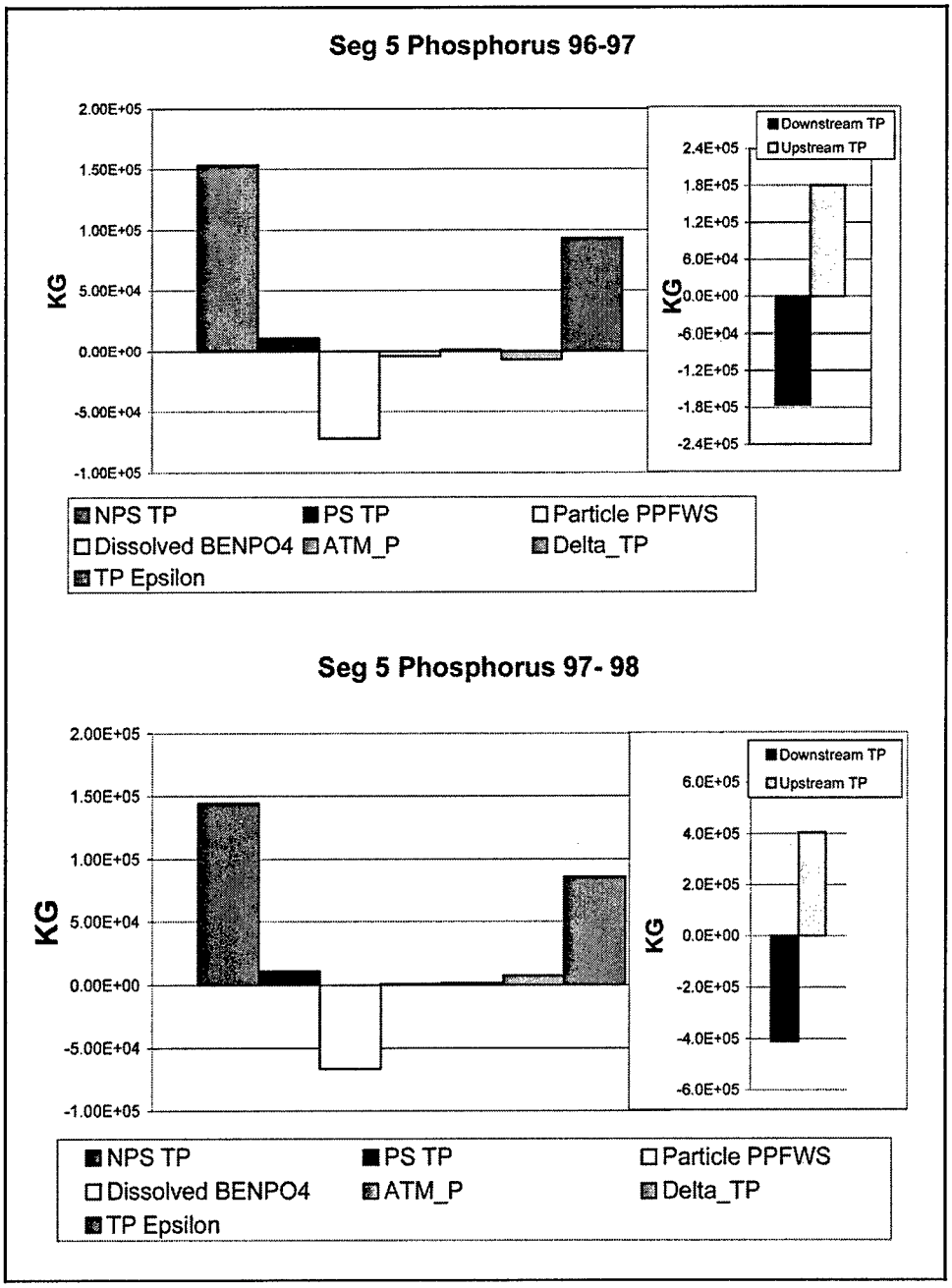

Figure 10-6. (Sheet 5 of 6)

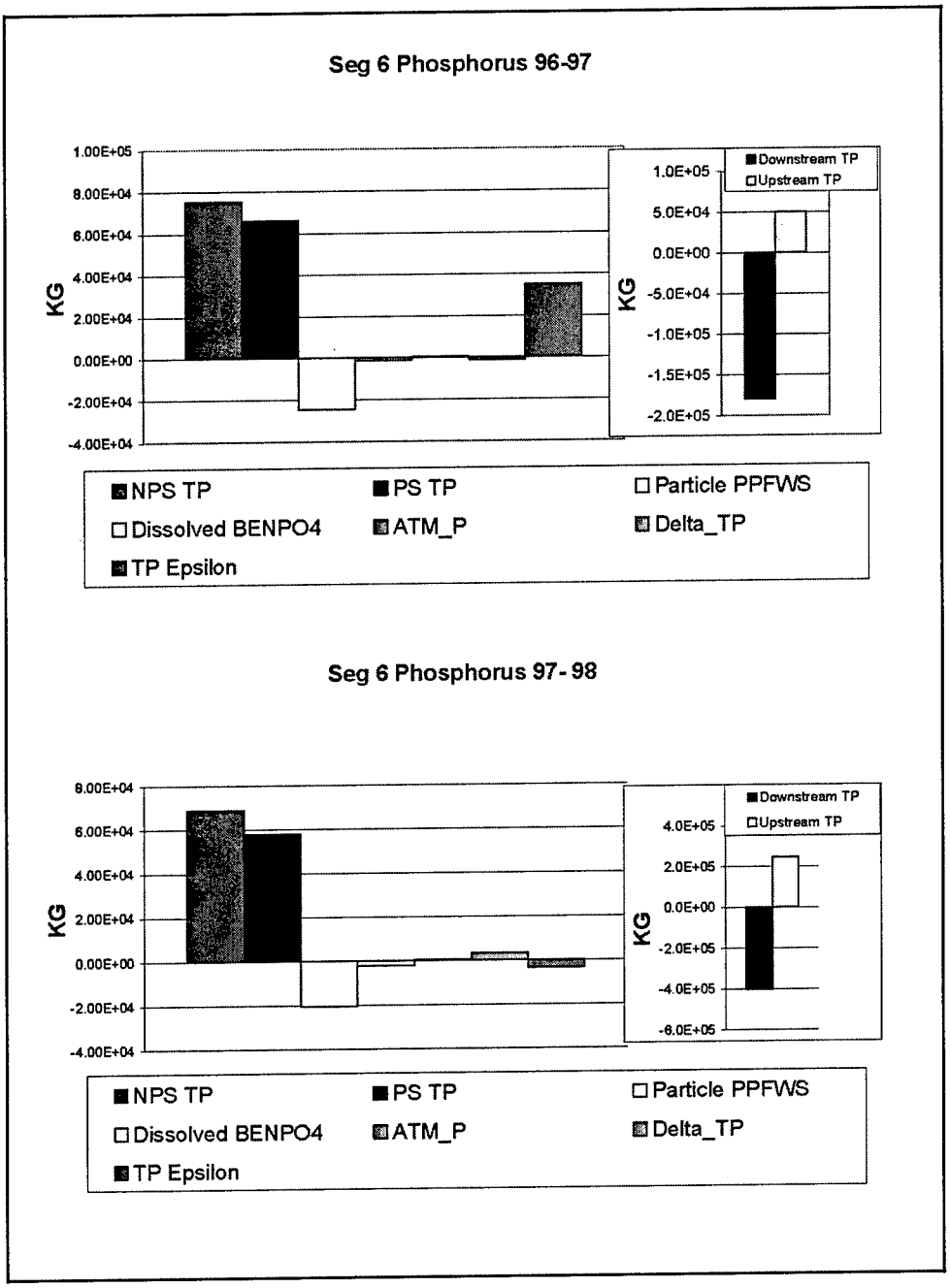

Figure 10-6. (Sheet 6 of 6)

b. Of the variables included in the TN and TP budgets, the budgets appear to be most affected by transport. Transport of TN and TP mass into and out of each segment is usually an order of magnitude larger than mass loads or other sources of mass. Overall transport through the system was in a downstream direction toward the ocean.

c. Besides transport for segments 1, 2, and 4, PS loads provide the largest source of TN mass for both years, and for segments 3, 5, and 6, NPS loads provide the largest source of TN mass for both years.

d. Like TN loadings, PS loads for segments 1, 2, and 4 provide the largest source of TP mass for both years after transport, and NPS loads for segments 3, 5, and 6 provide the largest source of TP mass for both years after transport.

e. Nitrogen fixation becomes a major source of TN in segments 5 and 6 during the 1997-1998-simulation year.

f. Besides transport out of the system as a mechanism of loss for nitrogen and phosphorus, particulate nitrogen and phosphorus settling is the next largest loss mechanism from the system. Losses of particulate phosphorus mass is about the same magnitude for all segments, but loss of particulate nitrogen mass from segments 4 and 5 is an order of magnitude greater than for all the other segments.

Ideally, the law of mass conservation requires that the mass balance within a segment should be zero. The ε is an indicator of the error amount of Equation 10-1. For this application, ε was found to be approximately 10 percent or less when computing TN and TP mass balance for each segment. Even though TN and TP mass balance were not zero, an error of 10 percent or less was deemed acceptable when one considers that loads are affected by numerous assumptions regarding sources, destination, attenuation, and round-off errors made during computations of the average yearly transport and mass load values.

Change in mass over a simulation year was included in the analysis as well. Estimates of delta TN and TP by year for each segment were computed by summing all components of TN (i.e., algal N, ammonium, nitrate, labile/refractory DON, and labile/refractory PON) and TP (i.e., algal internal P, labile/refractory DOP, and labile/refractory POP) for the first and last day of simulation and solving as:

Delta TP or TN = last day TP or TN (kg) minus 1st TP or TN (kg) (10-2)

The plots indicate that TP and TN mass has slightly changed over the year for all segments.

Reference

Hendrickson, J., and Konwinski, J. (1998). "Seasonal nutrient import-export budgets for the Lower St. Johns River, Florida," Contract Report WM598, Florida Department of Environmental Protection, Tallahassee, FL.

Appendix A
Acronyms

3D	three dimensional
ACR	areal community respiration
AME	average mean error
BOD	biochemical oxygen demand
CBOD	carbonaceous biochemical oxygen demand
CE-QUAL-ICM	Corps of Engineers Integrated Compartment Water Quality Model
CESAJ	U.S. Army Engineer District, Jacksonville
CH3D	computational hydrodynamics in three dimensions
DIC	dissolved inorganic carbon
DIN	dissolved inorganic nitrogen
DIP	dissolved inorganic phosphorus
DO	dissolved oxygen
DOC	dissolved organic carbon
DON	dissolved organic nitrogen
EFDC	Environmental Fluid Dynamics Code
EPA	U.S. Environmental Protection Agency
FDEP	Florida Department of Environmental Protection
GAP	gross areal production
HM	hydrodynamic model
ICM	integrated component model
LSJR	Lower St. Johns River
LTOC	labile total organic carbon
ME	mean error
NPS	non-point source
POC	particulate organic carbon

PON	particulate organic nitrogen
POP	particulate organic phosphorus
PS	point source
RE	relative error
RSME	root mean square error
RTOC	refractory total organic carbon
SAD	South Atlantic Division
SAS	Statistical Analysis System
SAV	submerged aquatic vegetation
SJRWMD	St. Johns River Water Management
SOW	scope of work
STORET	STOrage and RETrieval
SWIM	Surface Water Improvement and Management
TMDL	Total Maximum Daily Load
TN	total nitrogen
TOC	total organic carbon
TP	total phosphorus
USGS	U.S. Geological Survey
VCR	volumetric community respiration
WQM	water quality model

REPORT DOCUMENTATION PAGE

Form Approved
OMB No. 0704-0188

Public reporting burden for this collection of information is estimated to average 1 hour per response, including the time for reviewing instructions, searching existing data sources, gathering and maintaining the data needed, and completing and reviewing this collection of information. Send comments regarding this burden estimate or any other aspect of this collection of information, including suggestions for reducing this burden to Department of Defense, Washington Headquarters Services, Directorate for Information Operations and Reports (0704-0188), 1215 Jefferson Davis Highway, Suite 1204, Arlington, VA 22202-4302. Respondents should be aware that notwithstanding any other provision of law, no person shall be subject to any penalty for failing to comply with a collection of information if it does not display a currently valid OMB control number. PLEASE DO NOT RETURN YOUR FORM TO THE ABOVE ADDRESS.

1. REPORT DATE *(DD-MM-YYYY)*
August 2004

2. REPORT TYPE
Final report

3. DATES COVERED *(From - To)*

4. TITLE AND SUBTITLE
Three-Dimensional Eutrophication Model of the Lower St. Johns River, Florida

5a. CONTRACT NUMBER
CRDA 02-EL-03

5b. GRANT NUMBER

5c. PROGRAM ELEMENT NUMBER

6. AUTHOR(S)
Dottie H. Tillman, Carl F. Cerco, Mark R. Noel, James L. Martin, and John Hamrick

5d. PROJECT NUMBER

5e. TASK NUMBER

5f. WORK UNIT NUMBER

7. PERFORMING ORGANIZATION NAME(S) AND ADDRESS(ES)
U.S. Army Engineer Research and Development Center, Environmental Laboratory,
3909 Halls Ferry Road, Vicksburg, MS 39180-6199;
Mississippi State University, Department of Civil Engineering,
Mississippi State, MS 39762;
Tetra Tech Incorporated, Fairfax, VA 22030

8. PERFORMING ORGANIZATION REPORT NUMBER
ERDC/EL TR-04-13

9. SPONSORING / MONITORING AGENCY NAME(S) AND ADDRESS(ES)
St. Johns River Water Management District
Palatka, FL 32177

10. SPONSOR/MONITOR'S ACRONYM(S)

11. SPONSOR/MONITOR'S REPORT NUMBER(S)

12. DISTRIBUTION / AVAILABILITY STATEMENT
Approved for public release; distribution is unlimited.

13. SUPPLEMENTARY NOTES

14. ABSTRACT

The CE-QUAL-ICM three-dimensional eutrophication model was applied to the lower, estuarine, portion of the St. Johns River, Florida. Transport processes were obtained from the Environmental Fluid Dynamics Code. Model application period was December 1996 through November 1998. The model activated 28 state variables in the water column including physical variables, three algal groups, multiple forms of carbon, nitrogen, phosphorus and silica, and dissolved oxygen. Several features were added to the model for this application. These included representation of the internal algal phosphorus pool, distinction of labile and refractory dissolved organic matter, and representation of nitrogen fixation. The water column was coupled to a predictive sediment diagenesis model that computed sediment-water fluxes of dissolved oxygen, chemical oxygen demand, ammonium, nitrate, phosphate, and silica, based on computed inputs of particulate organic matter. Model results were compared to an extensive suite of observations in the water column and benthic sediments.

15. Subject Terms
CE-QUAL-ICM | Eutrophication | St. Johns River | Water quality model

16. SECURITY CLASSIFICATION OF:			17. LIMITATION OF ABSTRACT	18. NUMBER OF PAGES	19a. NAME OF RESPONSIBLE PERSON Carl F. Cerco
a. REPORT	b. ABSTRACT	c. THIS PAGE			19b. TELEPHONE NUMBER *(include area code)*
UNCLASSIFIED	UNCLASSIFIED	UNCLASSIFIED	SAR	318	